Contents

Hydrazide-Based Hypercoordinate Silicon Compounds

DANIEL KOST and INNA KALIKHMAN

Transition Metal Complexes Bearing a Phosphenium Ligand

HIROSHI NAKAZAWA

Synthesis of Organosilicon Compounds by New Direct Reactions

BOK RYUL YOO and IL NAM JUNG

Transition Metal Complexes Containing
All-Carbon Ligands

MICHAEL I. BRUCE and PAUL J. LOW

Contributors

Numbers in parentheses indicate the pages on which the authors' contributions begin.

DANIEL KOST and INNA KALIKHMAN (1), Department of Chemistry, Ben-Gurion University of the Negev, Beer-Sheva 84105, Israel

HIROSHI NAKAZAWA (107), Department of Chemistry, Graduate School of Science, Osaka City University, Sumiyoshi-ku, Osaka 558-8585, Japan

BOK RYUL YOO and IL NAM JUNG (145), Organosilicon Chemistry Laboratory, Korea Institute of Science & Technology, P.O. Box 131, Cheongryang, Seoul 130-650, Korea

MICHAEL I. BRUCE (179), Department of Chemistry, University of Adelaide, Adelaide, South Australia 5005, Australia

PAUL J. LOW (179), Department of Chemistry, University of Durham, South Road, Durham DH1 3HE, England

Hydrazide-Based Hypercoordinate Silicon Compounds

DANIEL KOST* and INNA KALIKHMAN*

Department of Chemistry, Ben-Gurion University of the Negev, Beer-Sheva 84105, Israel

I

INTRODUCTION

The chemistry of silicon compounds differs from that of carbon in the ease at which silicon can expand its coordination shell to five and six. The resulting hypercoordinate silicon complexes (sometimes referred to as "hypervalent compounds") have drawn considerable attention over the past decades, as is evident from the numerous review articles.[1–11] A relatively limited number of bidentate ligands have been utilized for the preparation of hypercoordinate silicon complexes. The present review describes the introduction and use of a new class of chelating agents, based on the hydrazide functional group.

Hydrazide-based silicon complexes are remarkably versatile, forming a variety of novel complexes, penta and hexacoordinate, neutral, cationic, or anionic, as well as zwitterionic compounds. Many of these complexes

*E-mail: kostd@bgumail.bgu.ac.il (D.K.); innakal@bgumail.bgu.ac.il (I.K.).

1

have intriguing stereochemical properties, show chemical (intermolecular) or stereochemical (intramolecular) ligand-exchange phenomena, which have been studied extensively using NMR spectroscopy.

The entire class of complexes which form the subject of this review have been synthesized utilizing a silicon-ligand exchange reaction ("transsilylation"), which is the thread connecting the various different types of compounds. The reaction (Eq. 1) consists of exchange of ligands between an *N*- or *O*-(trimethylsilyl)hydrazide (TMS-hydrazide) and a polyhalosilane, such that the only byproducts are volatile TMS halides, which are readily boiled off. The ease and cleanliness of this reaction allow real-time NMR monitoring, and led to the many compounds reviewed in this chapter. Their interest, however, derives from the rich chemical and stereochemical reactivity, and from the curiosity to understand the principles governing the multitude of structures and reactions found, and in particular the nature of the donor to silicon dative bond.

$$RSiMe_3 + SiX_nR'_{4-n} \longrightarrow Me_3SiX + R\text{-}SiX_{n-1}R'_{4-n}$$

$$(X = F, Cl, Br; \ n = 2\text{-}4)$$

(1)
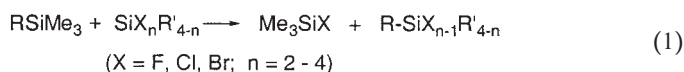
II

NEUTRAL PENTACOORDINATE COMPLEXES

A. *Chelates with Nitrogen–Silicon Coordination*

1. Dimethylamino Donor Coordination

i. Synthesis and structure

The reaction of dichlorosilanes (**2**, **3**) with *N*-dimethylamino-*O*-(trimethylsilyl)acylimidates (**1**)[12] produces neutral pentacoordinate silicon complexes (**4**, **5**), through ligand interchange (transsilylation) between the two silicon atoms (Eq. 2).[13–16] Three members of the series (**4a**,[14] **4c**,[15] **5c**[16]) were characterized by single crystal X-ray analysis and were shown to have a distorted trigonal bipyramid (TBP) geometry (Table I, Figs. 1 and 2).

$$
\begin{array}{l}
\text{Me}_3\text{SiO} \overset{R}{\underset{}{\diagdown}} \text{C=NNMe}_2 + \text{XPhSiCl}_2 \\[2pt]
\quad \textbf{1a}, R = Me \\
\quad \textbf{1b}, R = PhCH_2 \\
\quad \textbf{1c}, R = Ph \\
\quad \textbf{1d}, R = 4\text{-}MeC_6H_4 \\
\quad \textbf{1e}, R = 4\text{-}NO_2C_6H_4 \\
\quad \textbf{1f}, R = 3,5\text{-}(NO_2)_2C_6H_3 \\
\quad \textbf{1g}, R = CF_3 \\
\quad \textbf{1h}, R = Ph(Me)CH
\end{array}
$$

2, X = Me
3, X = H

−Me₃SiCl₃

4a-h, (X = Me)
5a-c, h (X = H)

(2)
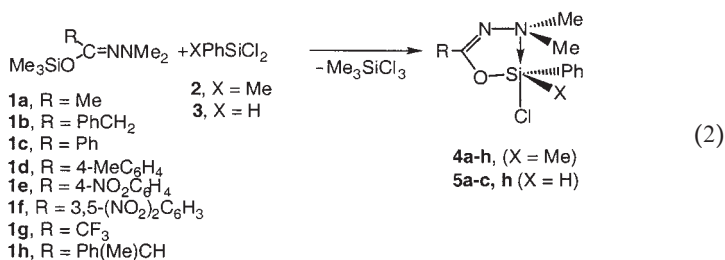
TABLE I

SELECTED BOND LENGTHS AND ANGLES FOR THE NEUTRAL PENTACOORDINATE COMPLEXES
4a,[14] **4c**,[15] AND **5c**[16]

Bond lengths (Å)			Angles (deg.)		
Bond	**4a**	**4c**	**5c**	Angle	**4a**	**5c**
Si–O	1.703(2)	1.684(2)	1.6948(14)	N–Si–Cl	166.7(1)	167.80(6)
Si–N	2.216(3)	1.843(3)	2.1582(17)	O–Si–C	112.5(1)	115.54(8)
Si–Cl	2.216(2)	2.192(9)	2.1602(8)	O–Si–C	127.5(1)	124.6(8)
Si–C	1.854(3)	1.843(3)	1.857(2)	O–Si–Cl	89.79(9)	91.33(5)
Si–C	1.863(3)	1.850(2)				
[Si–H]			[1.373(19)]			
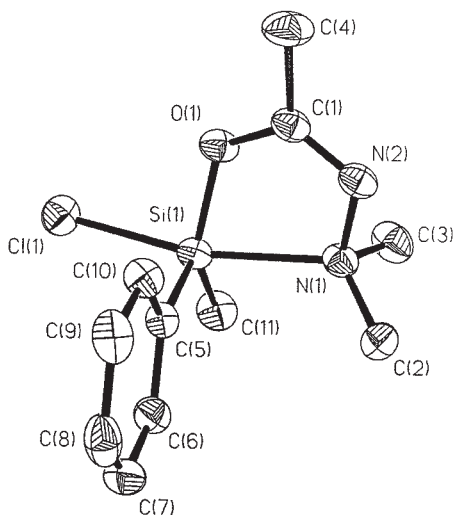
FIG. 1. Molecular structure of **4a** in the crystal.[14] Reproduced with permission from the American Chemical Society.
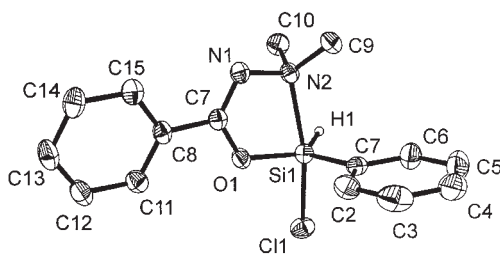
FIG. 2. Molecular structure of **5c** in the crystal.[16] Reproduced with permission from Wiley-VCH.

The ^{29}Si NMR spectra of **4** and **5** confirmed the TBP geometry and pentacoordination in solution: the ^{29}Si chemical shifts (Table II) fall within the pentacoordinate range.[14,16] However, the various compounds **4**, differing only in the remote substituents R, had substantially different ^{29}Si chemical shifts. This suggested that the substituents R had an effect on the donor strength of the nitrogen atom coordinated to silicon, and that the changes in ^{29}Si chemical shifts reflected changes in N $\rightarrow$ Si coordination strengths. Indeed, a correlation between ^{29}Si and ^{15}N chemical shifts (Table II, Fig. 3) gave a straight line, proving the connection between donor strength and intensity of coordination.[14] The comparison was made between coordinative silicon shifts, defined as the difference: $\Delta_1(^{29}\text{Si}) = \delta(^{29}\text{Si(pentacoordinate)}) - \delta(^{29}\text{Si(precursor}$ $\text{Me}_3\text{SiO(R)C}{=}\text{NNMe}_2))$, to eliminate the direct effect of R on the ^{29}Si chemical shift.

ii. Two ligand-exchange processes

Two intramolecular ligand exchange processes had been identified in neutral pentacoordinate N–Si chelate complexes: Si–N cleavage and pseudorotation.[17–19] Both were measured and reported for complexes with two or three halogen ligands attached to silicon, in which interchange of axial and equatorial ligands could be monitored.[17a,18] In complexes with a single halogen ligand, however, discrimination and exact assignment of both barriers had not been reported. Compounds **4** allowed such measurement and assignment of two intramolecular ligand-exchange processes in a monohalogeno pentacoordinate complex.[13,14,16]

The ^{1}H and ^{13}C NMR spectra of compounds **4** at ambient temperatures featured a single resonance for the two diastereotopic N-methyl groups, suggesting that rapid exchange relative to the NMR time scale took place and rendered the methyl groups equivalent. At lower temperatures typical coalescence phenomena of the methyl resonances were observed, enabling the determination of the free-energy activation barriers, listed in Table II. These barriers are also linearly correlated with the ^{29}Si coordinative chemical shifts, as is shown in Fig. 4. The correlation of activation barriers with ^{29}Si chemical shifts could readily be understood if the barriers were for the cleavage of the N $\rightarrow$ Si dative bond, because then *both* would be manifestations of the strength of coordination. However, the barriers could *a priori* be equally well for the inversion of configuration at silicon via pseudorotation.

To determine with certainty the nature of the exchange process, a second stereogenic unit, a chiral carbon center, was introduced

TABLE II
^{29}Si and ^{15}N NMR Data and Barriers for Ligand Exchange in **4a–4h**[14]

Compound	R	$\delta(^{29}Si)$ (ppm)	Δ_1 $(^{29}Si)^a$ (ppm)	$\delta(^{15}N)^b$ (ppm)	$\Delta(^{15}N)^c$ (ppm)	ΔG^* (kcal mol^{-1})
4a	Me	−32.8	−51.9	66.5	7.6	10.9
4b	PhCH$_2$	−31.8	−52.1	66.4	7.5	11.0
4c	Ph	−29.0	−47.8	66.8	6.6	10.6
4d	4-MeC$_6$H$_4$	−30.0	−48.2			10.7
4e	4-NO$_2$C$_6$H$_4$	−23.0	−44.5			9.4
4f	3,5-(NO$_2$)$_2$C$_6$H$_3$	−14.7	−38.5	68.2	3.7	8.9
4g	CF$_3$	−3.2	−30.0	64.7	2.4	< 7
4h	PhMeCH	−33.8	−54.2	65.7, 66.4	7.8, 5.7	11.4

^{a}Coordinative shift, defined by: $\Delta_1(^{29}Si) = \delta(^{29}Si(pentacoordinate)) - \delta(^{29}Si(precursor, Me_3SiO(R)C=NNMe_2))$.
^{b} ^{15}N shift for the $\underline{N}Me_2$ group, relative to external NH$_4$Cl.
^{c}Coordinative shift, defined by: $\Delta(^{15}N) = \delta(^{15}N(pentacoordinate)) - \delta(^{15}N(precursor, Me_3SiO(R)C=NNMe_2))$.
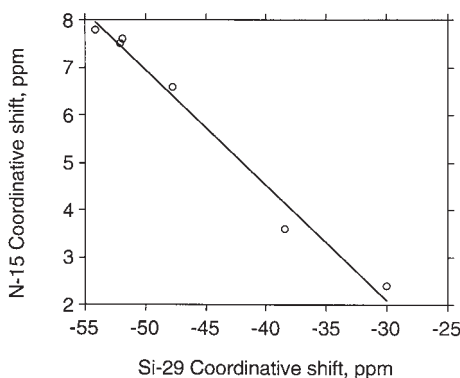
Fig. 3. Linear correlation between ^{15}N and ^{29}Si chemical shifts for differently substituted complexes **4**.[14] Reproduced with permission from the American Chemical Society.

in **4h**.[14] The resulting ^{1}H NMR spectra at various low temperatures (Fig. 5) provided the necessary evidence that the observed exchange process was the N → Si bond cleavage: at the slow-exchange limit temperature (200 K) the spectrum features doubling of all signals due to the presence of two diastereomers. When the temperature was raised, exchange took place *only* between the *N*-methyl groups, while the signals for all other groups remained essentially unchanged. This proved that the diastereomers were stable up to 300 K, i.e., no pseudorotation at silicon took place, and hence
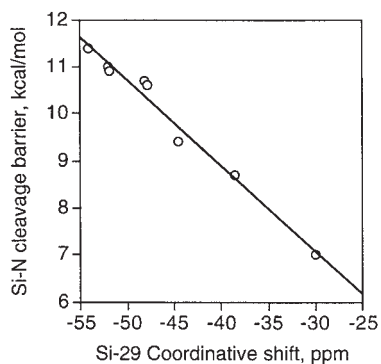
FIG. 4. Linear correlation between *N*-methyl exchange barriers and coordinative ^{29}Si chemical shifts for **4a–4g**.[14] Reproduced with permission from the American Chemical Society.

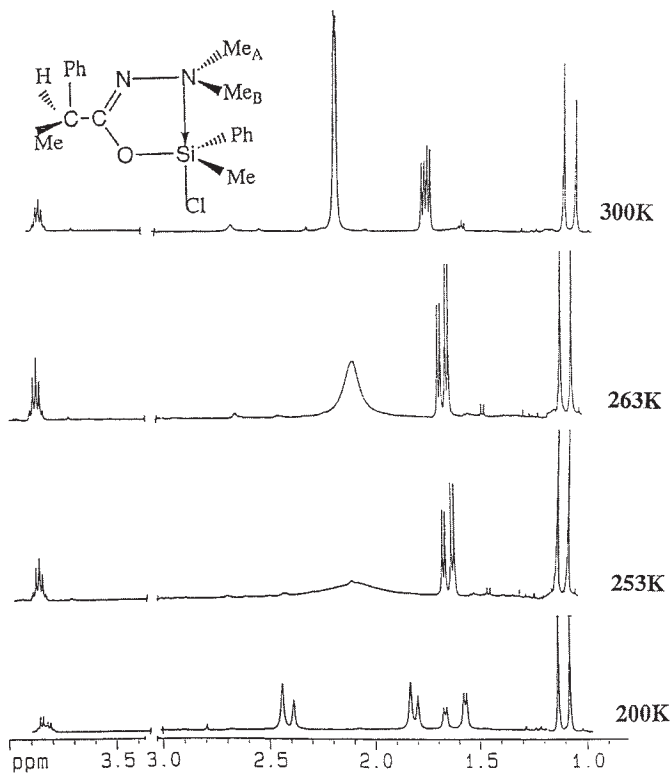FIG. 5. Variable temperature ^{1}H NMR spectra of **4h** (high-field region) in CD$_2$Cl$_2$ solution showing exchange of *N*-methyl groups without exchange of diastereomers.[14] Reproduced with permission from the American Chemical Society.

exchange of *N*-methyl groups must have resulted from N → Si cleavage, followed by rotation about the N–N bond and re-closure of the chelate ring (Eq. 3). It was thus shown that the remote R substituents effect the donor strengths such that electron withdrawing R (4-nitrophenyl) causes complexation to be weaker, resulting in lower ring-opening barrier, and relative shifts of the ^{29}Si–^{15}N resonances to lower field.[14]

$$(3)$$
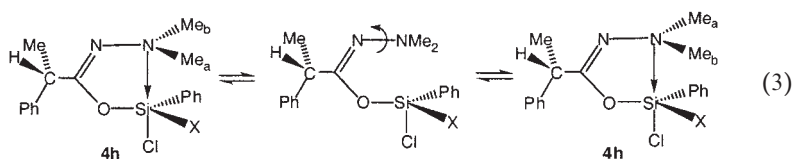
Complexes **4** undergo a second intramolecular exchange process, inversion of configuration at silicon, most likely by a Berry pseudorotation mechanism. However, this exchange is observable by NMR spectroscopy only for **4h**, through coalescence of signal pairs arising from the diastereomers due to epimerization at silicon.[14] This exchange was measured in $C_6D_5NO_2$ solution and the barrier was found to be remarkably high: $T_c = 380 \pm 1$ K, $\Delta G^* = 18.7 \pm 0.2$ kcal mol^{-1}. It was suggested that the high barrier associated with this monofunctional complex (possessing only one halogeno ligand) was the result of either forcing the halogen from the apical to the equatorial position, or forcing the ring to occupy two equatorial positions, during one of the pseudorotation steps.[14]

iii. Coupling constants across the dative bond

Complexes **5a–c,h** with a hydrido ligand behave essentially in a similar manner as **4a–h**: two consecutive intramolecular exchange processes are monitored by the NMR spectra, and can be assigned to dissociation of the N → Si bond and to inversion of configuration at the silicon center.[16] However, the presence of the hydrido ligand introduces an additional parameter, the spin–spin interactions between ^{1}H and ^{29}Si, ^{15}N, and even ^{13}C, through one, two, and three bonds, respectively, including the dative bond. Table III lists the coupling constants measured for **5a–c,h**, including the ^{15}N–^{29}Si interaction. Perhaps the most interesting observation in these compounds is the fact that spin–spin interactions across the dative bond are observed even at temperatures at which N → Si dissociation–recombination is rapid on the NMR time scale.[16]

A discussion on the correlation between crystal structure and coupling constants appears in Section V.

TABLE III

COUPLING CONSTANTS (HZ) THROUGH THREE, TWO, AND ONE BONDS ACROSS THE N → Si
COORDINATIVE BOND IN **5**, OBTAINED FROM ^{13}C (AT 243 K), ^{15}N, AND ^{15}N{^{1}H} SPECTRA
(AT 300 K), RESPECTIVELY[16]

Compound	R	$^3J(^{13}CNSi^1H)$	$^2J(^{15}NSi^1H)$	$^1J(^{15}N^{29}Si)$
5a	Me	1.6	10.8	3.2
5b	PhCH$_2$	1.7	10.8	2.4
5c	Ph	1.7	10.6	3.3
5h	PhMeCH	1.8		

2. Isopropylideneimino Donor Coordination

In order to study the effect of hybridization of the donor atom (nitrogen) on donor strength, a complex with the isopropylideneimino donor group (**7**) was prepared (Eq. 4) and compared with the dimethylamino complexes **4**. Compound **7** was obtained by the same exchange reaction (Eq. 1) as other hypercoordinate complexes from the isopropylideneimine **6a** and **2**. A crystal structure of **7** was determined, and is depicted in Fig. 6, and selected data are compared with those of the dimethylamino analog in Table IV.

$$\text{(4)}$$
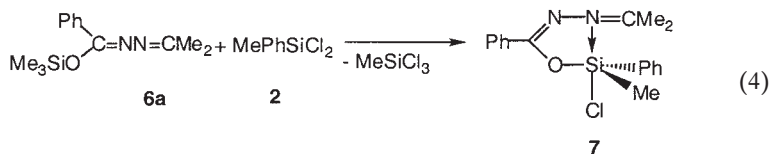
The crystallographic evidence, as well as the ^{29}Si NMR data, prove that the sp^2-hybridized nitrogen in **7** acts as a stronger donor towards silicon than the sp^3-hybridized nitrogen in **4c**. Table IV shows that in the two analogous complexes, differing only in the donor groups, the N → Si bond distance varies dramatically: it decreases by 0.18 Å from **4c** to **7**, indicating substantially stronger coordination.

The stronger coordination of the isopropylideneimino ligand to silicon is also confirmed by a substantial upfield shift of the silicon resonance, from −29.0 in **4c** to −52.8 ppm in **7** (in CDCl$_3$ solution at 300 K).[20] An additional manifestation of the stronger donor property of the isopropylideneimino group is found in the relative ease of ionization of hexacoordinate complexes with this ligand. This subject is discussed in Section III.B.2.

One may wonder why the isopropylideneimino group acts consistently as a stronger donor than the dimethylamino group: initially the reverse
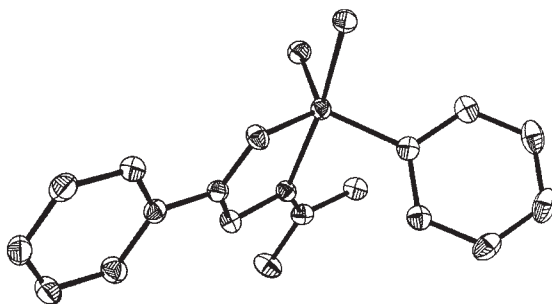
FIG. 6. Molecular structure of **7** in the crystal.[20]

TABLE IV

COMPARISON OF BOND DISTANCES IN ANALOGOUS PENTACOORDINATE COMPLEXES DIFFERING IN DONOR GROUPS: N–NMe$_2$ (**4c**)[15] AND N–N=CMe$_2$ (**7**)[20]

Bond	4c	7
Si–O	1.684(2)	1.7012(11)
Si–N	2.264(2)	2.0824(13)
Si–Cl	2.192(9)	2.2230(5)
Si–C (Me)	1.843(3)	1.8540(17)
Si–C (Ph)	1.850(2)	1.8665(16)

order might be expected, due to the higher-energy sp^3 lone-pair orbital in Me$_2$N relative to the sp^2 lone-pair in N=CMe$_2$. However, the planar conjugated C=N–N=C system in the isopropylideneimino donor is ideally oriented for coordination with silicon, and hence the probability of coordination is increased.

B. *Chelates with Oxygen–Silicon Coordination*

1. Amide-Based O → Si Coordinated Complexes

An effective route to O → Si pentacoordinate silicon chelates consists of the reaction of chloromethyl(dimethyl)chlorosilane (ClCH$_2$SiMe$_2$Cl, **8**) with a variety of *N*- or *O*-trimethylsilylamides,[21,22] lactams,[23–25] ureas,[26,27] acetylacetamide,[28,29] and 2-pyridones.[30–32] It is a two-step reaction: in the first step transsilylation takes place with evolution of the volatile trimethyl-chlorosilane, followed by an internal S$_N$2 type displacement of chloride by nitrogen, forming a five-membered heterocyclic chelate ring and a Si–Cl bond (Eq. 5).[11,21–25]

$$\text{(5)}$$

This reaction was applied to *O*-TMS-hydrazides **1**, and led to some interesting regioselective chemistry described below.

2. Regioselective Formation of Five- and Six-Membered O → Si Chelates

The transsilylation reaction described above was studied with **8** and the silylated hydrazides **1**.[33,34] The *E,Z* stereoisomers of **1a**[35] reacted in different ways, shown in Eqs. (6) and (7). Initially both isomers form unstable tetracoordinate silane intermediates (**9a-E**, **9a-Z**), which can be observed at low temperatures in CD_2Cl_2 solutions by ^{29}Si NMR spectroscopy. The intermediates **9a-E** and **9a-Z** could be observed for about 20 min at −70 °C, before reacting further to form five-membered and six-membered chelate products **10a** and **11a**, respectively. At ambient temperature the reaction proceeds immediately without observation of intermediates.

$$\text{(6)}$$

$$\text{(7)}$$

In the rearrangement reaction leading to **10a** and **11a** the nitrogen atom which is nearest and most accessible to the chloromethyl group displaces the chlorine atom in an internal S_N2 type substitution, followed by migration of the displaced chloride to silicon. This rearrangement leads to the two different products, with five- and six-membered chelate cycles, **10a** and **11a**. While five-membered chelate cycles as in **10a** are common in hypercoordinate silicon chemistry, the formation of six-membered chelates (**11a**) is unique.[33,34]

Other silylacylimidates **1** presumably reacted in a similar manner. However, since in all but **1a** only the *Z*-isomer was detectable by NMR spectroscopy, the only products obtained from all other **1** (**1c–e,g,i**) were the six-membered chelates **11c–e,g,i**.[34,36,37]

3. Evidence for Si ← Cl⁻ Coordination in Six-Membered Chelates

The structures of complexes **11** are of significant interest: **11** is a cyclic zwitterionic complex in which the ammonium nitrogen bears a formal positive charge, while the location of the negative charge is unclear. As Scheme 1 suggests, the negative charge may reside on the hydrazide nitrogen, on oxygen, on silicon, or on chloride ligand, depending on the relative contributions of the corresponding canonical structures **A–D**. The crystal structures obtained for two of these complexes, **11i** (R = 4-CH₃OC₆H₄)[36] and **11g** (R = CF₃),[37] are depicted in Figs. 7 and 8, and selected data are given in Table V. The O–Si bond distance in **11i** is relatively short, closer to a covalent (1.68 Å)[38] than to a dative O → Si bond (1.9–2.3 Å).[2] On the other hand, the Si–Cl distance (Table V) is substantially longer than a normal Si–Cl covalent bond (2.048 Å).[38] It follows that canonical structure **A** (Scheme 1) best describes the geometry of **11g,i**, that is, in these complexes the chloride, and not the oxygen part of the O–Si–Cl axial fragment, is coordinated to silicon.
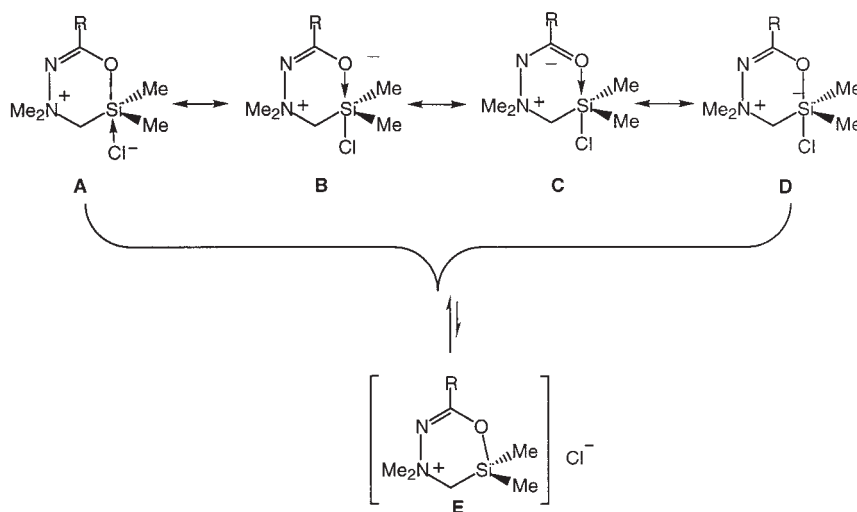
SCHEME 1. Canonical structures for complexes **11**, and their ionic dissociation.
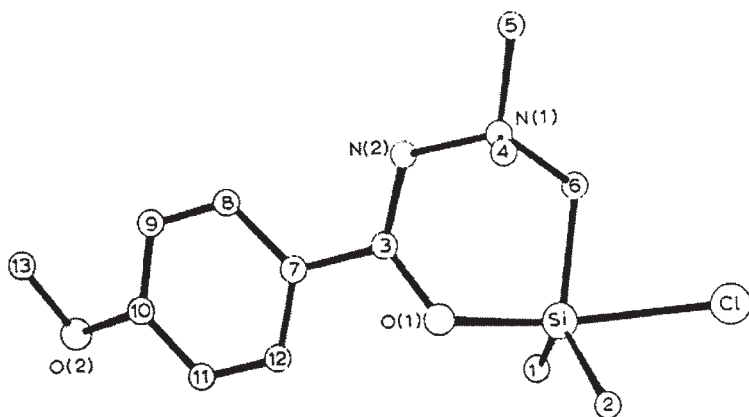
FIG. 7. Molecular structure of **11i** in the crystal.[36] Reproduced with permission from Elsevier Science.
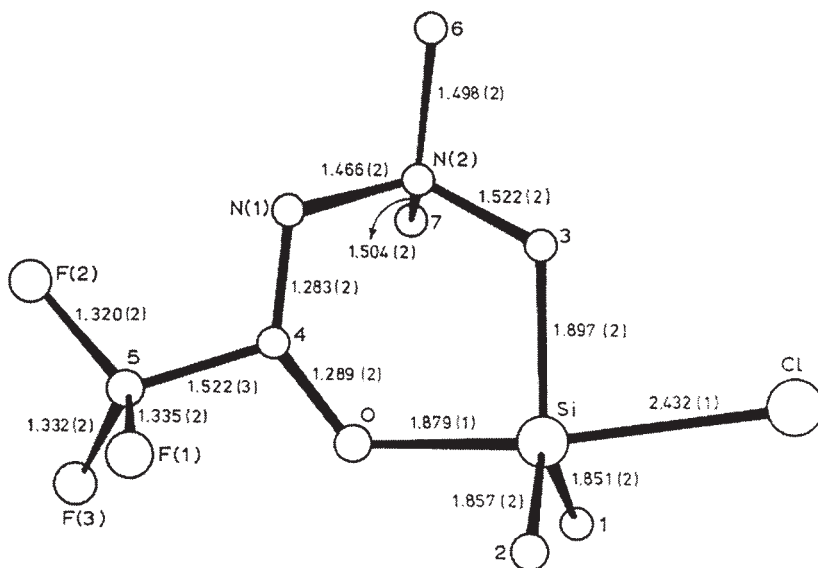

FIG. 8. Molecular structure of **11g** in the crystal.[37] Reproduced with permission from Elsevier Science.

This conclusion was also confirmed by multinuclear (^{13}C, ^{15}N, ^{29}Si) NMR spectroscopy (Table VI). The ^{29}Si resonances of complexes **11**, except that for **11g**, shifted to *lower* field upon cooling. This has been rationalized by the ionization reaction $A \rightarrow E$ (Scheme 1), which converts the pentacoordinate silicon to tetracoordinate, resulting in the shift of

TABLE V

SELECTED BOND LENGTHS (Å) FROM THE CRYSTAL STRUCTURES OF **10c,11g,i**, AND **13**

Bond	Si–Cl	Si–O	C–O	C–N	Ref.
10c	2.294(1)	1.975(1)	1.276(2)	1.325(2)	15,40
11g	2.432(1)	1.879(1)	1.289(2)	1.283(2)	37
11i	2.624(1)	1.788(1)	1.321(2)	1.289(2)	36
13	2.3438(13)	1.836(2)	1.296(4)	1.282(4)	41
	2.0758(12)				

TABLE VI

SELECTED ^{13}C, ^{29}Si, AND ^{15}N NMR CHEMICAL SHIFTS (δ, ppm) IN COMPLEXES **10a,c–e,g,i** AND **11a,c–e,g,i** (CD$_2$Cl$_2$, 308 K)

| Compound	R	$\delta(^{13}\text{C})^a$		$\delta(^{29}\text{Si})^a$ at T			$\delta(^{15}\text{N})^b$
		C=O	NCH$_3$	308 K	233 K	203 K	NCO
11a	Me	169.2	58.0	−33.5		−7.5	−114.4
11c	Ph	165.7	58.3	−20.8		−3.6	
11d	4-MeC$_6$H$_4$	165.5	59.4	−16.3		2.1	
11e	4-NO$_2$C$_6$H$_4$	165.5	58.1	−43.1		−31.4	
11g	CF$_3$	160.0	57.5	−42.9		−46.8	
11i	4-MeOC$_6$H$_4$	165.5	58.5	−17.4		−1.3	
10a	Me	175.5	43.1	−35.9	−38.3		−209.9
10c	Ph	171.7	43.2	−34.1	−37.9		
10d	4-MeC$_6$H$_4$	171.6	43.2	−36.3	−38.1		
10e	4-NO$_2$C$_6$H$_4$	170.2	43.2	−23.9	−30.7		
10g	CF$_3$	160.6	43.1	11.9	9.0		
10i	4-MeOC$_6$H$_4$	170.3	43.0	−23.9	−30.7		

^{a}Ref. 34.
^{b}Ref. 33.

resonance to lower field. The chloride coordination is also supported by the ^{15}N NMR spectrum: the resonance of the *N*CO atom in **11a** (Table VI) is characteristic of a C=N fragment, in agreement with canonical structure **A** and ruling out **C**.

4. Wawzonek-Like Rearrangement

For all of the complexes **1**, except **1a**, the only detectable product of the reaction with **8** was the six-membered chelate **11**. However, heating of compounds **11** up to their melting points (mp), or for prolonged periods of time in solution, led to conversion to **10** (Eq. 8).[33,34] This reaction is analogous to the Wawzonek rearrangement of hydrazide-ylides (Eq. 9).[39]

Indeed, canonical structure **C** (Scheme 1) for **11** is equivalent to the ylide in Eq. (9), and may explain the analogous rearrangement of **11**. The rearrangement in Eq. (8) is the only reported route to obtain complexes **10**, except **10a**. The structure assignment was confirmed by a crystal structure analysis of **10c** (Table V).[15,40]

$$(8)$$

$$(9)$$
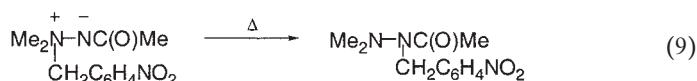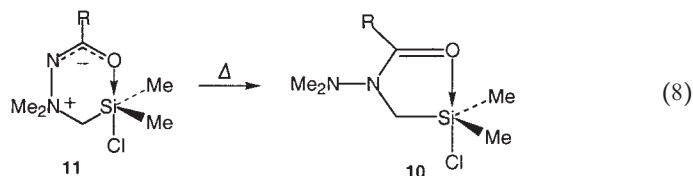
Complex **10c**, in contrast to its isomer **11c**, has a distinct $O \rightarrow Si$ coordination: relatively long O–Si and short Cl–Si distances (Table V). The ^{29}Si NMR spectra of compounds **10** also behave in the expected manner (Table VI): a decrease of temperature is associated with an *upfield* shift of the ^{29}Si resonance, again in contrast to **11**, presumably a manifestation of more intense coordination. The trend in the axial bond lengths (O–Si and Cl–Si) found in Table V may be viewed as a case of progress along the S_N2 reaction coordinate in a hypothetical nucleophilic displacement at silicon.[4a,6,40]

5. Six-Membered Chelate From ClCH₂Si(Me)Cl₂

A similar reaction to that described above (Eq. 7) occurs also with chloromethyl(methyl)dichlorosilane (**12**) (Eq. 10).[41] The reaction leads to a tautomeric equilibrium which interconverts a pentacoordinate with a hexacoordinate complex. This topic is discussed separately in Section III.A.6.
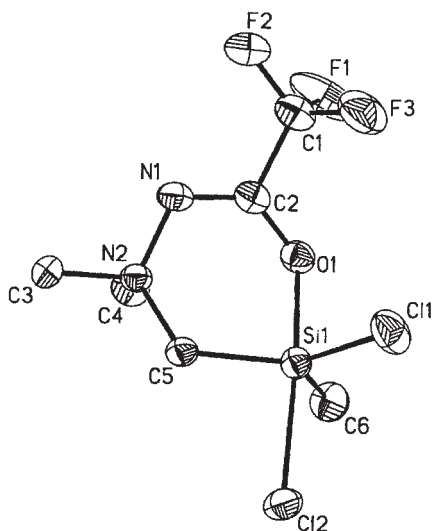

$$(10)$$
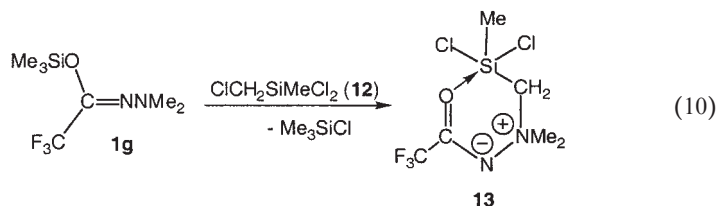
FIG. 9. Molecular structure of **13** in the crystal.[41] Reproduced with permission from the American Chemical Society.

The product **13** was subjected to a crystal structure analysis, and its structure is depicted in Fig. 9, and selected bond lengths are included in Table V. The overall geometry is a distorted TBP, with one chlorine atom at the apical and one at the equatorial position. The apical Si–Cl bond is significantly longer than the equatorial bond. Table V shows that **13** has relatively short Si–O and relatively long Si–Cl apical bonds, and hence that this is another rare case of Cl→ Si coordination. In accord with Cl→ Si coordination the silicon atom deviates from the equatorial plane toward the oxygen atom.[41]

6. Neutral Binuclear (O→ Si) Pentacoordinate Complexes

An interesting chiral binuclear pentacoordinate silicon chelate was obtained by the reaction of *O,O*-bis-TMS-diacetylhydrazine (**14**) with **8**. ^{29}Si NMR monitoring of the reaction at $-25\,^\circ$C reveals a stepwise reaction, leading to the stable rearranged heterocyclic 1-sila-2-oxa-4,5-diazacyclohexene-3 derivative (**15**, δ^{29}Si 18.0 ppm) (Eq. 11).[42] Compound **15** reacts further with excess **8** to give the binuclear pentacoordinate silicon chelate **16** (δ^{29}Si -8.8 ppm).

$$(11)$$
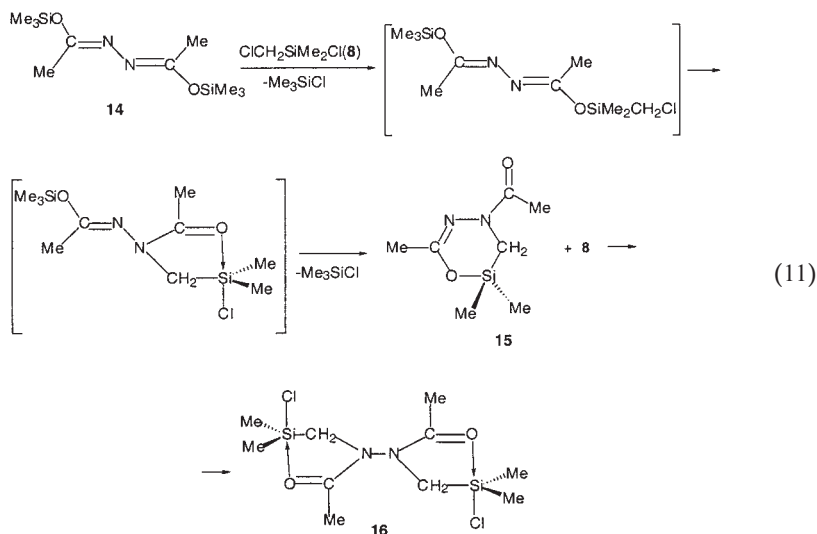
Compound **16** can be further transformed to several derivatives as shown in Eqs. (12) and (13), by replacement of the chloro ligands by methoxy (**17**, δ^{29}Si 9.1 ppm) or fluoro (**18**, δ^{29}Si 4.1 ppm) groups, or by partial replacement (**19**, δ^{29}Si 11.0, -16.9 ppm). Hydrolysis leads to the 4,5-diaza-2,7-disila-1-oxacycloheptane **20** (Eq. 14, δ^{29}Si 8.5 ppm).

$$(12)$$

$$(13)$$

$$(14)$$
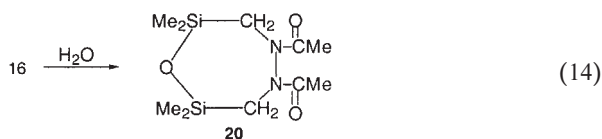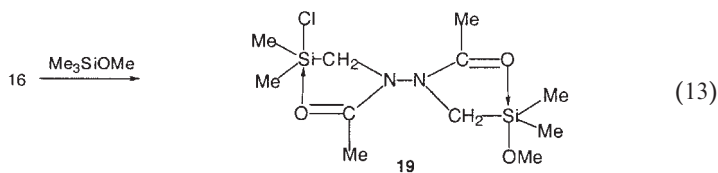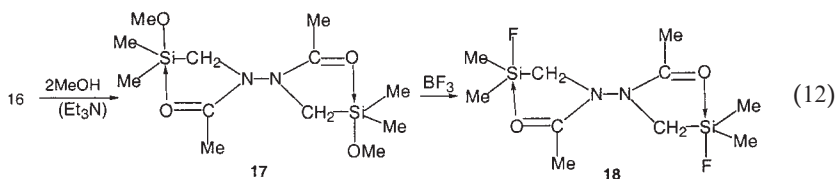
Compound **16** is a chiral molecule, as is evident from the diastereotopicity of the geminal Si-methyl groups and the methylene protons. Chirality results from the non-planar ground state about the hydrazine functionality (C_2 symmetry) and the substantially high barrier for rotation about this bond ($\Delta G^* > 24$ kcal mol^{-1}). A single crystal X-ray analysis for **16** confirmed the nearly 90° dihedral angle about the central N–N bond [C(O)NNC(O)] = 83.10°.[15,40a]

The stereodynamics of **16** were measured by variable temperature ^{1}H NMR spectroscopy, and revealed intermolecular exchange leading to coalescence of the geminal Si-methyl groups at 75 °C, without concomitant coalescence of the signals due to the geminal methylene protons. This was interpreted as intermolecular chelate exchange with other silicon compounds in solution while rotation about the N–N bond remained frozen relative to the NMR time scale. In fact, the latter process could not be observed up to 180 °C, leading to an estimated lower limit of 24 kcal mol^{-1} for the rotational barrier.

III

NEUTRAL HEXACOORDINATE SILICON COMPLEXES

A. *Bis-chelates with the Dimethylamino Donor Group*

The most widely studied group of hydrazide-based silicon complexes is the group of neutral hexacoordinate bis-chelates, with coordination of two dimethylamino donors to silicon.

1. Synthesis

In Section II.A.1.i the reaction of *N*-dimethylamino-*O*-(trimethylsilyl)-acylimidates (**1**), with dihalosilanes was shown to yield pentacoordinate monochelate complexes. When **1** is allowed to react with *tri*halosilanes (**21–26**) or with tetrahalosilanes (**27–29**), transsilylation leads to *two* ligand-exchange processes, producing neutral bis-(N → Si)-hexacoordinate silicon chelates (**30–38**, Eq. 15) in high yields.[43–48] The various complexes obtained as outlined in Eq. (15) are listed in Table VII, with their respective ^{29}Si chemical shifts. The reaction with the trichlorosilanes (**21–25**, as well as **28**) is fast and exothermic in all cases: NMR monitoring of the progress of the reaction does not permit observation of intermediates resulting from a single transsilylation process. Evidently these hexacoordinate neutral bis-chelates are substantially more stable than their di-(or tri-)-chloropentacoordinate precursors.
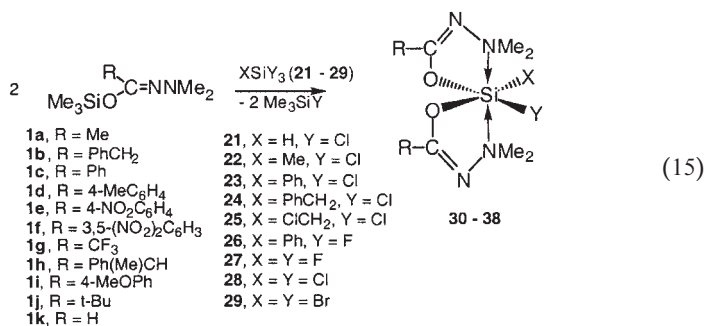
$$\text{(15)}$$

1a, R = Me
1b, R = PhCH$_2$
1c, R = Ph
1d, R = 4-MeC$_6$H$_4$
1e, R = 4-NO$_2$C$_6$H$_4$
1f, R = 3,5-(NO$_2$)$_2$C$_6$H$_3$
1g, R = CF$_3$
1h, R = Ph(Me)CH
1i, R = 4-MeOPh
1j, R = t-Bu
1k, R = H

21, X = H, Y = Cl
22, X = Me, Y = Cl
23, X = Ph, Y = Cl
24, X = PhCH$_2$, Y = Cl
25, X = ClCH$_2$, Y = Cl
26, X = Ph, Y = F
27, X = Y = F
28, X = Y = Cl
29, X = Y = Br

30 - 38

TABLE VII

^{29}Si NMR Chemical Shifts of Neutral Hexacoordinate Bis-(N → Si) Silicon
Complexes with the N–NMe$_2$ Donor Group [CDCl$_3$, 300 K, (^1J, Hz)]

Compound	R	X	Y	^{29}Si(CDCl$_3$)	Ref.
30a	Me	H	Cl	−137.7 (341.8)	44,45
30c	Ph	H	Cl	−137.2 (340.2)	44,45
30g	CF$_3$	H	Cl	−136.5 (344.4)	44,45
30j	t-Bu	H	Cl	−136.2 (344.8)	20
31a	Me	Me	Cl	−121.0	44,45
31c	Ph	Me	Cl	−121.7	44,45
31g	CF$_3$	Me	Cl	−124.5	44,45
31j	t-Bu	Me	Cl	−120.3	66
32a	Me	Ph	Cl	−128.8	45
32b	PhCH$_2$	Ph	Cl	−132.6	45
32c	Ph	Ph	Cl	−131.8	45
32g	CF$_3$	Ph	Cl	−132.7	45
32j	t-Bu	Ph	Cl	−132.9	66
33c	Ph	ClCH$_2$	Cl	−137.0[a]	51
33g	CF$_3$	ClCH$_2$	Cl	−135.3[a]	51
33k	H	ClCH$_2$	Cl	−139.9[a]	51
34a	Me	CH$_2$Ph	Cl	−125.4	66
34b	CH$_2$Ph	CH$_2$Ph	Cl	−128.5	66
34c	Ph	CH$_2$Ph	Cl	−127.8	66
35a	Me	Cl	Cl	−147.2	45
35c	Ph	Cl	Cl	−145.9	45
35g	CF$_3$	Cl	Cl	−146.2	45
36c	Ph	Ph	F	−148.6	45
36g	CF$_3$	Ph	F	−146.1(279.7)	50
37g	CF$_3$	F	F	−159.9(207.0)	66
38c	Ph	Br	Br	−169.8	66

See Eq. (15) for definitions of R, X, Y
[a]In toluene-d_8 solution.

In contrast, the reaction of **1** with polyfluorosilanes (**26**) proceeded slowly at room temperature (over several hours).[16] Indeed, in this reaction the neutral pentacoordinate complex resulting from a single ligand exchange (**4′a–c,h**) was formed as a stable intermediate and could be observed for several hours in the NMR spectra (Eq. 16).

$$(16)$$
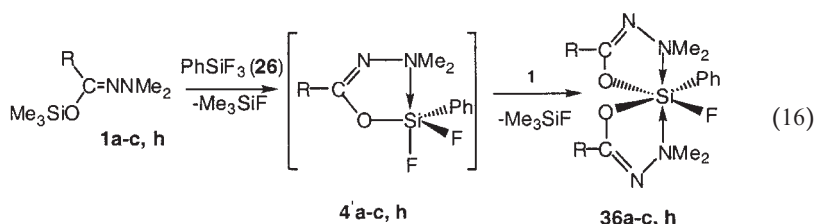
2. Structure

i. Molecular structure in the solid-state

The crystal structures of several complexes of series **30–38** have been determined and selected bond lengths and angles are given in Table VIII. The structures of representative molecules are also depicted in Fig. 10. All of these molecular structures feature slightly distorted octahedral geometries, and cis orientation of the two monodentate ligands. In addition, in all of the crystal structures obtained, the dimethylamino donor groups are in trans positions relative to each other. This particular molecular geometry is in contrast to structures reported earlier for hexacoordinate bis-(N → Si)-chelates (**39–42**, Scheme 2), in which the basic geometry about silicon was tetrahedral, with two nitrogen-donor moieties "capping" the tetrahedral faces at relatively large distances.[53–56]

The question arose as to which complexes formed octahedral and which bicapped-tetrahedral molecular structures. In the bicapped-tetrahedral complexes **39–42**, the number of electronegative ligands attached to silicon is smaller than in the octahedral complexes (**30–38**). A maximum of one Si–C bond is allowed in the octahedral complexes. When the number is greater than one, bicapped tetrahedral geometries are obtained in the solid-state.

Table VIII lists various bond lengths and angles extracted from the X-ray crystallographic determinations for **30–38**. Examination of the silicon–nitrogen distances shows that octahedral complexes are characterized by relatively short Si–N bond distances (∼1.95–2.2 Å), while in the bicapped-tetrahedral structures the Si–N distances are greater than 2.5 Å.[53–56]

TABLE VIII

Selected Bond Lengths (Å) and Angles (deg.) for Complexes of Series 30–38, 54

Compound	R, X, Y	Si–N	Si–O	Si–Cl (Si–Y)	N–Si–N	Ref.
30g	CF_3, H, Cl	2.002(3)	1.772(3)	2.184(2)	170.1(2)	50
		2.002(3)	1.772(3)			
30j	t-Bu, H, Cl	1.9825(1)	1.7490(8)	2.2454(4)	171.20(4)	87
		1.9883(10)	1.7757(9)			
31c	Ph, Me, Cl	2.015(7)	1.780(6)	2.197(4)	170.7(3)	49
		2.036(6)	1.771(6)			
32g	CF_3, Ph, Cl	2.042(4)	1.784(3)	2.187(2)	164.7(2)	47
		2.046(4)	1.808(3)			
		2.042(4)	1.790(3)	2.189(2)	166.2(2)	
		2.045(4)	1.804(3)			
35g	CF_3, Cl, Cl	2.011(2)	1.775(1)	2.141(1)	168.73(7)	47
		2.013(2)	1.777(1)	2.142(1)		
		2.010(2)	1.774(1)	2.147(1)	171.59(7)	
		2.017(2)	1.775(1)	2.138(1)		
33c	Ph, CH_2Cl, Cl	2.0145(13)	1.7606(11)	2.2140(8)	163.03(5)	51
		2.0463(13)	1.7625(11)			
36g	CF_3, Ph, F	2.021(3)	1.826(3)	1.638(2)	163.62(8)	50
		2.029(3)	1.817(2)			
37c	Ph, F, F	1.9591(10)	1.7764(9)	1.6353(7)	171.15(6)	20
		1.9591(10)	1.7764(9)	1.6353(7)		
37g	CF_3, F, F	1.962(2)	1.782(2)	1.615(2)	170.49(14)	50
		1.962(2)	1.782(2)	1.615(2)		
38c	Ph, Br, Br	2.067(4)	1.789(3)	2.3271(14)	170.95(17)	52
		1.985(4)	1.728(3)	2.3498(14)		
54c	Ph, OTf, OTf	1.967(3)	1.731(3)	1.793(3)	172.34(14)	66
		1.989(3)	1.724(3)	1.796(3)		

See Eq. (15) for definitions of R, X, Y.

Another question of interest relates to the relative orientation of the two nitrogen ligands: in all of the compounds of series **30**–**38**, the nitrogen atoms are trans relative to each other. However, in **43**, in which the immediate ligand environment around silicon is equal to that in **30**–**38**, the nitrogen-ligands occupy cis positions.[57] Comparison with the analogous *inter*molecular adducts: $SiF_4 \cdot 2NH_3$ (**44**),[58] $SiF_4 \cdot 2$pyridine (**45**),[59] shows that the latter adducts have the nitrogen ligands in trans positions, while the four fluoro ligands lie in an equatorial plane. It was concluded that in the absence of steric constraints the nitrogen ligands prefer the trans geometry, and apparently in the single structure **43** in which the cis orientation had been reported, the strained chelates forced a *cis* geometry. This conclusion is also supported by the observation that the Si–N distances in **30**–**38**
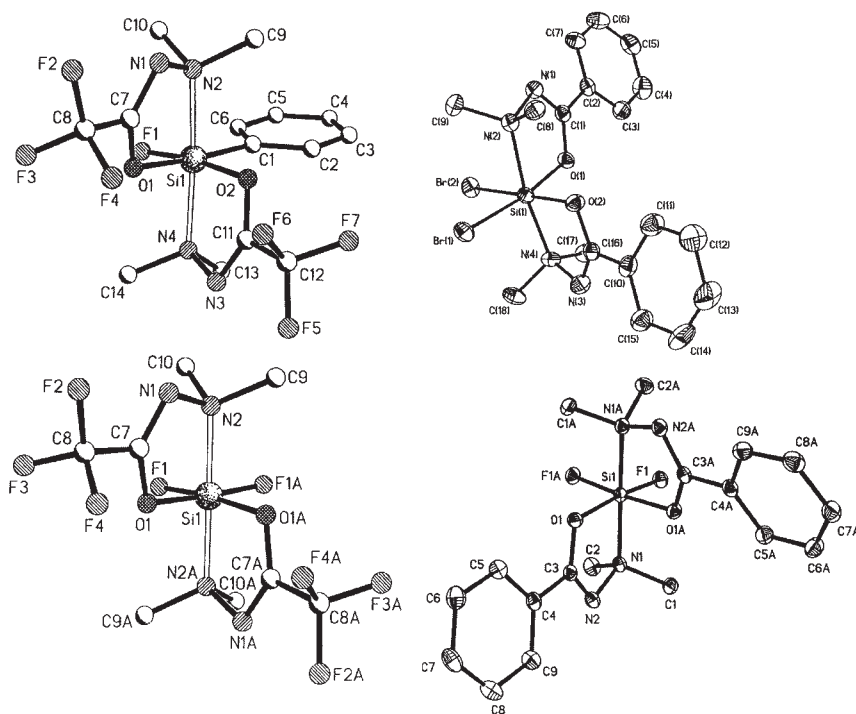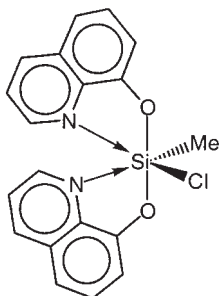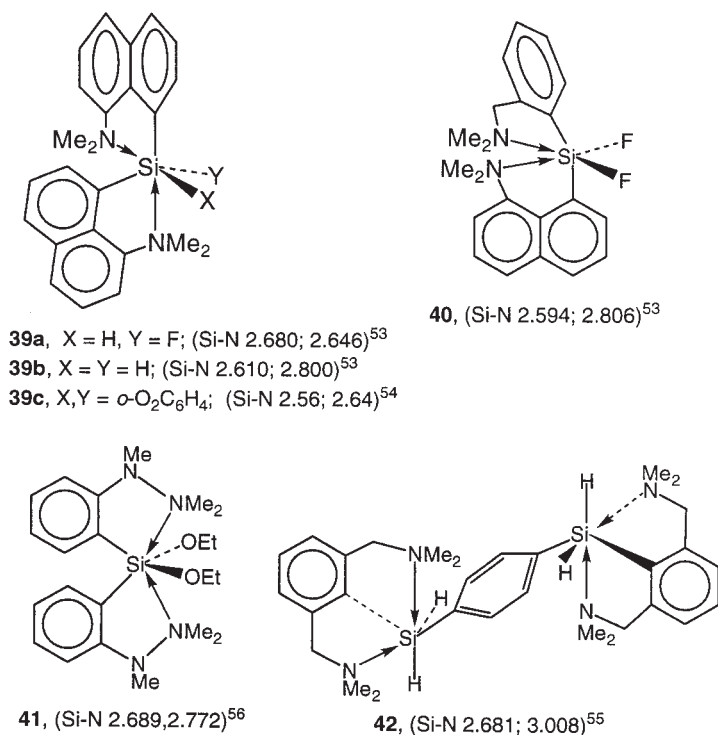
FIG. 10. Crystal structures of selected neutral hexacoordinate bis-chelates. Clockwise from top right: **38c**,[52] **37c**,[20] **37g**,[50] and **36g**.[50] Reproduced with permission from the American Chemical Society.

(Table VIII) are very close to those found in the strain-free **44** and **45**, 1.895[58] and 1.935 Å,[59] respectively.

43, (Si-N 2.014; 2.016)[57]

39a, X = H, Y = F; (Si-N 2.680; 2.646)[53]
39b, X = Y = H; (Si-N 2.610; 2.800)[53]
39c, X,Y = o-$O_2C_6H_4$; (Si-N 2.56; 2.64)[54]

40, (Si-N 2.594; 2.806)[53]

41, (Si-N 2.689,2.772)[56]   **42**, (Si-N 2.681; 3.008)[55]

SCHEME 2. Neutral hexacoordinate silicon bis-chelates with bicapped-terahedron structures.

ii. Bis-chelate topology

From a purely topological point of view,[60,61] there are 720 (6!) permutations by which six ligands can be arranged about a central atom in an (idealized) octahedral geometry.[45] For complexes of type M(AB)(CD)XY imposition of the constraint that bidentate ligands cannot assume trans positions reduces the number to 480. Elimination of all the permutations which are related by rotations of the whole molecule, represented by the four C_3 and three C_4 rotational axes of the octahedral skeleton (total of 24), reduces the number further to 20. When CD = AB [M(AB)$_2$XY] the interchange of AB pairs reduces the number of isomers further to 10. However, for structure **I** (Fig. 11) this AB $\rightleftarrows$ AB interchange is equivalent to a C_2 rotation, which has already been accounted for. The final number of independent isomers (including enantiomers) is therefore 11, represented by the six diastereomers depicted schematically in Fig. 11.
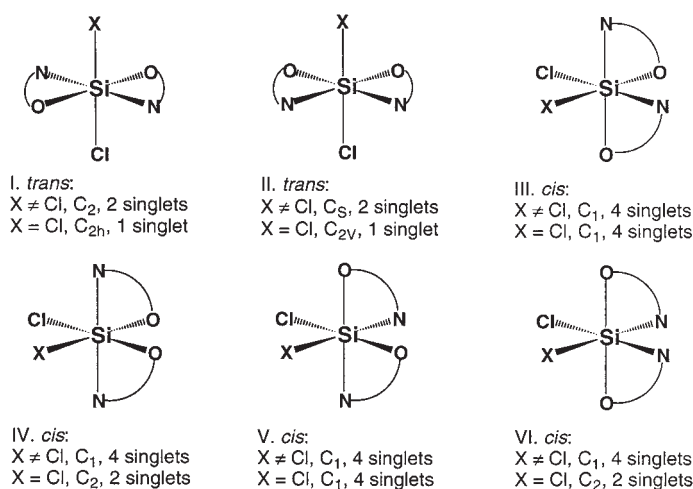
FIG. 11. Schematic representation of the six possible diastereoisomeric geometries; the symmetry point group and expected number of N-methyl NMR signals at the slow exchange limit for complexes with X = Y and for X ≠ Y are given under each structure.[45] Reproduced with permission from the American Chemical Society.

It seems quite extraordinary that all of the chelates of series **30–38** share the same geometry in the crystal, corresponding to only one (**IV**) of the possible six diastereomeric structures in Fig. 11.

iii. Structure in solution

X-Ray crystallographic analyses proved the octahedral geometry and ligand disposition in **30–38** in the solid-state. However, the structure in solution need not necessarily be the same. The structural assignment in solution came from the NMR spectral analysis: (a) the 2:1 stoichiometry was ascertained by the 2:1 signal-intensity ratios between the R and X groups. (b) The ^{29}Si NMR spectra readily confirmed hexacoordination of the compounds in toluene-d_8 or CDCl$_3$ solutions, since the ^{29}Si chemical shifts (Table VII) were characteristic of octahedral hexacoordination (as opposed to bicapped-tetrahedral structures reported for **39–42**, in which $\delta(^{29}$Si) was substantially downfield from the compounds described here).[53–56] (c) Finally, a decrease of ca. 40 Hz in the one-bond ^{29}Si–^{1}H coupling constants in **30a,c,g**, relative to a similarly substituted tetracoordinate silane, ClHSi(O-)$_2$ (381 Hz),[62] was reported as evidence for the decreased s-character of the Si–H bond associated with hexacoordination.[2]

The ^{1}H, ^{13}C, and ^{29}Si NMR spectra of **30–38** in toluene-d_8 solutions showed in all cases only one detectable diastereoisomer.[45] The number of

TABLE IX

TEMPERATURE DEPENDENCE OF THE ^{1}H NMR CHEMICAL SHIFTS (ppm) FOR **30–35** IN
TOLUENE-d_8 SOLUTIONS[45]

Compound	R, X, Y	Temperature (K)	δ(N–Me)				δ(C–Me)		δ(ortho-H)	
30a	Me, H, Cl	280	3.00	2.89	2.65	2.55	1.66	1.65		
		298		2.75			1.67			
30c	Ph, H, Cl	300	3.15	2.97	2.73	2.71				
		350		2.93						
30g	CF$_3$, H, Cl	298	2.65	2.51	2.36	2.34				
		345		2.55						
31a	Me, Me, Cl	250	2.89	2.84	2.73	2.64	1.63	1.58		
		298		2.75			1.61			
31c	Ph, Me, Cl	260	3.09	2.90	2.84	2.71				
		298		2.92						
31g	CF$_3$, Me, Cl	263	2.54	2.35	2.19	2.14				
		298		2.40						
32a	Me, Ph, Cl	243	3.02	2.42	2.40	2.12	1.73	1.71	8.80	7.71
		340		2.50			1.75		8.25	
32c	Ph, Ph, Cl	253	3.26	2.62	2.57	2.31			8.92	7.75
		340		2.75					8.35	
32g	CF$_3$, Ph, Cl	263	2.85	2.25	2.25	1.88			8.60	7.60
		320		2.20					8.00	
32b	PhCH$_2$, Ph, Cl	278	2.99	2.54	2.30	2.14	3.30	3.33	8.82	7.71
							3.06	3.30		
		350		2.20			3.18		8.10	
35a	Me, Cl, Cl	298		3.15		2.98	1.87			
		360		3.08			1.87			
35c	Ph, Cl, Cl	298		3.27		3.10				
		375		3.19						
35g	CF$_3$, Cl, Cl	298		3.33		3.26				
		398		3.30						

N-methyl signals is indicative of the configuration, and has been used to establish the stereochemistry of the single observed isomer, out of the six geometries given in Fig. 11. The symmetry point group for each geometry and the expected number of *N*-methyl signals at the slow-exchange limit temperature are shown in Fig. 11. At the slow-exchange limit temperatures, all complexes with different monodentate ligands (**30a,c,g–32a,c,g**) displayed four different signals in their ^{1}H and ^{13}C NMR spectra, for the four *N*-methyl groups (Tables IX and X). This is consistent only with the cis arrangement of ligands, as depicted in Fig. 11 (structures III–VI). This result was further supported by the observation that the two chelate cycles were diastereotopic: the R groups as well as the imide carbons on both rings were non-equivalent, as expected for structures III–VI. For compounds **35a,c,g**, in which both monodentate ligands are chlorine atoms, the slow

TABLE X

TEMPERATURE DEPENDENCE OF ^{13}C NMR CHEMICAL SHIFTS FOR **30–35** IN TOLUENE-d_8 SOLUTION[45]

Compound	R, X, Y	T (K)	δ(N–Me)				δ(C=N)		δ(ortho-C)	
30a	Me, H, Cl	298	50.8	50.5	49.8	49.0	166.9	166.7		
		330		50.4			166.8			
30c	Ph, H, Cl	298[a]	51.1	51.1	50.3	49.6	164.7	164.5		
30g	CF$_3$, H, Cl	298[a]	50.7	50.2	49.3	48.8	157.3	157.0		
31a	Me, Me, Cl	263	51.8	51.0	50.7	49.6	166.0	165.5		
		298		51.2			165.7			
31c	Ph, Me, Cl	263	52.6	51.6	51.2	50.4	164.0	163.8		
		298		51.4			163.9			
31g	CF$_3$, Me, Cl	263	51.3	50.4	50.3	49.3	156.3	156.1		
		298		50.7			156.2			
32a	Me, Ph, Cl	298	52.0	52.0	50.8	50.4	165.7	165.6	139.3	136.0
		330		51.4			165.7		137.4	
32c	Ph, Ph, Cl	298	52.7	52.5	51.4	50.9	165.0	163.9	139.3	136.2
		330		52.1			164.5		137.5	
32g	CF$_3$, Ph, Cl	270	51.6	51.6	50.5	50.2	156.9	156.2	138.9	135.8
		298		50.8			156.7		137.4	
32b	PhCH$_2$,Ph,Cl	270	51.8	51.8	50.9	50.2	166.7	166.6	138.9	136.0
		330		50.9			166.6		138.7	
35a[b]	Me, Cl, Cl	298[a]	52.0		51.2		165.6			
35c[b]	Ph, Cl, Cl	298[a]	52.9		52.2		163.0			
35g[b]	CF$_3$, Cl, Cl	298[a]	52.1		51.8		156.1			

[a] ^{13}C-Coalescence above 380 K.
[b] Nitrobenzene-d_5 solution.

exchange spectra showed only two *N*-methyl signals, as expected for structures IV and VI in Fig. 11. One of the two remaining possible structures, IV, is consistent with all of the crystallographic structures. It was therefore concluded that the geometry of **30–38** in toluene-d_8 solution is most likely the same as that in the solid-state, structure IV.

3. Stereodynamics

The hexacoordinate silicon complexes discussed here are highly flexible compounds, like some other hypercoordinate silicon compounds,[1–6] and undergo a variety of fluxional reorganization reactions, observable by temperature-dependent NMR spectroscopy. The dimethylamino-coordinated bis-chelates **30–38** are particularly suitable for an NMR study of ligand-site exchange processes (inter- or intramolecular), because of the pairs of diastereotopic *N*-methyl groups, which under certain

exchange conditions may interconvert and display typical coalescence phenomena.

i. NMR evidence for two ligand-site exchange processes

The ^{1}H and ^{13}C NMR evidence shows that *two distinct* ligand-site exchange processes take place in compounds **30–32**: the four signals due to the diastereotopic *N*-methyl groups coalesce, as the temperature is increased, initially to two and then to one singlet. The two, rate processes are not fully resolved in toluene-d_8 solutions, and have been followed by complete line-shape analysis. The best fits to the experimental spectra were obtained using six rate constants (for complete mutual exchange of four methyl groups) consisting of two pairs of equal (non-zero) rate constants and a pair of zeros. The resulting calculated rate constants and associated free-energy exchange barriers are listed in Table XI.

The two rate processes were well resolved and could be observed directly in acetone-d_6 solution only for complex **32a**. The low-temperature barrier was assigned to exchange of the two chelate rings, based on the simultaneous coalescence of *C*-methyl and *N*-methyl signals. The corresponding ^{1}H NMR spectra at various temperatures are shown in Fig. 12. This assignment was also supported by a difference-NOE experiment, which showed that exchanging methyl groups were *not*

TABLE XI

CALCULATED RATE CONSTANTS AND FREE ENERGIES OF ACTIVATION FOR EXCHANGE IN **30–32** IN TOLUENE-d_8 SOLUTION, AND FOR **35** IN NITROBENZENE-d_5[45]

Compound	Temp. (K[a])	$k_{12}=k_{34}$ (sec^{-1})	$k_{13}=k_{24}$ (sec^{-1})	$k_{14}=k_{23}$ (sec^{-1})	ΔG_1^* (kcal/mol)	ΔG_2^* (kcal/mol)	ΔG_3^* (kcal/mol)
30a	340	0	27	82	17.0	17.8	16.5(C$\underline{Me}$)
30c	345	0	60	14	17.5	18.5	
30g	345	0	60	30	17.5	18.0	
31a	280	0	96	16	13.8	14.8	
31c	285	0	100	13	13.7	14.8	
31g	283	0	162	32	13.7	14.6	13.8(CF$_3$)
32a	337	280	0	70	15.9	16.9	15.8(C$\underline{Me}$)
32c	337	330	0	165	15.8	16.4	15.8(*o*-H)
32g	335	300	0	150	15.9	16.3	15.4(*o*-H)
32b	335	280	0	70	15.9	16.9	15.8(*o*-H)
35a	346	11			17.9		
35c	363	13			19.5		
35g	393	26			20.7		

[a]Temperatures near the coalescence at which the corresponding rate constants were obtained by spectra simulation.
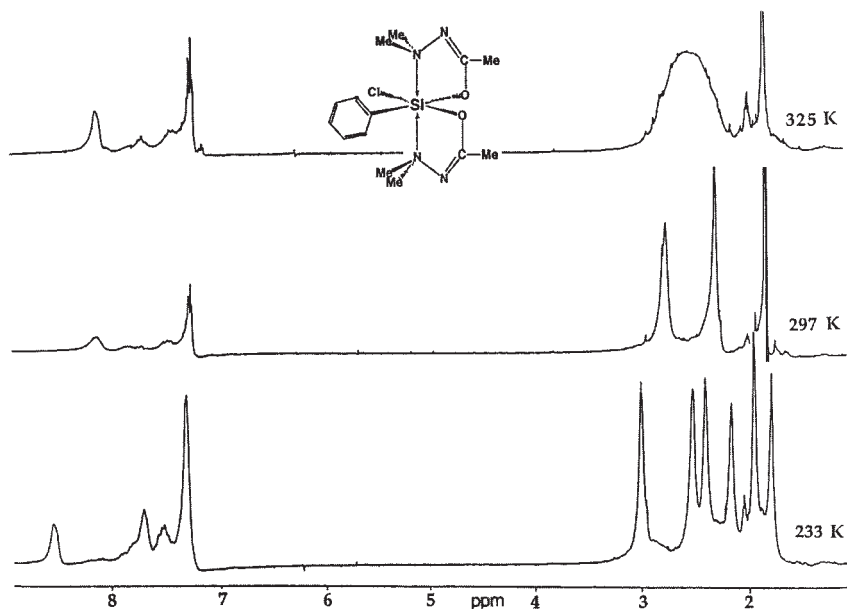
FIG. 12. ^{1}H DNMR spectra of **32a** in acetone-d_6 solution, featuring stepwise exchange of the four *N*-methyl groups.[45] Reproduced with permission from the American Chemical Society.

connected by NOE interactions, i.e., were far from each other and hence not geminal neighbors.

The exchange reactions are intramolecular, judged from the absence of a concentration dependence of the exchange rate. A possible intramolecular dissociative process, in which the Si–N dative bond dissociates, followed by rotation about the N–N bond and recombination of the N–Si bond could be ruled out: in compound **32b** with the diastereotopic methylene protons, the ^{1}H NMR spectra showed that the geminal *N*-methyl groups and the methylene protons exchanged at the same rate. However, cleavage of the Si–N bond as mentioned above would only exchange the *N*-methyl groups, but not the methylene protons. It follows that exchange must take place by a non-dissociative intramolecular process.[44,45]

ii. Ligand-site exchange mechanism

The fact that two consecutive intramolecular ligand-site exchange reactions took place in complexes **30–38**, and that the first exchange was between chelate rings, could best be rationalized in terms of a 1,2-shift mechanism. In this mechanism adjacent ligands (either the monodentate ligands, or the oxygen–oxygen ligands) exchange locations by twisting out of the horizontal plane to form a tetrahedral geometry, while the

nitrogen donors are pushed out and away from the silicon forming a bicapped-tetrahedral intermediate or transition state (Fig. 13). This mechanism is compatible with all of the observations: it offers two similar exchanges, which account for the observation of two rate processes with quite similar activation barriers; *both* (X,Y) and (O,O) exchanges effect interchange of the chelate rings, as observed for the lower-energy process; both processes correspond to topomerizations: the first is a true topomerization leading to the same geometry, while the second interchanges between enantiomers. In addition, the restricted rotation about the Si-phenyl bond observed in **32a–j**, and the coalescence of the ortho protons (or carbons) simultaneously with the lower of the two processes (Tables IX and X), may be accounted for by a "gear"-type rotation taking place with the (X, Ph) exchange.

Perhaps the strongest support for the exchange via bicapped tetrahedron geometry came from reports by Corriu[53–55] on stable hexacoordinate silicon chelates which had this structure in the solid-state and in solution: if the bicapped tetrahedral geometry was stable enough to be a ground-state geometry of some complexes, it certainly could serve as a very likely structure for an intermediate or transition state in the ligand exchange reactions.
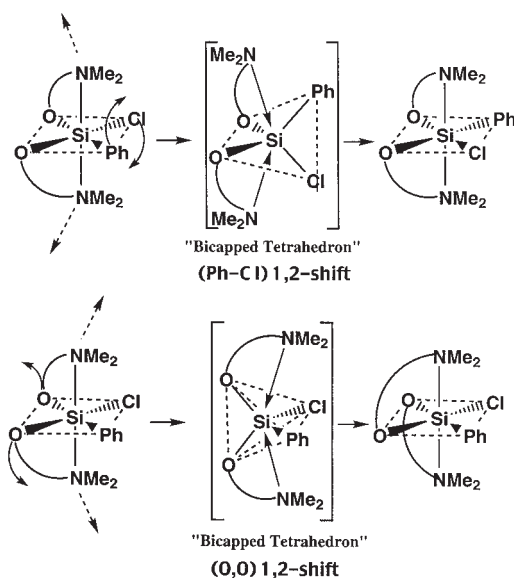
FIG. 13. Schematic representation of ligand-site exchange in **32** (1,2-shift, topomerization) through a bicapped-tetrahedral intermediate or transition state. Upper part: (Ph,Cl) interchange; lower part: (O,O) interchange.[45] Reproduced with permission from the American Chemical Society.

An alternative type of mechanism, a twist mechanism of one triangular face of the octahedron relative to the opposite face in a Bailar[63] or Ray–Dutt[64] type twist mechanism cannot be completely ruled out on the basis of available data. However, the following three arguments favor the bicapped-tetrahedron mechanism: (a) it takes at least *two* such consecutive twist steps to perform a complete topomerization, equivalent to the (X,Y) or the (O,O) exchange reactions (Figs. 14 and 15). (b) It would be difficult to account for the two different barriers for exchange with this mechanism and (c), the fact (mentioned above) that the bicapped-tetrahedron structures can be stable ground states suggests that they are excellent candidates for the intermediates or low-energy transition states in the proposed mechanism.

iii. Assignment of barriers to (X,Cl) and (O,O) exchange mechanisms

The evidence presented for the stereodynamic behavior of compounds **30–38** so far showed that they underwent two consecutive non-dissociative intramolecular ligand-site exchange reactions, assigned to exchange of adjacent ligands: (X,Y)- and (O,O)-exchange.[45] However, the presented data could not distinguish between these two processes, and hence it remained an open question which of the two corresponded to the low-energy barrier and which to the higher. This question was solved by introducing two homochiral carbon centers to the hexacoordinate complex, by the preparation of **46** from (R)-(−)-2-phenylpropionic acid.[47]

The difficulty in the assignment of the two processes to the two reactions observed by the coalescence of diastereotopic groups in **30–38** resulted from
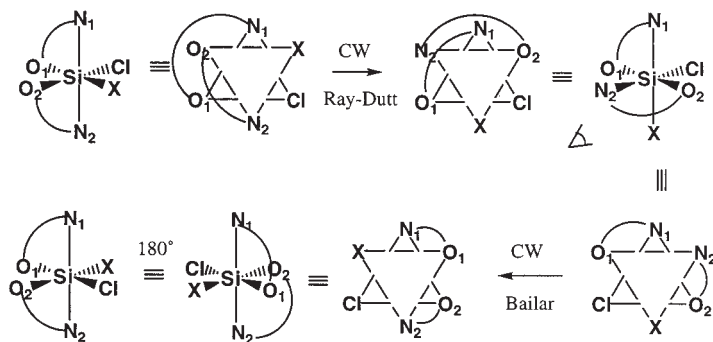
FIG. 14. A clockwise (CW) Ray-Dutt twist followed by a CW Bailar twist, applied schematically to a model complex like **30–32**. Each of the two processes exchanges diastereomers, but the combined action is a topomerization equivalent to a (X, Cl)-1,2 shift. The "eye" drawn near one of the structures shows which triangular face was selected for the second twist process.[45] Reproduced with permission from the American Chemical Society.
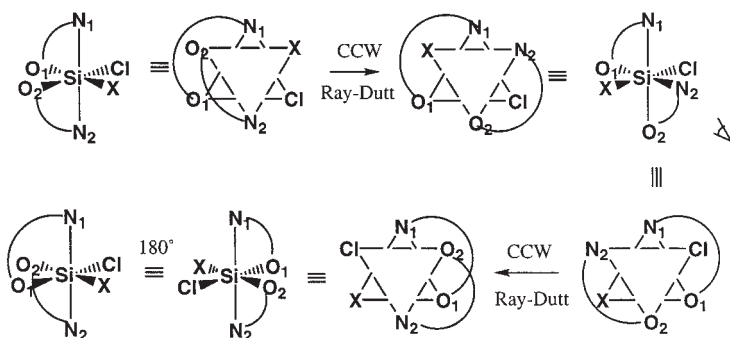
FIG. 15. Two consecutive counterclockwise (CCW) Ray-Dutt twists applied schematically to a model complex like **30–32**. While each of the two processes exchanges diastereomers, the combined action is topologically equivalent to an (O,O)-1,2 shift. The "eye" drawn near one of the structures shows which triangular face was selected for the second twist process.[45] Reproduced with permission from the American Chemical Society.

their similar NMR consequences: the four *N*-methyl signals first coalesced to a pair of singlets, followed by a second coalescence to one singlet. The lower-barrier process caused interchange of the two chelate rings. However, examination of models showed that the (X,Y)- and (O,O)-exchanges *both* effected exchange of chelate rings. This situation was changed in **46**: **46** has two diastereomers, *R*Δ*R* and *R*Λ*R*, differing only in the configuration of the silicon stereogenic unit. The (X,Y)-exchange process, which is a topomerization, does not invert the configuration at silicon, while the (O,O)-exchange does. This was of no consequence in the series **30–38**, because enantiomer-interconversion was indistinguishable from topomerization (in an otherwise achiral environment). However, in **46** the (X,Y)-exchange brings about coalescence of diastereotopic groups *within* a given diastereoisomer, while the (O,O)-exchange is an interchange of groups *between* the diastereoisomers (*R*Δ*R* ⇌ *R*Λ*R*).

46, (*R*Δ*R*) + (*R*Λ*R*)
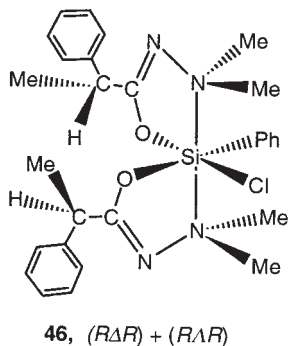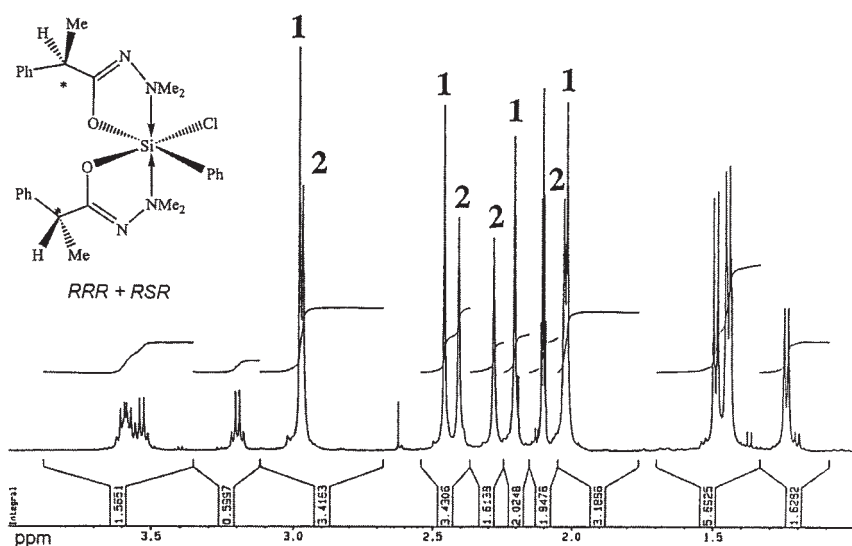
FIG. 16. High-field portion of the ^{1}H NMR spectrum of **46** at the slow-exchange limit temperature, 250 K (toluene-d_8), featuring two diastereomers.[47] Reproduced with permission from the American Chemical Society.

The ^{1}H NMR spectrum of **46** (Fig. 16) shows two unequally populated diastereoisomers: the four N-methyl groups in each diastereomer give rise to four singlets (labeled 1 and 2, respectively), with relative signal intensities between the two groups ca. 4:3. Exchange of signals due to N-methyl (and other) groups can take place in two different modes: if coalescence of signal-pairs *within* each stereoisomer is observed during the lower energy exchange process, this process constitutes a (Ph,Cl) exchange. Conversely, if the lower of the two processes exchanges signals belonging to one of the diastereomers with those of the other, then (O,O) exchange is observed. The NMR consequences of the two possible alternative exchange pathways are shown schematically in Fig. 17.

Because of the spectral complexity of the exchange of the N-methyl signals it was not possible to determine with certainty which signals interchanged upon heating. Therefore the exchange scheme was resolved by a 2D-NOESY spectrum at 250 K (Fig. 18), an intermediate temperature at which the lower-barrier exchange was effective while the second one was slow. The NOESY spectrum clearly reveals interchange only *within* each diastereoisomer: 1 ⇄ 1 and 2 ⇄ 2. It was concluded that the lower activation-energy process constituted a true topomerization, exchange of the monodentate ligands, while the higher-barrier belonged to the inversion of configuration at silicon through an (O,O)-exchange reaction.[47]
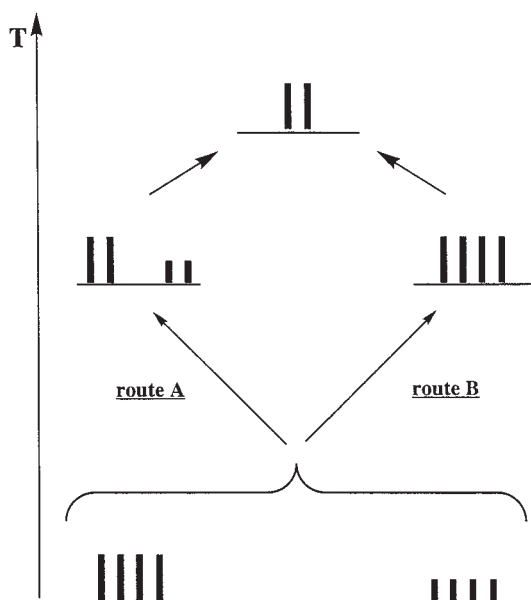
FIG. 17. Two schematic routes for the ^{1}H NMR spectral changes associated with N-methyl exchange in **46** upon increase of temperature: route A: exchange *within* each diastereomer; route B: exchange *between* diastereomers.[47] Reproduced with permission from the American Chemical Society.

iv. Correlation between SiCl distance and exchange barrier

Support for the assignment of (Ph,Cl) exchange to the lower of the two exchange processes came from an analysis of the X-ray crystallographic data. The activation barriers for this process for the chloro complexes (**30c–32c** and **35c**) in toluene-d_8 solutions inversely correlate with the Si–Cl bond lengths in the solid-state (Table XII). It was concluded that the (X,Cl)-exchange process involved elongation of the Si–Cl bond during the out-of-plane twist of ligands, and hence was more facile for complexes with *a priori* longer Si–Cl bonds. Persistence of the Si–F coupling constants in an analogous fluoro complex (**36c**) at elevated temperatures[45] suggested that the ligand exchange process was intramolecular.

v. Solvent effect on barriers in 32c

For one complex, **32c**, the two barriers were measured in a number of solvents, and a dramatic solvent dependence of the barriers was found (Table XIII).[45] The solvents were divided in three groups: the apolar solvents, including toluene-d_8, benzene-d_6, CCl$_4$, and hexachloro-butadiene, in which both activation barriers were relatively high and the
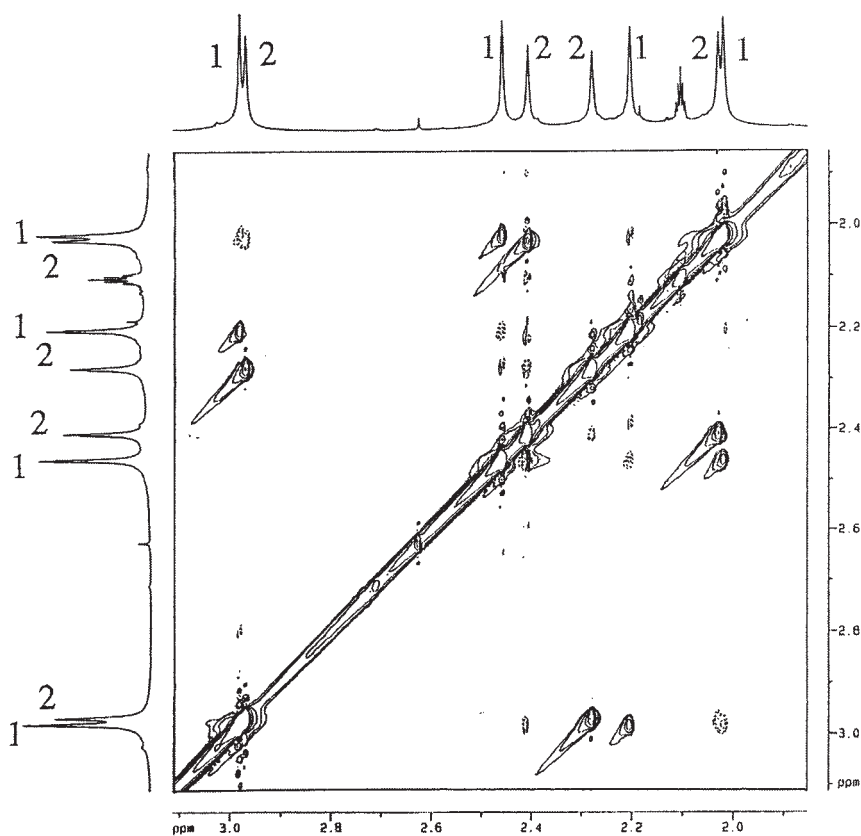
FIG. 18. 2D-NOESY spectrum of **46** (*N*-methyl region) in toluene-d_8 at 250 K. Solid lines: positive (exchange) signals; dotted lines: negative (NOE) signals. Exchange (and NOE) cross peaks connect *only* signals within the same diastereomer: 1 with 1 and 2 with 2.[47] Reproduced with permission from the American Chemical Society.

TABLE XII

Si–Cl Bond Distances and Free-Energy Barriers for the Low-Energy Ligand-Site Exchange in Hexacoordinate Complexes

Compound	R, X, Y	Si–Cl (Å)	Ref.	ΔG^* (kcal/mol)	Ref.
33c	Ph, CH$_2$Cl, Cl	2.2140(8)	51	12.8	51
31c	Ph, Me, Cl	2.197(4)	49	13.7	47
32g	CF$_3$, Ph, Cl	2.187(2)	47	15.9	47
30g	CF$_3$, H, Cl	2.184(2)	50	17.5	47
35g	CF$_3$, Cl, Cl	2.141(1)	47	20.7	47
		2.138(1)			

TABLE XIII

SOLVENT EFFECT ON ACTIVATION FREE ENERGIES FOR THE LIGAND-SITE EXCHANGE PROCESSES IN **32c**[45]

Solvent	Signal	Number of signals at 300 K	T_c (K)	ΔG_1^* (kcal/mol)	ΔG_2^* (kcal/mol)
CCl_4	NMe	4	340	16.4	16.9
	ortho H	2	350	16.4	
$CD_3C_6D_5$	NMe	4	337	15.8	16.4
	ortho H	2	340	15.8	
C_6D_6	NMe	4	340	16.3	16.7
	ortho H	2	350	16.4	
C_4Cl_6	NMe	4	345	16.6	16.9
	ortho H	2	355	16.6	
C_5D_5N	NMe_{12}	2	292	13.9	
	NMe_{34}	2	280	14.0	
	NMe	2	340		16.1
	ortho H	2	300	14.0	
$C_6D_5NO_2$	NMe_{12}	2	270	13.2	
	NMe	2	340		16.2
	ortho H	2	280	13.1	
$(CD_3)_2CO$	NMe_{12}	2	278	13.8	
	NMe_{34}	2	286	13.7	
	NMe	2	315		15.0
	ortho H	2	296	13.8	
$CDCl_3$	NMe	2	325		15.5
CD_2Cl_2	NMe_{12}	2	216	10.6	
	NMe_{34}	2	230	10.9	
	NMe	2	315		15.0
CD_3NO_2	NMe_{12}	2	< 240	~ 10.6	
	NMe	2	335		16.0

corresponding spectral changes occurred simultaneously and could be distinguished only by line-shape analysis. A second group of solvents consisted of the more polar acetone-d_6, nitrobenzene-d_5, and pyridine; in these solvents the two barriers were well separated and were observed directly. The third group included chloroform-d_1, dichloromethane-d_2, and nitromethane-d_3, in which the lower barriers were substantially lower (up to 5 kcal mol^{-1}) than those measured in apolar solvents. The variation in barriers as a function of solvent did not follow any simple solvent polarity parameter. Rather, solvents which are hydrogen-bond donors ($CDCl_3$ and CD_2Cl_2) and those which are powerful electron acceptors (deuterio-nitromethane and nitrobenzene) accelerate the exchange reaction. This suggested that association of a solvent molecule to the basic dimethylamino ligand assisted in the exchange reaction by

weakening the $N \rightarrow Si$ dative bond, and facilitating the bond-length increase necessary for the 1,2-shift.

In view of results obtained later,[65,66] (see following Section III.A.4) it now appears that the solvent effect is also to weaken (and polarize) the Si–Cl bond and facilitate its ionization. The substantially lower-barrier exchange process in $CDCl_3$ and CD_2Cl_2 may involve, in addition to the (X, Cl)-twist mechanism, ionization of the Si–Cl bond followed by re-entry of the chloride to a different position.

4. Reversible Ionization

All of the complexes **30–38** remain neutral and hexacoordinate in *apolar* solvents: toluene, carbon tetrachloride. However, most of these compounds undergo reversible ionization when dissolved in hydrogen-bond donor solvents: CD_2Cl_2, $CDCl_3$, $CHFCl_2$ (Eq. 17):[65–67]

31a, R = X = Me   **48a**, R = X = Me   (17)
31c, R = Ph, X = Me   **48c**, R = Ph, X = Me
31j, R = t-Bu, X = Me   **48j**, R = t-Bu, X = Me
32a, R = Me, X = Ph   **49a**, R = Me, X = Ph
32b, R = CH₂Ph, X = Ph   **49b**, R = CH₂Ph, X = Ph
32c, R = X = Ph   **49c**, R = X = Ph
32j, R = t-Bu, X = Ph   **49j**, R = t-Bu, X = Ph
34a, R = Me, X = CH₂Ph   **50a**, R = Me, X = CH₂Ph
34b, R = X = CH₂Ph   **50b**, R = X = CH₂Ph
34c, R = Ph, X = CH₂Ph   **50c**, R = Ph, X = CH₂Ph
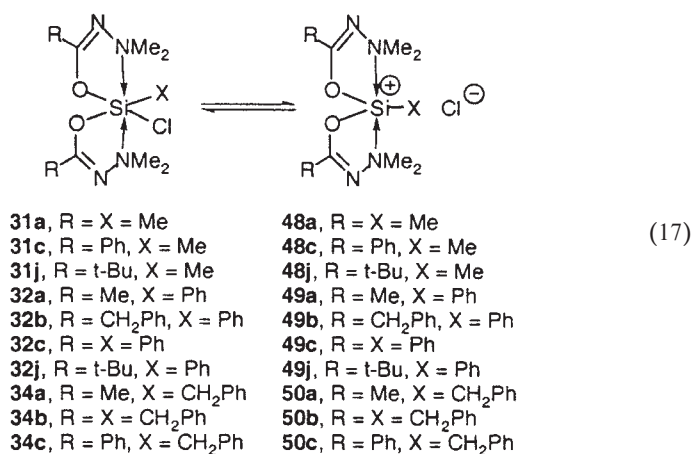
i. Temperature-dependent ^{29}Si NMR spectra

The ionization process was initially evident from a dramatic temperature dependence of the ^{29}Si NMR chemical shifts (Fig. 19): upon cooling of a solution of **31**, **32**, or **34** in CD_2Cl_2 a rapid downfield shift of the silicon resonance was found, followed by its disappearance in the baseline and emergence of two signals at low temperatures, near -70 and -130 ppm, corresponding, respectively, to ionic **48–50** and covalent **31**, **32**, or **34** (Table XIV).

This NMR spectroscopic study is of special significance, because for the first time, changes in ^{29}Si chemical shifts could be related directly to changes in coordination. It had been accepted for some time that
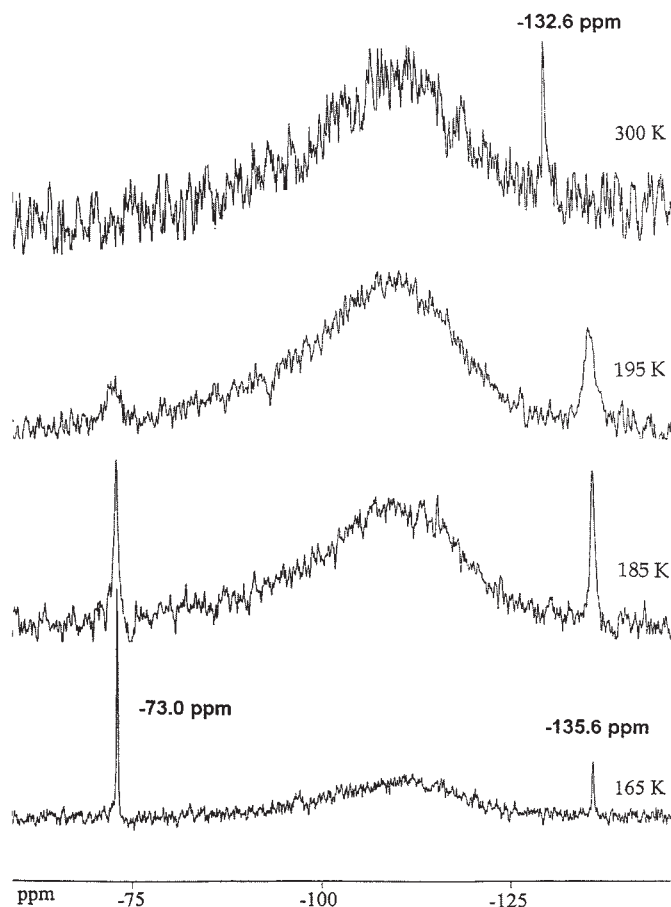
FIG. 19. ^{29}Si NMR spectra of **32a** in CD_2Cl_2 solution at different temperatures.[66] Reproduced with permission from the American Chemical Society.

changes in ^{29}Si chemical shift in pentacoordinate silicon complexes resulted from changes in coordination strength or coordination number.[68] However, never before could the ^{29}Si resonance actually be *resolved* into two individual resonances, assignable to differently coordinated complexes. The chemical-shift changes described above[66,67] and listed in Table XIV constitute the first report of low-temperature *resolution* of rapidly equilibrating penta- and hexacoordinate silicon complexes, and provide direct evidence for the correlation of ^{29}Si chemical shifts with coordination number.

TABLE XIV
^{29}Si Chemical Shifts for the Equilibrium Mixtures of **31**, **32**, **34**, and the
Corresponding Siliconium Chlorides **48**, **49**, **50** (Eq. 17) at Two Temperatures[66]

Compound	R, X	T (K)	$\delta(^{29}$Si), ppm CD$_2$Cl$_2$	tol-d_8 (solid-state)
31a ⇌ 48a	Me, Me	300	−121.3	−128.6 (−128.8)
		165	−65.0br	−130.0
31j ⇌ 48j	t-Bu, Me	300	−120.3	−128.8
		165	−65.0br	
31c ⇌ 48c	Ph, Me	300	−121.8	−127.9
32a ⇌ 49a	Me, Ph	300	−131.3	−135.6
		165	−73.0 −135.6	
32j ⇌ 49j	t-Bu, Ph	300	−132.9	
		165	−73.6 −135.9	
32b ⇌ 49b	PhCH$_2$, Ph	300	−133.7	
		165	−73.4 −135.9	
32c ⇌ 49c	Ph, Ph	300	−133.7	−136.9 (−136.4)
		165	−73.2 −136.9	
34a ⇌ 50a	Me, PhCH$_2$	300	−125.4	
		165	−65.9	
34b ⇌ 50b	PhCH$_2$, PhCH$_2$	300	−128.5	
		165	−66.3 −132.1	
34c ⇌ 50c	Ph, PhCH$_2$	300	−127.8	
		165	−64.7 −130.3	

ii. Ionization enthalpy and entropy: effect of substituent R on equilibrium

The ionization process is fully reversible with respect to temperature changes. From the temperature-dependent spectra, equilibrium constants were extracted and correlated with T^{-1} to afford enthalpies and entropies of the ionization reactions.[66,67] A list of typical reaction enthalpies and entropies for the ionization reactions of two complex families: **32**, having a phenyl group for monodentate ligand and **34**, with a common benzyl ligand, are given in Table XV. The data in Table XV are listed, for each of the **32** and **34** complex-families, in order of decreasing electron-releasing power of the remote substituents R.

It is evident from Table XV that the thermodynamic data for the ionization are strongly affected by the nature of the remote substituent R. All of the reactions are slightly exothermic, but the extent of exothermicity depends on R such that the more electron-releasing substituent is associated with the largest negative enthalpy (within each series, i.e., for the first four entries in Table XV). This was rationalized in terms of the effect of R on donor strength: the electron-releasing substituent transmits electron density

TABLE XV

REMOTE SUBSTITUENT (R) EFFECT ON REACTION ENTHALPIES AND ENTROPIES FOR THE
IONIZATION (Eq. 17) OF HEXACOORDINATE CHLORO COMPLEXES IN CD_2Cl_2 SOLUTIONS, LISTED
(FOR EACH GROUP) IN ORDER OF DECREASING ELECTRON-RELEASING POWER OF R[66]

Compound	R, X	ΔH° (kcal mol^{-1})	ΔS° (cal mol^{-1} deg^{-1})	Correlation coefficient	Number of points
32j	t-Bu, Ph	−3.9	−21.8	0.987	6
32a	Me, Ph	−2.8	−15.0	0.992	9
32b	CH_2Ph, Ph	−1.9	−9.4	0.996	5
32c	Ph, Ph	−0.8	−8.6	0.996	3
34a	Me, CH_2Ph	−3.9	−17.5	1	7
34b	CH_2Ph, CH_2Ph	−1.9	−12.3	0.997	9
34c	Ph, CH_2Ph	−1.8	−12.2	0.997	7

through the double bond to the dimethylamino donor group, increasing its donor strength. As a result the average electron density on silicon in the neutral complex (**32**, **34**) increases and, hence, it is easier for the negative ion to depart. This trend is manifested in the order of decreasing absolute enthalpies.

The trend in reaction entropies in Table XV parallels that of the reaction enthalpies, i.e., the more exothermic the ionization, the more ordered is the solvated ion pair. This was rationalized as a result of the increase in ion-pair separation as the reaction is more exothermic, due to the greater stability of the ions. Greater ion separation enables more intense solvation of the ions, and hence greater order of the solute–solvent system and greater negative entropy. The trends observed in enthalpies and entropies are essentially the same for both compound families, **32** and **34**, i.e., they depend primarily on the remote substituent R.

iii. Solvent effect on ionization

The major effect of solvent on the ionization process was first demonstrated by the temperature dependence of the ^{29}Si chemical shift of **34a** upon temperature in two solvents: CD_2Cl_2 and $CDCl_3$ (Fig. 20). In both solutions the average ^{29}Si resonance shifts to lower field as the temperature is decreased, as a result of an increase in the pentacoordinate (**50a**) to hexacoordinate (**34a**) concentration ratio. However, the rate of change with temperature (the first-order slope) is three times greater in $CDCl_3$ than in CD_2Cl_2 solution. This shows that the extent of ionization increases much faster upon cooling in the more hydrogen-bonding solvent than it does in dichloromethane, supporting the stronger and more ordered solvent–solute binding in chloroform.

$$y = 0.008x^2 - 4.937x + 615.145 \quad r = 1.000 \quad \textbf{CDCl}_3$$
$$y = 0.003x^2 - 1.615x + 121.386 \quad r = 0.999 \quad \textbf{CD}_2\textbf{Cl}_2$$
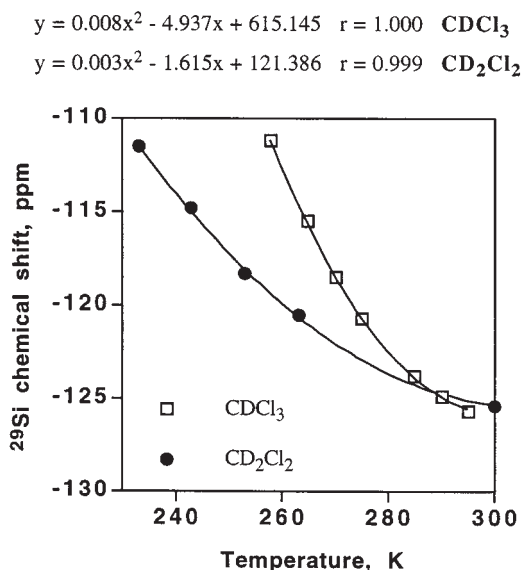
FIG. 20. Solvent effect on the ^{29}Si NMR chemical shift of **34a** in CD_2Cl_2 and $CDCl_3$ solutions at various temperatures.[66] Reproduced with permission from the American Chemical Society.

The solvent effect is clearly evident also from the thermodynamic data for the ionization, given in Table XVI for two representative cases: **31a** and **32a**, each measured in three different solvents: CD_2Cl_2, $CDCl_3$, and $CHFCl_2$. A dramatic change in reaction enthalpy and entropy of the ionization is observed as a function of solvent. Both the enthalpy and entropy of ionization are negative, and their absolute magnitudes increase with increasing hydrogen-bond donor strength of the solvent, in the order listed above. These observations were interpreted as a result of the ion-stabilizing effect of the solvents: the stronger the hydrogen bonding, the more stabilized are the ions and hence ionization is more exothermic. However, the stronger ion stabilization (in $CHFCl_2$) is associated with more intense solvation and greater solute–solvent order, manifest in the greater negative entropy.

Interestingly, the results presented in Table XVI are almost exactly equal for the two compounds, both in trends as well as in actual numbers. This suggests that the effect of the ligand X on the equilibrium constant is relatively small. The X-ligand does, however, have an effect on the equilibrium reaction *rate*, as is evident from the different ionization barriers found for these two complexes (Table XVI).

The data in Table XVI provide evidence that the major driving force for ionization is ion solvation. Indeed, in the absence of ion solvation, in apolar

TABLE XVI
SOLVENT EFFECT ON ENTHALPIES AND ENTROPIES OF IONIZATION FOR **31a** AND **32a**, AND
IONIZATION BARRIERS IN CD_2Cl_2[66]

Compound	R, X	Solvent	ΔH° (kcal mol^{-1})	ΔS° (cal mol^{-1} K^{-1})	Correl. coefficient	Number of points	ΔG^* (kcal mol^{-1})
31a	Me, Me	CD_2Cl_2	−2.6	−13.4	0.998	11	6.5 ± 0.5
31a	Me, Me	$CDCl_3$	−3.6	−18.1	0.990	8	
31a	Me, Me	$CHFCl_2$	−6.7	−23.8	0.998	8	
32a	Me, Ph	CD_2Cl_2	−2.8	−15.0	0.992	9	8.4 ± 0.5
32a	Me, Ph	$CDCl_3$	−3.6	−18.9	0.988	6	
32a	Me, Ph	$CHFCl_2$	−6.8	−22.9	0.996	6	

solvents such as toluene (Table XIV) or CCl_4 the ^{29}Si chemical shift is at its highest-field point, corresponding to the undissociated hexacoordinate chelate form.[66,67]

iv. Effect of counterion on ionization equilibrium

The ionization equilibrium (Eq. 17) can be shifted dramatically to the ionic side by replacement of the chloro ligand by other, better leaving-group ligands, such as bromo or triflato. The replacement itself proceeds in high yield by reaction with Me_3SiZ, where $Z = Br$ or CF_3SO_3, as shown in Eq. (18).[65–67] The shift of equilibrium is evident from the ^{29}Si NMR resonance at ambient temperature, which is at the extreme low-field end, corresponding to the ionic compound.

$$Z = Br, OTf \tag{18}$$
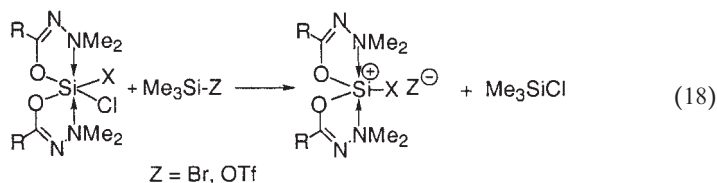
The siliconium salts of these counterions are stable (i.e., not in noticeable equilibrium with the hexacoordinate species) and are discussed in Section IV.B.1.

v. Ionization-resistant hexacoordinate complexes

Ionization of **31–34** proceeds smoothly as long as one of the mono-dentate ligands is a carbon-ligand group. When both of the monodentate ligands are electron-withdrawing groups, or when the R substituent is an electron-withdrawing group, ionization is prevented (Eq. 19).[66] This

TABLE XVII
^{29}Si CHEMICAL SHIFTS OF HEXACOORDINATE MONO- AND DITRIFLATO (51–54) COMPLEXES

Compound	51a	51c	52g	53g	54a	54c
$\delta(^{29}$Si), ppm	−150.8	−150.7	−130.2	−140.6	−161.7	−161.5

is evident from the ^{29}Si chemical shifts (Table XVII), which remain in the high-field region characteristic of hexacoordination, and is further confirmed by crystal structures. The crystal structures of two of these hexacoordinate complexes, the monotriflato **53g**, in which the CF$_3$ groups prevent ionization, and the ditriflato (**54c**) were determined and are depicted in Figs. 21 and 22, respectively.[65,66] The failure of these complexes to ionize was attributed to the lower electron density on silicon, resulting from the electronegative ligands, which makes it more difficult for silicon to release a negatively charged species.

(19)

35a, R = Me, X = Y = Cl
35c, R = Ph, X = Y = Cl
31g, R = CF₃, X = Me, Y = Cl
32g, R = CF₃, X = Ph, Y = Cl
38c, R = Ph, X = Z = Br

51a, R = Me, X = Cl
51c, R = Ph, X = Cl
52g, R = CF₃, X = Me
53g, R = CF₃, X = Ph

54a, R = Me
54c, R = Ph
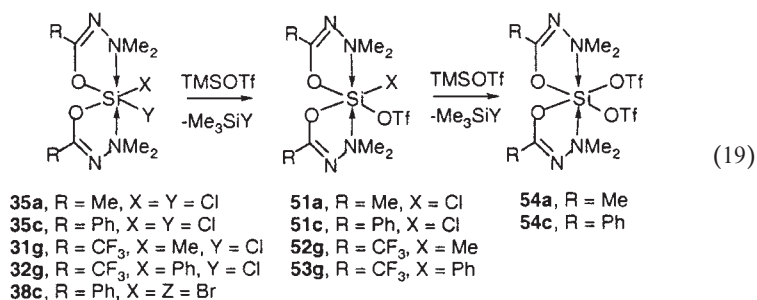
5. Binuclear Hexacoordinate Silicon Chelates

A subgroup of the neutral hexacoordinate silicon complexes discussed above is the family of binuclear complexes (**55a,c,g,j**).

55a, R = Me
55c, R = Ph
55g, R = CF₃
55j, R = t-Bu
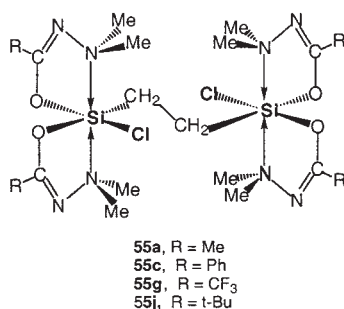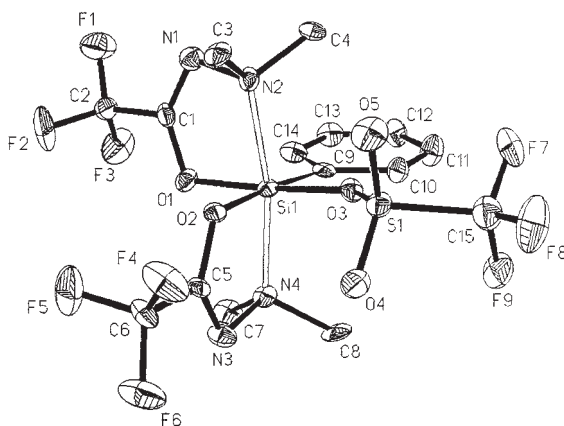
FIG. 21. Molecular structure in the solid-state of **53g**. Selected bond lengths: Si–N, 2.029(4), 2.037(4); Si–O, 1.775(4), 1.782(4); Si–O(3), 1.828(4), Si–C, 1.916(5).[66] Reproduced with permission from the American Chemical Society.
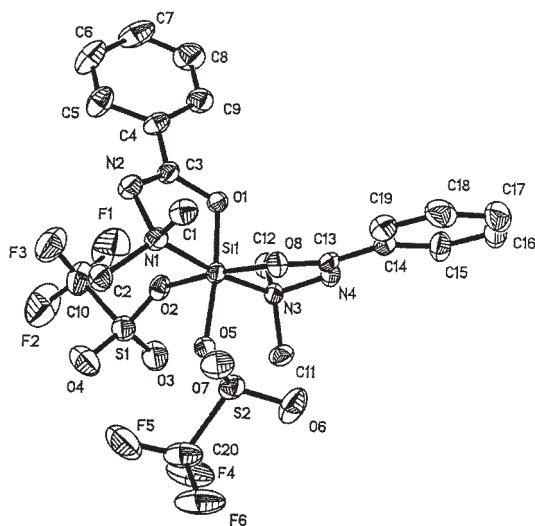
FIG. 22. Molecular structure in the solid-state of **54c**. Selected bond lengths: Si–N, 1.967(3), 1.989(3); Si–O, 1.731(3), 1.724(3); Si–O(2), Si–O(5), 1.793(3), 1.796(3).[66] Reproduced with permission from the American Chemical Society.

i. Synthesis and structure

Binuclear silicon chelates (**55a,c,g,j**) were prepared from 1,2-bis(trichloro-silyl)ethane and *N*-dimethylamino-*O*-trimethylsilylimidates (**1a,c,g,j**) in high yields.[69] The hexacoordination of these complexes is evident from a crystal structure analysis obtained for **55c** (Fig. 23), as well as from their

^{29}Si NMR chemical shifts at 300 K, which fall within the typical range of hexacoordinate complexes (Table XVIII).

The geometrical data for the crystal of **55c** (Fig. 23) are compared with those obtained previously (Table VIII) for the mononuclear analogs **31c** (R = Ph, X = Me) and **33c** (R = Ph, X = CH$_2$Cl):[45] as expected, in both compound types the basic geometry is a distorted octahedron, with N–Si–N, O–Si–Cl, and O–Si–C angles close to 180°.

ii. Equilibrium ionization of binuclear chelates

Like the mononuclear chelates,[66] binuclear **55a,c,j** (but not **55g**!) undergo reversible ionization which is enhanced at low temperature, as is evident from the temperature-dependent ^{29}Si NMR spectra (Fig. 24, Table XVIII). From the lowfield chemical shift already at 300 K (Table XVIII), relative to the mononuclear analogs **31a,c,j** (Table XIV), it was concluded that significant ionization takes place at ambient temperature, to a much greater extent than in **31**.[69]

The mode of ionization of **55** is of some interest: ionization may proceed stepwise, and result either in mixed penta-hexacoordinate monocations (**56**), or in dications (**57**, Eq. 20). The ^{29}Si NMR spectral changes with temperature provide evidence to answer this question (Fig. 24). At temperatures just below room temperature the average signal shifts to lowfield as the temperature decreases, as a result of ionization, leading to increased population of the ionic form (**56** or **57** or both). However, at lower temperatures (below the slow-exchange limit temperature) the two signals for the penta and hexacoordinate species reach *equal* intensities, which no longer change upon further cooling. This proves that the ionization produces the monoionic **56a,c,j**, and stops at this stage without further ionization to the dicationic **57**.

56a, R = Me
56c, R = Ph
56j, R = t-Bu

57a, R = Me
57c, R = Ph
57j, R = t-Bu

(20)
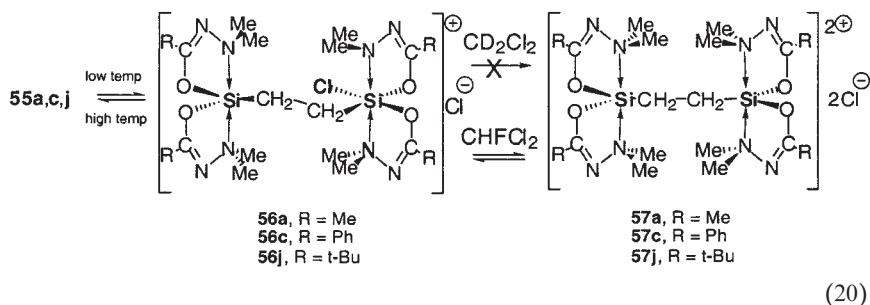
The second ionization step was, however, realized in a more polar solvent, CHFCl$_2$ (Fig. 25). In this solvent at low temperatures a second [29]Si
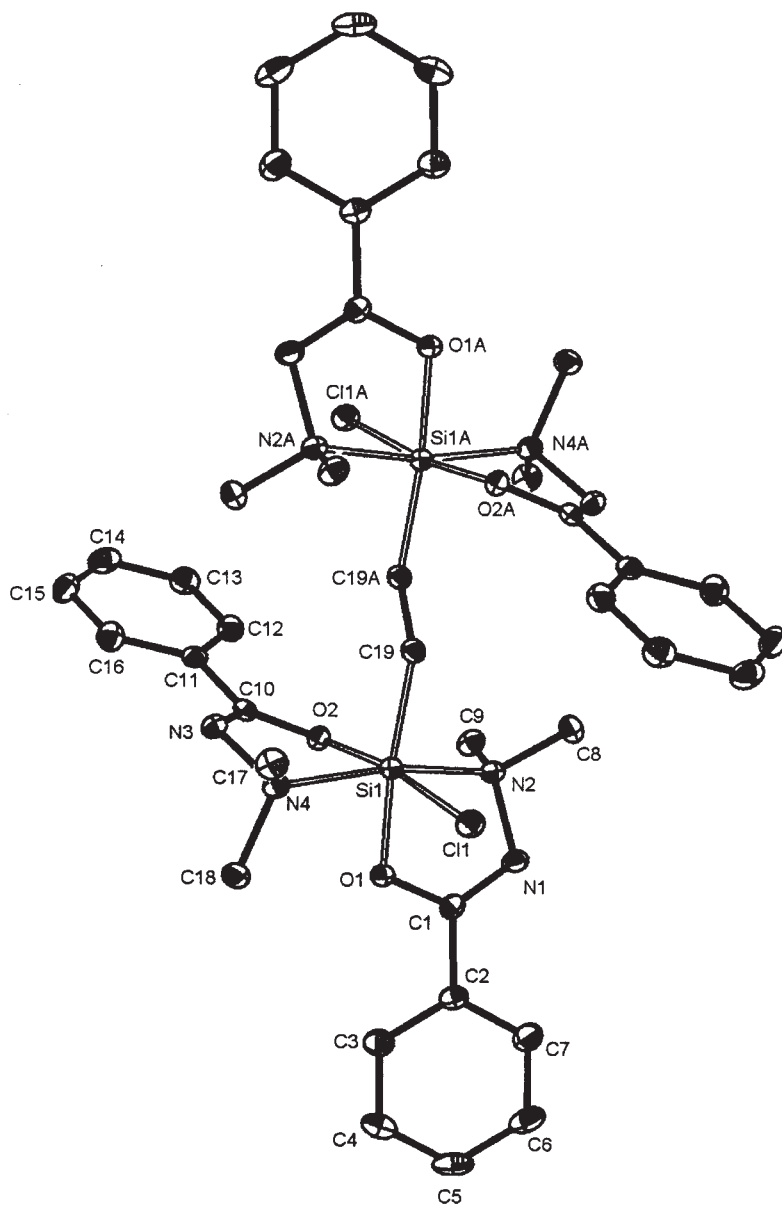
FIG. 23. Crystal structure of binuclear complex **55c**. Selected bond lengths (Å): Si(1)–O(1), 1.7892(15); Si(1)–O(2), 1.7768(15); Si(1)–N(1), 2.0578(17); Si(1)–N(2), 2.0441(17); Si(1)–Cl(1), 2.2410(7); Si(1)–C, 1.925(2). Angles (°): N–Si–N, 168.20(7); O–Si–O, 87.76(7); O–Si–C, 173.70(8); O–Si–Cl, 171.01(5).[69] Reproduced with permission from the American Chemical Society.

TABLE XVIII

^{29}Si Chemical Shifts for Binuclear Complexes **55a,c,g,j** (CD$_2$Cl$_2$ Solution, 180 K and 300 K)[69]

Compound	R	300 K	180 K
55a	Me	−110.3	−63.3; −132.3
55c	Ph	−116.6	−61.8; −130.8
55g	CF$_3$	−121.7	−123.6
55j	*t*-Bu	−103.1; −104.4	−62.6; −131.6
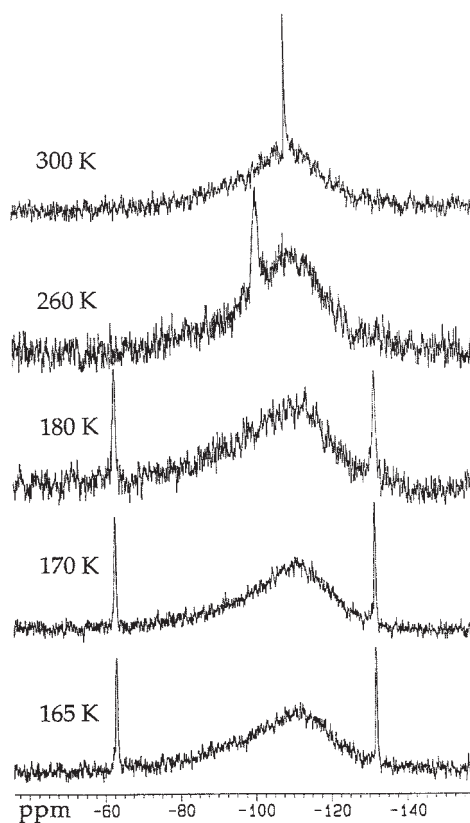
Fig. 24. Variable temperature ^{29}Si NMR spectra of **55a** in CD$_2$Cl$_2$ solution.[69] Reproduced with permission from the American Chemical Society.
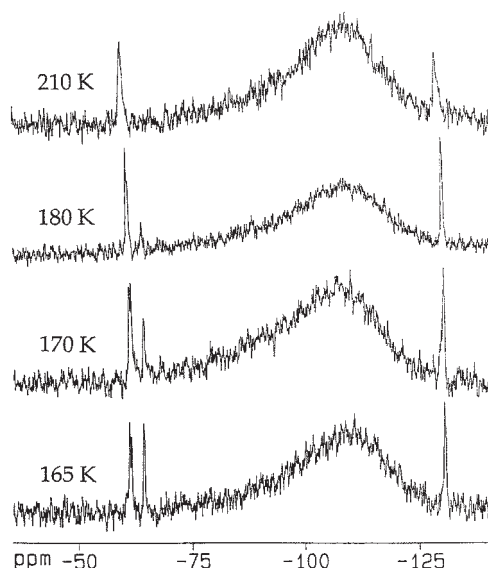
FIG. 25. ^{29}Si NMR spectra of **55j** $\rightleftarrows$ **56j**, **57j** in CHFCl$_2$ solution at low temperatures. Second ionization (**56j** $\rightarrow$ **57j**) is evident from the emergence of a new signal at -64.9 ppm below 180 K. The doubling of signals at -61 ppm appears to be due to the two diastereomeric **56j** complexes.[69] Reproduced with permission from the American Chemical Society.

resonance appeared at the pentacoordinate silicon region, which was assigned to the dicationic species **57**.[69]

Stable (i.e., not equilibrating) ionized binuclear complexes are discussed in Section IV.B.1.ii.

6. Tautomeric Equilibrium

i. Reversible chloride migration

A special case of reversible ionization of a hexacoordinate silicon complex has been described as a novel tautomeric equilibrium.[41] It differs from the formation of siliconium-ion salts in that the positive charge resides on nitrogen, in a dimethylammonium cation, and not on silicon. The transsilylation of **1g** with **12** in equimolar concentrations leads to the pentacoordinate zwitterionic complex **13** (Eq. (10), Section II.B.5). However, when the molar ratio was 2:1, respectively, an equilibrium mixture of tautomers (**58**, **59**) was obtained, as shown in Eq. (21). The same mixture was also obtained when a second mole-equivalent of **1g** was added to **13**.

In this reaction a chloride migrates between silicon and the ammonium nitrogen, converting a zwitterionic hexacoordinate chelate (**58**) to a

$$2 \; \underset{F_3C \quad 1g}{\overset{Me_3SiO}{\underset{}{C}}} =NNMe_2 + ClCH_2SiMeCl_2 \xrightarrow[- Me_3SiCl]{} \qquad\qquad\qquad (21)$$
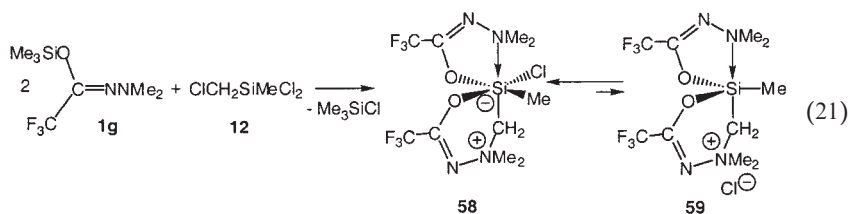
zwitterionic pentacoordinate chelate (**59**). Structural assignment of the latter was achieved by NMR-spectral comparison with two fully ionic analogs: the ammonium-triflate salt **59**(OTf) (Fig. 26), and the non-equilibrating **60** (Fig. 27).[41]

60
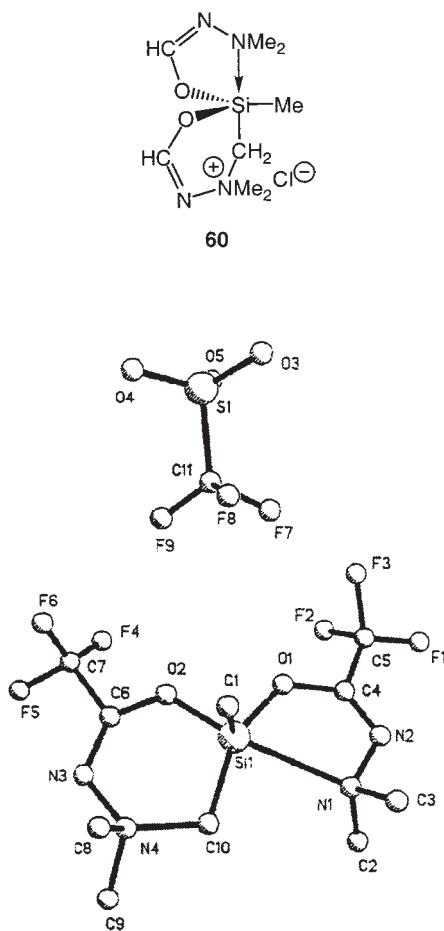
FIG. 26. Molecular structure of **59**(OTf) in the crystal.[41] Reproduced with permission from the American Chemical Society.
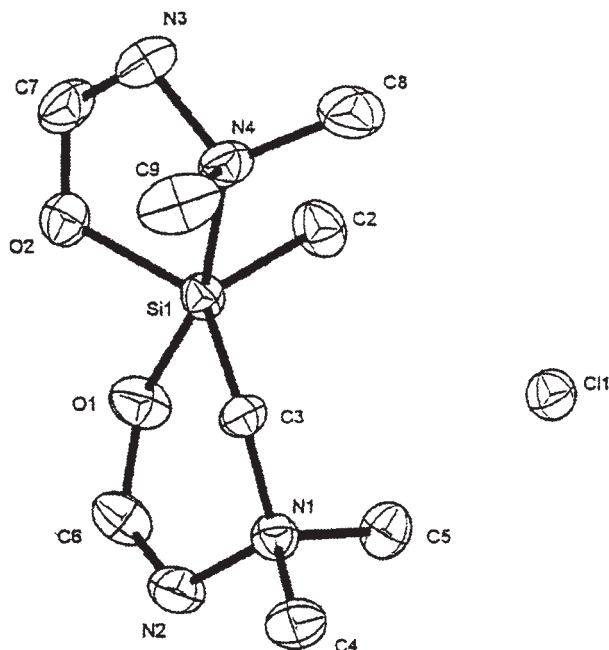
FIG. 27. Molecular structure of **60** in the crystal. Selected bond lengths: Si–O(1), 1.753(4); Si–O(2), 1.711(4); Si–N(4), 2.162(5); Si–C(2), 1.843(6); Si–C(3), 1.867(5). Angles: O(1)SiN(4), 163.6(2); O(2)SiC(3), 125.9(2); O(2)SiC(2), 112.3(3); O(1)SiO(2), 88.1(2).[41] Reproduced with permission from the American Chemical Society.

The ^{29}Si NMR spectra of this equilibrating system (**58/59**) behaves in a similar manner to that of the ionizing hexacoordinate complexes (Section III.A.4), showing remarkable temperature dependence (Fig. 28): the low-temperature ^{29}Si NMR spectrum of the mixture clearly features two signals, one typical of pentacoordination (δ^{29}Si $= -57.6$ ppm, assigned to **59**) and the other of hexacoordination (δ^{29}Si $= -134.0$ ppm, assigned to **58**). The intensity ratio of these two signals is temperature dependent in a fully reversible fashion, such that at lower temperatures the relative population of the pentacoordinate species (**59**) increases.

Interestingly, there is a significant difference between the present tautomeric system and the ionizing systems of Section III.A.4: the barrier for the equilibrium reaction is substantially higher in the present case than in the previous systems, resulting in well resolved resonances for the hexa- and
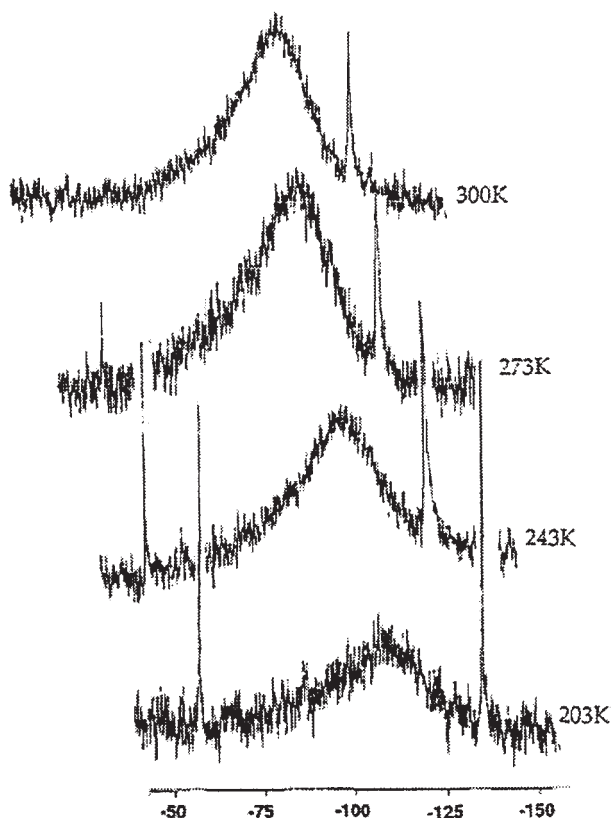
FIG. 28. Variable temperature ^{29}Si NMR spectra of the equilibrium mixture **58**/**59** in CD$_2$Cl$_2$ solution.[41] Reproduced with permission from the American Chemical Society.

pentacoordinate species already at 273 K (as opposed to 170–190 K in Section III.A.4).

ii. Reaction sequence by NMR-monitoring

The exact course of the reaction of **1g** with **12** (Eq. 21) was studied by monitoring the NMR spectra (^{1}H, ^{13}C, and ^{29}Si) of the reaction mixture at low temperatures.[41] The reagents (**1g** and **12**) were dissolved at liquid nitrogen temperature in CD$_2$Cl$_2$ and the solution was placed in a pre-cooled (200 K) NMR probe-head. The various NMR spectra were then measured at various temperatures. Equation (22) outlines the resulting reaction sequence.
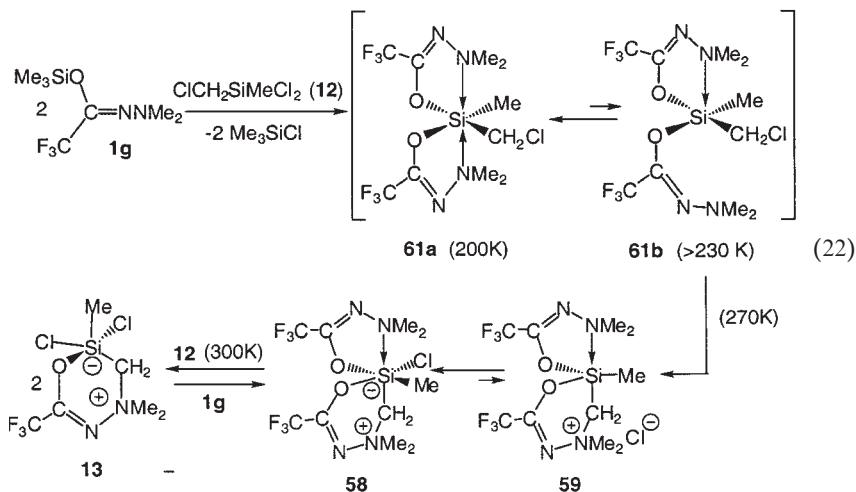
It is quite surprising to find that the monocyclic **13** is not an intermediate on the way to the bis-chelate **61a**, but rather the opposite, that **61a** forms initially at low temperature as an unstable intermediate. **61a** belongs to a large group of neutral hexacoordinate silicon complexes which have been studied extensively.[43–49] These complexes generally show a characteristic stereochemical non-rigidity (discussed in Section III.A.3), with two consecutive ligand-exchange processes observable by variable temperature NMR spectroscopy.[45,47] Indeed, in **61a** the N-methyl signals show typical line broadening and coalescence phenomena between 190 and 230 K, providing further confidence in the structural assignment, in the absence of a complete characterization of this unstable intermediate.

The structure of **61a** is surprising in that both of the monodentate ligands are carbon-ligands, in contrast to numerous analogs with electronegative ligands.[43–48] As a result **61a** is relatively unstable, and further increase in temperature leads to its N–Si dissociation to the pentacoordinate monochelate **61b**. This transformation is reversible, as shown in Eq. (22): at 200 K only **61a** is detected, while at temperatures between 230 and 250 K both isomers are observed, with the relative population of **61b** increasing with temperature up to ∼4:1 (**61a** : **61b**). The evidence for **61b** formation is the appearance of a highly-characteristic *temperature-dependent* ^{29}Si resonance between −8.3 and −4.8 ppm, as well as the equivalence of two N-methyl groups, and the non-equivalence of the other two in the ^{1}H and ^{13}C NMR spectra.

Further heating to 270 K leads to an irreversible transformation of the **61a,b** mixture to the mixture of tautomers, **58–59**.

iii. Chloride-bridged disiloxane by partial hydrolysis

An analogous case of tautomerization was attempted with complex **62**, without success (no equilibrium reaction could be observed), but with another interesting result: **62** partially hydrolyzed to form the first chloride-bridged disiloxane complex **63** (Eq. 23). The crystal structure of **63** is shown in Fig. 29, and selected bond lengths and angles are listed in Table XIX.[41] The bridging chloride clearly occupies the axial positions of *both* silicon
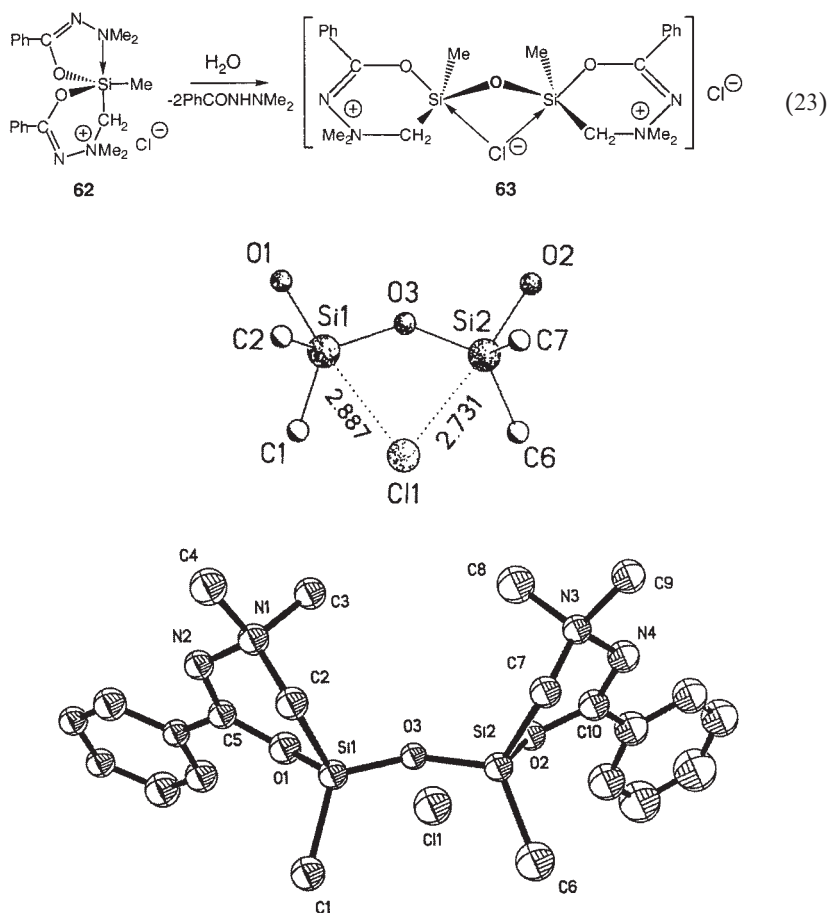
FIG. 29. Crystallographic molecular structure of **63** (lower part). Expansion of the bridge area, showing the critical Si–Cl distances and the TBP geometry around each silicon atom (upper part).[41] Reproduced with permission from the American Chemical Society.

TABLE XIX

SELECTED BOND LENGTHS AND ANGLES FOR **63**[41]

Bond	Bond length (Å)	Angle	Bond angle (deg.)	Angle	Bond angle (deg.)
Si(1)–O(1)	1.716(3)	O(1)–Si(1)–Cl(1)	173.08(12)	O(2)–Si(2)–Cl(1)	173.45(12)
Si(1)–O(3)	1.621(3)	O(1)–Si(1)–C(1)	102.1(2)	O(2)–Si(2)–C(6)	100.8(2)
Si(1)–C(1)	1.838(5)	O(1)–Si(1)–C(2)	97.4(2)	O(2)–Si(2)–C(7)	96.2(2)
Si(1)–C(2)	1.872(4)	O(1)–Si(1)–O(3)	99.3(2)	O(2)–Si(2)–O(3)	95.4(2)
Si(1)–Cl(1)	2.887(2)	C(1)–Si(1)–O(3)	117.2(2)	C(6)–Si(2)–O(3)	116.9(2)
Si(2)–O(3)	1.632(3)	C(2)–Si(1)–O(3)	115.4(2)	C(7)–Si(2)–O(3)	118.4(2)
Si(2)–O(2)	1.731(3)	C(1)–Si(1)–Cl(1)	84.7(2)	C(6)–Si(2)–Cl(1)	85.7(2)
Si(2)–C(6)	1.828(5)	C(2)–Si(1)–Cl(1)	80.06(14)	C(7)–Si(2)–Cl(1)	80.75(13)
Si(2)–C(7)	1.882(4)	O(3)–Si(1)–Cl(1)	76.30(11)	O(3)–Si(2)–Cl(1)	81.09(11)
Si(2)–Cl(1)	2.731(2)				

atoms, which have each a distorted TBP geometry, i.e., both silicon atoms are pentacoordinate.

Each of the two silicon atoms of **63** deviates from the central plane (defined by the corresponding equatorial ligands) toward the axial oxygen atom, indicating that the bridging chloride (Cl(1) in Fig. 29) forms a dative bond to each one of the silicon centers. This is fully confirmed by reference to the Si–Cl(1) distances: 2.887 and 2.731 Å, respectively, which are both substantially longer than normal covalent Si–Cl bonds (2.05 ± 0.03 Å),[38] and yet significantly shorter than the sum of the corresponding van der Waals radii (3.97 Å).[38,70]

In terms of the progress along a hypothetical S_N2 reaction coordinate, this structure may be viewed either as an early stage of a chloride anion displacing the axial oxygen leaving group, or as an almost complete displacement of a chloride by an oxygen nucleophile.

Evidence that **63** is pentacoordinate also in solution is provided by the typically pentacoordinate ^{29}Si chemical shift, and by its highly characteristic temperature dependence, as follows: [δ, ppm (T, K)]: -41.4 (330), -39.6 (300), -37.2 (275), -35.6 (243).[41] The inverse relationship is the evidence for the coordination of the chloride to silicon (Si $\leftarrow$ Cl$-$), rather than O $\rightarrow$ Si coordination (which was reported to have a regular dependence of $\delta(^{29}Si)$ on temperature, i.e., downfield shift as the temperature increases).[34] However, the present results do not permit the distinction of a bridged complex in solution from one in which a different chloride is attached to each silicon.

B. *Bis-chelates with the Isopropylideneimino Donor*

1. Preparation and Structure

A new donor ligand for coordination with silicon has been introduced: the isopropylideneimino ligand. Transsilylation of *N*-isopropy-lideneimino-*O*-(trimethylsilyl)acylimidates (**6a–b**) with tetrahalosilanes leads to direct replacement of two halogens and formation of the dihalo-complexes **64–66** (Eqs. 24, 25).[20,52] Only in the reaction of SiF$_4$ (Eq. 24) could the pentacoordinate intermediate be observed by NMR monitoring of the reaction progress. The intermediate was identified by its typical ^{29}Si quartet at δ −132.3 ppm, ($^1J_{Si-F} = 182$ Hz), but could not be isolated and fully characterized due to the formation of **64**. The crystal structures of **64a**, **65b**, and **66a** are depicted in Figs. 30–32, and selected bond lengths are listed in Table XX, along with data for the corresponding dimethylamino chelates for comparison. The remarkable differences are apparent immediately from the figures: the difluoro complex (**64a**) crystallized in the cis geometry, while the dichloro and dibromo **65b** and **66a** preferred the trans geometry.

$$(24)$$

6a, R = Ph
6b, R = PhCH$_2$

64a, R = Ph
64b, R = PhCH$_2$

$$(25)$$

6a,b

65a, X = Cl, R = Ph
65b, X = Cl, R = PhCH$_2$
66a, X = Br, R = Ph
66b, X = Br, R = PhCH$_2$
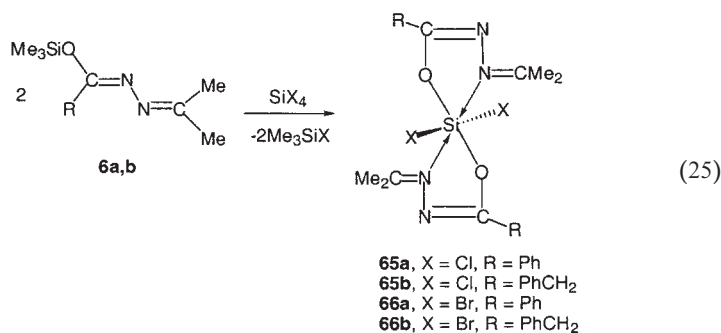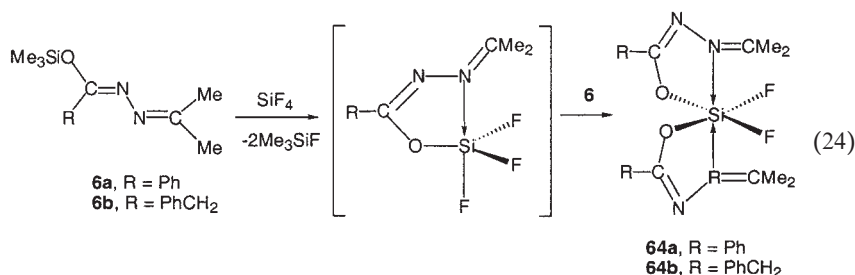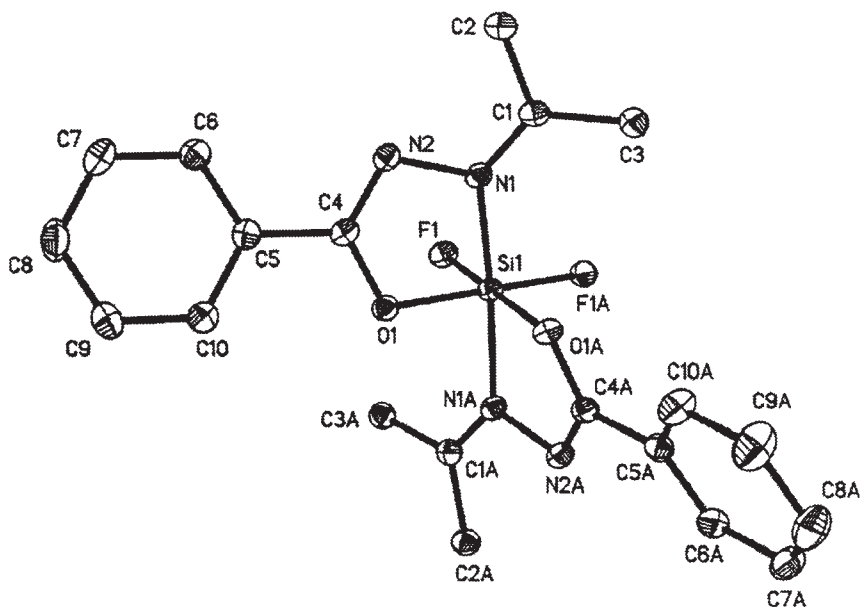
FIG. 30. Molecular structure of **64a** in the crystal.[20] Reproduced with permission from Elsevier.
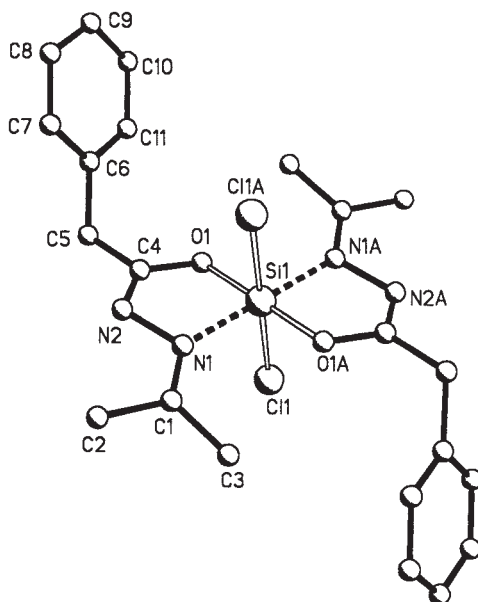
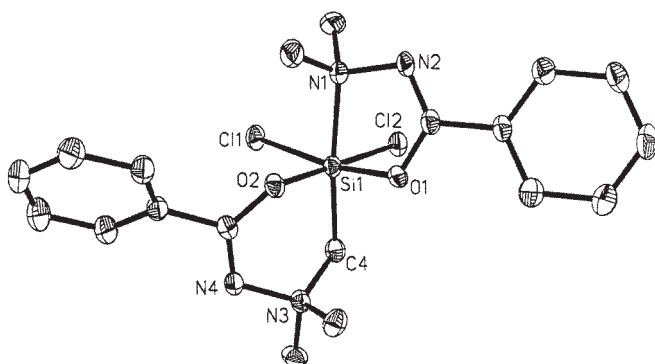FIG. 31. Molecular structure of **65b** in the crystal.[20] Reproduced with permission from Elsevier.
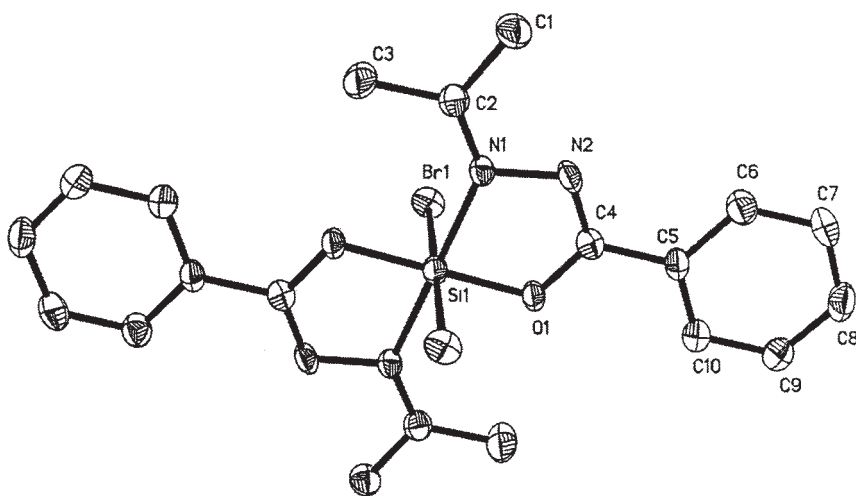
FIG. 32. Molecular structure of **66a** in the crystal.[52] Reproduced with permission from the American Chemical Society.

TABLE XX

COMPARISON OF ^{29}Si NMR CHEMICAL SHIFTS (CDCl$_3$, 300 K) AND SELECTED BOND LENGTHS
FOR ISOPROPYLIDENEIMINO- AND DIMETHYLAMINO-DIHALO-COMPLEXES

	Isopropylideneimino donor			Dimethylamino donor		
	64a	**65b**	**66a**	**37c**	**35g**	**38c**
Parameter	F	Cl	Br	F	Cl	Br
Si–N (Å)	1.9418(10)	1.9205(9)	1.933(3)	1.9591(10)	2.013(2)	2.067(4)
					2.011(2)	1.985(4)
Si–O (Å)	1.7867(8)	1.7381(8)	1.716(2)	1.7764(9)	1.6844 (15)	1.789(3)
					1.6964(14)	1.728(3)
Si–Hal (Å)	1.6543(7)	2.2088(7)	2.4050(6)	1.6353(7)	2.141(1)	2.3271(14)
					2.147(1)	2.3498(14)
δ^{29}Si (ppm)	−166.9	−163.7	−140.2	−160.0	−146.2	−170.0
($^1J_{Si-F}$, Hz)	(194 Hz)			(203 Hz)		
Reference	20	20	52	20	47	52

The fact that in **64a** the monodentate ligands are cis to each other, as has been found in numerous other hexacoordinate bis-acylimidato-*N,O* chelates **30–38**,[43–50] suggests that in the absence of special constraints the cis orientation is preferred. It follows that the uncommon trans geometry, found in **65** and **66**, is the result of steric repulsion between the bulkier Si–Cl and Si–Br bonds and the isopropylidene methyl group. All three dihalo-complexes (the *cis*-**64** and *trans*-**65** and **66**) react readily with
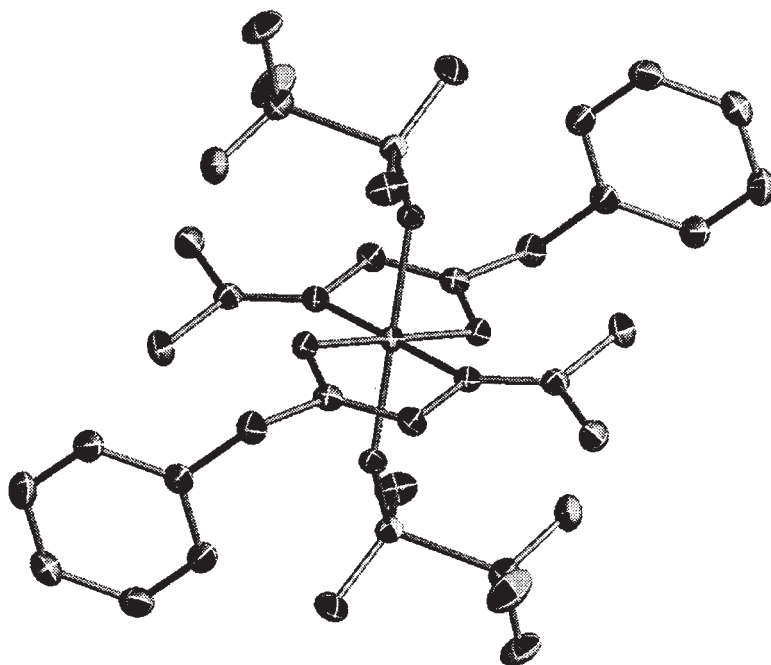
FIG. 33. Molecular structure of **67b** in the crystal.[20] Reproduced with permission form Elsevier.

TMSOTf, exchanging their halogeno ligands by triflate (Eq. 26), to yield *the same trans*-ditriflate chelates **67a,b** (Fig. 33).

(26)
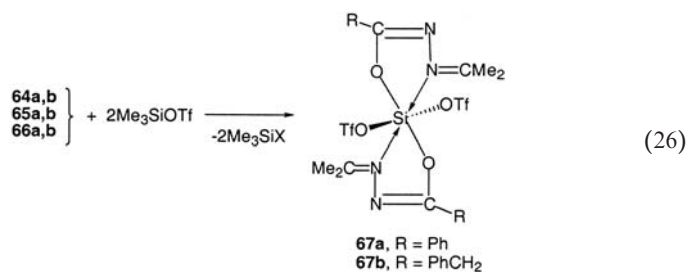
The trans geometry is confirmed in solution for **65b–67b** by the appearance of a singlet for the methylene protons in the ^{1}H NMR spectra due to C_{2h} symmetry of the trans chelates.

The data in Table XX permit an assessment of the donor strength of the new isopropylideneimino ligand.[20,52] Comparison of the bond lengths between the two chelate families (Table XX) clearly indicates stronger

TABLE XXI

SOLVENT AND TEMPERATURE DEPENDENCE OF ^{29}Si CHEMICAL SHIFTS FOR **66b**

Solvent	CCl$_4$	C$_6$D$_5$CD$_3$	CD$_2$Cl$_2$ + HMPTA	CDCl$_3$	CD$_2$Cl$_2$	CHFCl$_2$
δ^{29}Si (*T*, K)	−183.4 (300)	−182.0 (340)	−179.2 (300)	−165.5 (330)	−163.9 (300)	−124.1 (273)
				−159.2 (300)	−152.3 (263)	−122.0 (263)
				−133.7 (260)	−131.3 (213)	−118.7 (223)
				−118.2 (200)	−120.2 (170)	−118.4 (170)

coordination in the isopropylideneimino complexes, as evident from the consistently shorter N–Si and longer Si–X and Si–O distances, relative to the dimethylamino chelates. This is further enhanced by the observation that the ^{29}Si resonances in **64**–**65** are consistently shifted to higher field, relative to the dimethylamino analogs, indicating stronger coordination. The exception to this observation is **66a**, for which the ^{29}Si chemical shift is at *lower* field than the corresponding dimethylamino chelate **38c**. This is discussed in the following section.

2. Reversible Ionization

The unexpected downfield shift in **66a,b**, in connection with strong temperature and solvent effects on the ^{29}Si chemical shift (Table XXI), indicates that the dibromo complexes **66**, unlike the difluoro- (**64**) and dichloro- (**65**) analogs, undergo ionization to form the bromide salts (**68**) already at room temperature (Eq. 27).[20,52]

$$\text{(27)}$$

66   **68**

a, R = Ph; **b**, R = PhCH$_2$
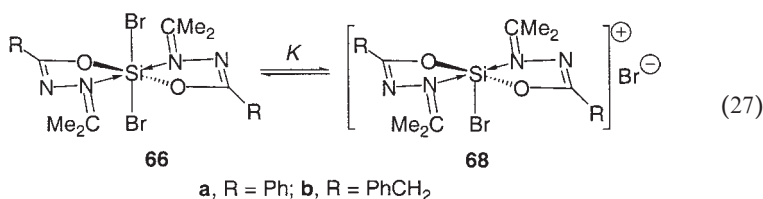
Ionization of **66** is unexpected not only because it is the only dihalo-complex in this series which ionizes, but because the previously reported dihalo-dimethylamino-coordinated complexes, **35**, **37**, and **38**, were completely resistant to ionization. Ionization of **66** thus constitutes additional evidence for the stronger donor property of the isopropylidene-imino ligand group.

A remarkable solvent dependence of the ^{29}Si chemical shift was observed for **66b** (Table XXI): the better hydrogen-bond donor solvents caused
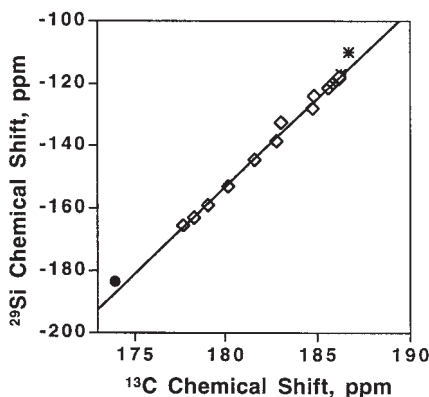
FIG. 34. Correlation of ^{29}Si and ^{13}C NMR chemical shifts (of the isopropylideneimino-carbon)
for **60b** with temperature variation. The point labeled ● was taken in CCl_4 solution
and represents the fully covalent hexacoordinate complex; the point labeled * belongs to the
fully ionic complex.[20]

increased ionization, manifest in lower-field ^{29}Si chemical shifts. The $\delta(^{29}Si)$
values measured in the apolar toluene-d_8 and CCl_4 solutions represent the
fully covalent, non-ionized **66b**. On the other hand, the slow-exchange limit
temperature and corresponding individual ^{29}Si NMR signals for the ionic
68b and neutral **66b** forms could not be observed, presumably due to rapid
bromide exchange, in contrast to exchange in dimethylamino complexes
in which the two species were well resolved at low temperatures (see
Section III.A.4.i).

Additional support for the ionization of **66b** at low temperatures
was provided by the linear correlation of the ^{29}Si with the
$(N=\underline{C}Me_2)$–^{13}C chemical shifts shown in Fig. 34. The linear relationship
is the evidence that both changes result from the same phenomenon, as
expected from ionization: reduced electron-density on silicon (resulting
from ionization) is accompanied by partial compensation from the
imino group, i.e., a parallel but smaller reduction in electron density near
the imino carbon. The point labeled ● in Fig. 34 represents the fully
covalent form (**66b** in CCl_4 solution), while the point on the other end of the
line labeled * is the fully ionic, BPh_4-salt. Both points fit in the line,
indicating that the entire line represents a gradual change from one end
(covalent) to the other (ionic).

Equilibrium constants were obtained for each temperature from the
temperature-dependent ^{29}Si chemical shifts, leading to the reaction enthalpy
and entropy of ionization for **66b**: -6.3 kcal mol^{-1} and -21 cal mol^{-1}
deg^{-1}, respectively. These values are in agreement with the reversible

ionizations reported for the dimethylamino complexes,[66,67] and indicate that also in this case the ionization is driven by the solvent.

C. *Irreversible Rearrangement*

1. Stepwise Synthesis

The transsilylation reaction of (chloromethyl)trichlorosilane (**69**) with **1** yields initially, under mild conditions, the bis-chelates **33**. Upon heating, or when left in solution for several days, **33** is quantitatively converted to the thermodynamically more favorable product **70** (Eq. 28). Representatives of both product-groups **33** and **70** have been isolated and characterized by single crystal X-ray analyses (**33c** and **70c**, Figs. 35 and 36).[51]

$$
\begin{array}{c}
\underset{\underset{R}{\overset{Me_3SiO}{|}}}{2}C{=}NNMe_2 + ClCH_2SiCl_3 \xrightarrow{-2Me_3SiCl}
\end{array}
$$

1   **69**

33   **70**

c, R = Ph; **g**, R = CF$_3$; **k**, R = H.
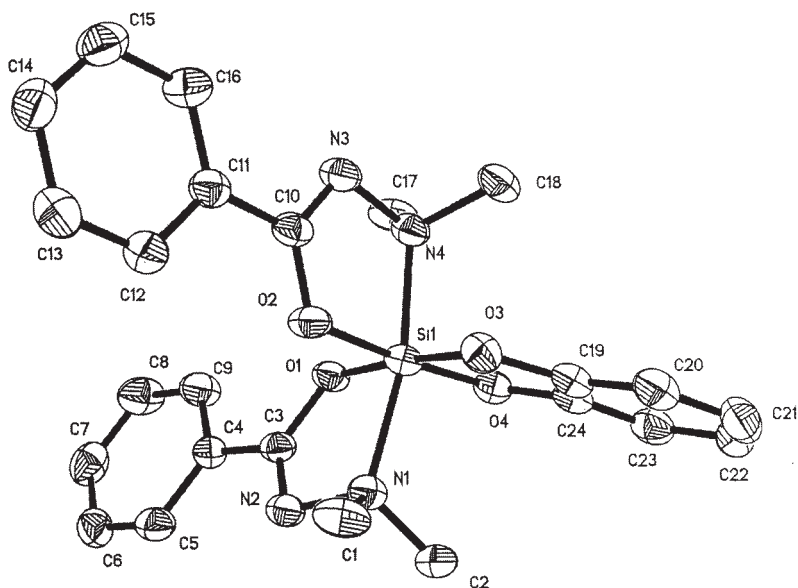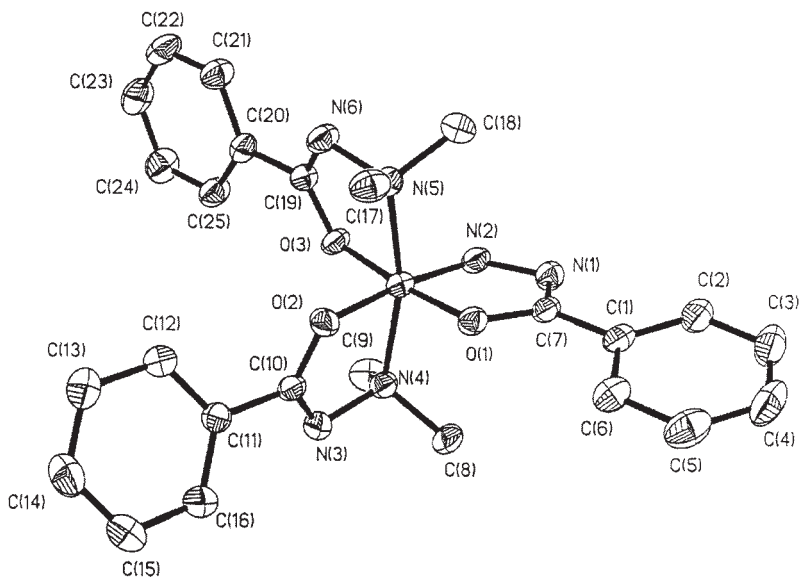
$$(28)$$
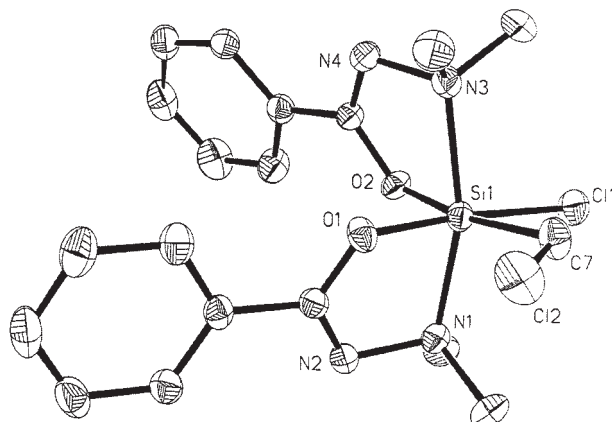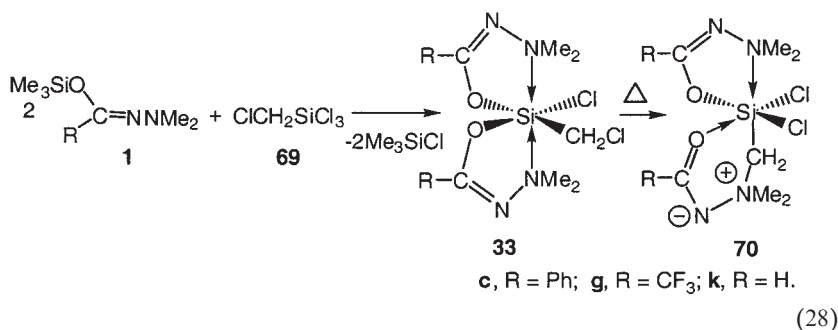
FIG. 35. Molecular structure of **33c** in the crystal.[51] Reproduced with permission from the American Chemical Society.

FIG. 36. Molecular structure of **70c** in the crystal.[51] Reproduced with permission from the
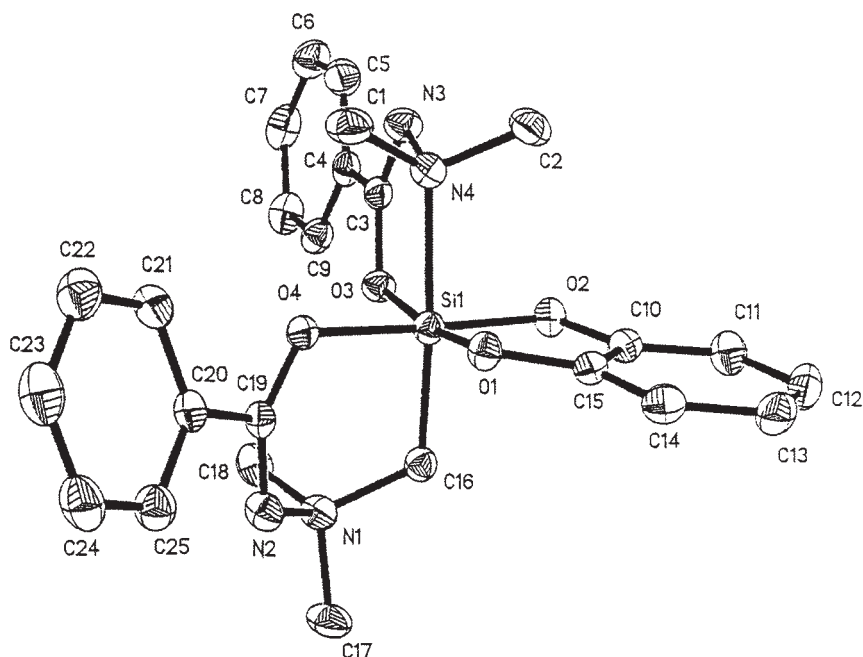American Chemical Society.

The initial intermediate **33** is the "normal" *bis*-(N → Si)-coordinated
complex, which is obtained in analogy to numerous other neutral
hexacoordinate complexes **30–38** (Eq. 15), prepared from SiCl$_4$ and various
trichlorosilanes and substituted *O*-trimethylsilylated hydrazides. The final
product **70** is the result of a novel molecular rearrangement, by which a
chloride has been displaced by the dimethylamino-nitrogen and has
migrated from carbon to silicon, accompanied by ring expansion and
conversion of the N → Si to O → Si coordination.

2. Structure of Rearranged Product

The exact molecular structure and charge locations in **70** are of interest.
From an analysis of bond lengths and angles (Table XXII) obtained from an
X-ray crystal structure of **70c** (Fig. 36) one can arrive at a reasonable
structural assignment. The bond angles listed in Table XXII show that the
geometry of **70c** is nearly octahedral. The mode of coordination and
charge distribution in **70c** can be represented by four canonical structures
shown in Eq. (29).

$$(29)$$
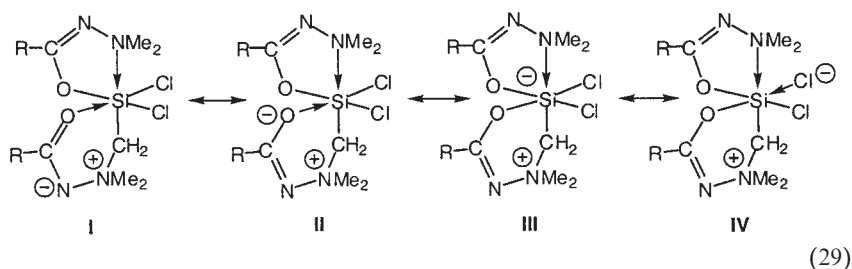
TABLE XXII

SELECTED INTERATOMIC DISTANCES AND BOND ANGLES IN COMPLEX **70c**[51]

Bond atoms	Distance (Å)	Angle	Degrees
Si–O(1)	1.755(2)	O(1)–Si–Cl(1)	170.22(6)
Si–O(2)	1.773(2)	O(1)–Si–O(2)	91.22(8)
Si–N(3)	2.0463(13)	O(2)–Si–N(1)	90.95(9)
Si–Cl(1)	2.2352(12)	O(2)–Si–C(4)	92.99(10)
Si–Cl(2)	2.2591(10)	C(4)–Si–Cl(1)	94.93(8)
Si–C(4)	1.911(3)	O(1)–Si–Cl(2)	89.89(7)
C(1)–O(1)	1.321(3)	C(4)–Si–Cl(2)	86.76(9)
C(1)–N(2)	1.285(3)	Cl(1)–Si–Cl(2)	90.09(4)
N(1)–N(2)	1.475(2)	O(1)–Si–C(4)	94.84(10)
C(5)–O(2)	1.319(3)	O(1)–Si–N(1)	81.25(8)
C(5)–N(4)	1.296(3)	O(2)–Si–Cl(1)	88.85(6)
N(3)–N(4)	1.477(3)	N(1)–Si–Cl(2)	89.37(7)
		N(1)–Si –Cl(1)	88.97(7)
		N(1)–Si–C(4)	174.51(9)
		O(2)–Si–Cl(2)	178.88(4)

An assessment of the relative contributions of each of I–IV is based on a comparison of the various bond lengths, relative to other hexa-coordinate silicon complexes. The Si–O and Si–Cl distances in **70c** fall well within the average covalent bonds in hypercoordinate silicon compounds (such as in **33**), and hence structures I and II, with an O → Si dative bond, as well as IV with a Cl⁻ → Si dative bond may be excluded. This leaves resonance hybrid III as the major contributor to the geometry and charge distribution of **70c**, suggesting that the complex may best be described as a zwitterionic silicate. Examination of the N–C and C–O distances in Table XXII is in agreement with this analysis: these bonds correspond to standard imidate bond lengths (O–C=N, average C–O 1.330 and C=N 1.279 Å[71]), ruling out the amide (O=C–N) geometry of hybrid I.

3. Stereodynamic Analysis of Rearranged Product

The variable temperature ^{1}H NMR spectra of **70g** (Fig. 37, Table XXIII) provided evidence for two consecutive ligand-site exchange processes. There are two pairs of diastereotopic *N*-methyl groups in **70g**, giving rise to two pairs of singlets, and an AB-quartet due to the CH$_2$-protons. Upon heating, *one* pair of *N*-methyl signals undergoes coalescence, due to rapid exchange of the methyl groups, while the other pair of signals and the AB-signals remain sharp. This selective exchange cannot result from
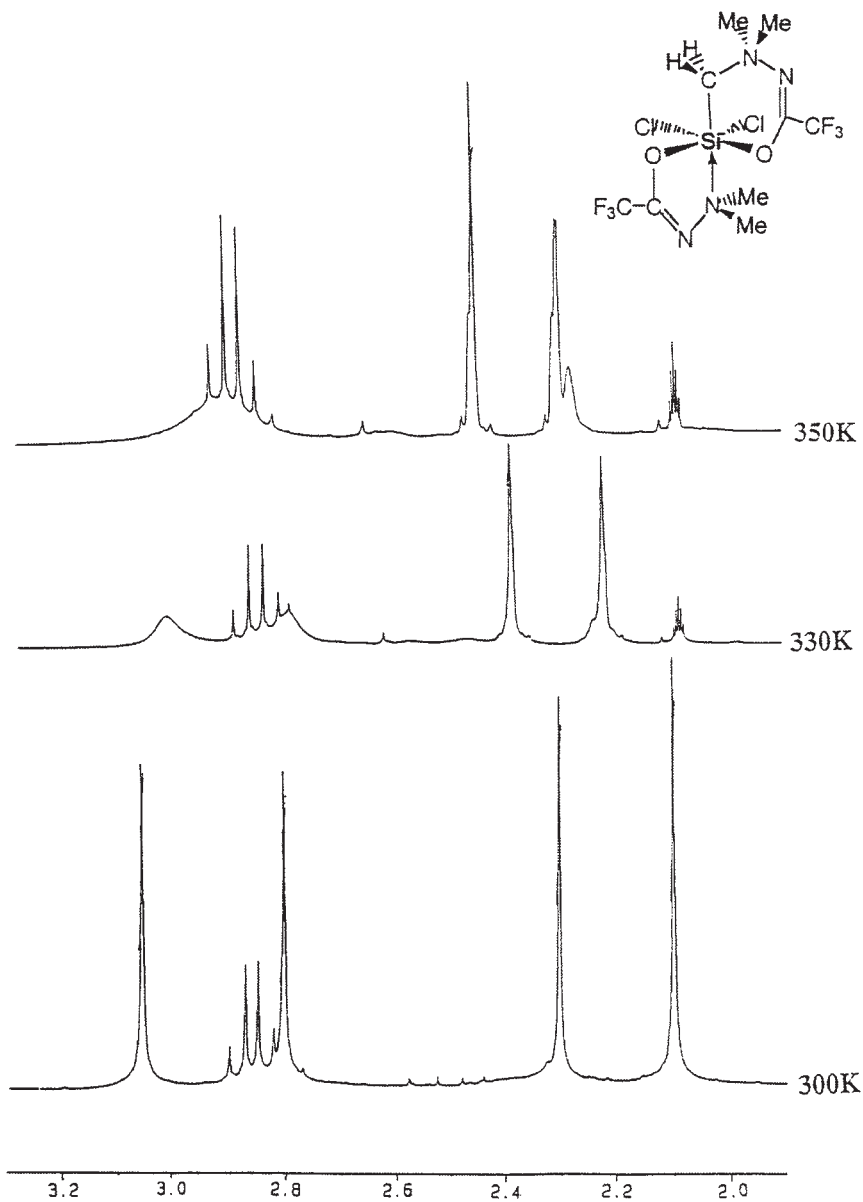
FIG. 37. Variable temperature ^{1}H NMR spectra of **70g** in toluene-d_8 solution.[51] Reproduced with permission from the American Chemical Society.

TABLE XXIII

VARIABLE TEMPERATURE ^{1}H NMR DATA FOR EXCHANGE OF N-METHYL GROUPS IN COMPLEXES **70**

Compound	Solvent	$\Delta\nu$ (Hz)	T_c (K)	ΔG^* (kcal mol^{-1})
70k	$C_6D_5CD_3$	30	332	16.7 ± 0.3
	$C_6D_5CD_3$	160	335	15.8 ± 0.3
	$CDCl_3$	12	263	13.6 ± 0.3
	$CDCl_3$	75	310	15.0 ± 0.3
70c	$C_6D_5CD_3$	89	360	17.4 ± 0.3
	$C_6D_5CD_3$	33	373	18.8 ± 0.3
70g	$C_6D_5CD_3$	133	350	16.6 ± 0.3
	$C_6D_5CD_3$	145	> 370	21.2 ± 0.2^a
	$C_6D_5NO_2$	103	350	16.8 ± 0.3
	$C_6D_5NO_2$	40	> 370	> 20

^{a}Measured by selective inversion recovery.

inversion of configuration at the silicon, and hence must be due to chelate-ring opening followed by rotation about the N–NMe$_2$ bond and reclosure of the chelate. The barrier for this exchange in toluene-d_8 is 16.6 ± 0.3 kcal mol^{-1}. Further heating eventually causes line broadening of the other signals, presumably as a result of inversion at silicon by (O,O)-exchange. However, the barrier for this process was too high to enable measurement by simple coalescence. The barrier for the second process was measured by utilizing the selective inversion recovery (SIR) technique,[72] which enables the determination of exchange rate constants at approximately 50° below the coalescence temperature.

The SIR spectra are depicted in Fig. 38. Chemical exchange of nuclei between the selectively-inverted site and the unperturbed-N-methyl site changes the population of the latter nuclei, causing an initial typical drop in intensity, followed by recovery. Equation (30) represents the corresponding changes in signal intensities (I_A, I_B) as a function of the variable delay-time τ. The first-order rate constant obtained from the experimental slope (Fig. 38c) is $k = 0.96$ s^{-1}, corresponding to a barrier for inversion of configuration at silicon $\Delta G^* = 21.2 \pm 0.2$ kcal mol^{-1} at 360 K.

$$\ln(1 - \frac{I_A + I_B}{I_A^\infty + I_B^\infty}) - \ln\frac{I_B - I_A}{I_B^\circ - I_A^\circ} = 2k\tau \tag{30}$$

This unusually high barrier for inversion of configuration at the chiral silicon atom in **70g** is probably due to (O,O)-exchange via a "bicapped tetrahedron" intermediate, in analogy to silicon inversion in compounds **30–38**.[45–48]
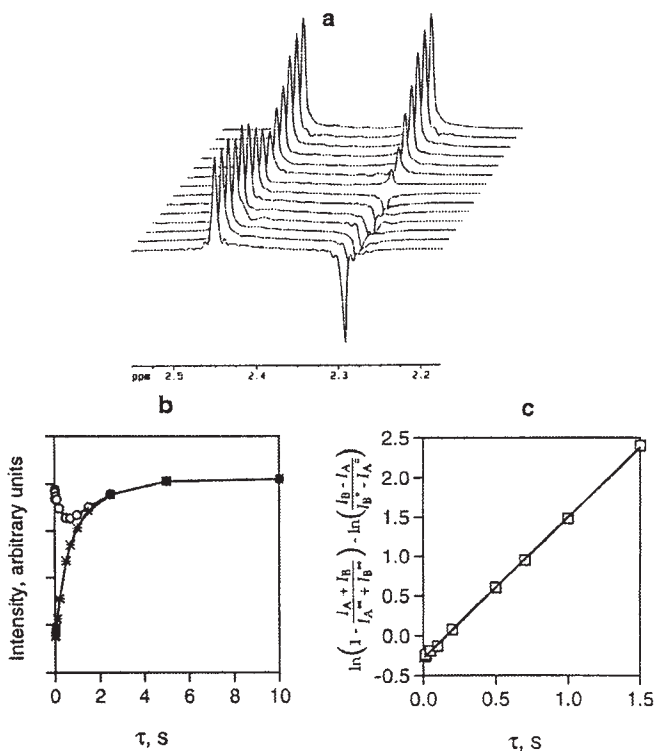
FIG. 38. Selective Inversion Recovery (SIR) ^{1}H NMR spectra for N-methyl exchange in **70g** in toluene-d_8 solution at 360 K: (a) stack plot of spectra; (b) a plot of signal intensity as a function of the variable delay τ; (c) linear correlation of data (Eq. 27).[51] Reproduced with permission from the American Chemical Society.

D. *Tris-chelates*

1. Synthesis and Structure

Dichloro neutral bis-chelates of hexacoordinate silicon were obtained by two methods: directly (**35**) by transsilylation of N-dimethylamino-O-(trimethylsilyl)acylimidates (**1**) with tetrachlorosilane, or by rearrangement as described in the previous section (**70**). The presence of two chloro ligands was utilized for further substitution, to form hexacoordinate silicon tris-chelates, by reaction with bis(trimethylsilyl)-precursors: **71** and **72**, as shown in Eqs. (31) and (32). The products (**73**, **74**, and **75**), are hexacoordinate *neutral* silicon tris-chelates, and **75** is the first reported zwitterionic tris-chelate with three different chelate rings.[73]

$$(31)$$

35c, R = Ph
35h, R = (R,S)-CH(Me)Ph
35h', R = (R)-CH(Me)Ph

71
-2Me₃SiCl

72
-2Me₃SiCl

73a, R = Ph
73b, R = (R,S)-CH(Me)Ph

74a, R = Ph
74c, R = (R)-CH(Me)Ph

$$(32)$$

70c   75
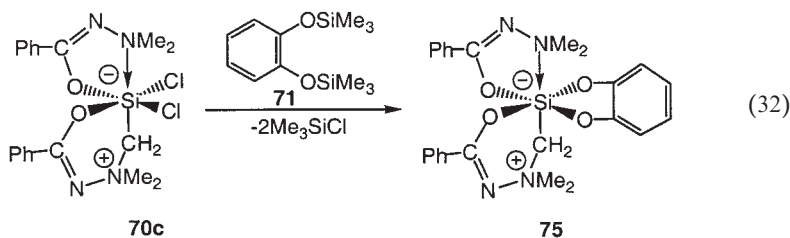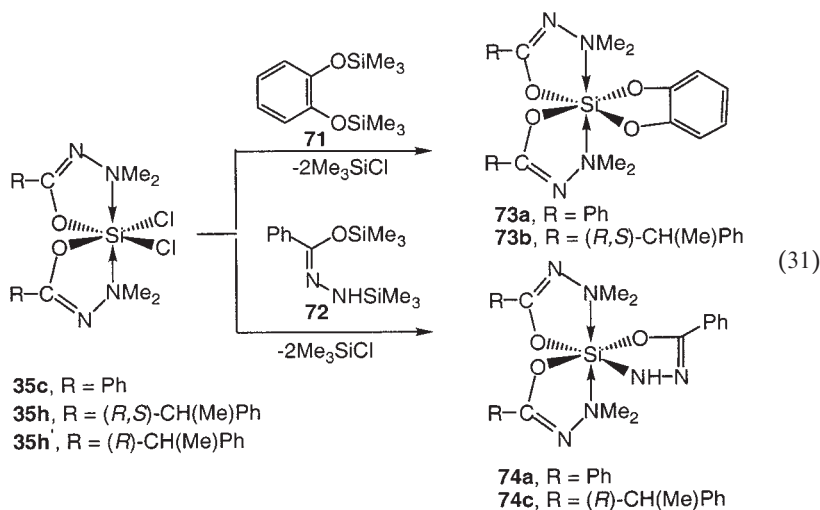
The crystal structures of **73a**, **74a**, and **75**, each representing one of the three types of tris-chelates, were reported. The structures are depicted in Figs. 39–41, and selected bond lengths and angles are listed in Table XXIV. It is evident that all three molecules have distorted octahedral geometries in the solid-state.

2. Dynamic Stereochemistry

The dynamic behavior of tris-chelates was of considerable interest due to the additional constraint of a third bidentate ligand, relative to the extensively studied bis-chelates, with two monodentate ligands (Section III.A.3). Also the question of whether N–Si dissociation takes place during multi-step ligand-site exchange processes was considered.

FIG. 39. Molecular structure of **73a** in the crystal.[73] Reproduced with permission from the American Chemical Society.

FIG. 40. Molecular structure of **74a** in the crystal.[73] Reproduced with permission from the American Chemical Society.

FIG. 41. Molecular structure of **75** in the crystal.[73] Reproduced with permission from the American Chemical Society.

TABLE XXIV

SELECTED BOND LENGTHS (Å) AND ANGLES (deg.) IN CRYSTALS OF **73a**, **74a**, AND **75**[73]

73a		74a		75	
Bond	Distance	Bond	Distance	Bond	Distance
Si(1)–O(1)	1.759(3)	Si(1)–O(1)	1.7401(17)	Si(1)–O(1)	1.7607(11)
Si(1)–O(2)	1.757(3)	Si(1)–N(2)	1.756(2)	Si(1)–O(3)	1.7707(11)
Si(1)–O(3)	1.731(3)	Si(1)–O(3)	1.7641(17)	Si(1)–O(2)	1.7784(11)
Si(1)–O(4)	1.735(3)	Si(1)–O(2)	1.7653(16)	Si(1)–O(4)	1.8023(11)
Si(1)–N(1)	2.010(3)	Si(1)–N(5)	2.016(2)	Si(1)–C(16)	1.9180(16)
Si(1)–N(4)	1.997(3)	Si(1)–N(4)	2.044(2)	Si(1)–N(4)	2.0809(14)
Angle	Degrees	Angle	Degrees	Angle	Degrees
O(1)–Si(1)–O(3)	174.72(13)	O(1)–Si(1)–O(3)	174.62(8)	O(1)–Si(1)–O(3)	170.85(6)
N(4)–Si(1)–N(1)	168.22(13)	N(2)–Si(1)–O(2)	173.32(9)	O(2)–Si(1)–O(4)	176.14(6)
O(4)–Si(1)–O(2)	175.40(13)	N(5)–Si(1)–N(4)	165.52(8)	C(16)–Si(1)N(4)	172.12(6)
O(3)–Si(1)–O(4)	90.19(12)	O(1)–Si(1)–O(2)	90.65(8)	O(3)–Si(1)–O(4)	91.80(5)
O(3)–Si(1)–O(2)	88.96(13)	O(3)–Si(1)–O(2)	91.56(8)	O(1)–Si(1)–O(4)	88.08(5)
O(3)–Si(1)–N(4)	95.44(13)	O(3)–Si(1)–N(2)	92.93(9)	O(1)–Si(1)–O(2)	89.42(5)
O(4)–Si(1)–N(4)	92.07(12)	O(1)–Si(1)–N(2)	85.30(8)	O(2)–Si(1)–O(3)	90.20(5)

i. Ligand-site exchange in 73a,b

Tris-chelate **73a** has C_2 symmetry, and hence its four N-methyl groups give rise to two signals in the ^{1}H and ^{13}C NMR spectra. Coalescence of these signals due to exchange could not be reached up to 370 K, and hence the SIR method[72] (Section III.C.3) was utilized at three temperatures, 360, 370, and 375 K, yielding rate constants of 1.86, 4.32, and 7.00 s^{-1}, respectively.[73] These led to estimated $\Delta H^* = 22.7$ kcal mol^{-1} and $\Delta S^* = 5.4$ cal mol^{-1} K^{-1}, in agreement with an intramolecular exchange. However, no assignment of the exchange to either N–Si dissociation–recombination or (O,O)-1,2-shift (see Fig. 13) could be made based on these results.

In order to assign the exchange process to one of these two reasonable mechanisms, a similar tris-chelate was prepared (**73b**), into which two chiral carbon centers were introduced. Compound **73b** can exist in three diastereomeric forms: $R\Delta R$, $R\Lambda R$, and $R\Delta S$ (identical with $S\Delta R$), and their respective enantiomers. The first two diastereomers have C_2 symmetry, and generate each two N-methyl signals. The remaining isomer $R\Delta S$ lacks symmetry, and hence gives rise to four N-methyl signals. A solution of **73b** indeed features in its ^{1}H and ^{13}C NMR spectra, eight nearly equal N-methyl signals.[73]

The stereochemical analysis for **73b** was done with the aid of ^{1}H NMR 2D-NOESY spectra at several temperatures (Fig. 42). At the lowest temperature, 325 K (Fig. 42a,b), ligand exchange is slow and hence only NOE (negative, dotted) cross signals are observed, unequivocally identifying geminal N-methyl pairs. At 340 K (Fig. 42c), in addition to NOE cross-signals, exchange (positive) signals can also be observed, proving interchange of sites between *non-geminal* N-methyl groups. Since Si–N dissociation followed by rotation about the N–N bond and recombination should obviously involve exchange of geminal methyl groups, this process is ruled out by the results, leaving the (O,O)-1,2-exchange as the most probable mechanism.

At 360 K the NOESY spectrum (Fig. 42d) is further modified by the addition of a second exchange cross-signal for each N-methyl group, indicating that now a second rate process is effective. This rate process *does* exchange geminal N-methyl groups, and thus may be assigned to N–Si dissociation–recombination. It is concluded that in **73b** two consecutive N-methyl exchange processes take place: the first is assigned to an (O,O)-shift (epimerization at silicon), and the higher barrier process is assigned to N–Si dissociation–recombination.[73]

ii. Ligand-site exchange in 74a,c

Compound **74a** has C_1 symmetry, and therefore displays four N-methyl signals in the ^{1}H and ^{13}C NMR spectra. There are three reasonable,
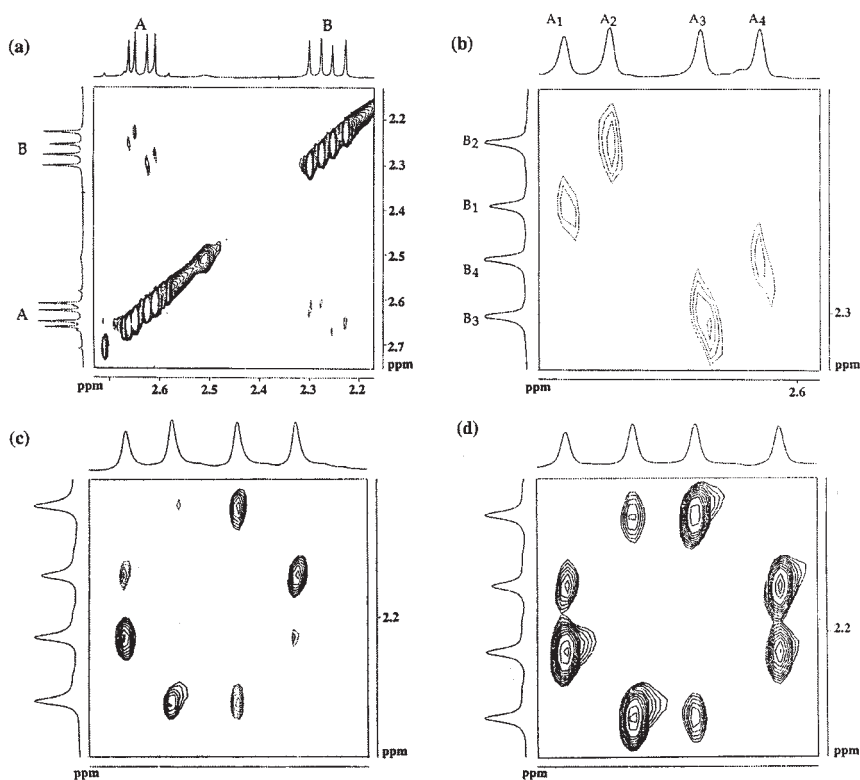
FIG. 42. ^{1}H NMR phase-sensitive NOESY and exchange spectra for **73b** (toluene-d_8): (a) full *N*-methyl range at 325 K, showing four A and four B signals for three diastereomers, with NOE (negative, dotted line) cross-signals identifying geminal pairs; (b) expansion of upper left part of (a): A-type signals are numbered arbitrarily and B-signals are numbered to correspond to their geminal A counterparts; (c) the same region at 340 K, showing *N*-methyl exchange (positive, solid lines) of *non-geminal* groups; (d) at 360 K two exchange processes are observed, without total scrambling.[73] Reproduced with permission from the American Chemical Society.

non-dissociative intramolecular processes which, in principle, can effect exchange between the various *N*-methyl pairs without changing the basic geometry of the complex: (1) Si–N dissociation–recombination; (2) (O,O)-exchange of the two dimethylhydrazido chelates; and (3) (O,N)-exchange of the third chelate ring. Each of these processes has different stereochemical consequences: process (1) should interchange, when rapid on the NMR time scale, between A and B geminal *N*-methyl groups (see Fig. 43). Process (2) results in the exchange A $\rightleftarrows$ B′ and B $\rightleftarrows$ A′, while process (3) exchanges between A and A′, and between B and B′ (A and B refer to geminal
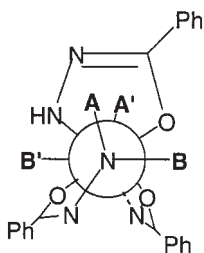
FIG. 43. Newman-like projection of **74a**, viewed along the N–Si–N axis. The *N*-methyl groups are labeled A, A′, B, B′.[73] Reproduced with permission from the American Chemical Society.
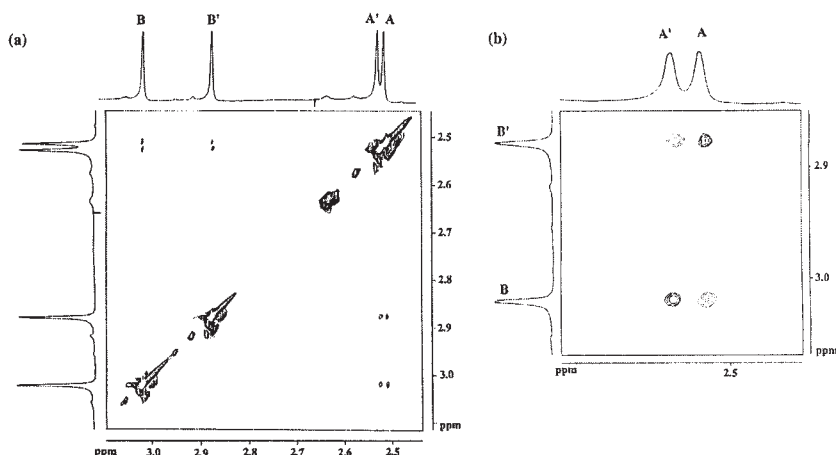
FIG. 44. 2D-NOESY and exchange ^{1}H-NMR spectrum of **74a**, (toluene-d_8, 300 K): (a) full *N*-methyl region; (b) expansion, showing geminal pairs (negative, dotted cross signals) and interchange of non-geminal pairs (positive cross peaks).[73] Reproduced with permission from the American Chemical Society.

N-methyl groups, while A, A′ and B, B′ refer to groups exposed to similar chemical environments: A and A′ flank the NH-hydrazido chelate ring on each side, while B and B′ point away from that ring. See Fig. 43).[73]

A 2D-NOESY experiment was used to observe and distinguish among the three exchange options in **74a** at 300 K (Fig. 44). NOE (negative) cross peaks (Fig. 44b) unequivocally identify signals due to the geminal (AB) *N*-methyl pairs. The exchange (positive) signals are clearly neither between geminal groups (A, B), nor between groups of similar chemical environments (A, A′ or B, B′), but represent the exchange A ⇄ B′ and B ⇄ A′. This result leads directly to the following two

conclusions: (a) that the exchange process must be non-dissociative (because dissociation of the $N \rightarrow Si$ bond would have caused the exchange A $\rightleftarrows$ B) and (b) that the observed exchange is 2, the interchange of the dimethylhydrazido chelates via (O,O)-shift. The free energy of activation for the process was determined by a 1D experiment, from the coalescence of signals due to the *ortho* protons of the phenyl rings: $T_c = 365$ K, $\Delta G^* = 18.5 \pm 0.2$ kcal mol^{-1}.[73]

Increasing the temperature of a toluene-d_8 solution of **74a** showed line broadening and exchange phenomena for a *second* exchange process. However, the mechanistic assignment between options 1 and 3 (above) could not be made on the basis of these results. A chelate with two chiral carbon centers was used again for the assignment, **74c**. **74c** was prepared from *optically pure R*-2-phenylpropionic acid. Two diastereomers were observed in the NMR spectra: $R\Delta R$ and $R\Lambda R$, with four unique N-methyl groups in each, for a total of eight singlets.

Assignment of N-methyl signals to the corresponding geminal pairs in **74c** was made, as for **73** and **74a**, by observation of NOE cross-signals in the 300 K (slow exchange) NOESY spectrum. At 345 K the NOESY spectrum (Fig. 45) features at least *two* exchange processes for each N-methyl group: one exchange of geminal pairs, resulting from the N–Si dissociation–recombination sequence, and the other one most likely due to epimerization at silicon via (O,O)-1,2-shift (judging from the similar process in **74a**). The possibility that at this temperature all three rate processes are rapid relative to the NMR time scale is ruled out by the fact that the spectrum in Fig. 45 does *not* feature complete scrambling of all N-methyl signals, as would be required by the simultaneous three exchanges.

iii. Ligand-site exchange in 75

The tris-chelate **75**, with three different chelate rings and lacking molecular symmetry (C_1), displays in the ^{1}H–^{13}C NMR spectra four N-methyl signals, and an AB quartet for the prochiral methylene protons in the ^{1}H spectrum. Two consecutive kinetic ligand exchange processes: N–Si dissociation–recombination, and (O,O)-exchange of the two hydrazido rings, were observed by ^{1}H NMR spectroscopy. The first of these exchange reactions was observed by the coalescence of two of the initial four N-methyl signals, in the absence of exchange of the prochiral CH_2 protons ($T_c = 363$ K, $\Delta G^* = 16.1 \pm 0.2$ kcal mol^{-1}). This could only result from a dissociation–recombination sequence, which renders the two N-methyl groups in the five-membered chelate ring homotopic.
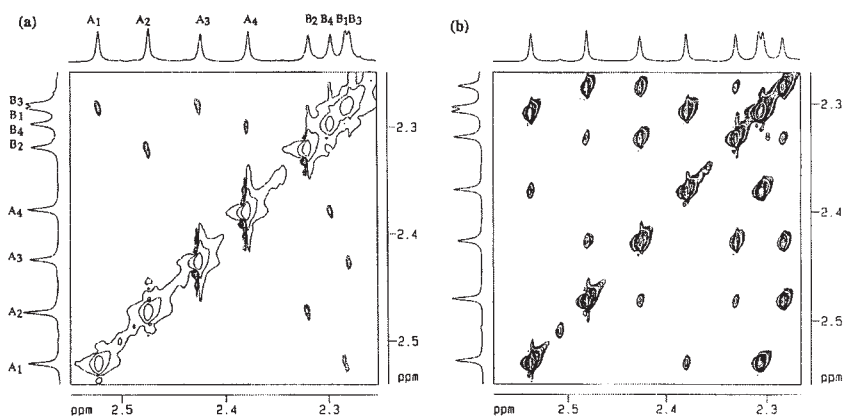
FIG. 45. ^{1}H 2D-NOESY and exchange spectrum of **74c** (toluene-d_8, 345 K), showing at least two exchange processes, *without* complete scrambling.[73] Reproduced with permission from the American Chemical Society.

The second process was too slow to permit measurement by the coalescence method, and the exchange barrier was determined using the SIR technique.[72] The first order rate constant obtained by this method at 355 K was $k = 1.02$ s^{-1}, corresponding to a free energy barrier $\Delta G^* = 20.9 \pm 0.1$ kcal mol^{-1}. This barrier was assigned to the inversion of configuration at silicon through a (O,O)-shift.[73]

IV

STABLE PENTACOORDINATE SILICONIUM COMPLEXES

We make a distinction between two types of ionic pentacoordinate complexes: those which are in dynamic equilibrium with neutral hexacoordinate complexes have been dealt with in Sections III.A.4, III.A.5.ii, and III.B.2. The second group includes those pentacoordinate siliconium-ion salts which are formed as such and are stable and do not equilibrate (to a noticeable extent) with their hypothetical neutral hexacoordinate counterparts. The present section discusses this group of persistent salts of pentacoordinate silicon cations.

Free tricoordinate silicon cations (silicenium) are exceedingly unstable, and have only recently been first realized.[74,75] A silicenium ion can be stabilized by coordination with two intramolecular donors, to form a stable (pentacoordinate) siliconium complex. These have been reported with

$N \rightarrow Si$ coordination (**76**, **77**[76] **78a**[77]) and most recently also with oxygen (**78b**,[78] **79**[79]), sulfur (**78c**),[78] and phosphorus (**78d**)[78] donor-ligands. The present section describes the chemistry of donor-stabilized silyl cations with hydrazido chelates.

76

77, X = I, Br, Cl, BF$_4$, OTf.

78

a, Do = NMe$_2$
b, Do = OMe
c, Do = SMe
d, Do = PMe$_2$

79, n = 3, 4; X = OTf, others
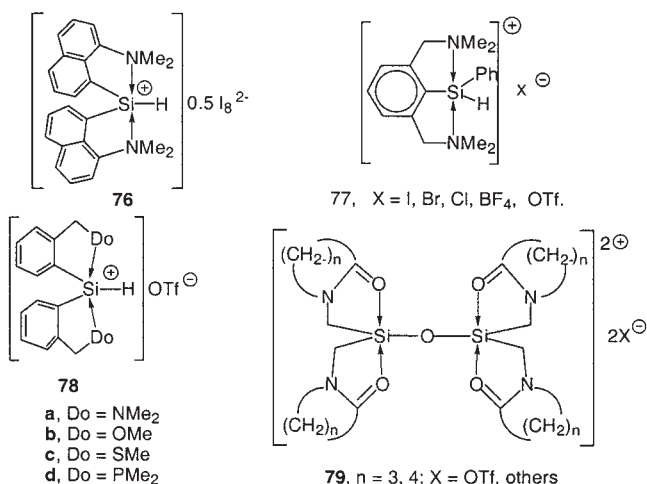
The terms "siliconium" or "donor-stabilized silyl cations" should be used in a formal sense, and not as an indication of the true charge on silicon: computational[75c,80] and experimental[75a,b] evidence suggests that while the silicon atom is positively charged in a free silicenium compound, it is effectively neutral in donor-stabilized siliconium complexes (i.e., most of the positive charge is transferred to the donor atoms); this is evident from the huge difference in ^{29}Si chemical shifts between the two classes of compounds (> 200 ppm in the former, and < -50 ppm in the latter). It also explains why the ^{29}Si chemical-shift ranges of neutral and cationic pentacoordinate silicon chelates are essentially the same.

A. *Silyl Cations Stabilized by Oxygen-Donors*

1. Synthesis and Structure

The first hydrazide-based siliconium-cation salts were obtained during an attempt to prepare neutral, hexacoordinate bis-chelates with $O \rightarrow Si$ coordination (**80**), in analogy to the extensively studied isomeric $N \rightarrow Si$ coordinated **30–38** (see Section III.A.1). In analogy to Eq. (15), the *N*-trimethylsilylhydrazides **81** were allowed to react with polyhalosilanes **22–25** (Eq. 33). However, in contrast to Eq. (15), the expected **80** were not

formed, but instead the salts of cationic pentacoordinate siliconium chelates **82–85** were obtained.[81]

80

81

22, X = Me
23, X = Ph
24, X = CH₂Ph
25, X = CH₂Cl

82, X = Me
83, X = Ph
84, X = CH₂Ph
85, X = CH₂Cl

$$(33)$$
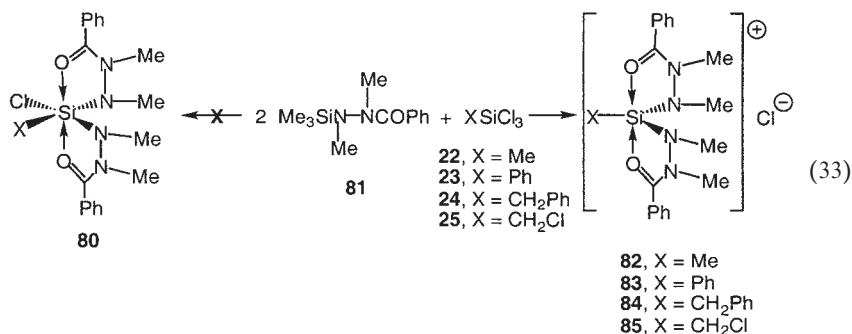
The salts **82–85** were characterized by their typical pentacoordinate ²⁹Si chemical shifts (Table XXV), by the equivalence of the two chelate rings resulting from the molecular C_2 symmetry, and by spectral analogy with a binuclear disiliconium dichloride salt (**86**) for which a crystal structure (Fig. 46) was obtained.

86
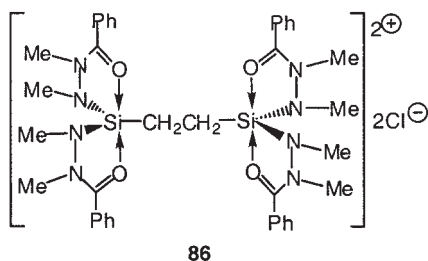
Compound **86** exists in two diastereomeric forms due to the chiral silicon centers, which are evident in the various NMR spectra (Table XXV). The crystal structure of **86** shows a molecular inversion center, and hence belongs to the *meso* diastereomer. The geometry around silicon in the crystal is a distorted TBP and the chloride is more than 7 Å away from silicon, in accord with a pentacoordinate siliconium chloride structure. The dative O → Si bonds are exceptionally short in **86** (1.802 and 1.807 Å) relative to those in other pentacoordinate complexes.[2,3,11b]

2. Analysis of Donor Strength by Bond Lengths

The question as to why these O → Si coordinated chelates, **82–86**, form donor-stabilized silyl cations, while the analogous N → Si chelates (**30–38**)

TABLE XXV
^{1}H, ^{13}C, AND ^{29}Si CHEMICAL SHIFTS (δ, ppm, AT 300 K IN CDCl$_3$) FOR
COMPLEXES **82–86** AND **89**

Compound	^{29}Si	^{13}C			^{1}H	
		C=O	CNCH$_3$	SiNCH$_3$	CNCH$_3$	SiNCH$_3$
82	−79.0	160.4	36.8	31.9	3.86	3.27
83	−94.8	160.3	37.2	32.6	3.79	3.30
84	−86.6	159.6	36.2	31.6	3.70	3.20
85	−91.7	159.4	36.7	32.0	3.64	3.07
86-I	−81.3	159.0	36.8	31.1	3.84	3.26
86-II	−81.6	158.9	36.8	31.1	3.84	3.28
89	−78.3	163.0	32.7[a]	30.9	3.60	3.07
	−78.9[a]	162.8[a]	32.7[a]	30.6[a]	3.56	3.05
	−78.9[a]	162.8[a]	32.6	30.6[a]	3.54	2.88
	−79.3	162.5	32.0	30.4	3.52	2.80

[a]Accidental equivalence of two groups.
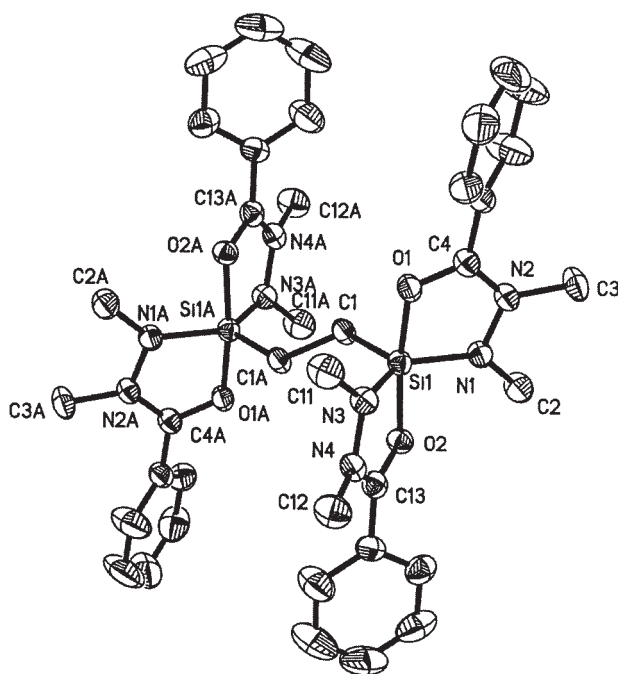
FIG. 46. Molecular structure of **86** in the crystal.[81] Reproduced with permission from the American Chemical Society.

are generally neutral and hexacoordinate is of interest. This is most likely because the two donor groups in **82**–**86** are more effective in dispersing the positive charge away from silicon, relative to the nitrogen donors in **30**–**38**. A bond-length analysis of **86** confirms this view: the relatively short O–Si distances are in agreement with stronger than usual coordination. This is further supported by comparison of the amide C=O and C–N bond lengths: the C=O bonds in **86** are substantially longer than average amide or hydrazide C=O bonds,[71] and the C–N bonds are shorter than typical amide C–N bonds.[71] In fact, the C–O and C–N distances in **86** are essentially equal, at 1.30 ± 0.01 Å. Examination of numerous relevant amide and hydrazide silicon complexes[14a],[82] shows that the C–O distance varies between 1.20 and 1.35 Å, while the C–N bond falls in the range 1.34–1.27 Å (depending on whether the sequence N–C=O $\rightarrow$ Si or N=C–O–Si is more important). In **86** both the C–O and C–N bonds are near the middle of their bond length range and, hence, **86** may best be described as a hybrid between equal parts of **87** and **88** (Eq. 34). The resulting charge distribution is 0.5 positive charge on each of the ammonium nitrogens, and zero charge on silicon. It follows that the formation of these formally cationic silicon complexes (**82**–**86**) is facilitated by the extraordinary ability of the hydrazide moiety to redistribute the charges so that the positive charge is effectively removed from silicon and transferred to the nitrogen atoms.

$$(34)$$
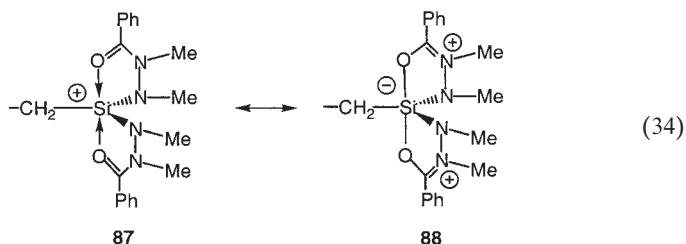
3. Inversion of Configuration at Silicon

The NMR spectra of **82**–**86** do not permit the observation of internal ligand-site exchange reactions. In order to enable an NMR kinetic study, the analogous complex **89** was prepared, having two additional chiral carbon centers (Table XXV) and three diastereomers: $R\Delta R$, $R\Lambda R$, and $R\Delta S = S\Delta R$ and their respective enantiomers.[81] The former two stereoisomers give rise to two N-methyl signals each (C_2 symmetry), while the third has four N-methyl signals (C_1), for a total of eight nearly equal N-methyl singlets in the ^{1}H NMR spectrum. Epimerization at silicon can be studied by observing the exchange of signals due to

different diastereomers. However, due to the relatively high barrier for epimerization the SIR technique had to be used,[72,81] for a nitrobenzene-d_5 solution of **89** at 360 K, resulting in a first-order rate constant $k = 2.74$ s^{-1} corresponding to $\Delta G^* = 20.5 \pm 0.2$ kcal mol^{-1}.

89
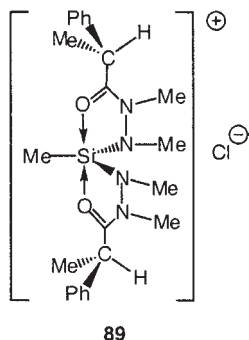
B. *Silyl Cations Stabilized by Nitrogen Donor Groups*

1. Dimethylaminoimidato-Coordinated Siliconium Complexes

i. *Mononuclear siliconium complexes*

The equilibrium reaction between neutral hexacoordinate chelates and pentacoordinate siliconium halide salts is discussed in Section III.A.4 (Eq. 17). This reaction can be driven completely to the ionic side by replacement of the chloro ligand by better leaving groups: triflate and bromide (Eq. (18), listed again with compound labels; see Section III.A.4.iv). The products of this counterion-exchange reaction are stable siliconium salts **90**(OTf)–**92**(OTf), **90**(Br)–**92**(Br), which no longer equilibrate with their hexacoordinate precursors (within detection limits).[65,66]

31a	Z = Br, OTf	**90a**(OTf), **90a**(Br), R = X = Me
31c		**90c**(OTf), **90c**(Br), R = Ph, X = Me
31j		**90j**(OTf), **90j**(Br), R = t-Bu, X = Me
32a		**91a**(OTf), **91a**(Br), R = Me, X = Ph
32b		**91b**(OTf), **91b**(Br), R = PhCH$_2$, X = Ph
32c		**91c**(OTf), **91c**(Br), R = X = Ph
32j		**91j**(OTf), **91j**(Br), R = PhCH$_2$, X = Ph
34a		**92a**(OTf), **92a**(Br), R = Me, X = PhCH$_2$
34b		**92b**(OTf), **92b**(Br), R = X = PhCH$_2$
34c		**92c**(OTf), **92c**(Br), R = Ph, X = PhCH$_2$

(18)
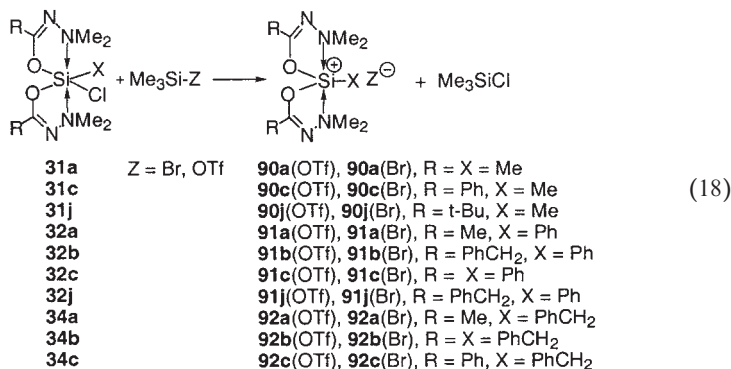
Stable siliconium-ion salts can also be prepared *without* exchange of ions, in the case of the bulky *t*-butyl ligand, directly from the TMS-hydrazide and *t*-BuSiCl$_3$ (Eq. 35).[66] The *t*-butylsiliconium chlorides **93**(Cl) are the only known stable chloride salts of this kind. The chloride can still be exchanged with other anions, as shown in Eq. (18), to produce **93a,c,j** bromide, iodide, and triflate.[83]

$$\text{(35)}$$

93a(Cl), R = Me
93c(Cl), R = Ph
93j(Cl), R = t-Bu
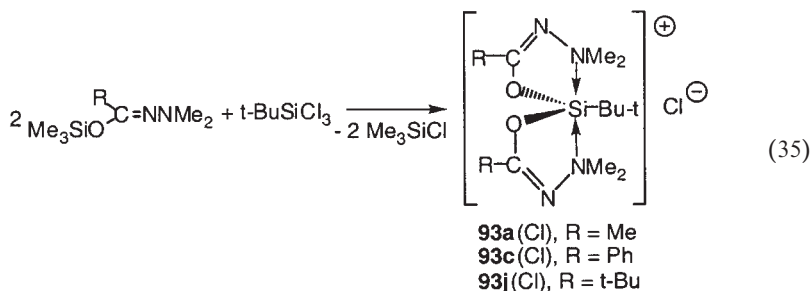
Even the ionization-resistant hexacoordinate complexes with two electron-withdrawing monodentate ligands form stable ionic siliconium salts when treated with AlCl$_3$, as shown in Eq. (36).[66]

$$\text{(36)}$$

35a, R = Me, X = Cl   **94a**, R = Me, X = Cl
35c, R = Ph, X = Cl   **94c**, R = Ph, X = Cl
38c, R = Ph, X = Br   **95c**, R = Ph, X = Br
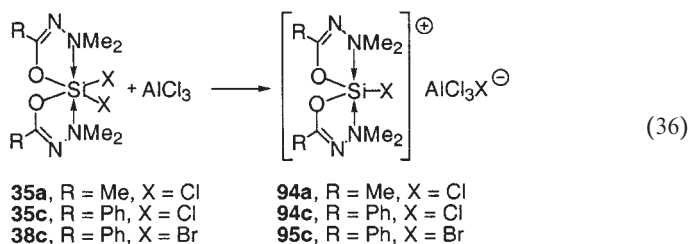
For several of the siliconium salts crystal structure analyses were obtained, confirming the pentacoordination and the ionic nature of the compounds (well separated cations and anions). The crystal structures for **90a**(OTf), **90c**(OTf), **91a**(OTf), **91a**(AlCl$_4$), and **93a**(OTf) are depicted in Figs. 47–51, respectively. Further structural support is found in the ^{29}Si NMR chemical shifts (Table XXVI). A remarkable observation in Table XXVI is the nearly equal ^{29}Si chemical shifts of siliconium salts sharing the same silicon complex, but with different anions [e.g.: **91a**(OTf), **91a**(Br), and **91a**(AlCl$_4$)]: the equal shifts are the evidence that the siliconium cations are essentially independent of
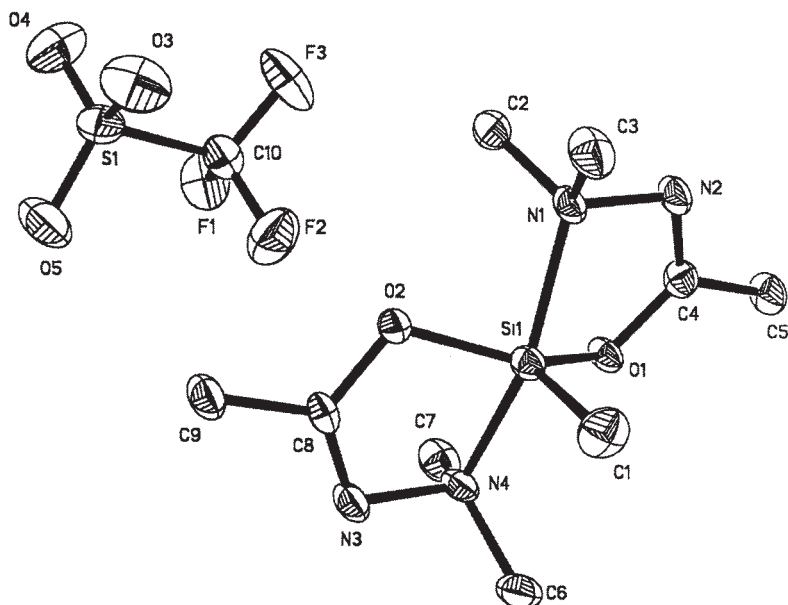
FIG. 47. Molecular structure of siliconium salt **90a**(OTf) in the crystal.[66] Reproduced with permission from the American Chemical Society.
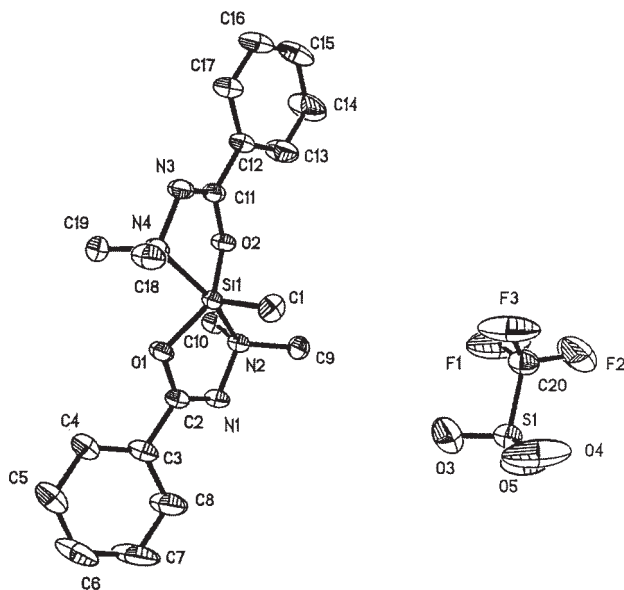
FIG. 48. Molecular structure of siliconium salt **90c**(OTf) in the crystal.[66] Reproduced with permission from the American Chemical Society.
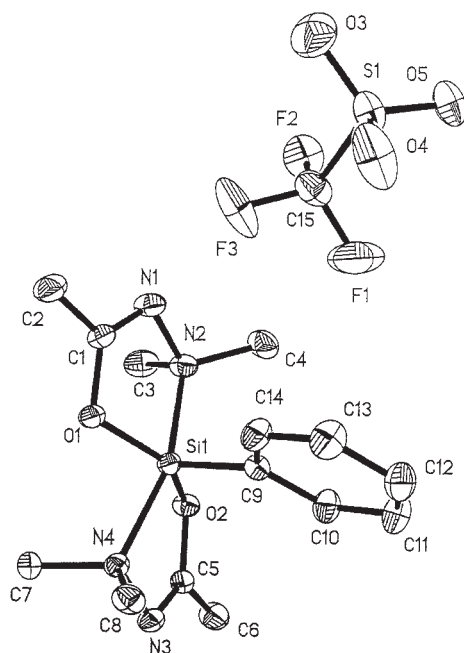
Fig. 49. Molecular structure of siliconium salt **91a**(OTf) in the crystal.[66] Reproduced with permission from the American Chemical Society.
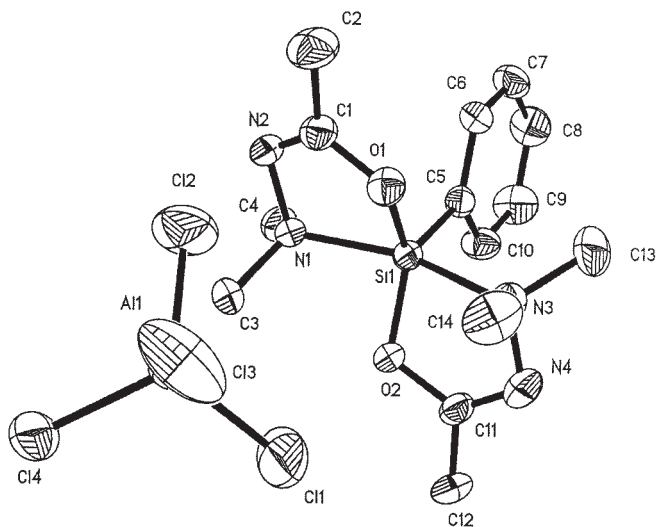
Fig. 50. Molecular structure of siliconium tetrachloroaluminate salt **91a**(AlCl₄) in the crystal.[66] Reproduced with permission from the American Chemical Society.
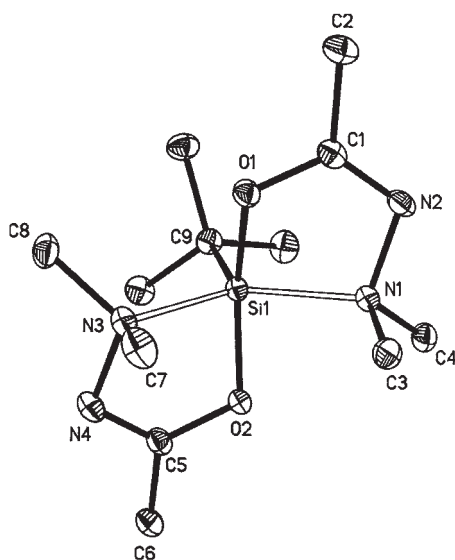
FIG. 51. Molecular structure of siliconium salt **93a**(OTf) in the crystal.[83] Reproduced with permission from Wiley-VCH.

TABLE XXVI

^{29}Si Chemical Shifts of Various Siliconium Salts (ppm, in CDCl$_3$, 300 K)

Compound	R, X	OTf$^-$	Br$^-$	AlCl$_4^-$	Cl$^-$ (I$^-$)	Ref.
90a	Me, Me	−61.7	−61.8			66
90c	Ph, Me	−60.9	−61.3	−62.5		66
91a	Me, Ph	−73.2	−73.0	−73.2		65,66
91b	PhCH$_2$, Ph	−73.4				66
91c	Ph, Ph	−72.6	−72.2	−72.0		66
91j	t-Bu, Ph	−73.6				66
92a	Me, PhCH$_2$	−65.8	−65.2	−65.3		66
92b	PhCH$_2$, PhCH$_2$	−66.1				66
92c	Ph, PhCH$_2$	−65.1	−65.0			66
93a	Me, t-Bu				−61.6	83
93c	Ph, t-Bu	−61.1			−61.1	83
93j	t-Bu, t-Bu				−61.1	83
94a	Me, Cl			−80.9		66
94c	Ph, Cl			−80.5		66
95j	Ph, Br			−80.6		66
57a	Me, −(CH$_2$)$_2$−	−64.7[a]				69
57c	Ph, −(CH$_2$)$_2$−	−63.3, −63.7[b]				69
57j	t-Bu, −(CH$_2$)$_2$−	−65.0	−66.4, −66.7[b]		(−65.0)	69

[a]In CD$_3$CN.
[b]Two diasteromers, CD$_2$Cl$_2$.

the counterions. These shifts also correspond to the low-temperature chemical shifts observed for the equilibrating systems (Sections III.A.4.i and III.A.4.iv), and provide further support for the identity of the stable siliconium cations with those equilibrating with the neutral hexacoordinate complexes.

ii. Binuclear disiliconium salts

The partial and reversible ionization of binuclear hexacoordinate silicon complexes **55a,c,j** is described in Section III.A.5.ii. Like the mononuclear siliconium chloride salts, these can also form stable binuclear disiliconium salts (**57a,c,j**) by replacement of the chloride by other counterions, which are better leaving groups (triflate, bromide, or iodide, Eq. 37).[69]

55a,c,j + Me₃SiY $\xrightarrow{\text{-2 Me}_3\text{SiCl}}$

Y = TfO, Br, I

57a(OTf), R = Me
57c(OTf), R = Ph
57j(OTf), **57j**(Br), **57j**(I), R = t-Bu

(37)
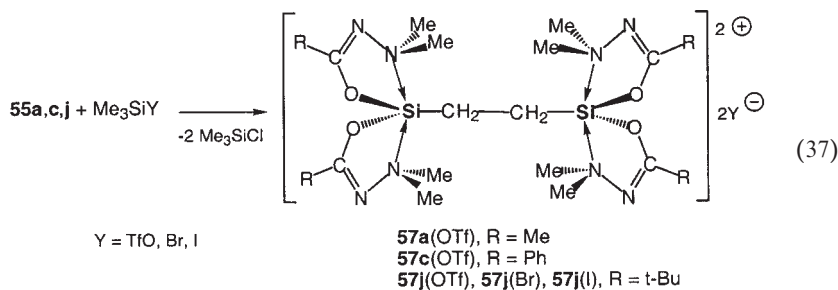
The binuclear siliconium salts **57** have two chiral centers at the silicons and hence exist as *d,l* and *meso* diastereomers. Only the latter isomers were isolated and characterized by crystallographic analysis: *meso*-**57a**(OTf) and *meso*-**57c**(OTf) (Figs. 52 and 53). The characterization is further confirmed by the [29]Si chemical shifts (Table XXVI) which are in agreement with those for similar mononuclear siliconium salts.

iii. Sterically-driven methyl-halide elimination

A surprising new reaction which some of the siliconium halides undergo has recently been reported.[83] The *t*-butylsiliconium [**93a,c,j**(Y)] chlorides, bromides, and iodides undergo, upon mild heating, an unprecedented methyl-halide elimination forming novel neutral pentacoordinate complexes (**96**, Eq. 38). In this reaction one of the two initially equivalent Me₂N groups loses a methyl, producing a complex with one covalent and one dative N–Si bond. The products of elimination were
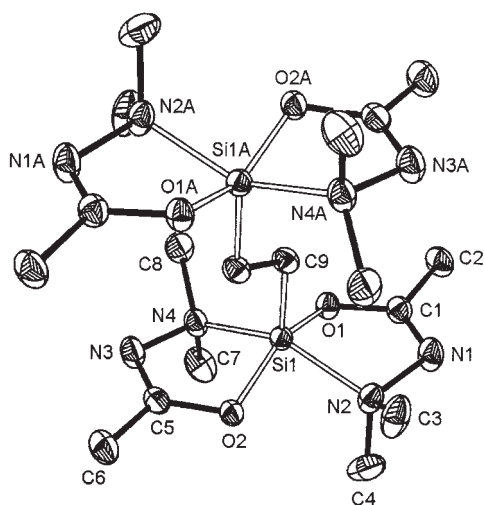
Fig. 52. Molecular structure of binuclear disiliconium triflate *meso*-**57a**(OTf) in the crystal.[69] Reproduced with permission from the American Chemical Society.
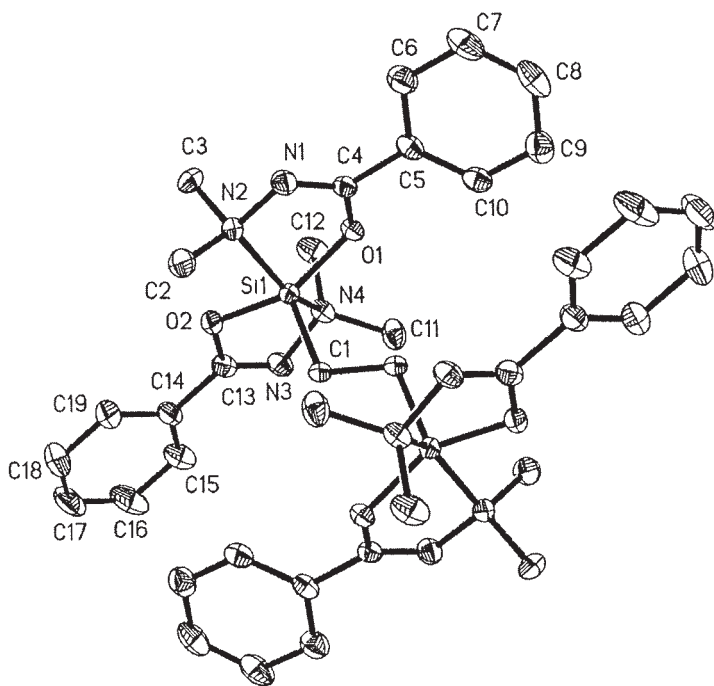
Fig. 53. Molecular structure of binuclear disiliconium triflate *meso*-**57c**(OTf) in the crystal.[69] Reproduced with permission from the American Chemical Society.

isolated and characterized by crystal structure (**96j**, Fig. 54), and by standard methods.[83]

$$Y = Cl, Br, I$$

93a(Y), R = Me
93c(Y), R = Ph
93j(Y), R = t-Bu

96a, R = Me
96c, R = Ph
96j, R = t-Bu

(38)
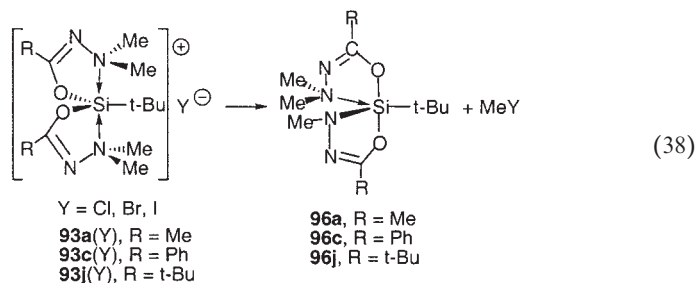
The progress of elimination (at 65 °C, in vacuum sealed CDCl$_3$ solutions) was monitored by ^{1}H and ^{29}Si NMR spectroscopy, and was found to depend on the counterion: among the halides the order of reactivity is I > Br > Cl [50% elimination after 85, 130, and 175 min, respectively, from **93c**(Cl), **93c**(Br), and **93c**(I)], whereas the siliconium triflate **93c**(OTf) did not react. It is thus evident that nucleophilic attack of the anion on one of the N-methyl groups is involved in the rate determining step of the elimination.

The scope of this reaction is as yet unknown, and is under investigation. It seems likely that the elimination of methyl halide is driven by steric repulsion between the t-butyl ligand and the bulky dimethylamino donor, since it has been observed only in t-butylsiliconium salts.
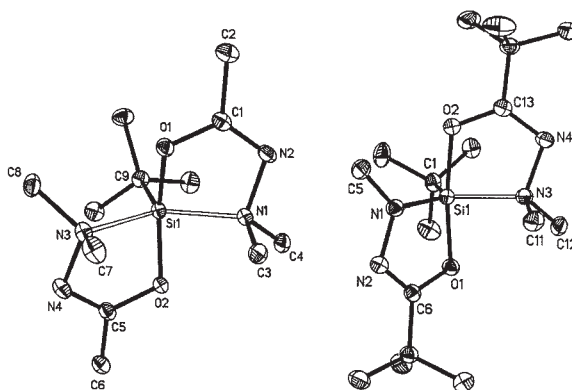
FIG. 54. Molecular structures of the siliconium salt **93a**(OTf) (left) and the elimination product **96j** (right) in the solid-state.[83] Reproduced with permission from Wiley-VCH.

iv. Crystal-structure comparison: a pseudorotation-coordinate model

Selected bond lengths and angles from the crystal structures for mono- and binuclear siliconium ion salts and from the elimination product **96j** are listed in Table XXVII. From the table and the figures it is evident that the geometry of the siliconium complexes **90a**(OTf), **90c**(OTf), **91a**(OTf), and **91a**(AlCl$_4$) corresponds to distorted TBP with two *trans*-diaxial nitrogen ligands. This is the common geometry for pentacoordinate bis-chelates with two nitrogen-donor ligands.[66,76,77] In addition, the bonds to silicon are generally shorter than the corresponding bonds in the neutral hexacoordinate precursors, **30–38**, as might be expected in positively-charged species. Interestingly, the deviation from TBP geometry for these crystals (**90**, **91**) is almost equal, as evident from the O–Si–O and N–Si–N angles, which are in the ranges 134–137° and 155–157°, respectively. These values correspond to a substantial deviation from TBP along the TBP → SP (square pyramid) coordinate, calculated from the difference between the N–Si–N and O–Si–O angles [%TBP = 100(NSiN − OSiO)/60].[66]

TABLE XXVII

Selected Bond Lengths and Angles from Crystal Structures of Pentacoordinate Siliconium Complexes and Elimination Product, and Calculated Percent TBP

Complex	Bond lengths (Å)			Bond angles (deg.)		%TBP1[a]	
	Si–O	Si–N	Si–C	O–Si–O	N–Si–N	(%TBP2)	Ref.
90a(OTf)	1.683(3) 1.680(3)	1.959(3) 1.954(3)	1.831(4)	134.33(13)	155.62(14)	35	66
90c(OTf)	1.6844(15) 1.6964(14)	1.9665(17) 1.9681(19)	1.835(2)	136.27(8)	154.78(8)	31	66
91a(OTf)	1.6833(11) 1.6911(11)	1.9645(13) 1.9747(13)	1.8453(15)	137.05(6)	157.24(6)	33	66
91a(AlCl$_4$)	1.6806(15) 1.6822(15)	1.9855(17) 1.9699(18)	1.838(2)	135.19(8)	157.89(8)	38	66
93a(OTf)	1.7240(8) 1.7266(8)	1.9397(10) 1.9470(10)	1.8964(11)	152.22(4)	133.54(4)	(31)	83
57a(OTf)	1.7070(16) 1.7073(16)	1.931(2) 1.936(2)	1.855(2)	146.01(9)	146.93(10)	0 (100% SP)	69
57c(OTf)	1.7134(19) 1.7216(19)	1.931(2) 1.931(2)	1.864(3)	149.62(10)	144.14(11)	(4) (96% SP)	69
96j	1.7844(7) 1.7591(7)	1.7265(9) 1.9496(9)	1.9115(10)	165.74(4)	121.51(4)	(74)	83

[a]Calculated by comparison of the N–Si–N and O–Si–O angles, see text.

In contrast to the nearly equal geometries of these mononuclear siliconium salts, the binuclear siliconium salts have a significantly different geometry: as the data in Table XXVII show, **57a,c** have equal O–Si–O and N–Si–N angles, and hence are further advanced along the TBP → SP coordinate to 100% SP, i.e., both binuclear molecules in the solid-state have essentially pure SP geometries.

Even more striking is the geometry found in the solid state for the *tert*-butylsiliconium triflate **93a**(OTf) (Fig. 54): in this compound, the O–Si–O angle is *greater* than the N–Si–N angle, i.e., the structure is advanced further from the pure SP to 31% of the TBP2, with axial-like oxygens. Finally, the elimination product **96j** has a slightly distorted TBP2 structure *with axial oxygens*, i.e., the dative $Me_2N → Si$ and the MeN–Si bonds are in nearly pure equatorial positions. This is the first report of equatorial coordination in a pentacoordinate silicon complex.

These gradual changes in geometry around silicon in the crystal structures discussed above may be viewed within a broader framework as points along a hypothetical reaction coordinate of the Berry pseudorotation process.[84] A single pseudorotation process is depicted schematically in Fig. 55. Each point along the pseudorotation coordinate has a corresponding crystal structure (beginning with the TBP1 model, **78a**[77a] through **90a**(OTf) → **57a**(OTf) → **93a**(OTf) and finally the TBP2 model **96j**, Table XXVII), and thus the entire process can be followed crystallographically, in the Bürgi-Dunitz sense.[85] TBP2 is essentially an inverted TBP1 in which axial and equatorial groups have exchanged their positions. Throughout this process the *t*-Bu group acts as "pivot" for the pseudorotation.

Most pentacoordinate bis-chelates of silicon with two N → Si dative bonds have the TBP1 geometry. Clearly this geometry is preferred. It is only

	TBP1	35% TBP1	SP	31% TBP2	TBP2
NSiN	171.2	155.6	146.9	133.5	121.5
OSiO (CSiC)	119.8	134.3	146.0	152.2	165.7
Compound	**78a**	**90a**(OTf)	**57a**(OTf)	**93a**(OTf)	**96j**
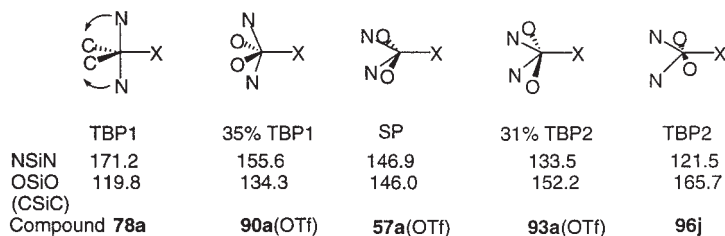
FIG. 55. Schematic progress along a Berry pseudorotation coordinate, with corresponding molecular structures and N–Si–N and O–Si–O angles (degrees).[83] Reproduced with permission from Wiley-VCH.

the steric strain introduced by the *t*-Bu group in **93** and **96**, or in the binuclear **57**, that pushes the geometry towards the other end of the reaction coordinate and enables the demonstration of stable points along the entire pseudorotation coordinate.

2. Isopropylideneimino-Coordinated Siliconium Chelates

In Sections II.A.2 and III.B it was shown that the isopropylideneimino donor group is a stronger donor than the dimethylamino group, based on three criteria: N–Si distance, ^{29}Si chemical shift and ease of ionization. The effect of this donor group on the formation of free siliconium-ion salts has also been studied and is described in this section.[20] Indeed, the transsilylation of **22** and **23** with the isopropylidenehydrazide precursors **6a,b** led to exclusive formation of pentacoordinate siliconium chlorides (**97**, **98**, Eq. 39), in contrast to the analogous reaction with the dimethyl amino-donor precursors (**1**), in which hexacoordinate chelates (**31**, **32**) were formed. These results further strengthen the evidence showing that the sp^2-hybridized isopropylideneimino group is a stronger donor than the sp^3-hybridized dimethylamino group.

$$(39)$$

6a, R = Ph
6b, R= PhCH$_2$

22, X = Me
23, X = Ph

97a, R = Ph, X = Me
97b, R = PhCH$_2$, X = Me
98a, R = Ph, X = Ph
98b, R = PhCH$_2$, X =Ph
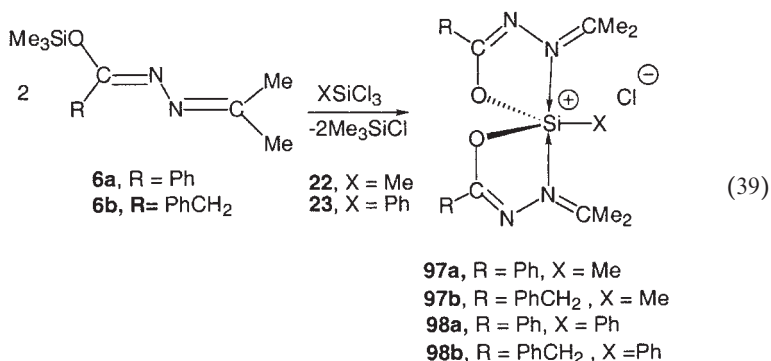
The structural evidence for **97**, **98** came from their characteristic ^{29}Si chemical shifts (Table XXVIII), and a crystal structure analysis for **97a**(OTf), the triflate salt derived from anion exchange with **97a** (Fig. 56, Table XXIX). Table XXVIII shows that these two salts, the chloride and triflate, have the same ^{29}Si chemical shifts, thus confirming the identical siliconium cation parts in both. In fact, from Table XXVIII it is also evident that the ^{13}C–^{1}H NMR spectra for the two siliconium salts are very similar, and hence the siliconium parts of the salts are identical.

TABLE XXVIII

COMPARISON OF ^{1}H, ^{13}C, AND ^{29}Si NMR SPECTRAL DATA FOR SILICONIUM CHLORIDES **97**, **98** AND THE SILICONIUM TRIFLATE **97a**(OTf) (CDCl$_3$, 300 K)[20]

Compound	δ ^{29}Si (ppm)	δ 9^{1}H, ppm (^2J, Hz)			δ ^{13}C (ppm)	
		CMe	SiMe	CH$_2$	C<u>Me</u>	C=N
97a	−81.0	2.74, 2.80	1.08		23.8, 25.1	162.0, 181.9
97b	−82.0	2.04, 2.40	0.61	3.57, 3.65 (15.2)	23.6, 24.2	166.5, 182.2
98a	−93.7	2.00, 2.53			23.7, 24.5	162.3, 185.5
98b	−94.3	1.49, 2.40		3.80, 3.83 (15.1)	24.0, 24.2	167.6, 184.2
97a(OTf)	−81.1	2.74, 2.76	1.03		23.7, 24.8	162.4, 182.0
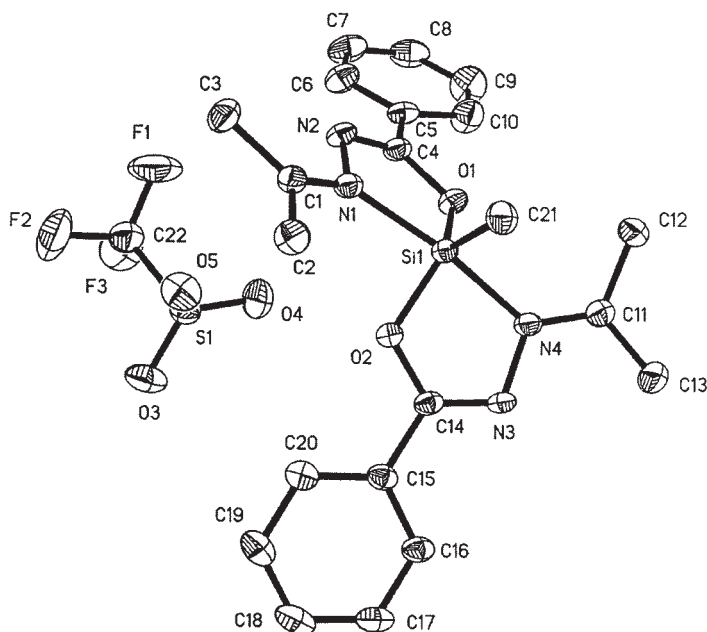
FIG. 56. Molecular structure of siliconium salt **97a**(OTf) in the crystal.[20] Reproduced with premission from Elsevier.

A further comparison of the isopropylideneimino complex **97a**(OTf) with the dimethylamino analog **90c**(OTf) is presented in Table XXIX. From the listed bond angles it is evident that **97a**(OTf) is a slightly distorted TBP with essentially axial nitrogens, whereas **90c**(OTf) is substantially more distorted along the TBP–SP coordinate (ca. 60%, see discussion in

TABLE XXIX

COMPARISON OF SELECTED BOND LENGTHS AND ANGLES AND ^{29}Si NMR CHEMICAL SHIFTS FOR ISOPROPYLIDENEIMINO- [97a(OTf)][20] AND DIMETHYLAMINO- [90c(OTf)][66] COMPLEXES

	97a(OTf)	90c(OTf)
Donor group	Isopropylideneimino	Dimethylamino
Si–N, Å	1.9337(17), 1.9659(17)	1.9665 (17), 1.9681 (19)
Si–O, Å	1.6747(14), 1.6811(14)	1.6844 (15), 1.6964 (14)
Si–C, Å	1.834(2)	1.835(2)
N–Si–N, deg	166.44(7)	154.78(8)
O–Si–O, deg	120.85(8)	136.27(8)
δ (^{29}Si), ppm	−81.1	−60.9

previous section). This means that in the dimethylamino complex the nitrogen atoms do not occupy axial positions, but rather an average axial-equatorial position. Judging from the ideal TBP and SP geometries, these bonds should be *shorter* than purely axial bonds. And yet, the comparison shows that the Si–N distances in 97a(OTf), which are "more axial", are shorter than those in 90c(OTf). It follows that coordination in 97a(OTf) is substantially stronger than in 90c(OTf), in agreement with previous conclusions.

This conclusion is fully supported by the higher-field ^{29}Si chemical shift found in 97a(OTf) relative to 90c(OTf) (Table XXIX).

V

SPIN–SPIN INTERACTIONS THROUGH THE N–SI DATIVE BOND

The nature of the coordination bond in silicon complexes has been of significant interest. One important property of this bond is its ability to transmit NMR spin–spin interactions. Despite the potential information on the nature of the dative-bond, which might be gained from the magnitude of spin–spin interactions, little has been reported on this subject. Ideally, one would like to measure directly the one-bond interaction between ^{29}Si and ^{15}N.[86] However, due to low natural abundance of both nuclei, as well as their low magnetogyric ratios (γ), this coupling constant is difficult to measure and provides little structural information. In order to study the coupling constants between nuclei extending on either side of the dative N $\rightarrow$ Si bond, several penta- and hexacoordinate complexes have been prepared with hydrido or fluoro ligands directly attached to silicon.[16,50]

In retrospect, we realize that the ability to observe coupling constants through two and three bonds across the dative bond in the present silicon complexes resulted from the favorable near 90° H–Si–N angle. In many of the previously reported N → Si coordinated silicon complexes this angle was near 180°, and no coupling could be observed.

Application of the transsilylation reaction using HSiPhCl$_2$, HSiCl$_3$, SiF$_4$, and PhSiF$_3$ led to formation of hydrido- and fluoro-, neutral penta- (**5b**)[16] or hexacoordinate (X = H, **30g**,[50] **30j**;[87] **36g**,[50] **37g**,[50] and **99**,[87] obtained from **30j** by reaction with Me$_3$SiBr) complexes, which have been mentioned in earlier chapters. In this section we describe the connection between geometrical parameters, extracted from crystal structures, and the corresponding one-, two, three, and even four-bond coupling constants. This information can serve as a tool for structure elucidation of silicon complexes in solution, in those cases for which crystal structures are unavailable.

A. *Two-Bond Coupling Constants*

1. Hydrido-Complexes

A compilation of NMR and crystallographic data for the hydrido complexes is given in Table XXX. The bond- and dihedral angles were obtained from crystal structures, and the two- and three-bond coupling constants were measured by natural abundance ^{15}N and by ^{13}C NMR spectroscopy, respectively. Table XXX shows that the ^{1}H–Si–^{15}N two-bond coupling constant is highly sensitive to the bond angle: it is maximal at 90°, and rapidly diminishes as the angle deviates from 90°. With the aid of two compounds (**100**, **101**[86]) which have substantially different H–Si–N angles (~109 and 180°, respectively) a plot of the dependence of geminal coupling constants on bond angles was generated, and is shown in Fig. 57 (note that in Fig. 57 ^2J is plotted against the *deviation* of bond angle form 90°, in either direction).

99   100   101
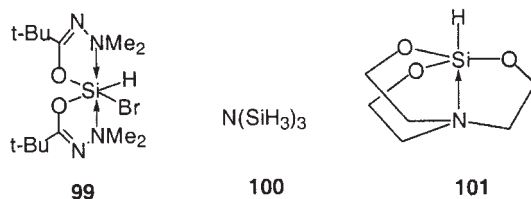
It is evident from Fig. 57 that the sensitivity of ^2J to bond angle (i.e., the greatest slope) is near 90°. This plot can be used effectively to estimate

TABLE XXX

BOND AND DIHEDRAL ANGLES (deg.) AND CORRESPONDING $^2J(^1HSi^{15}N)$ AND $^3J(^1HSiN^{13}C)$ IN PENTA- AND HEXACOORDINATE HYDRIDO-COMPLEXES

Compound	R, X	H–Si–N angle	$^2J(^1HSi^{15}N)$ (Hz)	H–Si–N–C angle	$^3J(^1HSiN^{13}C)$ Hz	Ref.
30g	CF$_3$, Cl	95.20(10)	10.2	157.4	2.4	50
		90.64(9)	12.0	31.9	1.1	
				49.3	0.4	
				−76.1	0	
30j	t-Bu, Cl	92.68(3)	10.17	136.0 (130.5)	1.0	87
		90.8(93)		6.6 (9.9)	2.2	
				79.3 (84.6)	0	
				−44.8 (40.70)	0	
99	t-Bu, Br			−3.9 (−7.2)	3.0	87
				36.5 (36.4)	0.7	
				−88.1 (−84.8)	0	
				−133.4(−129.5)	0	
5b	Ph, Cl		10.8	97.5	0	16
				28.3	1.7	
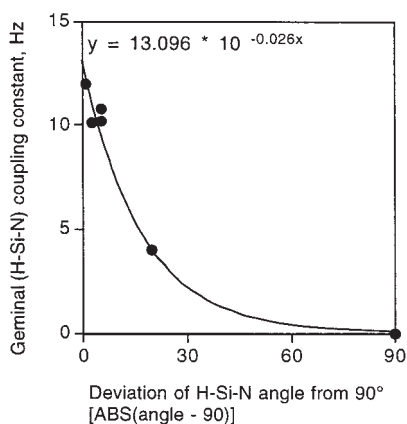
FIG. 57. Two-bond coupling constants as a function of the deviation of H–Si–N bond angle from 90° in hydrido complexes.[87]

unknown bond angles from solution coupling constants, especially for complexes in which the hydrido and nitrogen ligands are cis to each other (near 90° bond angle).

The geminal H–Si–N spin–spin interaction depends also on Si–N distance: the ionization process discussed above (Eq. 17) causes bond shortening. Scheme 3 demonstrates the effect of ionization (and resulting

31c
Si-N Bond length
2.015(7) and 2.036 (6)

91c(OTf)
Si-N Bond length
1.9665(17) and 1.9681 (19)

30j
^2J (HSiN) = 10.2 Hz

30j(AlCl₄)
^2J (HSiN) = 13.7 Hz
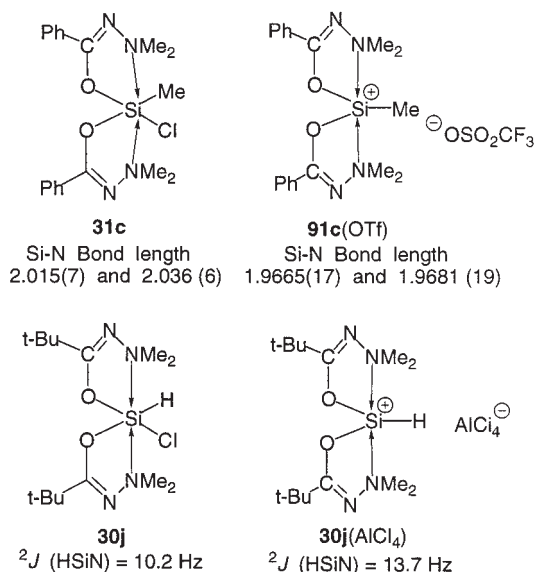
SCHEME 3. Demonstration of N → Si bond shortening upon ionization (**31c**[49] and **91c(OTf)**[66]), and corresponding increase in H–Si–N coupling constant in a similar complex-pair (**30j** and **30j(AlCl₄)**).[87]

bond shortening) on the H–Si–N coupling constant. The Scheme shows that shorter Si–N distances of the ionic vs. hexacoordinate species, are associated with an increase in geminal coupling constant from 10.2 to 13.7 Hz, as might be expected for more intense bonding.[87]

2. Fluoro Complexes

The mono- and difluoro complexes **36g** and **37g** enable measurement of spin–spin interactions across the dative N → Si bond.[50] The NMR data with the corresponding crystallographic bond lengths and angles are listed in Table XXXI. It is evident from the Table that, like in the hydrido case, the geminal (^{19}F–Si–^{15}N) coupling constants are strongly dependent on the bond angle: in **36g**, a change of ca. 5.5° (from 96.85 to 91.23°) led to doubling of the coupling constant, from $^2J = 4.5$ to 9 Hz.

In compound **37g** rapid exchange of the fluoro ligands prevents a direct comparison of bond angles and corresponding coupling constants. However, the two crystallographic F–Si–N bond angles in **37g** are similar to those in **36g**, and yet the average two-bond coupling, 12.2 Hz, is significantly greater than either coupling constant in **36g**. This is most likely the result of the shorter N–Si distance, generated by the two adjacent electronegative fluorine atoms.

TABLE XXXI

Si–N Bond Lengths (Å), Bond and Dihedral Angles (deg.), and Corresponding Two-
and Three-Bond Coupling Constants in Hexacoordinate Fluoro-Complexes[50]

Compound	R, X, Y	Si–N distance	F–Si–N angle	^2J(FSiN) (Hz)	F–Si–N–C angle	^3J(FSiNC) (Hz)	^3J(FSiNC)[a] (Hz)
36g	CF$_3$, Ph, F	2.021(3)	96.85(11)	4.5	138.9	0.5	
		2.029(3)	91.23(12)	9.0	14.6	9.1	
					40.4	3.4	
					−83.9	0	
37g	CF$_3$, F, F	1.962(2)	95.39(8)	12.2	143.08	1.4	0.8
		1.962(2)	91.12(9)		20.02	5.4	8.0
					49.28	0	2.2
					−73.78	0	0.6

[a]Interpolated, see text.

B. *Three-Bond Coupling Constants*

1. Hydrido-Complexes

Three-bond coupling constants in the series of hydrido complexes were determined by undecoupled ^{13}C NMR spectra. In each molecule there are four unique *N*-methyl groups, and hence four H–Si–N–C dihedral angles and corresponding vicinal coupling constants. The crystallographic dihedral angles and the three-bond coupling constants for hydrido complexes are shown in Table XXX.[16,50,87] A plot of ^3J(^{1}H–Si–N–^{13}C) coupling constants as a function of dihedral angles (Fig. 58), including data from several different complexes (five and six coordinate), shows a distinct Karplus-type relationship. This parabola correlation can be applied to extract reasonable dihedral angles from solution NMR data, for molecules for which crystal data are not available.

2. Fluoro Complexes

There are four unique *N*-methyl groups in **36g**, associated with four F–Si–N–C dihedral angles and three-bond coupling constants (Table XXXI). From the four data points for **36g** a Karplus-type plot of coupling constants vs. dihedral angles was constructed, and fitted to a best parabola (Fig. 59). In **37g** the structure/NMR analysis is further complicated by rapid exchange of the two fluoro ligands even at low temperatures. Since only two average coupling constants are available for **37g** (Table XXXI), the points for this compound in Fig. 59 were inserted using the crystallographic dihedral angles, and the corresponding coupling
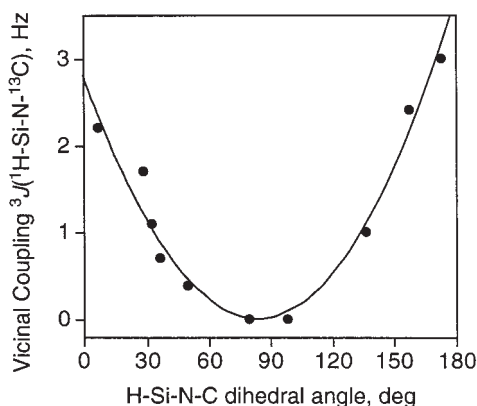
FIG. 58. Vicinal (^{1}H–Si–N–^{13}C) coupling constants of penta- and hexacoordinate hydridosilicon complexes vs. dihedral angle.[16,87] Reproduced with permission from Wiley-VCH.
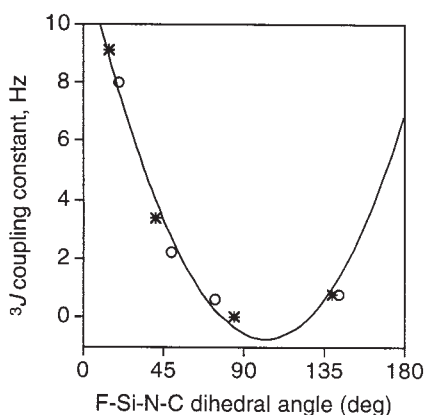
FIG. 59. Plot of three-bond $^3J(^{19}$F–Si–N–^{13}C) coupling constants against dihedral angles in **36g** (circles) and **37g** (*, interpolated from dihedral angles).[50] Reproduced with permission from the American Chemical Society.

constants were obtained from the plot by interpolation. Four J values were obtained, and are listed in Table XXXI.

There are several ways by which these four J values can be averaged pairwise; one option is $J_1 = 1.4$ and $J_2 = 4.4$ Hz, and it agrees well with the measured values, 1.4 and 5.4 Hz. In conclusion, despite the relatively small number of data points, a useful Karplus correlation was made for the three-bond ^{19}F–^{13}C coupling constants.

VI

ZWITTERIONIC PENTACOORDINATE (BENZIMIDATO-*N,O*) SILICATES

Interesting zwitterionic pentacoordinate silicate complexes have been developed and reported by Tacke and co-workers.[10] Similar (but cyclic) neutral zwitterionic complexes, in which a positive charge resides on an ammonium nitrogen and silicon may be formally negatively charged, have also been reported in Sections II.B.2 (**11**), II.B.5 (**13**), III.A.6 (**58**), and III.C (**70**, Eq. 29). Silicates of this series containing tri- and tetrafluoro silicon moieties[88] were subjected to transsilylation with the hydrazide-ligand precursors, producing mono- and bis-(benzimidato-*N,O*)silicates.[88] These new chelates undergo complex stereodynamic exchange reactions, including an ammonium-nitrogen inversion via deprotonation, nitrogen inversion, and reprotonation.

A. *Synthesis and Structure*

Transsilylation of zwitterionic λ^5Si-trifluorosilicates (**102a–c**) with the *N,O*-bis(trimethylsilyl)hydrazide **72** resulted in the zwitterionic monocyclic λ^5Si-monofluorosilicates **103a–c** (Eq. 40). Likewise, the tetrafluorosilicate (**104**) undergoes *stepwise* transsilylation, producing initially the monocyclic λ^5Si-difluorosilicate **105**, followed by the zwitterionic spirocyclic λ^5Si-silicate **106** (Eq. 41).

(40)

102   **a**, R = Me; **b**, R = *i*-Pr; **c**, R = *t*-Bu   **103**

(41)

104   **105**   **106**
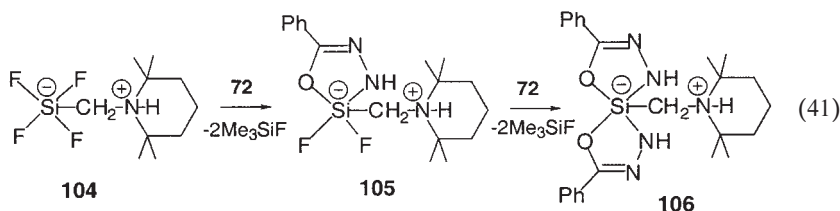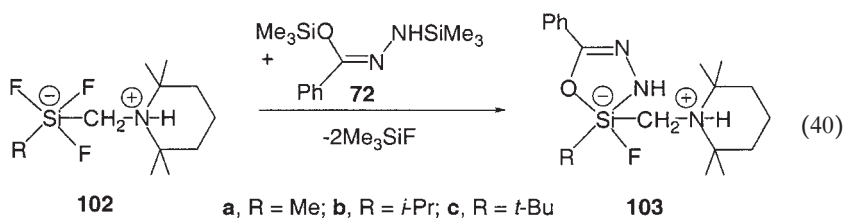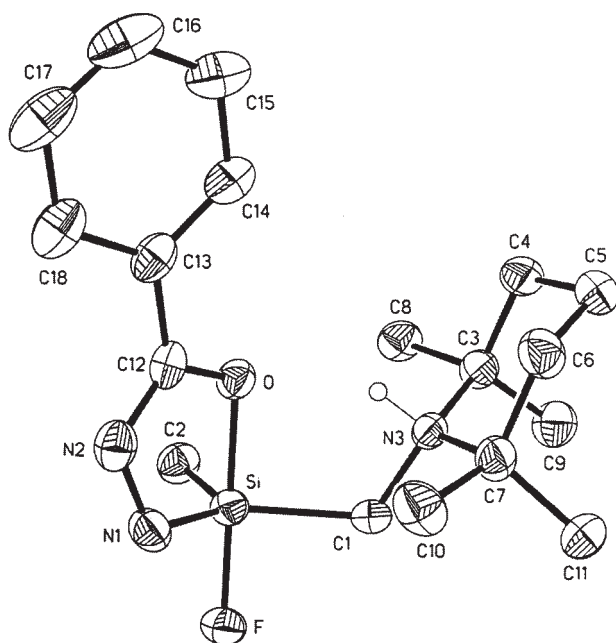
FIG. 60. Crystallographic molecular structure of zwitterionic silicate **103a**.[88] Reproduced with permission from the American Chemical Society.

The structures of the products (**103a**, **105**, and **106**) were analyzed and confirmed by single-crystal X-ray analyses (Figs. 60–62). The figures show the near TBP geometry of the complexes, with oxygen and fluorine (in **103a**, **105**) or oxygen and oxygen (in **106**) in axial positions. Selected interatomic distances and angles are presented in Table XXXII.
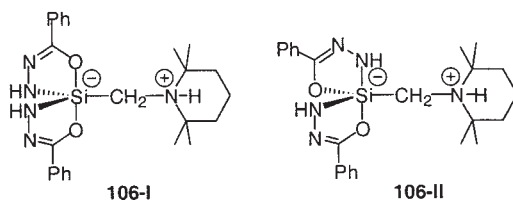
Complex **106** is formed in two diastereomers, **106-I** and **106-II**, differing in the chelate arrangement: in **106-I** the oxygen atoms are in trans diaxial positions, while in **106-II** one oxygen and one nitrogen are in
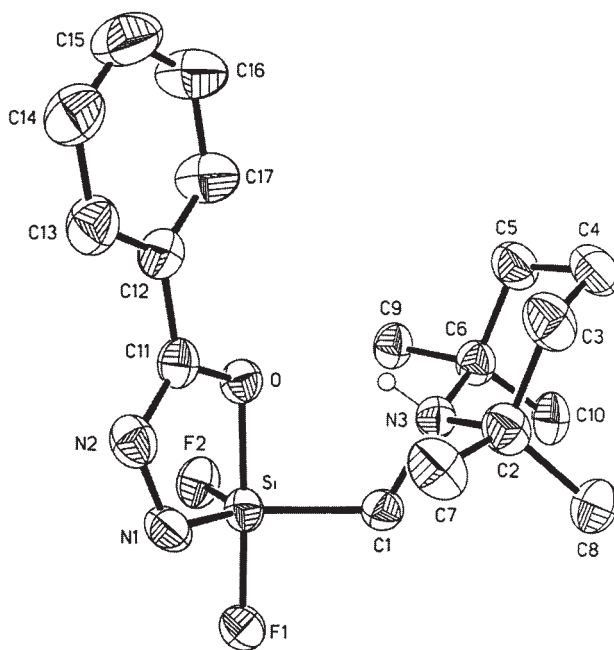
Fɪɢ. 61. Molecular structure in the crystal of zwitterionic silicate **105**.[88] Reproduced with permission from the American Chemical Society.

axial positions. Apparently the free energies of the diastereomers are nearly equal: both are formed simultaneously, and their population ratio depends on the reaction conditions. **106-I** is the predominant isomer, and is formed exclusively (within NMR detection limits) in CH_2Cl_2 at ambient temperature, after 14 days reaction time. In boiling chloroform a 9:1 population ratio in favor of **106-I** is obtained, while in nitrobenzene a 1:1 mixture is obtained at ambient temperature, and a 3:2 mixture at 100°. Once formed, the isomers appear to be stereostable: when a chloroform solution of pure **106-I** was kept for four days at ambient temperature, no **106-II** could be detected.

Suitable single crystals were obtained only for one of the diastereomers, **106-I**, when recrystallized from chloroform or acetonitrile. Crystal structures of **106-I** in either solvent were determined, and while the packing was substantially different, the molecular structures in both crystals were essentially equal, and only one is shown (Fig. 62) and included in Table XXXII.
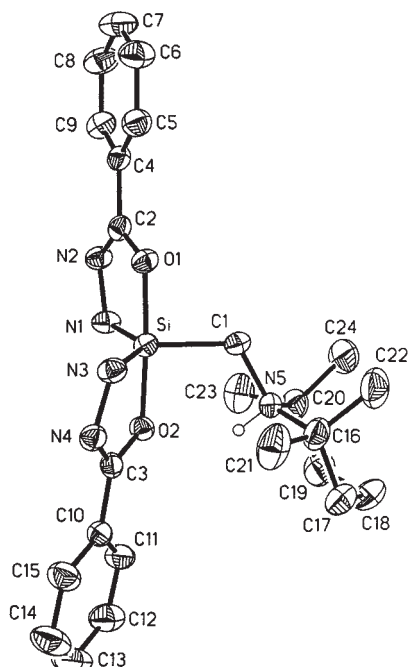
FIG. 62. Molecular structure in the crystal of zwitterionic silicate **106-I** · CHCl₃.[88] Reproduced with permission from the American Chemical Society.

TABLE XXXII

SELECTED INTERATOMIC DISTANCES (Å) AND ANGLES (deg.) FOR THE CRYSTAL STRUCTURES OF ZWITTERIONIC CHELATES **103a**, **105**, AND **106**

	103a		**105**		**106-I · CHCl₃**
Si–F	1.6868(14)	Si–F(1)	1.6676(16)	Si–O(1)	1.7827(14)
Si–O	1.8713(16)	Si–F(2)	1.6106(16)	Si–O(2)	1.8174(14)
Si–N(1)	1.740(2)	Si–O	1.8142(19)	Si–N(1)	1.7308(18)
Si–C(1)	1.927(2)	Si–N(1)	1.722(2)	Si–N(3)	1.7282(18)
Si–C(2)	1.869(2)	Si–C(1)	1.906(2)	Si–C(1)	1.910(2)
F–Si–O	169.83(8)	F(1)–Si–F(2)	92.95(9)	O(1)–Si–O(2)	176.52(7)
F–Si–N(1)	90.34(9)	F(1)–Si–O	174.05(8)	O(1)–Si–N(1)	85.59(8)
F–Si–C(1)	89. 24(8)	F(1)–Si–N(1)	91.31(11)	O(1)–Si–N(2)	93.62(8)
F–Si–C(2)	95.56(9)	F(1)–Si–C(1)	90.29(10)	O(1)–Si–C(1)	90.10(8)
O–Si–N(1)	81.42(8)	F(2)–Si–O	91.54(9)	O(2)–Si–N(1)	93.31(8)
O–Si–C(1)	90.56(8)	F(2)–Si–N(1)	121.31(10)	O(2)–Si–N(3)	84.44(8)
O–Si–C(2)	93.79(9)	F(2)–Si–C(1)	110.86(11)	O(2)–Si–C(1)	93.35 (8)
C(1)–Si–C(2)	114.26(11)	O–Si–C(1)	83.01(10)	N(1)–Si–N(3)	127.76(10)
N(1)–Si–C(2)	124.68(10)	N(1)–Si–C(1)	127.63(13)	N(1)–Si–C(1)	116.17(9)

B. *Stereodynamic Analysis*

1. Two Exchange Processes in **103a–c**

An unusual intramolecular ligand-site exchange reaction is found in the series **103a**–**c**: upon warming of a CDCl$_3$ solution of either of the compounds, coalescence of signals is observed in the ^{1}H–^{13}C NMR spectra resulting from exchange between the two arms of the piperidinium ring (C$_2$ with C$_6$, C$_3$ with C$_5$, and one of the C-methyl groups with another *non-geminal* group).[88] This exchange is *not* accompanied by parallel coalescence of the SiCH$_2$ proton signals, or by those of the isopropyl methyl groups in **103b**. This can only result from inversion of configuration at the ammonium nitrogen and piperidinium ring inversion, without inversion of absolute configuration at the pentacoordinate silicon moiety. The process responsible for these observations is a sequence of deprotonation of the ammonium proton, followed by inversion of the nitrogen pyramid and reprotonation at the opposite side of the nitrogen atom (Fig. 63).

Addition of external base (dry pyridine) or acid (4-nitrobenzoic) had no measurable effect on the rate of topomerization, suggesting that proton abstraction was done by one of the intramolecular heteroatoms: F, O, or N, adjacent to the NH group. The barrier for the topomerization was 17.0 ± 0.3 kcal mol^{-1} in all three compounds. A 2D-ROESY NMR experiment was carried out on a CDCl$_3$ solution of **103a** in support of the mechanism suggested in Fig. 63, which requires the exchange of A $\rightleftarrows$ B′ and B $\rightleftarrows$ A′ methyl groups. Indeed, distinct positive cross signals (Fig. 64) showed chemical exchange *only* as suggested by this mechanism. No exchange of geminal methyl groups was observed.

The barrier for inversion of configuration of the silicon environment was too high to be measured directly by the coalescence of signals. The SIR method,[72] which extends the range of accessible barriers, was applied to the exchange of the diastereotopic SiCH$_2$ protons in **103c** in PhNO$_2$-d_5 solution at 350 K, resulting in a barrier for enantiomerization $\Delta G^* = 20.7 \pm 0.3$ kcal mol^{-1}. This relatively high barrier for pseudorotation of a pentacoordinate silicon complex is in agreement with previous observations of high[14a] or inaccessible[17,18] barriers in pentacoordinate complexes possessing one highly electronegative ligand.

2. Two Exchange Processes in **105**

In contrast to the high barrier found in **103** for pseudorotation at silicon, the ^{1}H, ^{13}C, and ^{29}Si NMR spectra of **105** indicate rapid inversion about silicon already at room temperature: the two fluoro ligands are equivalent.
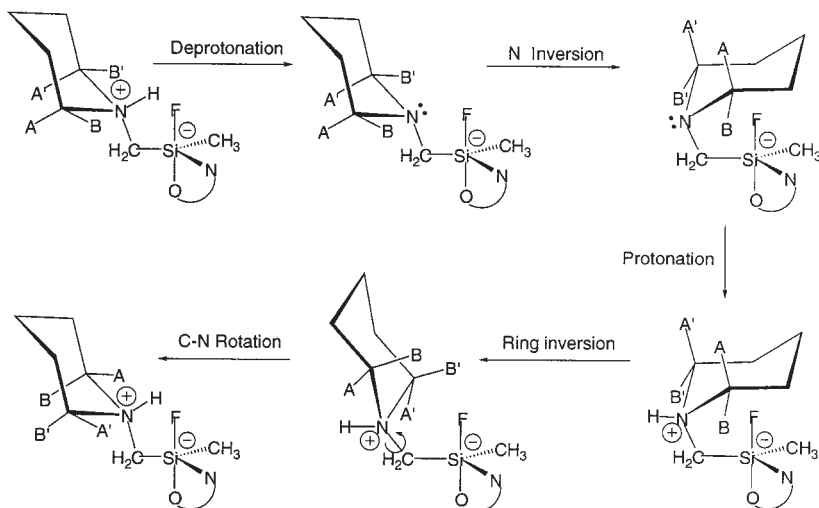
FIG. 63. Schematic representation of the topomerization of **103a** via deprotonation at the ammonium nitrogen, followed by N-inversion and reprotonation, resulting in the interchange A $\leftrightarrows$ B′, and B $\leftrightarrows$ A′.[88] Reproduced with permission from the American Chemical Society.
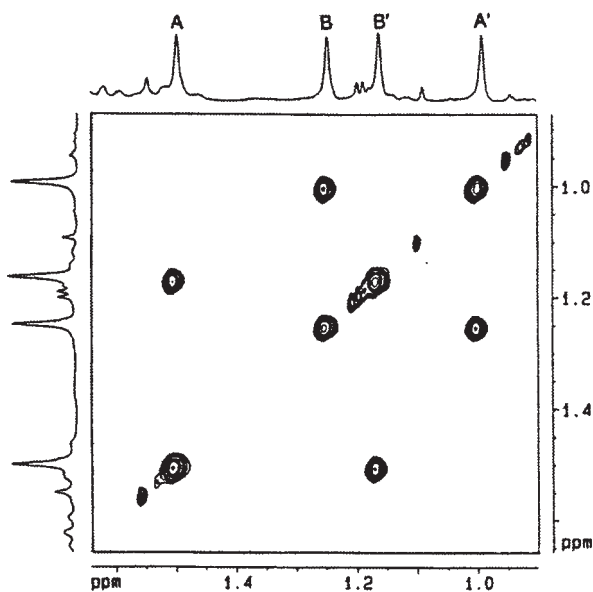
FIG. 64. 2D-ROESY spectrum of **103a** in CDCl$_3$ solution at 315 K, C–Me region. Positive cross signals represent chemical exchange between corresponding methyl groups.[88] Reproduced with permission from the American Chemical Society.
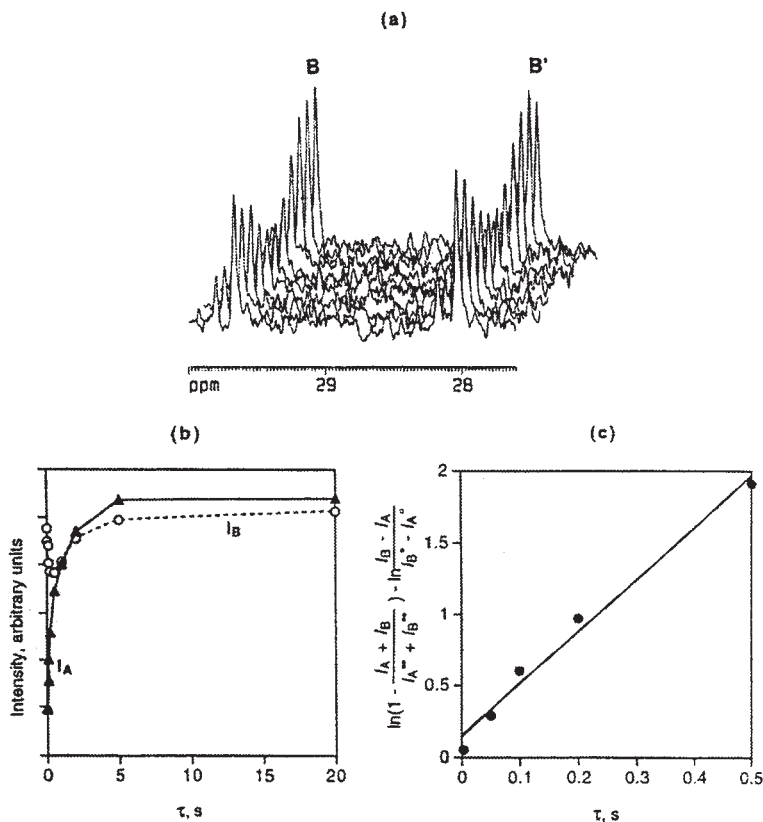
FIG. 65. ^{13}C NMR selective inversion recovery (SIR) experiment for the exchange of *C*-methyl groups in **106-I** (nitrobenzene-d_5, 360 K): (a) stack plot of spectra, showing only the signals B and B′; the signals due to **106-II** can be seen to the left of each signal, (b) plot of *C*-methyl signal intensities as a function of the variable delay τ, (c) corresponding linear plot of Eq. 30 (see Section III.C.3).[88] Reproduced with permission from the American Chemical Society.

At lower temperature the initial triplet observed in the ^{29}Si spectrum split in two doublets ($^1J_{\text{SiF}} = 215.7, 231.5$ Hz). The barrier for pseudorotation was determined from the coalescence of C-methyl signals in the ^{1}H NMR spectrum, $\Delta G^* = 11.7 \pm 0.3$ kcal mol^{-1}. The substantially lower barrier for pseudorotation in **105** relative to **103** is rationalized by the presence of two fluorine atoms: the energy required to promote the fluorine from the stable axial position to the less stable equatorial position is offset by the simultaneous transfer of the second fluorine from equatorial to axial position. In **103** the promotion energy of the single fluorine ligand is responsible for the high barrier. This explanation was first discussed by

Corriu and co-workers in similar mono- and dihalo pentacoordinate silicon complexes.[17a,18]

The second process, inversion of the ammonium nitrogen, was also observed in **105**, and had a barrier of 20.8 ± 0.3 kcal mol^{-1}, measured by the SIR technique at 360 K in nitrobenzene-d_5 solution.

3. Ligand-Site Exchange in **106-I**

The dynamic behavior of the major diastereomer of **106**, **106-I**, was investigated in nitrobenzene-d_5 solution. No coalescence of signals due pseudorotation at silicon could be observed, nor was any magnetization transfer observed from one of the SiCH$_2$ proton signals to the other in a SIR experiment up to 360 K. As expected, the barrier for pseudorotation in this bischelate is very high, because at some point along the pseudorotation sequence each of the chelate rings passes through a diequatorial position, associated with substantial steric strain.[17a]

The barrier for the unique process observed in these zwitterionic complexes, the "ammonium nitrogen inversion", was observed and measured by SIR, looking at transfer of magnetization between two C-methyl signals in the ^{13}C NMR spectrum (Fig. 65). The free energy barrier at 360 K in nitrobenzene-d_5 solution was $\Delta G^* = 20.8$ kcal mol^{-1}, the same as for **105**.

REFERENCES

(1) Tandura, S. N.; Voronkov, M. G.; Alekseev, N. V. *Top. Curr. Chem.* **1986**, *131*, 99.
(2) Kost, D.; Kalikhman, I., (Z. Rappoport, Y. Apeloig, Eds.) *The Chemistry of Organic Silicon Compounds*, Vol. 2, Part 2, Wiely, Chichester, U.K., 1998. pp. 1339–1445.
(3) Lukevics, E.; Pudova, O. A. *Chem. heterocycl. Compd. (Engl. Transl.)* **1996**, *32*, 1381.
(4) (a) Holmes, R. R. *Chem. Rev.* **1990**, *90*, 17. (b) Holmes, R. R. *Chem. Rev.* **1996**, *96*, 927.
(5) (a) Corriu, R. J. P.; Young, J. C., (S. Patai, Z. Rappoport, Eds.) *The Chemistry of Organic Silicon Compounds*, Vol. 1, Part 2, Wiely, Chichester, U.K., 1989. pp. 1241–1288. (b) Chuit, C.; Corriu, R. J. P.; Reyé, C.; Young, J. C. *Chem. Rev.* **1993**, *93*, 1371. (c) Chuit, C.; Corriu, R. J. P.; Reyé, C., (K. Akiba, Ed.) *The Chemistry of Hypervalent Compounds*, Wiley-VCH, New York, 1999. pp. 81–146.
(6) (a) Bassindale, A. R.; Taylor, P. G., (S. Patai, Z. Rappoport, Eds.) *The Chemistry of Organic Silicon Compounds*, Vol. 1, Part 1, Wiely, Chichester, U.K., 1989. pp. 839–892. (b) Bassindale, A. R.; Glin, S. J.; Taylor, P. G., (Z. Rappoport, Y. Apeloig, Eds.) *The Chemistry of Organic Silicon Compounds*, Vol. 2, Part 1, Wiely, Chichester, U.K., 1998. pp. 495–512.

 (7) Kira, M.; Zhang, L. C., (K. Akiba, Ed.) *The Chemistry of Hypervalent Compounds*, Wiley-VCH, New York, 1999. pp. 147–198.

 (8) Brook, M. A. *Silicon in Organic, Organometallic, and Polymer Chemistry*, Wiley, New York, 2000. pp. 97–114.

 (9) Verkade, J. G. *Coord. Chem. Rev.* **1994**, *137*, 233.

(10) Tacke, R.; Pülm, M.; Wagner, B. *Adv. Organomet. Chem.* **1999**, *44*, 221.

(11) (a) Pestunovich, V.; Kirpichenko, S.; Voronkov, M., (Z. Rappoport, Y. Apeloig, Eds.) *The Chemistry of Organic Silicon Compounds*, Vol. 2, Part 2, Wiely, Chichester, U.K., 1998. pp. 1447–1537. (b) Voronkov, M. G.; Pestunovich, V. A.; Baukov, Yu. I. *Organomet. Chem. USSR* **1991**, *4*, 593; *Chem. Abs.* **1992**, *116*, 41503y. (c) Negrebetsky, V. V.; Baukov, Yu. I. *Izv. Akad. Nauk SSSR, Ser. Khim.* **1997**, 1912.

(12) Kalinin, A. B.; Apasov, E. T.; Bugaeva, S. B.; Yoffe, S. L.; Tartakovskii, B. A. *Izv. Akad. Nauk SSSR, Ser. Khim.* **1983**, 1413; *Chem. Abs.* **1983**, *99*, 175871f.

(13) Kalikhman, I. D.; Gostevskii, B. A.; Bannikova, O. B.; Voronkov, M. G.; Pestunovich, V. A. *Metalloorg. Khim.* **1989**, *2*, 205; *Chem. Abs.* **1990**, *112*, 77291j.

(14) (a) Kalikhman, I.; Krivonos, S.; Ellern, A.; Kost, D. *Organometallics* **1996**, *15*, 5073. (b) Kalikhman, I.; Kost, D. (N. Auner, J. Weis, Eds.) *Organosilicon Chemistry III*, Wiley-VCH, Weinheim, 1998. pp. 446–451.

(15) Kalikhman, I. D. Ph.D. Dissertation, Institute of Organic Chemistry, Sib. Div. Acad. Science USSR, Irkutsk, 1989.

(16) Kalikhman, I.; Krivonos, S.; Kottke, T.; Stalke, D.; Kost, D., (N. Auner, J. Weis, Eds.) *Organosilicon Chemistry* IV, Wiley-VCH, Weinheim, 2000. pp. 494–499.

(17) (a) Carre, F.; Corriu, R. J. P.; Kpoton, A.; Poirier, M.; Royo, G.; Young, J. C.; Belin, C. *J. Organomet. Chem.* **1994**, *470*, 43. (b) Corriu, R. J. P.; Kpoton, A.; Poirier, M.; Royo, G.; De Saxce, A.; Young, J. C. *J. Organomet. Chem.* **1990**, *395*, 1.

(18) Corriu, R. J. P.; Kpoton, A.; Poirier, M.; Royo, G.; Corey, J. Y. *J. Organomet. Chem.* **1984**, *277*, C25.

(19) Corriu, R. J. P.; Mazhar, M.; Poirier, M.; Royo, G. *J. Organomet. Chem.* **1986**, *306*, C5.

(20) Kalikhman, I.; Gostevskii, B.; Girshberg, O.; Sivaramakrishna, A.; Kocher, N.; Stalke, D.; Kost, D. *J. Organomet. Chem.* **2003**, *686*, 202.

(21) Hillyard, R. W.; Ryan, C. M.; Yoder, C. H. *J. Organomet. Chem.* **1978**, *153*, 369.

(22) Yoder, C. H.; Ryan, C. M.; Martin, G. F.; Ho, P. S. *J. Organomet. Chem.* **1980**, *190*, 1.

(23) Albanov, A. I.; Baukov, Yu. I.; Voronkov, M. G.; Kramarova, E. P.; Larin, M. F.; Pestunovich, V. A. *Zh. Obshch. Khim.* **1983**, *53*, 246; *Chem. Abs.* **1983**, *98*, 215656c.

(24) Kalikhman, I. D.; Albanov, A. I.; Bannikova, O. B.; Belousova, L. I.; Voronkov, M. G.; Pestunovich, V. A.; Shipov, A. G.; Kramarova, E. P.; Baukov, Yu. I. *J. Organomet. Chem.* **1989**, *361*, 147.

(25) Baukov, Yu. I.; Kramarova, E. P.; Shipov, A. G.; Oleneva, G. I.; Artamkina, O. B.; Albanov, A. I.; Voronkov, M. G.; Pestunovich, V. A. *Zh. Obshch. Khim.* **1989**, *59*, 127; *Chem. Abs.* **1990**, *112*, 56003b.

(26) Voronkov, M. G.; Pestunovich, A. E.; Albanov, A. I.; Vlasova, N. N.; Pestunovich, V. A. *Izv. Akad. Nauk SSSR Ser. Khim.* **1989**, 2841.

(27) Bassindale, A. R.; Glynn, S. J.; Taylor, P. G.; Auner, N.; Herrschaft, B. *J. Organomet. Chem.* **2001**, *619*, 132.

(28) Belousova, L. I.; Gostevskii, B. A.; Kalikhman, I. D.; Vyazankina, O. A.; Bannikova, O. B.; Vyazankin, N. S.; Pestunovich, V. A. *Zh. Obshch. Khim.* **1988**, *58*, 407; *Chem. Abs.* **1989**, *110*, 114908x.

(29) Kalikhman, I. D.; Bannikova, O. B.; Belousova, L. I.; Gostevskii, B. A.; Liepinsh, E.; Vyazankina, O. A.; Vyazankin, N. S. *Metalloorg. Khim.* **1988**, *1*, 683; *Chem. Abs.* **1989**, *111*, 57840p.

(30) Bassindale, A. R., (B. Marciniec, J. Chojnowski, Eds.) *Progress in Organosilicon Chemistry*, Gordon and Breach Publ., Basel, 1995. pp. 191–208.

(31) Bassindale, A. R.; Borbaruah, M. *J. Chem. Soc., Chem. Commun.* **1991**, 1499.

(32) Bassindale, A. R.; Borbaruah, M.; Glynn, S. J.; Parker, D. J.; Taylor, P. G. *J. Organomet. Chem.* **2000**, *606*, 125.

(33) Kalikhman, I. D.; Bannikova, O. B.; Petuchov, L. P.; Pestunovich, V. A.; Voronkov, M. G. *Dokl. Akad. Nauk SSSR* **1986**, *287*, 870; *Chem. Abs.* **1987**, *106*, 50289d.

(34) Kalikhman, I. D.; Pestunovich, V. A.; Gostevskii, B. A.; Bannikova, O. B.; Voronkov, M. G. *J. Organomet. Chem.* **1988**, *338*, 169.

(35) Kalikhman, I. D.; Bannikova, O. B.; Kalinin, A. B.; Apasov, E. T.; Yoffe, S. L.; Tartakovskii, B. A.; Voronkov, M. G. *Izv. Akad. Nauk SSSR, Ser. Khim. 985*, 464.

(36) Macharashvili, A. A.; Shklover, V. E.; Struchkov, Yu. T.; Gostevskii, B. A.; Kalikhman, I. D.; Bannikova, O. B.; Voronkov, M. G.; Pestunovich, V. A. *J. Organomet. Chem.* **1988**, *356*, 23.

(37) Macharashvili, A. A.; Shklover, V. E.; Struchkov, Yu. T.; Voronkov, M. G.; Gostevskii, B. A.; Kalikhman, I. D.; Bannikova, O. B.; Pestunovich, V. A. *J. Organomet. Chem.* **1988**, *340*, 23.

(38) Kaftory, M.; Kapon, M.; Botoshansky, M., (Z. Rappoport, Y. Apeloig, Eds.) *The Chemistry of Organic Silicon Compounds*, Vol. 2, Wiely, Chichester, U.K., 1998. pp. 181–265.

(39) Wawzonek, S.; Yeakey, E. *J. Am. Chem. Soc.* **1960**, *82*, 5718.

(40) (a) Macharashvili, A. A. Ph.D. Dissertation, Institute of Organomet. Chem. Acad. Science USSR, Moscow, 1990. (b) Macharashvili, A. A.; Shklover, V. E.; Struchkov, Yu. T.; Oleneva, G. I.; Kramarova, E. P.; Shipov, A. G.; Baukov, Yu. I. *J. Chem. Soc., Chem. Commun.* **1991**, 1501. (c) Sidorkin, V. F.; Vladimirov, V. V.; Voronkov, M. G.; Pestunovich, V. A. *J. Mol. Struct.* **1991**, *228*, 1.

(41) Kalikhman, I.; Girshberg, O.; Lameyer, L.; Stalke, D.; Kost, D. *J. Am. Chem. Soc.* **2001**, *123*, 4709.

(42) Kalikhman, I. D.; Gostevskii, B. A.; Bannikova, O. B.; Voronkov, M. G.; Pestunovich, V. A. *J. Organomet. Chem.* **1989**, *376*, 249.

(43) Kost, D.; Kalikhman, I. *Bull. Magn. Reson.* **1995**, *17*, 108.

(44) Kalikhman, I.; Kost, D. *J. Chem. Soc., Chem. Commun.* **1995**, 1253.

(45) Kost, D.; Kalikhman, I.; Raban, M. *J. Am. Chem. Soc.* **1995**, *117*, 11512.

(46) Kalikhman, I. D.; Gostevskii, B. A.; Bannikova, O. B.; Voronkov, M. G.; Pestunovich, V. A. *Metalloorg. Khim.* **1989**, *2*, 704; *Chem. Abs.* **1990**, *112*, 139113p.

(47) Kost, D.; Kalikhman, I.; Krivonos, S.; Stalke, D.; Kottke, T. *J. Am. Chem. Soc.* **1998**, *120*, 4209.

(48) Kost, D.; Krivonos, S.; Kalikhman, I., (N. Auner, J. Weis, Eds.) *Organosilicon Chemistry III.* Wiley-VCH, Weinheim, **1998**. pp. 435–445.

(49) Mozzhukhin, A. O.; Antipin, M. Yu.; Struchkov, Yu. T.; Gostevskii, B. A.; Kalikhman, I. D.; Pestunovich, V. A.; Voronkov, M. G. *Metalloorg. Khim.* **1992**, *5*, 658; *Chem. Abs.* **1992**, *117*, 234095w.

(50) Kalikhman, I.; Krivonos, S.; Stalke, D.; Kottke, T.; Kost, D. *Organometallics* **1997**, *16*, 3255.

(51) Kalikhman, I.; Girshberg, O.; Lameyer, L.; Stalke, D.; Kost, D. *Organometallics* **2000**, *19*, 1927.

(52) Kalikhman, I.; Gostevskii, B.; Girshberg, O.; Krivonos, S.; Kost, D. *Organometallics* **2002**, *21*, 2551.

(53) (a) Breliere, C.; Carre, F.; Corriu, R. J. P.; Poirier, M.; Royo, G.; Zwecker, J. *Organometallics* **1989**, *8*, 1831. (b) Breliere, C.; Corriu, R. J. P.; Royo, G.; Zwecker, J. *Organometallics* **1989**, *8*, 1834.

(54) Carre, F.; Cerveau, G.; Chuit, C.; Corriu, R. J. P.; Reyé, C. *New J. Chem.* **1992**, *16*, 63.

(55) Carre, F.; Chuit, C.; Corriu, R. J. P.; Mehdi, A.; Reyé, C. *Organometallics* **1995**, *14*, 2754.

(56) Belzner, J.; Shär, D., (N. Auner, J. Weis, Eds.) *Organosilicon Chemistry II*, Wiley-VCH, Weinheim, 1996. pp. 459–465.

(57) Klebe, G.; Tran Qui, D. *Acta Cryst.* **1984**, *C40*, 476.

(58) Plitzko, C.; Meyer, G. *Z. Anorg. Allg. Chem.* **1996**, *622*, 1646.

(59) Bain, V. A.; Killean, R. C. G.; Webster, M. *Acta Crystallogr. Sect. B* **1969**, *25*, 156.

(60) Bickley, D. G.; Serpone, N. *Inorg. Chem.* **1976**, *15*, 948.

(61) Pignolet, L. H. *Top. Curr. Chem.* **1975**, *56*, 91.

(62) Horn, H. G.; Marsmann, H. C. *Makromol. Chem.* **1972**, *162*, 255.

(63) Bailar, J. C., Jr. *J. Inorg. Nucl. Chem.* **1958**, *8*, 165.

(64) Ray, P.; Dutt, N. K. *J. Indian Chem. Soc.* **1943**, *20*, 81.

(65) Kingston, V.; Gostevskii, B.; Kalikhman, I.; Kost, D. *Chem. Commun.* **2001**, 1272.

(66) Kost, D.; Kingston, V.; Gostevskii, B.; Ellern, A.; Stalke, D.; Walfort, B.; Kalikhman, I. *Organometallics* **2002**, *21*, 2293.

(67) Kost, D.; Kalikhman, I.; Kingston, V.; Gostevskii, B. *J. Phys. Org. Chem.* **2002**, *15*, 831.

(68) (a) Sidorkin, V. F.; Pestunovich, V. A.; Voronkov, M. G. *Magn. Res. Chem.* **1985**, *23*, 491. (b) Bassindale, A. R.; Borbaruah, M. *J. Chem. Soc., Chem. Commun.* **1991**, 1499. (c) Bassindale, A. R.; Borbaruah, M.; Glynn, S. J.; Parker, D. J.; Taylor, P. G. *J. Chem. Soc. Perkin Trans.* 2 **1999**, 2099. (d) Kummer, D.; Abdel Halim, S. H. *Z. Anorg. Allg. Chem.* **1996**, *622*, 57.

(69) Kalikhman, I.; Kingston, V.; Gostevskii, B.; Pestunovich, V.; Stalke, D.; Walfort, B.; Kost, D. *Organometallics* **2002**, *21*, 4468.

(70) Pauling, L. *The Nature of the Chemical Bond*, Cornell University Press, Ithaca and New York, 1960. pp. 257–264.

(71) Allen, F. H.; Kennard, O.; Watson, D. G.; Brammer, L.; Guy Opren, A.; Taylor, R. *J. Chem. Soc. Perkin Trans.* II, **1987**, S1.

(72) (a) Blanca, B. D. M.; Maimon, E.; Kost, D. *Angew. Chem. Int. Ed. Engl.* **1997**, *36*, 2216. (b) Orrell, K. G.; Sik, V. *Annu. Rep. NMR Spectrosc.* **1993**, *27*, 103.

(73) Kalikhman, I.; Kingston, V.; Girshberg, O.; Kost, D. *Organometallics* **2001**, *20*, 4713.

(74) (a) Lambert, J. B.; Kania, L.; Zhang, S. *Chem. Rev.* **1995**, *95*, 1191. (b) Lickiss, P. D. (Z. Rappoport, Y. Apeloig, Eds.) *The Chemistry of Organic Silicon Compounds*, Wiley, Chichester, U.K., 1998. pp. 557–594. (c) Olah, G. A.; Heiliger, L.; Li, X. Y.; Prakash, G. K. S. *J. Am. Chem. Soc.* **1990**, *112*, 5991.

(75) (a) Lambert, J. B.; Zhao, Y.; Wu, H.; Tse, W. C.; Kuhlman, B. *J. Am. Chem. Soc.* **1999**, *121*, 5001. (b) Lambert, J. B.; Zhao, Y. *Angew. Chem. Int. Ed.* **1997**, *36*, 400. (c) Müller, T.; Zhao, Y.; Lambert, J. B. *Organometallics* **1998**, *17*, 278.

(76) (a) Brelière, C.; Carré, F.; Corriu, R. J. P.; Wong Chi Man, M. *J. Chem. Soc., Chem. Commun.* **1994**, 2333. (b) Chauhan, M.; Chuit, C.; Corriu, R. J. P.; Reyé, C. *Tetrahedron Lett.* **1996**, *37*, 845. (c) Chuit, C.; Corriu, R. J. P.; Mehdi, A.; Reyé, C. *Angew. Chem. Int. Ed. Engl.* **1993**, *32*, 1311. (d) Chauhan, M.; Chuit, C.; Corriu, R. J. P.; Mehdi, A.; Reyé, C. *Organometallics* **1996**, *15*, 4326.

(77) (a) Belzner, J.; Schär, D.; Kneisel, B. O.; Herbst-Irmer, R. *Organometallics* **1995**, *14*, 1840. (b) Schär, D.; Belzner, J. (N. Auner, J. Weis, Eds.) *Organosilicon Chemistry III*, Wiley-VCH, Weinheim, **1998**. pp. 429–434.

(78) Berlekamp, U. H.; Jutzi, P.; Mix, A.; Neumann, B.; Stammler, H. G.; Schoeller, W. W. *Angew. Chem. Int. Ed.* **1999**, *38*, 2048.

(79) (a) Ovchinnikov, Yu. E.; Pogozhikh, S. A.; Razumovskaya, I. V.; Shipov, A. G.; Kramarova, E. P.; Bylikin, S. Yu.; Negrebetsky, V. V.; Baukov, Yu. I. *Russsian Chem. Bull.* **1998**, *47*, 967. (b) Kramarova, E. P.; Smirnova, L. S.; Artamkina, A. G.; Shipov, A. G.;

Baukov, Yu. I.; Ovchinnikov, Yu. E.; Mozzhukhin, A. O.; Struchkov, Yu. T. *Zh. Obshch. Khim.* **1993**, *63*, 2275.

(80) Kraka, E.; Sosa, C. P.; Gräfenstein, J.; Cremer, D. *Chem. Phys. Lett.* **1997**, *279*, 9.

(81) Kalikhman, I.; Krivonos, S.; Lameyer, L.; Stalke, D.; Kost, D. *Organometallics* **2001**, *20*, 1053.

(82) Macharashvili, A. A.; Shklover, V. E.; Struhkov, Yu. T.; Baukov, Yu. I.; Kramarova, E. P.; Oleneva, G. I. *J. Organomet. Chem.* **1987**, *327*, 167.

(83) Kost, D.; Gostevskii, B.; Kocher, N.; Stalke, D.; Kalikhman, I. *Angew. Chem. Int. Ed.* **2003**, *42*, 1023.

(84) (a) Berry, R. S. *J. Chem. Phys.* **1960**, *32*, 933. (b) Holmes, R. R.; Day, R. O.; Harland, J. J.; Sau, A. C.; Holmes, J. M. *Organometallics* **1984**, *3*, 341.

(85) Bürgi, H. B.; Dunitz, J. *Acc. Chem. Res.* **1983**, *16*, 153.

(86) Kupce, E.; Liepins, E.; Lapsina, A.; Urtane, I.; Zelcans, G.; Lukevics, E. *J. Organometal. Chem.* **1985**, *279*, 343.

(87) Kost, D.; Kingston, V.; Gostevskii, B.; Kalikhman, I., presented at the 16th IUPAC Conference on Physical-Organic Chemistry (ICPOC16), UCSD CA, San Diego, USA, August 2002.

(88) Kost, D.; Kalikhman, I.; Krivonos, S.; Bertermann, R.; Burschka, C.; Neugebauer, R. E.; Pülm, M.; Willeke, R.; Tacke, R. *Organometallics* **2000**, *19*, 1083.

Transition Metal Complexes Bearing a Phosphenium Ligand

HIROSHI NAKAZAWA

*Department of Chemistry, Graduate School of Science,
Osaka City University, Sumiyoshi-ku, Osaka 558-8585, Japan*

I

INTRODUCTION

A phosphenium cation is a two-coordinate phosphorus compound with a high degree of cationic charge accumulation at the phosphorus center, and thus it can be considered to be a member of an isoelectronic series in the third row of the periodic table involving silicenium $[SiR_3]^+$, phosphenium $[PR_2]^+$, sulfenium $[SR]^+$, and chloronium Cl^+. Moreover, focusing attention on both the lone pair electrons and the vacant p orbital at the central element, a phosphenium forms an apt parallel of a singlet carbene CR_2, silylene SiR_2, germylene GeR_2, stannylene SnR_2, and plumbylene PbR_2. Since the discovery of a phosphenium cation in 1972 by Fleming and co-workers,[1] considerable interest has been shown in both the phosphorus chemistry and the coordination chemistry.

The chemistry of transition metal complexes bearing a cationic phosphenium ligand dates back to the synthesis and characterization of $[(CO)_4Fe\{P(NR_2)_2\}][PF_6]$ by Parry in 1978.[2] Since then, many cationic phosphenium complexes have been investigated because a phosphenium may serve as a σ-donor (a Lewis base) and also as a π-acceptor (a Lewis acid) due to the lone pair electrons and a vacant p orbital, and a few review articles have appeared.[3–7] $[L_nM(PR_2)]$, being an electrically neutral transition metal complex, is sometimes treated as a phosphenium complex because it can be considered to consist of L_nM^- and PR_2^+.[8–11] In this chapter, the focus is on electrically cationic transition metal complexes described as $[L_nM(PRR')]^+$.

II

FORMATION OF CATIONIC PHOSPHENIUM COMPLEXES

A. *General Considerations*

Phosphines and their derivatives are known to be very useful ligands toward transition metals and a variety of complexes with phosphine as a ligand have been prepared for all kinds of transition metals. If one of the substituents on a coordinating tertiary phosphorus compound is abstracted as an anion, it would form a cationic phosphenium complex. Actually this strategy has been widely used, and halide, hydride, and alkoxide have been abstracted as an anion by an appropriate Lewis acid. An alternative method to prepare cationic phosphenium complexes is a direct reaction of a phosphenium cation with a transition metal complex having appropriate

leaving ligands. Although this is apparently the simplest method, there is a limitation that a transition-metal free stable phosphenium cation has to be obtained.

B. *Halide Abstraction*

Carbonyl complexes with $PF\{N(Me)CH_2\}_2$ (**1**) react with PF_5, serving as an F^- abstraction reagent, to give cationic phosphenium complexes as PF_6^- salts (**2**) [Eq. (1)].[2,12,13] An analogous noncyclic cationic phosphenium complex, $[Fe(CO)_4\{P(NMe_2)_2\}]^+$ is obtained in the reaction of $[Fe(CO)_4\{PF(NMe_2)_2\}]$ with PF_5.[2] Iron complexes with chloro-substituted phosphine (**3**) also can be converted into cationic phosphenium complexes (**4**) in the reaction with Al_2Cl_6 [Eq. (2)].[14,15] Trihalophosphine complexes, $Fe(CO)_4(PCl_3)$, $Fe(CO)_4(PClF_2)$, do not give phosphenium complexes in the reaction with Al_2Cl_6.

$$(CO)_nM-P\overset{F}{\underset{N}{\big|}}N \quad + \quad PF_5 \quad \longrightarrow \quad \left[(CO)_nM-P\overset{N}{\underset{N}{\big|}}\right]^+ \quad PF_6^- \tag{1}$$

1   **2**

$$M(CO)_n = Fe(CO)_4; Ni(CO)_3$$

$$(CO)_4Fe-P\overset{Cl}{\underset{Y}{\big|}}X \quad + \quad \tfrac{1}{2}\,Al_2Cl_6 \quad \longrightarrow \quad \left[(CO)_4Fe-P\overset{X}{\underset{Y}{\big\backslash}}\right]^+ \quad AlCl_4^- \tag{2}$$

3   **4**
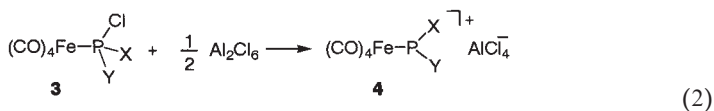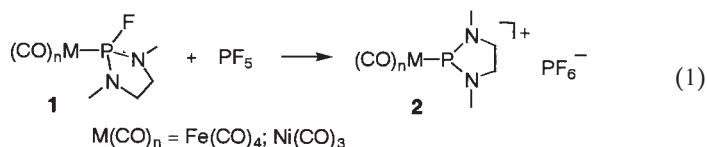
X	Cl	NEt_2	N^iPr_2	$N(SiMe_3)_2$	^tBu	$C_5H_4FeC_5H_5$
Y	NMe_2	NEt_2	N^iPr_2	$N(SiMe_3)_2$	NMe_2	$C_5H_4FeC_5H_5$

C. *Hydride Abstraction*

Hydride abstraction is not a common way to generate a cationic phosphenium complex. One example has been reported [Eq. (3)].[13] The hydride ion transfer is in equilibrium; at $-80\,°C$ the P–H compound (**5**) exists in solution dominantly, whereas at $-23\,°C$, **5** and phosphenium species (**6**) are present in approximately equal concentrations.

$$(CO)_3Ni-P\overset{H}{\underset{N}{\big|}}N \quad + \quad B(^{sec}Bu)_3 \quad \rightleftharpoons \quad \left[(CO)_3Ni-P\overset{N}{\underset{N}{\big|}}\right]^+ \quad HB(^{sec}Bu)_3^- \tag{3}$$

5   **6**
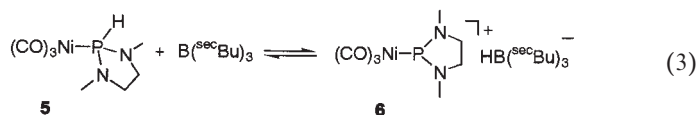
D. *Alkoxide Abstraction*

Trivalent phosphorus compounds containing one or more OR groups are known to react with a variety of transition metal complexes to give stable complexes having datively-bonded phosphorus compound(s). If heterolytic P–OR cleavage in the complex is attained, cationic phosphenium complexes would be generated. Actually, OR group abstraction as an anion from a coordinating phosphorus compound is one of the most applicable methods to produce a cationic phosphenium complex, because starting complexes are readily and widely accessible.

Treatment of a phosphite complex, $M\{P(OMe)_3\}_6$ ($M = Mo$, W) (**7**) with a protic acid such as HPF_6 results in P–OMe heterolytic cleavage to give $[M\{P(OMe)_3\}_5\{P(OMe)_2\}]^+PF_6^-$ (**8**) [Eq. (4)].[16–18] For Mo, the same cationic phosphenium complex was formed in the reaction with CF_3COOH, $(Me_3O)PF_6$, and MeOTf. Reactions with a proton of other transition metal phosphite complexes such as $Fe\{P(OMe)_3\}_5$, $HCo\{P(OMe)_3\}_4$, and $Ni\{P(OMe)_3\}_4$ lead solely to the formation of the protonation products at the metal center, $HFe\{P(OMe)_3\}_5^+$, $H_2Co\{P(OMe)_3\}_4^+$, and $HNi\{P(OMe)_3\}_4^+$, respectively.

$$M\{P(OMe)_3\}_6 \;+\; HPF_6 \longrightarrow \{P(OMe)_3\}_5M{-}P \begin{matrix} OMe \\ OMe \end{matrix} \Big]^+ \; PF_6^- \qquad (4)$$

7　　　　$M = Mo, W$　　　　　　　　　　　**8**
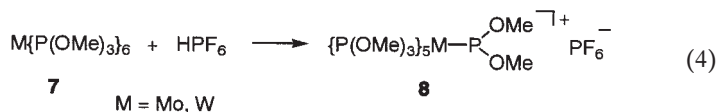
A group 6 transition metal complex bearing a diamino-substituted phosphite (**9**) reacts with a Lewis acid such as $BF_3 \cdot OEt_2$ to give a cationic phosphenium complex (**10**) [Eq. (5)].[19–21] The fac-**10** is formed first and then isomerizes to mer-**10**, indicating that the fac isomer is the kinetic product and the mer isomer is the thermodynamic one. The isomerization rate is Cr > Mo > W. A diamino-substituted ethylphosphite complex in place of a diamino-substituted methylphosphite complex gives exactly the same product in the reaction with $BF_3 \cdot OEt_2$. BCl_3 works as well as $BF_3 \cdot OEt_2$ as an OR^- abstracting reagent, whereas CH_3COOH does not. The diphenylphosphinoethane analogue (**11**) shows the same reactivity to afford **12** [Eq. (6)].[21]

9　　$M = Cr, Mo, W$　　　　fac-**10**　　　　mer-**10**　　　(5)

$$(6)$$

11   M = Mo, W   fac-**12**   mer-**12**
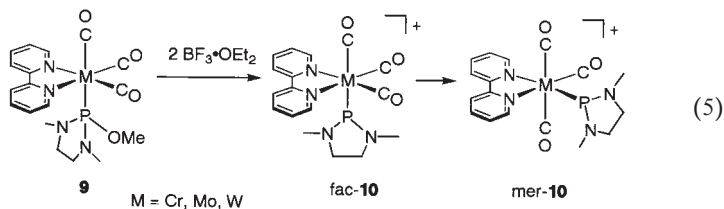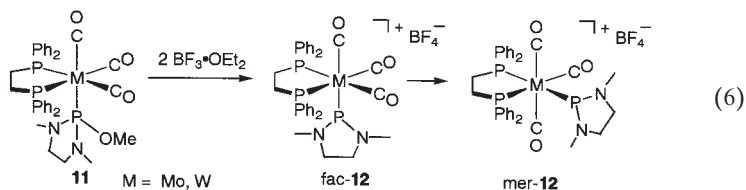
The alkoxide abstraction method can be applied to a piano stool type complex of group 8 transition metals as well. In the reaction of $Cp(CO)(Me)$-$Fe\{P(OMe)(NMeCH_2)_2\}$ with a Lewis acid, formation of a phosphenium complex $Cp(CO)(Me)Fe\{P(NMeCH_2)_2\}^+$ was postulated, but is not actually detected. However, the corresponding silyl, germyl, and stannyl complexes, $Cp(CO)(EMe_3)Fe\{P(OMe)(NMeCH_2)_2\}$ ($E = Si$, Ge, Sn) give phosphenium complexes, $Cp(CO)(EMe_3)Fe\{P(NMeCH_2)_2\}^+$, in the reaction with $BF_3 \cdot OEt_2$ [Eq. (7)].[22,23] Ruthenium complexes show the similar reactivity.[24]

$$(7)$$

M = Fe, Ru ER_3 = $SiMe_3$, $GeMe_3$, $SnMe_3$
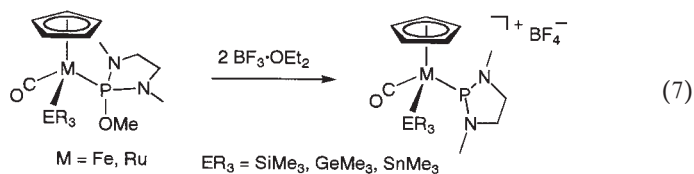
E. *Amide Abstraction*

The reaction of fac-$[(bpy)(CO)_3M\{PNMeCH_2CH_2O(NEt_2)\}]$ ($M = Cr$, Mo, W) (**13**) with $BF_3 \cdot OEt_2$ yields a cationic phosphenium complex, mer-$[(bpy)(CO)_3M\{PNMeCH_2CH_2O\}]^+$ (**14**) [Eq. (8)].[25] The results clearly show that BF_3 can abstract the amide group on the phosphorus as well. The reaction of fac-$[(bpy)(CO)_3M\{P(NEt_2)X(OMe)\}]$ (**15**) ($M = Mo$, W; $X = NEt_2$, OMe) with $BF_3 \cdot OEt_2$ shows interesting results concerning the preference of abstraction [Eq. (9)].[25] The phosphenium complex (**16**) resulting from selective OR abstraction was formed. Therefore, $BF_3 \cdot OEt_2$ is able to abstract an NR_2 group on a coordinating phosphorus to give a cationic phosphenium complex, but it prefers OR abstraction to NR_2 abstraction.

$$(8)$$

13   **14**
M = Cr, Mo, W

$$(9)$$

M = Mo, W   X = NEt₂, OMe
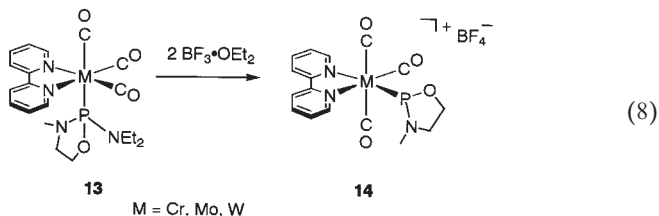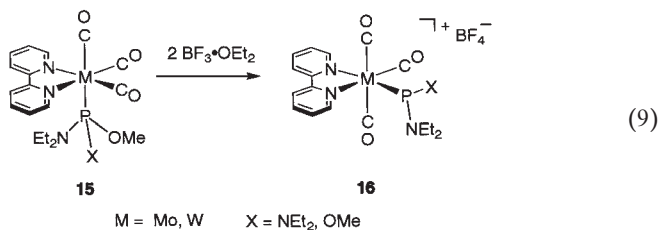
F. *Electrophilic Attack of a Phosphenium Cation*

A phosphenium cation reacts with a transition metal complex having an appropriate leaving ligand such as carbonyl, phosphine, and acetonitrile to generate a cationic phosphenium complex [Eqs. (10)–(14)].[2,26–29] This reaction seems to be the simplest method for the preparation of a cationic phosphenium complex. The drawback of this method is that known stable phosphenium cations are limited in number.

$$(10)$$

$$(11)$$

$$(12)$$

$$(13)$$

OTf⁻ = ⁻OSO₂CF₃

Ar = 2,6-ⁱPr-Ph, 2,4,6-Me₃-Ph, 4-MeO-Ph

(14)

17   **18**
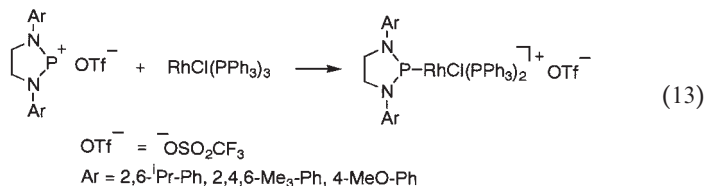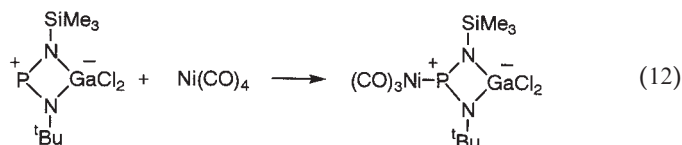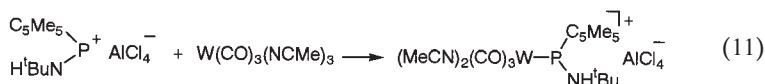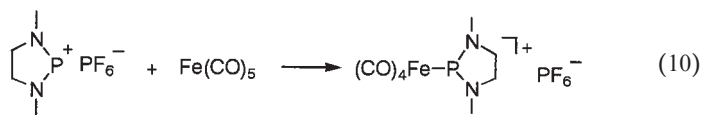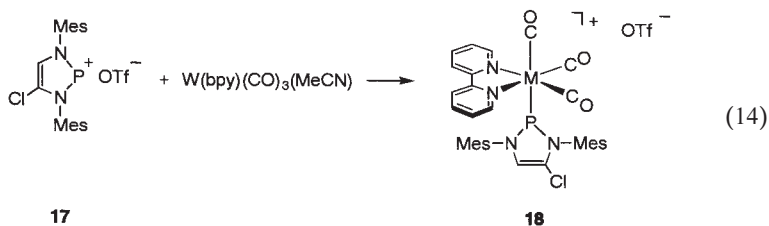
G. Others

As shown in Eq. (14), $W(bpy)(CO)_3(MeCN)$ reacts with the phosphenium cation (**17**) to give a cationic phosphenium complex (**18**). The same phosphenium complex (though the counter anion is different) (**19**) is also prepared in the reaction of the same starting W complex with the corresponding chlorophosphine [Eq. (15)].[29] In this reaction, P–Cl heterolytic cleavage spontaneously occurs to form the phosphenium complex. Complex **19** is unstable and is gradually converted into **20** by Cl^-/CO exchange.

(15)
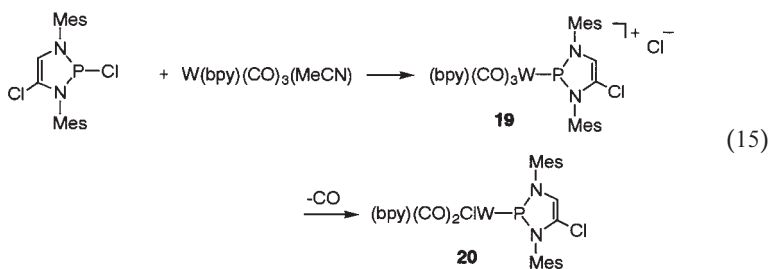
The ring-opening reaction of phosphorus-bridged[1]ferrocenophane (**21**) is proposed to produce a cationic phosphenium iron complex (**22**) [Eq. (16)].[30] Photolysis of **21** induces liberation of one carbonyl ligand to produce a coordinatively unsaturated species. Then the Cp–P bond cleavage results in the Cp ring migration from P to Fe, releasing the strain and yielding the phosphenium intermediate (**22**). This species picks up F^- from PF_6^- to give the final product (**23**).

(16)

21   **22**   **23**
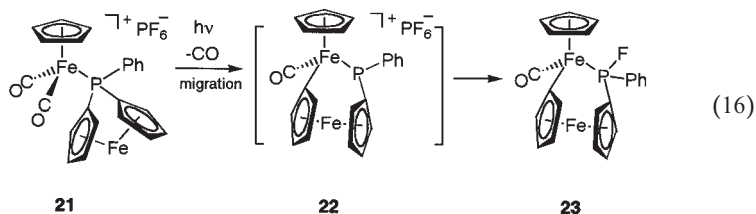
In the reaction of HBF_4 with the neutral complex $Cp(CO)_2W$-$[PPh\{N(SiMe_3)_2\}]$ (**24**) which possesses a planar geometry around the phosphorus, protonation takes place at the metal center to give a cationic phosphenium complex (**25**) [Eq. (17)].[31]

(17)
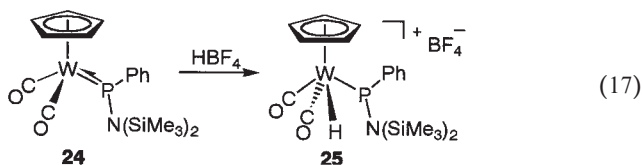
III

REACTIVITY OF CATIONIC PHOSPHENIUM COMPLEXES

A. *General Considerations*

A phosphenium ligand can be considered to have a vacant p orbital and a positive charge on the phosphorus to some extent even in a transition metal complex (see below). Thus, it serves as a π-acceptor resulting in the activation of other π-acceptor ligands existing on the same transition metal, and is susceptible to both intermolecular and intramolecular nucleophilic attack causing migration.

B. *Ligand Exchange Reaction Induced by a Phosphenium Ligand*

When $[Fe(CO)_4\{P(NMeCH_2)_2\}]^+$ is exposed to an atmosphere containing ^{13}C enriched CO, complete statistical exchange occurs within 0.5 h at 25 °C.[12,14] It should be noted that $Fe(CO)_5$ has a dissociation half-life of 4 years. Therefore, a phosphenium is a stronger π-acceptor than a CO ligand. For mer-**10**, a carbonyl ligand is readily replaced by trivalent phosphorus compounds to give **26** and **27** [Eq. (18)],[32] and thermolysis of **18** exhibits CO/OTf^- exchange reaction to generate **28** [Eq. (19)].[29]

(18)

$$(19)$$
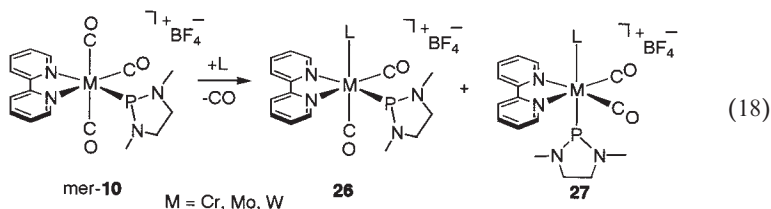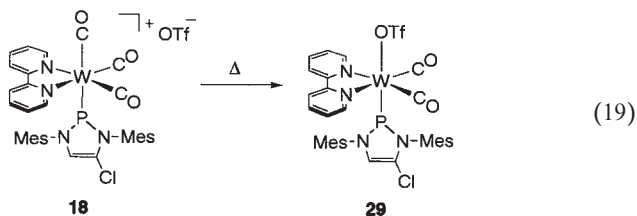
C. *Intermolecular Nucleophilic Attack at Phosphenium Phosphorus*

Although electrophilic character is expected for cationic phosphenium complexes, only a few examples have been reported. Mer-**10** readily reacts with Nu⁻ (Me⁻, OEt⁻) to generate **29** [Eq. (20)].[20] This shows that mer-**10** is susceptible to nucleophilic attack at the phosphenium phosphorus. Complex **29** is not obtained in the reaction of the corresponding phosphite complex (**30**) with Me⁻ or OEt⁻.

$$(20)$$
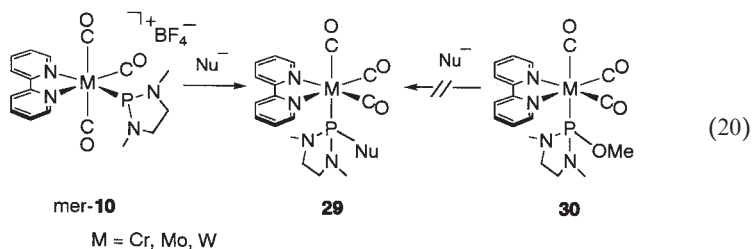
D. *Migration Reaction Involving Phosphenium Phosphorus*

Several types of migration involving a phosphenium ligand have been developed. These migrations seem to be intramolecular reactions, though most of them have not been verified. As mentioned above, $[Mo\{P(OMe)_3\}_5\{P(OMe)_2\}]^+$ is obtained in the reaction of $Mo\{P(OMe)_3\}_6$ with a protic acid. The structure of $[Mo\{P(OMe)_3\}_5\{P(OMe)_2\}]^+$ has been determined by X-ray analysis. It has an octahedral structure with five $P(OMe)_3$ and one $P(OMe)_2$ ligands around the Mo. In solution, the phosphenium complex shows OMe exchange phenomenon. The VT NMR studies reveal that at $-80\,°C$ the structure observed in the solid state is maintained, whereas above $-80\,°C$ OMe migration from $P(OMe)_3$ to $P(OMe)_2$ occurs, rendering all phosphorus nuclei and all OMe groups equivalent on the NMR time scale [Eq. (21)].[16,18]

$$\tag{21}$$
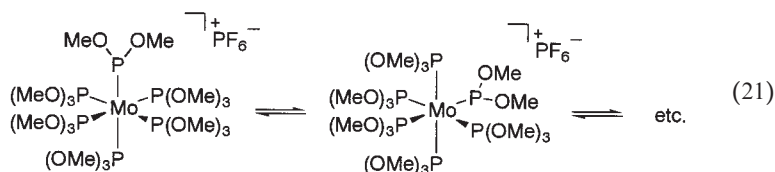
In the reaction of monoaminomonoalkoxy-substituted phosphenium complex **14** with diamino-substituted phosphite, the product is not a simple CO/phosphite exchange complex (which has monoaminomonoalkoxy-substituted phosphenium and diamino-substituted phosphite) but a complex with diamino-substituted phosphenium and monoamino-substituted phosphite (*cis*-**31** and *trans*-**31**) (Scheme 1).[33] This shows an OMe group migration from a phosphite P to a phosphenium P. The migration is irreversible. Similarly, OEt, SEt, and N(CH$_2$CH$_2$)$_2$ groups show this type of migration, but Me and Ph groups do not. Therefore, it can be said that a substituent on a tertiary phosphorus ligand migrates to the coordinating monoaminomonoalkoxy phosphenium ligand only when the substituent is a heteroatom, in other words, it has lone pair electrons. The proposed migration pathway is shown in Scheme 1. One of the CO ligands is readily replaced by the added phosphorus compound because the CO ligands are activated by a strong π-accepting phosphenium ligand. In the intermediate **32**, the Y group on the phosphorus cis to the phosphenium ligand may donate its lone pair electrons to the vacant p orbital of the phosphenium
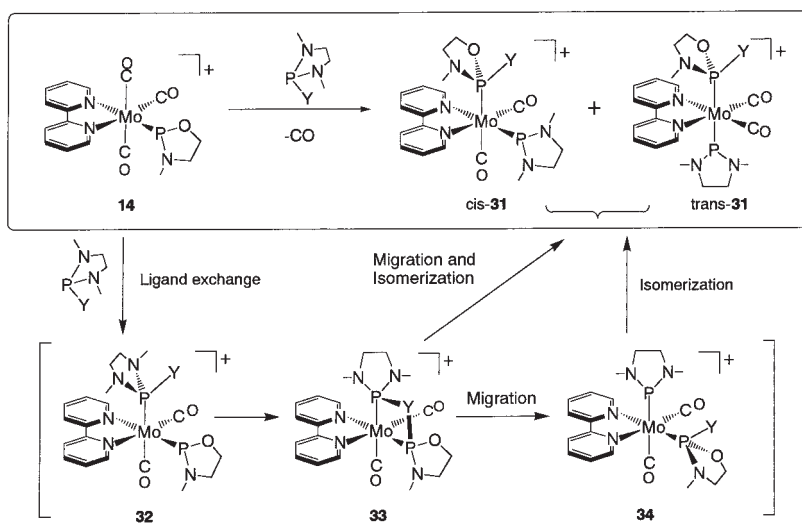
SCHEME 1

phosphorus to give **33**. Cleavage of the original P–Y bond with concomitant formation of the new P–Y σ-bond results in Y migration to give **34**. Then, **34** isomerizes to more stable geometrical isomers to give the final products *cis*-**31** and *trans*-**31**. Y migration may also be accomplished with the accompanying rearrangement around the Mo without the formation of **34**. As is mentioned above, a diamino phosphenium complex is more stable than a monoaminomonoalkoxy phosphenium. Therefore, the driving force of the migration is thought to be the formation of a more stable phosphenium ligand.

The conversion mentioned above is a migration from a tertiary phosphorus ligand to a phosphenium phosphorus in a transition-metal coordination sphere. The phosphenium ligand also shows another type of migration for transition metal complexes with a group 14 element ligand. Piano stool iron complexes having Cp, CO, phosphenium, and group 14 element ligand such as alkyl, silyl, germyl, and stannyl show interesting reactivity, which is summarized in Scheme 2. In the reaction of **35** with a Lewis acid such as $BF_3 \cdot OEt_2$ or TMSOTf, a cationic phosphenium complex (**36**) is uniformly formed irrespective of the kind of ER_3. The subsequent reaction is strongly dependent on E.

When E is carbon, the produced phosphenium complex is too reactive to be detected. The alkyl ligand immediately migrates to the phosphenium phosphorus to give **37**. The 16 electron species can be converted into an isolable complex **38** by the addition of PPh_3.[22,23]

When E is Si or Ge, the cationic phosphenium complex (**36**) is stable and Fe–Si and Fe–Ge bonds remain unreacted.[22,23] The formation of the silyl phosphenium complex, $[Cp(CO)(SiMe_3)Fe\{P(NMeCH_2)_2\}]BPh_4$ was confirmed by X-ray analysis.[23]

In contrast to the alkyl, silyl, and germyl complexes, when E is Sn, not SnR_3 but only one alkyl group on the Sn migrates to the phosphenium P to give a stannylene complex (**39**).[23,34] Since the transition metal–phosphorus bond has considerable double-bond character (see below), the conversion from **36** to **39** corresponds to a double-bond migration from Fe=P to Fe=Sn.

Similar behavior has been reported for Ru,[24] Mo,[35,36] and W[35,36] complexes. Cationic phosphenium complexes of a transition metal containing a group 14 element ligand are interesting in terms of migration because the different congeners exhibit different behavior in the coordination sphere: 1,2-migration for C, no migration for Si and Ge, and 1,3-migration for Sn.

Complex **40** is an iron complex with a phosphorus ylide ligand ($-CH_2^+PR_3$) (Scheme 3). It reacts with TMSOTf to give **42** which can be converted into an isolable complex **43** by the addition of *n*-Bu_4NBr.[37] The reaction sequence is shown in Scheme 3. Two points should be noted in this reaction: (i) an OMe^- anion is able to be abstracted by
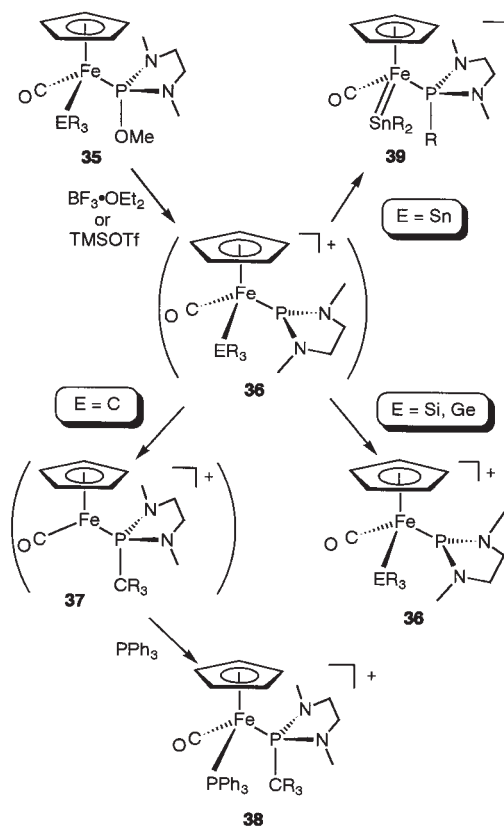
SCHEME 2

TMSOTf even in a cationic complex, and (ii) a cationic phosphorus ylide ligand can migrate to a cationic phosphenium ligand. The reaction has been confirmed to take place through intramolecular migration.

Hydride migration from a transition metal to a phosphenium phosphorus has been reported for a W complex (Scheme 4).[31] The cationic phosphenium complex (**44**) reacts with a two electron donor (PPh_3, PMe_3, OEt_2) to give **45** involving H migration from W to phosphenium phosphorus. The reaction with Cl^- also generates a H migration product (**46**).

E. Others

Treatment of $Rh(acac)(CO)_2$ with cationic phospheniums, $^+P(NEt_2)_2$, $^+P\{N(CHMePh)CH_2\}_2$ generates catalysts for hydroformylation of styrene

SCHEME 3

L (= PPh$_3$, PMe$_3$, OEt$_2$)
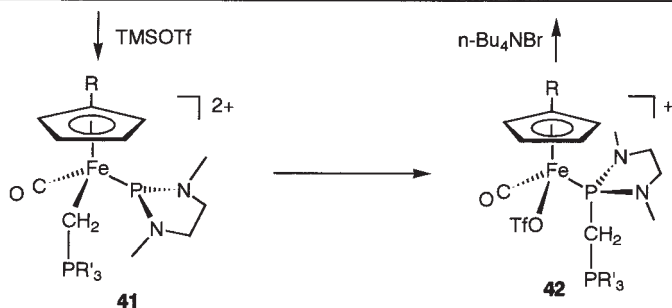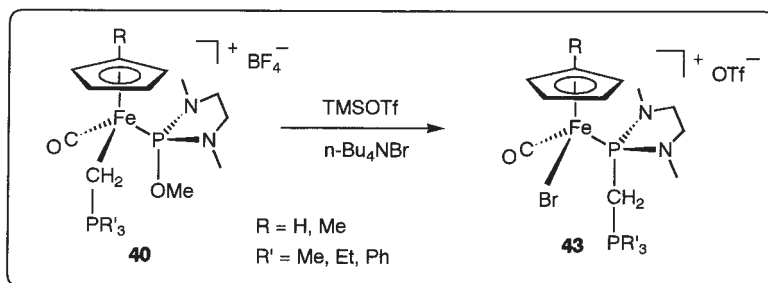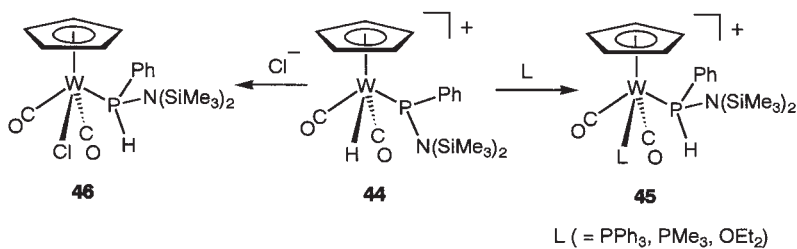
SCHEME 4

[Eq. (22)].[38] Although there is no evidence supporting the formation of a cationic phosphenium complex, it may be generated and serve as a catalyst for hydroformylation of styrene.
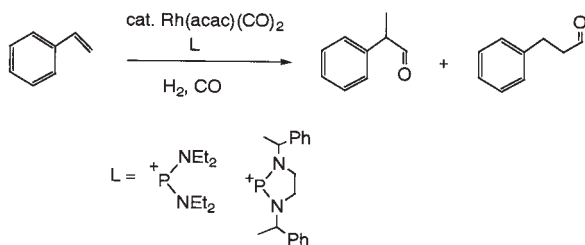
(22)

IV

COMPETITIVE REACTIONS WITH CATIONIC
PHOSPHENIUM COMPLEX FORMATION

A. *General Considerations*

Alkoxide anion abstraction by a Lewis acid from phosphorus ligand on a transition metal is one of the most useful methods to prepare cationic phosphenium complexes. It has been reported that OR anion abstraction from an alkoxyalkyl ligand, $C(OR)R'_2$, on a transition metal complex leads to the formation of a cationic carbene complex.[39–42] It is similarly expected that OR anion abstraction from an alkoxysilyl ligand, $Si(OR)R'_2$, would cause the formation of a cationic silylene complex. Therefore, increased attention has been focused on the reaction with a Lewis acid of transition metal complexes bearing both alkoxyalkyl and phosphite ligands and of complexes bearing both alkoxysilyl and phosphite ligands.

B. *Competition between Carbene Complex Formation and Phosphenium Complex Formation*

$Cp(CO)Fe(CH_2OMe)\{P(OR)(NMeCH_2)_2\}$ (**46**, **47**) has been subjected to a reaction with $BF_3 \cdot OEt_2$ in order to examine whether the OR group on the carbon or on the phosphorus is abstracted. Equation (23) shows the results.[22] An OR group on the carbon is selectively lost as an anion to give a cationic carbene complex, which is converted into an isolable ylide complex by the addition of PPh_3. Formation of **49** from **47** demonstrates the selective OR abstraction from the carbon and rules out the possibility that the OR on the phosphorus is first abstracted, and then the OR on the carbon migrates to the phosphorus to give the carbene complex eventually.

$$R = Me : \mathbf{46}$$
$$Et : \mathbf{47}$$

$$(23)$$

$$R = Me : \mathbf{48}$$
$$Et : \mathbf{49}$$
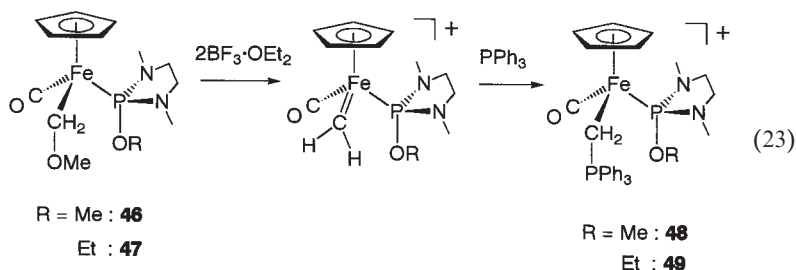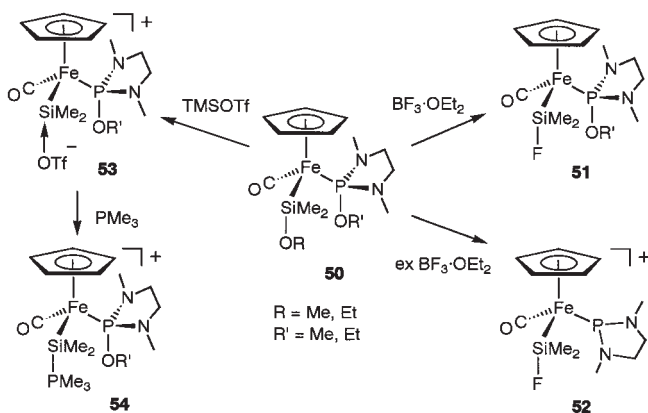
Scheme 5

C. *Competition between Silylene Complex Formation and Phosphenium Complex Formation*

In the reaction of $Cp(CO)Fe(SiMe_2OR)\{P(OR')(NMeCH_2)_2\}$ (**50**) with $BF_3 \cdot OEt_2$, when an equimolar amount of $BF_3 \cdot OEt_2$ is used, an OR/F substitution product (**51**) is obtained, and when excess $BF_3 \cdot OEt_2$ is used, a cationic phosphenium complex with a $SiFMe_2$ ligand (**52**) is obtained (Scheme 5).[43] It is deduced from the results that an OR group on the Si is first abstracted, then an OR group on the P is abstracted. In this reaction a silylene complex is not detected. Changing the Lewis acid from $BF_3 \cdot OEt_2$ to TMSOTf leads to the formation of silylene complex (**53**) though it is a base-stabilized one. Addition of PMe_3 produces an isolable complex (**54**), for which an X-ray structure was reported. The selectivity may be derived from a difference in basicity of the oxygen atom between Si–OR and P–OR in the complex and/or from the relative thermodynamic stability between the silylene and phosphenium complexes.

V

PHYSICAL PROPERTIES AND M–P BOND NATURE OF CATIONIC PHOSPHENIUM COMPLEXES

A. *Spectroscopic Properties*
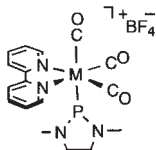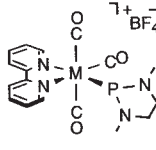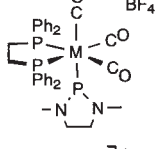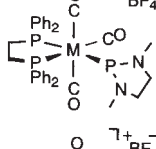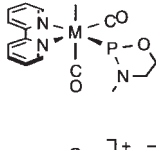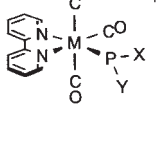
Needless to say, ^{31}P NMR data are undoubtedly indispensable and informative for preparation, characterization, and estimation of physical

properties of cationic phosphenium complexes. These data are listed in
Table I. ^{31}P NMR data have been reported to date for 76 cationic
phosphenium complexes. Out of the 76, 68 complexes show the chemical
shifts in a 100 ppm range (from 214 ppm to 314 ppm). Four resonances are
lower in magnetic field (324 ppm, 334.7 ppm, 349 ppm, and 441.5 ppm)
and four resonances are higher (172.4 ppm, 161.8 ppm, 150.0 ppm,
and 148.1 ppm). The latter resonances are for complexes with a
PN(Mes)CCl=CHN(Mes) ligand. Some tendencies can be noted. For
[(bpy)(CO)$_3$M(phosphenium)]$^+$, the chemical shift of a meridional isomer
is lower in magnetic field than that of the corresponding facial isomer,
and for [(bpy)(CO)$_2$(phosphite)M(phosphenium)]$^+$, the chemical shift of a
cis isomer is lower in magnetic field than that of the corresponding
trans isomer, though there are a few exceptions. This indicates that a
phosphenium ligand trans to an electron donating ligand exhibits a lower
chemical shift than that trans to a π-electron accepting ligand (CO).

The coupling constant between phosphenium phosphorus and tungsten
is readily available by ^{31}P NMR measurements, and is informative. In the
abstraction of an OR$^-$ anion from the coordinating phosphite, on going
from the parent phosphite complex to the fac-phosphenium complex, and to
the mer-phosphenium complex, the P–W coupling constant increases by
about 100 Hz; 334.6 Hz for fac-[(bpy)(CO)$_3$W{P(NMeCH$_2$)$_2$(OMe)}] →
441.7 Hz for fac-[(bpy)(CO)$_3$W{P(NMeCH$_2$)$_2$}]$^+$ → 561.1 Hz for mer-
[(bpy)(CO)$_3$W{P(NMeCH$_2$)$_2$}]$^+$; 338.2 Hz for fac-[(dppe)(CO)$_3$W{P-
(NMeCH$_2$)$_2$(OMe)}] → 419.1 Hz for fac-[(dppe)(CO)$_3$W{P(NMeCH$_2$)$_2$}]$^+$
→ 488.5 Hz for mer-[(dppe)(CO)$_3$W{P(NMeCH$_2$)$_2$}]$^+$. This indicates that
the P–W double bond character increases in this order.
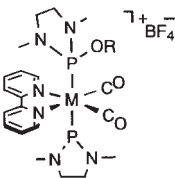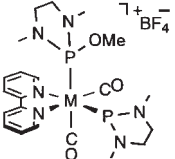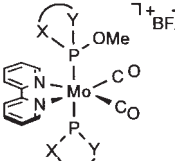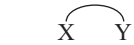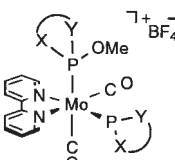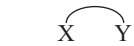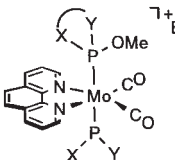
In addition to ^{31}P NMR data, transition-metal NMR data of cationic
phosphenium complexes of transition metals provide useful information
about bond character between a transition metal and a phosphenium
phosphorus. ^{95}Mo[44] and ^{183}W[29] NMR data have been reported. In the ^{95}Mo
NMR spectra, the chemical shifts, the coupling constants between Mo and
phosphenium P, and the line widths are shown in Table II for fac-[(bpy)
(CO)$_3$Mo{P(NMeCH$_2$)$_2$(OMe)}], fac-[(bpy)(CO)$_3$Mo{P(NMeCH$_2$)$_2$}]$^+$, and
mer-[(bpy)(CO)$_3$Mo{P(NMeCH$_2$)$_2$}]$^+$. In this order, deshielding of the
chemical shift, an increase in the Mo–P coupling, and an increase in the
line width are observed. These changes can be attributed to a dominant
contribution from the imbalance of electron density at the Mo in the
Ramsey equation due to a significant double-bond character between the
Mo and the phosphenium P.[44] ^{183}W NMR data for tungsten complexes
containing cationic phosphenium ligand, PN(Mes)CCl=CHN(Mes)
(Table III), revealed a linear correlation between δ^{183}W and $^1J_{WP}$,
suggesting the high π-acceptor ability of the phosphenium ligand.[29]

TABLE I
^{31}P NMR Data for a Phosphenium Group in Cationic Phosphenium Complexes

Complex			δ (ppm)	Notes	Ref.
{P(OMe)$_3$}$_5$Mo–P(OMe)(OMe) PF$_6$			214.4[a]	$-85\,°$C $^2J_{PP}=250$ Hz $^2J_{PP}=64$ Hz	16,18
	M = Cr		263.8		28
	M = Mo		252.5		28
	M = W		233.7	$^1J_{WP}=441.7$ Hz	28
	M = Cr		277.3		28
	M = Mo		268.2		28
	M = W		242.6	$^1J_{WP}=561.1$ Hz	28
	M = Mo		282.4		28
	M = W		257.1	$^1J_{WP}=419.1$ Hz $^1J_{PP}=22.1$ Hz	28
	M = Mo		283.4		28
	M = W		256.1	$^1J_{WP}=488.5$ Hz $^1J_{PP}=114.0$ and 19.0 Hz	28
	M = Cr		258.7		24
	M = Mo		253.8		24
	M = W		230.1	$^1J_{WP}=621.1$ Hz	24
M	X	Y			
Cr	NEt$_2$	NEt$_2$	296.3		24
Mo	NEt$_2$	NEt$_2$	290.0		24
W	NEt$_2$	NEt$_2$	261.5	$^1J_{WP}=558.1$ Hz	24
Mo	NEt$_2$	OMe	272.6		24
W	NEt$_2$	OMe	249.6	$^1J_{WP}=606.3$ Hz	24

(*Continued*)

TABLE I
Continued
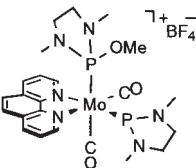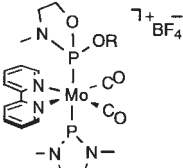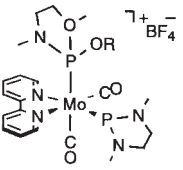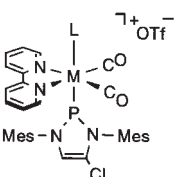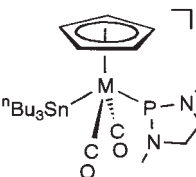
Complex		δ (ppm)	Notes	Ref.

	M	OR	δ (ppm)	Notes	Ref.
[structure: [(N N)(N N)P(OR)Mo(CO)₂] type]⁺ BF₄⁻	Cr	OMe	248.6	$^2J_{PP} = 91.6$ Hz	31
	Mo	OMe	242.2	$^2J_{PP} = 274.7$ Hz	31
	Mo	OEt	241.9	$^2J_{PP} = 274.6$ Hz	31
	W	OMe	222.2	$^2J_{PP} = 268.6$ Hz $^2J_{WP} = 518.8$ Hz	31

	M	OR	δ (ppm)	Notes	Ref.
[structure]⁺ BF₄⁻	Mo	OMe	257.7	$^2J_{PP} = 42.7$ Hz	31
	Mo	OEt	256.7	$^2J_{PP} = 42.7$ Hz	31
	W	OMe	234.0	$^2J_{PP} = 27.5$ Hz $^1J_{WP} = 589.0$ Hz	31

	X	Y	δ (ppm)	Notes	Ref.
[structure]⁺ BF₄⁻	MeNCH₂CH₂O		235.6	$^2J_{PP} = 326.5$ Hz	31
	^{t}BuNCH₂CH₂O		227.5	$^2J_{PP} = 320.5$ Hz	31
	OCMe₂CMe₂O		224.5	$^1J_{PP} = 369.2$ Hz	31

	X	Y	δ (ppm)	Notes	Ref.
[structure]⁺ BF₄⁻	MeNCH₂CH₂O		241.9	$^2J_{PP} = 54.9$ Hz	31
	OCMe₂CMe₂O		214.9	$^2J_{PP} = 58.0$ Hz	31

Complex	δ (ppm)	Notes	Ref.
trans-(bpy)(CO)₂(PPh₃)Mo−P[structure]⁺ BF₄⁻	246.9	$^2J_{PP} = 180.1$ Hz	31
cis-(bpy)(CO)₂(PPh₃)Mo−P[structure]⁺ BF₄⁻	257.6	$^2J_{PP} = 27.5$ Hz	31

	X	Y	δ (ppm)	Notes	Ref.
[structure]⁺ BF₄⁻	MeNCH₂CH₂Me		242.3	$^2J_{PP} = 271.6$ Hz	31
	^{t}BuNCH₂CH₂O		228.1	$^2J_{PP} = 347.4$ Hz	31
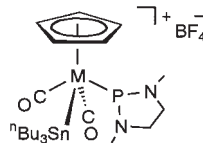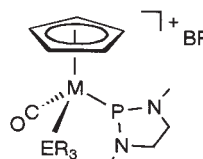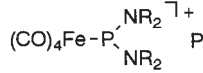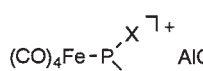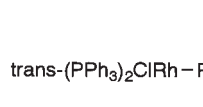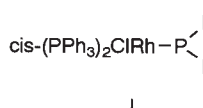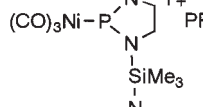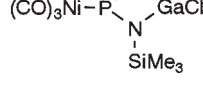
(*Continued*)

TABLE I
Continued

Complex		δ (ppm)	Notes	Ref.
		258.4	$^2J_{PP}=42.8$ Hz	31
	R = OMe	246.5	$^2J_{PP}=289.9$ Hz	32
	OEt	246.3	$^2J_{PP}=289.9$ Hz	32
	SEt	250.9	$^2J_{PP}=277.7$ Hz	32
	N(CH$_2$)$_2$	243.4	$^2J_{PP}=263.4$ Hz	32
	R = OMe	259.1	$^2J_{PP}=42.7$ Hz	32
	OEt	258.5	$^2J_{PP}=48.8$ Hz	32
	SEt	259.3	$^2J_{PP}=36.6$ Hz	32
trans-(bpy)(CO)$_2$ {P(OMe)(NMeCH$_2$CH$_2$O)Mo−P} BF$_4$		241.9	$^2J_{PP}=54.9$ Hz	32
cis-(bpy)(CO)$_2$ {P(OMe)(NMeCH$_2$CH$_2$O)Mo−P} BF$_4$		235.6	$^2J_{PP}=326.6$ Hz	32

	M	L			
	Mo	PPh$_3$	172.4		28
	W	PPh$_3$	150.0	$^1J_{WP}=598$ Hz	28
	W	MeCN	148.1	$^1J_{WP}=707$ Hz	28
	W	CO	161.8	$^1J_{WP}=497$ Hz	28

Complex		δ (ppm)	Notes	Ref.
[(MeCN)$_2$(CO)$_3$W{P(C$_5$Me$_5$)(NH^{t}Bu)}]$^+$[AlCl$_4$]$^-$		297.9	$^1J_{WP}=404$ Hz	25
[(MeCN)$_3$(CO)$_2$W{P(C$_5$Me$_5$)(NH^{t}Bu)}]$^+$[AlCl$_4$]$^-$		268.3	$^1J_{WP}=583$ Hz	25
	M = Mo	310.1		35
	W	282.8	−20 °C	35
			$^1J_{WP}=543.1$ Hz	
			$^2J_{SnP}=291.6$ Hz	

(Continued)

TABLE I
Continued

Complex		δ (ppm)	Notes	Ref.
	M = Mo	334.7		35
	W	298.8	−20 °C	35
			$^1J_{WP} = 516.4$ Hz	
			$^2J_{SnP} = 42.5$ Hz	
	M ER₃			
	Fe SiMe₃	309.3		21
	Fe SiFMe₂	311.1		38
	Fe GeMe₃	311.1		22
	Fe SnMe₃	307.9	$^2J_{SnP} = 547.9$ Hz	22
	Fe Sn^{n}Bu₃	307.5	$^2J_{SnP} = 301.5$ Hz	22
	Ru SiMe₃	286.6		38
	Ru SiMe₂SiMe₃	286.1		38
	Ru GeMe₃	289.1		38
	Ru Sn^{n}Bu₃	287.4	$^2J_{SnP} = 182.7$ Hz	38
	NR₂ = NMe₂	311		2
	NR₂ = NMeCH₂	300		2
	X = Y = NEt₂	307.6		14
	X = Y = N^{i}Pr₂	311.3		14
	X = Y = N(SiMe₃)₂	349.7	−20 °C	14
	X = Y = (C₅H₄)Fe(C₅H₅)	307.6		14
	X = Cl, Y = NMe₂	268.8		14
	X = ^{t}Bu, Y = NMe₂	441.5	−20 °C	14
		255.8	$^1J_{RhP} = 316$ Hz	28
		249.6	$^1J_{RhP} = 234$ Hz	28
			$^2J_{PP} = 448$ Hz	
		276		13
		324		26

^{a}The chemical shift was referenced to P(OMe)₃ in the original paper. The recalculated value based on 85% H₃PO₄ is listed in the table.

TABLE II

^{95}MO NMR DATA FOR A PHOSPHENIUM GROUP IN CATIONIC PHOSPHENIUM COMPLEXES

Complex	δ (ppm)	$^{1}J_{MoP}$ (Hz)	$W_{1/2}$ (Hz)
	−1081	193	35
	−1049	264	90
	−1015	337	300

TABLE III

^{183}W NMR DATA FOR A PHOSPHENIUM GROUP IN CATIONIC PHOSPHENIUM COMPLEXES

Complex	L	n	δ (ppm)	$^{1}J_{WP}$ (Hz)
	OTf	0	−1440	770
	NCMe	1	−1580	707
	Cl	0	−1680	703
	PPh$_3$	1	−1860	598
	CO	1	−2105	497

B. *Structural Properties*

In contrast to 76 cationic phosphenium complexes for which ^{31}P NMR data have been reported, only 7 complexes have been structurally characterized (Table IV). Five of them are diamino-substituted phosphenium complexes,[23,27,29,32,45] one is a monoaminomonoalkoxy phosphenium complex,[32] and one is a dialkoxy phosphenium complex.[16,18] The geometry

TABLE IV

M–P (Phosphenium) Bond Distances in Cationic Phosphenium Complexes

Complex	M–P Distance (Å)	Ref.
$[\{(MeO)_3P\}_5Mo\{P(OMe)_2\}]PF_6$	2.229(4)	16,18
trans-$[(bpy)(CO)_2\{P(NMeCH_2)_2(OMe)\}Mo\{P(NMeCH_2)_2\}]OTf$	2.254(1)	31
trans-$[(phen)(CO)_2\{P(N^tBu(CH_2)_2O)(OMe)\}Mo$- $\{P(N^tBu(CH_2)_2O)\}]OTf$	2.238(4)	31
trans-$[(bpy)(CO)_2(PPh_3)W\{P(N(Mes)CCl=CHN(Mes)_2)\}]OTf$	2.247(2)	28
$[(CO)_4Fe\{P(NEt_2)_2\}]AlCl_4$	2.10(5)	40
$[Cp(CO)(SiMe_3)Fe\{P(NMeCH_2)_2\}]BPh_4$	2.018(2)	22
$(CO)_3NiP(\mu\text{-}NSiMe_3)_2GaCl_2$	2.123(3)	26
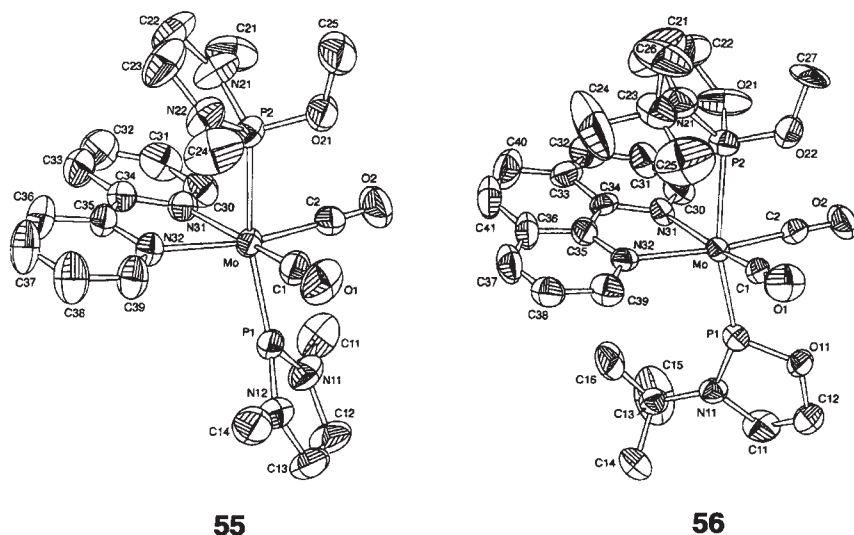
Fig. 1. Molecular structures of 55 and 56.

around the phosphenium phosphorus is planar without exception. The bond lengths range from 2.018 to 2.254 Å.

The structures of 55 and 56 are of interest because the central metal has both phosphite and phosphenium in mutually trans positions. The molecular structures are shown in Fig. 1. It should be noted that the bond distance of Mo–P(phosphenium) is significantly shorter than that of Mo–P(phosphite) for both complexes: for 55, Mo–P(phosphenium) = 2.254 Å, Mo–P(phosphite) = 2.495 Å; for 56, Mo–P(phosphenium) = 2.238 Å, Mo–P(phosphite) = 2.529 Å. Normal Mo–P dative bond distances are reported to fall in the range 2.40–2.57 Å.[3]

The observation that the Mo–P(phosphenium) bond is about 10% shorter than the Mo–P dative bond is consistent with double bond character in the phosphenium complex.

Another structural feature of interest is the P–N bond distance. The P–N bond distances (Å) in phosphenium and in phosphite ligands are almost equal: 1.642 (P1–N11), 1.644 (P1–N12), 1.648 (P2–N21), and 1.662 (P2–N22) for **55** and, 1.65 (P1–N11) and 1.63 (P2–N21) for **56**. This observation gives some insight into the role of an amino group on a phosphenium phosphorus (vide infra). For nitrogen atoms both in phosphenium and phosphite ligands, as well as phosphenium phosphorus atoms, trigonal-planar geometry is observed.

C. *M–P(Phosphenium) Bond Nature*

With transition-metal free cationic phosphenium, an amino substituent is known to stabilize the cation. Theoretical studies[46–50] support the existence of conjugation involving the nitrogen lone pairs and the vacant phosphorus p orbital, and estimate that the N–P$^+$–N lone pair conjugation in $[P(NH_2)_2]^+$ contributes 68.1 kcal/mol.[47]

With a cationic phosphenium complex of a transition metal, π-donation from the transition metal to phosphenium phosphorus is also conceivable. A cationic phosphenium complex can be described in the resonance forms shown in Scheme 6. **58** corresponds to a complex where a plus charge is located on the phosphorus and a phosphenium cation coordinates to a transition metal through its lone pair. Thus, the bond between M and P in **58** can be seen as a dative bond. If a sufficient electron density flows from the filled d orbital of a transition metal into the vacant p orbital on the phosphorus, the plus charge would be located on a transition metal and the M–P bond would become a double bond (**57**). The π-electron donation
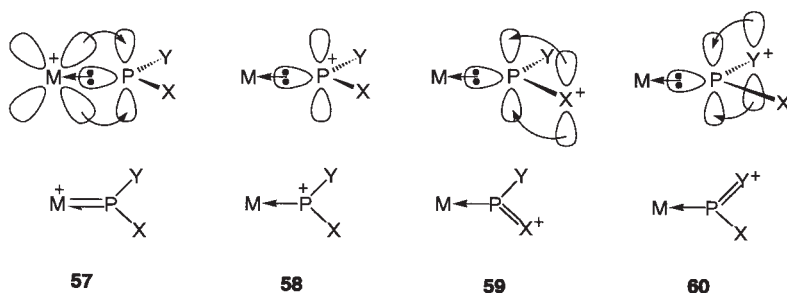
SCHEME 6

to the empty p orbital of the phosphorus may occur not only from M but also from the two other substituents on the phosphorus (X and Y). These features are depicted in **59** and **60**.

The results of X-ray structures mentioned above show that the P–N bond lengths are longer than those of transition-metal free phosphenium, such as $[P(N^iPr_2)_2][AlCl_4]$ (1.613 Å). Therefore, π-donation as depicted in **59** and **60** may not be dominant, in other words, π-back donation from a transition metal (**57**) may be the dominant contribution.

Systematic study on the influence of these substituents on the stability of cationic phosphenium complexes for $[(bpy)(CO)_3M\{PXY\}]^+$ revealed that the stability increases upon going to a heavier congener in terms of the transition metal, with increasing the number of amino substituents on the phosphorus, and with adding an ethylene bridge between X and Y.[25]

An amino substituent on the phosphenium phosphorus makes cationic phosphenium complexes stable, but the π-donation from an amino substituent is only a minor contribution. So what is the role of an amino substituent? The role may be, as is proposed for Arduengo carbene, to protect the approach of a nucleophile to phosphenium phosphorus by high pπ lone pair density flanking the phosphenium center.[32]

VI

THEORETICAL APPROACH TO CATIONIC PHOSPHENIUM COMPLEXES

A. *General Considerations*

Theoretical description of cationic phosphenium complexes has been reported in only a few papers. A simple representation is shown in Fig. 2 with diaminophosphenium and a 16e-ML_5 fragment.[6] There are two main interactions; an interaction of the phosphenium HOMO (lone pair) with the metal LUMO and that of the phosphenium LUMO with one of the occupied d orbitals. The former constitutes a dative bond from P to M, and the latter a π-back donation from M to P.

B. *Theoretical Studies for $[(bpy)(CO)_3M(phosphenium)]^+$*

More precise *ab initio* MO studies were reported for $[(bpy)(CO)_3M\{P(NMeCH_2)_2\}]^+$ (M = Mo, W).[51] The HOMO of the mer isomer
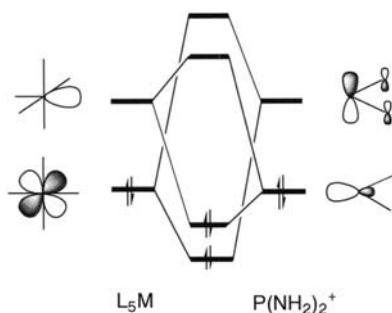
FIG. 2. Frontier orbital interactions between 16e-L$_5$M and a diaminophosphenium cation.
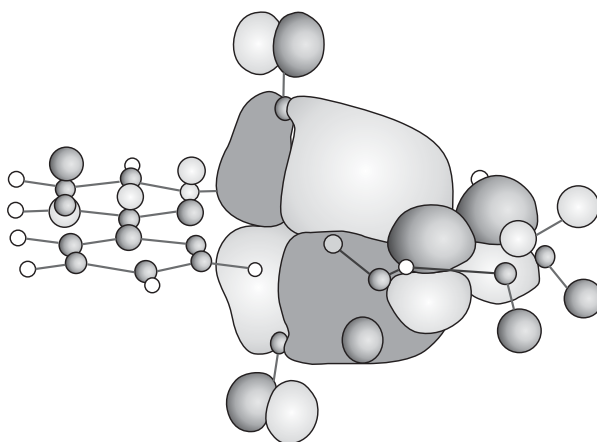
FIG. 3. HOMO of mer-[(bpy)(CO)$_3$Mo{P(NMeCH$_2$)$_2$}]$^+$.

of Mo is shown in Fig. 3, which corresponds to π-back donation from a filled d orbital of Mo to an empty p orbital of P. The *ab initio* calculation demonstrated that a phosphenium ligand has strong π-electron acceptor character, stronger than that of a CO ligand. A comparison between the optimized geometry of a free phosphenium and that of a transition-metal-bound phosphenium also shows strong π-back donation from M to P. The P–N distances in fac and mer isomers are almost the same (1.637–1.648 Å), but are considerably longer than that for the metal-free phosphenium (1.604 Å). This indicates that a phosphenium ligand gets π-donation predominantly from a transition metal and little from amino substituents. This is also demonstrated by Mulliken charge analysis. The charges assigned to N in the phosphenium complex are almost the same (ca. −0.41) regardless of the geometric isomers (fac, mer), or the kind of transition metals (Mo, W), but the charge assigned to N in a free phosphenium is more positive

TABLE V

ELECTRON POPULATIONS IN π-ORBITAL ON THE
PHOSPHENIUM RING IN [(bpy)(CO)₃Mo{P(NMeCH₂)₂}]⁺
AND IN A FREE PHOSPHENIUM

Atom	Fac-isomer	Mer-isomer	Metal-free
P	0.712	0.728	0.542
N	1.782	1.787	1.685

(ca. -0.35). Electron populations in π-orbitals on the phosphenium ring in
the Mo phosphenium complex and those in metal-free phosphenium are
shown in Table V. Less population on the N atom in the free ligand than in
the complex means more electron transfer from N to P in the former than
the latter. More population on the P atom in the complexes (0.712 for the
fac isomer, 0.728 for the mer isomer) than in metal-free phosphenium
(0.542) corresponds to π-back donation from the central metal.

C. *Theoretical Studies for [Cp(CO)(ER₃)Fe(phosphenium)]⁺*

One of the characteristic reactions of cationic phosphenium complexes
of transition metals is exhibited by a series of [Cp(CO)(ER₃)Fe{P-
(NMeCH₂)₂}]⁺. This is shown in Scheme 5; for ER₃ = CH₃, 1,2-methyl
migration from Fe to P, for ER₃ = SiMe₃, GeMe₃ no migration, and for
ER₃ = SnMe₃, 1,3-methyl migration from Sn to P. A DFT calculation
has been done for the model complex, [Cp(CO)(EH₂R)Fe{P(NHCH₂)₂}]⁺
(E = C, Si, Sn; R = H, CH₃).[52]
Figure 4 shows the energy diagram in kcal/mol for the 1,2-migration
of the CH₃ group and the optimized structures. The 1,2-migration for
61 proceeds with the formation of a three-centered transition state (**62**)
with a very small activation barrier of 1.3 kcal/mol. The transition state
62 leads to the formation of **63** where Fe⋯HC agostic interaction is
detected. Although the 1,2-migration is complete at this stage, this complex
further rearranges via transition state **64** to a more stable species **65**,
wherein one of the nitrogen lone pair coordinates to the Fe atom. Totally,
the 1,2-migration of the CH₃ group is 14.4 kcal/mol exothermic, and the
activation energy is 3.6 kcal/mol. Since the energy is small, the CH₃
migration is quite easy.
On the other hand, the SnH₃ 1,2-migration adopts a one-step mechanism
without an intermediate (**66 → 67 → 68**) (Fig. 5). The energy profiles
demonstrate a much higher activation barrier of 19.2 kcal/mol. A similar
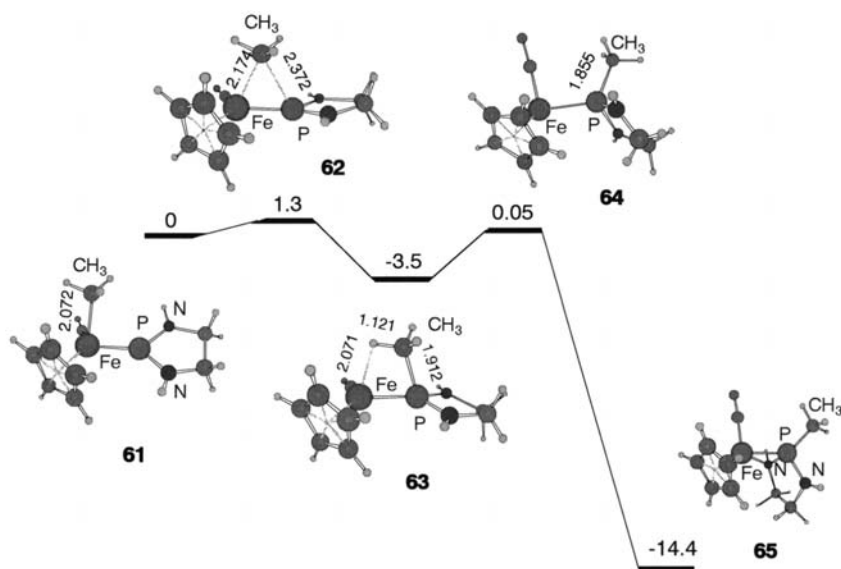
FIG. 4. Energy diagram (kcal/mol) of 1,2-migration of CH_3 in the iron complex having methyl and phosphenium ligands.
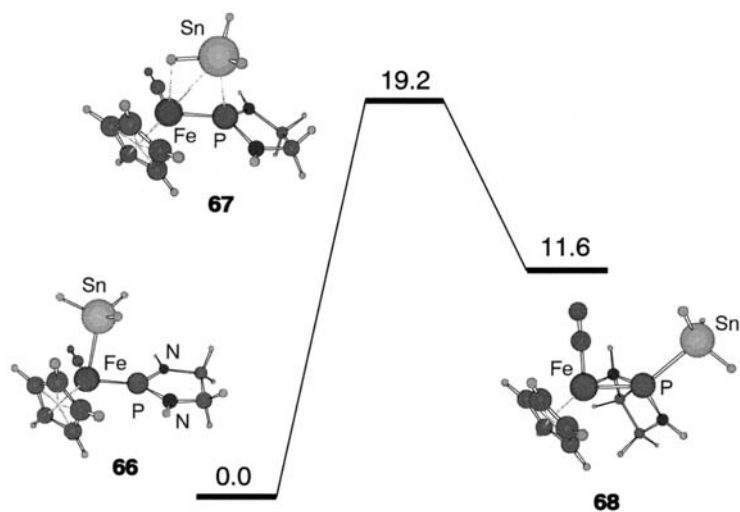
FIG. 5. Energy diagram (kcal/mol) of 1,2-migration of SnH_3 in the iron complex having stannyl and phosphenium ligands.

$$0.05 \qquad\qquad 0.32 \qquad\qquad 0.32$$
$$CH_3 \qquad\qquad SiH_3 \qquad\qquad SnH_3$$
$$| \qquad\qquad\quad | \qquad\qquad\quad |$$
$$[Fe]\!-\!\!-\![P] \qquad [Fe]\!-\!\!-\![P] \qquad [Fe]\!-\!\!-\![P]$$
$$0.07 \quad 0.88 \qquad -0.18 \quad 0.86 \qquad -0.13 \quad 0.81$$
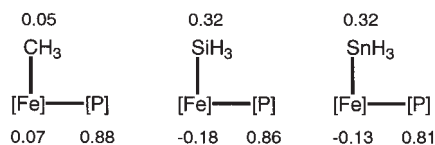
Fɪɢ. 6. Mulliken charge distribution where [Fe] and [P] stand for Cp(CO)Fe and $P(NHCH_2)_2$, respectively.

energy profile is obtained for SiH_3 migration with a 15.0 kcal/mol activation barrier. Endothermicity may results in large activation energies.

The 1,2-migration of methyl from Fe to P is highly favorable due to an exothermic reaction and the very small activation energy, whereas the 1,2-migrations of silyl and stannyl are endothermic and have relatively large activation energy. Theoretical studies have pointed out the following three reasons. (i) The $Fe\!-\!EH_3$ bond energy (kcal/mol) is in the order $Fe\!-\!CH_3$ (31.8) $<$ $Fe\!-\!SnH_3$ (36.3) $<$ $Fe\!-\!SiH_3$ (41.7). The Fe–C bond that is broken in the reactant is weaker than the Fe–Si and Fe–Sn bonds. (ii) The $P\!-\!EH_3$ bond energy (kcal/mol) is in the order $P\!-\!CH_3$ (93.7) $>$ $P\!-\!SiH_3$ (81.49) $>$ $P\!-\!SnH_3$ (72.1). The P–C bond that is formed in the product is stronger than the P–Si and P–Sn bonds. (iii) The Mulliken charges are depicted in Fig. 6. The CH_3 group shows a very small positive charge compared to SiH_3 and SnH_3, suggesting that the Coulombic repulsion between the migrating group and the phosphenium moiety is a minimum in the CH_3 migration.

In 1,3-methyl migrations for $[Cp(CO)(SnH_2CH_3)Fe\{P(NHCH_2)_2\}]^+$, the energy diagram (**69 → 70 → 71**) in kcal/mol and the optimized structures are shown in Fig. 7. The migration takes place through **70**. The energy barrier was estimated to be 32.7 kcal/mol. Similar energy diagrams were obtained with higher energies (42.7 kcal/mol) for the SiH_2CH_3 complex and 51.7 kcal/mol for the CH_2CH_3 complex. These relatively high activation energies suggest that these reactions are quite unlikely to occur. Among them a moderate barrier of 32.7 kcal/mol for the 1,3-methyl migration from SnH_2 shows the possibility of this reaction, which is consistent with the experimental results.

In the 1,3-methyl migrations, essentially $C\!-\!CH_3$, $Si\!-\!CH_3$, and $Sn\!-\!CH_3$ bonds are broken. These bond energies (kcal/mol) are in the order $C\!-\!CH_3$ (90.4) $>$ $Si\!-\!CH_3$ (86.6) $>$ $Sn\!-\!CH_3$ (69.9). During the course of the 1,3-methyl migrations, the Fe–C, Fe–Si, and Fe–Sn bonds become stronger Fe=C, Fe=Si, and Fe=Sn bonds by 45, 40, and 34 kcal/mol, respectively. The Coulombic factors are almost the same for these three reactions. Therefore, if only the Fe=E bond formation energies are considered, the migration from CH_2 would be the most exothermic. However, concerning
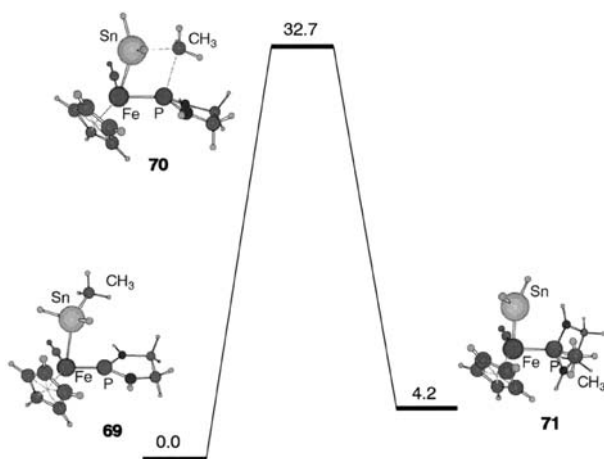
FIG. 7. Energy diagram (kcal/mol) of 1,3-migration of CH_3 from SnH_2 to phosphenium P in iron complex.
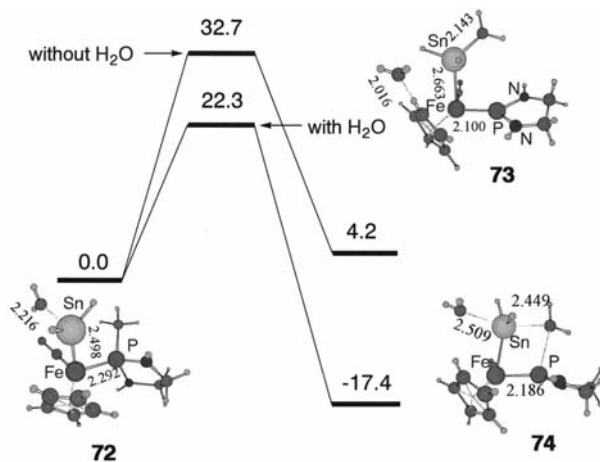
FIG. 8. Energy diagram (kcal/mol) of H_2O-mediated 1,3-migration of CH_3 from SnH_2 to phosphenium P in iron complex.

the bonds (E–C) to be broken, the Sn–C bond is weaker than the C–C and Si–C bond by 20 and 17 kcal/mol, respectively. The large difference indicates that because of the weak Sn–C bond, methyl migration from SnH_2 is the least endothermic.

 If the calculation is conducted in the presence of water as a simple base, the methyl 1,3-migration from Sn becomes exothermic and the activation energies are reduced by the coordination of water oxygen to the hetero atoms (**72 → 73 → 74**) (Fig. 8).

VII

COMPARISON BETWEEN CATIONIC PHOSPHENIUM COMPLEXES AND SILYLENE COMPLEXES

A. *General Considerations*

As mentioned above, cationic phosphenium is isoelectronic with carbene, silylene, germylene, stannylene, and plumbylene, because the central element has lone pair electrons and a vacant p orbital as well as two substituents. Therefore, their transition metal complexes have attracted considerable attention. It might be of special interest to compare cationic phosphenium complexes with silylene complexes because phosphorus and silicon are both situated in the third row of the periodic table.

B. *Base Stabilized Complexes*

A cationic phosphenium complex has positive charge. It has been estimated that the positive charge is located on the phosphorus atom to considerable extent and that the central metal is electronically neutral or slightly negative.[51,52] With regard to silylene complexes, strong $M^{\delta+} = Si^{\delta-}$ polarization has been reported.[53,54] Therefore, these species are expected to form an adduct with a 2e-donor base such as an amine or ether [Eq. (24)].

$$M = E \diagup \quad + \quad base \quad \longrightarrow \quad M = E \diagdown^{base} \quad \quad (24)$$

All cationic phosphenium complexes reported to date are base-free species. In contrast, silylene complexes tend to be stabilized by forming base adducts. Most silylene complexes are base-stabilized species[54–59] and base-free silylene complexes are still rare.[59–63] Typical examples are shown in Scheme 7. A phosphite–phosphenium complex exists in a solid state and even in solution, and does not take an OMe bridging form between the two P atoms,[64] whereas a silyl–silylene complex is not detected, but exists as an OMe bridging form between the two Si atoms.[65]

There are two plausible reasons explaining the difference. One is based on the difference in the substituents on the heteroatom. The substituents on a silylene ligand are alkyl and/or aryl groups, whereas those on a cationic phosphenium ligand are amino and/or alkoxy groups. Hetero
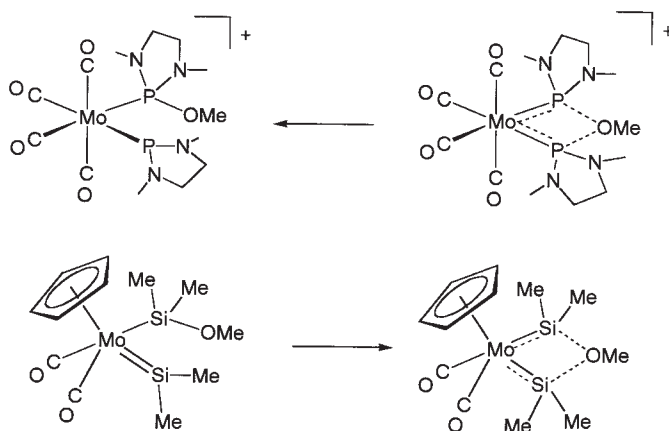
SCHEME 7

atoms may provide some electron density into the empty p orbital of phosphenium phosphorus. This would not lead to base-stabilized phosphenium complex formation. The other is the inherent character of P and Si. The real reason is not clear now, but should be an interesting point for further study.

C. 1,2-Alkyl Migration (Scheme 8)

1,2-Alkyl migration from a transition metal to phosphenium P has been demonstrated experimentally,[22–24,35,37] and calculation studies for an iron complex showed that it is exothermic by 14.4 kcal/mol with an activation energy of 3.6 kcal/mol.[52] Examples of 1,2-alkyl migration from a transition metal to silylene Si are still rare.[66–69] An MO calculation for the migration in Eq. (25) shows exothermicity by 22.4 kcal/mol and 3.8 kcal/mol of activation energy.[69]

$$(25)$$
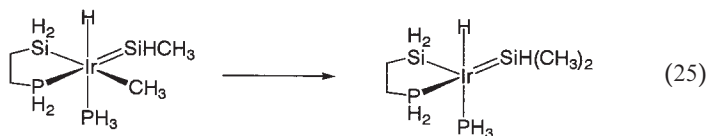
With 1,2-alkyl (or aryl) migration from a coordinating phosphorus compound to a transition metal, some examples[70–72] and theoretical
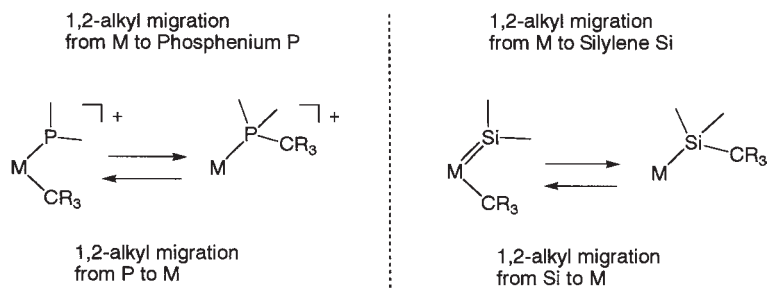
SCHEME 8

studies[73] have been reported. In contrast, the 1,2-alkyl migration from a silyl ligand to a transition metal is quite rare.[74,75]

D. *1,2-Silyl Migration (Scheme 9)*

Cationic phosphenium complexes of Fe and Ru, $[Cp(CO)(SiMe_3)$-$M\{P(NMeCH_2)_2\}]^+$, are stable unless exposed to air, and do not show 1,2-silyl migration from M to P.[23,24,43] The reverse reaction, that is, silyl migration from P to M has not been reported to date. 1,2-Silyl migration from M to silylene Si is postulated.[76] In contrast, there are many reports of 1,2-silyl migration from Si to M.[54,59,76] This reaction has been used to prepare silylene complexes.

E. *1,3-Alkyl Migration (Scheme 10)*

1,3-Alkyl migration from a silyl ligand to phosphenium P is demonstrated not to be feasible.[52] In contrast, 1,3-alkyl migration from a silyl ligand to silylene Si is widely known because it is involved in scrambling of substituents on silanes through silyl(silylene) complexes.[54,59,76] An energy diagram for 1,3-methyl migration from Si to phosphenium P and silylene Si is shown in Fig. 9. The activation energy for the migration to P is more than 3 times larger than that for the migration to Si.

There are three more 1,3-migrations which should be noted. One is 1,3-OR, -SEt, and -NR$_2$ migration from a tertiary phosphine to phosphenium P (from **32** to **31** in Scheme 1).[33] Another one is 1,3-alkyl migration from a stannyl ligand to phosphenium P (from **36** to **39** in Scheme 2).[23,24,34,36,48] In this reaction, a phosphenium complex is converted into a stannylene complex. This reaction corresponds to migration of a double bond from M=P to M=Sn. The last one is 1,3-alkoxy migration from a phosphite

1,2-silyl migration
from M to Phosphenium P

1,2-silyl migration
from M to Silylene Si

1,2-silyl migration
from P to M

1,2-silyl migration
from Si to M

SCHEME 9

1,3-alkyl migration
from Si to Phosphenium P

1,3-alkyl migration
from Si to Silylene Si
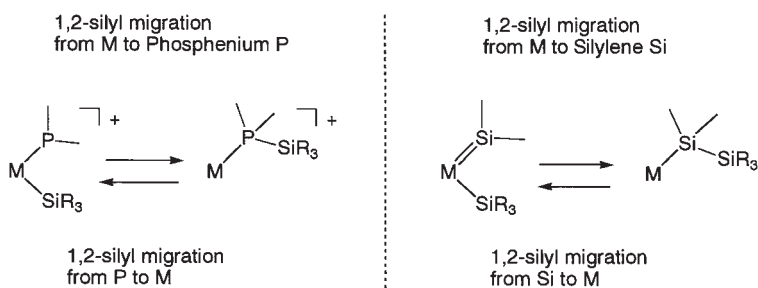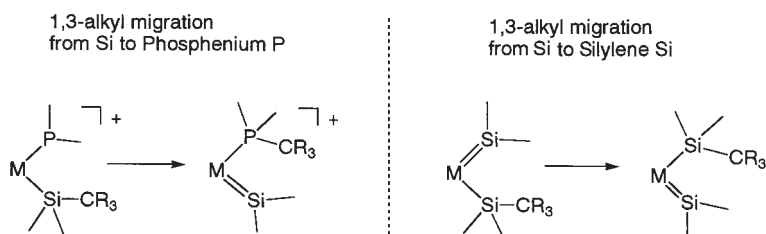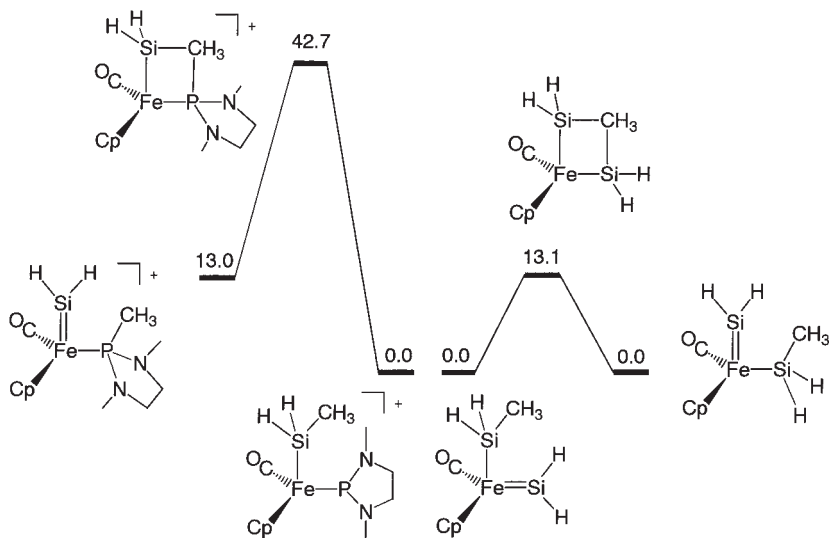
SCHEME 10

FIG. 9. Energy diagram (kcal/mol) of 1,3-migration of CH_3 from SiH_2 to phosphenium and silylene in iron complex.

1,3-alkoxy migration from a phosphite
ligand to silylene Si
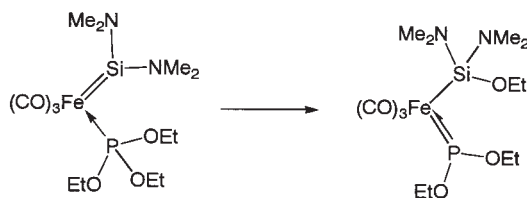
SCHEME 11

ligand to a silylene ligand (Scheme 11).[77,78] The photo-reaction of
$Fe(CO)_4\{P(OEt)_3\}$ with $HSi(NMe_2)_3$ has been reported to yield
$Fe(CO)_3\{P(OEt)(NMe_2)_2\}\{Si(OEt)_2 \cdot NHMe_2\}$. It has been proposed that
OEt migration from phosphite to silylene Si is involved.

VIII

CONCLUDING REMARKS

Since the first transition metal complex with a cationic phosphenium
ligand was reported in 1978, about a quarter of century has passed. More
than 70 phosphenium complexes have been synthesized and characterized,
and their spectroscopic data as well as X-ray structures demonstrated
that there is considerable double bond character between a transition
metal and a phosphenium phosphorus. Some interesting reactivities
have been observed involving 1,3-OR, -SR, and -NR_2 migration from
a tertiary phosphorus ligand to phosphenium P, 1,2-alkyl migration from a
transition metal to phosphenium P, and 1,3-alkyl migration from a stannyl
ligand to phosphenium P. Some theoretical considerations have also been
reported. Although considerable knowledge of phosphenium complexes
has accumulated, there are many unanswered questions. Investigation on
reactivity of phosphenium complexes with various reagents involving
heteroatom(s) remains to be done. Moreover, based on understandings
described here, an effort should be made to find reaction systems where
phosphenium complexes are involved in catalytic cycles.

REFERENCES

(1) Fleming, S.; Lupton, M. M.; Jekot, K. *Inorg. Chem.* **1972**, *11*, 2534.
(2) Montgomery, R. G.; Sauer, D. T.; Fleming, S. Sr.; Bennet, D. W.; Thomas, M. G.; Parry, R. W. *J. Am. Chem. Soc.* **1978**, *100*, 2231.
(3) Cowley, A. H.; Kemp, R. A. *Chem. Rev.* **1985**, *85*, 367.
(4) Sanchez, M.; Mazieres, M. R.; Lamande, L.; Wolf, R. (M. Regitz, O. J. Schere, Eds.) *Multiple Bonds and Low Coordination Chemistry*, Thieme, New York, 1990. Chapter D1.
(5) Schmodpeter, A. (M. Regitz, O. J. Schere, Eds.) *Multiple Bonds and Low Coordination Chemistry*, Thieme, New York, 1990. Chapter D2.
(6) Gudat, D. *Coord. Chem. Rev.* **1997**, *163*, 71.
(7) Nakazawa, H. *J. Organomet. Chem.* **2000**, *611*, 349.
(8) McNamara, W. F.; Duesler, E. N.; Paine, R. T.; Ortiz, J. V.; Kölle, P.; Nöth, H. *Organometallics* **1986**, *5*, 380.
(9) Hutchins, L. D.; Reisachen, H.-U.; Wood, G. L.; Duesler, E. N.; Paine, R. T. *J. Organomet. Chem.* **1987**, *335*, 229.
(10) Lang, H.; Leise, M.; Zsolnai, L. *J. Organomet. Chem.* **1990**, *389*, 3325.
(11) Malisch, W.; Hirth, U.-A.; Bright, T. A.; Köb, H.; Erter, T. S.; Hückmann, S.; Bertagnolli, H. *Angew. Chem. Int. Ed. Engl.* **1992**, *31*, 1525.
(12) Bennet, D. W.; Parry, R. W. *J. Am. Chem. Soc.* **1979**, *101*, 755.
(13) Snow, S. S.; Jiang, D.-X.; Parry, R. W. *Inorg. Chem.* **1987**, *26*, 1629.
(14) Cowley, A. H.; Kemp, R. A.; Wilburn, J. C. *Inorg. Chem.* **1981**, *20*, 4293.
(15) Baxter, S. G.; Collins, A. H.; Cowley, A. H.; Sena, S. F. *Inorg. Chem.* **1983**, *22*, 3475.
(16) Muetterties, E. L.; Kirner, J. F.; Evans, W. J.; Watson, P. L.; Abdel-Meguid, S.; Tavanaiepour, I.; Day, V. W. *Proc. Natl. Acad. Sci. USA* **1978**, *75*, 1056.
(17) Choi, H. W.; Gavin, R. M.; Muetterties, E. L. *J. Chem. Soc., Chem. Commun.* **1979**, 1085.
(18) Day, V. W.; Tavanaiepour, I.; Abdel-Meguid, S.; Kirner, J. F.; Goh, L.-Y. *Inorg. Chem.* **1982**, *21*, 657.
(19) Nakazawa, H.; Ohta, M.; Miyoshi, K.; Yoneda, H. *Inorg. Chem.* **1988**, *27*, 973.
(20) Nakazawa, H.; Ohta, M.; Miyoshi, K.; Yoneda, H. *Organometallics* **1989**, *8*, 638.
(21) Nakazawa, H.; Yamaguchi, Y.; Miyoshi, K. *J. Organomet. Chem.* **1994**, *465*, 193.
(22) Nakazawa, H.; Yamaguchi, Y.; Mizuta, T.; Ichimura, S.; Miyoshi, K. *Organometallics* **1995**, *14*, 4635.
(23) Nakazawa, H.; Yamaguchi, Y.; Kawamura, K.; Miyoshi, K. *Organometallics* **1997**, *16*, 4626.
(24) Kawamura, K.; Nakazawa, H.; Miyoshi, K. *Organometallics* **1999**, *18*, 4785.
(25) Yamaguchi, Y.; Nakazawa, H.; Itoh, T.; Miyoshi, K. *Bull. Chem. Soc. Jpn.* **1996**, *69*, 983.
(26) Gudat, D.; Nieger, M.; Niecke, E. *J. Chem. Soc. Dalton Trans.* **1989**, 693.
(27) Oberdörfer, R.; Nieger, M.; Niecke, E. *Chem. Ber.* **1994**, *127*, 2397.
(28) Arbams, M. B.; Scott, B. L.; Backer, R. T. *Organometallics* **2000**, *19*, 4944.
(29) Gudat, D.; Haghverdi, A.; Nieger, M. *J. Organomet. Chem.* **2001**, *617*, 383.
(30) Mizuta, T.; Yamasaki, T.; Nakazawa, H.; Miyoshi, K. *Organometallics* **1996**, *15*, 1093.
(31) Reisacher, H.-U.; Duesler, E. N.; Paine, R. T. *J. Organomet. Chem.* **1998**, *564*, 13.
(32) Nakazawa, H.; Yamaguchi, Y.; Mizuta, T.; Miyoshi, K. *Organometallics* **1995**, *14*, 4173.

(33) Yamaguchi, Y.; Nakazawa, H.; Kishishita, M.; Miyoshi, K. *Organometallics* **1996**, *15*, 4383.

(34) Nakazawa, H.; Yamaguchi, Y.; Miyoshi, K. *Organometallics* **1996**, *15*, 1337.

(35) Nakazawa, H.; Kishishita, M.; Yoshinaga, S.; Yamaguchi, Y.; Mizuta, T.; Miyoshi, K. *J. Organomet. Chem.* **1997**, *529*, 423.

(36) Nakazawa, H.; Kishishita, M.; Ishiyama, T.; Mizuta, T.; Miyoshi, K. *J. Organomet. Chem.* **2001**, *617*, 453.

(37) Nakazawa, H.; Kishishita, M.; Nakamoto, T.; Nakamura, N.; Ishiyama, T.; Miyoshi, K. *Chem. Lett.* **2000**, 230.

(38) Breit, B. *J. Mol. Catal.* **1999**, *143*, 143.

(39) Brookhart, M.; Studabaker, W. B. *Chem. Rev.* **1987**, *87*, 411.

(40) Davies, S. G.; Dordor-Hedgecock, I. M.; Sutton, K. H.; Whittaker, M. *J. Am. Chem. Soc.* **1987**, *109*, 5711.

(41) Guerchais, V.; Astruc, D.; Nunn, C. M.; Cowley, A. M. *Organometallics* **1990**, *9*, 1036.

(42) Vargas, R. M.; Theys, R. D.; Hossain, M. M. *J. Am. Chem. Soc.* **1992**, *114*, 777.

(43) Kawamura, K.; Nakazawa, H.; Miyoshi, K. *Organometallics* **1999**, *18*, 1517.

(44) Nakazawa, H.; Yamaguchi, Y.; Miyoshi, K.; Nagasawa, A. *Organometallics* **1996**, *15*, 2517.

(45) Cowley, A. H.; Kemp, R. A. *J. Organomet. Chem.* **1984**, *265*, C19.

(46) Cowley, A. H.; Cushner, M. C.; Lattman, M.; McKee, M. L.; Szobota, J. S.; Wilburn, J. C. *Pure Appl. Chem.* **1980**, *52*, 789.

(47) Trinquler, G.; Marre, M.-R. *J. Phys. Chem.* **1983**, *87*, 1903.

(48) Schoeller, W. W.; Busch, T. *Chem. Ber.* **1990**, *123*, 971.

(49) Suresh, C. H.; Koga, N. *Inorg. Chem.* **2000**, *39*, 3718.

(50) Gudat, D.; Haghverdi, A.; Hupfer, H.; Nieger, M. *Chem. Eur. J.* **2000**, *6*, 3414.

(51) Takano, K.; Tsumura, H.; Nakazawa, H.; Kurakata, M.; Hirano, T. *Organometallics* **2000**, *19*, 3323.

(52) Suresh, C. H.; Koga, N. *Organometallics* **2001**, *20*, 4333.

(53) Wada, H.; Tobita, H.; Ogino, H. *Organometallics* **1997**, *16*, 2200.

(54) Okazaki, M.; Tobita, H.; Ogino, H. *J. Chem. Soc. Dalton Trans.* **2003**, 493.

(55) Zybill, C.; Müller, G. *Angew. Chem. Int. Ed. Engl.* **1987**, *26*, 669.

(56) Straus, D. A.; Tilley, T. D. *J. Am. Chem. Soc.* **1987**, *109*, 5872.

(57) Ueno, K.; Tobita, H.; Shimoi, M.; Ogino, H. *J. Am. Chem. Soc.* **1988**, *110*, 4092.

(58) Tobita, H.; Ueno, K.; Shimoi, M.; Ogino, H. *J. Am. Chem. Soc.* **1990**, *112*, 3415.

(59) Ogino, H. *The Chemical Record* **2002**, *2*, 291.

(60) Straus, D. A.; Grumbine, S. D.; Tilley, T. D. *J. Am. Chem. Soc.* **1990**, *112*, 7801.

(61) Gehrhus, B.; Hitchcock, P. B.; Lappert, M. F.; Maciejewski, H. *Organometallics* **1998**, *17*, 5599.

(62) Mork, B. V.; Tilley, T. D. *J. Am. Chem. Soc.* **2001**, *123*, 9702.

(63) Ueno, K.; Asami, S.; Watanabe, N.; Ogino, H. *Organometallics* **2002**, *21*, 1326.

(64) Nakazawa, H., Miyoshi, Y., Katayama, T, Miyoshi, K. unpublished results.

(65) Ueno, K.; Masuko, A.; Ogino, H. *Organometallics* **1999**, *18*, 2694.

(66) Okazaki, M.; Tobita, H.; Ogino, H. *J. Chem. Soc. Dalton Trans.* **1997**, 3531.

(67) Okazaki, M.; Tobita, H.; Ogino, H. *J. Chem. Soc. Dalton Trans.* **1997**, 4829.

(68) Ozawa, F.; Kitaguchi, M.; Katayama, H. *Chem. Lett.* **1999**, 1289.

(69) Private communication from a research group led by Tobita, H. in Tohoku University.

(70) Garrou, P. E. *Chem. Rev.* **1985**, *85*, 171.

(71) Leeuwen, P. W. N. M.; Roobeek, C. F.; Orpen, A. G. *Organometallics* **1990**, *9*, 2179.

(72) Grushin, V. V.; Vymenits, A. B.; Yanovsky, A. I.; Struchkov, Y. T.; Vol'pin, M. E. *Organometallics* **1991**, *10*, 48.

(73) Ortiz, J. V.; Havlas, Z.; Hoffmann, R. *Helv. Chim. Acta* **1984**, *67*, 1.
(74) Burger, P.; Bergman, R. G. *J. Am. Chem. Soc.* **1993**, *115*, 10462.
(75) Klei, S. R.; Tilley, T. D.; Bergman, R. G. *Organometallics* **2001**, *20*, 3220.
(76) Sharma, H. K.; Pannel, K. H. *Chem. Rev.* **1995**, *95*, 1351.
(77) Bodensieck, U.; Braunstein, P.; Deck, W.; Faure, T.; Knorr, M; Stern, C. *Angew. Chem. Int. Ed. Engl.* **1994**, *33*, 2440.
(78) Braunstein, P.; Knorr, M; Stern, C. *Coord. Chem. Rev.* **1998**, *178–180*, 903.

Synthesis of Organosilicon Compounds by New Direct Reactions

BOK RYUL YOO and IL NAM JUNG

Organosilicon Chemistry Laboratory, Korea Institute of Science & Technology,
P.O. Box 131, Cheongryang, Seoul 130-650, Korea

I

INTRODUCTION

Si–C bond-forming reactions are the foundation of organosilicon chemistry and the silicone industry. Even though silicon (26%) is the second most abundant element after oxygen (49.5%) in the earth's crust, it is found in the form of silica and silicate minerals because of the high Si–O bond strength of 108 kcal/mol.[1a] There is little evidence that organosilicon compounds occur in nature. Organosilicon compounds are manmade

145

materials and have to be synthesized. The development of methodologies for forming Si–C bonds started in the 19th century.[1b,c] Historically, the alkylation of chlorosilanes using a variety of organometallic reagents such as organomagnesium halides,[2] organozinc, organomercury, organolithium, organosodium, organopotassium reagents, etc.[3] has been widely used for the preparation of organosilicon compounds in the laboratory since Friedel and Crafts reported the reaction of tetrachlorosilane with ethyl zinc to afford tetraethylsilane as the first Si–C coupling product in 1863 [Eq. (1)].[1b]

$$2 \, Zn(C_2H_5)_2 + SiCl_4 \rightarrow Si(C_2H_5)_4 + 2 \, ZnCl_2 \qquad (1)$$

Important advances in the synthesis of organosilicon compounds were made by F. S. Kipping who used Grignard reagents to replace chlorine groups on the silicon atom with hydrocarbon substituents (Eq. 2).[2] While his work provided a basis for the modern chemistry of organosilanes, the Grignard reaction is not a good synthetic method for large scale production of simple organosilanes useful to the silicone industry, because it requires flammable ether solvents and it is difficult to isolate the major product from byproducts and salts formed during the reaction.

$$-\underset{|}{\overset{|}{Si}}-Cl \; + \; R\text{-}Mg\text{-}X \; \longrightarrow \; -\underset{|}{\overset{|}{Si}}-R \; + \; MgXCl \qquad (2)$$
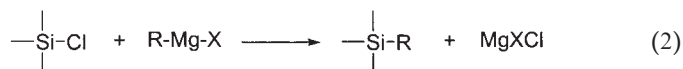
In 1940, E. G. Rochow discovered the direct reaction of elemental silicon with simple organic chlorides such as methyl chloride in the presence of copper catalyst to give methychlorosilanes. Since that discovery, the direct synthesis of organochlorosilanes from elemental silicon and organic chlorides has been intensively studied and the reaction has become the most widely used basic technique for the synthesis of simple organosilicon chlorides.[4–8] Subsequently, the hydrosilylation of unsaturated molecules with hydrosilanes[9–11] was developed and is also now of considerable industrial significance. Two new methods for organic substituents introduction to silicon have been recently developed and are expected to become commercially important processes. New methods for organic substituent-introducing to silicon atom recently developed are the dehydrochlorinative Si–C coupling reaction of alkyl halides[12,13] with hydrochlorosilanes and the double silylation of olefins with hydrosilanes[14] in the presence of organophosphonium salt as catalyst. By this catalytic coupling reaction, a wide variety of silyl-functionalized compounds may be prepared easily and in good yields.

Today's silicone industry is based on the direct reaction, which does not require a preformed organometallic reagent and a flammable solvent and

does not generate large quantities of metal halide. About 90% of the starting materials for the silicone industry are prepared by the direct reaction and the other portion by hydrosilylation reactions. Methylchlorosilanes, in particular dimethyldichlorosilane, the most important starting materials for the production of silicones, are produced by the direct reaction of elemental silicon with methyl chloride (Eq. 3).[4] Besides methyl chloride, the direct reaction of simple organic halides such as phenyl chloride and vinyl chloride has been also practiced on a large scale in industry.[7]

$$2\ CH_3Cl\ +\ Si\ \xrightarrow{\ Cu\ }\ (CH_3)_2SiCl_2 \tag{3}$$
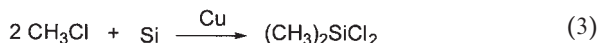
Although the direct reaction of elemental silicon with methyl chloride shown in Eq. (3) looks simple, it is a complicated reaction and gives many kinds of byproducts.[7,8] The yield of methylchlorosilane obtained from the direct reaction varies, and depends upon the reaction conditions such as temperature, pressure, flow rate of reactants, and other processing conditions including particle size and impurities of elemental silicon, catalyst, promoter, reactor type, etc.[7]

The direct reaction of elemental silicon with methyl chloride is usually carried out at around 300 °C to give 90% selectivity for dimethyldichlorosilane, while the carbon (sp^2-orbital)–chlorine bonds of chlorobenzene and vinyl chloride require more severe process conditions due to their lesser reactivity.[7] The selectivity of diorganosilicon dichlorides from these reactions are lower than that of dimethyldichlorosilane due to the decomposition of the starting materials at the higher reaction temperatures. For the direct reaction of chlorobenzene, silver is known as a superior catalyst to copper.[7,8] Although many organic halides have been applied for the syntheses of organochlorosilanes, alkyl chlorides other than methyl, phenyl, and vinyl chloride have not been used on a large scale in industry due to side reactions and low yields.[7,8]

Activated organic chlorides such as allyl choloride,[15] benzyl chloride,[16] polychloromethanes (methylene chloride[17,18] and chloroform[19]) have also been studied for the direct reaction with elemental silicon. As expected from their molecular structures having activation groups such as vinyl, phenyl, and chlorine next to the C–Cl bond, they are more reactive than methyl chloride, and react at lower temperatures. However, they undergo side reactions such as the elimination of hydrogen chloride, and give very poor yields. Carbon deposition resulting from decomposition and the production of polymeric products from the reaction of polychloromethanes on the surfaces of the silicon and copper catalysts deactivate the catalysts, resulting in loss of reactivity.[7,8]

Recently, it has been reported that organochlorosilanes having Si–C–Si linkages can be sucessfully synthesized by the direct reaction of elemental silicon with (chloromethyl)silanes[20] and with mixtures of (chloromethyl) silanes[21] or organic polychlorides[22–25] and excess hydrogen chloride. Hydrogen chloride-incorporated reactions of elemental silicon and activated alkyl chlorides[26,27] afford H–Si group(s)-containing chlorosilanes in relatively good yields. In such direct reactions, the decomposition of starting materials is suppressed and the deactivation problem of solid reactants due to polymer production was avoided.

Thousands of papers and patents have appeared on the direct synthesis of organochlorosilanes since 1940 when Rochow reported the direct reaction.[4] These results are comprehensively accounted for in a number of earlier reviews and books.[3–8] The purpose of this review is to describe the recent developing trend of the direct reaction of elemental silicon with activated or unactivated alkyl chlorides, in particular, emphasizing direct reactions with a mixture of hydrogen chloride and activated alkyl chlorides such as polychlorinated methanes, silylmethyl chlorides and dichlorides, allyl chloride, etc.

II

DIRECT REACTION OF ELEMENTAL SILICON WITH
ALKYL CHLORIDES

A. *Reaction with Methyl Chloride and its Mechanism*

Among the direct reactions of elemental silicon with a variety of alkyl chlorides, the reaction with methyl chloride has been intensively studied and utilized in both the laboratory and industry.[4,7,8] The distribution of methylchlorosilane products resulting from the direct reaction largely depends on the catalysts used, which are mostly transition metals. For example, dimethyldichlorosilane is obtained as the major product from the reaction using copper[1,7,8] or iron[28] catalysts, while methyldichlorosilane is the major product with lead catalyst,[29] and methyltrichlorosilane with tin catalyst,[29] and trimethylchlorosilane with calcium catalyst.[28] In particular, the direct reaction using methyl chloride in the presence of copper for selective dimethyldichlorosilane formation[7,30] has been well-studied and has led to an understanding of the direct reaction mechanism of alkyl halides.[7,8]

The direct reaction of elemental silicon with methyl chloride in the presence of copper affords dimethyldichlorosilane as the major product

along with other methylchlorosilanes (Me_nSiCl_{4-n}, $n = 1$, 3) and a variety of other silanes (Eq. 4): other monosilanes include Me_4Si, hydrogen-containing chlorosilanes such as Me_2SiHCl, $MeSiHCl_2$, H_nSiHCl_{4-n} ($n = 0$, 1, 2), and R_nSiCl_{4-n} (R > CH_3).[1a,31]

$$CH_3{-}CL + Si \xrightarrow{Cu} \underset{\text{main product}}{Cl{-}\underset{\underset{CH_3}{|}}{\overset{\overset{CH_3}{|}}{Si}}{-}Cl} + CH_3{-}\underset{\underset{CH_3}{|}}{\overset{\overset{CH_3}{|}}{Si}}{-}Cl + Cl{-}\underset{\underset{Cl}{|}}{\overset{\overset{CH_3}{|}}{Si}}{-}Cl + others \quad (4)$$
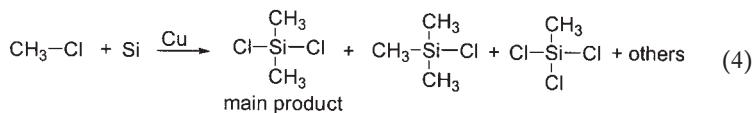
In addition to such monosilanes, many other higher molecular-weight compounds are also produced: disilanes ($Cl_{3-m}Me_mSiSiMe_nCl_{3-n}$: $m = 3, 2$, 1, 0; $n = 3, 2, 1, 0$), silaalkanes [$(Me_nSiCl_{3-n})_mCH_{4-m}$, $(SiCH_2CH_2Si)$ Me_nCl_{6-n}, and $Me_n(SiCH_2SiCH_2Si)Cl_{8-n}$], siloxanes ($Me_2HSiOSiHMe_2$, $Me_nCl_{6-n}Si_2O$), some hydrocarbons (CH_4, C_2H_6, C_2H_4), and H_2[8] indicating that it is a complex process. The composition of the products largely depends on reaction conditions such as the reaction temperature, catalyst, promoters, etc. Compounds containing two or more silicon atoms have high boiling points with high molecular weights. The disilane fraction can be converted to useful methylchlorosilanes by further reaction with HCl, Cl_2, alkyl chloride, etc.[7,8,32,33]

Many studies on the direct reaction of methyl chloride with silicon–copper contact mass and other metal promoters added to the silicon–copper contact mass have focused on the reaction mechanisms.[7,8] The reaction rate and the selectivity for dimethyldichlorosilane in this direct synthesis are influenced by metal additives, known as promoters, in low concentration. Aluminum, antimony, arsenic, bismuth, mercury, phosphorus, phosphine compounds[34] and their metal complexes,[35,36] Zinc,[37–39] tin[38–40] etc. are known to have beneficial effects as promoters for dimethyldichlorosilane formation.[7,8] Promoters are not themselves good catalysts for the direct reaction at temperatures < 350 °C,[6,8] but require the presence of copper to be effective. When zinc metal or zinc compounds (0.03–0.75 wt%) were added to silicon–copper contact mass, the reaction rate was potentiated and the selectivity of dimethyldichlorosilane was enhanced further.[34] These materials are described as structural promoters because they alter the surface enrichment of silicon, increase the electron density of the surface of the catalyst modify the crystal structure of the copper–silicon solid phase, and affect the absorption of methyl chloride on the catalyst surface and the activation energy for the formation of dimethyldichlorosilane.[38,39] Cadmium is also a structural promoter for this reaction, but cadmium presents serious toxicity problems in industrial use on a large scale.[41,42] Other metals such as arsenic, mercury, etc. are also restricted because of such toxicity problems. In the direct reaction of methyl chloride, tin in

combination with zinc is also known to be a good promoter. Tin is termed a textural promoter, since it is effective in enhancing the reaction rate and selectivity for dimethyldichlorosilane only in combination with optimum content of zinc.[38–40] Lead is a potent inhibitor in the direct reaction, and thus preferably kept below 0.005 wt% in elemental silicon materials.[7,8,43]

The study of the mechanism for the heterogeneous reaction between a gas (methyl chloride) and a solid (silicon–copper phase) consisting of two different elements and involving several phases is fraught with difficulties.[8,44–52] Obviously, the initial reaction must occur on the surface of the silicon–copper catalyst. In order to understand heterogeneous catalysis, a good understanding of the surface nature of the silicon–copper phase is required. Many reports dealing with the analysis of the silicon–copper surface formed during the reaction with methyl chloride[1a,7,30,53–56] have been published and have led to a great understanding of the physicochemical events leading to the formation of dimethyldichlorosilane and other products as well. It has been proposed by many researchers that methylchlorosilylene (MeClSi:) or silylenoid intermediates are formed by the chemisorption of methyl chloride on the copper-activated silicon surface.[7,8,50,57,58] The desorption of this silylene intermediate MeClSi: provides insight into the reaction mechanism because dimethyldichlorosilane can selectively be formed by the reaction of absorbed MeCl with absorbed MeClSi: as required by Langmuir-Hinshelwood kinetics.[7,8,50,57] Lewis[7] and Falconer[30,33] provided strong evidence that the direct reaction of elemental silicon with CH_3Cl in the presence of copper catalyst proceeds by way of surface-confined silylenes: CH_3ClSi: as the $(CH_3)_2SiCl_2$ precursor and Cl_2Si: as the precursor for CH_3SiCl_3, with all other organosilicon products except $(CH_3)_4Si$ originating from silylene intermediates. Key experimental support was provided by trapping experiments in which a desorbed species of mass 78 (CH_3ClSi:) was identified using mass spectrometry following CH_3Cl chemisorption on silicon-enriched surfaces of a silicon–copper catalyst.[7] Lewis et al. proposed that an intermediate such as MeClSi: behaves like a silylene, generated in the gas phase, and inserts into the carbon–chlorine bond of adsorbed methyl chloride to give dimethyldichlorosilane (Scheme 1).[7,59,60]

The formation of other monomeric methylchlorosilanes can be explained by the insertion of the corresponding divalent silicon species (silylenes) such as Cl_2Si:, ClHSi:, Me_2Si:, MeHSi:, and etc. into C–Cl or H–Cl bonds (Scheme 1).[7,61–72] The formation energies of silylenes calculated by Bell et al. increase as follows: Cl_2Si: (−39.95 kcal/mol) < CH_3ClSi: (−13.59 kcal/mol) < ClHSi: (9.6 kcal/mol) < Me_2Si: (16.3 kcal/mol) < MeHSi: (35.8 kcal/mol).[73] Thus, the stabilities of such silylenes, generated from the direct reaction of

$$Cu^{\delta+}-Si^{\delta-} \ + \ CH_3Cl \longrightarrow \begin{array}{c} Cl\text{-----}CH_3 \\ \vdots \quad \vdots \\ Cu^{\delta+}-Si^{\delta-} \end{array}$$

$$\downarrow -Cu$$

$$CH_3SiH_2Cl \xleftarrow{\ H_2\ } [CH_3ClSi:] \xrightarrow{\ HCl\ } CH_3HSiCl_2$$

$$\downarrow CH_3Cl$$

$$(CH_3)_2SiCl_2$$

$$Cu^{\delta+}-Si^{\delta-} \ + \ X^1-X^2 \longrightarrow [:SiX^1X^2] \xrightarrow{\ HCl\ } HSiClX^1X^2$$

$$X^1, X^2 = Me, H, Cl \qquad\qquad \downarrow CH_3Cl$$

$$CH_3SiClX^1X^2$$
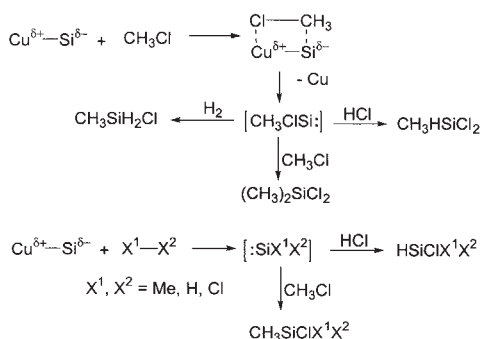
SCHEME 1. Silylene insertion reaction leading to the formation of methylchlorosilanes.

elemental silicon with methyl chloride in the presence of copper, decrease in the following order: $Cl_2Si: > HClSi: > (CH_3)_2Si: > CH_3HSi:$.[7,73] From the standpoint of efficient production of methylchlorosilanes, many studies have been carried out in industry.[34–36,74–77] In the formation of dimethyldichlorosilane, the observation of $CH_3ClSi:$ as a surface intermediate indicates that the rate-determing step of the direct reaction is its insertion into a C–Cl bond.

B. *Reaction with Long-Chained Alkyl Chlorides*

It is well-known that the direct processes for the synthesis of methylchlorosilanes and phenylchlorosilanes operate primarily on a large scale.[7,8] Mikhaylov *et al.*, reported that ethylchlorosilanes are also manufactured in the Soviet Union,[78] but the total production capacities of ethylchlorosilanes and ethylsilicones in the Soviet Union are unknown. The reaction of longer chain *n*-alkyl chlorides with elemental silicon gives alkylchlorosilanes in low yields due to the cracking and decomposition of the starting alkyl chlorides.[79] Under direct reaction conditions, those alkyl chlorides undergo dehydrochlorination reactions on the surface of silicon–copper contact mass to afford hydrogen chloride and alkene. It is well known that long-chain alkyl chlorides having hydrogen β to the C–Cl bond easily undergo β-elimination reactions during the direct reaction to give HCl and alkenes.[80,81] The hydrogen chloride formed participates simultaneously in the direct reaction to produce alkyldichlorosilanes having Si–H bonds.

In specific reaction conditions, formation of alkyldichlorosilanes with very high selectivity is observed from the reaction of elemental silicon with alkyl chlorides. For example, when a gaseous mixture of *n*-propyl chloride

and helium (inert gas) were fed in flow rates of 5 and 10 mmol/h into a reactor[82] charged with elemental silicon (7.1 mmol) and Cu(I)Cl (10 wt%) as a catalyst at 300 °C for 5 h, 2% of the silicon reactant was consumed to give *n*-propyldichlorosilane in 98% selectivity (Eq. 5).[82]

$$\text{(5)}$$
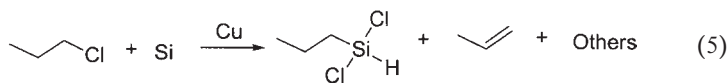
Under these reaction conditions, *n*-propyl chloride hardly decomposed to form propylene and hydrogen chloride with the amount of propylene being formed at a rate below 0.2 mmol/h. This probably accounts for the low silicon conversion, because hydrogen chloride is necessary for the formation of propyldichlorosilane.

When *iso*-propyl chloride was used instead of *n*-propyl chloride under the same reaction conditions as above, *iso*-propyldichlorosilane and other low boiling compounds were obtained (Eq. 6).

$$\text{(6)}$$
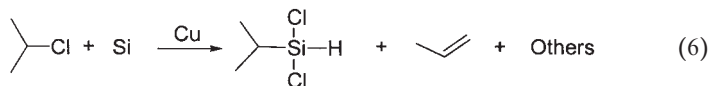
This reaction showed a greater reactivity than that involving *n*-propyl chloride. In a 5 h reaction period, *iso*-propyldichlorosilane in 85% selectivity was obtained with 86% consumption of elemental silicon.[82] In addition to *iso*-propyldichlorosilane, other products included isopropyltrichlorosilane, trichlorosilane, and dichlorosilane as minor components. These results indicate that the decomposition of isopropyl chloride to propylene and hydrogen chloride occurred. It seems likely that the hydrogen chloride reacted with elemental silicon to form the silicon–hydrogen bond containing intermediate, chlorosilylene (ClHSi:), followed by an insertion reaction with isopropyl chloride to give the *iso*-propyldichlorosilane product.

When reactions with *n*-, *sec*-, *iso*-, and *tert*-butyl chlorides were carried out under the same conditions for the *n*-propyl chloride reaction, butyldichlorosilanes were obtained as major products as observed in the analogous reactions of propyl chlorides. It has been reported that butyl chlorides undergo addition reactions to silylene intermediates to give the corresponding butylchlorosilane products.[68–72] Butene formation involving a zwitterion intermediate was proposed by Ishikawa *et al*. The tendency of alkyl chlorides to decompose to alkene and hydrogen chloride decreases

in the following order: *tert-* > *sec-* > *n*-alkyl chloride. The α,β-hydrogen chloride elimination of various alkyl chlorides on a copper catalyst has been reported.[80,81] The *sec-* and *tert*-butyl chlorides were more easily decomposed than *n*-butyl chloride to produce butenes and hydrogen chloride.

The decomposition rates of butyl chlorides decreased in the following order: *tert* > *sec* > *n*-butyl chloride. It is highly plausible that the formation of butene is caused by both the decomposition of butyl chloride over the copper surface and by the decomposition of zwitterion intermediate formed by the reaction of silylene on the surface of the silicon–copper contact mass with butyl chloride.[80,81] From the reaction with *n*-butyl chloride, *sec*-butyldichlorosilane is also obtained as a minor product along with *n*-butylchlorosilanes.[80]

The formation of *sec*-butyldichlorosilane can be explained by the reaction of elemental silicon with hydrogen chloride followed by insertion to 1-/2-butene resulting from the decomposition of *n*-butyl chloride, or by the reaction of elemental silicon with a gaseous mixture of hydrogen chloride and *sec*-butyl chloride formed by isomerization of *n*-butyl chloride under the direct reaction conditions. These results suggest that alkyldichlorosilane can be obtained both by the reaction of elemental silicon with a gaseous mixture of hydrogen chloride and alkyl chloride, and by the reaction of elemental silicon with a gaseous mixture of hydrogen chloride and alkene.[82]

In the direct reaction of cyclopentyl chloride using a stirred reactor equipped with a spiral band agitator (Fig. 1), cyclopentyl chloride was fed to the reactor containing the contact mass of elemental silicon (360 g) and Cu catalyst (40 g)/NiCl$_2$(dppb: 1,4-bis(diphenylphosphino)butane) promoter (0.7 g) at 260 °C to afford the corresponding cyclopentyl-containing chlorosilanes, cyclopentyldichlorosilane (21%) and cyclopentyltrichlorosilane (1%), along with cyclopentene (61%) (Eq. 7).[83]
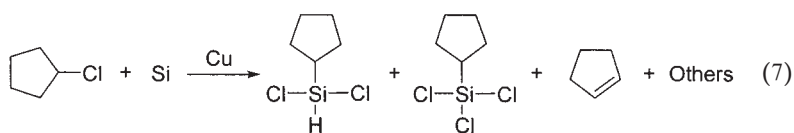
The main product, cyclopentyldichlorosilane, can be explained by the reaction of one equivalent of silicon with one equivalent of cyclopentyl chloride and hydrogen chloride. The hydrogen chloride used for the reaction should have been formed by the decomposition of cyclopentyl chloride.

1. Hydrogen Chloride   2. Nitrogen
3. Flowmeter   4. Preheater
5. Syringe Pump   6. Heating Wire
7. Insulation Jacket   8. Stirring Motor
9. Metal Inlet   10. Receiver
11. Cooler   12. Vent
13. Methyl Chloride
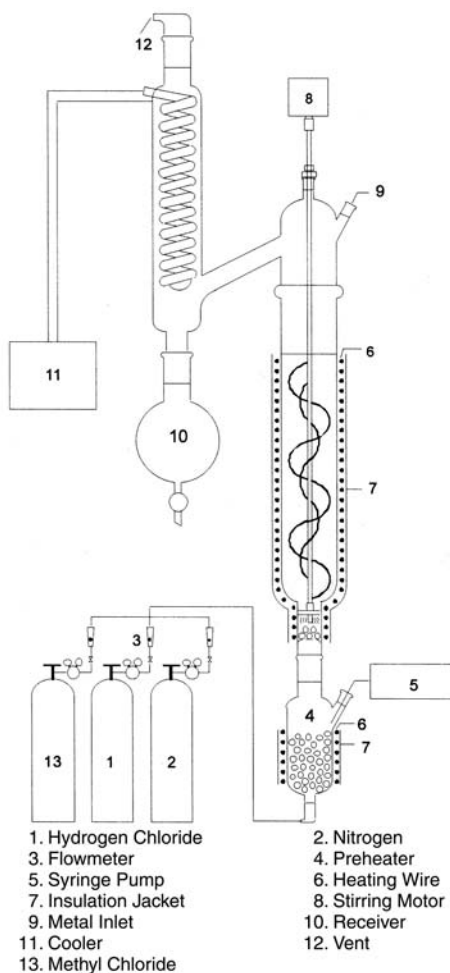
FIG. 1. Stirred bed reactor for direct reaction.

In this reaction, the decomposition of cyclopentyl chloride reactant was higher at 240 °C than at 260 °C. At higher reaction temperatures ranging from 280 to 300 °C, the total amounts of both cyclopentyl-containing chlorosilanes were similar to those at 260 °C, but the amount of cyclopentyltrichlorosilane increased slightly at higher temperatures. In this reaction, NiCl$_2$(dppb) was a good promoter for the preparation of cyclopentyldichlorosilane. This trend suggests that the optimum reaction temperature is 260 °C.

C. *Reaction with a Gaseous Mixture of Long-Chained Alkyl Chlorides and Hydrogen Chloride*

As described above, long-chain alkyl chlorides undergo α,β-elimination to give hydrogen chloride and alkene at the direct reaction temperature ($\doteq 300\,°C$). To increase the yield of alkylchlorosilanes from the direct reaction of elemental silicon with long-chain alkyl chlorides, this cleavage reaction must be suppressed. External addition of hydrogen chloride gas to the alkyl chloride reactants is expected to reduce the decomposition of long-chain alkyl chlorides. The effect of hydrogen chloride addition was studied using a stirred reactor equipped with a spiral band agitator (as shown in Fig. 1) at various reaction temperatures.[20]

As a mixture of *iso*-propyl chloride and hydrogen chloride was fed to a reactor containing the contact mass of elemental silicon (360 g) and Cu catalyst (40 g), *iso*-propyldichlorosilane was obtained as the major product along with *iso*-propyltrichlorosilane as a minor product (Eq. 8).[83]

$$\text{(CH}_3\text{)}_2\text{CHCl} \;+\; \text{HCl} \;+\; \text{Si} \;\xrightarrow{\text{Cu}}\; \text{Cl–Si(H)(}i\text{-Pr)–Cl} \;+\; \text{Cl–Si(Cl)(}i\text{-Pr)–Cl} \;+\; \text{Others} \qquad (8)$$
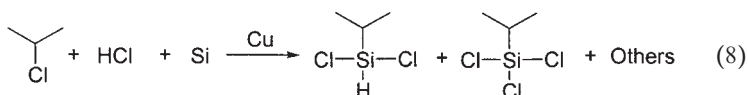
Other products were trichlorosilane and tetrechlorosilane, produced from the reaction of elemental silicon and hydrogen chloride. The formation of *iso*-propyldichlorosilane can be explained by the reaction of one equivalent of silicon with each equivalent of *iso*-propylchloride and hydrogen chloride.

At various temperatures ranging from 200 to 300 °C, *iso*-propyldichlorosilane was obtained in the highest yield at 220 °C, but decreased as the reaction temperature increased due to the decomposition of *iso*-propyl chloride. Under these reaction conditions, the yield of *iso*-propyldichlorosilane was higher compared to those obtained from the direct reaction without hydrogen chloride addition, indicating that the decomposition of *iso*-propyl chloride was suppressed as expected. The yields generally increased with increased ratios of hydrogen chloride to *iso*-propyl chloride.

The reaction of elemental silicon with a 1 : 2.5 mixture of *iso*-propyl chloride and hydrogen chloride using 0.17 wt% NiCl$_2$(dppb) as a promoter at 220 °C gave *iso*-propyldichlorosilane and *iso*-propyltrichlorosilane in 55 and 2% yields (based on *iso*-propyl chloride used), respectively. Zinc, known as a good promoter for the direct reaction of methyl chloride, was found to be an inhibitor in this reaction in addition to being an accelerator

of the decomposition of *iso*-propyl chloride. Tin was also shown to be a similar inhibitor. In contrast to the inhibiting zinc and tin, $NiCl_2(dppb)$ was found to be a good promoter and enhanced both the reactivity and selectivity for *iso*-propyldichlorosilane.

In the direct reaction of *n*-hexyl chloride, a 1:4 gaseous mixture of *n*-hexyl chloride and hydrogen chloride reacted with elemental silicon in the presence of copper/nickel catalyst at $280\,^\circ C$ to give the corresponding *n*-hexyl-containing chlorosilanes, *n*-hexyldichlorosilane (30%) and *n*-hexyltrichlorosilane (11%), along with 1-hexene (22%) (Eq. 9).[83]

$$(9)$$
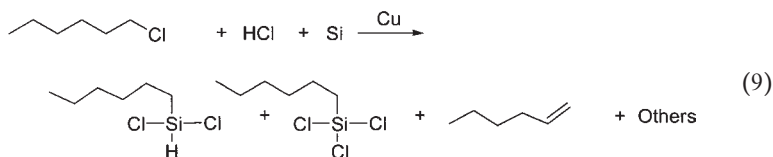
Unreacted *n*-hexyl chloride (11%) was recovered. The yield of *n*-hexyldichlorosilane increased from 14, 28, 30, to 41% as the ratio of hydrogen chloride/*n*-hexyl chloride increased from 1, 2, 4 to 8. However, a large excess of hydrogen chloride should be avoided because it increases the formation of byproducts such as trichlorosilane and tetrachlorosilane.

In this reaction, $NiCl_2(dppb)$ was also a good promoter for the preparation of *n*-hexyldichlorosilane. *tert*-Butyl chloride can be used instead of hydrogen chloride because it easily decomposes to give off hydrogen chloride. When *t*-butyl chloride was used, higher yields of *n*-hexyl containing chlorosilanes were obtained and the reaction using a 1:4 gaseous mixture of *n*-hexyl chloride and *t*-butyl chloride gave *n*-hexyldichlorosilane and *n*-hexyltrichlorosilane in 44 and 9% yields, respectively.

In the direct reation of cyclopentyl chloride, hydrogen chloride addition to the cyclopentyl chloride reactant did not have much effect but gave about the same result as without hydrogen chloride addition. This may be explained by the rapid decomposition of cyclopentyl chloride to provide enough hydrogen chloride to produce cyclopentyldichlorosilane.

D. *Reaction with Silylmethyl Chlorides*

In contrast to long-chain alkyl chlorides, silyl-group substituted methyl chlorides having no β-hydrogen do not decompose much under

the direct reaction conditions and react successfully with elemental silicon in the presence of copper catalyst to afford the Si–C coupled bis- or trisilaalkanes in good yields. The direct reaction of elemental silicon with a variety of silylmethyl chlorides 1 [$Cl_{3-n}Me_nSiCH_2Cl$: $n = 0$ (**a**), 1 (**b**), 2 (**c**), 3 (**d**)] in the presence of copper catalyst using a stirred reactor equipped with a spiral band agitator (Fig. 1) at various temperatures gave the corresponding trisilaalkanes **2a–d** and bis-silaalkanes **3a–d**.[20]

The formation of the expected 2,4,6-trisilaalkanes **2** can be explained by the 2:1 reaction of (chloromethyl)silanes **1** and elemental silicon. The byproducts, 1,3-disilaalkanes **3**, were obtained from the reaction of (chloromethyl)silane reactant **1** and hydrogen chloride (or chlorine) with the same silicon atom, as methyldichlorosilane (or methyltrichlorosilane) was obtained from the methyl chloride reaction. This result indicates that some of the (chloromethyl)silane reactant decomposed under the reaction conditions and acted as a chlorine or hydrogen chloride source. In the direct reaction of (chloromethyl)dimethylchlorosilane (**1c**), a significant amount of starting material was recovered at temperatures below 300 °C, but the reaction went to completion above 320 °C. 2,6-Dimethyl-2,4,4,6-tetra-chloro-2,4,6-trisilaheptane (**2c**) was obtained in much higher yields than 3-methyl-1,1,1,3-tetrachloro-1,3-disilabutane (**3c**) at reaction temperatures ranging from 280 to 320 °C, but the ratio of both compounds reversed above 340 °C.

The highest selectivity (82%) for the product **2c** was obtained at the reaction temperature of 320 °C. This reaction indicates that the amount of **3c** increased at higher temperatures because the chlorine produced from the decomposition of (chloromethyl)silane reactant **1c** increased at higher reaction temperatures. Although zinc is well-known as a good promoter for the direct reaction of methyl chloride, it was shown to act as an inhibitor for this reaction. In contrast to zinc addition, cadmium enhanced the reactivity and selectivity of (chloromethyl)silanes **2** and was found to be a good promoter for this particular reaction. Other (chloromethyl)silane reactants such as (chloromethyl)trichlorosilane (**1a**), (chloromethyl)methyldichlorosilane (**1b**), and (chloromethyl)trimethylsilane (**1d**) were used for this reaction. The yields and distribution of products depends on the substituents on the silicon reactants. As the number (n) of methyl-substituent(s) on the silicon atom of **1a–d** ($Cl_{3-n}Me_nSiCH_2Cl$: $n = 0$–3) increases from $n = 0$ to 3, the yields of trisilaalkanes increase from **2a** (51%), **2b** (62%), **2c** (82%), to **2d** (88%), respectively, but those of disilaalkanes generally decrease **3a** (14%), **3b** (19%), **3c** (2%), to **3d** (7%) (Eq. 10).[20]

$$\text{Cl}_{3-n}\text{Me}_n\text{Si}-\text{CH}_2-\text{Cl} \ + \ \text{Si} \ \xrightarrow[320\,°\text{C}]{\text{Cu/Cd}} \ \text{Cl}_{3-n}\text{Me}_n\text{Si}-\text{CH}_2-\underset{\underset{\text{Cl}}{|}}{\overset{\overset{\text{Cl}}{|}}{\text{Si}}}-\text{CH}_2-\text{SiMe}_n\text{Cl}_{3-n} \ +$$

1 a: n = 0
b: n = 1
c: n = 2
d: n = 3

2a (51%)
2b (62%)
2c (82%)
2d (88%)

(10)

$$\text{Cl}_{3-n}\text{Me}_n\text{Si}-\text{CH}_2-\underset{\underset{\text{Cl}}{|}}{\overset{\overset{\text{Cl}}{|}}{\text{Si}}}-\text{Cl} \ + \ \text{Others}$$

3a (14%)
3b (19%)
3c (2%)
3d (7%)
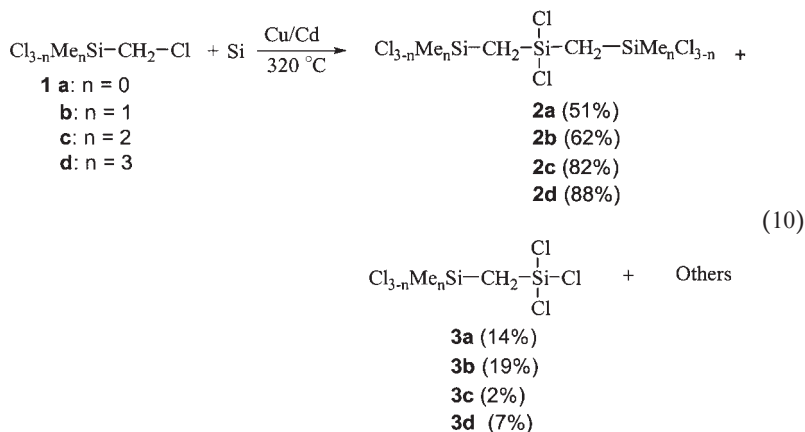
E. *Silylmethyl Chlorides and Hydrogen Chloride*

Organochlorosilanes having Si–H bond are interesting and useful starting materials for silicones, because they undergo hydrosilylation with unsaturated molecules and Si–H/C–Cl exchange reactions. The direct reaction of elemental silicon with silylmethyl chlorides **1a**–**d** having no β-hydrogen generally proceeds to give silaalkane products in good yields as described above. It was also described that external addition of hydrogen chloride to alkyl chlorides supresses the decomposition of alkyl chloride reactants and gives Si–H bond containing products.

The direct reaction of elemental silicon with a 1:3 gaseous mixture of silylmethyl chlorides **1a**–**d** and hydrogen chloride for the synthesis of Si–H containing organochlorosilanes [$\text{Cl}_2\text{HSiCH}_2\text{SiMe}_n\text{Cl}_{4-n}: = 0$ (**4a**), $n = 1$ (**4b**), $n = 2$ (**4c**), $n = 3$ (**4d**)] (Eq. 11) has been reported.[21] The direct reaction using a gaseous mixture of (chloromethyl)silanes **1** and hydrogen chloride in the presence of copper catalyst was carried out using a stirred reactor equipped with a spiral band agitator (Fig. 1) at various reaction temperatures. Both 1,3-disilaalkanes **4** containing Si–H bonds and (silylmethyl)trichlorosilanes **3** were obtained along with trichlorosilane and tetrachlorosilane. Trichlorosilane and tetrachlorosilane were formed from the reaction of elemental silicon with the excess hydrogen chloride used. Compounds **4a**–**d** obtained as major products suggest that the reactivities of **1** and hydrogen chloride are comparable. In the direct

reaction of elemental silicon with gaseous mixture of methyl chloride and hydrogen chloride, the yield of Si–H containing methylchlorosilanes is usually very low, because of the large reactivity differences between the two reactants.

In the direct reaction using a mixture of (chloromethyl)dimethylchlorosilane an hydrogen chloride, about 20% of the (chloromethyl)silane reactant was recovered at temperatures below 280 °C, indicating the temperature was not high enough for complete reaction. The recovery became 9% at temperatures above 300 °C. The yields of Si–H bond containing 1,1,3-trichloro-3-methyl-1,3-disilabutane (**4c**) as the major product increased from 47 to 55, and 59% as the reaction temperature increased from 280 to 300, and 320 °C, but dropped down again at 340 °C. At reaction temperatures ranging from 280 to 320 °C, 1,1,1,3-tetrachloro-3-methyl-1,3-disilabutane (**3c**) was obtained as a minor product in about 13–14% yield but increased to 21% at 340 °C, resulting from the increased decomposition of (chloromethyl)silane reactant **1c** or the reductive chlorination of 1,1,3-trichloro-3-methyl-1,3-disilabutane product **4c** at higher reaction temperatures. The selectivity for product **4c** was highest at 320 °C.

The formation of **4c** can be explained by the reaction in which 1 mol of each of the two reactants reacted simultaneously with an equivalent of elemental silicon. Besides 1,3-disilaalkanes **3c** and **4c**, **2c** was obtained in small amounts along with trichlorosilane and tetrachlorosilane. Cadmium was a good promoter for the reaction as observed in the direct reaction of reactant **1c** above, while zinc was found to be an inhibitor for this particular reaction. Other (chloromethyl)silanes **1a,b,d** were also applied for this reaction.[27]

The direct reaction using a gaseous mixture of the other (chloromethyl)silanes and hydrogen chloride under similar reaction conditions also gave the corresponding product mixtures of the two 1,3-disilaalkanes in relatively good yields. The yields and distribution of products depend on the substituents on the silicon of (chlromethyl)silane **1**. As the number of methyl-substituent(s) at the silicon of (chloromethyl)silanes [$Cl_{3-n}Me_nSiCH_2Cl$: $n = 0–3$] increases from $n = 0$ to 3, the yields of **4a–d** and other 1,3-disilabutanes **3a–d** were 41–59% and 14–19%, respectively, as shown in Eq. (11).

These carbosilane products can be used as precursors for silicon carbide materials, fine powders or continuous fibers. In particular, 1,3-disilabutane obtained by the reduction of 1,1,3,3-tetrachloro-1,3-disilabutane **4b** or 1,1,3,3,3-pentachloro-1,3-disilabutane **3b** by lithium hydride is a good precursor for silicon carbide.[84]

$$\text{Cl}_{3-n}\text{Me}_n\text{Si}-\text{CH}_2-\text{Cl/HCl} \quad + \quad \textbf{Si} \quad \xrightarrow[320\ ^\circ\text{C}]{\text{Cu/Cd}}$$

1a–d

$$\underset{\substack{\textbf{4a} (45\%) \\ \textbf{4b} (41\%) \\ \textbf{4c} (59\%) \\ \textbf{4d} (44\%)}}{\text{Cl}_{3-n}\text{Me}_n\text{Si}-\text{CH}_2-\overset{\text{Cl}}{\underset{\text{Cl}}{\text{Si}}}-\text{H}} \quad + \quad \underset{\substack{\textbf{3a} (19\%) \\ \textbf{3b} (19\%) \\ \textbf{3c} (14\%) \\ \textbf{3d} (16\%)}}{\text{Cl}_{3-n}\text{Me}_n\text{Si}-\text{CH}_2-\overset{\text{Cl}}{\underset{\text{Cl}}{\text{Si}}}-\text{Cl}} \quad + \quad \text{Others}$$

$$(11)$$
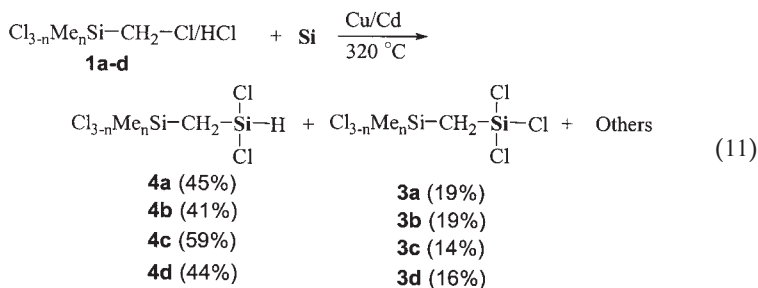
III

DIRECT REACTION OF ELEMENTAL SILICON WITH ACTIVATED ALKYL CHLORIDES

Unlike alkyl chlorides, activated benzyl chloride did not react with elemental silicon even with the addition of hydrogen chloride. Instead, benzyl chloride decomposed rapidly on contact with silicon–copper alloy at temperatures above 150 °C.[26] However, some activated alkyl chlorides such as, α,α-dichlorotoluene, α,α'-dichloro-o-xylene, and allyl chloride react with elemental silicon to give organochlorosilanes having Si–H bonds. In those reactions, a combined catalytic system of copper catalyst and cadmium promoter was advantageous: it accelerated the reaction rate so that lower reaction temperatures could be used. A fair selectivity favoring the $RSiHCl_2$ type of products was observed, but substantial amounts of organotrichloro-silanes, $RSiCl_3$, were also obtained and the yields increased at higher reaction temperatures.

A. Allyl Chloride and Hydrogen Chloride

Allylsilanes are known as interesting and useful reagents for organic synthesis.[85–88] Hurd first reported the direct reaction of elemental silicon with allyl chloride in the presence of copper catalyst to give a mixture of allylchlorosilanes and polymeric materials.[15] Among the volatile com-pounds, allyltrichlorosilane, formed by the 1:1:1 reaction of allyl chloride, hydrogen chloride and elemental silicon, was observed as the major product instead of the normally expected diallyldichlorosilane. Since diallyldichlorosilane thermally polymerizes at temperatures above 130 °C, the product mixture polymerized during the reaction or upon distillation.

To prepare allylchlorosilanes, the problems of allyl chloride decomposition and diallyldichlorosilane polymerization must be solved.[15] The hydrogen chloride addition technique was expected to work for this reaction.

When elemental silicon was reacted with a mixture of allyl chloride and hydrogen chloride in the presence of copper catalyst using a stirred reactor equipped with a spiral band agitator (Fig. 1) at temperatures ranging from 220 to 320 °C, allyldichlorosilane was successfully obtained as the major product along with allyltrichlorosilane as a minor product. Allyldichlorosilane was produced by the 1:1:1 reaction of allyl chloride, hydrogen chloride, and elemental silicon (Eq. 12).[27]

$$CH_2=CHCH_2\text{-Cl} \ + \ HCl \ + \ Si \ \xrightarrow[\text{260 °C}]{\text{Cu/Cd}}$$

$$CH_2=CHCH_2-\underset{\underset{Cl}{|}}{\overset{\overset{Cl}{|}}{Si}}-H \ + \ CH_2=CHCH_2-\underset{\underset{Cl}{|}}{\overset{\overset{Cl}{|}}{Si}}-Cl \ + Others \qquad (12)$$

31%   2%
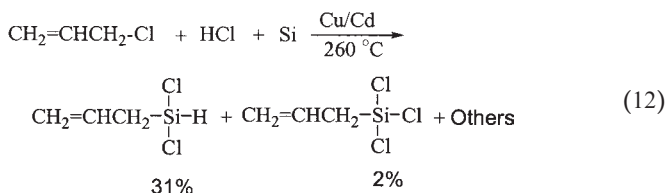
Allyl chloride did not react at temperatures below 220 °C. The total amount of products and the selectivity for allyldichlorosilane gradually increased as the temperature increased to 260 °C, but decreased beyond 280 °C. Reaction temperatures were significantly lower than those for unactivated alkyl chlorides, a reflection of the higher reactivity of allyl chloride. As hydrogen chloride content increased from 50 to 75 mol% in the mixture of allyl chloride and hydrogen chloride, the yield of allyldichlorosilane increased from 31 to 41% and that of diallyldichlorosilane decreased from 1.9 to 0.2%. However, the amount of trichlorosilane, formed from the reaction of elemental silicon with hydrogen chloride, also increased.

Zinc inhibited and cadmium promoted this particular reaction, consistent with the results observed for the direct reaction of elemental silicon with a mixture of alkyl chloride and hydrogen chloride, described above. In addition to allylchlorosilanes, several other compounds were also produced as minor products, including the following: 2-methyl-1,1,4,4-tetrachloro-l,4-disilabutane; 1,1,5,5-tetrachloro-1,5-disilapentane; and 3-(dichlorosilyl)-1,1,5,5-tetrachloro-1,5-disilapentane.

A 1:1 mixture of allyl chloride and hydrogen chloride reacted with elemental silicon in the presence of copper catalyst (10 wt%) and cadmium promoter (0.5 wt%) to give allyl-containing compounds, allyldichlorosilane (31%) and allyltrichlorosilane (2%), and other volatile compounds, 2-methyl-1,1,4,4-tetrachloro-1,4-disilabutane (1%); 1,1,5,5-tetrachloro-1,5-disilapentane (2%); 3-(dichlorosilyl)-1,1,5,5-tetrachloro-1,5-disilapentane (4%), etc. and polymeric materials.[27]

B. *Reaction with α,α′-Dichloro-o-xylene*

Although benzylic chlorides easily decompose above 150 °C, α,α′-dichloro-*o*-xylene having two benzylic chlorides undergoes the direct reaction to give 2,2-dichloro-2-silaindane in moderate yield (Eq. 13).[26] Alkyl-2-silaindanes are known to undergo ring opening polymerization to give the resulting polymers, which are high melting materials with good thermal stability. When 48 wt% solution of α,α′-dichloro-*o*-xylene in toluene was reacted with elemental silicon in the presence of copper catalyst (10% based on elemental silicon) in the reactor equipped with a spiral band agitator (Fig. 1) at temperatures ranging from 260 to 320 °C, 2,2-dichloro-2-silaindane was obtained with a best yield of 51% at 280 °C. Other products included α-(trichlorosilyl)-*o*-xylene (2%), *o*-xylene (3%), 5,6,11,12-tetrahydrodibenzo[*a,e*]cyclooctane (3%) and high boiling materials.

Even though 2,2-dichloro-2-silaindane was obtained from α,α′-dichloro-*o*-xylene in good yield, there was some deposition of solid materials, probably formed by the decomposition of α,α′-dichloro-*o*-xylene on the surface of the silicon. Zinc, known as a good promoter for the direct reaction of methyl chloride, was found to accelerate the decomposition of the reactant. Cadmium, known as a good promoter for the direct reaction of (chloromethyl) silanes, had no significant effect for this particular reaction, as was the case for silver.[26]
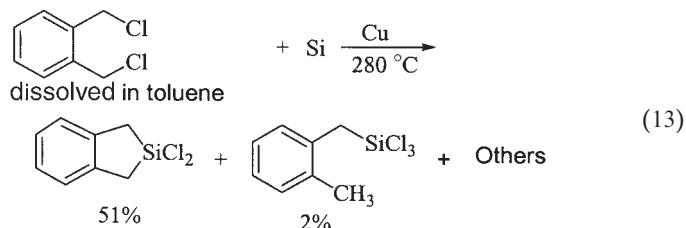
$$(13)$$

C. *α,α-Dichlorotoluene and Hydrogen Chloride*

The direct reaction of elemental silicon with α,α′-dichlorotoluene in the presence of copper catalyst around 300 °C was unsuccessful due to the decomposition of α,α-dichlorotoluene on the silicon–copper contact mass.[25] However, α,α-bis(silyl)toluenes were obtained when a mixture of α,α-dichlorotoluene and hydrogen chloride was reacted with silicon–copper

η-phase contact mass. The decomposition of α,α-dichlorotoluene was suppressed and the production of oligomeric and polymeric carbosilanes was reduced by the addition of hydrogen chloride to the α,α-dichlorotoluene reactant.

When a mixture of hydrogen chloride and 48 wt% solution of α,α'-dichloro-*o*-xylene in toluene was injected using a syringe pump into a reactor charged with Si (90%)–Cu (10%) η-phase contact mass and equipped with a spiral band agitator (Fig. 1) at temperatures ranging from 280 to 360 °C, α,α-bis(silyl)toluenes consisting of α,α-bis(dichlorosilyl)toluene, α-(dichlorosilyl)-α-(trichlorosilyl)toluenes, and α,α-bis(trichlorosilyl)toluenes were obtained as the major products along with monosilylated toluenes, α-(dichlorosilyl)toluenes and α-(trichlorosilyl)toluenes (Eq. 14). In this reaction, the total amount of products and the selectivity for α,α-bis(silyl)toluenes increased as the ratio of hydrogen chloride/α,α-dichlorotoluene increased. The highest yields of α,α-bis(silyl)toluenes were obtained when hydrogen chloride was used more than six-fold in excess.

$$X^1 = X^2 = H$$
$$X^1 = H, X^2 = Cl$$
$$X^1 = X^2 = Cl$$

$$X^3 = H \text{ or } Cl$$

(14)
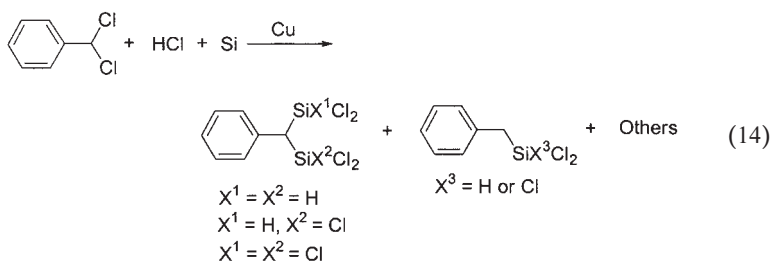
IV

DIRECT REACTION OF ELEMENTAL SILICON WITH POLYCHLOROMETHANES

Although the direct reaction of elemental silicon with alkyl chlorides has been extensively studied and a vast number of reports are available in the literature, the reactions with polychlorinated alkanes such as methylene chloride and chloroform are scarce, possibility due to the intractability of the non-volatile high molecular weight products often obtained.

A. *Methylene Chloride and Hydrogen Chloride*

Patnode and Schiessler (1945) first reported the direct reactions of methylene chloride with elemental silicon in the presence of copper catalyst. This reaction gave a mixture of both linear [Cl(Cl$_2$SiCH$_2$)$_n$SiCl$_2$X: X = H or Cl, $n = 1$–4] and cyclic carbosilanes [(Cl$_2$SiCH$_2$)$_n$, $n \geq 3$] as volatile compounds and unidentified high boilers (Eq. 15).[1a] Later, a study on the same reaction using a fluidized-bed reactor at 320 °C by Fritz and Matern was disclosed to give a similar mixture of volatile carbosilanes of over 40 compounds containing from one silicon atom to twelve silicon atoms.[32] The yield of non-volatiles was around 20%, partly due to the difficulty of efficient removal of the products out of the reactor.

$$\text{Cl-CH}_2\text{-Cl} \ + \ \text{Si} \ \xrightarrow{\text{Cu}} \ \overset{\overset{\displaystyle Cl}{|}}{\underset{\underset{\displaystyle Cl}{|}}{\left(\!\text{CH}_2\text{-Si}\!\right)_n}} \ + \ \text{Volatiles} \tag{15}$$

polycarbosilanes
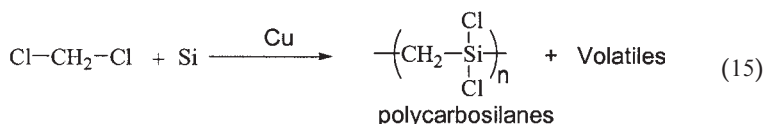
The volatile products obtained from the previously reported reactions always consisted of compounds having Si–H bonds, indicating that hydrogen chloride produced by the decomposition of methylene chloride participated in the direct reaction. The results also suggested that the hydrogen chloride incorporation technique would also work for this reaction. The direct reaction of elemental silicon with a mixture of methylene chloride and hydrogen chloride in the presence of copper catalyst using a stirred reactor equipped with a spiral band agitator (Fig. 1) at various temperatures gave bis(chlorosilyl)methanes containing Si–H bond(s) such as bis(dichlorosilyl)methane and bis(dichlorosilyl)(trichloro-silyl)methane as the major products and bis(trichlorosilyl)methane as a minor product along with trichlorosilane and tetrachlorosilane derived from the reaction of elemental silicon with hydrogen chloride (Eq. 16).[22] The decomposition of methylene chloride was suppressed and the production of polymeric carbosilanes reduced in this case.

$$\text{Cl-CH}_2\text{-Cl} \ + \ 4\,\text{HCl} \ + \ \text{Si} \ \xrightarrow[\text{Cu/Cd}]{280\ ^\circ\text{C}} \ \overset{\overset{\displaystyle Cl}{|}}{\underset{\underset{\displaystyle Cl}{|}}{X^1\text{-Si}}}\text{-CH}_2\text{-}\overset{\overset{\displaystyle Cl}{|}}{\underset{\underset{\displaystyle Cl}{|}}{\text{Si-X}^2}} \ + \ \text{Others} \tag{16}$$

$$X^1 = X^2 = \text{H: } 36\%$$
$$X^1 = \text{H, } X^2 = \text{Cl: } 31\%$$
$$X^1 = X^2 = \text{Cl: } 7\%$$
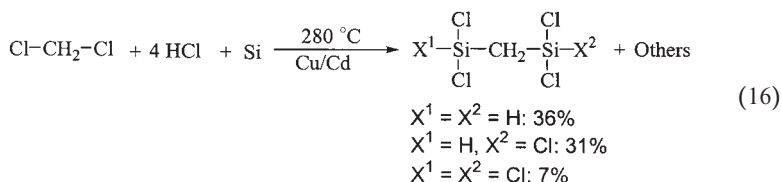
In this reaction, the required ratio of methylene chloride to hydrogen chloride was $1:2$ at the minimum to prevent polycarbosilane production. The highest selectivity for bis(dichlorosilyl)methane was observed and good yields of bis(silyl)methanes were obtained with a $1:4$ ratio of methylene chloride to hydrogen chloride. In this reaction, methylene chloride was recovered at temperatures below 260 °C. Product yields of bis(chlorosilyl)methanes did not differ greatly as the temperature increased from 280 °C to 340 °C, but the selectivity for bis(dichlorosilyl)methane decreased. More chlorinated bis(silyl)methanes increased in yield as the chlorine arising from the decomposition of methylene chloride increased at reaction temperatures higher than 340 °C. The optimum temperature for this reaction was 280 °C, considerably lower than the reaction temperature for methyl chloride.

Cadmium was a good promoter for this reaction, while zinc was found to be an inhibitor. Thus, the reaction of elemental silicon with a $1:4$ gaseous mixture of methylene chloride and hydrogen chloride at 280 °C using copper catalyst and cadmium promoter afforded bis(silyl)methanes consisting of bis(dichlorosilyl)methane (36%), bis(dichlorosilyl)(trichlorosilyl)methane (31%), and bis(trichlorosilyl)methane (7%).[22]

B. *Chloroform and Hydrogen Chloride*

Direct reaction of chloroform with elemental silicon in the presence of copper catalyst was first reported by Müller and Seitz in 1958.[19] This reaction gave branched compounds having formula $(Cl_2XSi)_3CH$ (X = H, Cl) and $Cl_3Si[XCl_2Si]_nSiCl_2Y$ (Y = CH_2SiCl_2X, $n = 1$–2) as well as cyclic carbosilanes having formula $[Cl_2SiCH(SiCl_2Z)]_n$ (Z = X or Y, $n = 3$) consisting of compounds containing one to seven silicon atoms (Eq. 17).[18]

$$\underset{\underset{Cl}{|}}{\overset{\overset{Cl}{|}}{H-C-Cl}} \quad + \quad Si \quad \xrightarrow{\ Cu\ } \quad H-C\left(\underset{\underset{Cl}{|}}{\overset{\overset{Cl}{|}}{Si}-X}\right)_3 \quad + \quad \text{Others} \tag{17}$$

$$X = H \text{ or } Cl$$
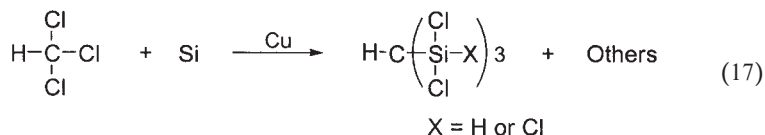
The deactivation of elemental silicon and copper catalyst was a major problem due in part to the decomposition of the starting chloroform and in part to the high boiling polycarbosilanes produced. Considering some of the products contained Si–H bonds, hydrogen chloride was likely produced during the reaction and involved in the reaction with elemental silicon.

Direct reaction of elemental silicon with a gaseous mixture of chloroform and hydrogen chloride has been studied in the presence of a copper catalyst

using a stirred reactor equipped with a spiral band agitator ([Fig. 1]) at various temperatures from 280 to 340 °C.[23] Tris(chlorosilyl)methanes with Si–H bonds were obtained from this reaction as the major products, along with bis(chlorosilyl)methanes, and trichlorosilane and tetrachlorosilane as byproducts ([Eq. 18]).[23]

$$H-\overset{\displaystyle Cl}{\underset{\displaystyle Cl}{\overset{|}{\underset{|}{C}}}}-Cl \ + \ 6\,HCl \ + \ Si \ \xrightarrow[300\,°C]{Cu/Cd} \ \text{Bis(chlorosilyl)methanes} \ +$$

$$\text{(17\%)}$$

$$H-\overset{\displaystyle SiHX^1Cl}{\underset{\displaystyle SiX^3Cl_2}{\overset{|}{\underset{|}{C}}}}-SiX^2Cl_2 \qquad + \qquad \text{Others} \qquad\qquad (18)$$

5a $X^1 = X^2 = X^3 = H$ (6%)
5b $X^1 = Cl, X^2 = X^3 = H$ (45%)
5c $X^1 = X^3 = Cl, X^2 = H$, (16%)
5d $X^1 = X^2 = X^3 = Cl$ (3%)
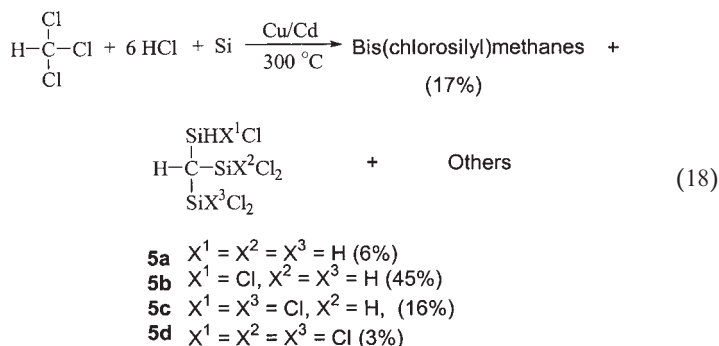
The bis(chlorosilyl)methanes were the same products as those obtained from the direct reaction of silicon with a mixture of methylene chloride and hydrogen chloride, indicating that some of the starting chloroform decomposed to methylene chloride during the reaction. When the isolated tris(chlorosilyl)methanes were fed into the reactor under the reaction conditions, they did not decompose to bis(chlorosilyl)methanes. The decomposition of chloroform was suppressed and the production of polymeric carbosilanes reduced by adding hydrogen chloride to chloroform. As a result, the deactivation problem of elemental silicon was eliminated. Cadmium was a good promoter for the reaction, while zinc was found to be an inhibitor.

The tris(silyl)methane products consisted mainly of four Si–H-containing tris(chlorosilyl)methanes: 2-(chlorosilyl)-1,1,3,3-tetrachloro-1,3-disilapropane (**5a**, 6%), 2-(dichlorosilyl)-1,1,3,3-tetrachloro-1,3-disilapropane (or tris (dichlorosilyl)methane) (**5b**, 45%), 2-(dichlorosilyl)-1,1,1,3,3-pentachloro-1,3-disilapropane (**5c**, 15%), and 2-(dichlorosilyl)-1,1,1,3,3,3-hexachloro-1,3-disilapropane (**5d**, 3%), and an all-chlorinated compound, 2-(trichlorosilyl)-1,1,1,3,3,3-hexachloro-1,3-disilapropane (trace). It is interesting that tris(silyl)methane, containing three Si–H bonds (**5b**), was obtained as the major product from the reaction of chloroform mixed with three equivalents of hydrogen chloride and of silicon, suggesting that the reactivities of chloroform and hydrogen chloride are comparable.

The selectivity for tris(dichlorosilyl)methane was the highest at 300 °C and decreased slightly at reaction temperatures below or above 300 °C. The total amount of products increased as the ratio of chloroform and

hydrogen chloride increased from $1:4.5$ to $1:9$. When the ratio increased from $4.5:1$ to $6:1$, the yield of tris(chlorosilyl)methanes and the selectivity for tris(dichlorosilyl)methane also increased. However, roughly the same amounts of products were obtained even when the ratio increased from $6:1$ to $9:1$, suggesting that the optimum-mixing ratio of hydrogen chloride to chloroform in the direct synthesis of chloroform from an industrial point, of view is $6:1$.[23]

C. *Tetrachloromethane and Hydrogen Chloride*

Using the same reaction procedure described in the direct reaction of elemental silicon with methylene chloride or chloroform, the reaction of elemental silicon with a gaseous mixture of tetrachloromethane and hydrogen chloride afforded no tetrakis(chlorosilyl)methane; instead, tris(chlorosilyl)methanes and bis(chlorosilyl)methanes were obtained, which were the same products derived from the reactions of chloroform and methylene chloride, respectively. This result may be rationalized by the decomposition of tetrachloromethane to chloroform and methylene chloride on the silicon–copper contact mass during the reaction, followed by reaction with elemental silicon to afford the products or by the decomposition reaction of partial silylated chloromethane intermediates.[16]

V

DIRECT REACTION OF ELEMENTAL SILICON WITH
(POLYCHLORINATED METHYL)SILANES

A. *(Dichloromethyl)chlorosilanes and Hydrogen Chloride*

As described above, a variety of new Si–H containing organochlorosilanes were successfully synthesized by the hydrogen chloride incorporating technique to activated alkyl chlorides such as allyl chloride, polychloromethanes and silyl-substituted methyl chlorides in the direct reaction of elemental silicon in the presence of copper-catalyst/cadmium promoter.

As an extension of these reactions, dichloromethyl-substituted silicon compounds have also been used for the direct reaction. Tris(chlorosilyl) methane products were obtained and their formation can be explained by the reaction of the two C–Cl bonds of (dichloromethyl)silane with

equivalent amounts of silicon and hydrogen chloride. The substituent effect on the silicon atom of the starting (dichloromethyl)silanes, **6** [$Cl_{3-n}Me_nSiCHCl_2$: $n=0$ (**a**), $n=1$ (**b**), $n=2$ (**c**), $n=3$ (**d**)] was investigated for the direct synthesis of tris(chlorosilyl)methanes.[24]

In order to find the optimum conditions for the direct reaction, (dichloromethyl)dichloromethylsilane (**6b**) was used as a representative among (dichloromethyl)silanes **6a–d**. A 1:4 mixture of **6b** and hydrogen chloride reacted with the contact mixture in the presence of copper catalyst using the stirred reactor (Fig. 1) at reaction temperatures from 240 °C to 310 °C. Tris(chlorosilyl)methanes consisting of three Si–H containing compounds were obtained as the major products: 2-(dichlorosilyl)-1,3,3-trichloro-1,3-disilabutane (**7b**), 2-(dichlorosilyl)-1,1,3,3-tetrachloro-1,3-disilabutane (**8b**), and 2-(dichlorosilyl)-1,1,1,3,3-pentachloro-1,3-disilabutane (**9b**); all chlorinated compound, 2-(trichlorosilyl)-1,1,1,3,3-pentachloro-1,3-disilabutane (**10b**). In addition to **7b–10b**, a mixture of bis(chlorosilyl) methanes **3b** and **4b** were produced as minor products along with trichlorosilane and tetrachlorosilane.

The production of Si–H containing compounds **7b–9b** as the major products suggests that both **6b** and hydrogen chloride reacted with the same silicon atom, and the reactivities of the two reactants are comparable. The minor products **3b** and **4b** are derived from the direct reaction of silicon with a gaseous mixture of (chloromethyl)dichloromethyl-silane, formed by the decomposition of the reactant **6b** during the reaction, and hydrogen chloride. It has been reported that tris(chlorosilyl) methanes do not decompose to bis(chlorosilyl)methanes under the reaction conditions.[20]

The formation of **8b** and the all-chlorinated compound **10b** can be explained by the reaction of one equivalent of **6b** with two equivalents of silicon and hydrogen chloride and by the reaction of one equivalent of **6b** with two equivalents of silicon and chlorine, respectively. Similarly, the formation of **9b** can be explained by the reaction of **6b** with two equivalents of silicon, and one equivalent each of hydrogen chloride and chlorine. The total amount of products and the percentage of the compound containing two Si–H bonds (**8b**) were the highest at 280 °C and decreased at temperatures below or above 280°C, while the percentages of the more chlorinated products, **9b** and **10b**, increased. These results indicate that the reactivity and selectivity were best at 280°C. Compared with the reaction of methylene chloride, the 73% yield of 2-(dichlorosilyl)-1,1,3,3-tetrachloro-1,3-disilabutane was more than double the corresponding bis(dichlorosilyl)methane production.

The optimum reaction temperature of 280 °C is the same as the temperature for the direct reaction of methylene chloride, indicating that

the silyl substitution of the starting compounds greatly improves the selectivity, but does not enhance the reactivity of the carbon–chlorine bonds towards the direct reaction. However, the optimal reaction temperature is about $40°$ lower than that for the direct reaction of monochlorinated methanes, such as methyl chloride and (chloromethyl)silanes **1a–d** without using hydrogen chloride. This result is consistent with the higher reactivity of (dichloromethyl)silane **6b** than those of monochlorinated organic compounds. The reaction even proceeded at a temperature as low as $240°C$, but the total mass of the product mixture and the selectivity for 2-(dichlorosilyl)-1,1,3,3-tetrachloro-1,3-disilabutane decreased as the temperature decreased below $240°C$, likely due to inefficient removal of the high boiling products from the reactor.

It is interesting to note that production of bis(chlorosilyl)methanes was the lowest at temperature below $280°C$ and increased at temperatures above, probably due to increased decomposition of the reactant. The percentage of polymeric carbosilanes obtained was 11% and comparable with the literature value for the reaction with chloroform.[23] The amounts and distribution of trisilylmethane products were measured using ratios of hydrogen chloride/**6b** ranging from 2 to 8 in the presence of copper catalyst with cadmium promoter at $280°C$.

In the formation of product **8b,** two moles of hydrogen chloride should be available for each mole of the reactant **6b**. Trichlorosilane and tetrachlorosilane as byproducts are also produced from the reaction of hydrogen chloride with silicon. Therefore, the required amount of hydrogen chloride for this reaction was more than a two-fold excess of **6b** to prevent polycarbosilane production. In this study, the total amount of products and the selectivity for the product **8b** increased as the ratio of **6b** to hydrogen chloride increased from $1:2$ to $1:4$, indicating that the decomposition of (dichloromethyl)silane **6b** reactant to hydrogen chloride and chlorine was suppressed under these reaction conditions as shown in other systems.[7–9] However, the results worsened as the ratio changed from $1:6$ to $1:8$, suggesting that the optimum mixing ratio of (dichloromethyl)silane **6b** to hydrogen chloride in the direct synthesis of (dichloromethyl)silane **6b** was $1:4$.

Promoters are normally incorporated in quantities less than 1%. Zinc is known as one of the most effective promoters for the direct synthesis methylchlorosilanes.[33] Cadmium is known as one of the most effective promoters for the direct synthesis of tris(sila)alkanes,[20] bis(chlorosilyl)methanes,[22] and tris(chlorosilyl)methane.[23] In the direct reaction of (dichloromethyl)silane **6b**, the total amounts (percentages) of (trisilyl)methane.[23] In the direct reaction of (dichloromethyl)silane **6b**, the total amounts (percentages) of (trisilyl)methane products **7b–10b** in the

product mixtures were 71%, 75%, and 76% with no promoter, cadmium, and zinc, respectively. The selectivity for tris(dichlorosilyl)methane **8b** in the direct reaction with cadmium as a promoter was slightly improved, while the reaction with zinc promoter resulted in the lowest yield. This indicates that zinc is not a promoter but an inhibitor, and cadmium is a good promoter for this reaction.

In the reaction using cadmium promoter, the selectivity for tris(chloro-silyl)methane **8b** was the highest among the four tris(chlorosilyl)methanes **7b–10b** and about 73% in the distribution of their four compounds. These are consistent with the results observed for the direct reactions of silicon with (chloromethyl)silanes,[20,21] allyl chloride,[27] methylene chloride,[22] and chloroform.[23]

The direct reaction was extended to other (dichloromethyl)silanes **6a,c,d** using the same optimized reaction conditions. A 1:4 mixture of (dichloromethyl)silanes **6a–d** ($Cl_{3-n}Me_nSiCHCl_2$: $n = 0$–3) and hydrogen chloride was reacted with the contact mixture[24] prepared from elemental silicon and copper catalyst using a stirred reactor equipped with a spiral band agitator (Fig. 1) at a flow rate of 6.93 g/h of (dichloromethly)silane reactants **6a–d** at a temperature of 280 °C for 3 h. The product mixtures consisted of three fractions, low boiling trichlorosilane and tetrachloro-silane, bis(chlorosilyl)methanes **3** and **4**, and tris(chlorosilyl)methanes **7–10** (Eq. 19).

(19)
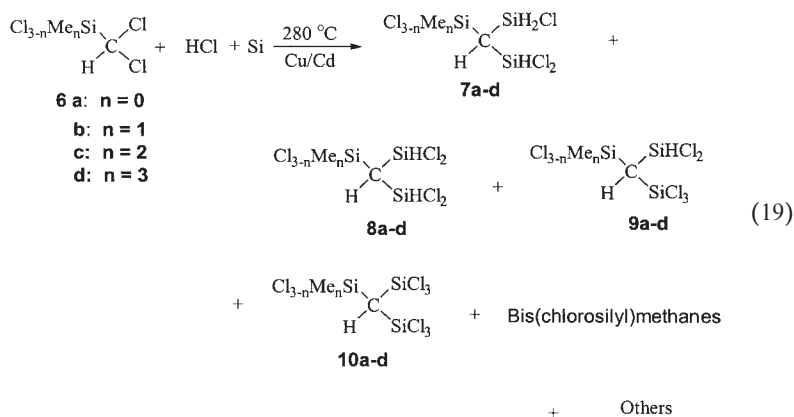
The products were purified by preparative GLC and subsequent spectral analysis led to the assignments of the structures for the products. The results obtained from the direct reaction of elemental silicon with mixtures of various (dichloromethyl)silanes **6a–d** and hydrogen chloride are summarized in Table I.

TABLE I

RESULTS OF THE DIRECT REACTIONS OF (DICHLOROMETHYL)SILANES **6a–d**

Reactant **6**[a]				Product yields (wt%)[c]				
				Tris(silyl)methanes **7–10**				
				Distribution (%)[d]				
n	g	g[b]	%	**7**	**8**	**9**	**10**	Bis[e]
0 (**a**)	22.9	28.5	75	7	72	18	3	19
1 (**b**)	20.8	27.0	75	4	73	21	2	14
2 (**c**)	18.6	27.5	86	6	71	21	2	13
3 (**d**)	16.5	25.9	85	4	72	12	11	14

[a]35 mmol of (dichloromethyl)silanes was used during 1 h; catalyst/promoter = Cu (10%)/ Cd (0.5%).
[b]Low boilers, $HSiCl_3$, and $SiCl_4$ are excluded for simplicity.
[c]Volatile carbosilanes.
[d]GLC area percentages of tris(chlorosilyl)methanes.
[e]Mixture of bis(chlorosilyl)methanes.

As shown in Table I, tris(silyl)methanes with two Si–H bonds **8a–d** $[Cl_{3-n}Me_nSiCH(SiHCl_2)]_2$ and tris(silyl)methanes with one Si–H bond **9a–d** $[Cl_{3-n}Me_nSiCH(SiHCl_2)(SiCl_3)]$ were obtained as the major products. Also obtained were the unexpected tris(silyl)methanes containing two hydrogen atoms on silicon **7a–d** $[Cl_{3-n}MeSiCH(SiH_2Cl)(SiCl_2)]$ and all chlorinated tris(silyl)methanes **10a–d** $[Cl_{3-n}Me_nSiCH(SiCl_3)_2]$ along with bis(chlorosilyl)methanes **3a–d** and **4a–d**, derived from the reaction of silicon with chloromethylsilanes **1a–d** formed by the decomposition of **6a–d**. In addition to those products, trichlorosilane and tetrachlorosilane were produced by the reaction of elemental silicon with hydrogen chloride.

The selectivity for products **8a–d** was higher than 71% for all four cases and was the highest for **6b** and the lowest for **6d**, although the differences were not great. These results suggest that the reactivity and selectivity of (dichloromethyl)silanes do not greatly depend upon the electronic nature of the substituents on silicon. In this reaction, the decomposition of **6a–d** was suppressed and the production of polymeric carbosilane reduced by adding hydrogen chloride to reactant **6**.

Cadmium was a good promoter for the reaction, and the optimum temperature for this direct synthesis was 280 °C.[24] Bis(chlorosilyl)methanes **3** and **4** were the same as those obtained in the direct reaction of silicon with a mixture of (chloromethyl)silanes **1** and hydrogen chloride,[21] indicating that some of the starting (dichloromethyl)silanes **6a–d** decomposed to

(chloromethyl)silanes **1a–d** during the reaction. Most of the tris(chlorosilyl)methane products **7–10** were different from the tris(chlorosilyl)methanes **5** obtained from the reaction of elemental silicon with a mixture of chloroform and hydrogen chloride, because the starting (dichloromethyl) silanes **6a–d** have substituents such as methyl or chlorine on the silicon atom. The optimum reaction conditions such as reaction temperature, the mixing ratio of the reactants, and catalyst/promoter effects for the synthesis of tris(silyl)methanes **7–10** were reported in detail.[24]

B. *(Trichloromethyl)chlorosilanes and Hydrogen Chloride*

The direct reaction of (trichloromethyl)chlorosilanes was applied under the same reaction condition described in the direct reaction of elemental silicon with (dichloromethyl)chlorosilanes above. In this reaction, an admixed gases of hydrogen chloride and 40 wt% (trichloromethyl)chlorosilanes in toluene injected using a syringe pump in pre-heater zone was fed into a reactor charged with elemental silicon (90%) and copper catalyst (10%) (Fig. 1). This reaction afforded no tetrakis (chlorosilyl)methane; instead, tris(silyl)methanes and bis(silyl)methanes were obtained, which were the same products derived from the reactions of (dichloromethyl)chlorosilanes or chloroform, and (chloromethyl)chlorosilanes or methylene chloride, respectively. This result may be rationalized by decomposition of (trichloromethyl)chlorosilanes to (dichloromethyl)-chlorosilanes and (chloromethyl)chlorosilanes on silicon–copper contact mass during the reaction, followed by reaction with elemental silicon to afford the products or the decomposition tetrakis(silyl)methane products.[16]

VI

DIRECT REACTION OF ELEMENTAL SILICON WITH A MIXTURE OF UNSATURATED HYDROCARBONS AND HYDROGEN CHLORIDE

The reaction of elemental silicon with a gaseous mixture of hydrogen chloride and unsaturated hydrocarbons such as alkenes (e.g., ethylene and propylene) and alkyne such as acetylene in the presence of copper catalyst also affords the corresponding organodichlorosilanes.

A. *Ethylene and Hydrogen Chloride*

The reaction of silicon with a gaseous mixture of ethylene and hydrogen chloride was carried out at temperatures ranging from 240 to 260 °C, after preheating a mixture of elemental silicon and copper(I) chloride in a helium stream at 450 °C.[82] Ethyldichlorosilane was formed along with trichlorosilane, dichlorosilane, and tetrachlorosilane (Eq. 20).

$$CH_2{=}CH_2 \ + \ HCl \ + \ Si \ \xrightarrow{\ CuCl\ } \ CH_3CH_2{-}\underset{\underset{Cl}{|}}{\overset{\overset{Cl}{|}}{Si}}{-}H \ + \ Others \qquad (20)$$
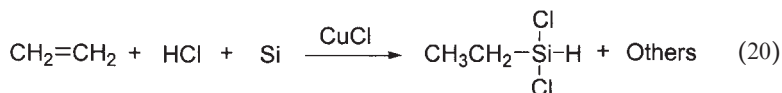
The selectivity for ethyldichlorosilane was higher at a lower temperature, while the silicon conversion was lower and the rate of formation of trichlorosilane decreased with decreasing reaction temperature. Using a 4:1 ratio of ethylene to hydrogen chloride, 36% of elemental silicon after 12 h was converted to give ethyldichlorosilane with 47% selectivity. The formation of ethyldichlorosilane can be explained by the formation of silacyclopropane from the addition of chlorosilylene (:SiHCl) to ethylene, followed by ring opening with hydrogen chloride.

B. *Propylene and Hydrogen Chloride*

Direct reaction of elemental silicon with hydrogen chloride and propylene in place of ethylene under the same reaction conditions gave isopropyldichlorosilane (22% selectivity) and *n*-propyldichlorosilane (8% selectivity) along with other chlorosilanes (Eq. 21).
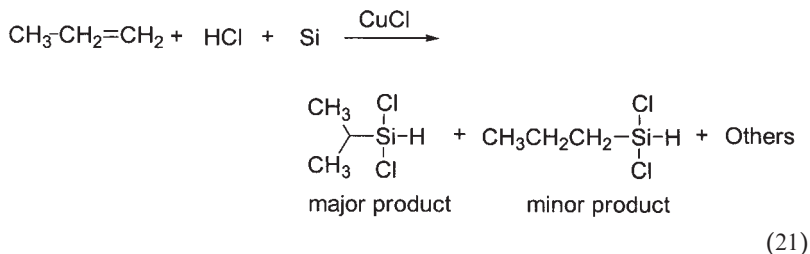
$$CH_3{-}CH_2{=}CH_2 \ + \ HCl \ + \ Si \ \xrightarrow{\ CuCl\ }$$

$$\underset{\text{major product}}{\overset{CH_3}{\underset{CH_3}{>}}{-}\underset{\underset{Cl}{|}}{\overset{\overset{Cl}{|}}{Si}}{-}H} \ + \ \underset{\text{minor product}}{CH_3CH_2CH_2{-}\underset{\underset{Cl}{|}}{\overset{\overset{Cl}{|}}{Si}}{-}H} \ + \ Others$$

$$(21)$$

The formation of isopropyldichlorosilane can be explained by the reaction of elemental silicon with hydrogen chloride and isopropyl chloride formed by the hydrochlorination of propylene. As an alternative, it is possible that a silicon–carbon bond is formed by the reaction of a silylene intermediate, generated on the surface of silicon metal powders, with alkene

or alkyne. In these reactions, a small part of the alkene undergoes hydrochlorination to yield alkyl chloride, which subsequently reacts with the surface silylene to form the silicon–carbon bond. The reaction of silicon with propyl or butyl chloride also gave alkyldichlorosilane as the main organosilicon product. Alkyl chloride is dehydrochlorinated over the copper surface, and the hydrogen chloride that is formed participates in the formation of the silicon–hydrogen bond.[82]

C. *Acetylene and Hydrogen Chloride*

The reaction of silicon with a mixture of hydrogen chloride and acetylene was carried out at various temperatures ranging from 240 to 260 °C, after a mixture of elemental silicon and copper(I) chloride in a helium stream was preheated at 450 °C.[82] Initially, activation of silicon–copper was required by feeding hydrogen chloride at 240 °C for 10 min; reaction did not proceed without this step. Subsequently, the mixture of hydrogen chloride and acetylene reacted with elemental silicon to give both dichlorovinylsilane and dichloroethylsilane (Eq. 22).[82]

$$CH{\equiv}CH \ + \ HCl \ + \ Si \ \xrightarrow{\ CuCl\ }$$

$$CH_2{=}CH{-}\underset{\underset{Cl}{|}}{\overset{\overset{Cl}{|}}{Si}}{-}X \ + \ CH_3CH_2{-}\underset{\underset{Cl}{|}}{\overset{\overset{Cl}{|}}{Si}}{-}X \ + \ \text{Others}$$

$$X = H \text{ or } Cl$$

$$(22)$$
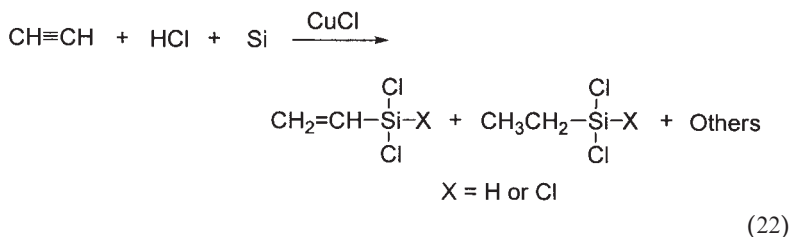
The rate of formation of ethyldichlorosilane was almost the same as those for dichlorovinylsilane and trichlorosilane. While the silicon conversion was 13% for 5 h, the overall selectivities for dichlorovinylsilane, dichloroethylsilane, and trichlorosilane were 39, 23, and 38%, respectively. The silicon conversion and the product distribution depended on the ratio of acetylene and hydrogen chloride. The selectivity for dichlorovinylsilane increased as the ratio of both reactants increased and reached 34% using a 0.26 : 1 mixture of acetylene and hydrogen chloride. The selectivities for dichlorovinylsilane and dichloroethylsilane were higher at lower temperatures and reached 36 and 26% at 223 °C, respectively.

In this reaction, vinyl chloride, which is formed by the hydrochlorination of acetylene with hydrogen chloride, was not observed from the reaction mixture. This result shows that vinyl chloride does not participate in the formation of dichlorovinylsilane.[82]

VII

CONCLUSIONS AND PROSPECTS

Recent studies on the direct reaction of elemental silicon with alkyl chlorides such as methyl chloride, activated alkyl chlorides, polychloromethanes, (chloromethyl)silanes, (dichloromethyl)silanes, etc. are summarized in this review. In the direct reaction of elemental silicon with activated alkyl chlorides and polychloromethanes, the decomposition of the reactants can be suppressed and the production of polymeric carbosilanes reduced by adding hydrogen chloride to the reactants. These reactions provide a variety of new organosilicon compounds containing Si–H and Si–Cl functionalities, which should find considerable application in the silicone industry.

REFERENCES

(1) (a) Seyferth, D. *Organometallics* **2001**, *202*, 4978. (b) Friedel, C.; Crafts, J. M. *Annalen* **1863**, *127*, 28. (c) Friedel, C.; Crafts, J. M. *Annalen* **1865**, *136*, 203.

(2) (a) Kipping, F. S. *Proc. Chem. Soc.* **1904**, *20*, 15. (b) Kipping, F. S.; Loyd, L. L. *J. Chem. Soc.* **1901**, *79*, 449.

(3) (a) Brook, M. A. *Silicon in Organic, Organometallic, and Polmer*, Wiley, New York, 2000. (b) Weber, W. P. *Silicon Reagents for Organic Synthesis*, Springer-Verlag, New York, 1983. (c) Colvin, E. W. *Silicon in Organic Synthesis*, Butterworths, London, 1981.

(4) Rochow, E. G. *J. Am. Chem. Soc.* **1945**, *67*, 963.

(5) Rochow, E. *An Introduction to the Chemistry of Silicones, Wiley, New York, 1951.*

(6) Petrov, A. D.; Mironov, B. F.; Ponomarenko, V. A.; Chernyshev, E. A. *Synthesis of Organosilicon Monomers, Consultants Bureau, New York, 1964.*

(7) Lewis, K. M.; Rethwisch, D. G. *Catalyzed Direct Reactions of Silicon, Elsevier Science Publisher, Amsterdam, 1993.*

(8) Voorhoeve, R. J. H. *Organohalosilanes, Precursors to Silicones, Elsevier, Amsterdam, 1967.*

(9) Lukevits, E. Y.; Voronkov, M. G. *Organic Insertion Reactions of Group IV Elements, Consultants Bureau, New York, 1966.*

(10) Marciniec, B. (Ed.), Comprehensive Handbook of Hydrosilylation, Pergamon Press, New York, 1992. References are therein.

(11) Song, Y. S.; Yoo, B. R.; Lee, G.-H.; Jung, I. N. *Organometallics* **1999**, *18*, 3109.

(12) Cho, Y. S.; Kang, S.-H.; Han, J. S.; Yoo, B. R.; Jung, I. N. *J. Am. Chem. Soc.* **2001**, *123*, 5584.

(13) Kang, S. H.; Han, J. S.; Yoo, B. R; Lee, M. E.; Jung, I. N. *Organometallics* **2003**, *22*, 529.

(14) Kang, S. H.; Han, J. S.; Yoo, B. R.; Lee, M. E.; Jung, I. N. *Angew. Chem. Int. Ed.* **2003**, submitted.

(15) Hurd, D. T. *J. Am. Chem. Soc.* **1945**, *67*, 1813.

(16) Jung, I. N. *et al.* Unpublished results.

(17) Patnode, W. I.; Schiessler, R. W. U.S. US 2,381,000; 2,381,001; 2,381,002; *Chem. Abstr.* **1945**, *39*, 4889.

(18) Fritz, G.; Matern, E. *Carbosilanes: Synthesis and Reactions, Springer, New York, 1986.* *pp. 46–53.*

(19) Müller, R.; Seitz, G. *Chem. Ber.* **1958**, *91*, 22.

(20) Jung, I. N.; Lee, G.-H.; Yeon, S.-H.; Suk, M.-Y. *Bull. Korean Chem. Soc*. **1991**, *12*, 445.

(21) Jung, I. N.; Han, J. S.; Yeon, S. H. *Organomerallics* **1993**, *12*, 2360.

(22) Yeon, S. H.; Han, J. S.; Yoo, B. R.; Jung, I. N. *Organomet. Chem*. **1996**, *516*, 91.

(23) Han, J. S.; Yeon, S. H.; Yoo, B. R.; Jung, I. N. *Organometallics* **1997**, *16*, 93.

(24) Lee, C. Y.; Han, J. S.; Yoo, B. R.; Jung, I. N. *Bull. Korean Chem. Soc*. **2000**, *21*, 1020.

(25) Yeon, S. H.; Han, J. S.; Jung, I. N. *Bull. Korean Chem. Soc*. **1995**, *16*, 692.

(26) Jung, I. N.; Yeon, S. H.; Han, J. S. *Bull. Korean Chem. Soc*. **1993**, *14*, 315.

(27) Yeon, S. H.; Lee, B. W.; Kim, S.-I.; Jung, I. N. *Organometallics* **1993**, *12*, 4887.

(28) Voorhoeve, R. J. H.; Vlugter, J. C. *J. Catal*. **1965**, *4*, 220.

(29) Voorhoeve, R. J. H.; Vlugter, J. C. *Rel. Trav. Chim*. **1963**, *82*, 605.

(30) Frank, T. C.; Kester, K. B.; Falconer, J. L. *J. Catal*. **1985**, *91*, 44.

(31) (a) Krylov, V. A.; Malarov, V. E.; Salaganskii, Y. M.; Sokolova, G. V. *Russ. J. Anal. Chem*. **1984**, *39*, 890. (b) Avdonin, G. V.; Alekseeva, Z. I.; Frangulyan, L. A.; Palamarchuk, N. A.; Syavtsillo, S. V.; Merkulov, V. *Sov. Chem. Ind*. **1972**, *48*, 305 (Engl. Trans.).

(32) Drake, J. E.; Riddle, C. R.; Glavincevski, B.; Gorzelska, K.; Henderson, H. E. *Inorg. Chem*. **1978**, *17*, 2333.

(33) Frank, T. C.; Kester, K. B.; Falconer, J. L. *J. Catal*. **1985**, *91*, 396.

(34) Ueno, S.; Shinohara, T.; Aramata, M.; Tanifuji, Y.; Inukai, T.; Fujioka, K. U.S. US 6,242,629 B1, **2001**, *Chem. Abstr*. **2001**, *135*, 5702.

(35) Ueno, S.; Shinohara, T.; Aramata, M.; Tanifuji, Y.; Inukai, T.; Fujioka, K. U.S: US 6,215,012 B1, **2001**, *Chem. Abstr*. **2001**, *134*, 252466.

(36) Lewis, L. N.; Bablin, J. M. U.S. US 6,005,130, **1999**, *Chem. Abstr*. **2000**, *132*, 23086.

(37) Gilliam, W. F. U.S. US 2,464,033, **1949**, *Chem. Abstr*. **1949**, *43*, 4286h.

(38) Lewis, L. N.; Childress, T. E. Eur. Pat. Appl. EP 191502, **1986**, *Chem. Abstr*. **1986**, *106*, 67480.

(39) Lewis, L. N.; McLeod, D.; Kanner, B., (J. Ward, Ed.) *Catalysis*, 1987, Elsevier Science Publishers, Amsterdam, 1988. pp. 415–434.

(40) Ward, J.; Ritzer, A.; Carroll, K. M.; Flock, J. W. *J. Catal*. **1986**, *100*, 240.

(41) Sax, (N. I. Sax, R. J. Lewis, Eds.) *Dangerous Properties of Industrial Materials*, Vol. II, 7th ed, Van Nostrand, New York, 1988. pp. 664–667.

(42) Sittig, M. *Handbook of Toxic and Hazardous Chemicals, Noyes Publications, Park Ridge, New Jersey, 1981. pp. 119–122.*

(43) Bhasin, M. *J. Catal*. **1974**, *34*, 356.

(44) Buechmer, W. *Organomet. Chem. Rev. Library* **1980**, *9*, 411.

(45) Mangalin, E. G.; Mosin, A. M.; Endovin, Y. P. *Russ. J. Appl. Chem*. **1977**, *50*, 605.

(46) De Cooker, M. G. R. T.; De Jong, J. W.; Van Den Berg, P. *J. Organomet. Chem*. **1975**, *86*, 175.

(47) De Cooker, M. G. R. T.; Van Den Hof, R. P. A.; Van Den Berg, P. J. *J. Organomet. Chem*. **1975**, *84*, 305.

(48) Golubtsov, S. A.; Ivanova, N. T.; Prigozhina, L. D.; Andrianov, K. A.; Ezeret, M. A.; Feldshtein, N. S. *Izv. Akad. Nauk. SSR Ser. Khim*. **1972**, *3*, 584.

(49) Bazant, V. *Pure Appl. Chem*. **1969**, *19*, 473.

(50) Bazant, V. *Pure Appl. Chem*. **1966**, *12*, 313.

(51) Müller, R.; Gumbel, H. *Z. Anorg. Allg. Chemie* **1964**, *327*, 286.

(52) Golubtsov, S. A.; Andrianov, K. A.; Turetskaya, R. A.; Belikova, Z. V.; Trofimova, I. V.; Morozov, N. G. *Dokl. Ahad. Nauk SSR* **1963**, *151*, 656.

(53) Banholzer, W. F.; Burrell, M. C. *J. Catal*. **1988**, *114*, 259.

(54) Gentle, T. M.; Owen, M. J. *J. Catal*. **1987**, *103*, 236.

(55) Banholzer, W. F.; Burrell, M. C. *Surf. Sci*. **1986**, *176*, 125.

(56) Sharma, A. K.; Gupta, S. K. *J. Catal.* **1985**, *93*, 68.

(57) Joklik, J.; Bazant, V. *Coll. Czech. Chem. Comm.* **1961**, *26*, 436.

(58) Clark, A. *The Theory of Adsorption and Catalysis, Academic Press, New York, 1970.*

(59) Gasper, P. (M. Jones, R. Moss, Eds.) *Reactive Intermediates*, Vol. 1, John Wiley & Sons, New York, 1978. pp. 229–277.

(60) Clarke, M. P. *Inorg. Chem.* **1965**, *7*, 387.

(61) Chernyshev, E. A.; Komalenkova, N. G.; Bashkirova, S. A. *J. Organomet. Chem.* **1984**, *271*, 129.

(62) Liu, C.; Hwang, T. *Adv. Inorg. Chem. Radiochem.* **1985**, *29*, 1.

(63) Atwell, W. H.; Weyenberg, D. R. *Angew. Chem.* **1969**, *8*, 469.

(64) Barton, T. J.; Burn, G. T. *J. Am. Chem. Soc.* **1978**, *100*, 5246.

(65) Sosa, C.; Schlegel, H. B. *J. Am. Chem. Soc.* **1984**, *106*, 5847.

(66) Barton, T. J.; Banasiak, D. S. *J. Am. Chem. Soc.* **1977**, *99*, 5199.

(67) Timms, P. L. *Inorg. Chem.* **1968**, *7*, 387–389.

(68) Kira, M.; Ishima, T.; Iwamoto, T.; Ichinohe, M. *J. Am. Chem. Soc.* **2001**, *123*, 1676.

(69) Moser, D. F.; Bosse, T.; Olson, J.; Moser, J. L.; Guzei, I. A.; West, R. *J. Am. Chem. Soc.* **2002**, *124*, 4186.

(70) Ishikawa, M.; Nakagawa, K.; Katayama, S.; Kumada, M. *J. Am. Chem. Soc.* **1981**, *103*, 4170.

(71) Ishikawa, M.; Nakagawa, K.; Katayama, S.; Kumada, M. *J. Organomet. Chem.* **1981**, *216*, C48.

(72) Ishida, S.; Iwamoto, T.; Kabuto, C.; Kira, M. *Chem. Lett.* **2001**, 1102.

(73) Bell, T. N.; Perkins, K. A.; Perkins, P. G. *J. Chem. Soc. Farad. Trans. I* **1981**, *77*, 1779.

(74) (a) Lewis, L. N.; Colborn, R. E.; Bablin J. M. U.S. US 6,407,276, **2002**, *Chem. Abstr.* **2002**, *137*, 20470d. (b) Lewis, L. N.; Ward, W. J., III; Bablin J. M. PCT Int. Appl. WO 2001081354 A2, **2001**, *Chem. Abstr.* **2001**, *135*, 344592.

(75) Lewis, M. K.; Ritscher, S. J. PCT Int. Appl. WO 02 44,186; *Chem. Abstr.* **2002**, *137*, 7790p.

(76) (a) Kalchauer, W.; Straussberger, H.; Streckel, W.; Gross, J. Ger. DE 19951773, **2001**, *Chem. Abstr.* **2001**, *134*, 207965. (b) Kalchauer, W.; Straussberger, H.; Streckel, W.; Goetze, U. Ger. DE 19919337, **2000**, *Chem. Abstr.* **2000**, *132*, 308505.

(77) Kalchauer, W.; Straussberger, H.; Streckel, W.; Gross, J. Ger. DE 19937908, **2000**, *Chem. Abstr.* **2000**, *132*, 321981.

(78) Mikhaylov, V. M.; Penskii, V. N. *Production of Monomer and Polymer Organosilicon Compounds*, pp. 18–22 (English transtated), AD-779129 from NTIS, US Dept. Commerce, Springfield, VA22151.

(79) Fritz, G.; Thielking, H. *Z. Anorg. Allg. Chem.* **1960**, *306*, 39.

(80) Petrov, A. D.; Smetankina, N. P.; Nikishin, G. I. *J. Gen. Chem. USSR* **1955**, *25*, 2305.

(81) Lin, J.-L.; Teplyakov, A. V.; Bent, B. E. *J. Phys. Chem.* **1996**, *100*, 10721.

(82) Okamoto, M.; Onodera, S.; Yamamoto, Y.; Suzuki, E.; Ono, Y. *J. Chem. Soc., Dalton Trans.* **2001**, 71.

(83) Kim, M. Y.; Lim, Y. C.; Han, J. S.; Yoo, B. R.; Jung, I. N. **2003**, in preparation for publication.

(84) Boo, J.-H.; Yu, K.-S.; Kim, Y.; Yeon, S. H.; Jung, I. N. *Chem. Mater.* **1995**, *7*, 694.

(85) Jung, I. N.; Yoo, B. R. *Adv. Organomet. Chem.* **2001**, *46*, 145.

(86) Jung, I. N.; Yoo, B. R. *Synlett.* **1999**, 519.

(87) Masse, C. E.; Panek, J. C. *Chem. Rev.* **1995**, *95*, 1293.

(88) Hosmi, A.; Sakurai, H. *Tetrahedron Lett.* **1976**, 1295.

Transition Metal Complexes Containing All-Carbon Ligands

MICHAEL I. BRUCE*

*Department of Chemistry, University of Adelaide,
Adelaide, South Australia 5005, Australia*

PAUL J. LOW*

*Department of Chemistry, University of Durham,
South Road, Durham DH1 3HE, England*

*Corresponding authors. (MIB) Fax: +61 8 8303 4358; E-mail: michael.bruce
@adelaide.edu.au. (PJL) Fax: +44 191 384 4737; E-mail: p.j.low@durham.ac.uk

I

INTRODUCTION

While small carbon molecules have been found in locations as diverse as interstellar molecular clouds, carbon stars, hydrocarbon flames and laser-ablated carbon, bulk quantities are much less easily produced and have therefore been little studied. However, as with many organic intermediates, stabilization of these reactive molecules by coordination to metal centers can be achieved and is the subject of this review. The preparation of systems containing metal centers linked by carbon-atom chains is both a synthetic challenge (in spite of the first such being obtained over 45 years ago) and of considerable current relevance.

In the solid state, three allotropes of carbon (diamond, graphite, and fullerene; Fig. 1) are well-established. Synthetic approaches to other carbon allotropes, including poly-ynes, cyclo[n]carbons and other carbon networks have been surveyed.[1] The chemistry of fullerenes, the so-called "third form" of carbon, and of the closely related carbon nanotubes, has been extensively detailed.[2–4] The molecule C_{20} may be the smallest fullerene, although other structures have been suggested (Fig. 2).[5] It is highly reactive and has been produced in only miniscule amounts in a mass spectrometer from a highly brominated dodecahedrane.

In the free state, carbon molecules containing less than 60 carbon atoms are generally unstable, although many smaller ones have been
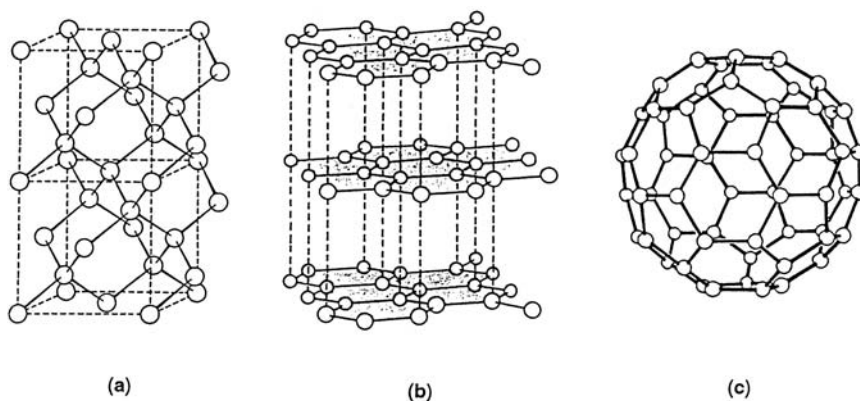
FIG. 1. Atomic arrangements in (a) diamond, (b) graphite, and (c) fullerene (C_{60}).

Cage   Bowl   Ring
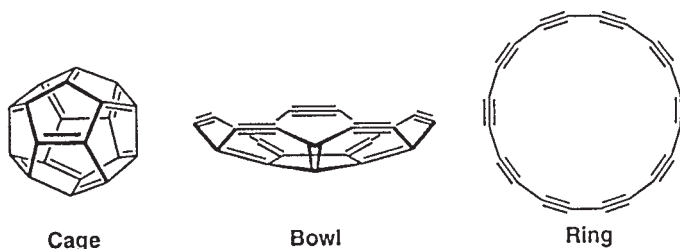
FIG. 2. Possible structures of C_{20}.

detected in comets,[6] interstellar molecular clouds,[7] and in the atmospheres of carbon stars.[8] Other sources include ion-molecule reactions under high vacuum conditions where subsequent reactions are precluded.[9] The preparation, structure, and chemistry of carbon molecules or clusters C_n ($n = 1$–20) have been reviewed;[10,11] hybrid molecules, such as cyclic poly-ynes and related molecules, have also been considered.[12] It has been suggested that chains of C(sp) atoms may form a "fourth stable allotrope of carbon", also known as "carbyne" or "chaoite".[13,14] Approaches to this material have been described, bulk quantities of C_n (n up to 28) with bulky organic groups having been made and CF_3-capped species with up to 300 carbon atoms have been observed in the gas phase.[15–20] Closely related are the dicyanopoly-ynes, obtained by vaporization of graphite in the presence of cyanogen.[21]

In addition to discussions of unnatural carbon allotropes constructed from C(sp^2) and C(sp^3) atoms,[22–24] several imaginative approaches to the construction of molecular "carbon scaffolds" and other novel molecular
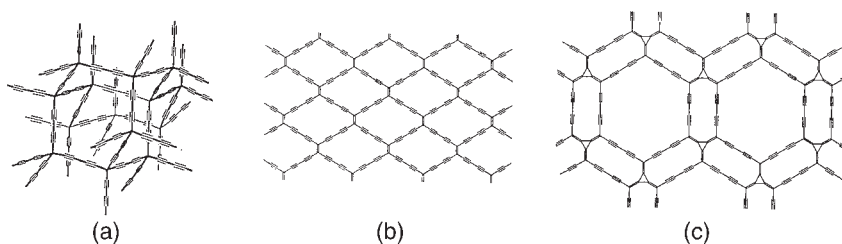
FIG. 3. Extended carbon networks containing diyne fragments linked by (a) sp^3 carbons, (b) sp^2 carbons, and (c) [3]-radialenes.

(a)   (b)
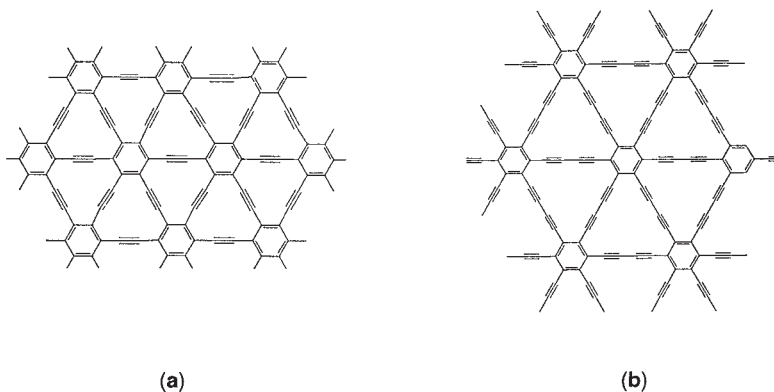
FIG. 4. Carbon networks: (a) graphyne, (b) graphdiyne.

architectures have involved acetylenic carbons.[25–27] Some examples built from sp, sp^2, and sp^3 carbon atoms are shown in Fig. 3. Novel stable molecular scale materials with attractive and specialized properties, such as electrical and non-linear optical properties, result from the presence of two-dimensional π electron systems.[28,29] Monodisperse π-conjugated oligomers can now be made with multi-nanometer dimensions.[30] Combination of benzene and alkyne units gives "graphdiyne";[31] several other systems have been proposed (Fig. 4).

This chapter surveys the rapidly burgeoning field comprising the chemistry of transition metal complexes containing ligands which are made up only of carbon atoms within their coordination spheres. Interest in this area is related to the search for new materials, of which molecular scale electron (or hole) conductors ("wires") form but one group. Possible stabilization of one-dimensional carbon (carbyne) by addition of metal fragments has been noted.[1,25,32] The role of transition metal complexes in building up the molecular topologies related to those described above [see a proposed Fe(CO)$_3$ derivative in Fig. 5] together with the well-known
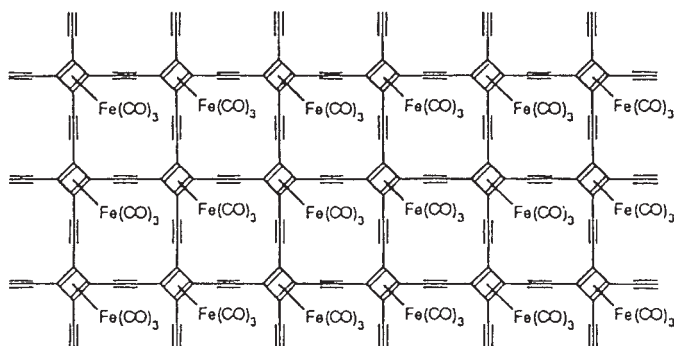
FIG. 5. An extended carbon network stabilized by $Fe(CO)_3$ groups coordinated to cyclobutadiene fragments.

propensity of transition metal centers to stabilize reactive molecules and intermediates allows the preparation of complexes containing C_n ligands as stable entities with a chemistry of their own.[33] This is the chemistry described below. However, whether one describes the compound $\{(Me_3P)_2ClPd\}C\equiv CC\equiv C\{PtCl(PMe_3)_2\}$ as containing a complexed C_4 molecule, or as a diyndiyl complex, is a matter of personal choice. Aspects of this and related chemistry have been reviewed elsewhere[30,34,35] but this account is intended to be comprehensive to the end of 2002. Our recent article on the chemistry of 1,3-diynes and related species is also relevant.[36]

In order to limit this account to a reasonable length, we have decided to cover metal complexes which contain linear or cyclic ligands of composition C_n ($n < 60$). We shall also survey metal cluster complexes containing all-carbon molecules containing two or more carbon atoms; the chemistry of mono-carbido clusters is too extensive to be included here and has been reviewed.[37–40] There have been several recent reviews of metal complexes containing fullerenes of various sizes;[41–44] the largest to date is C_{84} in $Ir(C_{84})Cl(CO)(PPh_3)_2$,[45] while multiple addition of $Pt(PR_3)_2$ (R = Et, Ph) units to several fullerenes has also been reported.[46,47] We shall not cover these here, nor shall we discuss the *endo*-metallofullerenes.[48,49] Similarly, we shall not include any molecules which have been produced in the gas-phase, but have not been isolated or structurally characterized in the solid-state. These include "simple" metal carbides, such as Ta_4C_4,[50] the metallacarbohedrenes, $M_8(C_2)_6$ (M = Ti, Zr, Hf, V, Nb, etc.) (Fig. 6),[51–56] and $M_{14}C_{13}$.[54,57] The presence of C–C bonds in the former has been confirmed by gas-phase IR spectroscopy.[58] Finally, transition metal carbides, although having been shown structurally to contain C_n species of various sizes, will not be included.[59,60] In this regard, however,
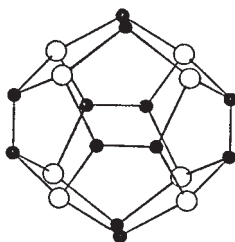
FIG. 6. Proposed structure for metallacarbohedrenes, $M_8(C_2)_6$.

the reader may be interested to consult the recent articles by King,[61,62] in which he rationalizes various observed structures in terms of well-known organometallic fragments.

Our treatment will cover firstly mononuclear complexes (the term mononuclear refers to the end-capping metal groups, not to the complex as a whole) containing linear C_n ligands, in order of increasing carbon content of the ligand. Following will be a short section (reflecting only the paucity of current results) devoted to complexes of cyclic all-carbon ligands, such as $[C_3\{Fe(CO)_2Cp\}_3]^+$. Complexes containing C_n ligands associated with binuclear metal–metal bonded systems are followed by an account of metal cluster complexes containing C_n ligands. This section also includes hybrid complexes where a cluster supports a C_n ligand also attached to a mononuclear metal–ligand fragment. The survey will be broadly based on a Group-by-Group approach and will include salient details of synthesis, properties, chemistry and electronic structure. Where appropriate, data for individual complexes are tabulated.

A. *Possible Chemical Sources of C_n Molecules*

Although smaller, short-lived and highly reactive C_n molecules have usually been prepared using plasmas and studied in matrices or in the gas phase, there have been several reports of molecular species which have been designed as possible precursors for C_n molecules under conventional laboratory conditions. Thus, pyrolysis of 5-diazotetrazole in the presence of an appropriate substrate has been used as a source of atomic carbon.[63–65] The reaction of C_3O_2 with $WCl_2(PMePh_2)_4$ gives $WCl_2(CO)(PMePh_2)_2$ $(\eta^2\text{-}OC_2PMePh_2)$ which loses CO at r.t. affording the phosphinocarbyne $WCl_2(CO)(PMePh_2)_2(CPMePh_2)$.[66] The $CPPh_3$ analogue is obtained directly from $WCl_2(PMePh_2)_4$ and $O=C=C=PPh_3$.

Thermolysis of $[IPh(C\equiv CH)]OTf$ in the presence of substrate affords products resulting from formal addition of C_2;[67] related iodonium cations

$[PhI(C\equiv C)_nIPh]^{2+}$ ($n=1$, 2) are also known.[68] Dehydrochlorination of Diels–Alder adducts of 2-chloro-1,4-benzodithiin-S,S'-tetroxide, followed by addition of a second molecule of diene and desulfonylation, gives compounds expected from the addition of C_2 to the dienes.[69] Both of these compounds can be considered to be C_2 synthons. Complexes of the carbonyl ylid $Ph_3P^+C\equiv C^-$ have been made from $Ph_3P=C=PPh_3$, e.g., $MnBr(CO)_4(CCPPh_3)$,[70] $[Ru(CCPMeR_2)(PPh_3)_2Cp^*]^+$,[71] and are considered to be donor/acceptor-stabilized forms of C_2.

Stabilization of even C_n molecules by simultaneous coordination of electron-rich phosphine and electron-deficient borane groups has been used in the case of $R_3B–C_n–PR'_3$ ($n=2$,[72] 4[73]), whereas for odd n, stabilization requires two donor groups at the ends of the C_n chain, as in $R_3P–C_n–PR_3$ ($n=1$,[74] 3[73]). Evidence for the formation of the analogous diylid, $Ph_3P=C=C=PPh_3$, in the reaction of E-$[Ph_3PCH=CH(PPh_3)](OTf)_2$ with LiBu has been given.[75] The use of these species as sources of C_n ligands in transition metal chemistry is in its infancy.

II

COMPLEXES CONTAINING C_n CHAINS

The contemporary challenge of preparing carbon allotropes containing "infinite" one-dimensional arrays of C(sp) atoms has been approached by extensions of poly-yne chemistry to end-groups which stabilize, solubilize, and provide other desirable properties for characterization, as way-points. The presence of poly-yne chains promotes strong electronic communication between the end-groups in rigid-rod structures.[76,77] Several reviews and highlights which address the importance of these complexes have appeared.[34,78,79] The function of carbon chains as "molecular wires" has been considered on several occasions[80–82] and potential applications in areas as diverse as electronics, optical technology, electrochemistry and the synthesis of highly unsaturated compounds have been remarked upon. Rigid-rod compounds containing these and related groups, such as $\{(ML_x)–C_m–Y–C_n–(M'L'_y)\}$ ($Y=C_6H_4$, $C_6H_4C_6H_4$, C_5H_2S, etc.), are expected to show liquid crystalline and NLO properties[83–86] and can also act as monomers for carbon-rich polymers. However, the effects of other spacers within the chain, such as C_6H_4, thien-2,5-diyl, etc., will not be discussed below.

Metal-capped carbon chains can exist in several forms (**A–D**; Chart 1), with uneven-numbered chains only as cumulenic or alkynyl-carbynic tautomers and to date, up to 20 carbon atoms have been used to join two

M——(C≡C)$_m$——M   M══(C≡C)$_m$══M

(A)   **(B)**

M≡C——(C≡C)$_m$——C≡M   M——(C≡C)$_m$——C≡M

(C)   **(D)**
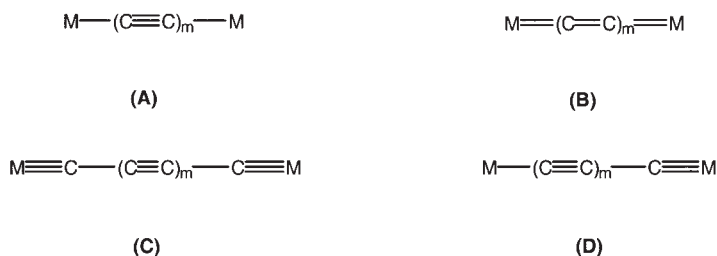
CHART 1

metal centers. Major synthetic routes involve:

(a) oxidative coupling of terminal poly-ynes (Glaser-Eglinton [Cu(OAc)$_2$/ hot pyridine], Hay [CuCl, tmeda/O$_2$, r.t.]).[87] It is remarkable that for such reactive organometallic species, the M–C(sp) bond is not cleaved in these reactions. In general, oxidative coupling affords carbon chains capped at each end by ML$_n$ fragments;

(b) lithiation and condensation with appropriate halides;

(c) copper-catalyzed coupling of halo- (bromo-) alkynes (Cadiot–Chodkiewicz);

(d) radical dimerization, with prior or subsequent deprotonation.

Routes to complexes containing longer carbon chains linking two metal centers have used either a combination of the approaches discussed above (for even-numbered chains) or methods dependent on a single reactive metal-bonded carbon center. The synthetic methods employed depend heavily on the nature of the metal fragment. Thus while Re(C≡CC≡CH)(NO)(PPh$_3$)Cp* and Fe(C≡CC≡CH)(dppe)Cp* are sufficiently robust to be coupled to give the bis(metallated) tetrayndiyls using the Glaser conditions, the carbonyl complexes M(C≡CC≡CH)(CO)$_3$Cp (M = Mo, W) and Fe(C≡CC≡CH)(CO)$_2$Cp are more successfully coupled using the milder Hay conditions. The Glaser coupling has also been applied with success in the preparation of bimetallic complexes with metal centers spanned by longer poly-yne chains.

Descriptions of the major features of the spectroscopy, molecular and electronic structures, and the electrochemistry of the resulting complexes are given in Section IV below. Key electronic properties (including electronic communication between the metal centers) and changes in bond order along the C$_n$ chain as oxidation proceeds can be studied by IR, NIR and UV/vis spectroscopy, and electrochemical methods. Intra-molecular electron transfer processes have been studied in many C$_n$ systems with a variety of end-caps [α,ω-CN, Me, Bu^t, Ph, SiR$_3$; organometallic, ML$_x$ (L = N-donor ligand: bpy, tpy, porph); mixed organic/metal, e.g., ML$_x$/NMe$_2$].[30]

As summarized by Lapinte,[88] the role of the carbon chain can be perceived as providing rigidity to the molecular backbone and it allows the whole molecule to acquire properties not found in the individual constituents. Electronically, this arises by mixing of carbon orbitals with the metal orbitals, favored by the large degree of covalency of the C_n system. Attachment of different groups to each end results in polarization of the C_n system, which may be reversed by suitable redox processes, possibly allowing construction of a molecular switch. A discussion of the use of two metal centers linked by an unsaturated spacer (C_n) for synthesis of molecular wires concludes that the terminal metal–ligand fragments play a crucial role in determining the degree of electronic communication along the wire. Particularly, the authors' work with derivatives containing the Fe(dppe)Cp* fragment has been high-lighted.[89]

Introduction of two or more terminal diyne units, either at a metal center or, for example, on an η-ring-metal complex, gives the possibility of generating metal-based polymers. In the case of alkynes, many examples of polymers have been described, but studies of similar systems derived from di- or poly-ynes are in their infancy.[90] Two- and three-dimensional polymers can be constructed in similar fashion, extension leading (conceptually, at least) to the formation of novel carbon allotropes.

A recent development has been the characterization of discrete complexes containing carbyne anions (see below) and the metallated derivatives (with Li, for example) of C_n chains. Lithiation of $\{L_xM\}(C{\equiv}C)_mH$ has given derivatives which are useful intermediates en route to bicapped carbon chains, although at present their structures remain unknown. By analogy with the carbyne anions, the characterization of species containing anionic naked carbon chains may be anticipated.

A. *Monocarbon Ligands*

1. Mononuclear C₁ Complexes

Perhaps the most unusual complexes here are the anionic species containing one-coordinate carbon. Successive reactions of $Mo\{NBu^t(Ar)\}_3$ ($Ar = C_6H_3Me_2$-3,5) with CO to give **1** (Scheme 1), reduction and acylation with pivaloyl chloride is followed by cleavage of the acyl group with Na and protonation with MeCN to give **2**, also formed in low yield from $Mo\{NBu^t(Ar)\}_3$ and CH_2Cl_2.[91] Deprotonation of **2** with $LiBu^t$ or KCH_2Ph gives tan **3**/**Li** (assumed to be a dimer) (δ 470.1) and crystallographically characterized **3**/**K**. An alternative route which affords gram quantities of **3**/**K** has been developed, whereby the reaction of 7-chloronorbornadiene

Ar = $C_6H_3Me_2$-3,5
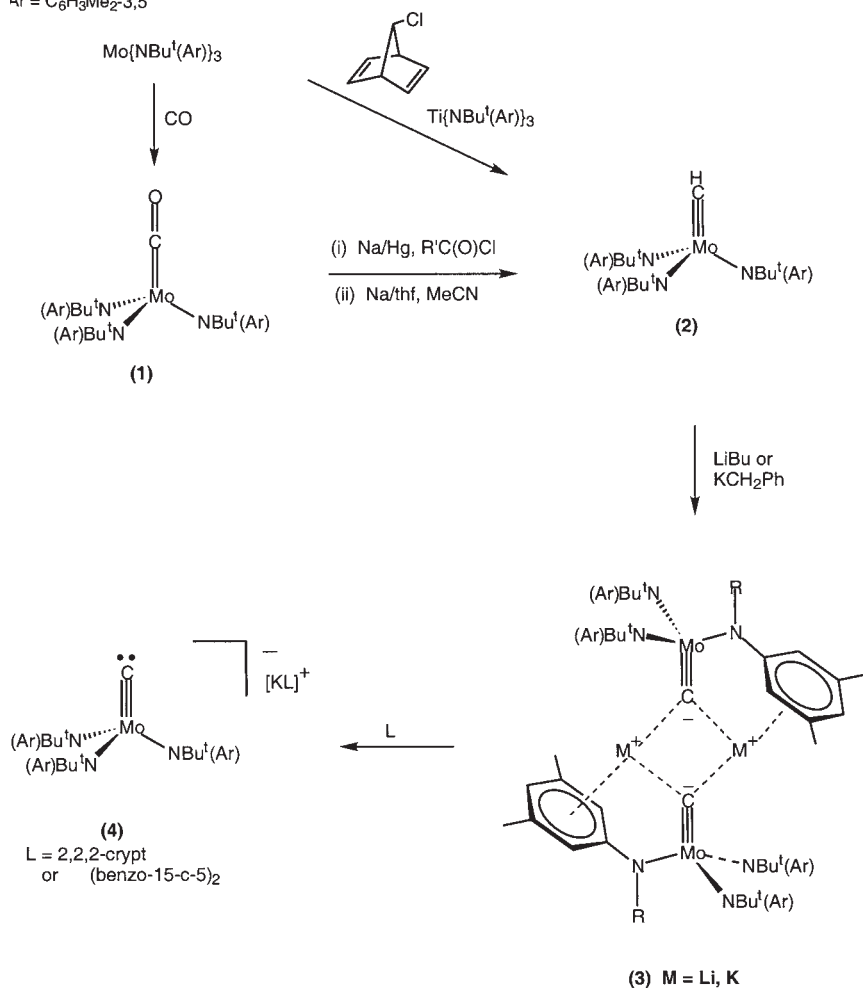
SCHEME 1

with a mixture of Mo{NBu^t(Ar)}$_3$ and Ti{NBu^t(Ar)}$_3$ resulted in loss of chlorine and benzene to give **2** (70%).[92] Addition of KCH$_2$Ph afforded **3/K** (40%). The square M$_2$C$_2$ unit is cleaved by macrocyclic ethers to give the ion-separated complex **4**, which contains an exposed carbide ligand.[93–95] The Mo≡C bond length is 1.713(9) Å [cf. 1.68(3) in **3**, 1.702(5) Å in HC≡ Mo(NR$_2$)$_3$].

The carbide resonance of **4** is found between δ ca. 474 and 501 (Table I), which may be compared with δ 288 for **1**. The τ_1 for the carbon atom is

0.14 s. Solvation occurs in thf as shown by ^{13}C resonances for **3**/**K** (δ 489) and **4** [L = (thf)$_n$] (δ 501), the former being favored at low temperatures [K_{eq} 22.5 M^{-1}, ΔH 13.3 kJ mol^{-1}, ΔS −23 J mol^{-1} K^{-1}]. While no C–Mo coupling is seen in solution, ^{13}C CP/MAS spectra of solid ^{13}C-enriched **4** give J(CMo) 60(5) Hz and the Mo nuclear quadrupole coupling constant of ca. −2.9 MHz.

The NMR parameters indicate that the carbon 2s^2 pair is largely localized on the carbon atom, giving the largest ^{13}C chemical shift tensors so far found. Significant deshielding occurs in **3**/**K**. The electronic structure involves a high-lying HOMO with σ symmetry and a low-lying LUMO which has largely Mo–C$_{\pi*}$ character. DFT calculations carried out on [CMo(NH$_2$)$_3$]$^-$ and HCMo(NH$_2$)$_3$ show the charge distribution to be −0.5334 and −0.2379 (on C), and 0.3628 and 0.5992 (on Mo), respectively. The added negative charge in the anion leads to an increase in overlap population from 0.4462 in **2** to 0.5795 in **4**, interpreted as the formal C^{4-} anion being a stronger donor than HC^{3-}, leading to a greater bond order for the C–Mo bond in **4**.[95]

Very fast degenerate proton transfer occurs between **4** and **2** [$k = 7 \times 10^6$ (20°), 4×10^5 (−60°), 1×10^5 M^{-1} s^{-1} (−90°), E_a 17 kJ mol^{-1}]. The anion in **4** is sufficiently basic to deprotonate MeCN and HC≡CPh, while only partial conversion of **2** to the anion is achieved with KCPh$_3$. Accordingly, the pK_a of **2** is estimated to be ca. 30.7. The strong nucleophilic properties and synthetic utility of **3** are shown in its reactions with PCl$_2$X (X = Cl, Ph), the chalcogens and SC$_2$H$_4$ (Scheme 2). The products all contain a sterically undemanding substituent on the carbon and unusual chemistry is foreseen.[95] Reduction of **5** with Na/Hg affords the phospha-isocyanide complex as ion-pair **6**, while a neutral diamagnetic dimer was obtained from the reaction between **5** and **6**.[92]

Deprotonation (LiBu, LiBu^t, LDA) of the methylidyne complex Tp′(OC)$_2$W≡CH (**7**; Scheme 3) affords orange Tp′(OC)$_2$W≡CLi (**8**) which was not isolated but could be characterized by its broad ^{13}C signal at δ 556.[96] The ν(CO) spectrum indicates the negative charge is mainly in the carbon s orbital. The pK_a of the methylidyne is estimated at 28.7 (vs. 2-benzylpyridine), it being less acidic than HC≡CPh or HC≡CBu^t (pK_a 23.2, 25.5, both vs. NH$_2$Cy). Nucleophilic properties of the carbide anion are shown in reactions with electrophiles such as MeI, SiMe$_3$(OTf), I$_2$, and acyl compounds.

The optimized geometries (DFT/B3LYP) of FeC(CO)$_4$ (Fig. 7) show the trigonal pyramidal form with axial C is a minimum on the singlet potential energy surface, while the equatorial isomer is a transition state.[97] The Fe–C bond dissociation energy is calculated between 350 and 395 kJ mol^{-1}. The complex should behave as a nucleophile, with the

Ar = C₆H₃Me₂-3,5
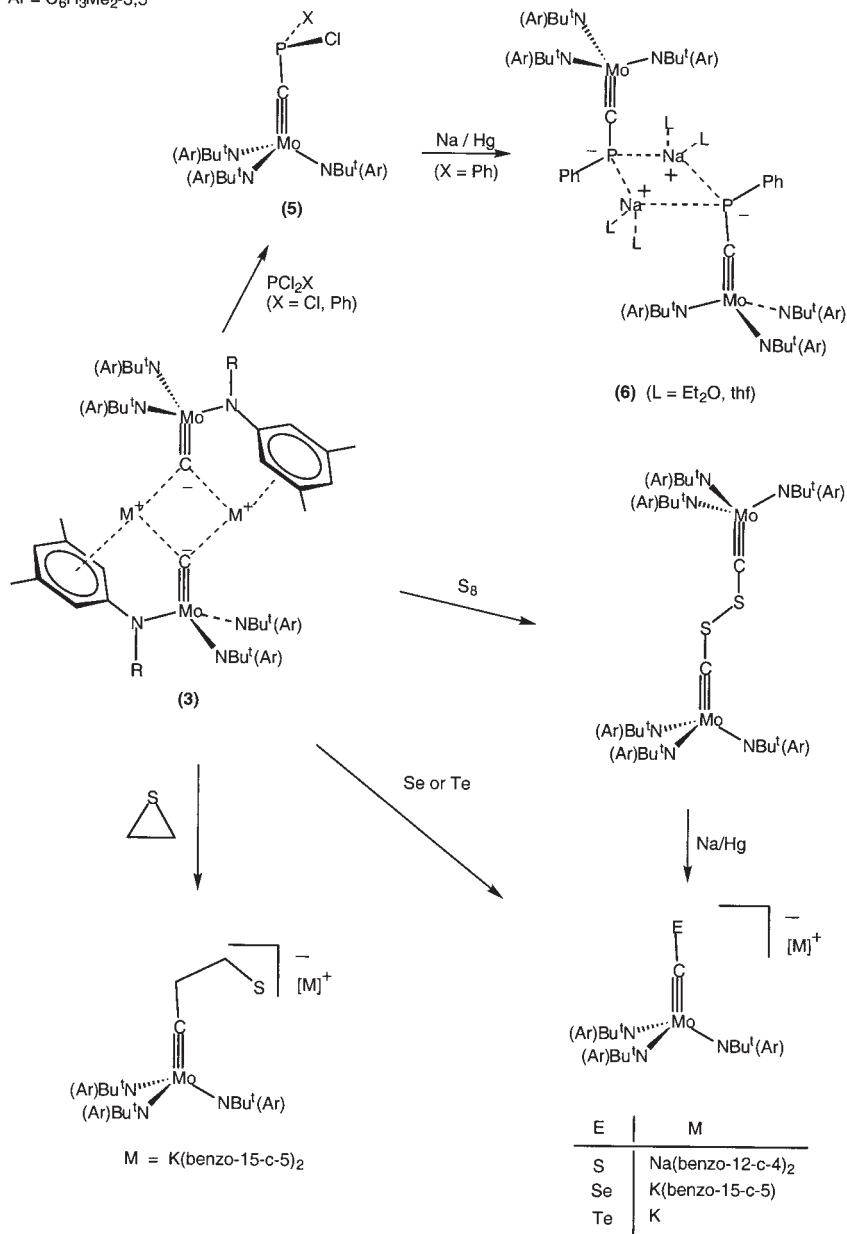
Scheme 2

TABLE I

COMPLEXES CONTAINING C_1 LIGANDS, $\{L_nM\}-C-\{M'L'_m\}$

ML_n	$M'L'_m$	δ_C	M–C	M–C–M'	Notes	Ref.
(a) Mononuclear						
Mo{N[CMe(CD$_3$)$_2$]xy}$_3$	–		1.713(9)	–	[a]	93
Mo{N[CMe(CD$_3$)$_2$]xy}$_3$	–	482.8		–	[b]	93
Mo{N[CMe(CD$_3$)$_2$]xy}$_3$	–	494.5		–	[c]	93
Mo{N[CMe(CD$_3$)$_2$]xy}$_3$	–	474.2		–	[d]	93
W(CO)$_2$Tp'	–	556		–	[e]	96
RuCl$_2$(PCy$_3$)$_2$	–	471.8		–		98
RuCl$_2$(PCy$_3$){I(mes)}	–	479.64	1.650(2)	–		98
(b) Binuclear						
Nb(calix-O$_4$) (μ-O)(μ-Na)$_2$	Nb(calix-O$_4$)	268.9	1.966, 1.968(5)	92.0(2)	[f]	99
Nb(calix-O$_4$) (μ-Na)$_3$	Nb(calix-O$_4$)		1.925(4), 1.919(3)	173.9(2)	[f]	99
Nb(calix-O$_4$) (μ-Na)$_2$	Nb(calix-O$_4$)	257			[f]	99
Mo(CO)$_2$Tp*	Fe(CO)$_2$Cp	381	1.819(6) (Mo), 1.911(8) (Fe)	172.2(5)		101
W(O)(silox)$_2$	WCl$_2$(silox)$_2$	379.14 (J_{CW} 200, 187)			[g]	100
W(Nxy)(silox)$_2$	WCl$_2$(silox)$_2$	406.25 (J_{CW} 194)	1.994(17), 1.769(17)	176.0(12)	[g]	100
W(OBu^t)$_3$	Ru(CO)$_2$Cp	237.3 (J_{CW} 290.1)	1.75(2) (W), 2.09(2) (Ru)	177(2)		103
Fe(oep)	Fe(oep)		1.664			210
Fe(tpp)	Fe(tpp)		1.675, 1.683(1)	180		109,114,117,210
Fe(tpp)(thf)	Fe(pc)(thf)		1.71, 1.65(1)	179(1)		117
Fe(pc)	Fe(pc)					113,114,117
Fe(thf)(pc)	Fe(thf)(pc)		1.71, 1.64(2)			114,117
FeF(pc)	FeF(pc)		1.687(4)	179.5(3)	[h]	114,116

(Continued)

TABLE I
Continued

ML_n	$M'L'_m$	δ_C	M–C	M–C–M'	Notes	Ref.
FeX(pc)	FeX(pc)				[h]	114,116
Fe(py)(pc)	Fe(py)(pc)		1.69(2)	177.5(8)		113–115
Fe(4-Mepy)(pc)	Fe(4-Mepy)(pc)					113
Fe(pip)(pc)	Fe(pip)(pc)					113
Fe(Me-im)(pc)	Fe(Me-im)(pc)		1.70(1)	178(1)		112,113
Fe(OCMe₂)(pc)	Fe(OCMe₂)(pc)					113
Fe(tpp)	Re(CO)₄Re(CO)₅		1.605(13) (Fe), 1.957(12) (Re)	173.3(9)		118
Ru(py)(pc)	Ru(py)(pc)		1.77(2)	174.5(8)		115

Notes: [a][K(benzo-15-crown-5)]⁺ salt; [b][K(2,2,2-crypt)]⁺ salt; [c]Dimer; [d]Na salt in solution, not isolated; [e]Li derivative; [f]calix-O₄ = 4-Buᵗ-calix[4]arene; [g]silox = OSiBuᵗ₃; [h][NBu₄]⁺ salts, X = Cl, Br, NO₃ (radical cations), CN, OCN, SCN.

SCHEME 3

E-X = Me-I, Me$_3$Si-OTf, I$_2$, PhC(O)-Br

= HB(dmpz)$_3$ (Tp*)
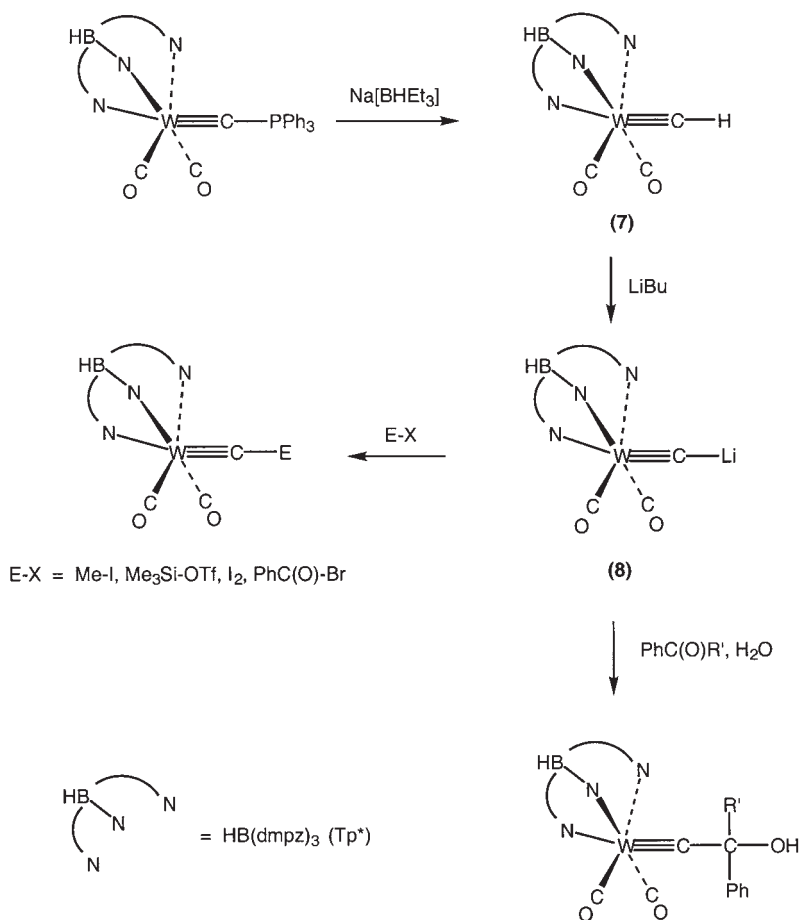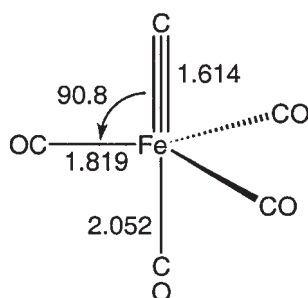
FIG. 7. Computed distances (Å) and C≡Fe–CO angle (°) for FeC(CO)$_4$.
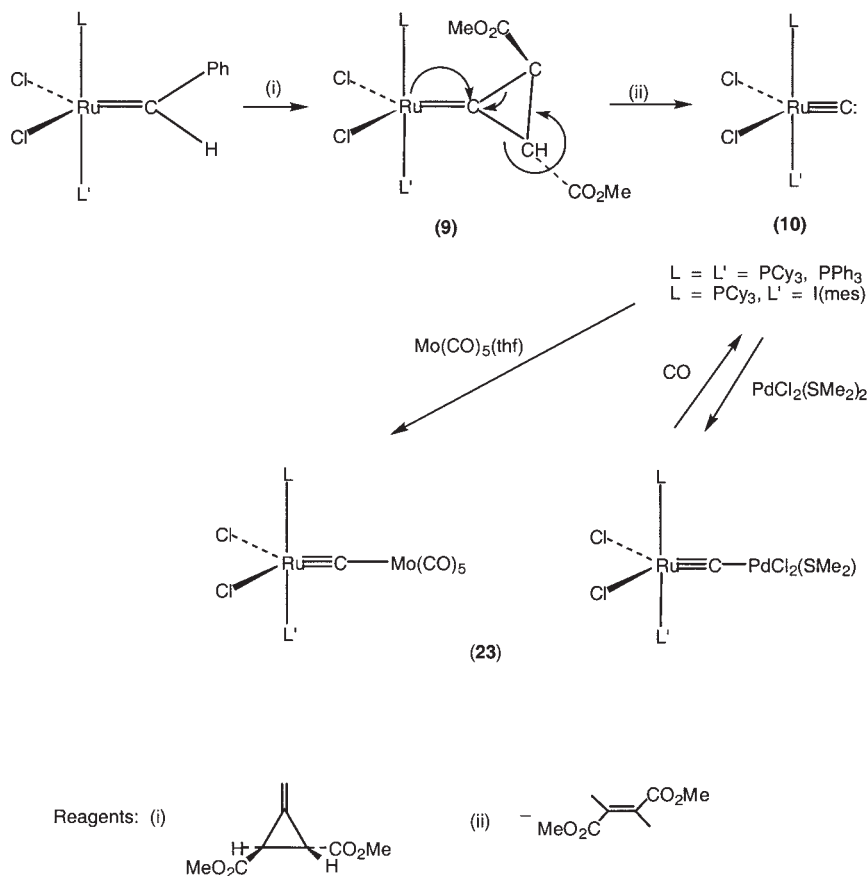
SCHEME 4

carbide ligand being a strong π acceptor and even stronger σ donor, polarized towards the Fe atom. Stabilization by coordination to Lewis acids such as BCl_3 (strongly bonded) may give isolable compounds.

Elimination of dimethyl fumarate from intermediate **9**, obtained from reactions between Grubbs-type complexes $RuCl_2(=CHPh)(PCy_3)(L)$ [L = PCy_3, I(mes)] and the substituted methylenecyclopropane $CH_2=CCH(CO_2Me)CH(CO_2Me)$, gives air- and moisture-stable $Ru(\equiv C)$ $Cl_2(PCy_3)(L)$ (**10**) (Scheme 4).[98] The I(mes) complex has a very short Ru–C distance [1.650(2) Å]; in both, the carbido resonance is found at δ ca. 475. Complex **10** (L = PCy_3) is also obtained (70% yield) directly from **9** [$L_2 = (PPh_3)_2$] by addition of an excess of PCy_3.

(11)   (12)   (13)

(15)   (14)
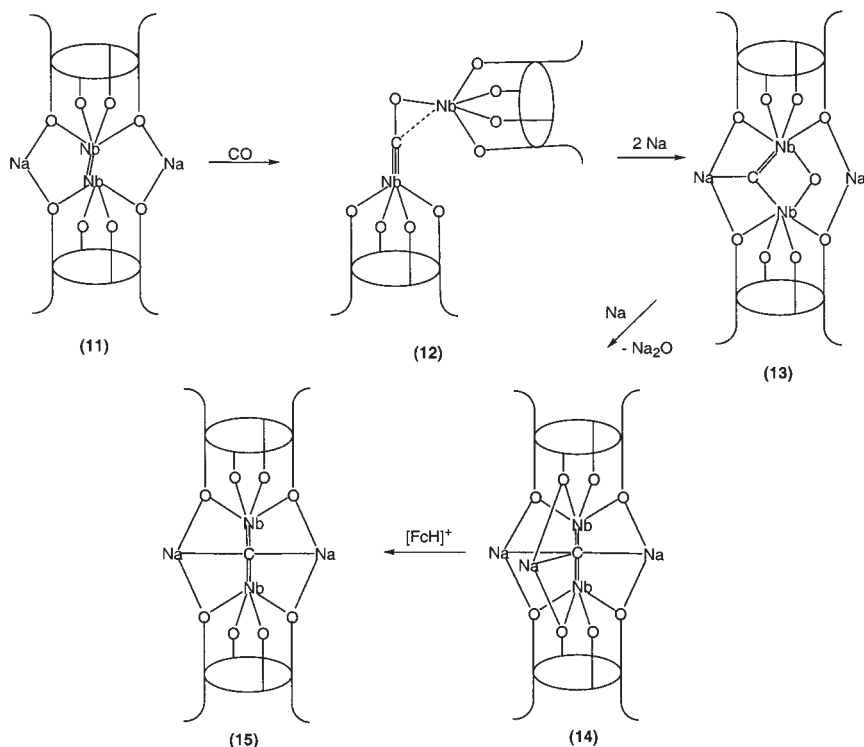
SCHEME 5

2. Bi- and Poly-Nuclear C_1 Complexes

The reductive cleavage of CO to carbide and oxide, then to carbide, has been modeled on an Nb–O framework (Scheme 5).[99] Reduction of a calixarene–niobium complex **11** with CO affords oxyalkylidyne **12** in which one Nb atom forms an Nb≡C bond and the other engages in η^2-CO bonding. Treatment with sodium resulted in reductive cleavage to **13** and deoxygenation to paramagnetic **14**; oxidation ([FcH]$^+$) gives **15**. The interactions shown result from electrophilic attack of Na$^+$ on the electron-rich carbide ligand.

Dissociation of CO about a W≡W triple bond is found in the reaction of (silox)$_2$ClW≡WCl(silox)$_2$ (**16**, Scheme 6; silox = OSiBu$_3^t$) which affords initially **17**. On heating (120 °C, 4 h) in toluene, (silox)$_2$(O)W= C=WCl$_2$(silox)$_2$ (**18**) is formed.[100] A similar reaction of **16** with xylyl isocyanide gave W$_2$Cl$_2$(silox)$_4$(CNxy), which in less than 1 h at 80 °C gave the imido analogue (silox)$_2$(Nxy)W=C=WCl$_2$(silox)$_2$ (**19**). The carbide

Silox = $OSiBu^t_3$

(16)   CO   (17)

xyNC;
80°C   120°C

(19)   (18)
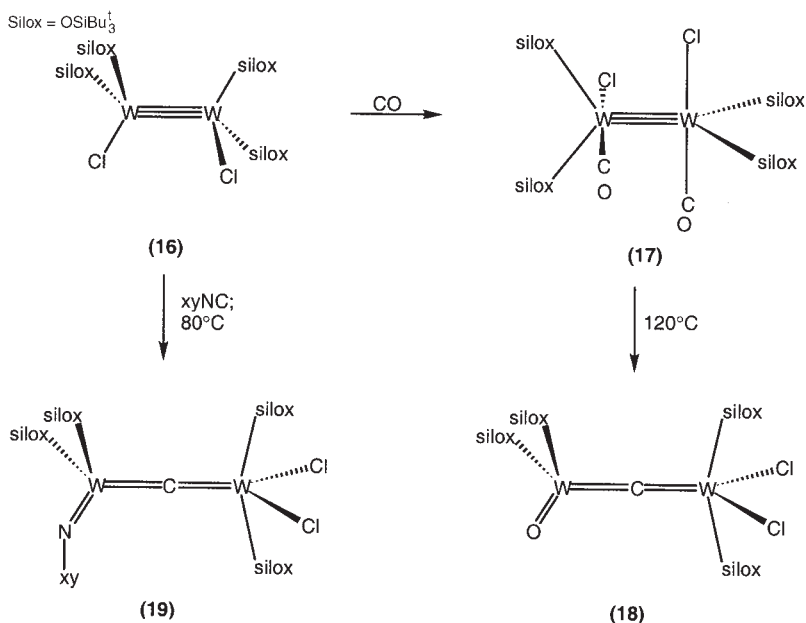
SCHEME 6

resonances in **18** and **19** are at δ 379.14 [J(CW) 200, 187 Hz] and 406.25 [J(CW) 194 Hz], respectively. The latter contains two W–C distances [1.769, 1.994(17) Å], with W–C–W 176.0(12)°, consistent with the W≡C–W formulation. Treatment of either with acid (HCl) affords methane.

The chlorocarbyne–molybdenum complex $Mo(\equiv CCl)(CO)_2Tp^*$ reacts with $[Fe(CO)_2Cp]^-$ to give $Tp^*(OC)_2Mo\equiv C–Fe(CO)_2Cp$ (**20**; Scheme 7), for which the carbide resonance is found at δ 381. Structural data are consistent with the Mo≡C–Fe formulation.[101] Protonation (HBF_4) affords the μ-CH complex, in which the proton is agostic, adopting a position bridging the C and Mo atoms [$δ_C$ 344, J(CH) 72 Hz]. Photolytic substitution of both CO ligands on iron by PMe_3 or $CNBu^t$ is found, while insertion of CS_2 into the Fe–C bond gives $Tp^*(OC)_2Mo\equiv CCS_2Fe(CO)Cp$. Related heterometallic carbides obtained from $M(\equiv CX)(CO)_2Tp^*$ (M = Mo, W; X = Cl, Br) have been described briefly and include complexes with M≡C–M′ bonds (**21**, M′ = Ni, Pd, Pt).[102]

Metathesis of $W(\equiv CEt)(OBu^t)_3$ or $W_2(OBu^t)_6$ with $Ru(C\equiv CMe)(CO)_2$ Cp' (Cp' = Cp, Cp^{Me}) occurs readily at r.t. with elimination of MeC≡CEt to give $(Bu^tO)_3W\equiv C–Ru(CO)_2Cp'$ (**22**; Scheme 8); the analogous iron derivative could not be prepared in this way.[103–105] The carbide resonance is at δ 237.3 [J(CW) 290.1], while the W≡C and Ru–C distances are 1.75(2) and 2.09(2) Å, respectively. The W≡C–Ru fragment is essentially linear [177(2)°].
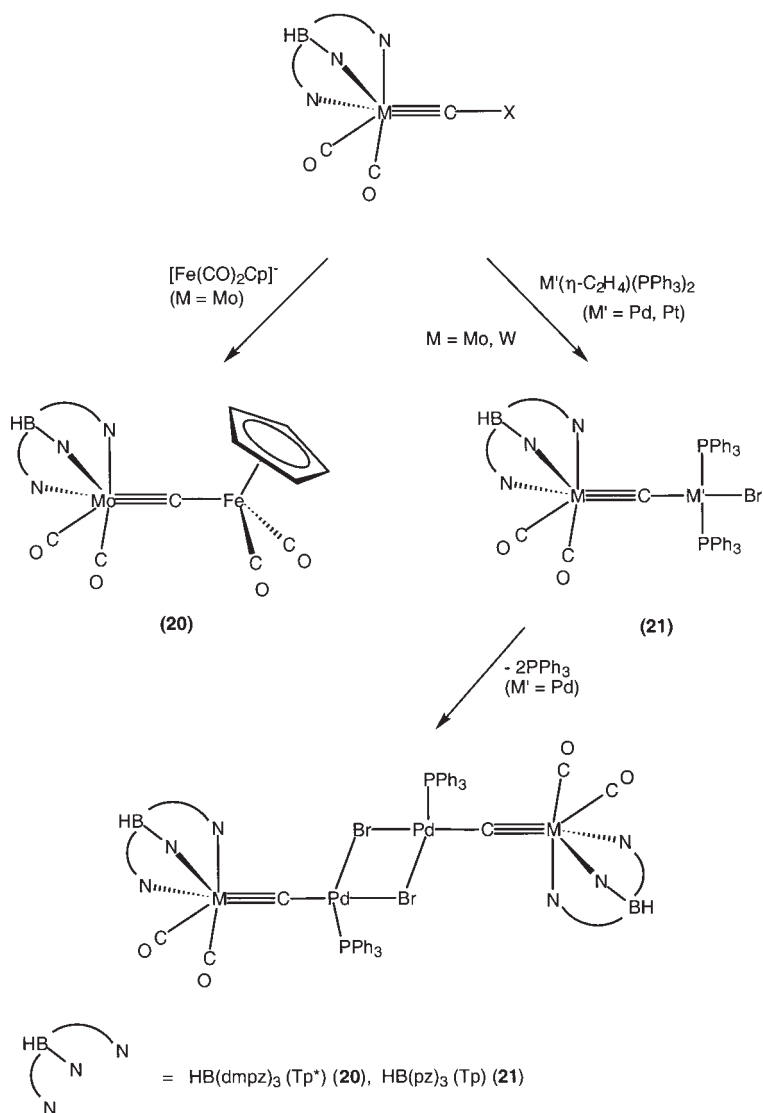
Scheme 7

Complex **10** behaves as a σ-donor in the complexes $(PCy_3)_2Cl_2Ru{\equiv}C{-}ML_n$ [**23**; $ML_n = Mo(CO)_5$ (not isolated), *trans*-$PdCl_2(SMe_2)$] (Scheme 4),[106] as predicted for $Fe({\equiv}C)(CO)_4$ (above). The μ-C ligands resonate between δ 381.2 and 446.3, respectively, and structural data are consistent with the $Ru{\equiv}C{-}M$ formulation.

$(Bu^tO)_3W \equiv CEt$ or $(Bu^tO)_3W \equiv W(OBu^t)_3$

$MeC \equiv C - Ru(CO)_2Cp'$

$(Bu^tO)_3W \equiv C - Ru(CO)_2Cp'$
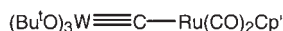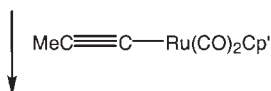
(22)

SCHEME 8
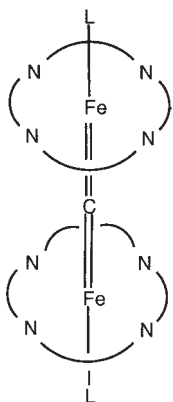
(24) N_4 = tpp, L = -
(25) N_4 = pc, L = -
(26) N_4 = tpp, L = Me-im
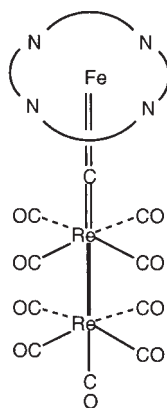
(27) N_4 = tpp

The earliest example of a μ-carbido complex, {Fe(tpp)}$_2$C (**24**), was obtained by reactions of Fe(tpp) (tpp = tetraphenylporphin) with CI$_4$, CCl$_3$SiMe$_3$, CH$_2$Cl$_2$ and LiBu, or by reaction with Fe(CBr$_2$)(tpp).[107,108] The X-ray structure of **24** reveals a single carbon atom bridging the two Fe(tpp) moieties with Fe–C 1.675(1) Å and a linear Fe–C–Fe unit, i.e., it has an Fe=C=Fe structure.[109] Theoretical calculations (EH MO) confirm that there is strong Fe–C π bonding in {Fe(tpp)}$_2$C.[110] The Mössbauer spectrum, measured at 131 K, with an isomer shift of 0.10 mm s^{-1} and quadrupole splitting of 1.88 mm s^{-1}, is similar to that of the analogous μ-N complex.[111]

Similarly, reaction of Fe(pc) (pc = phthalocyaninato) with CI$_4$ in 1-chloronaphthalene, in the presence of sodium dithionite, gives

{(pc)Fe}=C={Fe(pc)} (**25**); addition of 1-methylimidazole affords {(pc)(Me-im)Fe}=C={Fe(Me-im)(pc)} (**26**).[112] A band at ca. 990 cm^{-1} is assigned to ν_{as}(FeCFe) in the parent carbide, which shifts to 940 cm^{-1} upon coordination of the *N*-donor ligand. The 1-methylimidazole adduct has Fe–C bonds of 1.70(1) Å and Fe–C–Fe of 178(1)°; the pc rings are staggered. Other complexes containing acetone, pyridine, 4-methylpyridine, and piperidine have been reported.[113] Mössbauer data for these complexes are consistent with their being Fe(IV) derivatives.[113,114]

Recent papers have described a series of related derivatives, including crystal structure determinations, for {M(py)(pc)}$_2$(μ-C) (M = Fe, Ru),[115] [NBu$_4$]$_2$[{FeX(pc)}$_2$(μ-C)] (X = F, Cl, Br),[116] and {(pc)Fe}=C={Fe(tpp)}, {Fe(tpp)}$_2$(μ-C) and their thf adducts.[117] Synthetic methods include direct addition of the Lewis base (*N*-ligand, halide) to the parent carbide complex, and reaction of [Fe(pc)]$^{2-}$ with Fe(CCl$_2$)(tpp).

Heterometallic carbide complexes have been obtained from Fe(CCl$_2$)(tpp) and carbonylmetal anions. Thus, with [Re(CO)$_5$]$^-$, (tpp)Fe=C=Re(CO)$_4$Re(CO)$_5$ (**27**) was formed, with Fe–C and Re–C distances of 1.605(13) and 1.957(12) Å, respectively, and Fe–C–Re 172.8(4)°. The carbene resonance is at δ 211.7. The tpp ligand is unusually distorted from planarity.[118] Briefly mentioned are (tpp)Fe=C=Cr(CO)$_5$ and (tpp)Fe=C=Fe(CO)$_4$, obtained similarly using [Cr(CO)$_5$]$^{2-}$ and [Fe(CO)$_4$]$^{2-}$, respectively.[102]

An early report described (tpp)Sn{C[Re(CO)$_3$]}$_2$ from SnCl$_2$(tpp) and Re$_2$(CO)$_{10}$, together with a crystal structure[119] but calculations (EH MO) suggest its reformulation as a μ-O or μ-CH$_2$ complex.[110,120]

3. Tetrametallomethanes

Some tetra-metal-substituted methanes are known. While reactions of C{B(OMe)$_2$}$_4$ with AuCl(PR$_3$) have usually given the aurophilic carbide clusters such as [C{Au(PPh$_3$)}$_5$]$^+$ or [C{Au(PPh$_3$)}$_6$]$^{2+}$,[122,123] use of sterically demanding phosphines afforded neutral C{Au(PR$_3$)}$_4$ (R = Cy, C$_6$H$_4$Me-2).[124]

Similarly, reactions of C{B(OMe)$_2$}$_4$ with Hg(OAc)$_2$ afforded C(HgOAc)$_4$;[125] a series of tetra-mercuro-methanes, C(HgX)$_4$ (X = Cl, Br, I, CN, SCN) has been obtained from reactions of C{Hg(OAc)}$_4$ with halides or pseudohalides.[126] In turn, the acetoxy compounds derived from "Hofmann's base", previously thought to contain a C$_2$ unit, are now believed to be a polymeric oxonium ion formed by condensation of C{Hg(OH)}$_4$. Treatment of this compound with acetic or trifluoroacetic acids afforded C{Hg(O$_2$R)}$_4$ (R = Me, CF$_3$). Extensive spectroscopic studies of these derivatives have been carried out.[127–129] Further reactions with

MeSH or H_2S give $C\{Hg(SMe)\}_4$ and $\{CHg_4S_2\}_n$, respectively.[130] Several of these compounds have been used as sources of heavy-atoms in X-ray crystallography of macromolecules such as nucleic acids, membrane proteins and ribosomes.[131–133]

4. Molecular Ti–Al Carbides

Reactions of $TiMe_2(N{=}PR_3)Cp'$ (**28**, $Cp' = Cp$, $R = Pr^i$, Ph, Cy; $Cp' =$ ind, $R = Pr^i$; Scheme 9) with $AlMe_3$ afford clusters containing carbide ligands, $Cp'Ti(\mu\text{-Me})(\mu\text{-N}{=}PR_3)(\mu_4\text{-C})(\mu\text{-AlMe}_2)_2(AlMe_2)$ (**29**) (Table II).[134,135] An excess of $AlMe_3$ gives **30**, containing a five-coordinate trigonal bipyramidal carbide, which has been compared to that in $[\{Au(PPh_3\}_5C]^+$ and other hypervalent carbon species. One Al atom in **29** is three-coordinate and takes up Lewis bases, L, to give $CpTi(\mu\text{-Me})(\mu\text{-N}{=}PPr^i_3)(\mu_4\text{-C})$ $(AlMe_2)_2\{AlMe_2(L)\}$ (**31**; $L = OEt_2$, thf, PMe_3). The phenyl analogue of **29** was obtained from $TiMe_2(N{=}PPh_3)Cp$ and an excess of $AlMe_3$ and crystallographically identified [Ti–C 1.975(3) Å]. The carbide resonances of the ^{13}C-enriched compounds are found between δ 298 and 313.

Related chemistry occurs in reactions of the thiolates $Ti(SR)_2(N{=}PPr^i_3)Cp$ (**32**, $R = Ph$, CH_2Ph, Bu^t) with $AlMe_3$ which result in the unusual complete C–H bond activation of a Me group to give $CpTi(\mu\text{-SR})(\mu\text{-N}{=}PPr^i_3)(\mu_4\text{-C})(AlMe_2)_2(SRAlMe)$ (**33**). The same compounds are formed by addition of HSR to **29**. The carbide is coordinated by Ti and three Al atoms, with Ti–C distances of between 1.900(3) and 1.945(6) Å and severely distorted tetrahedral geometry resulting from the presence of three fused four-membered rings.[136,137]

B. *Complexes Containing C_2 Ligands*

Consideration of the degree of metal substitution at the carbons of the C_2 fragment and the separations of the two carbon atoms, has led to the formulation of polymetallic species as "permetallated" ethyne (**E**), ethene (**F**), or ethane (**G**) (Chart 2).[35] Addition of metal fragments to the unsaturated species **E** leads to sequential formation of **F** and **G** and progressive saturation of the C≡C triple bond. These ideas are broadly consistent with the results of computational studies (Section IX.D). Compounds of type **E** are described below, while the more highly metallated species are discussed in Sections VII, VIII, and IX.

Although the ethynediide dianion, $[C{\equiv}C]^{2-}$, in the form of its Group 1 and 2 salts, is a useful if somewhat specialized reagent in organic chemistry, transition metal complexes containing C_2 ligands have been sparsely studied until recently. Compounds such as M_nC_2 [M = Group 11

Cp′ = Cp, R = Cy, Pr^i
Cp′ = ind, R = Pr^i

(28)

$\xrightarrow[\text{- CH}_4]{\text{AlMe}_3}$

(29)

L

AlMe$_3$

RSH

(31) L = OEt$_2$, thf, PMe$_3$

(30)

R = Ph, CH$_2$Ph

(32)

$\xrightarrow[\text{- CH}_4]{\text{xs AlMe}_3}$

(33)
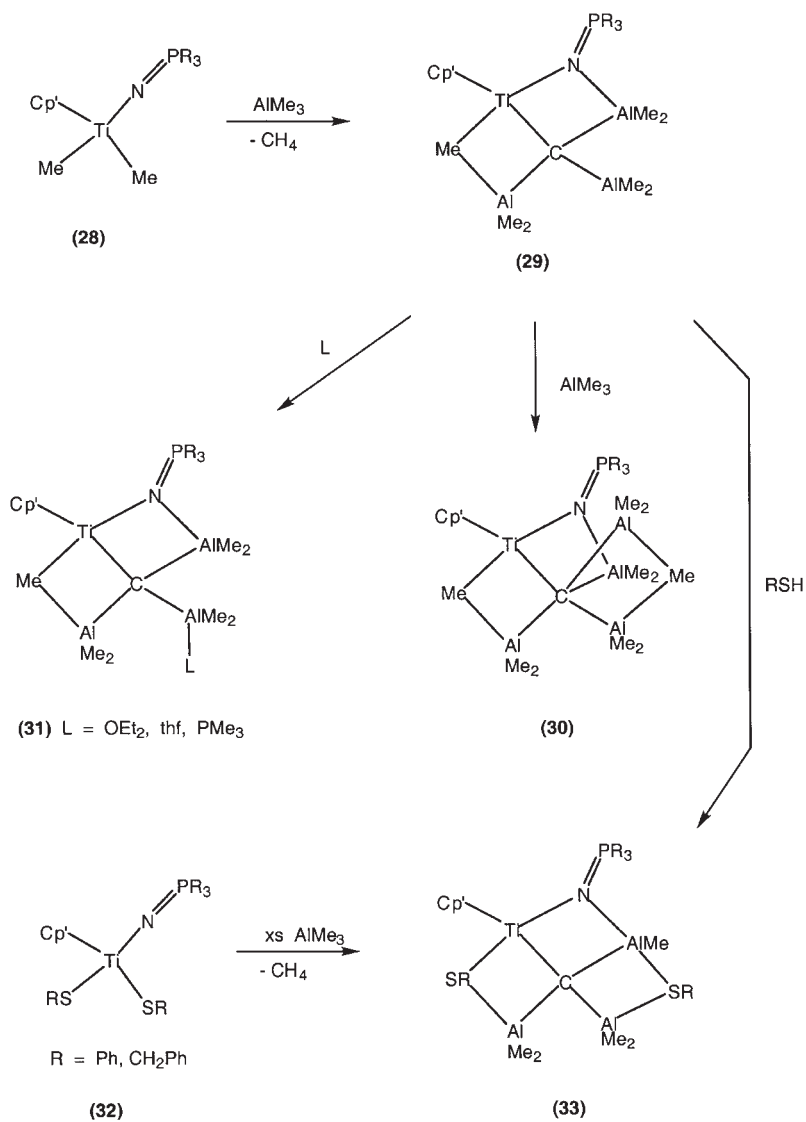
SCHEME 9

TABLE II

Some Spectroscopic and Structural Data for Molecular Ti–Al Carbides

Complex	Cp′	R	R′	L	δ_C	Ti–C/Å	Ref.
29	Cp	Cy	–	–	–	1.891(6)	135
29	Cp	Pr^i	–	–	304.7	1.874(4)	134,135
29	ind	Pr^i	–	–	310.8	1.878(4)	135
30	Cp	Ph	–	–	–	1.972(3)	134,135
30	Cp	Pr^i	–	–	298.2	1.972(3)	134,135
31	Cp	Pr^i	–	OEt_2	312.8	–	134,135
31	Cp	Pr^i	–	PMe_3	309.1	1.887(5)	135
31	Cp	Pr^i	–	thf	312.4	–	135
33	Cp	Pr^i	CH_2Ph	–	–	1.900(3)	136,137
33	Cp	Pr^i	Ph	–	–	1.902(2)	137
33	Cp	Pr^i	Bu^t	–	–	1.945(6)	137

permetallated ethyne
(E)

permetallated ethene
(F)

permetallated ethane
(G)
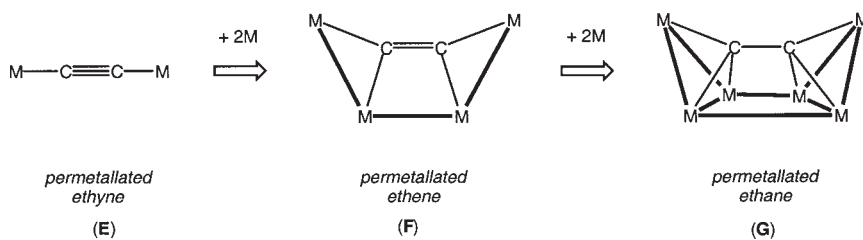
CHART 2

($n=2$) or 12 metal ($n=1$)] have been known for many decades and, although structural studies are limited, they are thought to be polymers with extended frameworks. Detailed studies are often precluded by the extreme tendency towards detonation with mechanical shock. Apart from the complexes reviewed herein, transition metals are also found in association with C_2 units in solid-state ternary dicarbides together with the electropositive lanthanides or actinides, e.g., $DyCoC_2$ or $ScCrC_2$,[62,138] and the lanthanide cluster species, such as $Cs_3[Tb_{10}(C_2)_2]I_{21}$ and $Gd_{10}(C_2)_2I_{16}$.[139,140] The C–C separations are longer than that found in ethyne (1.205 Å), ranging from 1.32 to 1.47 Å and even to 1.60 Å in $ScCrC_2$ (above), leading to their interpretation as C_2^{n-} ($n=4$ or 6), i.e., deprotonated ethene or ethane.

Transition metal derivatives assume μ-η^1:η^1 bridging modes which are assigned electronic structures **H**, **I** or **J** (Chart 3) on the basis of the central C–C separation, which can be related to those in ethyne (1.21 Å), ethene (1.34 Å), or ethane (1.53 Å), respectively.

$$L_nM\text{---}C\equiv C\text{---}ML_n \qquad L_nM\text{==}C\text{==}C\text{==}ML_n \qquad L_nM\text{≡≡}C\text{---}C\text{≡≡}ML_n$$

(H)   **(I)**   **(J)**
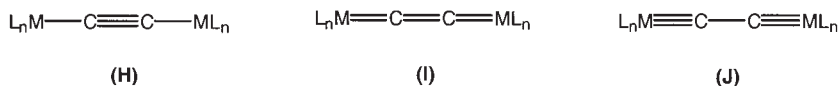
<center>CHART 3</center>

Possible routes to C_2 complexes include the following:

(a) reaction of alkali metal ethynyls or ethynyl Grignard reagents with metal halides, alkyls, or triflates;

(b) reaction of anionic metal carbonyls with $HC\equiv CX$ or C_2X_2 ($X =$ halide or triflate);

(c) oxidative addition of dihaloethynes, 1,3-diynes or alkynyliodonium cations to metal substrates; this may be followed by substitution of the second halogen;

(d) deprotonation of vinylidene complexes (from metal halides or alkyls with alkyne complexes containing acidic protons) or $\mu\text{-}\eta^1 : \eta^2\text{-}C\equiv CH$ complexes (in which the alkyne protons are rendered more acidic by coordination);

(e) from metal alkyls and ethyne;

(f) by modification of another two-carbon ligand, e.g., by dehydrogenation;

(g) by metathesis of carbyne-metal complexes with alkynyl-metal complexes, or of complexes containing $M\equiv M$ triple bonds with 1,3-diynes.

However, the ethynediide dianion often reacts as a 2-e reducing agent rather than giving any C_2 complexes.[141]

The chemistry of haloalkynes with low-valent metal complexes has been reviewed.[142] Two competing reactions of anionic metal carbonyls $[M(CO)_n]^-$ with halo-alkynes are (i) abstraction of X^+ to give $MX(CO)_n$ and (ii) nucleophilic displacement of X^- to give $M(C\equiv CX)(CO)_n$ and $\{M(CO)_n\}_2(\mu\text{-}C\equiv C)$. A recent study of reactions of haloalkynes with $[M(CO)_3Cp']^-$ ($M =$ Cr, Mo, W; $Cp' =$ Cp, Cp*)] has clarified the reaction conditions, which are determined by the nucleophilicity of the anionic metal carbonyl and the electron-withdrawing power of any substituent on the $C\equiv C$ triple bond. Cross-coupling of the anion with a chloroalkyne is catalyzed by palladium.[143]

1. Complexes Containing Isolated C_2 Ligands

At the time of writing, there are no reported examples of complexes containing C_2 ligands attached to only one metal atom, although in principle, it should be possible to access species such as $[W(C\equiv C)(CO)_5]^{2-}$, using alkali metal cations surrounded by crown ethers. Deprotonation

(with LiR) of ethynyl or vinylidene ligands gives lithiated derivatives which are valuable synthons for C_2 compounds, although their use has been limited. As a result of the presence of the metal fragment, which is both electropositive and a π-donor, the pK_a of the acetylenic proton (ca. 22–34) is more acidic than the Cp protons in $ReMe(NO)(PPh_3)Cp$, but less acidic than organic alkynes. Thus, the reaction between $Re(C{\equiv}CH)(NO)$ $(PPh_3)Cp$ and LiBu (thf, $-80\,^{\circ}C$) gives lithiocarbide complexes $Re(C{\equiv}CLi)$ $(NO)(PPh_3)Cp$ and $Re(C{\equiv}CLi)(NO)(PPh_3)(\eta\text{-}C_5H_4Li)$, as demonstrated by the formation of the corresponding methylated derivatives after treatment with MeI.[144,145] The dilithiated complex was formed in ca. 90% yield if 2 equiv. LiBu were used; however, both products were formed even when 1 equiv. LiBu was used (66/26 at $-80\,^{\circ}C$, 80/10 at $20\,^{\circ}C$). In some cases, addition of CuCl gave an insoluble and as yet uncharacterized copper(I) derivative, which was used with advantage in the reactions with metal halides. Reactions of the lithiated complex with $SnClPh_3$ afforded similar amounts of $Re(C{\equiv}CSnPh_3)(NO)(PPh_3)Cp$ and $Re(C{\equiv}CSnPh_3)(NO)(PPh_3)$ $(\eta\text{-}C_5H_4SnPh_3)$. More extensive reactions were carried out with $Re(C{\equiv}$ $CH)(NO)(PPh_3)Cp^*$, which afforded the corresponding $C{\equiv}CR$ ($R = D$, Me, $SiMe_3$, $SnPh_3$) complexes. Double deprotonation of $[Ru(=C=CH_2)$ $(PPh_3)_2Cp^*]^+$ with $LiBu^t$ ($-78\,^{\circ}C$) affords $Ru(C{\equiv}CLi)(PPh_3)_2Cp^*$, which reacts with $SiClMe_3$ to give $Ru(C{\equiv}CSiMe_3)(PPh_3)_2Cp^*$.[146] The Cp analogue gave inseparable mixtures of products formed from $Ru(C{\equiv}CLi)$ $(PPh_3)_2Cp$ and $Ru(C{\equiv}CLi)(PPh_3)_2(\eta\text{-}C_5H_4Li)$, as found for the rhenium analogue.

2. Binuclear Complexes Containing C_2 Ligands

Selected spectroscopic data for homo-binuclear C_2 complexes are given in Table III.

(a) Group 3

Reactions of ethyne with $ScRCp_2^*$ ($R = H$, Me, CH_2SiMe_3, $CMe=CMe_2$, $C{\equiv}CMe$, Ph, NMe_2) afford $Sc(C{\equiv}CH)Cp_2^*$; excess ethyne is converted to various oligo- and poly-alkynes.[147] Rapid conversion of the ethynyl to off-white $\{ScCp_2^*\}_2(\mu\text{-}C{\equiv}C)$ (**34**) occurs on attempted isolation.

While several products were obtained from ethyne and $SmCp_2^*$, the reaction with $Sm(thf)_nCp_2^*$ ($n = 1, 2$) in toluene at $-196\,^{\circ}C$ afforded yellow $\{Sm(thf)Cp_2^*\}_2(\mu\text{-}C{\equiv}C)$ (**35**); the monometallated derivative could not be obtained, nor was there any evidence for the formation of an $\eta^2\text{-}C_2H_2$ intermediate.[148]

Reduction of $M(thf)\{oepg\text{-}Na(thf)_2\}$ [$M = Pr$, Nd; oepg = *meso*-octaethyl-porphyrinogen tetra-anion] with sodium in the presence of ethyne results

$$L_nM\text{-}C\equiv C\text{-}ML_n$$
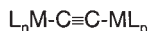
(34) ScCp*$_2$

(35) Sm(thf)Cp*$_2$

(37) Ti(PMe$_3$)Cp$_2$

(39) Zr(CR=CHR')Cp$_2$ (R = H, R' = SiMe$_3$; R = Ph, R' = Me)

(41) Zr(NHBu^i)Cp'$_2$ (Cp' = Cp, Cp^{Me})

(42) Hf(C≡CH)Cp*$_2$

(43) [V(mes)$_3$]$^-$

(45) M(CO)$_3$Cp (M = Cr, Mo, W)

(51) M(CO)$_5$ (M = Mn, Re)

(52) ReO$_3$

(53) Fe(CO)$_2$Cp*

(55) Ru(CO)$_2$Cp

(58) trans-PtCl(PR$_3$)$_2$ (R = Bu, Ph)

(59) Pt{C$_6$H$_3$(CH$_2$NMe$_2$)$_2$-2,6}

(61) Au(PR$_3$) [R = Ph, 3- and 4-tol, C$_6$H$_4$-OMe-4, nap; PR$_3$ = PPh$_2$(bp), PPhFc$_2$]

(63) HgR (R = Me, Cy, Ph)
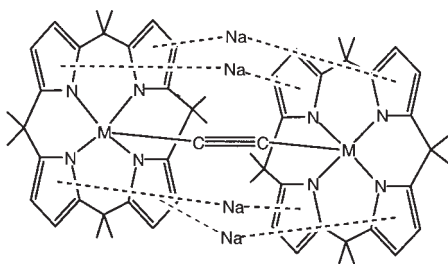
(36) M = Pr, Nd

in formation of {M(oepg)(μ-Na)$_2$}$_2$(μ-C≡C) (36), in which the saddle-shaped ligand is attached to M in the N,η^5-mode, the sodium cations being incorporated into the cavities formed by bridging of two M(oepg) fragments by the C$_2$ unit.[149]

(b) Group 4

An otherwise unsubstantiated account describes air-sensitive blue {(TiCp$_2$)$_2$(μ-C≡C)}$_n$, isolated from the reaction of C$_2$(MgBr)$_2$ with

TABLE III

SELECTED SPECTROSCOPIC PROPERTIES OF $\{ML_x\}_2(\mu\text{-}C_2)$

ML_x	IR (Raman) $\nu(CC)/cm^{-1}$	δ_C (J/Hz)	λ nm (ε M^{-1} cm^{-1})	Ref.
Group 3				
$ScCp_2^*$	(1899)	179.4		147
Group 4				
$Ti(PMe_3)Cp_2$		258.1 (m)		151
$Zr(NHBu^t)Cp_2$		169.9		156
$Zr(NHBu^t)(Cp^{Me})$		171.0		156
$Zr(CPh=CHPh)Cp_2$		178.5		153
$Hf(C{\equiv}CH)Cp_2^*$	(1938)	153.3		157
Group 5				
$Ta(silox)_3$	709/695 (^{13}CC)/682 ($^{13}C_2$) (1617)			157,160
Group 6				
$Cr(CO)_3Cp$		116.1		162
$W(CO)_3Cp$	obscured by CO	101.1		163,165
$W(CO)_3Cp^{Me}$	obscured by CO	106.3		165
$W(OBu^t)_3$	not observed	278.6	470 (170), 425 (460), 370 (1800), 350 (2100), 295 (3100), 248 (24,000)	167,168
$W(OBu^t)_3{}^3$	not observed		430 (2490), 354 (7590), 294 (11,300), 254 (27,800), 246 (26,800)	170
$W(OCMe_2CF_3)_3$	not observed		460 (220), 420 (460), 373 (1700), 354 (1900), 289 (2900), 247 (26,000), 241 (26,000)	168
$W(OCMe_2Et)_3$	not observed		464 (210), 428 (520), 370 (2300), 353 (2500), 296 (3700), 249 (30,000)	168
Group 7				
$Re(CO)_5$	(2002)		319 (12,000), 242 (50,000), 223 (68,000)	171,175
ReO_3		143.7		177

Group 8				
Fe(CO)$_2$Cp^{Et}		98.1		182
Fe(CO)$_2$Cp*		98.1		178
Ru(CO)$_2$Cp		74.7		104
Ru(CO)$_2$Cp^{Me}		81.9		105
Os(CO)$_2$Cp		65.9		105
Group 10				
trans-PdCl(PMe$_3$)$_2$	(2008)	101.91 (CP 15.6)		187,188
trans-PdI(PMe$_3$)$_2$	(2004)			187,188
trans-PtCl(PMe$_3$)$_2$	(2024)			187,188
trans-PtI(PMe$_3$)$_2$	(2022)			187,188
Group 11				
Au{PPh(nap)$_2$}	(2012)		322 (10,100), 315 (20,100), 306 (36,500), 296 (51,000), 284 (42,500), 274 (35,800), 232 (169,000)	209,211
Au{PPh$_2$(nap)}	(2007)		318 (4100), 306 (12,600), 295 (19,500), 284 (17,400), 261 (20,000), 230 (90,500)	209,211
Au{PPhFc$_2$}	(2003)	145.0 (dd)	406 (5170), 300 (10,400), 285 (15,600), 270 (27,300), 258 (58,200), 242 (63,800)	209
Au{P(nap)$_3$}	(2008)		308, 297, 287, 230 (ε not determined)	209
Au(PCy$_3$)			331 (50), 315sh (120), 303 (330), 283 (3500), 270 (6840), 256 (55,020), 239 (47,260)	288
Au(PPh$_3$)	(2040)/(2002)		288 (4150), 265 (18,800), 234 (48,800)	206,209
Au{P(tol)$_3$}	(2025)			206
Au{P(C$_6$H$_4$OMe-4)$_3$}		89.95 (CP 24.4)		380
Group 12				
HgMe		155.8		216
HgCy		158.7 (CHg 880, 200)		216
HgPh		155.0 (CHg 956, 260)		216

(38)
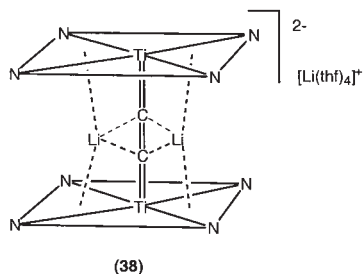
TiClCp$_2$, as being "undoubtedly polymeric".[150] A poor yield of deep green {Ti(PMe$_3$)Cp$_2$}$_2$(μ-C≡C) (**37**) was obtained by from TiCl$_2$Cp$_2$ with Li$_2$C$_2$ and treating the resulting {TiClCp$_2$}$_2$(μ-C≡C) *in situ* with PMe$_3$ and magnesium.[151] The reaction of 2-methylene-1,1-diphenylcyclopropane with Ti(PMe$_3$)$_2$Cp$_2$ gives the red η^2 complex which over six weeks in thf solution gives a higher yield of **37**, enabling it to be characterized crystallographically. It is very sensitive to air and water, and reacts with HCl to give an 85/15 mixture of ethyne and ethene. The formation of this complex probably occurs by ring-opening, loss of CH$_2$=CPh$_2$ and then 1,1-diphenyl-2-methylcyclopropane after dimerization, and hydrogen transfer.

The reaction of Ti(thf)$_2$(oepg) with lithium in the presence of ethene gives red [Li(thf)$_4$]$_2$[{Ti(oepg)(μ-Li)}$_2$(μ-C$_2$)] (**38**), in which two Ti(oepg) units are joined by a C$_2$ unit, together with two Li atoms. The latter are η^3 bonded to the porphyrinogen ligands and the Li$_2$Ti$_2$ portion is square-planar. The C–C bond is longer than expected for a bridging ethyndiyl group, with the structural data consistent with a Ti=C=C=Ti formulation, although the paramagnetism is in accord with the Ti–C≡C–Ti form.[152] The C$_2$ unit is stabilized by coordination to electron-rich Ti centers and protected by the Li cations which can also interact with the periphery of the oepg ligands (cf. the Nb–calixarene complex above).

Ethyne reacts with the zirconacyclobutene $\overline{\text{Zr(CH}_2\text{CPh=CPh)}}$(PMe$_3$)Cp$_2$ with ring-opening to give yellow {Zr(CPh=CMePh)Cp$_2$}$_2$(μ-C≡C) (**39**, R = Ph).[153] The complexes M(L){η^2-C$_2$(SiMe$_3$)$_2$}Cp$_2$ (M = Ti, L = –; M = Zr, L = thf) are useful precursors.[121,154,155] The zirconium derivative reacts with ethyne to give a mixture of {Zr[C(SiMe$_3$)=CH(SiMe$_3$)]Cp$_2$}$_2$ (μ-C≡C) (**39**, R = SiMe$_3$), which contains an agostic Zr⋯H interaction to the vinyl H, and zirconacyclopentadiene Zr{CH=CHC(SiMe$_3$)= C(SiMe$_3$)}Cp$_2$. Reactions of Zr(NBu^t)(thf)Cp$_2'$ (**40**; Cp' = Cp, Cp^{Me}) with ethyne give {ZrCp$_2'$}$_2$(μ-NBu^t)(μ-CHCH=NBu^t), which on heating are converted to light yellow {Zr(NHBu^t)Cp$_2'$}$_2$(μ-C≡C) (**41**) via fragmentation into Zr(NBu^t)Cp$_2'$ and Zr(CH=CHNBu^t)Cp$_2'$ (Scheme 10).[156]

An excess of NaC$_2$H is required for the synthesis of Hf(C≡CH)$_2$Cp$_2^*$ from the dichloride; if the reaction is carried out in refluxing thf, light yellow

R = H, Me

(40)

+ thf   - thf

HC≡CH

Δ

(41)
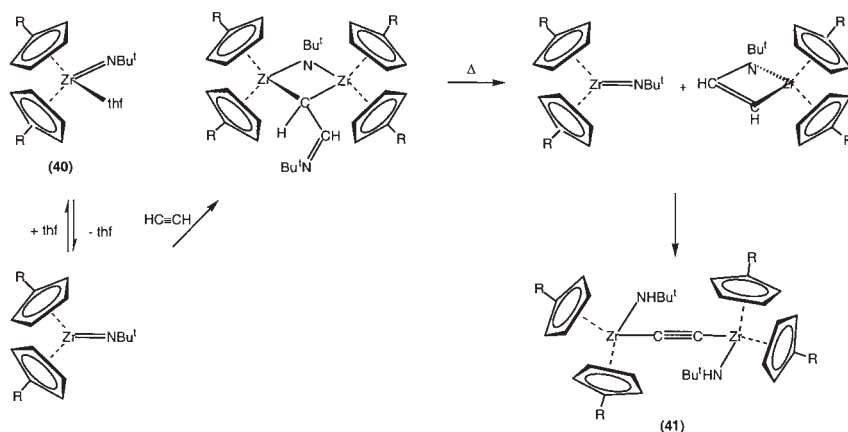
SCHEME 10

$\{Hf(C\equiv CH)Cp_2^*\}_2(\mu\text{-}C\equiv C)$ (**42**) is obtained in 50% yield.[157] Fluxional ^1H NMR spectra arise by rotation of the two Hf sites about the Hf–C–C–Hf axis (barrier to rotation 19.5 kcal mol^{-1}).

(c) Group 5

The reaction between Li_2C_2 and $V(mes)_3$ in thf afforded grey-blue paramagnetic $[Li(thf)_4]_2[\{V(mes)_3\}_2(\mu\text{-}C\equiv C)]$ (**43**).[158]

The formation of a C_2 complex from CO and a tantalum siloxide (Scheme 11) provides significant support for intermediate steps in the Fischer–Tropsch reaction. Cleavage of CO in the reaction with $Ta(silox)_3$ (silox $= OSiBu_3^t$) in benzene at r.t. gave a 2/1 mixture of brick-red $\{Ta(silox)_3\}_2(\mu\text{-}C_2)$ (**44**) and $TaO(silox)_3$.[159–161] Structural data are consistent with the presence of the Ta=C=C=Ta fragment, in which the HOMOs are a fully occupied C=C π^b and a half-occupied HOMO localized on the Ta=C bond (π) with partial C=C π^* character. Magnetic properties indicate a singlet ground state. Hydrolysis required drastic conditions (thf, 110 °C, 15 h) and gave C_2H_4 and H(silox); dioxygen required 30 min at r.t. to give $Ta(=C=C=O)(silox)_3$ and $TaO(silox)_3$. The same mixture was obtained from $Ta(silox)_3$ and CO in toluene between -78 °C and r.t., while treatment of the ketenylidene with $Ta(silox)_3$ rapidly formed the dicarbide and $TaO(silox)_3$. Labeling studies suggest the transformations shown in Scheme 11, and these are supported by the direct reaction of $Ph_2C=C=O$ with $Ta(silox)_3$ to give $Ta(\eta^2\text{-}OC=CPh_2)(silox)_3$ at -78 °C in hexane. Extended thermolysis (benzene, 155 °C, 8 h) resulted in extrusion of C_2Ph_2
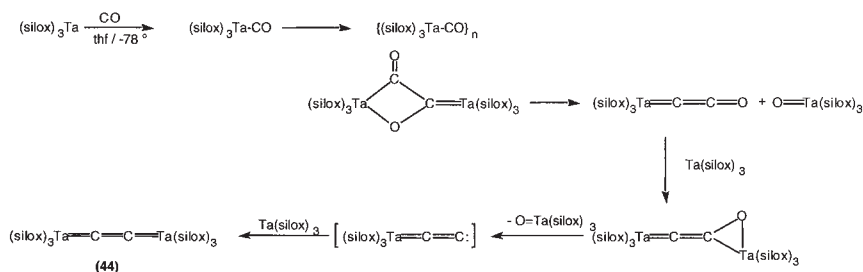
SCHEME 11

and formation of TaO(silox)$_3$. The suggested intermediate vinylidene, such as Ta($=$C$=$CPh$_2$)(silox)$_3$, could not be detected or trapped. The selectivity of this reaction is the result of the strong reducing and oxophilic nature of the formally Ta(III) center.

(d) Group 6

Chloroethynyl complexes of Mo and W are obtained from [M(CO)$_3$Cp]$^-$ (M $=$ Mo, W) with C$_2$Cl$_2$, with only trace amounts of W(CCl$=$ CHCl)(CO)$_3$Cp and {W(CO)$_3$Cp}$_2$(μ-C$\equiv$C) being isolated.[162] Pale brown {Cr(CO)$_3$Cp}$_2$(μ-C$\equiv$C) (**45/Cr**) is the major product obtained with M $=$ Cr, together with a black pyrophoric powder containing Cr. With C$_2$X$_2$ (X $=$ Br, I), only MX(CO)$_3$Cp was formed. The dark yellow tungsten complex **45/W** is also obtained from the reaction of LiC$_2$H with WCl(CO)$_3$Cp.[163]

Reactions between [W(CO)$_3$Cp$'$]$^-$ (Cp$'$ $=$ Cp, Cp^{Me}) and CH$_2$I$_2$ in MeCN give {W(CO)$_3$Cp$'$}$_2$(μ-C$\equiv$C) (**45/W$'$**) in 31% yield [together with WX(CO)$_3$Cp$'$ (X $=$ Me, I) in similar amounts].[164,165] In MeOH, intermediate formation of W(CH$_2$I)(CO)$_3$Cp$'$ and the ketene complexes W$_2$(μ-η^1: η^2-CH$_2$CO)(CO)$_5$Cp$'_2$ (**46**) is seen (Scheme 12). The latter are probably formed by insertion of CO into the μ-CH$_2$ derivative; when dissolved in MeCN, they are converted to the dicarbide by formal loss of H$_2$O. The Cp complexes are the less stable.

Generation of the C$_2$ ligand by modification of another two-carbon ligand has been achieved in the reactions of [M($=$C$=$CH$_2$)(CO)$_2$Tp*]$^-$ (M $=$ Mo, W), itself obtained by deprotonation (KOBu^t) of the methyl–carbyne complexes (Scheme 13).[166] Reactions of the anion with WI(CO)(η^2-C$_2$Ph$_2$)Tp afford Tp*(OC)$_2$M$\equiv$CCH$_2$W(CO)(η^2-C$_2$Ph$_2$)Tp (**47**) which are converted to the anions [Tp*(OC)$_2$M$\equiv$CCHW(CO)(η^2-C$_2$Ph$_2$)Tp]$^-$ (**48**) by treatment with KOBu^t. Further addition of an equivalent of KOBu^t and half an equivalent of I$_2$ afforded Tp*(OC)$_2$M$\equiv$CC$\equiv$W(CO)(η^2-C$_2$Ph$_2$)Tp (**49**) (by net removal of 2H). In contrast to the Cp complexes described above, the presence of a dicarbide bridge is suggested by the two resonances

R = H, Me
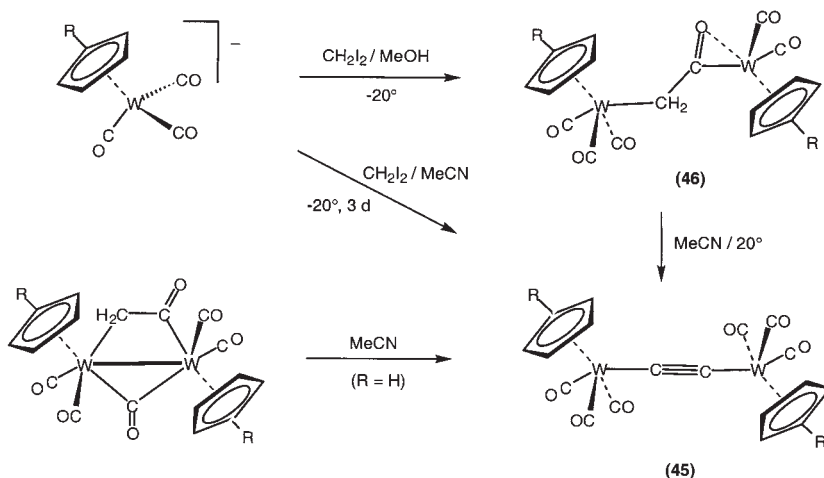
SCHEME 12

M = Mo,
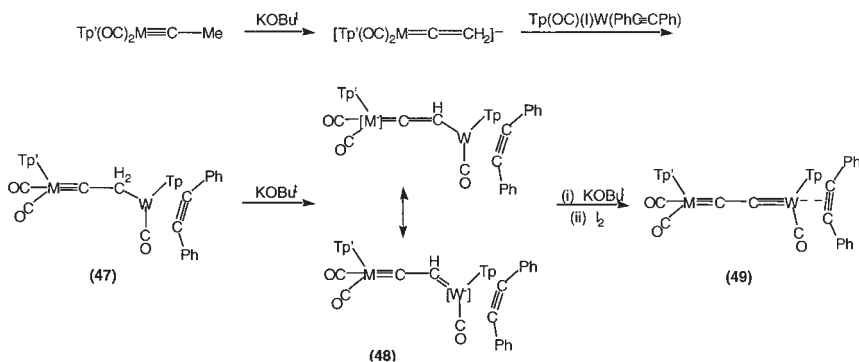
SCHEME 13

at δ 343 and 277 (M = Mo) or 347 and 274 (W). In the vinylidene precursor, the C₂Ph₂ ligand is a four-electron donor, whereas in the dicarbyne complex, it donates only two electrons, allowing formation of the dicarbyne bridge.

The dark red dicarbyne complex {W(OBuᵗ)₃}₂(μ-C₂) **(50)** was first reported from metathesis of W₂(OBuᵗ)₆ and EtC≡CC≡CEt (Scheme 14).[167] Two structure determinations revealed that the three OBuᵗ groups on each tungsten are staggered (D₃ᵈ). The structure of the toluene hemisolvate has rather longer W–C and shorter C–C bonds; both are consistent with the W≡C–C≡W formulation.[168–170] This complex is not a metathesis catalyst

$$(OBu^t)_3W\equiv C\!-\!\!-\!C\equiv W(OBu^t)_3$$

(50)

$$(Bu^tO)_3W\equiv\!\!\equiv\!\!W(OBu^t)_3 \qquad\qquad (Bu^tO)_3W\equiv C\!-\!\!-\!C\equiv W(OBu^t)_3$$

$$\xrightarrow{\hspace{3cm}}$$

(50)

$$+ \qquad\qquad\qquad\qquad +$$

$$EtC\equiv C\!-\!\!-\!C\equiv CEt \qquad\qquad EtC\equiv CEt$$
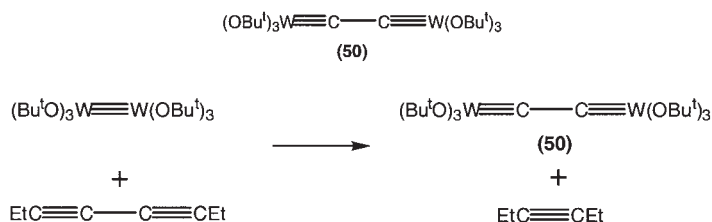
SCHEME 14

for alkynes and is probably formed as the most stable of the three possible alkylidyne products. However, when the reaction is carried out in the presence of quinuclidine (quin), slow formation of $W(\equiv CC\equiv CEt)(OBu^t)_3(quin)$ occurs. Several derivatives were obtained from $W(\equiv CEt)(OR)_3$ [R = Bu^t, $CMe_2(CF_3)$, CMe_2Et] and $EtC\equiv CC\equiv CEt$; use of more bulky deca-4,6-diyne gave only $W(\equiv CR')\{OCMe_2(CF_3)\}_3$ (R' = Pr, $C\equiv CPr$).[168]

(e) Group 7

Several reports have shown that general routes to complexes containing $M\text{–}C\equiv C\text{–}M$ fragments (M = Mn, Re) are not available, Li_2C_2 and $MnBr(CO)_5$ giving only $Mn_2(CO)_{10}$[141] while Li_2C_2 or Na_2C_2 with $Re(FBF_3)(CO)_5$ also does not give the desired product.[171] Similarly, the reaction between $MnBr(CO)_5$ and $C_2(SnMe_3)_2$ gives only $Mn(SnMe_3)(CO)_5$ and $\{Mn(CO)_5\}_2SnMe_2$.[172]

Comparison of the reactions of $[M(CO)_5]^-$ (M = Mn, Re) with C_2I_2 showed that, while the rhenium anion abstracts I^+ to give $ReI(CO)_5$ and $\{Re(\mu\text{-}I)(CO)_4\}_2$, the manganese anion gives pale yellow $\{Mn(CO)_5\}_2(\mu\text{-}C\equiv C)$ (**51/Mn**) accompanied by $\{Mn(\mu\text{-}I)(CO)_4\}_2$.[173] This C_2 complex can also be obtained from $Mn(FBF_3)(CO)_5$ and $HC\equiv CSiMe_3$, followed by deprotonation of the resulting $[\{Mn(CO)_5\}_2(\mu\text{-}\eta^1:\eta^2\text{-}C_2H)]BF_4$ with $K[BHEt_3]$.[172]

In the course of studies of the synthesis of binuclear hydrocarbon-bridged complexes by nucleophilic attack of anionic metal carbonyls on coordinated unsaturated hydrocarbons,[34,174] reaction of $Re(FBF_3)(CO)_5$ with $Re(C\equiv CH)(CO)_5$, itself obtained from $Re(FBF_3)(CO)_5$ and $HC\equiv CSiMe_3$, afforded $[\{Re(CO)_5\}_2(\mu\text{-}\eta^1:\eta^2\text{-}C_2H)]^+$ which could be deprotonated with $K[BHEt_3]$ to $\{Re(CO)_5\}_2(\mu\text{-}C\equiv C)$ (**51/Re**; Scheme 15).[175,176] The latter reaction can be reversed with $[Et_2OH]BF_4$ and methylation ($[Me_3O]^+$) gives $[\{Re(CO)_5\}_2(\mu\text{-}\eta^1:\eta^2\text{-}C_2Me)]BF_4$, although reactions with HX (X = Cl, OTf) afford $ReX(CO)_5$.

The reaction between $Re_2O_7(thf)_2$ and $Bu_3SnC\equiv CSnBu_3$ gives the extremely unstable $\{ReO_3\}_2(\mu\text{-}C\equiv C)$ (**52**) in quantitative yield (by NMR). Hydrolysis rapidly produces $ReO_3(C\equiv CH)$, which is further converted to $H[ReO_4]$.[177]

SCHEME 15

SCHEME 16

(f) Group 8

Iron. Deprotonation of $[Fp_2^*(\mu\text{-}\eta^1:\eta^2\text{-}C_2H)]^+$ $[Fp^* = Fe(CO)_2Cp^*]$ with NaOMe gives brick-red $Fp^*C{\equiv}CFp^*$ (**53**) in a reaction which is reversed with acid (HOTf).[178–180] The reactions of the cation with other carbon nucleophiles [LiMe, LiCuMe$_2$, NaCH(CO$_2$Me)$_2$] also give **53**,[180,181] but LiR (R = Bu, Bu^t) gives acylvinylidene **54** by further attack on a CO group of the C$_2$ complex (Scheme 16). In the solid-state, a solvent MeOH molecule interacts with the C${\equiv}$C triple bond of **53** inducing a bending of the iron

[Ru] = Ru(CO)$_2$Cp
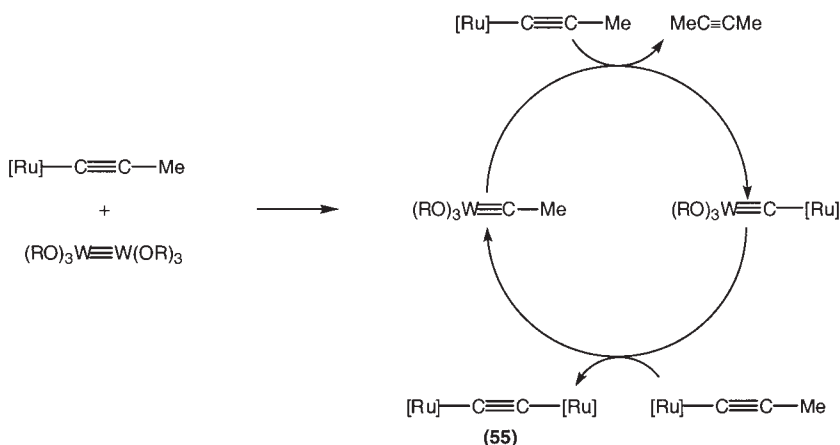
SCHEME 17

substituents away from the MeOH [Fe–C–C, 173.0, 173.3(8)°], while no distortion is seen in the solvent-free molecule. The H atom of MeOH is 2.41, 2.45(5) Å distant from the two C atoms, with some elongation of the C≡C triple bond [1.202(5) vs. 1.173(4) Å].[182]

Ruthenium. Although the reaction between W(≡CEt)(OBu^t)$_3$ and Ru(C≡CMe)(CO)$_2$Cp in toluene gives (Bu^{t}O)$_3$W≡C–Ru(CO)$_2$Cp (Section II.A), loss of volatile C$_2$Me$_2$ and precipitation of yellow {Ru(CO)$_2$Cp}$_2$(μ-C≡C) (**55**) occurs if the reaction is carried out in iso-octane (Scheme 17).[104,105] The latter can be obtained in 66% yield if W$_2$(OBu^t)$_6$ is used as a catalyst (up to nine turnovers per W atom); the Cp^{Me} analogue is also known.[104] Extension of the reaction to a mixture of Ru(C≡CMe)(CO)$_2$Cp^{Me} and (Bu^{t}O)$_3$W≡C–Ru(CO)$_2$Cp^{Me} afforded {Cp^{Me}(OC)$_2$Ru}$_2$(μ-C≡C).

(g) Group 10

Nickel. The only mention of a nickel-C$_2$ system appears to be as an intermediate in the reactions of NiCl$_2$(PR$_3$)$_2$ (R = Me, Pr, Bu) with C$_2$Cl$_2$, in which an intermediate nickel(I) species NiCl(PR$_3$)$_n$ may react with NiCl(C≡CCl)(PR$_3$)$_2$ to give {NiCl(PR$_3$)$_2$}C≡C{NiCl$_2$(PR$_3$)} (**56**; Scheme 18).[183] Elimination of NiCl(PR$_3$)$_n$ then generates the observed product, [NiCl(C≡CPMe$_3$)(PMe$_3$)$_2$]$^+$.

Palladium and platinum. Reactions of alkali metal acetylides, M$_2$C$_2$ (M = Na, K) with Pd or Pt (550 °C, in argon) gave black M$_2$(Pd/Pt)C$_2$,
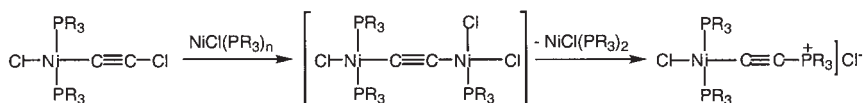
(56) R = Me, Pr, Bu

SCHEME 18
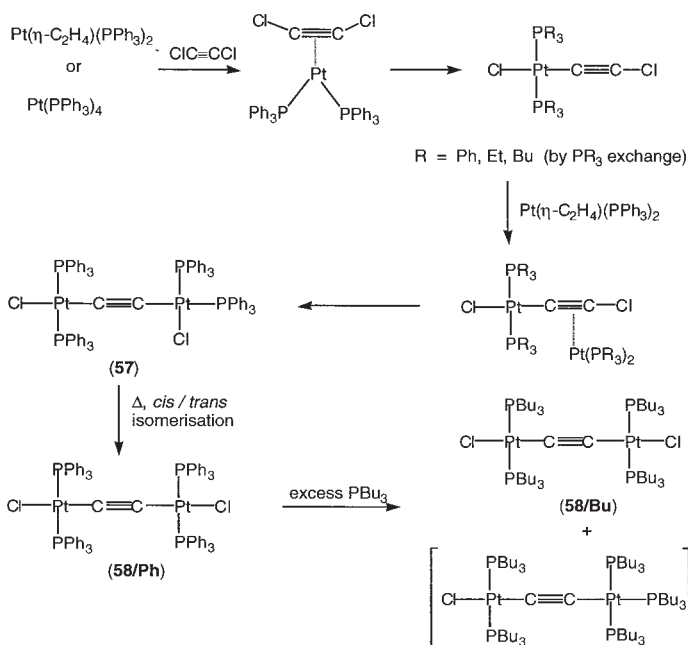
SCHEME 19

which are air- and moisture-sensitive.[184,185] They contain $-\{M-C-C\}_n-$ chains, which interact with the alkali metal cations via the C_2 units; each Pd/Pt atom is octahedrally surrounded by six M atoms. The C–C separations are lengthened [1.263(3) (Pd), 1.289(4) Å (Pt)] and $\nu(CC)$ reduced [ca. 1850 cm^{-1}] as a result of significant back-bonding into the C_2 unit. The compounds are semi-conductors with an indirect band gap of ca. 0.2 eV.

Isomerization of Pt(η^2-C_2Cl_2)(PPh$_3$)$_2$ [from C_2Cl_2 and Pt(η^2-C_2H_4)(PPh$_3$)$_2$ or Pt(PPh$_3$)$_4$] to *trans*-PtCl(C≡CCl)(PPh$_3$)$_2$ occurs upon refluxing in toluene for several hours. Further reaction of the latter with Pt(η^2-C_2H_4)(PPh$_3$)$_2$ gives {*trans*-PtCl(PPh$_3$)$_2$}C≡C{*cis*-PtCl(PPh$_3$)$_2$} **(57;** Scheme 19).[186] Ready exchange of PEt$_3$ for PPh$_3$ occurs. A similar reaction with *trans*-PtCl(C≡CCl)(PEt$_3$)$_2$ gives a mixture of the binuclear μ-η^1:η^2-C≡CCl complex, which isomerizes to the C_2 complex upon warming in

solution, and {*trans*-PtCl(PEt$_3$)$_2$}C≡C{*cis*-PtCl(PPh$_3$)$_2$}. Complex **57** converts to the *trans, trans* isomer **58/Ph** on heating in refluxing toluene for several hours. The two Pt(PPh$_3$)$_2$ groups are staggered, the angle between the two P–Pt–P vectors being 82°, generating an ovoid molecule with diameters ca. 10–11 and 12.5 Å. An excess of PBu$_3$ reacts with **58/Ph** to give a mixture of {*trans*-PtCl(PBu$_3$)$_2$}$_2$(C≡C) (**58/Bu**) and [{*trans*-PtCl(PBu$_3$)$_2$}C≡C{Pt(PPh$_3$)$_3$}]Cl.

Copper-catalyzed coupling (CuCl/NHEt$_2$) of *trans*-M(C≡CH)$_2$(PMe$_3$)$_2$ with MCl$_2$(PMe$_3$)$_2$ gives lemon yellow (Pd) or white (Pt) {*trans*-MCl(PMe$_3$)$_2$}$_2$(μ-C≡C) (M = Pd, Pt); the corresponding Pd/PR$_3$ (R = Et, Bu) complexes require longer reaction times.[187,188] The reaction proceeds via MCl(C≡CH)(PR$_3$)$_2$ which then reacts with further dichloro complex. Exchange of Cl for I occurs with KI (for the PdCl/PMe$_3$, PEt$_3$, and PtCl/PMe$_3$ compounds) while with C$_2$H$_2$, the palladium complex gave only Pd(C≡CH)$_2$(PMe$_3$)$_2$. In the presence of PhCN, the cationic derivatives [{Pd(NCPh)(PEt$_3$)$_2$}$_2$(μ-C≡C)]X$_2$ (X = Cl, PF$_6$) are formed.[189]

The synthesis of {[C$_6$H$_3$(CH$_2$NMe$_2$)$_2$-2,6]Pt}$_2$C$_2$ (**59**) from the chloro complex and Li$_2$C$_2$ has been described.[190] Zwitterionic μ-η^1:η^2-C$_2$SiMe$_3$ complexes {*cis*-Pt(C$_6$F$_5$)$_2$(CO)(μ-η^1:η^2-C$_2$SiMe$_3$)}{*trans*-Pt(C≡CSiMe$_3$)(PR$_3$)$_2$} (R = Et, Ph) have been obtained from *trans*-Pt(C≡CSiMe$_3$)$_2$(PR$_3$)$_2$ and *cis*-Pt(C$_6$F$_5$)$_2$(CO)(thf). Treatment with MeOH or EtOH gives alkoxycarbene complexes {*cis*-Pt(C$_6$F$_5$)$_2$(CO)}C≡C{*trans*-Pt[CMe(OR)](PR$_3$)$_2$} (**60**) from reactions which involve protodesilylation and the possible intermediacy of vinylidene complexes (Scheme 20).[191]
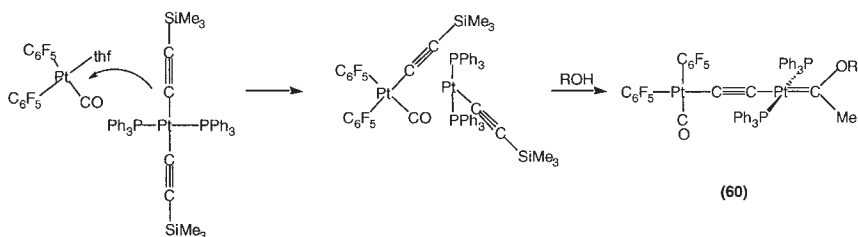
SCHEME 20

(h) Group 11

The extensive early chemistry of the Group 11 acetylides, M$_2$C$_2$, has been summarized in Gmelin.[192] The structures of polymeric copper(I) and silver(I) acetylides, M$_2$C$_2$ (M = Cu, Ag) are unknown, but have been assumed to involve both σ and π bonding of the C$_2$ unit as it bridges the Group 11 atoms (**K**). However, they either react with ligands or dissolve in solutions of silver(I) salts to give more tractable products.

(**K**)
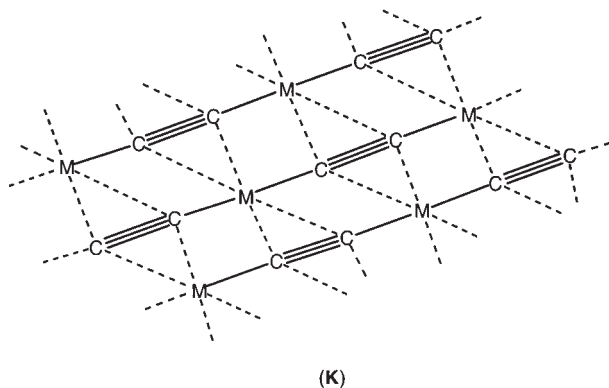
Copper. The compound $\{Cu_2C_2\}_n$ is formed readily from ethyne and sources of copper(I) in aqueous or aqueous ammoniacal solution as an explosive orange monohydrate, or from Cu_2I_2 and $KC\equiv CH$ in liquid ammonia as dark red crystals.[193–195] It is also formed by decomposition of orange $CuC\equiv CH$ above $-45°$, or from the reaction between CuCl and $\{[C_6H_3(CH_2NMe_2)_2\text{-}2,6]Pt\}_2C_2$.[190] The acetylide is insoluble in all solvents with which it does not react; with HCl or KCN solutions, ethyne is liberated. If copper(II) salts are used, red CuC_2 is formed.

Extensive studies of its chemistry have been carried out in conjunction with the use of Cu(I) as a catalyst for the synthesis of various acetylenic derivatives from ethyne and aldehydes or ketones. On standing in air at r.t., it appears to disproportionate, evidence for the formation of Cu_2C_4 being presented,[196] and higher members of the series Cu_2C_n ($n \leq 20$) have been obtained by oxidation of Cu_2C_2 with $CuCl_2$. Thermal decomposition gives a fine powder, suggested to be "carbyne".[197,198] Treatment of the oxidized material with HCl has given mixtures of $H(C\equiv C)_mH$ ($m = 1$–6).

Silver. Similarly, extensive reports about the chemistry of Ag_2C_2 are available, which emphasize its greater explosive power compared with Cu_2C_2. In liquid ammonia, $AgNO_3$ reacts with $KC\equiv CH$ to give a deep yellow precipitate (probably $AgC\equiv CH$) which spontaneously loses ethyne at $0\,°C$ to give explosive white Ag_2C_2. The reaction between Ag_2C_2 and KC_2H in liquid ammonia gives a mixture of $K[Ag(C\equiv CH)_2]$ and insoluble $KC\equiv CAg$.[199] The latter reacts with water to give Ag_2C_2 and dissolves in aqueous KCN, forming $K[Ag(CN)_2]$, both reactions proceeding with the evolution of ethyne. Other preparations are from $AgNO_3$ and $Hg_2(C\equiv CH)_2$ or $C_2(CO_2Na)_2$.

A large number of multiple salts containing Ag_2C_2 have recently been shown to contain C_2 units within Ag_n cages ($n = 7$–24) (Section IX.C). Ternary carbides $MAgC_2$ (M = alkali metal), which are not explosive, have been prepared from an excess of MC_2H and AgI in liquid ammonia via $M[Ag(C_2H)_2]$, which loses ethyne at 120–130 °C to give insoluble $MAgC_2$.[200] The insoluble Li compound could also be obtained by heating $Li[Ag(C_2H)_2]$ in boiling pyridine. They contain $-\{Ag-C-C\}_n-$ chains, the alkali metal cation being associated with three (Li) or four $C\equiv C$ units in separate chains.

Gold. Explosive Au_2C_2 has been known for over a century.[201,202] Yellow polymeric gold(I) alkynyl compounds are readily prepared from the alkyne and $AuCl_3$ and KBr in aqueous acetone after reduction with SO_2. The brown, explosive precipitate of $Au_2C_2 \cdot NH_3$, from AuI and $K[C\equiv CH]$ in liquid NH_3, is touch-sensitive, and with an excess of $K[C\equiv CH]$ dissolves to form white $K_2[\{Au(C\equiv CH)\}_2(\mu-C\equiv C)]$, which reacts with ethyne to give $K[Au(C\equiv CH)_2]$.[202] The C_2 complex reacts with KCN to give $[Au(CN)_2]^-$ and ethyne. Extension to similar derivatives $K[\{AuR\}_2(\mu-C\equiv C)]$ (R = CN, $C\equiv CH$, $C\equiv CMe$, $C\equiv CPh$) from reactions of $\{Au_2C_2\}_n$ with CN^- or $[C\equiv CR]^-$ was also reported, these anions being isolated as their $[PPh_4]^+$ salts; characterization was limited to IR and ^{31}P NMR spectroscopy.[203]

More recently, reactions of alkali metal acetylides, HC_2M (M = Li–Cs), with AuI in liquid NH_3 and subsequent heating of the solid product in pyridine (Li–K) or in vacuum (Rb, Cs) gave pale yellow M_2AuC_2.[184,185] They contain $-\{Au-C-C\}_n-$ chains, which interact with the alkali metal cations via the C_2 units, and are generally similar to the analogous silver compounds.[204]

Treatment of $AuCl(PR_3)$ with ethyne in the presence of base (NaOEt) gives firstly, $Au(C\equiv CH)(PR_3)$ (R = Ph, tol-3 and -4, C_6H_4OMe-4) and then $\{Au(PR_3)\}_2(\mu-C\equiv C)$ (**61**), a process which may proceed directly if the intermediate ethynyl complex is soluble.[205–207] Modifications of the synthetic procedure have included addition of thf to improve solubility, use of the colloidal solution of $AuCl(PR_3)$ obtained by running this solution into EtOH, and the use of $KOBu^t$ or KOH in EtOH. Prolonged reaction times with ethyne results in increasing amounts of $Au(C\equiv CH)(PR_3)$ being formed, which can be sometimes separated from the C_2 complex only with difficulty. Treatment of $Au(C\equiv CSiMe_3)(PPh_3)$ with K_2CO_3 in methanol gave a quantitative yield of $\{Au(PPh_3)\}_2(\mu-C\equiv C)$, possibly via an intermediate $[Au(C\equiv C)(PPh_3)]^-$ anion.[208] Other examples of complexes with $PR_3 = P(nap)_3$, $PPh_2(bp)$ (bp = biphenylyl) and $PPhFc_2$ have been described.[209] Facile metathesis of $W_2(OBu^t)_6$ or $W(\equiv CEt)(OBu^t)_3$ and $Au(C\equiv CMe)(PR_3)$ (R = Et, Ph) gives $\{Au(PR_3)\}_2(\mu-C\equiv C)$.[105] In their fast-atom bombardment mass spectra, aggregation processes predominate,
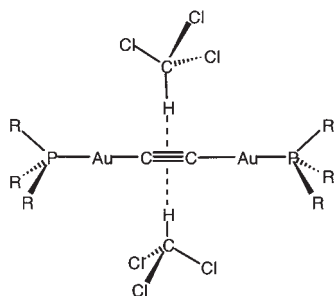
(62) $PR_3 = PPh_{3-n}(nap)_n$, n = 1,2

the highest mass ions being found around m/z 4000, corresponding to $[M_4 + Au_2C_2]^+$ $[M = C_2\{Au(PR_3)\}_2]$, other fragment ions being assigned as $[M_n + Au]^+$ and $[M_n + Au(PR_3)]^+$.[207]

Most of these complexes form strong solvates with CH_2Cl_2 or $CHCl_3$, or with C_6H_6. The solid-state structure of the the PPh_3 complex contains a benzene molecule included in an octahedral cavity formed by the Ph groups of the PPh_3 ligand. Similarly, the $P(C_6H_4Me-3)_3$ derivative forms an elongated cavity that has been likened to a wine barrel with the Ph rings as the staves and the Me groups as the ends.[207] Other features include the aromatic ring stacking of naphthyl groups in the $PPh_2(nap)$ and $PPh(nap)_2$ complexes.[209] There are no aurophilic interactions in the solid-state structures of $CHCl_3$ solvates of $\{Au(PR_3)\}_2(\mu\text{-}C\equiv C)$ [**62**; $PR_3 = PPh_{3-n}(nap)_n$, $n = 1$, 2].[209,211] The chloroform solvate molecules are arranged so that the C–H bond points to the center of the $C\equiv C$ triple bond 2.42 Å away. For the $PPh(nap)_2$ complex, two $CHCl_3$ molecules "dock" with the same π orbital, while for the $PPh_2(nap)$ complex, four $CHCl_3$ molecules are found, two interacting with each $C\equiv C$ π orbital at 2.50, 2.58 Å. These arrangements have been likened to a "reversed coordination" (square-planar and octahedral, respectively) of the C_2 moiety; the bulky $Au(PR_3)$ substituents generate cavities in which the solvate molecules are protected. DFT calculations indicate that the bonding is strong (10–15 kJ mol^{-1}), with the $C\equiv C$ triple bond becoming more electron rich than in ethyne as a result of the $Au(PR_3)$ groups.[212]

(i) Group 12

Very little is known about white mercury(I) acetylide, which is formed as a monohydrate by passing ethyne into aqueous solutions of mercury(I) acetate, while white HgC_2 was similarly obtained from HgI_2/KI or $K_2[Hg(CN)_4]$ solutions.[213] This material decomposes at 100 °C and with dilute HCl, affords ethyne. The mercury(I) compound $Hg_2C_2 \cdot H_2O$, from

ethyne and $Hg_2(OAc)_2$ in the dark, cannot be freed from water without decomposition.

A series of white organomercury complexes $\{HgR\}_2(\mu\text{-}C\equiv C)$ (63; R = Me, Et, Pr, Bu, C_5H_{11}, C_6H_{13}, Ph, C_6H_4Me-2, and -4, CH_2Ph), which are volatile enough to have a garlic odour, were prepared by passing ethyne into solutions of HgXR (X = Cl, Br, I) containing 10% KOH.[214] The compounds, which precipitate out from the reaction medium, can be crystallized from organic solvents. Reactions with HCl give ethyne and with iodine give C_2I_2 and HgI_2. Similar compounds have been obtained from HgClR (R = CH_2Ph, Ph) and $C_2(SnBu_3)_2$.[215] With $HgCl_2$, an oligomeric compound, formulated as $Cl(HgC\equiv C)_nSnBu_3$ ($n \sim 5$) was formed, while with a 2/1 ratio of reactants, the product is $Cl(HgC\equiv C)_2HgCl$. Little is known about these derivatives, although ^{13}C and ^{199}Hg NMR data for compounds with R = Me, Et, Cy, Ph have been reported. Large variations in $J(CHg)$ are explained in terms of varying contributions to the Fermi contact interaction as a result of differing polarization of the Hg–C(sp) bond.

(j) Mixed metal systems

Table IV lists hetero-binuclear C_2 complexes with some spectroscopic data.

Zr–Fe, Zr–Ru. In contrast to $Ru(C\equiv CH)(PMe_3)_2Cp$, which is hydro-zirconated to $\{ZrClCp_2\}CH=CH\{Ru(PMe_3)_2Cp\}$ by $\{ZrHClCp_2\}_n$,[217] the dark red iron analogue $Fe(C\equiv CH)(dppe)Cp^*$ reacts to form $\{ZrClCp_2\}C\equiv C\{Fe(dppe)Cp^*\}$ (64) in quantitative yield.[218] The difference probably results from the increased steric hindrance about the iron atom.

Reactions of $Ru(C\equiv CH)(PMe_3)_2Cp$ with $ZrCl(X)Cp_2$ (X = Me or better, NMe_2) give orange $\{ZrClCp_2\}C\equiv C\{Ru(PMe_3)_2Cp\}$ (65) as an example of a complex with electron-poor and electron-rich metal centers at each end of the C_2 ligand ("push–pull alkyne").[219] The complex is thermally stable but extremely sensitive to water. A contribution from the zwitterionic form $Ru^+=C=C=Zr^-$, resulting from the disparity in electron density at the two metal centers tending to equalize through the C_2 ligand, accounts for a somewhat longer C–C distance [1.251(20) Å] than found in $\{Ru(CO)_2Cp\}_2(\mu\text{-}C\equiv C)$, and lower $\nu(CC)$ absorption (1868 cm^{-1}) and ^{13}C chemical shifts [δ 178.3 (CRu), 190.4 (CZr)].

W–Fe, W–Ru. In the presence of $TlBF_4$, reactions of $WCl(CO)(\eta^2\text{-}C_2Ph_2)Cp$ with $M(C\equiv CH)(L)_2Cp$ [M = Fe, L = PMe_3, $P(OMe)_3$, L_2 = dppp; M = Ru, L = PMe_3, $P(OMe)_3$] give the μ-η^1_M:η^2_W-C_2H cations (66), which can be deprotonated with $KOBu^t$ or $NaN(SiMe_3)_2$ to $\{W(CO)(\eta^2\text{-}C_2Ph_2)Cp\}C\equiv C\{ML_2Cp\}$ (67).[220] The μ-ethynyl cation is regenerated by addition of HBF_4 to the $Ru(PMe_3)_2Cp$ derivative. Unusually, the W–C–C

$$L_nM\text{-}C\equiv C\text{-}M'L'_m$$
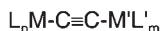
ML$_n$	**M'L'**$_m$
(64) ZrClCp$_2$	Fe(dppe)Cp*
(65) ZrClCp$_2$	Ru(PMe$_3$)$_2$Cp
(67) W(CO)(η-C$_2$Ph$_2$)Cp	M(L)$_2$Cp
	[M = Fe, L = PMe$_3$, P(OMe)$_3$; L$_2$ = dppp;
	M = Ru, L = PMe$_3$, P(OMe)$_3$]
(69) [Mn(CO)$_2$Cp']$^-$	Fe(CO)$_2$Cp*
(70) Re(NO)(PPh$_3$)Cp*	Rh(CO)(PPh$_3$)$_2$
(71) Re(NO)(PPh$_3$)Cp*	trans-PdCl(PEt$_3$)$_2$
(72) Fe(dppm)Cp,	Au(PPh$_3$)
Ru(PPh$_3$)$_2$(η^5-C$_9$H$_7$)	
(73) trans-PdCl(PBu$_3$)$_2$	trans-PtCl(PBu$_3$)$_2$

M = Fe, L = PMe$_3$, P(OMe)$_3$, dppp/2
M = Ru, L = PMe$_3$, P(OMe)$_3$
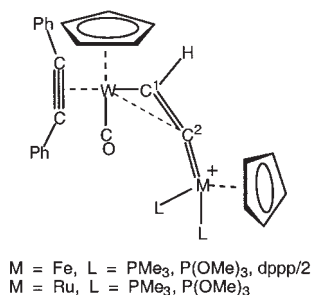
(66)

angle in the cation [97.3(8)°] suggests that there is some bonding interaction between the tungsten and C(2), although W–C(1) is long at 2.53(1) Å, leading to a description of this complex as containing a metallated (tungsten) vinylidene ligand (alternatively a 3-center, 2-electron system).

Mo–Cu, Ag. Reactions of [NH$_4$]$_2$[MoS$_4$] with M$_2$C$_2$ (M = Cu, Ag) give violet or brown materials formulated as [NH$_4$]$_2$[MoS$_4$M$_2$C$_2$].[221] Analytical and spectroscopic studies suggest that these contain polymeric bridged anions (**68**). Addition of Lewis bases L (py, bpy, phen, nicotinamide, PPh$_3$) give monomeric species formulated as [S$_2$Mo(μ-S)$_2$MC≡CML$_2$]$^{2-}$.

TABLE IV

Selected Spectroscopic Properties of Hetero-Binuclear Complexes, $\{ML_x\}-C_n-\{M'L'_y\}$

		IR (Raman)	δ_C (J/Hz)		λ nm	
ML_x	$M'L'_y$	ν(CC) cm^{-1}	C(1)	C(2)	(ε M^{-1} cm^{-1})	Ref.
Group 4						
ZrClCp$_2$	Ru(PMe$_3$)$_2$Cp	1868[a]	190.4	178.3	418	217
		1872[b]		(PC 22.8)	(ε not given)	
ZrClCp$_2$	Fe(dppe)Cp*	1843[a]	207.1	192.2		218
				(PC 40)		
Group 6						
Mo(CO)$_2$Tp*	W(CO)(C$_2$Ph$_2$)Tp	not observed	277.0	342.7		166
			(CW 43)	(CW 184)		
W(CO)$_2$Tp*	W(CO)(C$_2$Ph$_2$)Tp	not observed	274.4	347.5		166
			(CW 171)	(CW 185)		
W(CO)(C$_2$Ph$_2$)Cp	Ru(PMe$_3$)$_2$Cp	not observed	144.7	195.0		220
W(CO)(C$_2$Ph$_2$)Cp	Fe(PMe$_3$)$_2$Cp	not observed	160.6	211.2		433
W(CO)(C$_2$Ph$_2$)Cp	Fe{P(OMe)$_3$}$_2$Cp	not observed	158.9	179.5		433
W(CO)(C$_2$Ph$_2$)Cp	Fe(dppp)Cp	not observed	165.1	198.1		433
W(CO)(C$_2$Ph$_2$)Cp	Ru{P(OMe)$_3$}$_2$Cp	not observed	144.5	168.4		433
Group 7						
Re(NO)(PPh$_3$)Cp*	Rh(CO)(PPh$_3$)$_2$	1961[b]	134.6	153.4		223,224
		1961[a]	(CP 10.5)	(CRh 37.7,		
				CP 21.2)		

Re(NO)(PPh₃)Cp*	PdCl(PEt₃)₂-*trans*	1989[b] 1994[a] (1971)	111.7 (CPPh 15.1, CPEt 4.3)	116.2 (CPPh 1.5, CPEt 17.5)	390 (4000), 314 (17,000), 268 (35,000), 234 (76,000)	223,224
Group 8						
Fe(dppm)Cp	Au(PPh₃)	1966[a]	overlap with Ph (128.8–133.0)			225
Ru(CO)₂Cp	Ru(CO)₂Cp^Me		82.3, 83.6			105
Ru(PPh₃)₂(η⁵-C₉H₇)	Au(PPh₃)	1933[a]	226.39 (CP 19.4), overlap with Ph (127.3–138.7)			225
Ru(dppe)(η⁵-C₉H₇)	Au(PPh₃)	1935[a]	220.80 (CP 19.7), overlap with Ph (128.1–134.6)			225
Ru(PMe₃)(PPh₃) (η⁵-C₉H₇)	Au(PPh₃)	not observed	227.70, overlap with Ph (127.65–139.6)			225
Group 10						
cis-Pt(C₆F₅)₂(CO)	*trans*-Pt{CMe(OEt)} (PEt₃)₂	2021[c]	173.3 (CP 4.5)			191
cis-Pt(C₆F₅)₂(CO)	*trans*-Pt{CMe(OMe)} (PEt₃)₂	2026[c]				191
cis-Pt(C₆F₅)₂(CO)	*trans*-Pt{CMe(OEt)} (PPh₃)₂	2030[c]				191
cis-Pt(C₆F₅)₂(CO)	*trans*-Pt{CMe(OMe)} (PPh₃)₂	2019[c]				191
trans-PdCl(PEt₃)₂	*trans*-PtCl(PEt₃)₂		94.26 (CP 16, CPt 363)	88.62 (CP 14, CPt 1339)		226

[a]Enantiomeric pair. [b]thf. [c]Nujol.
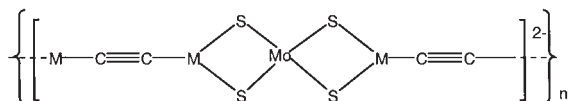
(68) M = Cu, Ag

Mn–Fe. Deprotonation (LiBu) of Mn(=C=CHFp*)(CO)$_2$Cp′ gives the anionic species Li[{Mn(CO)$_2$Cp′}C≡CFp*] (**69**).[222] An excess of LiBu attacks an iron-bonded CO group to give eventually the μ-acylvinyl complex {Mn(CO)Cp′}(μ-CO){μ-η^1:η^2-CH=CHC(O)Bu(Fp*)} (Scheme 16).[181] Calculations indicate preferred sites of electrophilic attack are C$_\beta$ (to Mn) and Mn, which is found for protonation (or deuteration). In contrast, methylation affords Mn{η^2-MeC$_2$[Fp*]}(CO)$_2$Cp′ by attack at C$_\alpha$, a result explained by the bulky Cp* ligand preventing attack on C$_\beta$ by anything larger than a proton. No reaction is found with SiClMe$_3$.

Re–Rh, *Re–Pd*. Metallation of Re(C≡CH)(NO)(PPh$_3$)Cp* with LiBu, followed by addition of RhCl(CO)(PPh$_3$)$_2$ or *trans*-PtCl$_2$(PEt$_3$)$_2$, gives the red heterobimetallic C$_2$ complexes {Re(NO)(PPh$_3$)Cp*}C≡C{ML$_n$} [ML$_n$=Rh(CO)(PPh$_3$)$_2$ (**70**), *trans*-PdCl(PEt$_3$)$_2$ (**71**)].[223,224] In both cases, steric interactions between the bulky PR$_3$ ligands on Rh or Pd and the Cp* and PPh$_3$ ligands on Re probably account for restricted rotation about the C≡C bond indicated by low temperature ^{31}P NMR spectra.

Fe, Ru–Au. A series of mixed-metal C$_2$ complexes is obtained from reactions between M(C≡CH)(PP)Cp′ [M = FeCp, PP = dppm; MCp′ = Ru(η^5-C$_9$H$_7$), PP = (PPh$_3$)$_2$, dppe, (PMe$_3$)(PPh$_3$)] and AuCl(PPh$_3$) in the presence of Tl(acac) as halide abstractor. Stille couplings of AuCl(PPh$_3$) with Fe(C≡CSnPh$_3$)(dppm)Cp or Ru(C≡CSnPh$_3$)(PPh$_3$)$_2$(η^5-C$_9$H$_7$) also give the respective Fe–Au and Ru–Au complexes (**72**).[225]

Pd–Pt. The heterometallic {*trans*-PdCl(PR$_3$)$_2$}C≡C{*trans*-PtCl(PR$_3$)$_2$} (**73**, R = Me, Et, Bu) were best prepared from *trans*-PdCl$_2$(PR$_3$)$_2$ and *trans*-Pt(C≡CH)$_2$(PR$_3$)$_2$; the reaction between *trans*-PdCl(C≡CH)(PEt$_3$)$_2$ and *trans*-PtCl$_2$(PEt$_3$)$_2$ gave the Pd/Pt–C$_2$ complex together with some of the homonuclear products as a result of ready self-disproportionation.[226]

C. *Complexes Containing C$_3$ Ligands*

Possible reactions which lead to C$_3$ ligands bridging two transition metals include:

(a) reaction of lithiated ethynyl-metal complexes with metal carbonyls, followed by treatment of the intermediate anion with [OMe$_3$]BF$_4$ to

give methoxycarbene derivatives. Subsequent abstraction of the OMe group (BF_3) gives the C_3 complex;

(b) removal of H atoms from hydrocarbon fragments bridging two metal centers, such as methylene-bridged bis-carbyne complexes;

(c) metathesis of $C \equiv C$ and $M \equiv C$ triple bonds.

1. Tp*M Systems (M = Mo, W)

The vinylidene anions $[M(=C=CH_2)(CO)_2Tp^*]^-$ (M = Mo, W), obtained by deprotonating $M(\equiv CMe)(CO)_2Tp^*$, react with $Mo(\equiv CCl)(CO)_2Tp^*$ to give $Tp^*(OC)_2M \equiv CCH_2C \equiv Mo(CO)_2Tp^*$ (**74**, Scheme 21).[227] The Mo–W derivative is deprotonated ($KOBu^t$) to the dianion $[Tp^*(OC)_2W=C=C=C=Mo(CO)_2Tp^*]^{2-}$ (**75**), which reacts with H^+ or
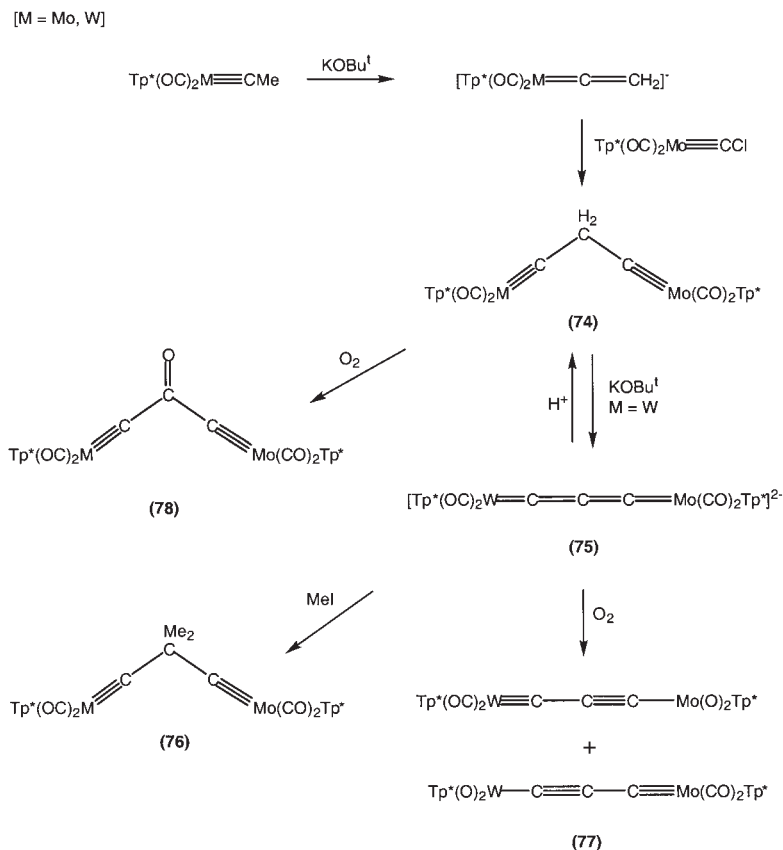
SCHEME 21

MeI to give $Tp^*(OC)_2W\equiv CCR_2C\equiv Mo(CO)_2Tp^*$ (**74** or **76**, respectively). In the dianion, the carbons of the C_3 unit are found at δ 238.4 (WC), 234.4 (MoC) and 153.8 (CCC). After addition of $KOBu^t$, the anion can be oxidized (air) to give a separable mixture of $Tp^*(OC)_2W\equiv CC\equiv CMo(O)_2Tp^*$ (**77/Mo**) and $Tp^*(O)_2WC\equiv CC\equiv Mo(CO)_2Tp^*$ (**77/W**), the former predominating. The green dimolybdenum analogue is formed from $Tp^*(OC)_2Mo\equiv CCH_2C\equiv Mo(CO)_2Tp^*$ and $KOBu^t$, followed by exposure to air. Aerial oxidation of $Tp^*(OC)_2W\equiv CCH_2C\equiv Mo(CO)_2Tp^*$ or direct reaction between the dianion and 2-PhSO$_2$-3-Ph-oxaziridine and HCl, affords the unsaturated ketones $Tp^*(OC)_2M\equiv CC(O)C\equiv Mo(CO)_2Tp^*$ (**78**).

2. Complexes Derived from Re(C≡CH)(NO)(PPh$_3$)Cp*

Lithiation of $Re(C\equiv CH)(NO)(PPh_3)Cp^*$ ($LiBu/thf$, $-80\,^\circ C$) and reaction with $W(CO)_6$ or $Mn(CO)_3Cp'$ ($Cp' = Cp$, η-C$_5$HCl$_4$, η-C$_5$Cl$_5$) and addition of $[OMe_3]BF_4$ gave $\{Re(NO)(PPh_3Cp^*\}\{\mu$-C$\equiv CC(OMe)=\}\{M(CO)_x\}$ (**79**, M = W, $x = 5$; M = MnCp', $x = 2$; Scheme 22).[228–230] Many attempts to remove the OMe group from the W complexes were unsuccessful, but treatment of the Mn derivatives with BF$_3$ gave $[\{Mn(CO)_2Cp'\}CCC\{Re(NO)(PPh_3)Cp^*\}]BF_4$ (**80**). Spectroscopic and structural data are consistent with the cumulenylidene, formulation $Re^+=C=C=C=Mn$ for the bridge. For the Mn complexes, the most intense UV–vis bands show progressive red-shifts from Cp to η-C$_5$Cl$_5$ (392, 396, 414 nm). The blue-grey Re–C$_3$–Fe analogue $[\{Re(NO)(PPh_3)Cp^*\}CCC\{Fe(CO)_4\}]BF_4$ was obtained similarly, but neither this nor the SbF$_6$ salt could be structurally characterized.[229]

The same approach applied to $Re_2(CO)_{10}$ afforded cis-$\{Re(NO)(PPh_3)Cp^*\}\{\mu$-C$\equiv CC(OMe)=\}\{Re(CO)_4Re(CO)_5\}$ (**81**) which with BF$_3$ gave $[\{Re(NO)(PPh_3)Cp^*\}\{\mu$-CCC[Re(CO)$_4$]\}\{Re(CO)_5\}]BF_4$ (**82**) for which resonance forms **a**–**d** can be written. Of these, form **a** with an Re=C double bond [Re–C 1.94(3) Å] is favored.[231,232] The C$_3$ chain is end-capped by two rheniums, while the Re(CO)$_4$ group is attached by an asymmetric η^3 interaction to all three carbons. As a result, the C$_3$ unit is bent [CCC 152(4)$^\circ$]. The ^{13}C NMR spectrum contains three resonances at δ 297.1, 146.6, and 95.1 for the C$_3$ group, the former having J(CP) 10 Hz, indicating attachment to the Cp*Re fragment. With BF$_3\cdot$OEt$_2$, an air-stable orange-red material is formed, for which structure **83** has been suggested.

Metathesis of $(Bu^tO)_3W\equiv W(OBu^t)_3$ with $Re(C\equiv CC\equiv CR)(NO)(PPh_3)Cp^*$ (R = H, Me, but not SiMe$_3$) gives deep red $\{Re(NO)(PPh_3)Cp^*\}C\equiv CC\equiv\{W(OBu^t)_3\}$ (**84**) together with $W(\equiv CR)(OBu^t)_3$.[233] In the solid-state structure, a dimer is formed with two μ-OBu^t groups.

$ML_n = Re(NO)(PPh_3)Cp^*,$
$M'L'_m = M(CO)_n$ (M = W, n = 5; M = Fe, n = 4; M = MnCp', n = 2)

$$\{L_nM\}\!-\!C\!\equiv\!O \xrightarrow[\text{(ii) } [OMe_3]BF_4]{\text{(i) } LiC\!\equiv\!C\{M'L'_m\}} \{L_nM\}\!=\!C\diagdown$$

(79)

BF₃

$[\{L_nM\}\!=\!C\!-\!C\!\equiv\!C\!-\!\{M'L'_m\}]^+$

(80)
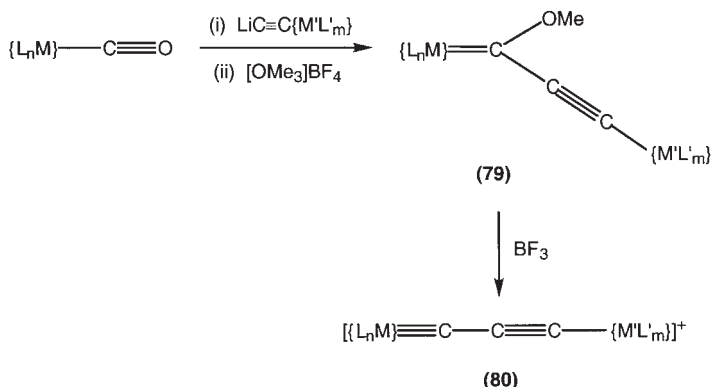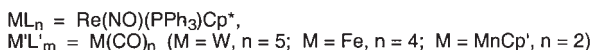
SCHEME 22

D. *Complexes Containing C₄ Ligands*

The subset of bimetallic complexes $\{ML_x\}_2(\mu\text{-}\eta^1,\eta^1\text{-}C_4)$ is dominated by the diyndiyl (**L**) sub-group, although a smaller number of complexes displaying carbon ligands better considered as cumulenic (**M**) or as metal complexes of acetylenic dicarbynes (**N**) are also known (Chart 4). Theoretical analyses of these various forms have been carried out, with the structural type being found to depend heavily on the nature of the metal and its oxidation state, as well as the type of supporting ligands. A more detailed description of these studies is given in Section IV.D.

The chemistry and physical properties of diyndiyl complexes are similar to those of both bimetallic acetylide complexes and typical of somewhat sterically congested and electron-rich, diynes. Buta-1,3-diyne and its derivatives have been used in the preparation of a wide variety of C₄ complexes, although due care must be exercised in the preparation and manipulation of this potentially explosive reagent. The nucleophilic dilithio derivative LiC≡CC≡CLi is obtained either by lithiation (BuLi) of buta-1,3-diyne[234] or from *cis*-HC≡CCH=CH(OMe) after treatment with three equivalents of BuLi at low temperature.[235] The corresponding disodium salt has been prepared by reaction of butadiyne with $NaNH_2$.[234] The silyl derivative $Me_3SiC\equiv CC\equiv CSiMe_3$, which is commercially

L_xM—$C{\equiv}C$—$C{\equiv}C$—ML_x $L_xM{=}C{=}C{=}C{=}C{=}ML_x$ $L_xM{=}C$—$C{\equiv}C$—$C{=}ML_x$

(L)   (M)   (N)

CHART 4
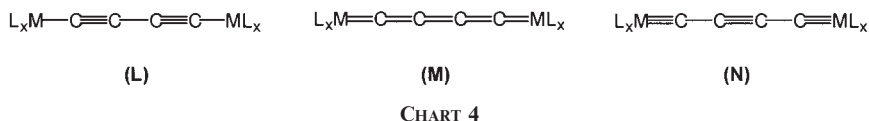
available or readily prepared by Hay coupling of $Me_3SiC{\equiv}CH$,[236] is a stable crystalline butadiyne synthon and reaction with two equivalents of MeLi affords Li_2C_4.[237] Reaction of Li_2C_4 with $SnClMe_3$ affords the tin derivative $Me_3SnC{\equiv}CC{\equiv}CSnMe_3$, which has been shown to enter into a Pd-catalyzed cross-coupling reaction with $FeI(CO)_2Cp$ to give $\{Fe(CO)_2Cp\}_2(\mu\text{-}C{\equiv}CC{\equiv}C)$.[238] The electrophilic iodonium salt $[PhIC{\equiv}CC{\equiv}CIPh][OTf]_2$ has been employed in the preparation of Rh and Ir complexes.[239] Very recently, remarkably stable 1-iodo-4-trialkylsilyl-buta-1,3-diynes have been prepared by direct iodination of $LiC{\equiv}CC{\equiv}CSiR_3$ ($R = Me$, Pr^i),[240] although the use of these materials in the synthesis of C_4 complexes remains unexplored at present. Manipulation of the non-metal end-cap in diynyl complexes $\{ML_n\}C{\equiv}CC{\equiv}CR^{36}$ has also enabled entry to many M_2C_4 systems.

Many of the common synthetic routes to C_4 complexes are similar to those employed in C_2 chemistry, and can be summarized:

(a) reactions of alkali metal or di-Grignard derivatives of buta-1,3-diyne with metal halides and pseudo-halides;
(b) oxidative addition of buta-1,3-diyne to low-valent metal substrates;
(c) metallation or transmetallation of η^1-diynyl complexes $\{ML_n\}C{\equiv}CC{\equiv}CR$ ($R = H$, $SiMe_3$, SnR_3');
(d) reactions of Group 14 diyne reagents $R_3EC{\equiv}CC{\equiv}CER_3$ ($E = Si$, Sn) with metal halides;
(e) oxidative coupling of terminal η^1-acetylide complexes;
(f) modification of the supporting ligand configuration around existing MC_4M species.

1. Homodimetallic Compounds

Table V summarizes selected spectroscopic data for homo-binuclear C_4 complexes.

(a) Groups 3–5

At the time of writing, no compounds containing metals of Groups 3–5 as end-caps to C_4 chains are known.

TABLE V
SELECTED SPECTROSCOPIC PROPERTIES OF {ML$_x$}$_2$(μ-C$_4$)

ML$_x$	IR (Raman) v(CC) cm^{-1}	δ$_C$ (J/Hz) C(1)	δ$_C$ (J/Hz) C(2)	λ nm (ε M^{-1} cm^{-1})	Ref.
Group 6					
Mo(CO)$_3$Cp	not observed	limited solubility			241,293
Mo(CO)$_2$Tp′		279.8	258.2		245
Mo(CO)$_2$Tp′		279.8	258.2		245
	not observed	248.9	107.0		245
W(CO)$_3$Cp	2145[a]	limited solubility			241,293
W(CO)$_3$Cp*	obscured by CO	119.7	106.5		243
W(O)$_2$Cp*	2017[a]	119.6	110.5		243
W(CO)$_2$Tp′	not observed	243.7	88.0		245
Group 7					
trans-Mn(I)(dmpe)$_2$	2127, 1805[b]			1164 (1400), 908 (39,360), 572 (4960), 504 (3820), 390 (40,430)	246
trans-Mn(C≡CH)(dmpe)$_2$	not observed				247
Re(NO)(PPh$_3$)Cp*[c]	1964w/1888[a] 1968w;[b] 1967w[d] (2056)	95.8 (CC 96.5/47.1; CP 10.9)	117.5 (CC 97.2/47.6)	350 (17,000)	248,249
Re(NO){P(tol)$_3$}Cp*	1963[a]	95.7, 96.6[c]	118.0	232 (63,900), 270sh (22,300), 352 (13,500)	251

(*Continued*)

TABLE V
Continued

ML_x	IR (Raman) $\nu(CC)$ cm^{-1}	δ_C (J/Hz) C(1)	C(2)	λ nm (ε M^{-1} cm^{-1})	Ref.
Re(CO)$_3$(Bu$^t_2$-bpy)	1981^e	117	124	330 (15,140), 362 (8510), 458 (3010)^a	253
Group 8					
Fe(CO)$_2$Cp	2144^a	66.84	101.58		238,255,256
Fe(CO)$_2$Cp^{Et}					446
Fe(CO)$_2$Cp*	2141	79.8	98.5		182
	2150	101.6	66.8		306
Fe(dippe)Cp*	1949^e				258
Fe(dppe)Cp*	1955, 1880^a	99.7	110.2		270
Ru(PPh$_3$)$_2$Cp	*cis* 1970/*trans* 1990, 1976^e				260–262
Ru(PMe$_3$)(PPh$_3$)Cp	1972, 1957^a				262
Ru(dppe)Cp	1970				267
Ru(dppm)Cp*	1966	93.25 (CP 27)	100.38		264
Ru(dppe)Cp*	1973	94.63 (CP 27)	99.47		264
Os(PPh$_3$)$_2$Cp	1972				271
Os(dppe)Cp*	1965				271
Group 9					
Rh(H)(Cl)(P^{i}Pr$_3$)$_2$	2010^b				275
Rh(H)(Cl)(py)(P^{i}Pr$_3$)$_2$	2000^b	110.22 (CRh 13.3)			275
Rh(C=C=CPh$_2$)(PPr$^i_3$)$_2$	1947^e				278
Rh(C=C=CBu^{t}Ph)(PPr$^i_3$)$_2$	1952^e	133.7 (CRh 39.7; CP 19.3)	149.8 (m)		278
Rh(C=CHPh)}(PPr$^i_3$)$_2$	not observed	123.1 (CRh 37.2, CP 21.3)	obscured by solvent		277,279
Rh(C=CMe$_2$)(PPr$^i_3$)$_2$	not observed	123.8 (CRh 38.2, CP 19.1)	127.4 (CRh 10.1)		277

RhH(py)(C≡CPh)(PPr$^i_3$)$_2$	2086^e	124.5 (m) or 96.9 (m)	110.8 or 99.3 (both CRh 7)		277
Rh(C=CH$_2$)(PPr$^i_3$)$_2$	not observed	122.2 (CRh 38.1, CP 19.3)	125.0 (CRh 8.7)		279
Rh(C=CHBu^t)(PPr$^i_3$)$_2$	not observed	122.7 (CRh 37.6, CP 19.3)	127.4 (CRh 8.1)		279
Rh(CNxy)(PPr$^i_3$)$_2$	2031, 2005, 1965 (CN and CC)^e	not observed			279
Rh(CO)(PPr$^i_3$)$_2$	not observed	108.1m, 109.5m			280
[*trans*-IrCl(CO) (NCMe)(PPh$_3$)$_2$]$^+$	2183^f	46.9 (CP 12)	95.6		239
IrHCl(PPr$^i_3$)$_2$		67.8 (CP 13.4)	101.0 (CP 1.9)		276
IrHCl(py)(PPr$^i_3$)$_2$	2010^g	57.6 (CP 11.4)	88.2 (br)		276
Group 10					
cyclo-Pt(PEt$_3$)$_2$	2144^e				285
cyclo-Pt(dppe)	2148^e				285
cyclo-Pt(dppp)	2148^e				285
cyclo-Pt(dcype)	2075, 2142	94.7 (*trans*-CP 139, *cis*-CP 12, CPt 1084)	98.9 (*trans*-CP 32, *cis*-CP < 0.1, CPt 313)		284
cyclo-Pt(dcpe) {C≡CC≡C[Pt(PBu$_3$)$_2$]}	2001, 2074, 2139				284
Group 11					
Au(PCy$_3$)	(2150, 2087)	123.8 (CP 134.1)	88 (CP 25.8)	413 (20), 381 (40), 361 (80), 339sh (130), 328 (580), 309 (1410), 291 (1770), 264 (119,880), 252sh (27,350), 245 (77,930)	288
Au(PPh$_3$)	2102				267
Au{P(tol)$_3$}	2157	119.89 (CP 140)	88.11		267
cyclo-Au$_2$(dppm)	2141				289

Note: ^{a}CH$_2$Cl$_2$; ^{b}KBr; ^{c}enantiomeric pair; ^{d}thf; ^{e}nujol; ^{f}CCl$_4$; ^{g}CHCl$_3$.

(b) Group 6

Copper(I)-catalyzed reactions of $MCl(CO)_3Cp'$ (M = Mo, Cp' = Cp; M = W, Cp' = η^5-C$_5$H$_5$, η^5-C$_5$Me$_5$) with an excess of buta-1,3-diyne in amine solvents readily afford the diynyl complexes $M(C\equiv CC\equiv CH)(CO)_3Cp'$ which react further under similar conditions with a stoichiometric amount of the halide $MCl(CO)_3Cp'$ to give diyndiyl complexes $\{M(CO)_3Cp'\}_2(\mu$-$C\equiv CC\equiv C)$ (85) in good yield (Scheme 23).[241–243] While the Cp derivatives were generally insoluble, the Cp* analogue $\{W(CO)_3Cp^*\}_2(\mu$-$C\equiv CC\equiv C)$ has much greater solubility in common organic solvents, and chemical oxidation (H_2O_2/H_2SO_4) of this complex afforded the bis(dioxo) complex $\{W(O)_2Cp^*\}_2(\mu$-$C\equiv CC\equiv C)$ (86) via an intermediate bis (oxo–peroxo) complex which could not be isolated in a pure state (Scheme 23).[243] The asymmetric homobimetallic species $\{Cp(dppe)(CO)Mo\}(\mu$-$C\equiv CC\equiv C)\{Mo(CO)_2(PPh_3)Cp^{CO_2Me}\}$ was isolated as a mixture of cis (34%) and trans (66%) isomers (with respect to the CO ligands) from the CuI-catalyzed reaction of $Mo(C\equiv CC\equiv CH)(CO)(dppe)Cp$ with cis/trans-$MoI(CO)_2(PPh_3)Cp^{CO_2Me}$.[244]

$$\{L_nM\}\!-\!\!-\!C\!\equiv\!C\!-\!\!\cdots\!\!-\!C\!\equiv\!C\!-\!\!-\!\{ML_n\}$$
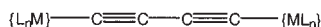
ML_n

(85)	$M(CO)_3Cp'$ (M = Cr, Mo, W; Cp' = Cp, Cp*)
(86)	$W(O)_2Cp^*$
(93)	$MnI(dmpe)_2$
(95)	$Mn(C\equiv CH)(dmpe)_2$
(96)	$Re(NO)(PR_3)Cp^*$ (R = Ph, tol, C$_6$H$_4$Bu^t-4)
(98)	Fp
(99)	$Fe(dippe)Cp^*$
(103)	$Ru(PPh_3)_2Cp$
(104)	$Ru(PMe_3)(PPh_3)Cp$
(105)	$Ru(dppe)Cp$
(106)	cis-$RuCl(bpy)_2$
(107)	$Fe(dppe)Cp^*$
(109)	$Ru(dppe)Cp^*$
(110)	$Ru(dppm)Cp^*$
(111)	$Os(dppe)Cp^*$
(114)	cis-[RhH(PMe$_3$)$_4$]$^+$
(115)	trans-RhHCl(PPr$^i_3$)$_2$
(116)	trans-RhHCl(py)(PPr$^i_3$)$_2$
(121)	trans-Rh(=C=CHPh)(PPr$^i_3$)$_2$
(122)	trans-RhH(C≡CPh)(PPr$^i_3$)$_2$
(123)	trans-Rh(CO)(PPr$^i_3$)$_2$
(124)	[trans-IrCl(CO)(NCMe)(PPh$_3$)$_2$]$^+$
(125)	$Ni(CN)(NH_3)_5$
(126)	$Ni(PPh_3)Cp$
(127)	$MCl(PR_3)_2$ (M = Pd, Pt; R = Bu, Ph)
(128)	PtMe(cod)
(131)	$Au(PR_3)$ (R = Cy, Ph)

M,M' = Mo, W; R = H, Me

(85)   **(86)**
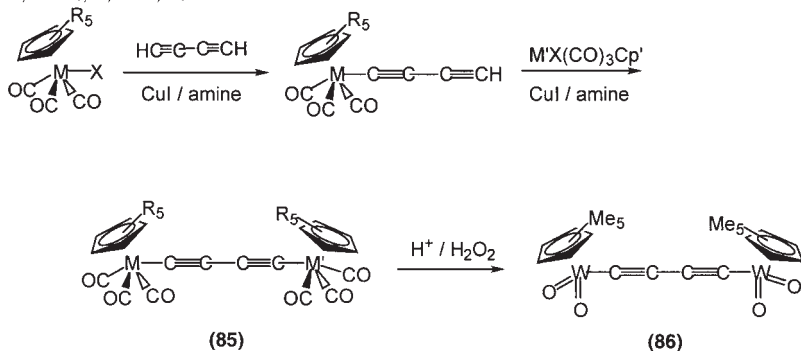
SCHEME 23

Complexes of types **L** and **M** containing Group 6 metal fragments have been obtained via a beautiful sequence of reactions (Scheme 24), commencing with deprotonation (BuLi) of M($\equiv$CCH$_3$)(CO)$_2$Tp' (**87**) (M = Mo, W; Tp' = hydridotris(3,5-dimethylpyrazolyl)borate) to give the anionic vinylidene (**88**), which is oxidized (ferricinium, iodine, or nitrobenzene) to afford bright yellow {M(CO)$_2$Tp'}$_2$(μ-CCH$_2$CH$_2$C) (**89**). A second sequence of deprotonation/oxidation reactions gives {M(CO)$_2$Tp'}$_2$(μ-CCH=CHC) (**90**). Further deprotonation of **90** with KOBu^t affords the blue–green anionic cumulene complexes **91**, which are finally oxidized to give the neutral complexes of type **M** (**92**).[245] Overall, the

M = Mo, W
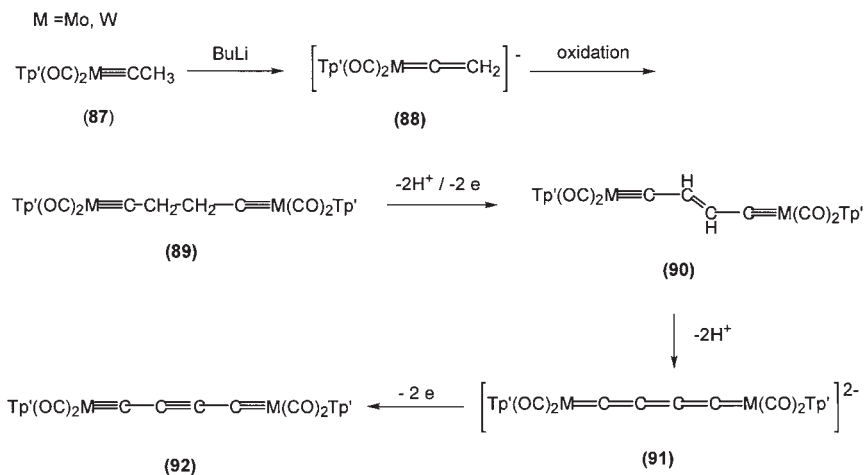
SCHEME 24

reaction sequence amounts to the removal of two molecules of dihydrogen from the CH_2CH_2 linkage between the robust metal carbyne cores.

(c) Group 7

Green, paramagnetic $\{MnI(dmpe)_2\}_2(\mu\text{-}C\equiv CC\equiv C)$ (**93**) was obtained from the reaction of $MnI(dmpe)(\eta^5\text{-}C_5H_4Me)$ with $Me_3SnC\equiv CC\equiv CSnMe_3$ in the presence of dmpe.[246] The complex was sequentially oxidized by ferrocinium to afford the mono and dications. In turn, these were readily reduced in reactions with $CoCp_2$. Desilylation and subsequent deprotonation of $[\{Mn(dmpe)_2(C\equiv CSiMe_3)_2]^+$ (**94**) (Scheme 25) affords the radical complex $Mn(dmpe)_2(C\equiv CH)(C\equiv C^\cdot)$ which is best described in terms of a triplet ground state. This radical undergoes a spontaneous homo-coupling reaction to give $\{Mn(dmpe)_2(C\equiv CH)\}_2(\mu\text{-}C_4)$ (**95**), which is oxidized by $[\{Mn(dmpe)_2(C\equiv CH)_2]^+$ present in the solution to give $[\{Mn(dmpe)_2(C\equiv CH)\}_2(\mu\text{-}C_4)]^+$ ($[\mathbf{95}]^+$), isolated in ca. 65% yield.[247]

Glaser oxidative coupling $[Cu(OAc)_2/py]$ of the rhenium ethynyls $Re(C\equiv CH)(NO)(PR_3)Cp^*$ $(R = Ph;^{248–250}$ tol, $C_6H_4Bu^t\text{-}4^{251})$ affords the corresponding diyndiyls $\{Re(NO)(PR_3)Cp^*\}_2(\mu\text{-}C\equiv CC\equiv C)$ (**96**) as diastereotopic mixtures. Fractional crystallization leads to diastereotopic enrichment, or resolution for $R = Ph$, which permitted cystallographic assignment of the configuration. ^{13}C-Labeled complexes were prepared and
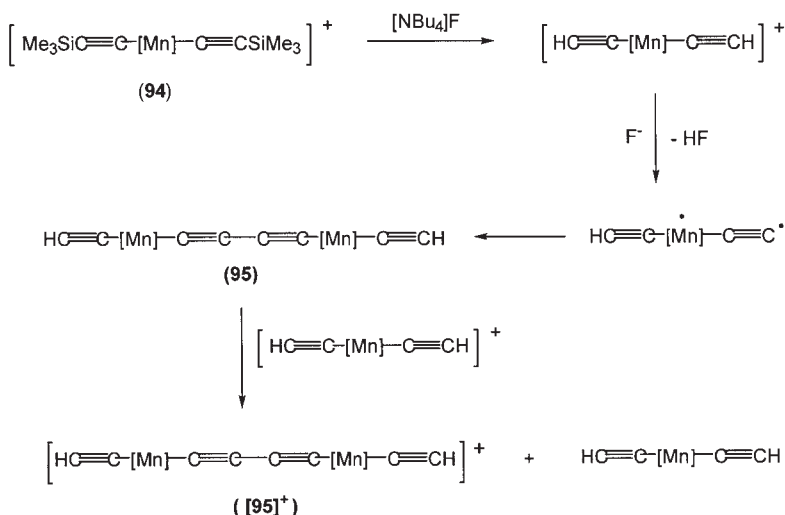
SCHEME 25

isolated in an analogous manner. Ethynyl complexes bearing bulkier phosphines (R = 4-C_6H_4Ph, Cy) did not afford the corresponding diyndiyls under comparable conditions.[249,252] The binuclear rhenium α,α'-diimine complex {Re(CO)$_3$(Bu$^t_2$-bpy)}$_2$(μ-C≡CC≡C) has been prepared by Glaser coupling of Re(C≡CH)(CO)$_3$(Bu$^t_2$-bpy).[253]

(d) Group 8

The first report of a transition metal complex containing a bridging C_4 ligand, K_8[{(NC)$_5$Fe}C≡CC≡C{Fe(CN)$_5$}], appeared in 1957.[254] Arguably, Wong's report in 1990 describing the synthesis and characterization of a series of μ-η^1,η^1-C≡CC≡C complexes by sequential reactions of Fe(C≡CC≡CH)(CO)(L)Cp (L = CO, PPh$_3$) with Bu^{s}Li and a metal halide (Scheme 26) was responsible for renewing interest in this area.[255] In this manner, {Cp(L)(CO)Fe}(μ-C≡CC≡C){Fe(CO)$_2$Cp} (**97**) was obtained, as were several heterobimetallic derivatives (Scheme 26) (see Section II.D.2). The Cp* derivative has been prepared in a similar fashion.[182] Complex **98** has also been prepared by reaction of Li$_2$C$_4$ with two equiv. of FeCl(CO)$_2$Cp,[255,256] and via the Pd-catalyzed coupling of Me$_3$SnC≡CC≡CSnMe$_3$ with FeI(CO)$_2$Cp in thf or dmf.[238]

Application of Cu(I)-amine coupling of the appropriate metal halides to Fe(C≡CC≡CH)(CO)$_2$Cp^R has given a range of complexes {Cp^R(CO)$_2$Fe} (μ-C≡CC≡C){ML$_n$}   [Cp^R = Cp*,   ML$_n$ = Fe(CO)$_2$Cp*,   Fe(CO)$_2$ (η-C$_5$H$_4$Et);   Cp^R = η-C$_5$H$_4$Et,   ML$_n$ = Fe(CO)$_2$(η-C$_5$H$_4$Et)] (see also Section II.D.2 below).[182,257] The more electron-rich dippe complex {Cp*(dippe)Fe}$_2$(μ-C≡CC≡C) (**99**) was prepared by coupling FeCl(dippe) Cp* with Fe(C≡CC≡CH)(dippe)Cp* in the presence of both KPF$_6$ and KOBu^t in methanol.[258] It is likely that the reaction involves either an ethynylvinylidene or butatrienylidene intermediate (Scheme 27). Analogous procedures have been used to prepare {Cp*(L)$_2$Fe} (μ-C≡CC≡C){Fe(CO)$_2$(η^5-C$_5$R$_5$)} from FeCl(L)$_2$Cp* and the appropriate
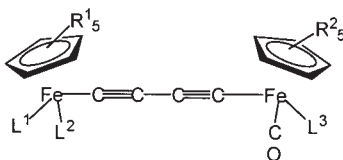
	R^1	R^2	L^1	L^2	L^3
(97)	H	H	CO	CO	PPh$_3$
(100)	Me	Me	dppe		CO
(101)	Me	Ph	dppe		CO
(102)	Me	Me	dippe		CO

L = CO, PPh$_3$;
M = Fe (x = 2) (L = PPh$_3$ **97**, CO **98**)
M = Mo, W (x = 3) (**134**)

SCHEME 26

	R^1	(L^1)$_2$	R^2	(L^2)$_2$
(**97**)	H	(CO)$_2$	H	(CO)(PPh$_3$)
(**99**)	Me	dippe	Me	dippe
(**100**)	Me	(CO)$_2$	Me	dppe
(**101**)	Ph	(CO)$_2$	Me	dppe
(**102**)	Me	(CO)$_2$	Me	dippe
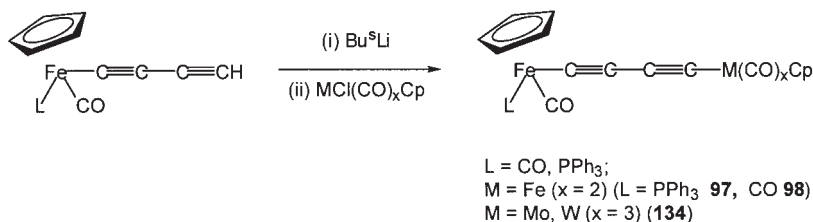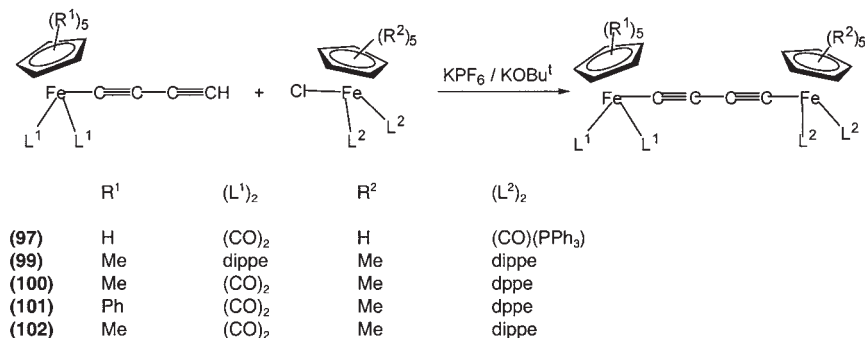
SCHEME 27

diynyl reagent Fe(C≡CC≡CH)(CO)$_2$(η^5-C$_5$R$_5$) [L$_2$ = dppe, R = Me **100**, Ph **101**;[88] L$_2$ = dippe, R = Me **102**].[259]

The ruthenium complex {Ru(PPh$_3$)$_2$Cp}$_2$(μ-C≡CC≡C) (**103**) was first obtained by displacement of the labile thf ligand in [Ru(thf)(PPh$_3$)$_2$Cp]$^+$ by Li$_2$C$_4$.[260] Alternatively, the reaction of RuCl(PPh$_3$)$_2$Cp with Me$_3$SiC≡CC≡CSiMe$_3$ in the presence of KF and a strong non-nucleophilic base affords **103** in good yield,[261] and ligand exchange at elevated temperatures affords the mixed phosphine derivatives {Ru(PPh$_3$)(PMe$_3$)Cp}$_2$(μ-C≡CC≡C) (**104**)[262] and {Ru(dppe)Cp}$_2$(μ-C≡CC≡C) (**105**) (Scheme 28).[263]

In general terms, the direct metalla-desilylation of SiMe$_3$-protected diynes has proven to be of great use in the preparation of Group 8 metal complexes.[261,264–266] For example, metallation of the diynyl ligand in Ru(C≡CC≡CSiMe$_3$)(PPh$_3$)$_2$Cp with RuCl(dppe)(η^5-C$_5$R$_5$) (R = H, Me) is achieved upon reaction with KF and dbu in methanol to give {Cp(Ph$_3$P)$_2$Ru}(μ-C≡CC≡C){Ru(dppe)(η^5-C$_5$R$_5$)}.[267]

The reagent Me$_3$SiC≡CC≡CSiMe$_3$ is suitable for the preparation of the octahedral complex cis-{RuCl(bpy)$_2$}$_2$(μ-C≡CC≡C) (**106**) from cis-RuCl$_2$(bpy)$_2$ in the presence of NaF and NaBF$_4$.[268] The same complex was also obtained from Me$_3$SiC≡CSiMe$_3$, but the mechanism responsible for the coupling process was not identified. In the case of iron, the reaction

RuCl(PPh$_3$)$_2$Cp

(i) or (ii)

Cp(Ph$_3$P)$_2$Ru—C≡C—C≡C—Ru(PPh$_3$)$_2$Cp

(103)

(iii)

Cp(L)$_2$Ru—C≡C—C≡C—Ru(L)$_2$Cp
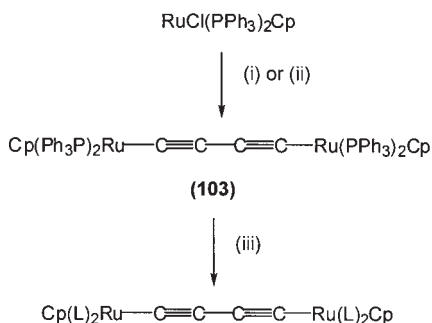
Reagents: (i) AgPF$_6$, Li$_2$C$_4$; (ii) Me$_3$SiC$_2$C$_2$SiMe$_3$ / KF / DBU;
(iii) PMe$_3$ [L$_2$ = (PMe$_3$)(PPh$_3$) (**104**)] or dppe [L$_2$ = dppe (**105**)] 110°C

SCHEME 28

of FeCl(dppe)Cp* with RC≡CC≡CSiMe$_3$ (R = H, 0.6 equiv; SiMe$_3$, 1.2 equiv) in refluxing methanol containing a halide abstracting agent (R = H, NaBPh$_4$; R = SiMe$_3$, KPF$_6$) and a suitable nucleophilic base (R = H, KOBu^t/MeOH; R = SiMe$_3$, KF) gave {Fe(dppe)Cp*}$_2$(μ-C≡CC≡C) (**107**) in up to 73% yield.[266] It is interesting to note that for both iron and ruthenium, binuclear species were formed from Me$_3$SiC≡CC≡CSiMe$_3$ regardless of the stoichiometry employed.

   An alternative approach to C$_4$ metal complexes of the Group 8 metals involves oxidative coupling (ferrocinium cation) of the ethynyls M(C≡CH)(dppe)Cp* (M = Fe, Ru, Os) at low temperature to give the bis(vinylidene)s [{Cp*(dppe)M}$_2$(μ-C=CH–CH=C)]$^{2+}$ (**108**) via a 17-e radical ethynyl cation. Deprotonation of **108** (KOBu^t) gave the diyndiyls {Cp*(dppe)M}$_2$(μ-C≡CC≡C) [Scheme 29; M = Fe (**107**),[269,270] Ru (**109**)[264] (the analogous dppm complex **110** was also prepared), Os (**111**)[271]]. Oxidation and rearrangement of the Ru porphyrin **112** afforded the bis(vinylidene) **113** although this has not been converted to the C$_4$ derivative (Scheme 30).[272] The original authors note that this complex represents an entry point for dimetallacumulene and carbene chemistry.

(e) Group 9

   The first Group 9 C$_4$ complex was reported by Marder and his colleagues in 1991.[84,273,274] Facile oxidative addition of each C–H moiety in butadiyne to [Rh(PMe$_3$)$_4$]$^+$ gave the bimetallic Rh(II) species {cis-RhH(PMe$_3$)$_4$}$_2$ (μ-C≡CC≡C) (**114**) in a single-pot reaction. The only by-product of the reaction is the volatile PMe$_3$, which is readily removed. Similarly, double

(108)   M = Fe (**107**), Ru (**109**), Os (**111**)

SCHEME 29

(112)   **(113)**
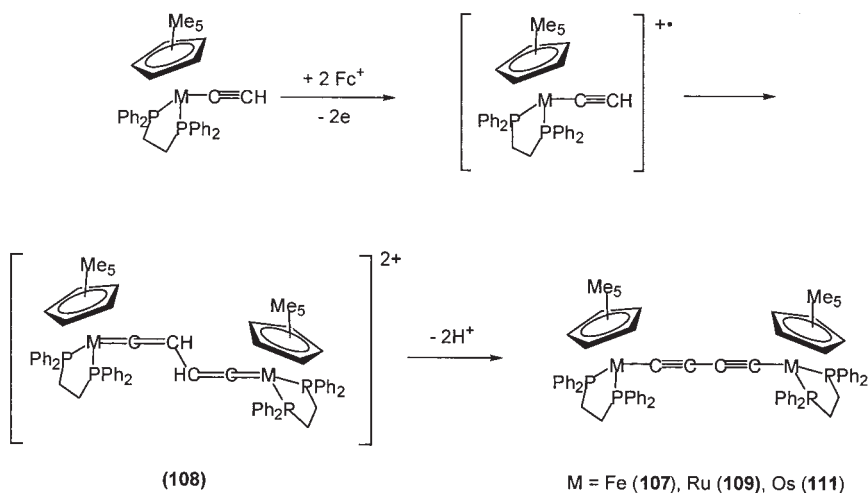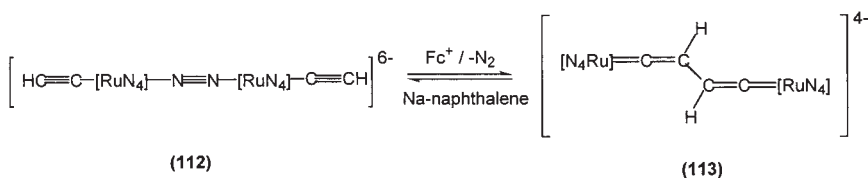
[RuN$_4$] = Ru(*meso*-octamethylporphrynogen)

SCHEME 30

oxidative addition of HC≡CC≡CH to {RhCl(PPr$_3^i$)$_2$}$_n$ affords the Rh(III) complex {RhHCl(PPr$_3^i$)$_2$}$_2$(μ-C≡CC≡C) (**115**), which with pyridine gives {RhHCl(py)(PPr$_3^i$)$_2$}$_2$(μ-C≡CC≡C) (**116**).[275] The same product was obtained from reaction of the bis(vinylidene) complex {RhCl(PPr$_3^i$)$_2$}$_2$ (μ-C=CHCH=C) (**117**), formed by thermolysis of **115** or photolysis of wet benzene solutions of Rh(C=CHC≡CSiMe$_3$)(Cl)(PPr$_3^i$)$_2$ containing {RhCl (PPr$_3^i$)$_2$}$_n$, with pyridine (Scheme 31). The iridium analogues have also been described.[276]

Stannylated diynes have proven to be especially useful in the preparation of Rh(I) complexes containing C$_4$ ligands (**118**) via the elimination of Ph$_3$SnX from Rh(X)(L)(PPr$_3^i$)$_2$ and Ph$_3$SnC≡CC≡CSnPh$_3$ [X=OH, F; L=C=CHR (R=H, Ph, Bu^t), C=CMe$_2$, C=C=CPhR (R=Ph, Bu^t), CNxy, CO].[277–279] Reactions of fluorinated starting materials were greatly expedited by the formation of insoluble SnFPh$_3$ in organic

[Rh] = $trans$-Rh(PPr$^i_3$)$_2$
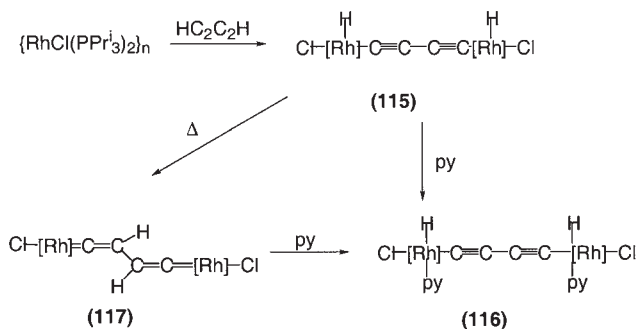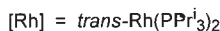
SCHEME 31

solvents. The fluoro(isocyanide) precursor reacts sufficiently slowly with Ph$_3$SnC≡CC≡CSnPh$_3$ to permit the isolation of the diynyl complex Rh(C≡CC≡CSnPh$_3$)(CNxy)(PPr$^i_3$)$_2$ (**119**). The second carbon–tin bond was subsequently cleaved upon reaction with RhF(C=CHPh)(PPr$^i_3$)$_2$ to afford the asymmetric C$_4$ complex $trans,trans$-{Rh(CNxy)(PPr$^i_3$)$_2$} (μ-C≡CC≡C){Rh(=C=CHPh)(PPr$^i_3$)$_2$} (**120**) in excellent yield (Scheme 32). In the case of {Rh(=C=CHPh)(PPr$^i_3$)$_2$}$_2$(μ-C≡CC≡C) (**121**), reaction with an excess of pyridine gave {RhH(C≡CPh)(PPr$^i_3$)$_2$}$_2$(μ-C≡CC≡C) (**122**). Similar chemistry occurs with Me$_3$SiC≡CC≡CSiMe$_3$ and two equiv. of Rh(OH)(CO)(PPr$^i_3$)$_2$ to give {Rh(CO)(PPr$^i_3$)$_2$}$_2$(μ-C≡CC≡C) (**123**).[280]

An alternative single source C$_4$ precursor is the electrophilic bis(iodonium) triflate [PhIC≡CC≡CIPh](OTf)$_2$, which reacts with Vaska's complex in acetonitrile to give unstable pale brown [{$trans$-IrCl(CO)(NCMe)(PPh$_3$)$_2$}$_2$(μ-C≡CC≡C)](OTf)$_2$ (**124**).[239] With $trans$-RhCl(CO)(PPh$_3$)$_2$, only uncharacterized polymeric material was formed.

(f) Group 10

Homo-bimetallic nickel derivatives of C$_4$ are rare, only {Ni(CN)(NH$_3$)$_5$}$_2$(μ-C≡CC≡C) (**125**)[254] and {Ni(PPh$_3$)Cp}$_2$(μ-C≡CC≡C) (**126**)[256] having been reported. The C$_4$ chemistry of the Group 10 metals, especially Pd and Pt, was largely advanced by interest in metal-containing poly-ynyl polymers (Section II.H), with several of these species being prepared as intermediates for polymer synthesis or resulting from polymer degradation or ligand exchange reactions.

The CuI-catalyzed reaction of an excess of MCl$_2$(PBu$_3$)$_2$ with $trans$-M(C≡CC≡CH)(PBu$_3$)$_2$ in piperidine/toluene or NHEt$_2$ afforded

[Rh] = *trans*-Rh(PPr$^i_3$)$_2$

$$L-[Rh]-X \xrightarrow[- 2SnXPh_3]{0.5\ Ph_3SnC_2C_2SnPh_3} L-[Rh]-C\equiv C-C\equiv C-[Rh]-L$$
(118)

Ph$_3$SnC$_2$C$_2$SnPh$_3$
- SnXPh$_3$

RhF(CNR)(PPr$^i_3$)$_2$

$$L-[Rh]-C\equiv C-C\equiv C-SnPh_3 \xrightarrow{RhF(C=CHPh)(PPr^i_3)_2} L-[Rh]-C\equiv C-C\equiv C-[Rh]-L'$$
(119)   **(120)**

X = OH, F;   L, L' = C=CR'$_2$, C=C=CR'$_2$, CNxy, CO

SCHEME 32

{L$_n$M}————C≡C—C≡C——{M'L'$_m$}
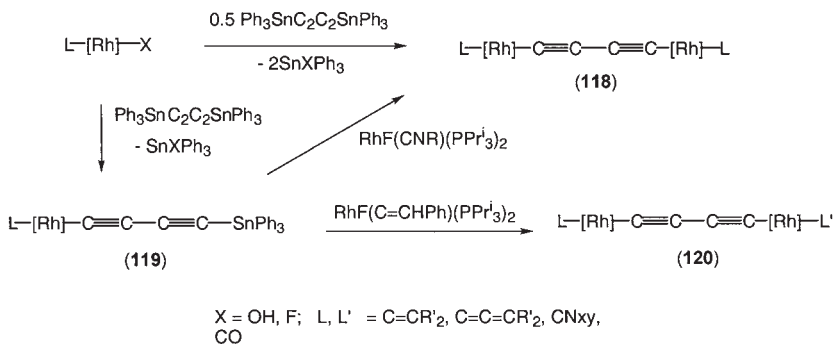
	ML$_n$	M'L'$_m$
(120)	Rh(CNxy)(PPr$^i_3$)$_2$	Rh(=C=CHPh)(PPr$^i_3$)$_2$
(133/M)	W(CO)$_3$Cp	M(CO)$_5$ (M = Mn, Re)
(134)	W(CO)$_3$Cp	Fe(CO)$_2$Cp
(135)	W(CO)$_3$Cp	Ru(PPh$_3$)$_2$Cp
(136/M)	W(CO)$_3$Cp	M(CO)(PPh$_3$)$_2$ (M = Rh, Ir)
(137)	Re(NO)(PPh$_3$)Cp*	Fe(dppe)Cp*
(137a)	Re(NO)(PPh$_3$)Cp*	*trans*-PdCl(PEt$_3$)$_2$
(138)	Fe(CO)$_2$(η-C$_5$Me$_4$Et)	Ru(CO)$_2$Cp' (Cp' = Cp, Cp*)
(139)	Fe(dppe)Cp*	Ru(PPh$_3$)$_2$Cp
(142)	Cu(triphos)	Au{P(tol)$_3$}

{MCl(PBu$_3$)$_2$}$_2$(μ-C≡CC≡C) (**127**; M = Pd,[281] Pt[282]). The palladium polymer {Pd(PBu$_3$)$_2$(μ-C≡CC≡C)}$_n$ reacts with PdCl$_2$(PBu$_3$)$_2$ to give {*trans*-PdCl(PBu$_3$)$_2$}$_2$(μ-C≡CC≡C) (**127/Pd**), while the platinum analogue is inert under similar conditions, due to the increased Pt–C bond strength.[281] The complex Pt(OH)Me(cod) reacts directly with buta-1,3-diyne to afford {PtMe(cod)}$_2$(μ-C≡CC≡C) (**128**) in moderate yield.[283]

The *cis*-bis(diynyl) complexes, *cis*-Pt(C≡CC≡CH)$_2$(PP) (PP = dppe, dppp, dcype) react with *cis*- or *trans*-PtX$_2$(PP) (X = Cl, OTf) under high dilution conditions to afford molecular squares **129** and **130** (Scheme 33).[284,285] The smaller squares have been shown to have high binding affinity for alkylammonium and Group 11 metal cations.

(129)

(130)
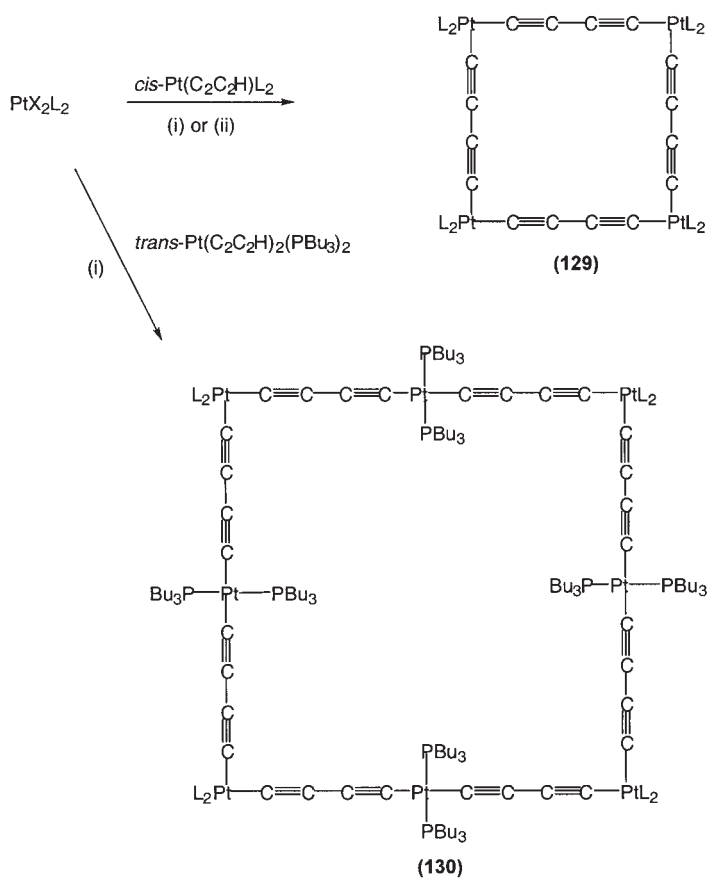
Reagents:

(i) CuI / NHEt$_2$ (X = Cl, L$_2$ = dcpe)
(ii) NaOAc (X = OTf, L$_2$ = dppe, dppp)

SCHEME 33

(g) Group 11

The structures of Group 11 diyndiyl derivatives M$_2$C$_4$ (M = Cu, Ag) are unknown; they are explosive materials, prone to detonation upon mechanical shock. The preparation of Cu$_2$C$_4$ from buta-1,3-diyne and ammoniacal solutions of CuI has been reported, and this material is thought to convert to the linear carbon allotrope carbyne during thermal decomposition.[196,198,286] Evidence has also been given for the formation of Cu$_2$C$_4$ in aged samples of Cu$_2$C$_2$.[198] A yellow solid which precipitates when buta-1,3-diyne is passed into solutions of AgPF$_6$ containing NHEt$_2$

is thought to be Ag_2C_4, although this material has not been investigated in detail.[287]

More readily manipulated C_4 complexes have been isolated using $Au(PR_3)$ endcaps. An elegant synthesis of the luminescent complex $\{Au(PCy_3)\}_2(\mu\text{-}C{\equiv}CC{\equiv}C)$ (80%) (**131/Cy**) involves treatment of a methanolic solution of $AuCl(PCy_3)$ containing $Me_3SiC{\equiv}CC{\equiv}CSiMe_3$ with $NaOH$.[288] The $P(tol)_3$ derivative $\{Au[P(tol)_3]\}_2(\mu\text{-}C{\equiv}CC{\equiv}C)$ (**131/tol**) is prepared similarly.[267] Analogous PPh_3-substituted materials were obtained from the CuI-catalyzed reaction between $Au(C{\equiv}CC{\equiv}CH)(PPh_3)$ and $AuCl(PR_3)$ ($R = Ph$, tol).[267] The condensation reaction of $\{Au(C{\equiv}CC{\equiv}CH)_2\}(\mu\text{-dppm})$, in which aurophilic interactions are expected to impose a "U"-shape, with $\{Au(OTf)\}_2(\mu\text{-dppm})$ in $NHEt_2$ under high dilution conditions affords $cyclo\text{-}\{Au_2(\mu\text{-}C{\equiv}CC{\equiv}C)(\mu\text{-dppm})\}_2$ (**132**) in 87% yield.[289]
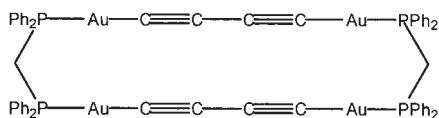
(132)

2. Heterobimetallic Complexes

The chemical reactivity of the $C{\equiv}CH$ portion of terminal 1,3-diynyl ligands is often found to resemble that of conventional organic 1-alkynes.[36] Consequently, numerous examples of heterometallic diyndiyl complexes have been prepared (Table VI). The most frequently used methods involve metallation of terminal diynyl complexes $\{ML_x\}C{\equiv}CC{\equiv}CH$, usually with similar synthetic protocols to those described for the preparation of diynyl and homometallic diyndiyls. General methods include:

(a) CuI-catalyzed coupling of $\{ML_x\}C{\equiv}CC{\equiv}CH$ with metal halides in amine solvents;

(b) lithiation of terminal diynyl ligands with any of a range of organolithium bases, such as n-, sec- or t-BuLi, or $Li(NPr_2^i)$ (LDA), followed by treatment with the metal halide or pseudo-halide. If CO ligands are present, more bulky and less nucleophilic reagents ($LiBu^s$, LDA) may be required;

(c) copper(I) derivatives of the diynyl-metal complex, prepared *in situ* by addition of CuI to the lithio compound, are useful reagents employed in Cadiot–Chodkiewicz couplings;

(d) a copper(I)-free procedure uses the terminal diynyl and the metal triflate in the presence of $NHEt_2$ or NaOAc;

(e) metalladesilylation of silylated diynes is achieved using electron-rich metal fragments in the presence of fluoride.

Copper(I) derivatives of metal diynyl complexes have proven to be useful synthetic intermediates in Cadiot–Chodkiewicz coupling reactions,[290–292] and similar species are implicated in coupling of metal diynyls with aryl halides under Pd/Cu catalyzed (Sonogashira) conditions[241,242] and in the CuI-catalyzed coupling reactions of metal diynyl species with other metal halides.[293]

The following sub-sections describe the preparation of hetero-bimetallic complexes, and are grouped in terms of the earliest metal present in the complex.

(a) Group 6

The chloride ligand is readily displaced from complexes $MCl(CO)_3Cp$ (M = Mo, W) by diynyl anions. For example, $\{Cp(CO)_3Mo\}(\mu\text{-}C{\equiv}CC{\equiv}C)$ $\{Fe(CO)_2Cp\}$ is readily obtained from sequential reaction of $Fe(C{\equiv}CC{\equiv}CH)(CO)_2Cp$ with Bu^sLi and $MoCl(CO)_3Cp$.[255] The Group 6 diynyl complex $W(C{\equiv}CC{\equiv}CH)(CO)_3Cp$ is also a convenient source of these complexes and, for example, $\{Cp(CO)_3W\}(\mu\text{-}C{\equiv}CC{\equiv}C)\{Mn(CO)_5\}$ (133) is prepared from $W(C{\equiv}CC{\equiv}CH)(CO)_3Cp$, $MnI(CO)_5$, and LDA. The use of the bulkier lithiated bases seems to be essential in order to avoid complications arising from inadvertent attack of this reagent at the carbonyl ligands.[293]

In the presence of a CuI catalyst, $W(C{\equiv}CC{\equiv}CH)(CO)_3Cp$ couples with $FeCl(CO)_2Cp$ to give the mixed Group 6/8 complex $\{Cp(CO)_3W\}(\mu\text{-}C{\equiv}CC{\equiv}C)\{Fe(CO)_2Cp\}$ (134). Treatment of $W(C{\equiv}CC{\equiv}CSiMe_3)(CO)_3Cp$ with $RuCl(PPh_3)_2Cp$ in a methanolic solution of KF gave $\{Cp(CO)_3W\}$ $(\mu\text{-}C{\equiv}CC{\equiv}C)\{Ru(PPh_3)_2Cp\}$ (135).[294]

Copper(I)-catalyzed reactions have also been used to make W/Rh- and W/Ir-diyndiyl complexes, although the products are often contaminated by the corresponding O_2 adducts.[293] Better is a Cu-free procedure in which $W(C{\equiv}CCC{\equiv}CH)(CO)_3Cp$ and $M(OTf)(CO)(PPh_3)_2$ (generated *in situ*) react in the presence of diethylamine to give $\{Cp(CO)_3W\}(\mu\text{-}C{\equiv}CC{\equiv}C)$ $\{M(CO)(PPh_3)_2\}$ (136/M; M = Rh, Ir).[295]

Reaction of the bimetallic reagents $\{AuCl\}_2(\mu\text{-}dppm)$ with $W(C{\equiv}CC{\equiv}CH)_2(CO)_3Cp$ requires the CuI catalyst, and affords the tetrametallic species $[\{Au(C{\equiv}CC{\equiv}C[W(CO)_3Cp])\}_2(\mu\text{-}dppm)]$. It is thought that the steric requirements of the $W(CO)_3Cp$ groups would overcome the Au$\cdots$Au aurophilic interactions and twisting of the Au-phosphine backbone would result.[289]

TABLE VI

SELECTED SPECTROSCOPIC PROPERTIES OF HETERO-BINUCLEAR COMPLEXES $\{ML_x\}$–C_4–$\{M'L'_y\}$

			δ_C (J/Hz)					
ML_x	$M'L'_y$	IR (Raman) ν(CC) cm^{-1}	C(1)	C(2)	C(3)	C(4)	λ nm (ε M^{-1} cm^{-1})	Ref.
Group 6								
Mo(CO)(dppe)Cp	Mo(CO)$_2$(PPh$_3$)Cp^{CO2Me}	2145, 2052[g]	106.8, 101.7, 92.7, 70.9					244
Mo(CO)$_3$Cp	W(CO)$_3$Cp	2145[d]	insoluble					293
W(CO)$_3$Cp	Mn(CO)$_5$	2150, 2128[d]	114.88 (CW 22)	101.49, 80.83, 55.65				293
W(CO)$_3$Cp	Fe(CO)$_2$Cp	2135[d]	115.45 (br)	63.32	42.32	101.00		255,293
W(CO)$_3$Cp	Fe(CO)(PPh$_3$)Cp	2127[d]	117.6	105.1	52.0	98.1 (CP 41.3)		255
W(CO)$_3$Cp	Ru(CO)$_2$Cp	2142[d]	115.26	87.45	52.01	95.43		293
W(CO)$_3$Cp	Ru(PPh$_3$)$_2$Cp	2110, 1976[f]						294
W(CO)$_3$Cp	Rh(CO)(PPh$_3$)$_2$	2145[d]	not observed					293,295
W(CO)$_3$Cp	Rh(O$_2$)(CO)(PPh$_3$)$_2$	2145[e]	not observed					293
W(CO)$_3$Cp	Rh(tcne)(CO)(PPh$_3$)$_2$	2142[d]	not observed					295
W(CO)$_3$Cp	Ir(CO)(PPh$_3$)$_2$	2156[d]	not observed					293
W(CO)$_3$Cp	Ir(O$_2$)(CO)(PPh$_3$)$_2$	2147[d]	not observed					293
W(CO)$_3$Cp	Au(PPh$_3$)	2145[d]						293
Group 7								
Re(NO)(PPh$_3$)Cp*	Fe(dppe)Cp*	2093, 2058, 1955[e]	121.3, 106.4, 76.7				356sh (14,000), 330sh (19,000), 298 (40,000)	296

Re(NO)(PPh$_3$)Cp*	Rh(CO)(PPh$_3$)$_2$	2110^d					224
Re(NO)(PPh$_3$)Cp*	PdCl(PEt$_3$)$_2$-*trans*	1988^d	90.8	116.1	95.0	83.9	224
		1988^c	(CP 17.6)		(CP 3.7)	(CP 17.3)	
		(2128, 2093)					
Group 8							
Fe(CO)$_2$Cp	Fe(CO)(PPh$_3$)Cp						255
Fe(dppe)Cp*	Fe(CO)$_2$(η^5-C$_5$Ph$_5$)	2102^c	107.4	108.5	102.4	68.3	88
			(CP 41)	(CP 2)	(CP 3)		
Fe(dippe)Cp*	Fe(CO)$_2$Cp*	2112^e	111.7	106.5	102.5	65.0	259
			(CP 39)	(CP 2)	(CP 2)		
Fe(dppe)Cp*	Ru(PPh$_3$)$_2$Cp	2037, 1959					267
Ru(PPh$_3$)$_2$Cp	Ru(dppe)Cp	1966					267
Ru(PPh$_3$)$_2$Cp	Ru(dppe)Cp*	1965					267
Group 9							
Rh(CNxy)(PPr$^i_3$)$_2$	Rh(C=CHPh)(PPr$^i_3$)$_2$	2030, 2004 (NC and CC)^e	110.0 (CRh 36.6, CP 20.3)	107.5 (CRh 12.2)			279
Group 10							
Pt(C≡CC≡CH) (dppe)	AuPPh$_3$	2140, 2084^e	not reported				285
Group 11							
Au{P(tol)$_3$}	Cu(triphos)	2158, 2127					267
Au(PPh$_3$)	Au(Ptol$_3$)	2153	126.96, 125.80, 88.23, 85.78				267

Note: ^{a}Di-potassium salt; ^{b}BF$_4$ salt; ^{c}KBr; ^{d}CH$_2$Cl$_2$; ^{e}nujol; ^{f}cyclohexane; ^{g}thf.

(b) Group 7

The complex {Cp*(NO)(PPh₃)Re}(μ-C≡CC≡C){Fe(dppe)Cp*} (137) was prepared from the reaction of Re(C≡CC≡CSiMe₃)(PPh₃)(NO)Cp* with FeCl(dppe)Cp* in the presence of KF, the halide abstracting agent KPF₆ and 18-crown-6.[296] Sequential reactions of Re(C≡CC≡CH)(PPh₃)(NO)Cp* with LiBu and PdCl₂(PEt₃)₂ give {Cp*(NO)(PPh₃)Re}(μ-C≡CC≡C){PdCl(PEt₃)₂},[224] while Re(C≡CC≡CCu)(PPh₃)(NO)Cp*, of presently unknown structure, is prepared in a similar manner.[290]

(c) Group 8

In the presence of CuI and an amine solvent, Fe(C≡CC≡CH)(CO)₂(η⁵-C₅Me₄Et) couples with RuCl(CO)₂Cp′ to give {(η⁵-C₅Me₄Et)(CO)₂Fe}(μ-C≡CC≡C){Ru(CO)₂Cp′} (138; Cp′ = Cp, Cp*).[182,257] The more electron rich mixed iron/ruthenium complex {Fe(dppe)Cp*}(μ-C≡CC≡C){Ru(PPh₃)₂Cp} (139) is readily prepared from reaction of Ru(C≡CC≡CH)(PPh₃)₂Cp with FeCl(dppe)Cp* following reaction in the presence of NEt₃ and NaBPh₄.[297]

(d) Group 10

Curiously, while sequential treatment of the *cis*-bis(diynyl) reagent *cis*-Pt(C≡CC≡CH)₂(dppe) with two equivalents of BuᵗLi and MeI affords the bis(pentadiynyl) complex Pt(C≡CC≡CMe)₂(dppe), only monoauration is observed after a similar reaction with AuCl(PPh₃) with Pt(C≡CC≡CH){C≡CC≡C[Au(PPh₃)]}(dppe) (140) being the only isolated product. The same product was obtained from a CuI-catalyzed coupling of Pt(C≡CC≡CH)₂(dppe) and AuCl(PPh₃) in a mixed NHEt₂/thf solvent. Molecular modeling studies failed to reveal any obvious steric interactions which might be responsible for this anomalous behavior.[285] Nevertheless, *cis*-Pt(C≡CC≡CH)₂(dppe) reacts with [ppn][Au(acac)₂] to afford a tetra-anionic, heterometallic expanded molecular square (141).[289]

(e) Group 11

Lithiation (LiBu) of Au(C≡CC≡CH){P(tol)₃} followed by treatment with CuCl(triphos) gave {[(tol)₃P]Au}C≡CC≡C{Cu(triphos)} (142) in good yield.[267]

3. Trimetallic Complexes

Aside from the edges of the molecular squares mentioned above, there are few complexes of the type M(μ-C≡CC≡CM′)₂ known (Table VII). These have been prepared using the same types of reactions described previously. For example, a CuI-catalyzed reaction between *trans*-Pt(C≡CC≡CH)₂

PPh$_2$

Ph$_2$P—Pt—C≡C—C≡C—Au(PPh$_3$)

C
‖
C
‖
C
≡
C
|
H

(140)

4+

L$_2$Pt—C≡C—C≡C—Au—C≡C—C≡C—PtL$_2$

Au

L$_2$Pt—C≡C—C≡C—Au—C≡C—C≡C—PtL$_2$

(141) L$_2$ = dppe

(PBu$_3$)$_2$ and MCl$_2$(PBu$_3$)$_2$ (M = Pd, Pt) gives the linear trimetallic species *trans*-Pt{C≡CC≡C[MCl(PBu$_3$)$_2$]}$_2$(PBu$_3$)$_2$ (**143**).[281] Selective cleavage of the Pd–C bonds occurs in the reaction between PdCl$_2$(PBu$_3$)$_2$ and *trans,trans*-{Pd(PBu$_3$)$_2$}(μ-C≡CC≡C){Pt(PBu$_3$)$_2$(μ-C≡CC≡C)}$_n$ to give *trans,trans*, *trans*-Pt(PBu$_3$)$_2${(μ-C≡CC≡C)[PdCl(PBu$_3$)$_2$]}$_2$ (**143/Pd**).
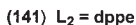
Lithiation of Re(C≡CC≡CH)(NO)(PPh$_3$)Cp* and subsequent reaction with a stoichiometric amount of *trans*-PdCl$_2$(PEt$_3$)$_2$ affords *trans*-Pd{C≡CC≡C[Re(NO)(PPh$_3$)Cp*]}$_2$(PEt$_3$)$_2$ (**144**).[224] The Pd(PEt$_3$)$_2$ group efficiently insulates the remote Re centers, and there is no evidence of electronic "communication" between the terminal metal fragments. Coupling W(C≡CC≡CH)(CO)$_3$Cp with *cis*-PtCl$_2$(PP) species [PP = (PEt$_3$)$_2$,

TABLE VII

Trimetallic Bis(diyndiyl) Complexes

Complex	IR (Raman) ν(CC) cm^{-1}	δ_c (J/Hz)	Ref.
Hg{C≡CC≡C[W(CO)$_3$Cp]}$_2$	2161[a]	unassigned	293
trans-Pd{C≡CC≡C[Re(NO)(PPh$_3$)Cp*]}$_2$(PEt$_3$)$_2$	2114, 1984[a]	100.5 (CP 11.1) [C(1)], 98.2 (CP 3.3)	224
	2114, 1988[c]	[C(2)], 117.0 [C(3)], 87.4 (CP 18.4) [C(4)]	
	(2111/2128)		
cis-Pt{C≡CC≡C[W(CO)$_3$Cp]}$_2$(PEt$_3$)$_2$	not observed	116.15, 93.69, 58.90	293
Pt{C≡CC≡C[PtCl(PBu$_3$)$_2$]}$_2$(PBu$_3$)$_2$	2280w, 1990m[b]		281
Pt{C≡CC≡C[PdCl(PBu$_3$)$_2$]}$_2$(PBu$_3$)$_2$	2290w, 1992m[b]		281
[ppn]$_4$[cyclo-Pt(dppe){C≡CC≡CAuC≡CC≡C}]$_4$	2142, 2073[b]	99.56 (Au–C), 97.26, 76.08, 60.31	289
Hg{C≡CC≡C[Au(PPh$_3$)]}$_2$	2100, 2014		267
Hg{C≡CC≡C[AuP(tol)$_3$]}$_2$	2166, 2052	88.17 (CP 29) (Au–C), 102.52, 72.52	267
Hg{C≡CC≡C[Ru(dppe)Cp*]}$_2$	2156, 2095, 1992		298
Hg{C≡CC≡C[Ru(PPh$_3$)$_2$Cp]}$_2$	2108, 1955		298
[ppn][Au{C≡CC≡C[W(CO)$_3$Cp]}$_2$]	2029[b]	63.57	267
[ppn][Au{C≡CC≡C[Au(PPh$_3$)]}$_2$]	2140, 2080[b]	118.78, 88.34	267
[ppn][Au{C≡CC≡C[Au(Ptol$_3$)]}$_2$]	2145		267

Note: [a]CH$_2$Cl$_2$; [b]nujol; [c]KBr.

dppe, dppp] to give *cis*-Pt{C≡CC≡C[W(CO)$_3$Cp]}$_2$(PP) (**145**) is catalyzed by CuI.[293]

The salts [ppn][Au{C≡CC≡C[Au(PR$_3$)]}$_2$] (**146**; R = Ph,[289] tol[267]) contain a linear 13-atom P–Au–C$_4$–Au–C$_4$–Au–P sequence in the anions and were obtained from Au(C≡CC≡CH)(PR$_3$) and [ppn][Au(acac)$_2$] in the presence of NHEt$_2$ through the elimination of acacH. The reaction between [ppn][Au(acac)$_2$] and W(C≡CC≡CH)(CO)$_3$Cp gives the linear trimetallic species [ppn][Au{C≡CC≡C[W(CO)$_3$Cp]}$_2$] (**147**).[289]

The diynyl complexes Ru(C≡CC≡CH)(dppe)Cp*, W(C≡CC≡CH) (CO)$_3$Cp and Au(C≡CC≡CH)(PR$_3$) (R = Ph, tol) react with 0.5 equiv. Hg(OAc)$_2$ to give the trimetallic complexes Hg{C≡CC≡C[ML$_n$]}$_2$ (**148**).[267,293,298] The limited mixing of the Hg-based metal orbitals with the carbon π-orbitals results in the terminal metal groups being essentially electronically isolated.

{L$_r$M}—C≡C—C≡C—M'—C≡C—C≡C—{ML$_n$}
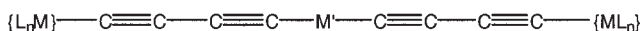
	M'	ML$_n$
(**143**)	*trans*-Pt(PBu$_3$)$_2$	*trans*-MCl(PBu$_3$)$_2$ (M = Pd, Pt)
(**144**)	*trans*-Pd(PEt$_3$)$_2$	Re(NO)(PPh$_3$)Cp*
(**145**)	*cis*-Pt(PP) [PP = (PEt$_3$)$_2$, dppe, dppp]	W(CO)$_3$Cp
(**146**)	[Au]⁻	Au(PR$_3$) (R = Ph, tol)
(**147**)	[Au]⁻	W(CO)$_3$Cp
(**148/W**)	Hg	W(CO)$_3$Cp
(**148/Ru**)	Hg	Ru(dppe)Cp*
(**148/Au**)	Hg	Au(PR$_3$) (R = Ph, tol)

E. *Complexes Containing C$_5$ Ligands*

1. Group 7

The methodology used to prepare the first C$_3$ complexes has been applied to the synthesis of a C$_5$ analogue. Lithiation of Re(C≡CC≡CH) (NO)(PPh$_3$)Cp*, followed by successive reactions with Mn(CO)$_3$(η-C$_5$Cl$_5$) and [OMe$_3$]BF$_4$, gives dark purple {Re(NO)(PPh$_3$)Cp*}{μ-C≡CC≡ CC(OMe)=}{Mn(CO)$_2$(η-C$_5$Cl$_5$)} (**149**, Scheme 34).[230] Removal of the OMe group with BF$_3$ then affords dark brown [{Re(NO)(PPh$_3$)Cp*} CCCCC{Mn(CO)$_2$(η-C$_5$Cl$_5$)}][BF$_4$] (**150**). This complex is very light sensitive and decomposes readily to paramagnetic materials. Similar derivatives with Mn(CO)$_2$(η-C$_5$Br$_5$) and Fe(CO)$_4$ groups were prepared.[229]

$(\eta\text{-}C_5Cl_5)(OC)_2Mn\text{---}C\equiv O$

(i) $Li(C\equiv C)_2Re(NO)(PPh_3)Cp^*$
(ii) $[OMe_3]BF_4$

OMe

$\{(\eta\text{-}C_5Cl_5)(OC)_2Mn\}=C$

$C\equiv C$

$C\equiv C$

$\{Re(NO)(PPh_3)Cp^*\}$

(149)

BF$_3$

$[\{(\eta\text{-}C_5Cl_5)(OC)_2Mn\}=C=C=C=C=C=\{Re(NO)(PPh_3)Cp^*\}]^+$

(150)
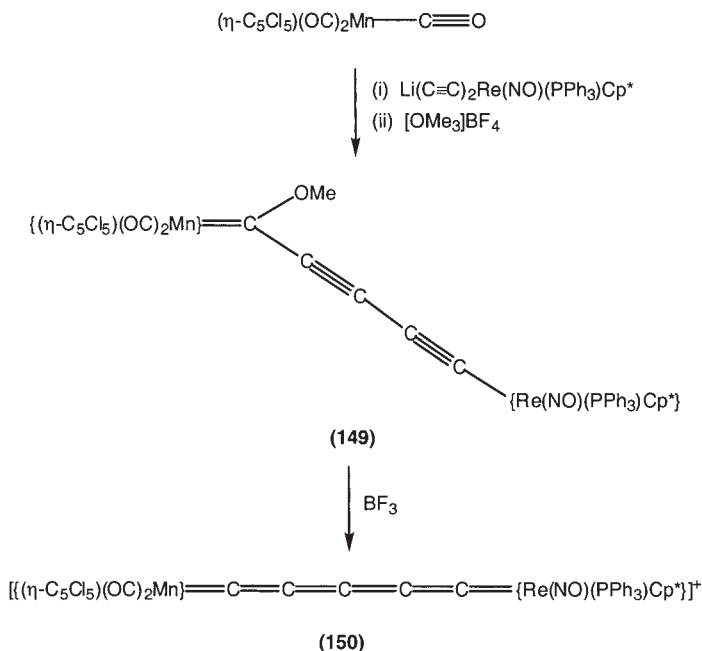
SCHEME 34

Spectroscopic properties are consistent with the cumulenic structure shown, with $\nu(CC)$ at 1953 cm^{-1} and ^{13}C NMR signals for the C$_5$ chain at δ 218.4 [J(CP) 12.5 Hz, ReC], 296.2 (MnC), and at 119.1, 110.6, and 107.0 (CCCCC). No reactions were found with tcne, C$_2$H$_4$, or SMe$_2$.

The complex cis-$\{Re(NO)(PPh_3)Cp^*\}\{\mu\text{-}C\equiv CC\equiv CC(OMe)=\}\{Re(CO)_4$ Re(CO)$_5\}$ **(151)**, obtained from Re(C$\equiv$CC$\equiv$CLi)(NO)(PPh$_3$)Cp* and Re$_2$(CO)$_{10}$, did not give the C$_5$ derivative with BF$_3$.[232]

PPh$_3$ OMe

Re $-$ C$\equiv$C $-$ C$\equiv$C $-$ C

NO   Re $-$ Re(CO)$_5$
                           (CO)$_4$

(151)
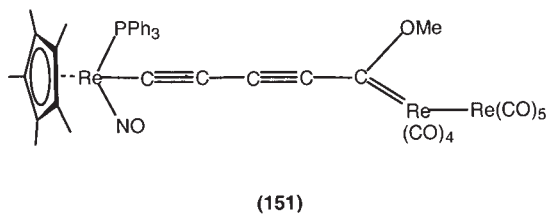
2. Group 8

Attempts to obtain complexes containing C$_5$ chains linking electron-rich ruthenium or osmium centers have been reported, with several complexes

$[M(PR_3)_2 = Fe(dppe), Ru(PPh_3)_2, Os(PPh_3)_2]$

(152)

(153)
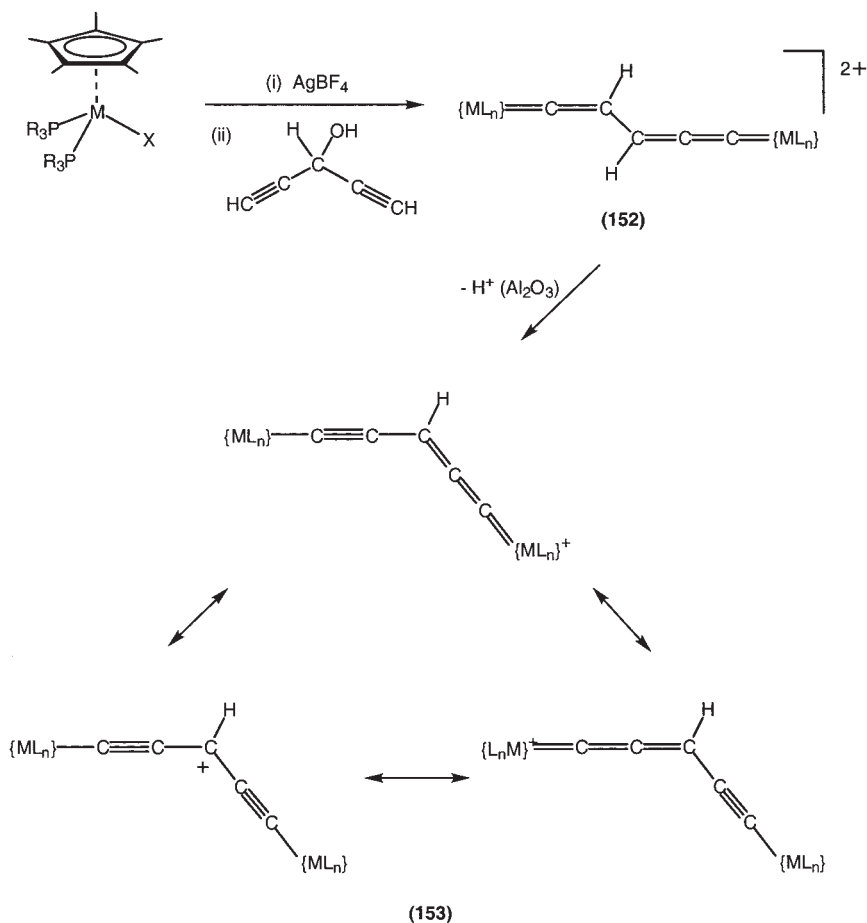
SCHEME 35

containing μ-C_5H ligands having been prepared. The reaction of CH(OH)
$(C{\equiv}CH)_2$ with $[M(L)_2Cp^*]^+$ (M = Fe, L_2 = dppe; M = Ru, L = PPh$_3$,
L_2 = dppe; M = Os, L = PPh$_3$) gave $[\{M(L)_2Cp^*\}{=}C{=}C{=}CHCH{=}C{=}$
$\{M(L)_2Cp^*\}]^{2+}$ (**152**, Scheme 35) which were deprotonated on alumina
to give stable blue $[\{M(L)_2Cp^*\}{=}C{=}C{=}CHC{\equiv}C\{M(L)_2Cp^*\}]^+$
(**153**).[299–301] The symmetrical μ-C_5H bridge is V-shaped. It was not possible
to convert the Ru compound into a complex containing a C_5 bridge, either
with $[CPh_3]^+$ (to remove H$^-$) or with strong base (to remove H$^+$).

Comparing the ^{1}H NMR spectra, the signals for the central H on the
C_5 chain occur at δ 6.50 (Fe), 8.30 (Ru), and 10.55 (Os), suggesting
increasing carbocationic nature as the Group is descended. Strong
absorptions at 722 (Fe), 600 (Ru), and 583 nm (Os) are assigned to
transitions involving the M–C_5–M bridges. The solid-state structures of
the Ru and Os complexes are similar, with the V-shaped C_5H chain
[130.3(11), 128.2(8)° (Os)] probably reflecting the degree of steric interaction
between the phosphine Ph groups on the two metal centers. Electrochemical
studies show a reduction wave between −1.10 and −1.30 V and two
oxidation waves, which are reversible for iron (at +0.12 and +0.47 V)
but irreversible for ruthenium and osmium (+0.68, +0.74 and +1.04,
+1.10 V). These have been assigned to reduction of the C_5H ligand, the
LUMO of which is largely centered on the CH group (C p orbital
character), and to oxidation of the metal centers (Scheme 36).[301]
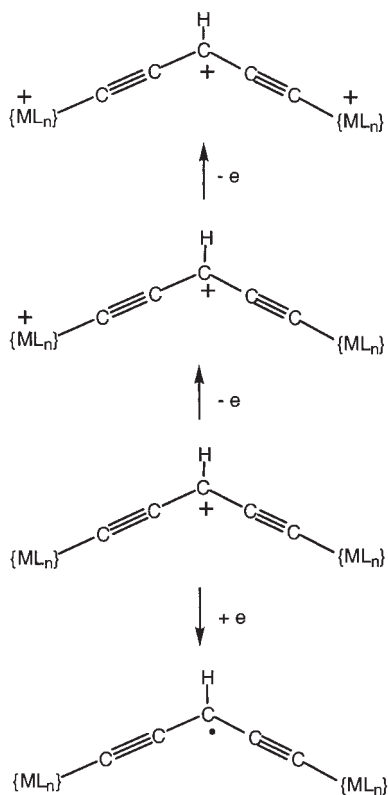
SCHEME 36

F. *Complexes Containing C_6–C_{20} Ligands*

Terminal poly-ynes containing chains with six or more carbon atoms are generally highly sensitive to thermolysis or photolysis and are therefore not readily available for use in the construction of complexes of the type being reviewed here. Trialkylsilyl-capped chains are somewhat more stable, and reliable syntheses of $R_3Si(C{\equiv}C)_mSiR_3$ ($R = Me$, Pr^i, $m = 3$, 4) are available. Very recently, several series of poly-ynes containing up to ten $C{\equiv}C$ triple bonds were described, making use of bulky aromatic polyether dendrimers to separate the carbon chains.[302] An alternative approach is the use of cyano end-groups and the series $N{\equiv}C{-}(C{\equiv}C)_m{-}C{\equiv}N$ ($m = 1$–8) is known.[21,303]

Complexes containing C_6 and C_8 ligands bridging two metal centers were first described in 1970 but only partly characterized.[256] Several complexes of this type have also been obtained by depolymerization of $H\{(C{\equiv}CC{\equiv}C)Pt(PBu_3)_2(C{\equiv}CC{\equiv}C)\}_nH$ (Section II.H). More recently, construction of derivatives of longer carbon chains is achieved by sequential application of metallation or oxidative coupling reactions to suitable precursors containing one or two $C{\equiv}C$ triple bonds. In this way, derivatives containing up to 20 carbon atoms, such as $\{Re(NO)(PPh_3)Cp^*\}_2\{\mu\text{-}(C{\equiv}C)_{10}\}$, have been prepared and satisfactorily characterized. Usually, this has been carried out to give homonuclear systems, since it is not yet clear whether coupling of poly-ynes with different end-groups can be directed to give specific combinations preferentially, rather than giving statistical mixtures of all possible products.

There are four general reactions which have been applied to lengthen the carbon chain commencing with the complexes $\{ML_x\}C{\equiv}CC{\equiv}CH$:

(a) Lithiation (LiBu), which may or may not be followed by cupration with CuI, to give $\{ML_x\}C{\equiv}CC{\equiv}CLi(Cu)$, which is condensed *in situ* with halo-poly-alkynes, such as $Br(C{\equiv}C)_mSiR_3$ ($m = 1$, 2; $R = Me$, Et) to give $\{ML_x\}C{\equiv}CC{\equiv}C(C{\equiv}C)_mSiR_3$;

(b) In some cases, the free poly-yne can be generated *in situ* by proto-desilylation reactions (base, fluoride). If these reactions are carried out in the presence of a metal halide, subsequent reaction gives the desired complexes end-capped by transition metal–ligand fragments.

(c) Oxidative coupling (Eglinton, Hay) of 1-alkynes containing ML_x groups, $H(C{\equiv}C)_m\{ML_x\}$, doubles the chain length to give $\{ML_x\}_2\{\mu\text{-}(C{\equiv}C)_{2m}\}$. Note that a variant of this reaction, carried out in the presence of $HC{\equiv}CSiR_3$, results in lengthening of the poly-alkynyl chain by one C_2 unit. The desilylated complexes may be obtained *in situ* by proto-desilylation as in (b).

These compounds will be described below, together with the trends in properties (spectroscopic, structural) as the chain length increases. In the limit, the properties may resemble those of "carbyne", the (presently) unknown C(sp) allotrope. If redox-active metal centers are linked by unsaturated C_n chains, electronic interactions between the two metal centers may occur, and have been demonstrated for up to C_{10} chains so far. Further complexation of metal centers by π-bonding to the chain generally reduces communication along the chain, but more recent studies of cobalt carbonyl complexes and their phosphine derivatives have suggested that both through-bond and through-space interactions may occur. This remains a topic of active investigation.

1. Molybdenum and Tungsten Complexes

Oxidative coupling (Hay conditions: CuCl/tmed in acetone, O_2 or air, r.t.) of $M(C{\equiv}CC{\equiv}CH)(CO)_3Cp$ (M = Mo, W) gives orange $\{M(CO)_3Cp\}_2\{\mu\text{-}(C{\equiv}C)_4\}$ (**154**; Scheme 37) in excellent yield.[241,242]

2. Rhenium Complexes

The major synthetic routes to binuclear complexes containing longer $-(C{\equiv}C)_m-$ chains (**155**/**m**) have been established by Gladysz and his co-workers, who have employed $Re(NO)(PR_3)Cp'$ (R generally Ph, $Cp' = Cp$, Cp*) as end-capping groups.[290] The $Re(NO)(PPh_3)Cp*$ fragment is chiral, although in most syntheses racemic mixtures of the initial mono-rhenium complexes have been used. Reactions give mixtures of *meso* and *dl* diastereomers, which in some cases are distinguishable by NMR methods (Table VIII). For example, ^{13}C and ^{31}P resonances for both isomers can be seen for the C_6 complex, but for the C_8 derivative, separate resonances were not seen (probably because of a greater separation of metal centers); a similar isomeric formulation is assumed. As mentioned above (Section II.D), the diastereomers of the C_4 complex can be separated by crystallization. However, in no case longer than C_4 has it been possible to separate the isomers and difficulties in getting X-ray quality crystals have been ascribed to the presence of mixtures of diastereomers. For the C_8

$$[L_xM]\text{-}C{\equiv}C\text{-}C{\equiv}C\text{-}H \quad \xrightarrow[{[Cu(tmeda)]^+}]{O_2} \quad [L_xM]\text{-}C{\equiv}C\text{-}C{\equiv}C\text{-}C{\equiv}C\text{-}C{\equiv}C\text{-}[ML_x]$$

(**154**)

$$L_xM = Mo / W(CO)_3Cp$$

SCHEME 37

$L_xM-(C\equiv C)_m-ML_x$
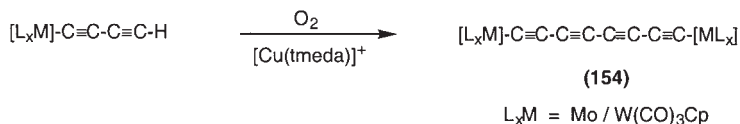
	m	ML_x
(154)	4	$M(CO)_3Cp$ (M = Mo, W)
(155)	2,3,4,5,6,8,10	$Re(NO)(PPh_3)Cp^*$
(158)	3,6	$Fe(CO)_2Cp^*$ (Fp*)
(159)	4	$Fe(dppe)Cp^*$
(160)	3,4	$Ru(PPh_3)_2Cp$
(161)	4,6	*trans*-$Pt(tol)(PAr_3)_2$
(165)	4,6,8	*trans*-$Pt(C_6F_5)\{P(tol)_3\}_2$
(169)	3,4	$Au(PR_3)$ (R = Cy, tol)

complex, a preliminary X-ray study suggests that the Re center is less sterically hindered than that in the C_4 complex.

Oxidative cross-coupling $[Cu(OAc)_2/py]$ of a mixture of $Re(C\equiv CH)(NO)(PPh_3)Cp^*$ and $Re(C\equiv CC\equiv CH)(NO)(PPh_3)Cp^*$ gives a mixture of the $\{Re(NO)(PPh_3)Cp^*\}_2\{\mu\text{-}(C\equiv C)_m\}$ complexes (**155/m**; $m = 2$, 14; 3, 44; 4, 15%) which could be separated by chromatography on silica gel.[250,290] An alternative synthesis of the C_8 complex was also obtained by a sequence of reactions between $Re(C\equiv CC\equiv CCu)(NO)(PPh_3)Cp^*$ and $BrC\equiv CC\equiv CSiMe_3$ in the presence of $NHEt_2$ to give $Re\{(C\equiv C)_4SiMe_3\}(NO)(PPh_3)Cp^*$, which was desilylated and oxidatively coupled to give **155/4**.[304] This complex is also formed by thermal decomposition of *trans*-$Pd\{C\equiv CC\equiv C[Re(NO)(PPh_3)Cp^*]\}_2(PPh_3)_2$ in refluxing benzene.[250,290]

Syntheses of complexes containing poly-ynediyl chains, $-(C\equiv C)_m-$ ($m = 3\text{--}10$), spanning rhenium centers involves a methodology involving four well-established reactions applied sequentially to $Re(C\equiv CC\equiv CH)(NO)(PPh_3)Cp^*$ (Scheme 38).[248,290,291] Conversion to an incompletely characterized copper(I) derivative (see below) was achieved with LiBu and CuI, after which reaction with bromo(silyl)alkynes (Cadiot–Chodkiewicz) and protodesilylation of the resulting C_6 and C_8 complexes ([NBu$_4$]F in wet thf) afforded $Re\{(C\equiv C)_mH\}(NO)(PPh_3)Cp^*$ ($m = 3$, 4). Oxidative coupling $[Cu(OAc)_2/py]$ then gave the binuclear C_{12} and C_{16} complexes. In one case, reaction of $BrC\equiv CC\equiv CBr$ with $Re(C\equiv CC\equiv CCu)(NO)(PPh_3)Cp^*$ afforded **155/6** directly. Lithiation and cupration of $Re\{(C\equiv C)_4H\}(NO)(PPh_3)Cp^*$, followed by coupling with $SiR_3C\equiv CBr$ (R = Me, Et) gives $Re\{(C\equiv C)_5SiR_3\}(NO)(PPh_3)Cp^*$. Alternatively, this compound can

TABLE VIII

SELECTED SPECTROSCOPIC PROPERTIES OF $\{ML_x\}_2(\mu\text{-}C_n)$ ($n = 6\text{–}20$)

ML_x	n	IR (Raman) $\nu(CC)/cm^{-1}$	δ_C (J/Hz) C(1)	C(2)	C(3)	C(4)	Unassigned	λ nm (ε M^{-1} cm^{-1})	Ref.
Group 6									
Mo(CO)₃Cp	8	2140[a]	112.24	92.22	63.47	59.95			242
W(CO)₃Cp	8	2190[a]	112.39	91.60	63.70	60.91			241,242
Group 7									
Re(NO)(PPh₃)Cp*	6	2061m[a] 2064m[b] 2058m[c] (2100s, 1951s)	104.2, 103.3[a] (CP 15.7/16.0)	114.3, 113.9				232 (62,000), 328 (39,000), 354 (37,000)	250
	6		106.8, 106.5[a] (CP 16.8/16.0)	112.6	65.0, 64.9			232 (62,000), 328 (39,000), 354 (37,000)	290
	8	2108s, 1959m[a] 2112s, 1956m[b] 2107s, 1954m[c] (2100s, 2000s)	109.7 (CP 16.9)	113.3				360 (67,000), 390 (60,000)	250,290
	8		111.0 (CP 18.4)	112.7	66.8 (CP 2.9)	63.8		234 (58,000), 262sh (36,000), 340sh (56,000), 360 (67,000), 390 (60,000)	290
	10	2120s, 2000m[b] 2114s, 1993m[c]	117.3 (CP 15.7)	112.7	66.1 (CP 2.7)		66.3, 64.1	230 (58,000), 268 (32,000), 274 (32,000), 338sh (41,000), 366sh (59,000),	290

							394 (76,000), 426 (50,000), 474 (10,000)	
	12	2117m, 2056vs, 1952s[b] 2112m, 2050s, 1946s[c] (2135w, 2030m 1951s)	116.8 (CP 15.6)	113.7	66.0 (CP 3.3)	67.1, 66.3, 64.4	230 (60,500), 280 (47,600), 364sh (47,300), 390 (63,400), 422 (82,700), 470 (37,350) 512sh (16,600), 568 (3900)	290,291
	16	2074m, 2014vs, 1941vs[b] 2069m, 2012s, 1938s[c] (2101vw, 2000w, 1921s)	125.1 (CP 15.2)	113.2	66.6 (CP 2.4)	66.7, 66.4, 65.6, 65.5, 65.2	232 (62,600), 328 (61,700), 348 (65,300) 402sh (81,500), 430 (142,000), 470 (128,000), 548 (61,200), 644 (9900)	290,291
	20	2164w, 2116w, 2058s, 2031vs, 1962vs[b] 2136w, 2101w, 2036s, 1949s[c] (2102vw, 2068vw, 1984w 1899s)	127.3 (CP 14.6)	113.2	66.6	67.0, 66.5, 65.5, 65.4, 65.3, 64.9, 64.8	228 (78,000), 384sh (110,000), 430 (131,000), 466 (191,000), 508 (136,000), 582 (73,000), 602 (73,000)	290,291
Re(NO){P(tol)₃}Cp*	4[f]	1963[a]	95.7, 96.6	118.0			232 (63,900), 270sh (22,300), 352 (13,500),	251
	6[f]	2059w[a]	104.9	114.8,	66.6		232 (82,000),	251

TABLE VIII
Continued

ML_x	n	IR (Raman) $v(CC)/cm^{-1}$	δ_C (J/Hz) C(1)	C(2)	C(3)	C(4)	Unassigned	λ nm (ε M^{-1} cm^{-1})	Ref.
			(CP 16.6)	114.7				320 (38,200), 358 (37,800)	
	8	2107s, 1954m[a]	110.7 (CP 12.7)	114.6	67.9	66.0		234 (83,000), 362 (75,000), 394 (71,000)	251
Re(NO){P(C$_6$H$_4$Bu^t)$_3$}Cp*	8	2108s, 1954m[a]	110.3 (CP 15)	114.5	67.7 (CP 3.0)	66.0		232 (90,200), 362 (65,600), 394 (61,000)	251
Re(NO){P(C$_6$H$_4$Ph)$_3$}Cp*	8	2108s, 1954m[a]	109.8 (CP16.9)	114.4	67.5	65.8		228 (74,500), 270 (164,000), 362 (74,200), 392 (61,000)	251
Re(NO)(PCy$_3$)Cp*	8	2110s, 1953w[a]	not observed					274 (27,300), 340 (39,400), 366 (55,100), 398 (52,800)	251
Group 8									
Fe(CO)$_2$Cp*	6	2094[a]	99.7				94.9, 54.0		182,306
	8	2136, 2088[a]	110.8				94.8, 61.6, 51.4		182,306
	12	2123, 2087[a]	118.3				94.6, 64.8, 62.2, 58.9, 50.5		306
Fe(dppe)Cp*	8	2109s, 1949s[d]	139.5 (CP 4.2)	101.8	62.7 (CP 3)	50.6		389 (100,500), 481 (10,000)	307

Ru(PPh$_3$)$_2$Cp	6	2135w, 2066s, 1965w[a]							261
	8	2110s, 1956m[a]							308
Group 10									
trans-Pt(tol)(Ptol$_3$)$_2$	8	2135s, 1987m[a]	111.6 (CP 13.5)	98.3	64.5	58.4		233 (200,000), 305 (95,000), 343 (100,000)	310
	12	2121m, 2083s, 1982m[a]	120.9 (CP 14.4, CPt 875)	96.7 (CPt 212.5)			66.6, 63.8, 61.2, 56.9	231 (151,000), 322 (60,000), 347 (125,000), 371 (215,000)	310
trans-Pt(tol){PPh$_3$}$_2$	8	2139s, 1984m[a]	112.9	98.6	64.3	58.4			310
	12	not observed	not observed						310
trans-Pt(C$_6$F$_5$){P(tol)$_3$}$_2$	8	2152s, 2011m[e]	100.6 (CPt 998)	96.7 (CPt 265)	64.1	58.1		295 (80,000), 325 (113,000)	311
	12	2127m, 2088s, 1992m[e]	106.5	95.5			65.7, 63.0, 61.0, 57.1	315 (101,000), 336 (267,000), 359 (432,000)	311
	16	2154w, 2088w, 2054s, 1984m[e]	109.1	95.0			66.7, 64.9, 63.1, 61.5, 60.1, 56.8	290 (46,000), 306 (42,000), 326 (54,000), 346 (151,000), 369 (397,000), 397 (602,000)	311
Group 11									
Au(PCy$_3$)	6	2109[d]	131.3 (CP 131.4)	85.9 (CP 25)	75.1			see original literature	315
	8	2147, 2066, 2007[d]	136.0 (CP 122.2)	87.4 (CP 24.9)	67.4	62.8		290, 274, 260, 252	315

Note: [a]CH$_2$Cl$_2$; [b]thf; [c]KBr; [d]nujol; [e]powder film; [f]enantiomeric pair.

[Re*] = Re(NO)(PPh₃)Cp*

$[Re^*] = Re(NO)(PPh_3)Cp^*$

$[Re^*]-C{\equiv}C-C{\equiv}C-H$ $\xrightarrow[{[Cu(tmeda)]^+}]{O_2}$ $[Re^*]-C{\equiv}C-C{\equiv}C-C{\equiv}C-[Re^*]$

(155/4)

LiBu, CuI

$[Re^*]-C{\equiv}C-C{\equiv}C-Cu$ $\xrightarrow{Br-C{\equiv}C-SiR_3}$ $[Re^*]-C{\equiv}C-C{\equiv}C-C{\equiv}C-SiR_3$

$\downarrow K_2CO_3 / MeOH$

(i) Br-C≡C-C≡C-SiR₃
(ii) K₂CO₃ / MeOH

$[Re^*]-C{\equiv}C-C{\equiv}C-C{\equiv}C-H$ $\xrightarrow{Cu(OAc)_2 / py}$ $[Re^*]-C{\equiv}C-C{\equiv}C-C{\equiv}C-C{\equiv}C-C{\equiv}C-[Re^*]$

(155/6)

$[Re^*]-C{\equiv}C-C{\equiv}C-C{\equiv}C-H$

$[Re^*]-C{\equiv}C-C{\equiv}C-C{\equiv}C-Cu$

(i) LiBu, CuI
(ii) Br-C≡C-SiR₃

$\downarrow Br-C{\equiv}C-C{\equiv}C-SiMe_3$

Cu(OAc)₂ / py

$[Re^*]-C{\equiv}C-C{\equiv}C-C{\equiv}C-C{\equiv}C-C{\equiv}C-SiR_3$

(i) K₂CO₃ MeOH
(ii) Cu(OAc)₂py

$[Re^*]-C{\equiv}C-C{\equiv}C-C{\equiv}C-C{\equiv}C-C{\equiv}C-C{\equiv}C-C{\equiv}C-C{\equiv}C-[Re^*]$

(155/8)

$[Re^*]-C{\equiv}C-C{\equiv}C-C{\equiv}C-C{\equiv}C-C{\equiv}C-C{\equiv}C-C{\equiv}C-C{\equiv}C-C{\equiv}C-[Re^*]$

(155/10)
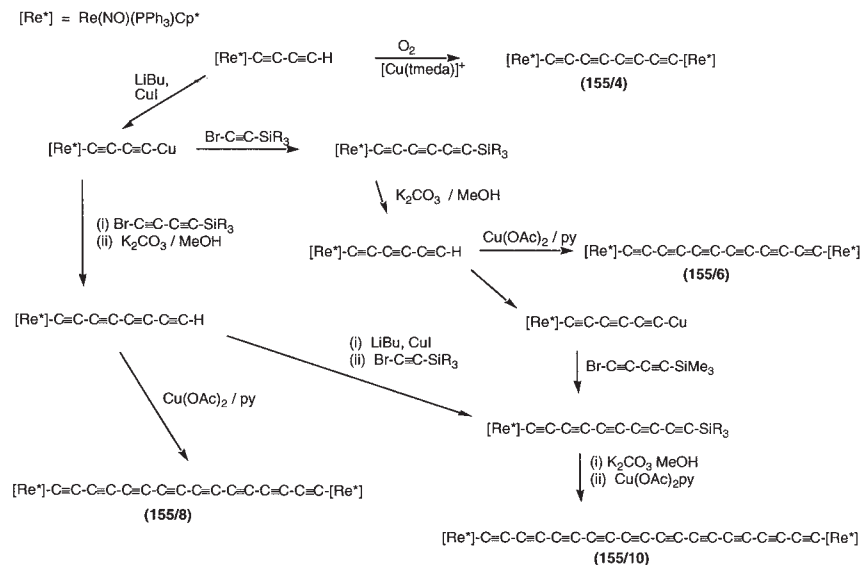
SCHEME 38

be obtained from $SiEt_3C{\equiv}CBr$ and the copper compound to give $Re\{(C{\equiv}C)_3SiEt_3\}(NO)(PPh_3)Cp^*$, which after conventional desilylation, lithiation and reaction with CuI, is converted to the putative $Re\{(C{\equiv}C)_3Cu\}(NO)(PPh_3)Cp^*$. Further reaction with $SiMe_3C{\equiv}CC{\equiv}CBr$ affords $Re\{(C{\equiv}C)_5SiMe_3\}(NO)(PPh_3)Cp^*$. Desilylation and oxidative coupling $[Cu(OAc)_2/py]$ then affords **155/10**.[291]

Rapid decomposition of the product from reaction of $Re\{(C{\equiv}C)_6 SiMe_3\}(NO)(PPh_3)Cp^*$ with wet $[NBu_4]F/PhMe$ precluded the synthesis of **155/12**. Compounds with up to 16 carbon atoms in the chain form orange powders which are stable in air, but **155/10** is black. While no obvious trends in stability are apparent, decomposition points indicated by DSC range between 155 (for C_{20}) to 217 °C (for C_8). Complexes containing long carbon-chain links between two metal centers are generally stable in air at r.t. for a week and decompose > 100 °C without explosion.

Complexes containing a range of different phosphines PR_3 (R = tol, $C_6H_4Bu^t$-4, C_6H_4Ph-4, Cy) could be prepared from the appropriate $ReMe(NO)(PR_3)Cp^*$ derivative by a reaction sequence involving treatment with HBF_4 in PhCl, displacement of the labile PhCl ligand by $HC{\equiv}CC{\equiv}CSiMe_3$, conversion to the σ-diynyl compound with $KOBu^t$, followed by protodesilylation ($[NBu_4]F$ in wet thf) and oxidative coupling $[Cu(OAc)_2/py, 50–80$ °C] to $\{Re(NO)(PR_3)Cp^*\}_2\{\mu-(C{\equiv}C)_4\}$.[251]

These orange to dark red compounds were obtained in 23–54% yields as inseparable diastereomeric mixtures. Oxidative coupling of Re{(C≡C)$_m$H}(NO){P(tol)$_3$}Cp* ($m = 1$ and 2) afforded the orange C$_6$ complex (23%), accompanied by only 8% of the C$_8$ derivative.

Similar synthetic sequences have been employed to prepare {Re(NO)[PPh$_2$(CH$_2$)$_6$CH=CH$_2$] Cp*}$_2${μ-(C≡C)$_4$} (**156**) as a mixture of diastereomers, which with Grubbs's catalyst underwent olefin metathesis to give **157** (Scheme 39).[305] An ion from the intermolecular metathesis product (m/z 2728) was detected in the mass spectrum of **157**, while the NMR spectra suggested that the compound was a mixture of configurational (at Re) and geometrical (Z/E) isomers. CV data (two one-electron oxidations at $E°(1) = +0.24$, $E°(2) = +0.52$, both only partially reversible) showed oxidation to be thermodynamically slightly more favorable than for the PPh$_3$ analogue.

3. Iron Complexes

Copper(I)-catalyzed coupling of Fp*Cl with Fp*(C≡C)$_3$H (from Fp*Cl, Me$_3$Si(C≡C)$_3$SiMe$_3$ and LiMe, followed by proto-desilylation) gives orange Fp*(C≡C)$_3$Fp* (**158/m**, $m = 3$) (71%).[182] This complex has only one ν(C≡C) band at 2094 cm^{-1}, and the chain carbons resonate at δ 99.7, 94.9, and 54.0 (C$_\alpha$, C$_\beta$, C$_\gamma$). Similar coupling (CuCl/tmeda, O$_2$, 30 °C) of Fp*(C≡C)$_3$H gives yellow-brown Fp*(C≡C)$_6$Fp* (**158/6**; 76%).[306] The Fe–C$_{12}$–Fe chain adopts an S-configuration (individual angles 171.7(9)–178(1), av. 175.2°). Changes in Fe–C and C–C bond lengths compared with the ethyn- and butadiyn-diyl complexes are rationalized in terms of contributions from a vinylidene tautomer. While C$_\alpha$ and C$_\beta$ resonate at δ 118.3 and 94.6, respectively, the other carbon chain atoms are found between δ 50.5 and 64.8. Two ν(C≡C) bands are found at 2123 and 2087 cm^{-1}. Oxidative coupling (CuCl/tmeda/O$_2$) of Fp*(C≡C)$_2$H gave Fp*(C≡C)$_4$Fp* (75%).[182] This paper gives an extensive table of ^{13}C NMR shifts and assignments. Two ν(C≡C) bands occur in the IR spectrum, while the four carbons of the chain resonate at δ 139.5, 101.8, 62.7, and 50.6, with ^4J(CP) (3 Hz) being larger than ^3J(CP) (∼ 0 Hz), and ^2J(CP) 42 Hz.

Similar oxidative coupling [Cu(OAc)$_2$/pyridine/dbu, 40 °C] of Fe(C≡CC≡CH)(dppe)Cp* gives {Fe(dppe)Cp*}$_2${μ-(C≡C)$_4$} (**159**) as an air- and thermally-stable burnt-orange compound.[307] Oxidation with [FcH]$^+$ gave forest-green [{Fe(dppe)Cp*}$_2$(μ-C$_8$)]$^{+•}$, which has two ν(CC) absorptions at lower frequencies (1784, 1879 cm^{-1}), intermediate between the diyndiyl and cumulenic forms. The UV/vis spectra contain MLCT bands at 389, 481 nm (neutral) and 403, 423, 556, 624, 707 nm (cation), while the near IR spectrum contains a narrow intense intervalence CT band

(156)

(157)
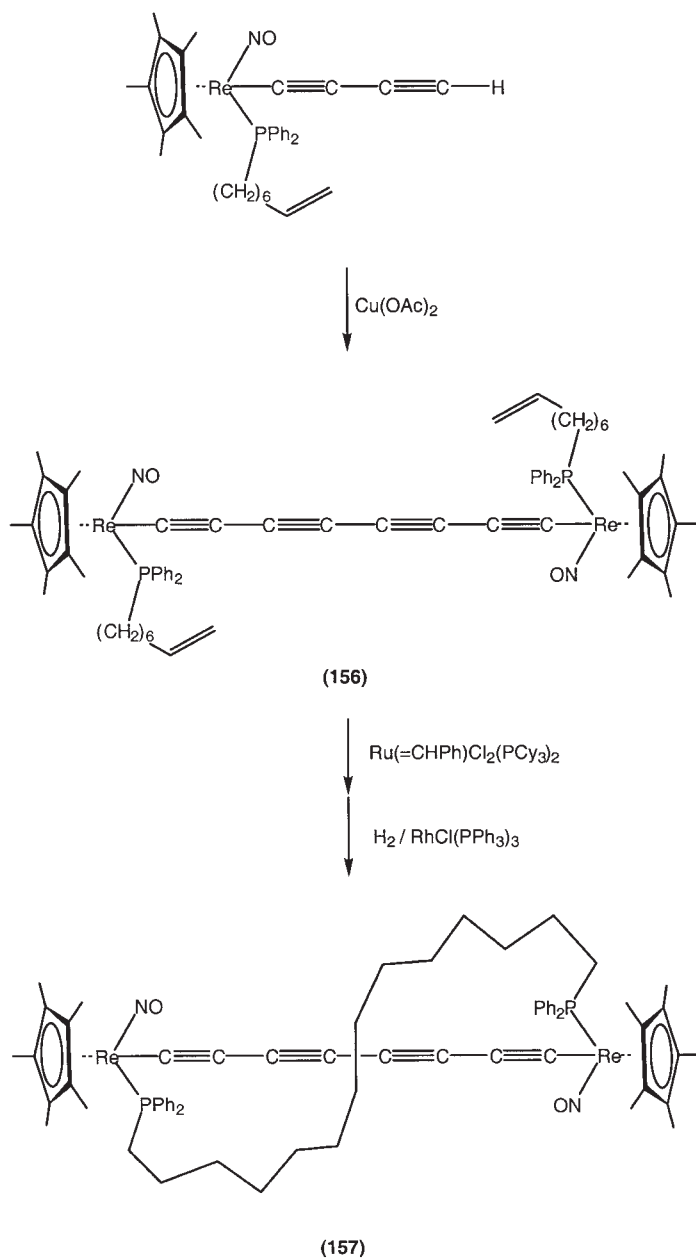
SCHEME 39

(1958 nm). There is a strong electronic coupling between the two Fe centers ($V_{ab} = 0.32$ eV).

4. Ruthenium Complexes

Facile cleavage of the C(sp)–Si bond of silylated alkynes occurs in reactions with $RuCl(PPh_3)_2Cp$ carried out in the presence of fluoride ion. Application of this reaction to $Me_3Si(C≡C)_mSiMe_3$ ($m = 3$, 4) has given orange ${Ru(PPh_3)_2Cp}_2{\mu-(C≡C)_m}$ (**160**/**m**, $m = 3$, 4).[261,308] In the solid state, the two metal–ligand groups take up a *trans* conformation, intermolecular interactions resulting in bending of the carbon chain at C_α [172.2(4)°]. Oxidative coupling [$Cu(OAc)_2$, pyridine/dbu] of $RuCl{(C≡C)_3H}(dppe)_2$ afforded ${RuCl(dppe)_2}_2{\mu-(C≡C)_6}$.[309]

5. Platinum Complexes

Commencing with *trans*-$PtCl(tol)(PAr_3)_2$ (Ar = Ph, tol), conventional copper(I)-catalyzed coupling with buta-1,3-diyne to give *trans*-$Pt(C≡CC≡CH)(tol)(PAr_3)_2$, followed by oxidative cross-coupling reactions involving $HC≡CSiEt_3$, have given bright yellow or orange ${trans-Pt(tol)(PAr_3)_2}_2{\mu-(C≡C)_m}$ (**161**/**m**, $m = 4$, 6).[310] Extension to C_{16} complexes is limited by the apparent instability of $Pt{(C≡C)_4H}(tol){P(tol)_3}_2$, while PPh_3 derivatives have much lower solubilities. The spectral properties are similar to those of other long chain complexes, although the UV/vis bands are less intense than those of the rhenium analogues. The CVs contained two irreversible oxidation waves. In the solid-state, these complexes stack with the C_n chains parallel and with C_α aligned near the mid-point of the chain of an adjacent molecule. The carbon chains show slight bending, mostly at the Pt-bonded ends, but in general the geometrical parameters are unexceptional. Bond lengths approach limiting values of 1.24 and 1.34 Å for C≡C and C–C bonds, respectively.

A series of complexes containing *trans*-$Pt(C_6F_5){P(tol)_3}_2$ end-groups have been prepared similarly from the chloro complex.[311] Conversion to the buta-1,3-diynyl derivative *trans*-$Pt(C≡CC≡CH)(C_6F_5){P(tol)_3}_2$ (**162**) and oxidative cross-coupling ($CuCl$/tmeda, O_2, acetone) with an excess of $HC≡CSiEt_3$ gives *trans*-$Pt{(C≡C)_3SiEt_3}(C_6F_5){P(tol)_3}_2$ (**163**), which in turn could be protodesilylated (wet [NBu_4]F) and oxidatively coupled again with $HC≡CSiEt_3$ in the presence of $SiClMe_3$ to remove fluoride ion, to give *trans*-$Pt{(C≡C)_4SiEt_3}(C_6F_5){P(tol)_3}_2$ (**164**) (Scheme 40). Binuclear compounds are formed by oxidatively coupling either **162** directly, or after treatment of **163** or **164** with [NBu_4]F, with $CuCl$/tmeda. Complexes ${trans-Pt(C_6F_5)[P(tol)_3]_2}_2{\mu-(C≡C)_m}$ (**165**/**m**, $m = 4,6,8$) are formed as

[Pt] = *trans*-Pt(C$_6$F$_5$)(P(tol)$_3$)$_2$

[Pt]-C≡C-C-C≡C-C≡C-[Pt]
(165/4)

[Pt]-C≡C-C-C≡C-H   —O$_2$ / CuCl / tmeda→
(162)

—O$_2$ / HC≡CSiEt$_3$→   [Pt]-C≡C-C-C≡C-C≡C-SiEt$_3$
(163)

wet [NBu$_4$]F ↓

[Pt]-C≡C-C-C≡C-C≡C-H   —O$_2$ / CuCl / tmeda→   [Pt]-C≡C-C-C≡C-C-C≡C-C-C≡C-[Pt]
(165/6)

HC≡CSiEt$_3$ ↗

[Pt]-C≡C-C-C≡C-C≡C-C≡C-SiEt$_3$ —wet [NBu$_4$]F→   [Pt]-C≡C-C-C≡C-C≡C-C≡C-H   —O$_2$ / CuCl / tmeda→   [Pt]-C≡C-C-C≡C-C-C≡C-C≡C-C-C≡C-C≡C-[Pt]
(164)   **(165/8)**
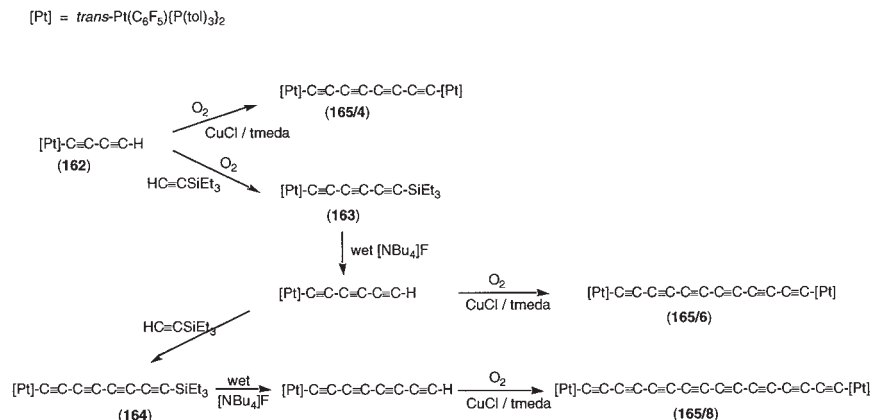
SCHEME 40

air-stable yellow to apricot powders. Unlike some of their mononuclear precursors, they are thermally stable, with m.p. between 234 and 288 °C.

The C$_6$ complex {*trans*-PtPh(PEt$_3$)$_2$}$_2${μ-(C≡C)$_3$} was formed in 18% yield during treatment of *trans*-PtPh{C≡CSiPh$_2$(C≡CH)}(PEt$_3$)$_2$ with Cu(OAc)$_2$/O$_2$ in pyridine, in reactions involving cleavage of Si–C(sp) bonds.[312] The C$_6$ chain is almost linear (maximum deviation 1.7°). The UV–visible spectrum shows well-resolved coupling to vibronic levels in the excited state, as found in {–Pt(PBu$_3$)$_2$(–C≡CC≡CC≡C–)}$_n$.[313] Similarly, sharp structured emissions are found in the photoluminescence spectra, probably from the triplet state associated with the carbon chain. The vibronic progression (2090 cm^{-1}) reflects the ν(C≡C) mode.

A fascinating development of this chemistry has been the construction of molecules containing double helices formed by wrapping poly-methylene chains around a –(C≡C)$_m$– chain.[314] This was achieved by linking two Pt end-caps with diphosphine ligands, themselves containing –(CH$_2$)$_n$ (n ≥ 12) chains. Simple phosphine substitution reactions of {*trans*-Pt(tol)(PPh$_3$)$_2$}$_2${μ-(C≡C)$_m$} by PR$_2$(CH$_2$)$_{12}$PR$_2$ (R = Ph, *c*-C$_6$H$_9$) gave one product which, however, oligomerized or polymerized upon workup. Use of PAr$_2$(CH$_2$)$_{14}$PAr$_2$ (Ar = Ph, tol) and {*trans*-Pt(C$_6$F$_5$)[P(tol)$_3$]$_2$}$_2${μ-(C≡C)$_m$} afforded similar complexes **166** in high yield (Scheme 41), together with some of the corresponding chelate complexes. Several combinations of –(C≡C)$_m$– and –(CH$_2$)$_n$– chain lengths were prepared, structural studies suggesting that helical conformations are adopted with sp^3/sp carbon ratios > 1.5. Interconversion of enantiomeric double helices has a low barrier

(166)
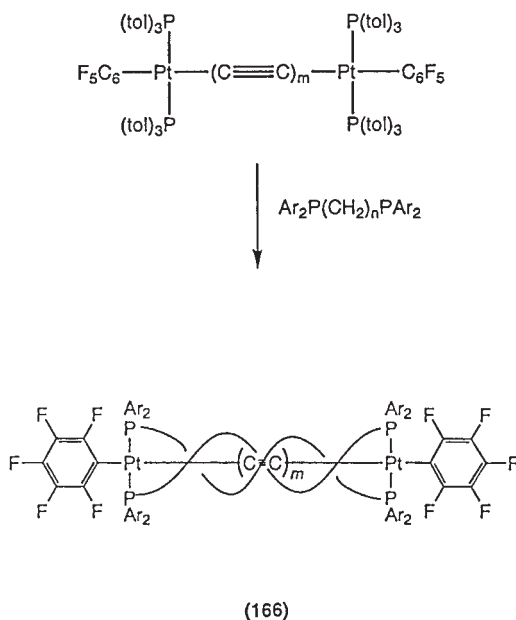
SCHEME 41

(ca. 12 kcal mol^{-1}). For $m = 4$, $n = 10$, 11, only non-helical complexes were obtained.

An alternative approach used as precursor trans-$Pt(C_6F_5)(C{\equiv}CC{\equiv}CH)$ $\{PPh_2(CH_2)_6CH{=}CH_2\}_2$, which was oxidatively coupled ($CuCl/tmeda/O_2$) to the C_8 complex. Again, linking of vinylphosphines by olefin metathesis with Grubb's catalyst and subsequent hydrogenation of the C=C bonds (H_2/Pd on C) gave **167** in 32% yield, together with the chelate complex **168** (Scheme 42).[314] The –$(CH_2)_{14}$– chains are inter-twined and have more than a half twist (196.5°), as defined by the two P–Pt–P planes.

6. Gold Complexes

Reactions of $Me_3Si(C{\equiv}C)_mSiMe_3$ ($m = 3$, 4) with $AuCl(PR_3)$ (R = Cy,[315] tol[267]) in the presence of NaOH in methanol give air-stable pale yellow $\{(R_3P)Au\}_2\{\mu\text{-}(C{\equiv}C)_m\}$ (**169**). The C_8 complex was also obtained by oxidative coupling of $Au(C{\equiv}CC{\equiv}CH)\{P(tol)_3\}$.[267] The complexes are unstable in chlorinated solvents, although no C–H···C≡C π-type association is found. In all cases, the carbons of the chain resonated between δ 60 and 130. Extension of these studies to tetra-ethynylethene afforded the unusual branched chain C_{10} derivatives
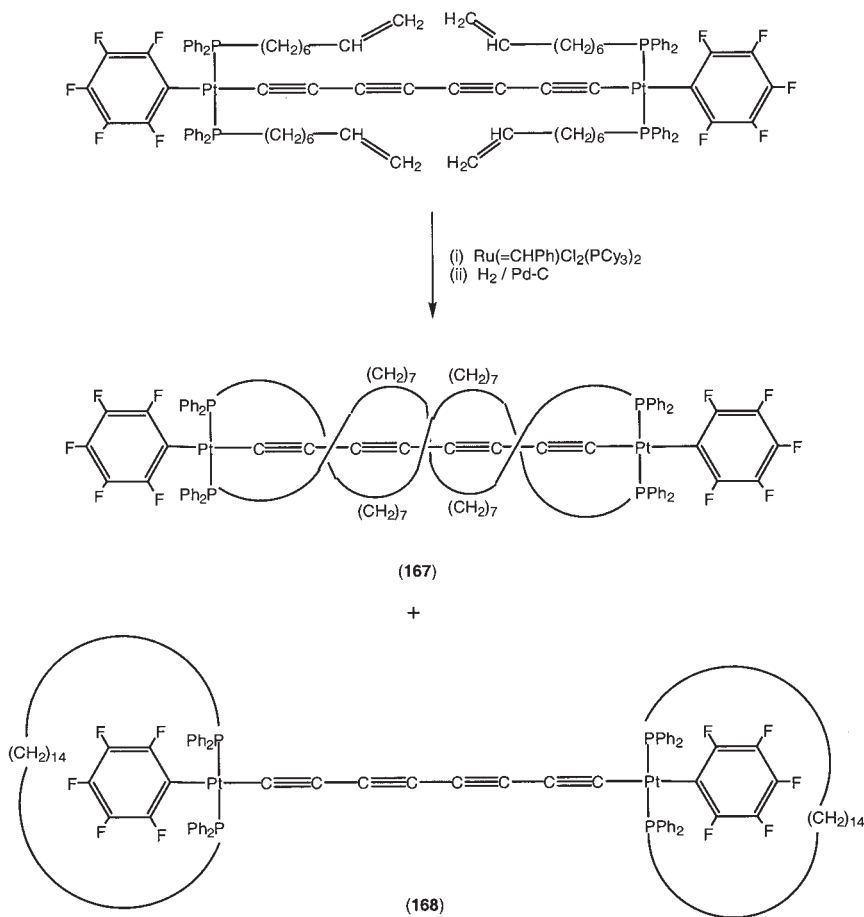
SCHEME 42

{(R$_3$P)AuC≡C}$_2$C=C{C≡C[Au(PR$_3$)]}$_2$ (**170**; R = Cy,[316] Ph[317]). The former shows carbon-centered ^{1}(ππ*) fluorescence at 428 nm.

7. Heterometallic Compounds

(a) W–Cu

The red copper(I) derivative, formulated as {CuC≡CC≡C[W(CO)$_3$Cp]}$_n$, has been obtained serendipitously as a by-product from copper(I)-catalyzed coupling reactions of W(C≡CC≡CH)(CO)$_3$Cp.[317] It is shock-sensitive and attempts to characterize it further have been unsuccessful to date.
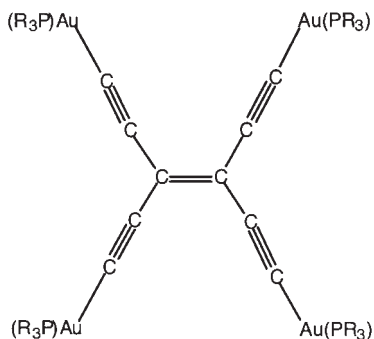
(170) R = Cy, Ph

(b) Re–Cu

Lithiation of poly-ynyl-rhenium complexes $Re\{(C\equiv C)_mH\}(NO)(PPh_3)$ Cp^* ($m = 1, 2, 3$), followed by treatment with CuI, gives incompletely characterized mixed-metal derivatives of composition $\{Cu(C\equiv C)_m[Re(NO)(PPh_3)Cp^*]\}_x$ as red-brown thermally stable powders which are likely oligomeric.[292,304] Alternatively, the $SiMe_3$-alkyne can be converted to the Cu derivative directly by reaction with $Cu(OBu^t)$ and $[NH_4]F$ in one pot.[290] The Cu–C_4 derivative is a useful synthon (see above) en route to C_6 and longer derivatives, subsequent reactions with bromo-alkynes giving the corresponding di-rhenium complexes. Attempts to characterize the copper derivatives by addition of phosphines or other ligands to break the supposed oligomeric linkages were unsuccessful.

G. *Complexes Containing Binuclear End-Caps*

1. Homonuclear

An excess of Li_2C_2 reacts with $Ru_2(\mu\text{-ap})_4Cl$ to give red-purple $\{Ru_2(\mu\text{-ap})_4\}_2(\mu\text{-}C\equiv C)$ (**171/1**; ap = 2-anilinopyridinate) in which mutual strengthening of the Ru–C and weakening of the $C\equiv C$ π bonds is found, and for which CV data indicate that significant electronic communication occurs between the two Ru_2 centers.[318,319] This complex has also been isolated from reactions of the ethynyl under Glaser coupling conditions.

Black $\{Ru_2(C\equiv CC\equiv CSiMe_3)(\mu\text{-dpf})_4\}_2\{\mu\text{-}(C\equiv C)_4\}$ (**172**; dpf $= N,N'$-diphenylformamidinate) is formed by homo-coupling (CuCl/py) of the butadiynyl $Ru_2(C\equiv CC\equiv CH)(C\equiv CC\equiv CSiMe_3)(\mu\text{-dpf})_4$ (**173**).[320] In the solid-state, the C_8 complex has two toluene molecules over the significantly
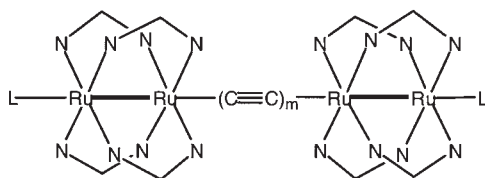
	M	N-N	L
(171)	Ru	ap	-
(172)	Ru	dpf	C≡CC≡SiMe$_3$
(175)	Rh	ap	-
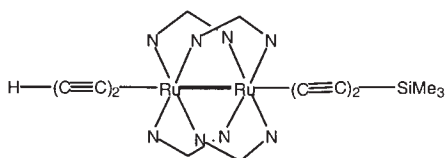
(**173**) N-N = dpf

bent carbon chain, with the Me groups pointing to the chain. It shows two quasi-reversible reduction waves at −1.68 and −0.74 V together with two irreversible oxidations at +0.50 and +0.81 V. Similar coupling of **173** with Ru$_2$(C≡CC≡CH)$_2$(μ-dpf)$_4$ gives **174**, which contains a 32-atom Si–C$_4$–Ru$_2$–C$_8$–Ru$_2$–C$_8$–Ru$_2$–C$_4$–Si chain with a length ca. 45–50 Å.

Glaser-type coupling of terminal alkynes with Ru$_2$(C≡CC≡CH)(ap)$_4$ affords, in addition to the diyne and hetero-coupled products, the homometallic complex {Ru$_2$(μ-ap)$_4$}$_2${μ-(C≡C)$_4$} (**171/4**, M = Ru, LL = ap)[321] or, in better yield, from Ru$_2$Cl(μ-ap)$_4$ and Li$_2$C$_4$.[318] Eglinton/Hay-type coupling of Ru$_2${(C≡C)$_m$H}(μ-ap)$_4$ (m = 1–3) has given {Ru$_2$(μ-ap)$_4$}$_2${μ-(C≡C)$_{2m}$} (**171/2m**).[322] The C$_8$ complex shows complex electrochemical behavior, with separations between redox couples being less than those found in the C$_4$ complex.

The structurally analogous rhodium complex {Rh$_2$(μ-ap)$_4$}$_2$(μ-C≡CC≡C) (**175**, M = Rh, LL = ap) was obtained stepwise from Rh$_2$(μ-ap)$_4$Cl with LiC≡CSiMe$_3$, desilylation with LiBu and further reaction with Rh$_2$(μ-ap)$_4$Cl.[323] However, in this case UV spectroscopy indicates little electronic communication between the two Rh$_2$ centers.

(174) N-N = dpf

(176)
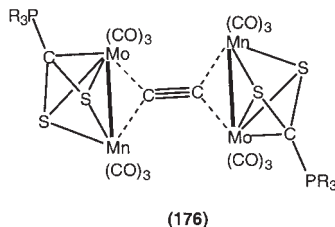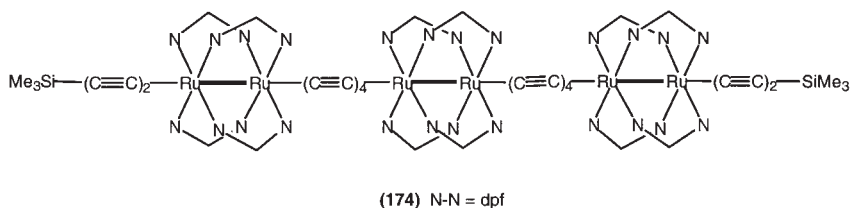
2. Heteronuclear

The reaction of Na_2C_2 with $\{(OC)_3Mo\}(\mu\text{-Br})(\mu\text{-S}_2PCy_3)\{Mn(CO)_3\}$ gives emerald-green $\{[(OC)_3Mo](\mu\text{-S}_2PCy_3)[Mn(CO)_3]\}_2(\mu\!:\!\mu\text{-C}\!\equiv\!C)$ **(176)** in which the four metal atoms are staggered (CMoMn interplanar angle 49.2°).[324] The Mo–C and Mn–C distances support its formulation as a 3-center/2-electron CMoMn system, i.e., as a tetrametallated ethyne.

H. *Polymeric Complexes Containing C_n Chains*

Conjugated polymeric materials containing metal centers in the main chain have been a source of considerable interest due to both the rigid rod-like structure adopted by these materials, which can lead to liquid crystalline phase behavior,[85] and the extended conjugated π-system which can result in large non-linear optical responses.[325–327] While there have been many reports of polymeric materials based upon poly(ethynylated) repeat units $\{ML_n(C\!\equiv\!CRC\!\equiv\!C)\}_n$,[328,329] metallo-carbon main chain polymers are rather more sparsely described. The vibrational spectra of polymeric poly-yndiyl Pt(II) species are consistent with there being considerable $C\!\equiv\!C$ character in the polycarbon fragment, despite the π-conjugation which is evident through the metal centers in vibrational and optical studies.[330] Vibrations in these rod-like materials are strongly coupled to the electronic transitions along the metallo-carbon backbone which results in resonant enhancement of the vibrations parallel to the backbone relative to perpendicular motions. The π-conjugation through these materials is

reduced by insertion of aromatic (phenylene) substructures, which may reflect a combination of the energy differences between the acetylenic and phenylene ring orbitals, as well as the orientation of the ring π-system relative to the π-system associated with the platinum-poly-ynyl chain. However, recent studies have shown that the 2,5-C≡C–C_4H_2S–C≡C– spacer may have an effect on the ground-state interactions between iron centers similar to that of a –C_8– spacer, when measured using a Hush-style method of analysis.[331]

The first reports of poly-yndiyl polymers were made by the Hagihara group in the 1970s. The regular polymer {trans-Pt(PBu$_3$)$_2$C≡CC≡C}$_n$ (177) was prepared by the CuI-mediated condensation of trans-Pt(C≡CC≡CH)$_2$ (PBu$_3$)$_2$ with PtCl$_2$(PBu$_3$)$_2$ in diethylamine.[332] The resulting pale yellow material was isolated and purified by repeated precipitation in methanol and characterized by IR [ν(C≡C) at 1999 cm^{-1}] and ^{31}P NMR spectroscopy [δ −4.2 ppm, J(PPt) 2384 Hz]. A weight-average molecular weight M_w of 119,000–122,000 was determined by sedimentation equilibrium in toluene. Despite the high molecular weight, the polymer was highly soluble in a range of organic solvents, including CH$_2$Cl$_2$, thf, benzene, and refluxing hexane. The analogous Pd polymer 178 (M_w 63,000, $λ_{max}$ 342 nm, log ε 4.32) was prepared in an identical manner.[281,333] The blue shift of the lowest energy UV absorption band (metal-alkynyl charge transfer) in the Pd material relative to the Pt analogue reflects the decreased metal–carbon interactions (see electronic structures below). The Pd-containing material was rather more reactive than its Pt analogue, and the CuI-catalyzed reaction of 178 with PdCl$_2$(PBu$_3$)$_2$ in NHEt$_2$ gave the palladium dimer {PdCl(PBu$_3$)$_2$}$_2$(μ-C≡CC≡C).[281,334]

Mixed ligand polymers have also been reported. For example, room temperature reactions of {PtCl(PBu$_3$)$_2$}$_2$(μ-C≡CC≡C) with 1,4-diethynyl benzene in amine solvents catalyzed by CuI afforded {[Pt(PBu$_3$)$_2$] C≡CC≡C[Pt(PBu$_3$)$_2$]C≡CC$_6$H$_4$C≡C}$_n$ (M_w = 34,000) (179). The related polymer {[Pt(PBu$_3$)$_2$]C≡CC≡C[Pt(PBu$_3$)$_2$]C≡CC≡C[Pt(PBu$_3$)$_2$]C≡CC$_6$H$_4$ C≡C}$_n$ (180) is obtained from trans-Pt(C≡CC≡CH)$_2$(PBu$_3$)$_2$ and trans-Pt(C≡CC$_6$H$_4$C≡CH)$_2$(PBu$_3$)$_2$. At elevated temperatures, CuI-mediated ligand redistribution reactions result in more irregular polymer structures.[282] Palladium analogues containing mixed C$_4$ and Ar (Ar = benzene-1,4-diethynyl, 2,5-Me$_2$- or Et$_2$-benzene-1,4-diethynyl) moieties spaced along the polymer backbone are also known.[333]

Polymers containing alternating Pd and Pt metal centers linked by C≡CC≡C groups in the backbone were obtained by entirely analogous methods from 1:1 reactions of trans-M(C≡CC≡CH)$_2$(PBu$_3$)$_2$ and M′Cl$_2$ (PBu$_3$)$_2$ (181/MM′, M = Pt, M′ = Pd). Oligomeric model complexes trans-M{C≡CC≡C[M′Cl(PBu$_3$)$_2$]}$_2$(PBu$_3$)$_2$ were obtained from reactions
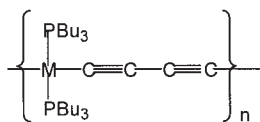
(177) M = Pt
(178) M = Pd
(182) M = Ni
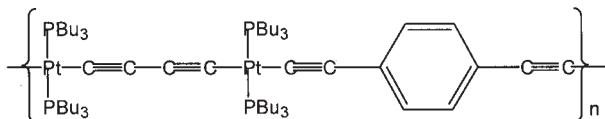
(179)
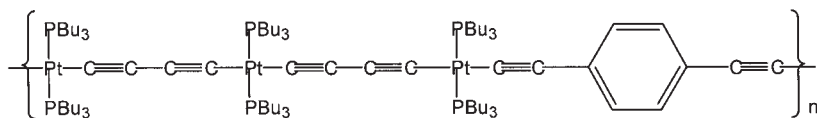
(180)
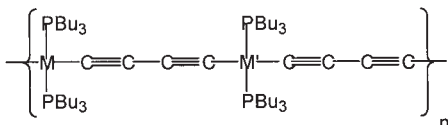
(181) M = Pd, M' = Pt
(183) M = Ni, M' = Pd
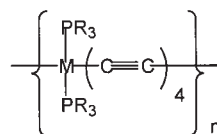
(184)

employing a 1:2 stoichiometry (Section II.D.3).[281] While polymer **181/PtPd** gave a well-resolved UV spectrum and is the more well-defined, the spectrum of **181/PdPt** was considerably broader, suggesting a degree of randomization in the metal arrangement in the main chain. This is possibly induced by CuI-promoted ligand redistribution reactions (scrambling) of the palladium precursor Pd(C≡CC≡CH)$_2$(PBu$_3$)$_2$, with its weaker Pd–C bond, under the reaction conditions. The suggestion of metal disorder in **181/PdPt** was further supported by depolymerization reactions with CuI, from which a series of unspecified oligomers was obtained. Depolymerization of the regular polymer **181/PtPd** afforded Pt{C≡CC≡C[PdCl(PBu$_3$)$_2$]}(PBu$_3$)$_2$ in 75% isolated yield.[281]

Nickel centers have been introduced into these Group 10 poly-yndiyl polymers by reactions of bis(diynyl)metal reagents with Ni(C≡CH)$_2$(PBu$_3$)$_2$.

Loss of gaseous acetylene drives the reactions to completion. In this manner, polymers {$trans$-Ni(PBu$_3$)$_2$(C≡CC≡C)}$_n$ (**182**) (M_w 15,000) and {$trans$-[Ni(PBu$_3$)$_2$]C≡CC≡C[Pt(PBu$_3$)$_2$]C≡CC≡C}$_n$ (**183**) were obtained.[335] The presence of additional PBu$_3$ was found to be beneficial in preventing decomposition of the polymer by phosphine dissociation. Similar syntheses involve copper-catalyzed coupling of nickel dihalides with Ni(C≡CC≡CH)$_2$(PBu$_3$)$_2$.[336]

Oxidative homocoupling of Pd(C≡CC≡CH)$_2$(PBu$_3$)$_2$ under Hay conditions (CuCl/tmeda/O$_2$) afforded the oligomeric tetrayndiyl $trans$-H{C≡CC≡C[Pd(PBu$_3$)$_2$]C≡CC≡C}$_n$H (**184**/**Pd**) (n ca. 9.5) in 75% yield. In the IR spectrum ν(C≡C) bands were observed at 2200, 2160, 2100, and 1980 cm^{-1}, while the UV spectrum was characterized by a single absorption band (λ_{max} 378 nm, ε 520,000).[337] The corresponding Pt polymer (**184**/**Pt**) was rather insoluble, precipitating from the reaction solvent as a rather low molecular weight material (M_w < 20,000). The lowest molecular weight fractions of this polymer, which were soluble in CH$_2$Cl$_2$, gave two ^{31}P resonances which were assigned to the phosphines coordinated to the external (δ −4.94 ppm) and internal (δ −5.16 ppm) metal centers. The IR spectrum contained ν(C≡C) bands at 2135 and 2005 cm^{-1}. The polymer **184**/**Pt** was cleanly depolymerized by CuI in piperidine to afford the tetrayndiyl complex {PtCl(PBu$_3$)$_2$}$_2${μ-(C≡C)$_4$} in 80% yield, which provides indirect evidence for the regularity of the polymer.[338]

Reactions of the bis(trimethylstannyl)poly-ynes Me$_3$Sn(C≡C)$_m$SnMe$_3$ (m = 2, 3) with PtCl$_2$(EBu$_3$)$_2$ (E = P, As), sometimes in the presence of catalytic CuI, affords high molecular weight polymers {Pt(EBu)$_2$(C≡C)$_m$}$_n$ (E = P, M_w = 130,000–210,000) in ≥ 90% isolated yields.[339,340] The polymers were purified by a column chromatography and repeated precipitation from methanol. The IR spectra of these materials were characterized by strong ν(C≡C) bands at 1999 cm^{-1} (m = 2) or 2096 cm^{-1} (m = 3).

Optical absorption and photoluminescence (PL) spectra reveal a series of features assigned to π → π* transitions involving the poly(yndiyl) portion of the main chain. The triyndiyl polymers give rise to the lowest energy absorption bands, indicative of a lower band gap in these materials. The absorption spectra are particularly well-resolved as a consequence of coupling of the ground-to-excited state transition with transitions to the various vibrational levels of the excited state. Interestingly, the main peak in the PL spectrum of each material was found to be long-lived (μs), indicating that it arises from a forbidden transition likely involving a triplet state. It was noted by Friend and colleagues that the large spin–orbit coupling associated with heavy transition metals could facilitate singlet–triplet conversion and as a result differentiate metallo-polymers

from the simple hydrocarbon species.[340] This later point has been a source of a considerable body of attention. Since emission from triplet states is spin forbidden, triplet states can usually only be probed by a number of indirect methods. An understanding of the effects of electron spin on the electronic interactions in conjugated polymers is necessary to underpin the technological development of optoelectronic devices which might employ these materials. By using heavy metal centers in the main chain of the conjugated polymer, radiative transitions between singlet and triplet states become possible, allowing triplet states to be studied directly.[341–343]

The black polymeric material which is deposited from methanolic solutions of $\{Co_2(CO)_6\}_2(\mu-\eta^2:\eta^2-Me_3SiC_2C_2SiMe_3)$ gave microanalytical data consistent with the formation of a polyacetylene, or arguably a fragment of the linear carbon allotrope carbyne, with each, or most, triple bonds coordinated to a $Co_2(CO)_6$ fragment $\{Co_2(\mu-C_2)(CO)_6\}_n$ (n ca. 30). However, related poly-yne complexes have been shown to accommodate only two adjacent $C_2Co_2(CO)_6$ units, which are separated from the next pair by an uncoordinated $C\equiv C$ triple bond. The nature of the end-capping groups was not discussed, but is probably $SiMe_3$ or H.[344] Theoretical analysis of the structure using Hückel methods revealed a degree of residual conjugation along the carbyne-like backbone. However, the band structure of the ideal polymer shows the valence and conduction bands to be separated by a large band-gap and predominantly metal-centered, and the polymer is thought to be of little use as a conductive material.[345]

Liquid crystal polymers (LCPs) have been a source of considerable interest for some time, as they have been shown to offer particular advantages in terms of their processability and physical properties which make them attractive in a wide range of engineering applications.[346] Serrano and his colleagues have reviewed metallomesogenic polymers, including the liquid crystalline properties of several of the platinum poly-yndiyl polymers described above.[85,86]

The second and third order non-linear optical (NLO) properties of metal-containing systems, including polymeric materials, have been comprehensively reviewed.[347–349] For the Hagihara-type polymeric materials $\{M(PBu_3)_n(C\equiv CC\equiv C)\}_n$ (M = Ni, Pt) the third order NLO responses were measured using degenerate four-wave mixing (DFWM) methods, with the observed hyperpolarizablility decreasing from Ni (CHCl$_3$, λ 410 nm, $|\gamma|$ 3.57×10^{-42} m^5 V^{-2}) to Pt (CHCl$_3$, λ 364 nm, $|\gamma|$ 2.28×10^{-42} m^5 V^{-2}).[336,350–352] However, direct comparisons should be made with caution as the polymer length and average molecular weight vary with the metal.

III

COMPLEXES CONTAINING CYCLIC C_n LIGANDS

Included in this Section are the few complexes which contain per-metallated C_n rings, often π-bonded to another metal center.

A. C_3

Reactions of $Na[Fe(CO)_2Cp]$ with $[C_3Cl_3]SbF_6$ afford a reasonable yield of dark amber $[\{Fe(CO)_2Cp\}_3C_3]SbF_6$ (185) in which the three iron residues are σ-bonded to the three-membered ring.[353,354] The chloride salt is obtained from the anion and C_3Cl_4. The three Cp rings are disposed two above, the third below, the C_3 ring plane; the ring itself is nearly equilateral. The Fe–C bonds [av. 1.916(7) Å] are similar in length to Fe–C(sp) bonds, the NMR spectra indicating free rotation about the Fe–C bonds. The C_3 carbons resonate at δ_C 256.6.

Approaches to complexes containing neutral cyclo[3]carbon (cyclopropenylidene) by reaction of Fp^- with $M(CO)_5\{=C_3(OEt)_2\}$ (M = Cr, Mo, W) afforded the σ-bonded derivatives $M(CO)_5\{=C_3(OEt)[Fe(CO)_2Cp]\}$ (186).[355] Structural data suggest that the zwitterionic formulation is important. Replacement of the OEt group with a third ML_n fragment was unsuccessful, although $NHMe_2$ reacted with 186/Cr to give $Cr(CO)_5\{=C_3(NMe_2)[Fe(CO)_2Cp]\}$.

(185)

(186) M = Cr, Mo, W
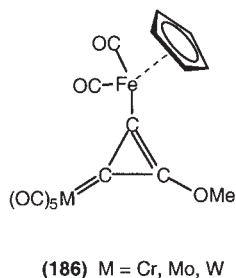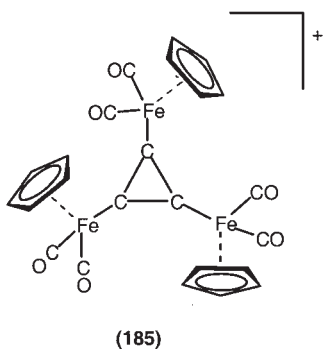
Analogous complexes with $M(CO)_3Cp$ (M = Mo, W), $Re(CO)_5$, and $Ru(CO)_2Cp$ substituents, prepared by similar routes, are also known. The rhenium complex is unstable, but gives a resonance at δ_C 237.8 for the C_3 ring carbons.

LCAO density functional calculations on the iron complex show that the most important bonding interactions correspond to σ and π bonding in the C_3 ring plane, together with those of iron d_π orbitals with the C_3 π system.[356] The latter is the smaller one, although $M \rightarrow C_3^+$ back-bonding is not negligible. Half of the positive charge is delocalized onto the CO and Cp ligands. Calculations on $[\{Fe(CO)_2Cp\}C_3H_2]^+$ indicate that both extreme orientations of the iron group are almost isoenergetic, consistent with the free rotation found by NMR; the observed orientations in the crystal are determined by crystal packing effects.

B. C_4

Facile mercuration of $Fe(CO)_3(\eta\text{-}C_4H_4)$ occurs with $Hg(OAc)_2$ in acetic acid (30 min, r.t.) to give an equilibrium mixture of all possible products, including $Fe(CO)_3\{\eta\text{-}C_4(HgOAc)_4\}$, which were characterized by iodination (KI_3).[357] In acetic acid, disproportionation occurs, even with the tetra-substituted product. This system has a reactivity similar to that of ferrocene.

C. C_5

Per-mercuration of $Mn(CO)_3Cp$ with $Hg(O_2CCF_3)_2$ in CH_2Cl_2 or Et_2O at r.t. to give a yellow, poorly soluble $Mn(CO)_3\{\eta\text{-}C_5[Hg(O_2CCF_3)]_5\}$ was first reported in 1983.[358] This compound is the likely intermediate in the formation of $Mn(CO)_3(\eta\text{-}C_5I_5)$ by treatment of $Mn(CO)_3Cp$ with $Hg(O_2CCF_3)_2$ followed by NaI_3.[359] Per-mercuration of $M(CO)_3Cp$ (M = Mn, Re) occurred with $Hg(OAc)_2$ (1,2-dichloroethane, reflux, 4 h) to give pale yellow $M(CO)_3\{\eta\text{-}C_5(HgOAc)_5\}$ (Mn 73, Re 90%).[360] NMR studies indicate that rotation of the OAc groups is fast. Mercury–halogen exchange occurred between the manganese complex and CuCl or CuBr in acetone, or with aqueous KI. The rhenium complex decomposed under similar conditions.

Deca-mercuration of ferrocene with $Hg(O_2CCF_3)_2$ in $EtOH/Et_2O$ (r.t.) was first described in 1977;[361] similar reactions with FcR (R = Me, Et, CN, CHO, Ac) gave $Fe\{\eta\text{-}C_5R(HgOAc)_4\}\{C_5(HgOAc)_5\}$.[362] A later improved study, in which the reaction is carried out with added HgO to remove CF_3CO_2H, gave yellow-orange $Fe\{\eta\text{-}C_5(HgO_2CCF_3)_5\}_2$ (60%). Low solubility precluded obtaining ^{13}C and ^{199}Hg NMR spectra.[363] Halogenation $(CuCl_2, KBr_3, KI_3)$ gave mixtures of partly halogenated ferrocenes. Treatment of ferrocene with $Hg(OAc)_2$ in refluxing 1,2-dichloroethane gave yellow $Fe\{\eta\text{-}C_5(HgOAc)_5\}_2$ (95%), which could be satisfactorily per-halogenated.

Per-mercuration of ruthenocene to give off-white $Ru\{\eta\text{-}C_5(HgOAc)_5\}_2$ occurs nearly quantitatively with $Hg(OAc)_2$ in refluxing 1,2-dichloroethane (88%).[364] Similar reactions with RuCpCp* occur in EtOH/Et$_2$O at r.t. to give $RuCp*\{\eta\text{-}C_5(HgOAc)_5\}$.[365] The rate of the first mercuration is slower than subsequent steps. The ^{1}H NMR spectrum shows that rotation of the OAc groups occurs rapidly at $60\,^{\circ}$C, but is frozen out at $-80\,^{\circ}$C (O or Me pointing up from ring plane). Halogenation with CuCl$_2$ or KX$_3$ in water (X = Br, I) gives $Ru(\eta\text{-}C_5X_5)_2$ (X = Cl, Br, I) (39–73%) or $RuCp*(\eta\text{-}C_5X_5)$ (35–67%).

D. C_9

The brown raft-like complex $[\{Fe(CO)_2Cp\}_3\{\mu_3C_3(C\equiv C)_3\}]SbF_6$ (**187**) is formed from the reaction of $[C_3Cl_3]SbF_6$ and $Fe(C\equiv CSiMe_3)(CO))_2Cp$.[354]

(187)
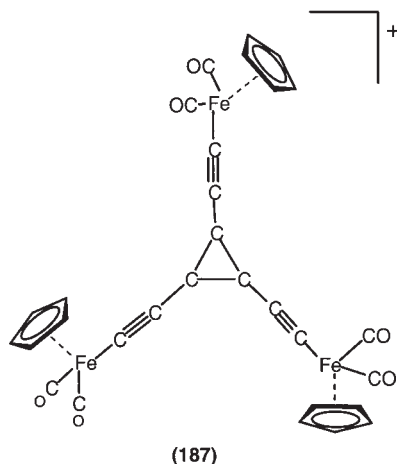
E. C_{18}, C_{24}

The larger all-carbon molecules, C_n ($n = 10$–24), are predicted to have mono-cyclic structures (cyclo[n]carbons), molecules with $n = 14$, 18, 22, being expected to be aromatic, with closed $4n + 2$ electron shells.[1,25,26,32] The smallest cyclocarbon for which a reasonable stability is predicted is cyclo[18]carbon, C_{18}.[366–368] Both in-plane and out-of-plane π systems are aromatic. In contrast, the larger molecules ($n = 30$–40), are very reactive, while more stable polycyclic structures predominate for higher values of n, culminating in fullerene structures for $n \geq 60$.

Several approaches to the synthesis of C_{18} and other cyclo[n]carbons have been made, including fragmentation of propellane- or anthraceno-annulated dehydroannulenes with loss of indane or anthracene, respectively, using flash vacuum pyrolysis (FVP).[369–371] Fragmentation of higher carbon oxides ($C_{4n}O_n$, $n=6, 8, 10$) under laser desorption with loss of CO has also been studied[372,373] and other routes have been explored.[374,375]

The total strain energy of a free cyclo[n]carbon ($n=18, 24, 30$; alternating C–C single and C≡C triple bonds) is calculated at 76 kcal mol^{-1}, which agrees with the sum of distortion of acetylenic or allenic angles from 180° to 160° (ca. 4 kcal mol^{-1}). The well-known bending of acetylenic bonds that occurs after complexation to a metal center (between 136 and 145°) was used to design a synthesis of cyclo[n]carbons ($n=18, 24$) as their $Co_2(CO)_6$ complexes, in which the ring would be relatively free of strain.[371,376] The more stable $Co_2(\mu\text{-dppm})(CO)_4$ adduct of $Pr^i_3Si(C\equiv C)_3SiPr^i_3$ was proto desilylated ([NBu$_4$]F in moist thf) and oxidatively coupled [Cu(OAc)$_2$/pyridine, 55 °C] to give the tri- and tetra-mers in 33 and 5.4% yields, respectively, containing cyclo[18]carbon (**188**) and cyclo[24]carbon. The X-ray structure of the former confirmed bending at the complexed C_2 units between 131 and 134°. The UV–vis spectra contain bands at 370 and 380 nm, respectively, indicating that partial macrocyclic conjugation exists. The cyclocarbons have not been successfully released from the complexes (for example, using Ce(IV), 4-methylmorpholine-N-oxide, or I$_2$), probably because of the greater stability of the dppm-substituted complexes compared to the analogous $Co_2(CO)_6$ adducts, or because of the inherent instability of the cyclo[n]carbons.

(188)
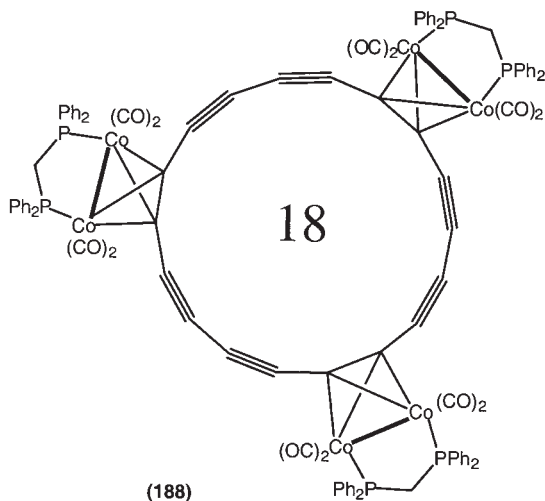
IV

SPECTROSCOPIC PROPERTIES, MOLECULAR STRUCTURES, ELECTROCHEMISTRY, AND ELECTRONIC STRUCTURES OF $\{ML_x\}_2(\mu\text{-}C_n)$ COMPLEXES

A. *Spectroscopic Properties*

Of the various techniques routinely available, IR and ^{13}C NMR spectroscopy usually provide the most valuable information in terms of the determination of the most appropriate valence description (**A–D**, Chart 1) of the carbon fragment. Mössbauer spectroscopy has also been used with good effect with iron-containing poly-carbon complexes.[89] This solution-based work is complemented by a significant number of solid-state structural studies, which are described in greater detail below. Electronic spectroscopic methods, including luminescence methods, have been used to probe the electronic structures of a small number of poly-yndiyl complexes and polymers.[288,315,340–342,377–380] Selected IR, ^{13}C NMR, and UV–vis data have been given in Tables I–VIII, above.

1. Vibrational Spectroscopy

(a) $\nu(CC)$ bands

The great majority of C_2 complexes are of type **A**, being well described as dimetallated acetylenes. As such, the IR or Raman spectra of these compounds very often contain a band between 1900 and 2050 cm^{-1}, which can be confidently assigned to the $\nu(C\equiv C)$ mode. In light of the selection rules, symmetrical complexes $\{ML_x\}_2(\mu\text{-}C_2)$ rarely give IR-active $\nu(C\equiv C)$ bands, and in these cases Raman spectroscopy is more useful. In the case of $[Li(thf)_4]_2[\{Ti(oepg)(\mu\text{-}Li)\}_2(\mu\text{-}C_2)]$, for which the structural data are consistent with a Ti=C=C=Ti formulation, the $\nu(C=C)$ band was not IR active.[152] The Raman spectrum of $\{Ta(silox)_3\}_2(\mu\text{-}C=C)$ has been measured, and $\nu(C=C)$ is found at 1617 cm^{-1}, also consistent with the cumulenic structure **B**.[159,160] The asymmetry inherent in heterometallic examples gives rise to a greater proportion of complexes which show IR-active $\nu(CC)$ bands. While the $\nu(C\equiv C)$ frequencies associated with these heterometallic complexes are for the most part similar to those of homometallic derivatives, it is interesting to note that the complex $\{ZrClCp_2\}(\mu\text{-}C\equiv C)\{Cp(PMe_3)_2Ru\}$ in which the $C\equiv C$ system spans electron-rich and electron-poor metal fragment, gives rise to an unusually low energy, high intensity $\nu(C\equiv C)$ band at 1868 cm^{-1}.[217]

The $\nu(C{\equiv}C)$ bands were not observed for any of the Group 6 C_3 complexes with $M{\equiv}C{-}C{\equiv}CM'$ valence structures.[227] However, the presence of characteristic strong $\nu(C{=}C{=}C)$ bands between 1870 and 1900 cm^{-1} in the IR spectra of the C_3 complexes [{Cp*(NO)(PPh$_3$)Re}(μ-C$_3$){ML$_x$}]$^{n+}$ [$n=1$, ML$_x$ = Mn(CO)$_2$Cp', Cp' = Cp, η^5-C$_5$H$_4$Cl, η^5-C$_5$Cl$_5$; $n=0$, ML$_x$ = Fe(CO)$_4$] strongly supports the description of these materials in terms of cumulenic $M{=}C{=}C{=}C{=}M'$ structures.[229]

Poly-yndiyl structures (**L**) dominate the C_4 and higher sub-groups, and it is useful to compare the properties of these species with those of their organic analogues. In organic poly-ynes, broad $\nu(C{\equiv}C)$ absorptions are found, the wavelengths being essentially independent of the end-group. The number of bands increases with chain length, and if silyl groups are present sharper bands are found. In general, the $\nu(C{\equiv}C)$ stretches of the metal complexes {ML$_x$}$_2${μ-(C$\equiv$C)$_m$} are found between 1900 and 2200 cm^{-1}. The number of IR-active $\nu(C{\equiv}C)$ bands increases with increasing number of C≡C moieties and the new $\nu(C{\equiv}C)$ bands are generally found at higher frequencies. Of course, symmetrical dimetal complexes show only half the number of $\nu(C{\equiv}C)$ bands. For example, while the IR spectrum of {Re(NO)(PPh$_3$)Cp*}$_2$(μ-C≡CC≡C) contains a single $\nu(C{\equiv}C)$ band at 1968 cm^{-1} (KBr), the decayndiyl complex {Re(NO)(PPh$_3$)Cp*}$_2${μ-(C$\equiv$C)$_{10}$} exhibits five $\nu(C{\equiv}C)$ bands between 2164 and 1962 cm^{-1},[250,290] while for Pt compounds **165/4**, **6**, **8**, two, three, and four $\nu(CC)$ bands were found for $m=4$, 6, and 8, respectively.[311] Similar multiplicities are found for Fe and Ru, but not Mo or W, based series.

In a limited number of cases, Raman spectroscopy has been employed, and while the amount of data available is greatly reduced, the range of frequencies observed is comparable with those found in the IR spectra.[224,249,290]

(b) Other bands

With Re(NO)(PPh$_3$)Cp* end-groups, $\nu(NO)$ frequencies increase from 1627–1637 ($m=1$) to a limiting value of ca. 1660–1662 cm^{-1} (for $m=$ 5–6),[250,290] and similar trends in the $\nu(CO)$ frequencies are also observed in the series Fp*(C≡C)$_m$Fp*.[306] While this trend was initially thought to be due to the increased electron-withdrawing power of the poly-yne with increasing chain length, and progressive reduction in back-bonding, more recent computational results suggest that these trends are more likely due to a decrease in the electron-donating properties of the longer chain ligands.

For complexes containing cumulenic ligands (**M**), such as [{Ru(PPh$_3$)$_2$Cp}$_2$(μ-C=C=C=C)]$^{2+}$, the IR-active $\nu(C{=}C)$ band is observed near 1750 cm^{-1}.[262] While the $\nu(C{=}C)$ band in [{Re(NO)(PPh$_3$)Cp*}$_2$ (μ-C=C=C=C)]$^{2+}$ was not observed, a strong Raman band at 1883 cm^{-1}

was found and attributed to the carbon fragment.[249] The infra-red spectra of the ethynyl-bridged dicarbyne complexes $\{M(CO)_2Tp'\}_2\{\mu\text{-}(\equiv CC\equiv CC\equiv)\}$ (**N**) were dominated by the $\nu(CO)$ bands, and do not provide clear evidence for the valence structure of the carbon chain.[245]

There are few examples of complexes in which a linear chain containing an odd number of carbons C_n ($n \geq 5$) spans two metal centers. In the case of $[\{Cp^*(NO)(PPh_3)Re\}(\mu\text{-}C_5)\{Mn(CO)_5(\eta^5\text{-}C_5Cl_5)\}]^+$ a single, strong $\nu(CC)$ band was observed at ca. 1950 cm^{-1} and assigned to the cumulenic $C{=}C{=}C{=}C{=}C$ moiety.[229]

2. ^{13}C NMR Spectroscopy

As with the vibrational spectroscopic techniques, the ^{13}C NMR spectra of poly-yndiyl and cumulated carbon ligands are distinct, providing a complementary technique for use in the assignment of formal valence structure. In organic poly-ynes, the resonances of the two carbons out from the end-group appear down-field from the remainder, which are concentrated between δ 62 and 67.[302] For the most part, ^{13}C chemical shifts associated with C_n complexes follow the trends established for these organic analogues and the appropriate metal ynyl or metallacumulene mono-metallic complexes.[36,381] While there is great variation in the ^{13}C NMR parameters associated with poly-yndiyl complexes, due at least in part to the difficulty in unambiguously assigning these spectra, in general ^{13}C resonances near 100–120 ppm and 80–100 ppm can be assigned to the M–C$\equiv$C and M–C$\equiv C$ carbons, respectively. Internal carbons give resonances which asymptotically approach 60 ppm with increasing chain length.

The cumulenic carbon atoms in complexes of type **M** give rise to resonances M$=$C$=$C (200–300 ppm) and M$=$C$=C$ (150–250 ppm).[227,229,245,249] As the length of the carbon chain increases, the internal $=C=C=$ resonances tend towards 100 ppm, although data are scarce. For example, the ^{13}C NMR signals for the C_3 chain in $[\{Re(NO)(PPh_3)Cp^*\}CCC\{Mn(CO)_2(\eta\text{-}C_5Cl_5)\}][BF_4]$ are found at δ 287.8 (MnC), 221.1 [J(CP) 11, ReC] and 168.9 (CCC) while for $[\{Re(NO)(PPh_3)Cp^*\}CCCCC\{Mn(CO)_2(\eta\text{-}C_5Cl_5)\}][BF_4]$ (**150**) the C_5 resonances are at δ 218.4 [J(CP) 12.5, ReC], 296.2 (MnC), and at 119.1, 110.6, and 107.0 ($CCCCC$).[229]

The acetylene-bridged dicarbyne form **N** shows both low-field M$\equiv$C signals (ca. δ 350 ppm) and higher field acetylenic resonances for the $C\equiv C$ nuclei near δ 80–100 ppm.[166,227,245]

Definitive assignment of the ^{13}C resonances has been possible only in few cases where ^{13}C labeling studies have been carried out[249] or when additional information is provided by coupling to other spin-active nuclei associated with the supporting metal–ligand fragments. In this respect, J(CP) values

have been most widely exploited, but coupling to metal nuclei such as ^{183}W has also been reported and used in the assignment of ^{13}C NMR data. The data collected in Tables I–VIII are based upon the assignments given in the original literature, although there are now sufficient data reported to indicate several inconsistencies within closely related compounds.

3. UV–Vis Spectroscopy and Luminescent Properties

The UV–vis absorptions of organic poly-ynes occur in two distinct regions, one at higher wavelength showing little dependency on chain length, whereas that at lower wavelength shows markedly increased extinction coefficients as n increases and a limit of $\lambda = 569$ nm has been estimated for $R(C\equiv C)_{\infty}R$. Bands in this latter region dominate the spectral profile, with ε values approaching 6×10^5 M^{-1} cm^{-1}.[302] Absorptions in both regions are assigned to $\pi \rightarrow \pi^*$ transitions.

The UV–vis spectra of bimetallic complexes containing linear C_n ligands contain transitions which have been assigned to $\pi \rightarrow \pi^*$ transitions associated with the $(C\equiv C)_m$ fragment and also to MLCT processes, which could be approximated by n (or d) $\rightarrow \pi^*$ transitions. Rich UV–vis spectra are found for $\{W(OBu^t)_3\}_2(\mu\text{-}C_2)$ and closely related complexes. While definitive assignments of most of these transitions were not possible, the lowest energy (430 nm) was attributed to the singlet HOMO $\rightarrow$ LUMO transition. In the excited state, π conjugation along the chain occurs.[170] The lowest energy band in the UV–vis spectrum of $\{Re(CO)_5\}_2(\mu\text{-}C\equiv C)$ (319 nm) was assigned to the $\pi(C\equiv C) \rightarrow \pi^*(CO)$ transition.[171]

In complexes $\{ML_x\}_2\{\mu\text{-}(C\equiv C)_m\}$ containing longer poly-ynyl ligands, absorption bands assigned to n (or d) $\rightarrow \pi^*$ transitions shift to lower energy and become more intense with increasing chain length[251,290,310,311,315] in a manner similar to that associated with organic poly-ynes.[21,302] Extinction coefficients for the allowed $\pi \rightarrow \pi^*$ bands are typically greater than for the forbidden n $\rightarrow \pi^*$ (MLCT) bands, and the $\pi \rightarrow \pi^*$ transition associated with, for example, $\{Pt(C_6F_5)(PEt_3)_2\}_2\{\mu\text{-}(C\equiv C)_8\}$ is $> 600,000$ M cm^{-1}. For the series of complexes $\{Re(NO)(PPh_3)Cp^*\}_2\{\mu\text{-}(C\equiv C)_m\}$ there appears to be a correlation between $1/m$ and band energy, which permits an estimate of 565 nm ($\pi \rightarrow \pi^*$) and 1082 nm (n $\rightarrow \pi^*$) as the respective limiting values for compounds of infinite chain length.[290]

The heterometallic complexes $\{Cp^*(PPh_3)(NO)Re\}(\mu\text{-}C\equiv C)\{trans\text{-}PdCl(PEt_3)_2\}$ and $trans\text{-}Pd\{C\equiv CC\equiv C[Re(NO)(PPh_3)Cp^*]\}_2(PEt_3)_2$ give rise to similar UV–vis spectra, featuring three shoulders on the intense PPh$_3$ centered absorption at 234 nm, indicating similar underlying electronic structures.[224]

The UV–vis spectrum of $\{Re(CO)_3(Bu_2^t$-bpy)$\}_2(\mu$-C≡CC≡C) contains a solvent-dependent low energy absorption which appears between 430 and 495 nm (450 nm in acetone).[253] Excitation at λ 350–400 nm gives long-lived (μs at 77 K, shorter at 298 K) orange-red emissions at ca. 660–690 nm which are not solvent-dependent, originating from a ^{3}MLCT $d_\pi(Re) \rightarrow \pi^*$(bpy) transition. Excitation at $\lambda > 350$ nm gives emission at 750 nm, likely from ^{3}MLCT $d_\pi(Re) \rightarrow \pi^*(C_4Re)$ or ^{3}LLCT $\pi(C_4Re) \rightarrow \pi^*$(bpy) transitions.

Gold complexes of general form $\{Au(PR_3)\}_2\{\mu$-(C≡C)$_m\}$ give rise to absorption spectra which display vibronic structure and luminescent properties which assist in making assignments. Electronic absorption spectra of complexes with $PPh_{3-n}(nap)_n$ ($n = 1$–3) have an intense band at ca. 296 nm, assigned to promotion of an electron from the phosphorus lone pair (now σ) to a naphthyl π^* orbital, i.e., $\sigma \rightarrow \pi^*$(nap). Excitation with $\lambda > 330$ nm results in long-lived emissions, which are reduced in the $PPhFc_2$ complex. For the $PPh(nap)_2$ derivative, multiple emission is found, dependent upon the exciting wavelength: for $\lambda = 350$ nm, a $\sigma \rightarrow \pi^*$ transition is involved, while for $\lambda = 380$ nm, the emission originates in a $\pi \rightarrow \pi^*$ transition.[209]

Photo-excitation of $\{Au[P(C_6H_4OMe-4)_3]\}_2(\mu$-C≡C) at 320 nm results in emission between 400 and 600 nm which has vibronic structure [spacing 2100 cm^{-1}, ν(C≡C)], arising from the $^3(\pi \rightarrow \pi^*)$ excited state of C_2^{2-}.[380] The absorption, excitation and emissive properties of $\{AuPCy_3\}_2\{\mu$-(C≡C)$_n\}$ ($n = 1$–4) have been investigated in some detail as the heavy atom permits sufficient spin–orbit coupling to allow observation of the lowest energy $^3(\pi \rightarrow \pi^*)$ state in both the absorption and emission spectra for the more soluble complexes $n = 1$, 2. For the C_2 complex, [5d(Au)] $\rightarrow$ [6p(Au), π^*(phosphine)] (singlet–triplet parentage) are at 270, 283 nm, while [5d(Au) $\rightarrow$ [6p(Au), π^*(phosphine)] (singlet–singlet) are more intense, at 239, 256 nm.[288,315] This is interpreted in terms of the C_2 ligand acting as a π-acceptor, with $\pi^*(C_2^{2-})$ higher in energy than $p_{x,y}$(Au). There is a near-UV emission which has a ca. 2000 cm^{-1} vibronic progression, assigned to $^3(\pi \rightarrow \pi^*)$ transitions. In the excitation spectra, similar bands with a ca. 1700 cm^{-1} progression are assigned to ν(C≡C) in the $^3(\pi \rightarrow \pi^*)$ excited state. Other broad emissions in the solid-state are tentatively assigned to exciplex formation involving strong hydrogen bonds between the excited C_2 fragment and solvent H atoms. Similar observations are made for the longer chain complexes, although solubility problems prevented the observation of the weak, forbidden acetylenic $^3(\pi \rightarrow \pi^*)$ band in the absorption spectra. While the acetylenic $^1(\pi \rightarrow \pi^*)$ transitions in $\{AuPCy_3\}_2\{\mu$-(C≡C)$_m\}$ ($m = 1$–3) are buried beneath the [5d(Au)] $\rightarrow$ [6p(Au), π^*(phosphine)] transitions, in the $m = 4$ complex a vibronic absorption at 274–290 nm (vibrational progression 2010 cm^{-1}) is assigned to the

dipole-allowed $\pi \to \pi^*$ transition of the tetrayndiyl bridge.[315] Both the triyndiyl and tetrayndiyl complexes are emissive and vibronically structured (2120 cm^{-1} progression) λ_{0-0} emissions are observed at 498 and 575 nm, respectively, arising from the $^3(\pi \to \pi^*)$ excited state. Linear regression analysis indicates that the energy of the 0–0 transition decreases with increasing conjugation length, and a limiting λ_{0-0} value (corresponding to the $n = 8$ complex) for the acetylenic $^3(\pi \to \pi^*)$ emission is estimated to be 910 nm.[315]

The UV–vis spectra of the odd-carbon chain compounds [{Cp*(PPh$_3$)(NO)Re}(μ-C$_n$){ML$_x$}]BF$_4$ [$n = 3$,   ML$_x$ = Mn(CO)$_2$Cp,   Mn(CO)$_2$(η^5-C$_5$H$_4$Cl),   Mn(CO)$_2$(η^5-C$_5$Cl$_5$),   Fe(CO)$_4$; $n = 5$,   ML$_x$ = Mn(CO)$_2$(η^5-C$_5$Cl$_5$)] are dominated by intense bands near the visible region which have no counterpart in the corresponding mono-metallic model complexes, with weaker bands trailing into the visible. The ReC$_3$Mn complexes show a progressive red shift of the most intense band (392, 396, 414 nm), with the lower energy transitions appearing to follow the same trend, as the number of chlorine atoms on the Cp ring is increased. The longest wavelength bands ($\geq$ 376 and 562 nm) in the UV–vis spectrum of {Re(NO)(PPh$_3$)Cp*}{μ-C≡CC≡CC(OMe)=}{Mn(CO)$_2$(η-C$_5$Cl$_5$)} are substantially red-shifted from the comparable absorption bands in the C$_3$(OMe)-bridged analogue, and the most intense band in the C$_5$ analogue (λ 480 nm) was found to be virtually independent of solvent. These trends suggest that charge transfer from a rhenium- (or ReC$_n$)-based orbital to an orbital with appreciable Mn or MnC$_n$ π^* character, i.e., involving orbitals with appreciable ReC$_x$ π or C$_x$Mn π^* character rather than being purely metal-based transitions.[229]

B. *Structural Studies*

Examples of metal complexes containing linear carbon ligands have been characterized for metals from across the transition series (Tables IX, X, and XI) and the structural forms **A**–**D** can generally be differentiated on the basis of an examination of the structural parameters. However, the variable precision of the structure determinations, the different size of the various metals and variations in the electrostatic contribution to the M–C bond with metal oxidation state and the nature of the other supporting ligands (e.g., phosphine vs. carbonyl) make detailed comparisons of the molecular parameters within a structural subset somewhat arbitrary.

Structural parameters associated with M–C$_2$–M complexes are summarized in Table IX. For the majority of complexes, the C–C bond length falls within the range 1.13–1.25 Å, and these compounds are considered to be of type **A**. Such classifications based upon bond lengths are also supported by the IR and ^{13}C NMR data. Fewer C$_2$ complexes of type **B** and **C** have been

TABLE IX

Bond Lengths (Å) and Angles at C(n) in C$_2$ Complexes

ML$_x$	Bond lengths		Ref.
	M–C(1)	C(1)–C(2)	
	Bond angles at		
	C(1)	*C(2)*	
(a) Homo-binuclear C$_2$ complexes {ML$_x$}$_2$(μ-C$_2$)			
Group 3			
ScCp$_2^*$	2.194(7)	1.224(9)	147
	175.1(6)		
Sm(thf)Cp$_2^*$	2.438(7), 2.448(8)	1.213(10)	148
	173.3(6)	*176.3(6)*	
Pr(oepg)(μ-Na)$_2$	2.670(4)	1.250(8)	149
	180.0		
Nd(oepg)(μ-Na)$_2$	2.790(7)	1.490(17)	149
	84.8(6)		
Group 4			
Ti(PMe$_3$)Cp$_2$	2.051(2)	1.253(2)	151
	177.1(1)		
[Ti(oepg)(μ-Li)]$^-$	1.809(9), 1.757(7)	1.301(11)	152
	178.7(9)	*178.7(8)*	
Zr(NHBu^t)Cp$_2$	2.240(3)	1.226(7)	156
	173.8		
Zr{C(SiMe$_3$)=CH	2.258(6)	1.212(12)	401
(SiMe$_3$)}Cp$_2^*$	*177.0*		
Hf(C≡CH)Cp$_2^*$	2.25(2)	1.24(3)	157
	171(2)		
Group 5			
Ta(silox)$_3$	1.95(2)	1.37(4)	159,160
	173(3)		

Group 6			
W(CO)$_3$Cp	2.172(22)	1.18(3)	164
	172.3(18)	*173.1(17)*	
W(CO)$_3$Cp^{Me}	2.135(9)	1.216(19)	165
	176.4(8)		
W(OBu^t)$_3$	1.79(1)	1.38(2)	168,169
	180		
W(OBu^t)$_3$	1.819(16)	1.34(3)	
	178.6(17)		
Group 7			
Mn(CO)$_5$	2.011(2)	1.201(2)	173
	179.5(2)		
Re(CO)$_5$	2.141(16)	1.195(33)	171
	179.2(23)		
Group 8			
Fe(CO)$_2$Cp$^{Et\ a}$	1.929/1.932(3)	1.206/1.211(6)	182
	178.6(6)/178.4(5)		
Fe(CO)$_2$Cp*	1.935(3), 1.939(4)	1.202(5)	182
	173.0(3)	*173.8(3)*	
Ru(CO)$_2$Cp	2.05, 2.04(1)	1.19(1)	104
	179.6(9)		
Ru(CO)$_2$Cp^{Me}	2.055(2)	1.205(3)	105
Os(CO)$_2$Cp	2.071(6)	1.169(9)	105
Group 10			
trans-PtI(PMe$_3$)$_2$	1.973(30), 1.980(38)	1.179(48)	187,188
	175.6(30)	*177.1(33)*	
trans-PtCl(PPh$_3$)$_2$	1.958(4)	1.221(9)	186
	177.8		
Group 11			
Au(PEt$_3$)	1.95, 1.99(2)	1.22(2), 1.29(3)	105
Au(PPh$_3$)	2.00(1)	1.19(2)	207
	180.0		

(*Continued*)

TABLE IX

Continued

	Bond lengths			
	M–C(1)		C(1)–C(2)	
	Bond angles at			
ML$_x$	*C(1)*		*C(2)*	Ref.
Au{P(tol)$_3$}	2.02(1), 2.002(9)		1.13(2), 1.19(2)	206
Au{P(C$_6$H$_4$Me-3)}	2.002(9)		1.19(2)	207
Au{PPh(nap)$_2$}	1.986(17)		1.225(34)	209,211
	177.8(23)			
Au{PPh$_2$(nap)}	1.983(8)		1.222(16)	209
	174.2(10)			
Au(PPhFc$_2$)	2.002(6)		1.196(12)	209
	177.9(11)			

		M–C(1)	C(1)–C(2)	
ML$_x$	M'L'$_x$	C(1)	C(2)	Ref.
(b) Hetero-nuclear C$_2$ complexes {ML$_x$}(μ-C$_2$){M'L'$_y$}				
W(CO)(C$_2$Ph$_2$)Cp	Ru(PMe$_3$)$_2$Cp	2.05(1), 1.96(1)	1.25(2)	220
		97.3(8), 163(1)		
Re(NO)(PPh$_3$)$_2$Cp*	*trans*-PdCl(PEt$_3$)$_2$	2.079(9), 1.967(9)	1.21(1)	223,224
		173.2(9), 169.5(9)		
ZrClCp$_2$	Ru(PMe$_3$)$_2$Cp	1.989(13), 2.141(15)	1.251(20)	217
		174(2), 169.9(3)		
cis-Pt(C$_6$F$_5$)$_2$(CO)	*trans*-Pt{CMe(OEt)}(PEt$_3$)$_2$	2.00(2), 2.02(1)	1.22(3)	191
		171.7(23), 174.6(9)		

[a] Values for molecules 1, 2.

structurally characterized. However, from the data in Table IX, it is clear that the complex anion [Ti(oepg)(μ-Li)]$_2$(μ-C$_2$) is better described in terms of a cumulated Ti=C=C=Ti structure (Ti–C 1.809(9)/1.757(7) Å, C–C 1.301(11) Å, cf. {Ti(PMe$_3$)Cp}$_2$(μ-C≡C) Ti–C 2.051(2) Å, C–C 1.253(2) Å). Similarly, the long C–C separation in {Ta(silox)$_3$}$_2$(μ-C$_2$) points to a Ta=C=C=Ta valence structure, which is confirmed by the ν(C≡C) stretching frequency. A combination of ^{13}C NMR and structural data indicate the C$_2$ unit in {W(OBu^t)$_3$}$_2$(μ-C$_2$) to be a bis(carbyne).[168–170] Structural comparisons of related dimetalla-alkyne, -alkene, and -alkane complexes have been made in both the rhenium[171] and mixed Zr–Ru series,[217] the M–C and C–C bonds showing the expected shortening. In the last two entries, there are agostic interactions between H atoms on the Ru–C atom and the Zr center.

Complex[a]	C–C	M–C (M = Re or Zr)	Ru–C
[Re]–C≡C–[Re]	1.20(3)	2.14(2)	
[Re]–CHR=CHR–[Re][b]	1.37(1)	2.18(1)	
[Re]–CH$_2$CH$_2$–[Re]	1.52(2)	2.30(1)	
[Zr]–C≡C–[Ru]	1.251(20)	1.989(13)	2.141(15)
[Zr]–CH=CH–[Ru]	1.304(22)	2.095(16)	2.185(19)
[Zr]–CH$_2$CH$_2$–[Ru]	1.485(14)	2.186(9)	2.276(10)

[a][Re] = Re(CO)$_5$, [Zr] = ZrClCp$_2$, [Ru] = Ru(PMe$_3$)$_2$Cp; [b]CHR=CHR = cyclobutenedione-1,2-diyl.

In both the manganese[173] and rhenium[171] complexes {M(CO)$_5$}$_2$(μ-C≡C),[171] the M(CO)$_5$ groups are eclipsed, in contrast to the staggered geometry found about the C≡C bond for Pt complexes.[188]

As might be expected from the limited number of examples that have been prepared so far, there are few structurally characterized examples of M–C$_3$–M complexes. However, these include examples of structural types **B** and **C**. The C–C bond lengths in [{Cp*(NO)(Ph$_3$P)Re}(μ-C$_3$){Mn(CO)$_2$Cp}]$^+$ are in the range 1.27–1.31(2) Å, which spans the values reported for allene and butatriene (1.28–1.31 Å). These distances are similar to those reported for [{Re(NO)(PPh$_3$)Cp*}$_2$(μ-C=C=C=C)]$^{2+}$ [1.260–1.305(10) Å]. The Re=C distances are also similar in these cations [C$_3$: 1.91–1.93(1); C$_4$: 1.909–1.916(7) Å]. The Mn=C distance in the C$_3$ cation [1.75(1) Å] is closer to the distances found in vinylidene and allenylidene complexes (ca. 1.80 Å) than in manganese carbyne derivatives (ca. 1.66 Å).

The OBu^t-bridged dimer found for {(Bu^{t}O)$_3$W}(μ-C$_3$){Re(NO)(PPh$_3$)Cp*} in the solid-state has alternating short and long C–C separations, consistent with the W≡C [1.769(8) Å], ≡C–C≡[1.398(11) Å], –C≡C– [1.227(10) Å] and ≡C–Re [2.039(8) Å] formulation.[233]

TABLE X
BOND LENGTHS (Å) AND ANGLES AT C(n) IN C$_4$ COMPLEXES

		Bond lengths				
		M–C(1)	C(1)–C(2)	C(2)–C(3)	C(3)–C(4)	
			Bond angles at			
ML$_x$	n	*C(1)*	*C(2)*	*C(3)*	*C(4)*	Ref.
(a) Homo-binuclear complexes [{ML$_x$}$_2$(μ-C$_4$)]$^{n+}$						
Group 6						
W(CO)$_3$Cp*	0	2.127(7)	1.226(10)	1.376(14)		243
		178.9(8)	*179.3(10)*			
W(O)$_2$Cp*	0	2.072(4)	1.217(5)	1.375(7)		243
		177.6(3)	*179.3(5)*			
Group 7						
trans-MnI(dmpe)$_2$	0	1.798(15)	1.263(17)	1.33(3)		246
		176.1	*177.4*			
	1 [PF$_6$]	1.763(2)	1.275(3)	1.313(5)		246
		179.1	*179.3*			
	2 [BF$_4$]$_2$	1.768(4), 1.770(4)	1.289(5)	1.295(5)	1.298(5)	246
trans-Mn(C≡CH)(dmpe)$_2$	1 [PF$_6$]	1.818(4)	1.285*6)	1.307(9)		247
		180.0(4)	*180.0(3)*			
SS/RR-Re(NO)(PPh$_3$)$_2$Cp*	0	2.037(5)	1.202(7)	1.389(5)		248,249
		174.4(5)	*176.8(6)*			
	2 [PF$_6$]$_2$	1.909(7), 1.916(7)	1.263(10)	1.305(10)	1.260(10)	248,249
		168.5(7), 171.4(7)	*177.8(9)*	*175.4(9)*		
Re(CO)$_3$(Bu$_2^t$-bpy)	0	2.13(2)	1.19(2)	1.43(4)		253
		176(1)	*178(2)*			
Group 8						
Fe(CO)$_2$Cp*	0	1.993(4)	1.917(4)	1.396(7)		182
		178.0(4)	*178.0(6)*			

Fe(dppe)Cp*	0	1.889(9), 1.885(8)	1.22(1)	1.37(1)	1.22(1)	450
		175(1)	*177(1)*	*176(1)*	*179(1)*	
	1 [PF$_6$]	1.830(8)	1.236(9)	1.36(1)		269,270
		167.0(6)	*177(1)*			
Fe(dippe)Cp*	3 [PF$_6$]$_3$	1.79(1)	1.27(1)	1.33(1)		258
		175.2(9)	*178.7(9)*			
Ru(PPh$_3$)$_2$Cp	0[a]	2.001(3)	1.217(4)	1.370(6)		260
		178.9(2)	*177.2(3)*			
	0[b]	2.01(3)	1.24(4)	1.31(4)		260
		174(2)	*176(3)*			
	0[c]	2.00, 2.01(1)	1.20(2)	1.38(2)	1.25(2)	261
		177(1)	*178(2)*	*175(1)*	*170(1)*	
	0[d]	2.00(1)	1.22(1)	1.39(1)		261
		175(1)	*177(1)*			
Ru(dppm)Cp*	0	2.017(2), 2.019(2)	1.216(3)	1.385(3)	1.223(3)	264
		175.2(2)	*179.1(2)*	*177.7(3)*	*170.6(2)*	
Ru(dppe)Cp	0	2.016(7), 2.007(8)	1.22(1)	1.40(1)	1.22(1)	267
		177.1(9)	*176(1)*	*172(1)*	*171.4(9)*	
Ru(dppe)Cp*	0	2.001(3), 2.003(3)	1.223(4)	1.382(4)	1.2128(4)	264
		176.6(3)	*176.9(3)*	*178.0(3)*	*177.1(3)*	
	1 [PF$_6$]	1.931(2)	1.248(3)	1.338(3)		264
		165.6(2)	*178.0(2)*			
	2 [PF$_6$]$_2$	1.858(5), 1.856(5)	1.280(7)	1.294(7)	1.269(7)	264
		175.6(5)	*176.7(6)*	*174.2(6)*	*170.1(4)*	
		174.5(8)				
Ru$_2$(μ-ap)$_4$	0	2.047(14)	1.258(16)	1.33(2)		318
		177.8(12)	*176.1(19)*			
Os(dppe)Cp*	0	2.010(3), 2.015(3)	1.220(4)	1.380(4)	1.224(4)	271
		177.4(3)	*176.2(3)*	*177.3(3)*	*177.2(3)*	

TABLE X
Continued

		Bond lengths				
		M–C(1)	C(1)–C(2)	C(2)–C(3)	C(3)–C(4)	
		Bond angles at				
MLₓ	*n*	*C(1)*	*C(2)*	*C(3)*	*C(4)*	Ref.

ML_x	n	M–C(1) / *C(1)*	C(1)–C(2) / *C(2)*	C(2)–C(3) / *C(3)*	C(3)–C(4) / *C(4)*	Ref.
Group 9						
trans-Rh(C=CMe₂)(PPr$^i_3$)₂	0	2.023(7) *173.1(7)*	1.221(9) *176(1)*	1.38(1)		277
trans-Rh(CO)(PPr$^i_3$)₂	0	2.021(4) *178.5(4)*	1.205(5) *178.9(5)*	1.388(7)		280
Au{P(tol)₃}	0	1.996(5), 1.996(5) *176.3(6)*	1.196(6) *178.6(6)*	1.390(6) *178.8(5)*	1.215(6) *169.2(6)*	267

ML_x	$M'L'_y$	M–C(1) / *C(1)*	C(1)–C(2) / *C(2)*	C(2)–C(3) / *C(3)*	C(3)–C(4) / *C(4)*	Ref.
(b) Hetero-binuclear complexes {MLₓ}(µ-C₄){M′L′$_y$}						
W(CO)₃Cp	Ir(O₂)(CO)(PPh₃)₂	2.13(5), 2.03(4) *166(4)*	1.21(7) *170(5)*	1.41(7) *170(5)*	1.21(7) *154(4)*	293
W(CO)₃Cp	Rh(tcne)(CO)(PPh₃)₂	2.10(1), 2.00(1) *178(1)* *179.5(2)*	1.23(2) *173(1)*	1.38(2) *176(1)*	1.20(2) *170(1)*	295
Re(NO)(PPh₃)Cp*	Mn(CO)₂Cp^f	1.92/1.93(1), 1.75/1.75(2) *173/175(1)*	1.26/1.28(2) *175/170(2)*	1.32/1.28(2) *178/178(1)*		228,229

Re(NO)(PPh$_3$)Cp*	Fe(dppe)Cp*	1.895(6), 2.029(6)	1.209(8)	1.370(9)	1.224(9)	296
		176.6(5)	*178.3(7)*	*177.4(7)*	*169.6(6)*	
Fe(dppe)Cp*	Fe(CO)$_2$Cp*	1.886(9), 1.90(1)	1.21(1)	1.36(1)	1.24(1)	88
		177.8(8)	*175(1)*	*178.4(9)*	*172.0(1)*	
Fe(dppe)Cp*	Ru(PPh$_3$)$_2$Cp	1.989(5), 2.019(5)	1.226(7)	1.392(7)	1.238(7)	267
		176.6(5)	*178.3(7)*	*177.4(7)*	*169.6(6)*	
cyclo-Pt(dppe)	Pt(dppe)	2.027(8), 2.00(1), 2.019(8), 2.00(1)	1.17(1), 1.24(2)	1.40(1), 1.38(2)	1.22(1), 1.21(2)	285
		176(1), 175.9(8)	*179(1), 177.5(9)*	*178(1), 177(1)*	*177(1), 177.3(8)*	
(c) Trimetallic complexes						
cis-Pt(PEt$_3$)$_2$	{W(CO)$_3$Cp}$_2$	1.99(1), 2.14(1)^e	1.20(3)	1.39(1)	1.21(2)	293
		172(1)	*177(1)*	*176(1)*	*177(1)*	

Note: ^{a}*trans* isomer, thf solvate; ^{b}*cis* isomer; ^{c}*cis* isomer, thf solvate; ^{d}*cis* isomer, MeOH solvate; ^{e}averaged values; ^{f}values for molecules 1, 2.

TABLE XI
Bond Lengths (Å) and Angles at C(n) in $\{ML_x\}_2(\mu\text{-}C_n)$ ($n = 6\text{--}20$)

ML_x	n	M–C(1) / *C(1)*	C(1)–C(2) / *C(2)*	C(2)–C(3) / *C(3)*	C(3)–C(4) / *C(4)*	C(4)–C(5) / *C(5)*	C(5)–C(6) / *C(6)*	C(6)–C(7) or C(6′)	Ref.
					Bond angles at				
Fe(CO)$_2$Cp*	12	1.878(9), 1.888(8)	1.23(1), 1.20(1)	1.36(1), 1.38(1)	1.20(1), 1.19(1)	1.35(1), 1.36(1)	1.22(1), 1.23(1)	1.35(1)	306
		175.2(6), 173.3(7)	*172.7(8), 171.9(9)*	*175.5(8), 173.8(9)*	*176.8(9), 175.1(9)*	*176.3(9), 176.9(9)*	*177(1), 178(1)*		
Ru(PPh$_3$)$_2$Cp	6	2.001(6)	1.210(8)	1.382(8)	1.212(8)				261
		172.2(4)	*178.8(6)*	*177.3(6)*					
Ru$_2$(μ-dpf)$_4$ (C≡CC≡CSiMe$_3$)	8	1.939(12) *176.7(12)*	1.22(2) *176.3(18)*	1.37(2) *176.0(19)*	1.22(2) *177.2(30)*	1.31(3)			320
Os(dppe)Cp*	6	2.001(6) *171.8(3)*	1.210(8) *177.4(3)*	1.382(4) *178.2(4)*	1.212(8)				271
trans-Pt(tol)(PPh$_3$)$_2$	8	2.011(4) *178.0(4)*	1.2118(6) *176.5(5)*	1.368(6) *177.8(5)*	1.223(6) *179.5(9)*	1.367(9)			310
trans-Pt(tol){P(tol)$_3$}$_2$	12	1.990(3) *174.0(3)*	1.233(4) *174.5(4)*	1.358(4) *178.6(4)*	1.210(5) *178.3(4)*	1.356(5) *177.5(4)*	1.211(5) *178.9(6)*	1.344(7)	310
trans-Pt(C$_6$F$_5$){P(tol)$_3$}$_2$	8	1.951(2) *177.6(4)*	1.252(6) *179.2(5)*	1.365(6) *177.1(5)*	1.209(6) *178.5(6)*	1.351(8)			311
	12	1.972(6), 1.983(5)	1.234(8), 1.223(7)	1.361(8), 1.374(7)	1.209(8), 1.208(7)	1.363(7), 1.356(7)	1.216(7), 1.210(7)	1.358(8)	311
		172.9(5), 171.6(5)	*173.2(7), 171.8(6)*	*178.3(7), 176.2(6)*	*175.6(7), 173.4(6)*	*175.3(6), 175.3(6)*	*175.7(6), 175.7(6)*		
	16	1.981(2) *175.7(2)*	1.220(3) *176.9(3)*	1.355(3) *178.2(3)*	1.214(3) *178.0(3)*	1.350(3) *178.7(3)*	1.217(4) *179.1(3)*	1.349(3) *178.3(3)*	311
Au(Pcy$_3$)	6	2.011(8)	1.170(1)	1.40(1)	1.18(1)				315

dpf = N,N'-diphenylformamidinate.

The majority of structurally characterized examples of $\{ML_n\}_2(\mu\text{-}C_4)$ complexes belong to the poly-yndiyl (**L**) subset (Table X). The structures typically display M–C bond lengths of ca. 2.0 Å, with distinctly shorter bond lengths being observed only in the case of complexes of the smaller and lighter metals, such as Mn. Along the poly-yndiyl carbon chain, clear short-long-short alternation of the C–C separations is in evidence, with C≡C bonds lengths near 1.20 Å, and C–C bond lengths of 1.35 Å being typical. The effects of metal size are most clearly demonstrated in the rare examples of hetero-bimetallic complexes which have been structurally characterized. Thus in complexes such as $\{Fe(dppe)Cp^*\}(\mu\text{-}C{\equiv}CC{\equiv}C)\{ML_x\}$ $[ML_x =$ $Re(NO)(PPh_3)Cp^*,$[296] $Ru(PPh_3)_2Cp$[267]], the shorter M–C distance is associated with the smaller Fe center. Of the two alkynyl moieties, the C≡C adjacent the more electron-releasing metal fragment is the longer. In the case of the tungsten complexes $\{W(CO)_3Cp^*\}_2(\mu\text{-}C{\equiv}CC{\equiv}C)$ [W–C 2.127(7) Å] and $\{W(O)_2Cp^*\}_2(\mu\text{-}C{\equiv}CC{\equiv}C)$ [W–C 2.072(4) Å], the shortening of the W–C_{diynyl} bond distance has been attributed to both the decreased size of the W(VI) center in the dioxo complex, and the greater electrostatic attraction between the high oxidation state metal and the carbon center.[243]

Lengthening of the carbon chain (Table XI) does not alter these generalized observations, although the extension of the conjugated M–$(C{\equiv}C)_m$–M π-system results in a small lengthening of the C≡C moieties and contraction of the C–C bond lengths. For H–$(C{\equiv}C)_m$–H, theoretical calculations predict limiting values for C–C and C≡C of 1.1956–1.2031 and 1.3574–1.3726 Å, respectively.[382] The complex $\{trans\text{-}Pt(C_6F_5)[P(tol)_3]_2\}_2$ $\{\mu\text{-}(C{\equiv}C)_8\}$ contains the longest metal-stabilized carbon fragment structurally characterized during the period covered by this chapter.[311] In general, individual parameters (Pt–C, C–C, C≡C bond distances, M–C–C, C–C–C bond angles) do not differ significantly from values found in analogous alkynylmetal complexes. For increasing n in the Pt series **165**/**m**, the C≡C and C–C distances tend to values of 1.20 and 1.35 Å, respectively.[311]

A striking feature is the bending of the M–C_n–M chain to a greater or lesser extent, which appears to arise from the low bending force constants of M–C, C≡C, and ≡C–C bonds. This was first observed in $Re\{(C{\equiv}C)_m tol\}$ $(NO)(PPh_3)Cp^*$ ($m = 3, 4$), where the bond angles average 174.7 and 175.7°, respectively.[292] The degree of bending does not appear to be related to any one of van der Waals contacts, π interactions or the presence of solvent molecules. Computational studies have failed to identify any underlying electronic effects which may be responsible for these gracefully bent structures, and, at present, these structural phenomena are best considered to be a result of "crystal packing forces". Angles at individual atoms do not

differ much from 180° but the bending may be either cumulative, leading to inter-metal distances less than the sum of the intervening bond distances, e.g., for **165**/**m** ($m = 4$, 6, 8),[311] or pseudo-symmetrical, resulting in an *S*- or transoid conformation. The C_n chain shows the greatest degree of bending for **165**/**6**, with an average angle at C of 174.6°. The chain in the Pt–C_{16}–Pt complex is straighter, with an average angle of 178.0°, leading to a difference in Pt $\cdots$ Pt separations of only 0.3%. Some degree of curvature is also found in $\{Fe(CO)_2Cp^*\}_2\{\mu\text{-}(C\equiv C)_6\}$, with angles at C ranging between 171.7 and 178° (av. 175.2°).[306] In this case, crystal packing is determined by interactions between the Fp* groups.

As mentioned above, in derivatives containing π-bonded metal–ligand fragments, changes to the geometries of the carbon chains also parallel those found in analogous alkyne-ML_n complexes.[383]

C. Electrochemistry

The combination of multiple metal centers linked by a conjugated polycarbon bridge often results in a rich electrochemical response. Details of the electrochemical studies which have been performed to date are summarized in Table XII. Rather than correct the original data, which has been collected using a wide range of solvents, electrolytes and reference electrodes, to a common reference potential, we cite the results as reported in the literature together with an indication of the conditions employed.[384] While comparisons between complexes featuring significantly different metal centers holds some value, a more illustrative comparison of the properties of these metallated polycarbon species comes from an analysis of trends observed in a closely related series of compounds, and it is this latter approach around which we base the following discussion.

1. Complexes Containing C_2 Ligands

The complex $\{W(OBu^t)_3\}_2(\mu\text{-}C_2)$ shows two irreversible 1-e oxidation processes at E_p +0.362 and +0.816 V (vs. SCE), consistent with a delocalized (rather than mixed-valence) cation.[170] Electrochemistry of $\{Re(CO)_5\}_2$ $(\mu\text{-}C\equiv C)$ shows two irreversible oxidations occur at $E =$ +1.12, +1.35 V (CH_2Cl_2) or +1.02, +1.55 V (MeCN) indicating that the C≡C triple bond oxidizes more easily than the Re–Re bond in $Re_2(CO)_{10}$ [E +1.40 V (MeCN)].[171]

2. Complexes Containing C_3 and C_5 Ligands

The electrochemical responses of the complexes $\{ML_x\}_2(\mu\text{-}C_n)$ ($n = 3$, 5) have not yet been described.

3. Complexes Containing C_4 Ligands

(a) Homometallic Complexes

Group 6. An electrochemical study of $\{M(CO)_2Tp'\}_2\{\mu\text{-}(\equiv C\text{–}C\equiv C\text{–}C\equiv)\}$ (M = Mo, W) revealed two reversible oxidation processes in each case, with the tungsten complex both easier to oxidize than the Mo analogue and giving rise to a larger separation of the redox events [ΔE(Mo) = 0.239, $K_c = 1 \times 10^4$; ΔE(W) = 0.278 V, $K_c = 5 \times 10^4$].[385] The separation of redox events, often taken as a rough "rule of thumb" estimate of the ground state interactions between the metal centers in such bridged bimetallic complexes, is smaller than in many of the diyndiyl systems described below, and has been attributed to a limited contribution from the carbon bridge orbitals to the HOMO of the oxidized form.

Group 7. The paramagnetic manganese complexes [$\{trans\text{-}Mn(X)(dmpe)_2\}_2(\mu\text{-}C\equiv CC\equiv C)$] [X = I (**93**),[246] C≡CH (**95**)[247]] can be oxidized in two fully reversible steps, with the CVs indicating the electrochemical formation of the corresponding mono (Mn^{II}/Mn^{III}) and dications (Mn^{III}/Mn^{III}). In the case of **95** an irreversible reduction (−2.29 V) was also observed, and assigned to the Mn^{II}/Mn^{II}–Mn^{II}/Mn^{I} couple. The large potential difference between each oxidation process [$\Delta E = 0.63$ V (**93**), 0.576 V (**95**)] gives rise to large comproportionation constants K_C [5.4×10^{10} (**93**), 7.5×10^9 (**95**)], which indicate the thermodynamic stability of the monocations [**93**]$^+$ and [**95**]$^+$ towards disproportionation.[386]

The CV of (SS,RR)-$\{Re(NO)(PPh_3)Cp^*\}_2(\mu\text{-}C\equiv CC\equiv C)$ (**96**/Ph) also displays two reversible oxidation waves. Samples enriched in the SR,RS diasteromer give identical electrochemical results.[248,249,251] Racemic mixtures of **96**/tol, which bears the P(tol)$_3$ ligand, displayed two reversible one-electron oxidation processes in the CV which were approximately 230 mV more facile than the corresponding processes in **96**/Ph.[251]

The complex $\{Re(CO)_3(Bu^t_2\text{-}bpy)\}_2(\mu\text{-}C\equiv CC\equiv C)$ undergoes three irreversible oxidations and a Bu$^t_2$-bpy-centered reduction (−1.62 V). Oxidation processes near +1.8 V are also observed in related alkynyl complexes, and suggests that this redox event is associated with the Re(I/II) couple. The remaining redox events were tentatively assigned to oxidation of the carbon chain.[253]

Group 8. The iron complexes [$\{Cp^*L_2Fe\}_2(\mu\text{-}C\equiv CC\equiv C)$] [$L_2$ = dppe (**107**), dippe (**99**)] are characterized by a series of three one-electron oxidation processes (L_2 = dppe,[258,269,270] dippe[258]). Substitution of the dppe ligand for dippe results in positive shifts of the three electrode potentials by 0.29, 0.14, and 0.14 V respectively, and that the difference between these processes increases with increasing electron density at the metal centers.

TABLE XII

ELECTROCHEMICAL PROPERTIES OF COMPLEXES CONTAINING LINEAR C_n LIGANDS

Complex	$E_{1/2}$/V	K_c	Notes[a]	Ref.
Group 6				
{W(OBu^t)$_3$}$_2${μ-(≡C–C≡)}	+0.36 (irr), +0.82 (irr)			170
{Mo(CO)$_2$Tp$'$}$_2${μ-(≡C–C≡C–C≡)}	+0.29 (r), +0.53 (r)	1×10^4		385
{W(CO)$_2$Tp$'$}$_2${μ-(≡C–C≡C–C≡)}	+0.17 (r), +0.45 (r)	5×10^4		385
Group 7				
[{MnI(dmpe)$_2$}$_2$(μ-C=C=C=C)][BPh$_4$]$_2$	−0.02 (r), −0.66 (q)	5.4×10^{10}	b	246
[{Mn(C≡CH)(dmpe)$_2$}$_2$(μ-C≡CC≡C)]PF$_6$	−0.89 (r), −1.46 (r), −2.29 (irr)	7.5×10^9	c	247
{Re(CO)$_3$(Bu$^t_2$-bpy)}$_2$(μ-C≡CC≡C)	+0.72 (irr), +1.33 (irr), +1.84 (irr), −1.62 (irr)		d	253
{Re(CO)$_5$}$_2$(μ-C≡C)	+1.12, +1.35			171
SS,RR-{Re(NO)(PPh$_3$)Cp*}$_2$(μ-C≡CC≡C)	+0.01, +0.54	1.1×10^9		248,249,251
{Re(NO)[P(tol)$_3$]Cp*}$_2$(μ-C≡CC≡C)	−0.22, +0.31	1.1×10^9		251
{Re(NO)(PPh$_3$)Cp*}$_2${μ-(C≡C)$_3$}	+0.10, +0.48	3.0×10^6		251
{Re(NO)[P(tol)$_3$]Cp*}$_2${μ-(C≡C)$_3$}	+0.02, +0.41	4.4×10^6		251
{Re(NO)(PPh$_3$)Cp*}$_2${μ-(C≡C)$_4$}	+0.24, +0.52	5.9×10^4		251
{Re(NO)(Ptol$_3$)Cp*}$_2${μ-(C≡C)$_4$}	+0.16, +0.45	8.8×10^4		251
{Re(NO){P(C$_4$H$_4$Bu^t-4)$_3$}Cp*}$_2${μ-(C≡C)$_4$}	+0.18, +0.48	1.3×10^5		251
{Re(NO){P(C$_4$H$_4$Ph-4)$_3$}Cp*}$_2${μ-(C≡C)$_4$}	+0.25, +0.54	8.8×10^4		251
{Re(NO)(PCy$_3$)Cp*}$_2${μ-(C≡C)$_4$}	+0.11, +0.43	2.8×10^5		251
{Re(NO)(PPh$_3$)Cp*}$_2${μ-(C≡C)$_5$}	+0.43, +0.63	2.6×10^3	e	290,291
{Re(NO)(PPh$_3$)Cp*}$_2${μ-(C≡C)$_6$}	+0.46, +0.65	1.7×10^3	e	290,291
{Re(NO)(PPh$_3$)Cp*}$_2${μ-(C≡C)$_8$}	+0.57, +0.66	34	e	290,291
{Re(NO)(PPh$_3$)Cp*}$_2${μ-(C≡C)$_{10}$}	+0.64		e	290,291
Group 8				
{Fe(dppe)Cp*}$_2$(μ-C≡CC≡C)	−0.68, −0.40, +0.95	1.6×10^{12}		258,266,269,270
{Fe(dippe)Cp*}$_2$(μ-C≡CC≡C)	−0.18, 0.81, −0.97			258

Compound				
{Cp*(dppe)Fe}(μ-C≡CC≡C){Fe(CO)$_2$Cp*}	−0.36, +0.74			88,259
{Cp*(dppe)Fe}(μ-C≡CC≡C){Fe(CO)$_2$(η-C$_5$Ph$_5$)}	−0.28, +0.93			88
{Cp*(dippe)Fe}(μ-C≡CC≡C){Fe(CO)$_2$(η-C$_5$Me$_5$)}	−0.53, +0.69			259
{Ru(PPh$_3$)$_2$Cp}$_2$(μ-C≡CC≡C)	−0.23, +0.41, +1.03, +1.68	1.5×10^{11}, 1.5×10^{11}		262,265
{Ru(PPh$_3$)(PMe$_3$)Cp}$_2$(μ-C≡CC≡C)	−0.26, +0.33, +0.97, +1.46	2.1×10^{10}, 2.7×10^8		262,265
{Ru(dppm)Cp*}$_2$(μ-C≡CC≡C)	−0.48, +0.15, +1.04, +1.41	4.46×10^{10}, 1.11×10^{15}, 1.80×10^6	f	264
{Ru(dppe)Cp*}$_2$(μ-C≡CC≡C)	−0.43, +0.22, +1.04, +1.51	9.70×10^{10}, 7.26×10^{13}, 8.80×10^7	f	264
{cis-RuCl(bpy)$_2$}$_2$(μ-C≡CC≡C)	−1.61, −1.42, +0.35, +0.87, +2.05, +2.47	6.13×10^8	b	268
{Ru$_2$(μ-ap)$_4$}$_2$(μ-C≡CC≡C)	−1.17, −0.78, +0.33, +0.49, +1.12	3.8×10^6 (red), 506 (ox)	g	318
Group 9				
{Rh$_2$(ap)$_4$}$_2$(μ-C≡CC≡C)	−0.65, −0.52, +0.60		h	323
Heterometallics				
{Cp*(NO)(Ph$_3$P)Re}(μ-C≡C){PdCl(PEt$_3$)$_2$}	+0.08, +1.25		i	224
{Cp*(NO)(Ph$_3$P)Re}(μ-C≡CC≡C){PdCl(PEt$_3$)$_2$}	+0.32, +1.29 (irrev)		i	224
trans-Pd{C≡CC≡C[Re(NO)(PPh$_3$)Cp*]}$_2$(PEt$_3$)$_2$	+0.32, +1.29 (irrev)		i	224
{Cp*(NO)(Ph$_3$P)Re}(μ-C≡CC≡C){Fe(dppe)Cp*}	−0.50, +0.23, +1.33			296
{Cp*(NO)(Ph$_3$P)Re}(μ-C≡CC≡C){Fe(dppe)Cp*}	−0.50, +0.23, +1.33			296
Os$_3$(μ-H){μ$_2$-η^1-C≡C[Re(NO)(PPh$_3$)Cp*]}	+0.78			434
Os$_3$(μ-H){μ$_2$-η^1-C≡CC≡C[Re(NO)(PPh$_3$)Cp*]}	+0.43			434
Os$_3$(μ-H){μ$_2$-η^1-(C≡C)$_3$[Re(NO)(PPh$_3$)Cp*]}	+0.48			434

Notes: ^{a}Measured in CH$_2$Cl$_2$ containing 0.1 M [NBu$_4$]PF$_6$ vs. SCE, referenced to FcH/[FcH]$^+$ couple at 0.46 V. ^{b}In MeCN, [NBu$_4$]PF$_6$ vs. Ag/AgCl. ^{c}In NCMe, vs. Fc/Fc$^+$. ^{d}In NCMe, 0.1 M NBu$_4$PF$_6$ vs. SCE, FcH/[FcH]$^+$ internal reference. ^{e}In CH$_2$Cl$_2$, 0.1 M [NBu$_4$]BF$_4$, vs. Ag wire. ^{f}In CH$_2$Cl$_2$. ^{g}In thf, 0.2 M [NBu$_4$]PF$_6$, vs. Ag/AgCl. ^{h}In thf, 0.2 M [NBu$_4$]ClO$_4$ vs. SCE. ^{i}In CH$_2$Cl$_2$, 0.1 M [NBu$_4$]BF$_4$, Ag pseudo-reference (FcH/[FcH]$^+$ = 0.56 V).

The large separation between the redox events indicates the thermodynamic stability of $[107]^{n+}$ and $[99]^{n+}$ ($n = 0$–3), and chemical oxidation of **107** and **99** by $[FcH]PF_6$ or $AgPF_6$ afforded $[107]^{n+}$ ($n = 1, 2$)[270] and $[99]^{n+}$ ($n = 1$–3)[258] in good to excellent yields.

In the case of the homo-bimetallic diyndiyl complexes {Cp*(dppe)Fe}(μ-C≡CC≡C){Fe(CO)$_2$(η^5-C$_5$R$_5$)} (R = Me **100**, Ph **101**) CV analyses reveal two oxidation processes, the latter becoming reversible at faster scan rates. The first oxidation processes is rather more thermodynamically favorable than was found for the mononuclear species Fe(C≡CC≡CSiMe$_3$)(dppe)Cp* under the same conditions (0.00 V), while the much greater chemical reversibility of the second oxidation process suggests there is a significant interaction between the two metal centers. The results are consistent with significant electron-donating properties associated with the metallo-carbon fragment, despite the presence of the supporting carbonyl ligands.[88] Similar data were reported for {Cp*(dippe)Fe}(μ-C≡CC≡C){Fe(CO)$_2$(η^5-C$_5$Me$_5$)} (**102**) under the same conditions (-0.53, $+0.69$ V).[259]

The ruthenium diyndiyl complexes {Ru(PP)Cp′}$_2$(μ-C≡CC≡C) [Cp′ = Cp, PP = (PPh$_3$)$_2$ **103**, (PPh$_3$)(PMe$_3$) **104**] undergo a series of four oxidations, the first three being well-defined reversible one-electron processes, the fourth complicated by subsequent chemical reactions.[262,265] The chemical reversibility of the fourth oxidation process is improved in the complexes **109**, **110** (Cp′ = Cp*, PP = dppe, dppm, respectively), although some decomposition of **110** in the higher oxidation states occurs.[264] These data indicate that a total of five accessible oxidation states is associated with the Ru–C$_4$–Ru framework. The $3+/4+$ couple has not been found in any related iron system to date. The first oxidation potentials of the more electron-rich complexes **110** and **109** at -0.48 and -0.43 V, respectively, are lower than those determined for **103**, **104** but not as low as the $0/1+$ potential observed for the Fe(dppe)Cp* analogue (-0.68 V) measured under the same conditions. Similar comments apply to the second oxidation potentials ($1+/2+$) of these complexes. However, as oxidation proceeds, the $2+/3+$ couples are essentially identical for the ruthenium compounds, while the $3+/4+$ couples of **110** and **109** (at $+1.41$, $+1.51$ V) are lower than those for the RuCp complex [$+1.68$ V (irr.)] and in both cases they are reversible. In the case of **110**, an irreversible wave was also observed in the cathodic sweep (0.724 V), which was found to decrease at higher scan rates. This is most likely due to a product resulting from the decomposition of the higher oxidized species under the conditions used in the experiment and is presently uncharacterized. In each case, the large potential difference between these processes gives rise to large values for the comproportionation constants associated with the oxidized materials and provides an indication of their thermodynamic stability.[264]

The cyclic voltammogram of {cis-RuCl(bpy)$_2$}$_2$(μ-C≡CC≡C) displays two quasi-reversible oxidation waves at +0.351 and +0.871 V (vs. Ag/AgCl) which have been attributed to the Ru^{II}/Ru^{III} and Ru^{III}/Ru^{III} couples. Two irreversible oxidations above +2 V were observed and may arise from oxidation to formal Ru^{III}/Ru^{IV} and Ru^{IV}/Ru^{IV} states. Ligand (bpy)-centered reduction processes were observed at −1.42 and −1.61 V.[268]

(b) Heterobimetallic Complexes

Electrochemical studies have also been performed on a number of heterometallic systems, which may be broadly distinguished by the extent of interaction between the dissimilar metal fragments mediated by the μ-polycarbon ligand. Gladysz and his co-workers have investigated the electrochemical properties of the binuclear species [{Cp*(NO)(PPh$_3$)Re}(μ-C≡C){PdCl(PEt$_3$)$_2$}], [{Cp*(NO)(PPh$_3$)Re}(μ-C≡CC≡C){PdCl(PEt$_3$)$_2$}] and the linear trimetallic complex trans-Pd{C≡CC≡C[Re(NO)(PPh$_3$)Cp*]}$_2$(PEt$_3$)$_2$.[224] In each case, two oxidation waves were detected by CV, the first being chemically reversible. By analogy with model complexes, the oxidations can be attributed to sequential processes largely centered on the electron-rich Re(PPh$_3$)(NO)Cp* fragment, and the PdX(PEt$_3$)$_2$ moiety. It is apparent that the Pd(PEt$_3$)$_2$ fragment is not efficient at transmitting electronic information between the rhenium centers.

The mixed rhenium/iron complex {Cp*(NO)(PPh$_3$)Re}(μ-C≡CC≡C){Fe(dppe)Cp*} (137) gives three oxidation waves in the CV at −0.50, +0.23, and +1.33 V, the first two being reversible, the third being partially obscured by the edge of the solvent electrochemical window (CH$_2$Cl$_2$).[296] Comparisons of the values obtained from Re(C≡CC≡CSiMe$_3$)(PPh$_3$)(NO)Cp* (+0.35 V) and Fe(C≡CC≡CSiMe$_3$)(dppe)Cp* (0.00 V) and the homobimetallic complexes 96/Ph (+0.01, +0.54 V) and 107 (−0.69, +0.03, +0.95 V), measured under the same conditions, suggest that the initial oxidation process in 137 is likely to be predominantly iron in character, while the second would be more rhenium-centered. Assuming that the solvation energies associated with these species in their various oxidation states are similar, a strong interaction between the Fe and Re metal end-caps is apparent. It appears that the Fe(dppe)Cp* moiety is more electron-rich than the rhenium end-cap, and that even the mono-oxidized form of the iron end-cap is capable of acting as a good electron-releasing group in comparison to SiMe$_3$. The second oxidation process in the heterobimetallic species is also thermodynamically more favorable than the oxidation event associated with Re(C≡CC≡CSiMe$_3$)(PPh$_3$)(NO)Cp*, clearly indicating that the iron center plays a role in stabilising the oxidized product.[296]

4. Higher Poly-yndiyl Complexes

It is generally observed that electronic interactions between metal centers bridged by linear carbon fragments are strongly attenuated by the length of the bridge. For example, the CV trace of the octatetrayndiyl complex {Fe(dppe)Cp*}$_2${μ-(C≡C)$_4$} (**159**) displays two reversible oxidation waves at −0.23 and +0.20 V (vs. FcH, +0.420 V), which gives a wave separation of 0.43 V, somewhat less than the 0.71 V separation found for the diyndiyl **107**.[307] Nevertheless, while the interaction between the metal centers in **159** is some what less than in **107**, the radical cation has suffient thermodynamic stability with respect to disproportionation ($K_C = 2 \times 10^7$) to be isolated by oxidation with [FcH]PF$_6$. The observation of a unique ν(CC) profile for [**159**]PF$_6$ together with a strong NIR band (λ_{max} 1958 nm, ε 31,000), which is narrower than predicted by the Hush relationship for localized mixed-valence systems, indicates that the cation is best described with a delocalized electronic structure ($V_{ab} = 0.32$ eV).[307]

Gladysz and his group have carried out systematic analyses of the effect of chain length on coupling between rhenium centers in complexes of general form {Re(PR$_3$)(NO)Cp*}$_2${μ-(C≡C)$_m$} (R = Ph, m = 1–10;[250,290,291] R = C$_6$H$_4$Me-4, m = 2–4;[251] R = C$_6$H$_4$Bu^t-4, C$_6$H$_4$Ph-4, Cy, m = 4[251]). Each complex undergoes two oxidation processes, the reversibility of which decreases with increasing chain length. In addition, as the chain is lengthened, the first oxidation potential becomes less thermodynamically favorable, and shifts to more positive potentials. The second oxidation potential is less susceptible to the influence of the carbon fragment, and as a result the differences between the two formal electrode potentials decrease, such that only a single, possibly two-electron, oxidation is observed for [{Re(PPh$_3$)(NO)Cp*}$_2${μ-(C≡C)$_{10}$}].[290] The reversibility of the electrochemistry of the longer chain examples was improved by the presence of bulky phosphines, but in no case could oxidized materials be isolated for complexes with bridging poly-yndiyl ligands other than C≡CC≡C.[251]

5. Complexes Containing Bimetallic Fragments

Complexes containing multiple polymetallic fragments bridged by poly-yndiyl ligands have also been shown to display a rich electrochemical response. The bis(dirhodium) complex {Rh$_2$(ap)$_4$}$_2$(μ-C≡CC≡C) (**175**) (ap = 2-anilinopyridinate) exhibits two overlapping oxidation processes at 0.60 V together with two resolved one-electron reductions at −0.52 and −0.65 V (vs. SCE, thf, 0.2 M TBAP).[323] The CV results were verified by normal pulse voltammetry, which gave a current–voltage curve with limiting currents in the ratio 2:1:1 for the oxidation and two reductions respectively. ESR data suggest the electronic configuration of $(\sigma)^2(\pi)^4$

$(\delta)^2(\pi^*)^4(\delta)^1$ is appropriate for the neutral material, with the unpaired electron most likely localized on the rhodium center which is not σ-bonded to the diyndiyl ligand. Consequently, while oxidation involves orbitals which are not mixed with the polycarbon bridge, upon reduction, the additional electron density can be delocalized across the Rh–C_4–Rh portion of the complex, and this interaction is responsible for the separation of the reduction potentials.

The closely related bis(diruthenium) complexes, $\{Ru_2(ap)_4\}_2\{\mu\text{-}(C{\equiv}C)_m\}$ (**171/m**) ($m = 1$, 2) undergo a total of five identifiable redox processes.[318,319] The first four events are partially chemically reversible, while the most positive oxidation event is more irreversible. These redox processes have been assigned to two sequential reduction processes, (**171/1** −1.555, −0.888 V; **171/2** −1.173, −0.784 V), and three sequential oxidation processes (**171/1** 0.223, 0.508, 1.079 V; **171/2** 0.334, 0.491, 1.115 V). As was observed for the Rh analogues, coupling between the bimetallic centers is most pronounced upon reduction, with the greater difference between the reduction potentials of each complex [**171/1** 667 mV, $K_C(\text{red}) = 1.9 \times 10^{11}$; **171/2** 389 mV, $K_C(\text{red}) = 3.8 \times 10^6$] than was observed for the oxidations [**171/1** 285 mV, $K_C(\text{ox}) = 6.6 \times 10^4$; **171/2** 157 mV, $K_C(\text{ox}) = 506$]. This is consistent with these complexes being better carriers for electrons than holes. The oxidation waves merge for the C_8 complex and become an apparent 2-electron event (or two superimposed 1-electron events) with C_{12}, whereas even in the latter, the reduction waves are resolved. Regardless of the nature of the electrochemical event, the trend of exponentially decreased coupling with increasing poly-yndiyl bridge length is apparent.

D. *Electronic Structures*

Several structures may be envisioned for compounds $\{ML_x\}_2(\mu\text{-}C_n)$, which are broadly distinguished by whether or not they describe closed-shell singlet states or open-shell triplet states, and the number and combination of bonds between the metal and carbon as well as adjacent carbon centers. There have been several reports rationalising the valence bond descriptions of complexes containing even[387–389] or odd values of n[390,391] and related polymeric materials[3,392,393] and Sponsler has offered a comparison of the electronic properties of $\{Fe(CO)_2Cp\}_2(\mu\text{-}L)$ as a function of the structure of the bridging ligand L (L = CH=CHCH=CH, C≡CC≡C, C_6H_4, N=CHCH=N).[394] These various analyses suggest that the structural type depends heavily on the nature of the metal and its oxidation state, as well as the type of supporting ligands, and the number of carbon atoms in the C_n

ligand. It is this latter aspect which suggests a natural break of this survey
in terms of even and odd numbered chains.

1. Even-Numbered C_n Chains

The σ-bonded $M–C_n–M$ framework is similar in all complexes, and
the variation in valence bond descriptions of the M–C and C–C bonds,
and associated bond orders, are associated with the changes in the com-
position and occupancy of the π- and δ-frontier orbitals. In general terms, it
is therefore possible to forecast the valence structures for the C_n-bridged
complexes (n even) based on the metal d^x configuration, since a total of
$[2(x-1)+2n]$ electrons is contributed to the π-skeleton from the metal and
carbon fragments.

A qualitative model for a metal complex $M–C_n–M$ can be derived by
considering the interactions between two metal fragments M with the
orbitals of a C_n fragment. The $M–C_n–M$ σ-framework (taken to define
the z coordinate) comprises two low energy M–C σ bonds formed from
the M d_{z^2} and C(sp) orbitals of the terminal carbons, with the other
C(sp) hybrids forming $(n-1)$ C–C bonds of lower energy. This strongly
σ-bonded framework is complemented by two orthogonal sets of
$(n+2)$-centered MOs derived from linear combinations of M d_{xz} with C
p_x and M d_{yz} with C p_y orbitals, giving rise to $(n+2)$ orbitals which
are either degenerate or closely spaced in energy, depending on symmetry.
The scheme is completed by the metal-centered orbitals of δ symmetry,
formally derived from the in and out of phase combinations of the metal d_{xy}
and $d_{x^2-y^2}$ orbitals. For octahedral fragments, the $d_{x^2-y^2}$ levels are
destabilized by σ interactions with the supporting ligands and are likely
to be well removed from the lower lying π-orbitals. This π-scheme is
illustrated in Fig. 8 for octahedral metal fragments and a C_2 ligand.[387]

This generic bonding scheme can be fine-tuned by allowing for different
metals, the donor or acceptor properties of the supporting ligands and
symmetries of the metal ligand fragments, all of which affect the energies of
the metal d orbitals and consequently the extent to which they interact with
carbon orbitals of appropriate symmetry, and the occupancy of the resulting
frontier orbitals. In general terms, π-donor ligands destabilize the metal
d orbitals, and as a result these metal d orbitals are found at much higher
energies than the C_n π-orbitals. Consequently, the lower lying frontier
π-MO's (1π) tend to be predominantly C-centered π-bonding, while the
higher lying ($2\pi-4\pi$) orbitals exhibit more metal character.[395] The converse
is true of complexes containing π-accepting ligands.[387,396]

In the case of early d metal systems, in which the presence of π-donor
ligands is necessary to stabilize the complex, the δ orbitals are likely to lie
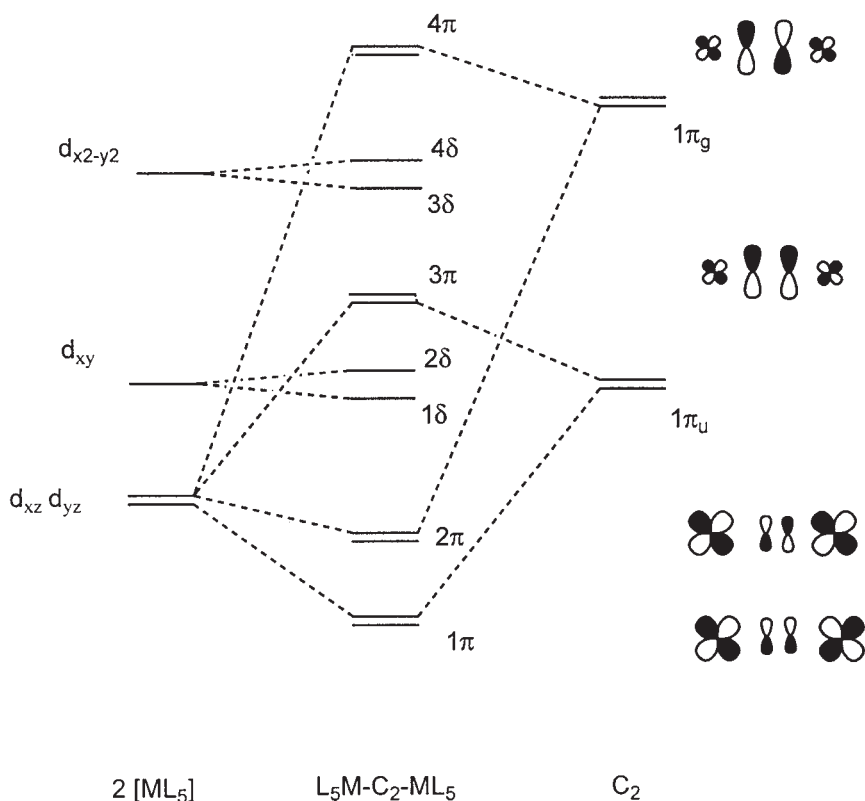
FIG. 8. Schematic MO diagram for $\{L_5M\}C_2\{ML_5\}$ complexes depicting the main interactions between the frontier orbitals of the ML_5 fragments (M = mid-late transiton metal, L = π-accepting ligand) and C_2. Adapted from Ref. 387.

above the 2π level. Thus in the case of C_2 complexes containing d^1 metal fragments (i.e., with 4π electrons), the 1π levels which are essentially localized between the carbon centers are occupied and form the HOMO, giving rise to the M–C≡C–M valence description. Increasing the electron count by the introduction of d^2 metals results in occupation of the 2π level, which is π-bonding between metal and carbon and C–C anti-bonding in nature, leading to M=C=C=M descriptions, as observed for $\{Ti(PMe_3)Cp\}_2(\mu\text{-}C_2)$,[151] potentially with triplet ground state character. Further occupation of the 2π level leads to a valence description as a dimetallo-carbyne, M≡C–C≡M, as is found experimentally for $\{(^tBuO)_3W\}_2(\mu\text{-}C_2)$.[170] As the metal d-electron count increases and π-accepting supporting ligands become more likely to be encountered, more care is required to

establish the relative positions of the non-bonding δ orbitals with respect to the 3π level. For example, a bonding scheme for $\{W(OH)_3\}_2(\mu\text{-}C_2)$ has the HOMO derived from metal d_π (e_g) and C_2 π-orbitals (74 and 26%, respectively), while the LUMO is largely metal-centered (Fig. 9).[170]
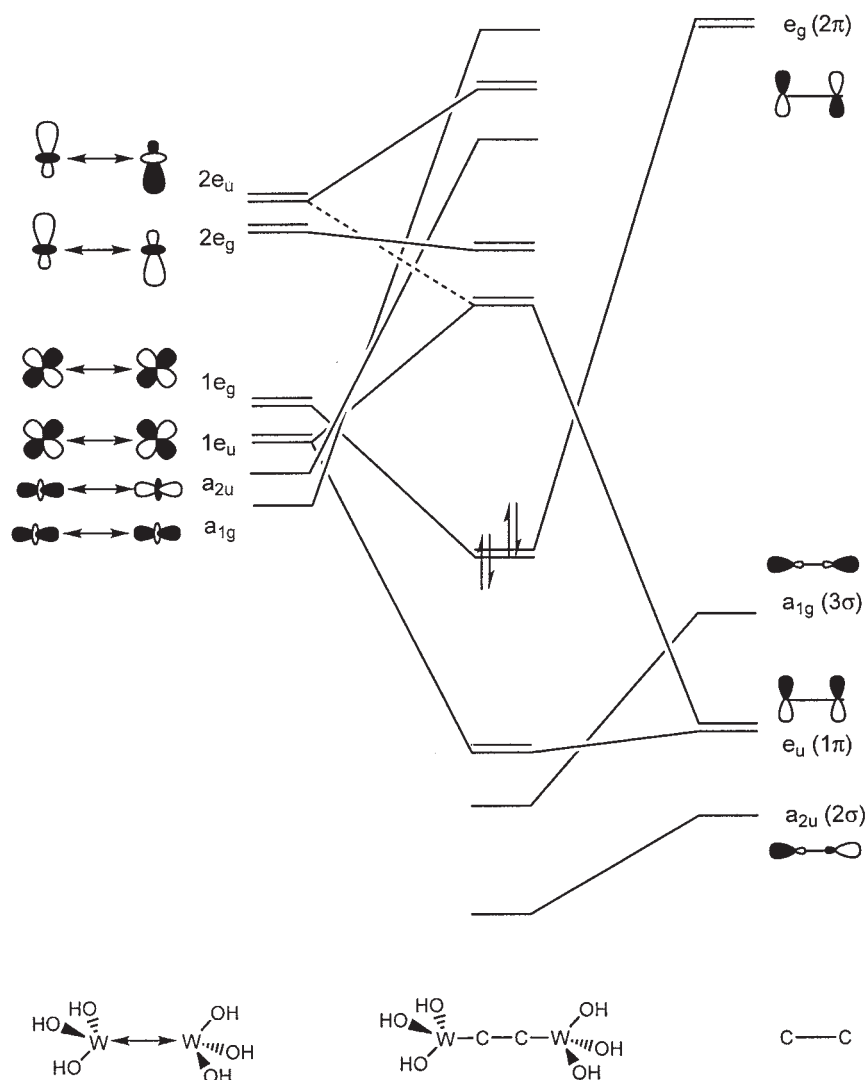
FIG. 9. Schematic MO diagram for $\{W(OH)_3\}_2(\mu\text{-}C_2)$ depicting the main interactions between the frontier orbitals of the two $W(OH)_3$ fragments and C_2. Adapted from Ref. 170.

For more electron-rich (low oxidation state) complexes, progressive occupation of the 3π levels, which are M–C antibonding and C–C bonding in nature, results in a shift in structure back through cumulenic forms towards the acetylenic substructure. The C_2 π^*-orbitals are well removed in energy from the metal d orbitals, and π-back bonding is therefore limited. Thus, the HOMOs of $\{Re(CO)_5\}_2(\mu$-C≡C) consist predominantly of the C≡C π-orbitals; no Re–C_2 back-bonding occurs because of the large separation (3.16 eV) from the π^*-orbital.[171] This precludes the observation of a second series of cumulenic and carbyne-like structures for the metals at the far right of the periodic table. On this basis it is possible to predict poly-yne-like structures (**L**) for metal fragments, such as $M(L)_2Cp$ (M = Fe, Ru, Os, L = CO, PR_3) and $Re(NO)(PPh_3)Cp^*$, which become more cumulenic (**M, N**) as the number of electrons available to fill the 3π levels is reduced.

As the carbon chain is extended, the energies of the occupied π-orbitals from the C_n fragment increase, while the energies of the $C(\pi^*)$-orbitals decrease dramatically. This shift of fragment orbital energies can play a significant role in tuning the composition and order of the resulting MOs.[396] This point is addressed in more detail below with reference to specific complexes.

Detailed DFT studies have been carried out on several C_4 complexes,[246,249,262] with the intention of understanding the electronic structures of these complexes and their redox-related analogues. The complex $\{MnI(dmpe)_2\}_2(\mu$-C≡CC≡C) (**93**), was found to have a triplet ground state[246] as predicted from the studies on the isoelectronic model compounds $\{Mn(CO)_2Cp\}_2(\mu$-C≡CC≡C)[396] and $\{MnI(PH_3)_4\}_2(\mu$-C≡CC≡ C).[246] Sequential oxidation of this compound serves to depopulate the 4π levels to give [**93**]$^+$ and [**93**]$^{2+}$ which possess more cumulenic structures, as is evidenced by the decreased ν(CC) frequencies and the trends in C–C bond lengths observed in their solid-state structures.

The isoelectronic complexes $\{Re(NO)(PPh_3)Cp^*\}_2(\mu$-C≡CC≡C) (**96/Ph**),[249] $\{Fe(dppe)Cp^*\}_2(\mu$-C≡CC≡C) (**107**)[258,270] and $\{Ru(PPh_3)(L)Cp\}_2$ $(\mu$-C≡CC≡C) (**109**)[262] all feature fully occupied, closed-shell singlet structures for their HOMOs. The experimental structures are in accord with this description, and display bond lengths consistent with a poly-yne-like structure. These complexes, and closely related phosphine derivatives, display two (Re), three (Fe) or four (Ru) 1-e oxidation processes.

While computations involving [**96**]$^+$ did not converge, the calculated structure of the dication is in good agreement with the experimentally observed cumulenic form. In terms of the simple Hückel model, double oxidation of **96** is consistent with the depopulation of the higher lying 4π level. In the case of the iron complex **107**, the first two oxidation processes resulted in an *increase* in the acetylenic character of the carbon chain and

the resulting dication $[\mathbf{107}]^{2+}$ was found to be diamagnetic at room temperature.[270] Two interpretations have been given for this point, which differ only in the fine detail of the explanation. Sgamellotti and his colleagues[396] have argued that the strongly electron donating dppe ligand destabilizes the metal d orbitals which form the 2δ MO, raising the level of this orbital relative to 4π to become the HOMO. In this scheme, the HOMO is thought to be derived from the metal orbitals which are δ-bonding with respect to the carbon fragment. The first two oxidation processes of **107** depopulate the δ orbital(s) and do not affect the gross bonding picture associated with the C_4 portion of the molecule. Halet and colleagues have performed DFT calculations on $\{Fe(PH_3)_2Cp\}_2(\mu\text{-}C\equiv CC\equiv C)$ and found the HOMO to be delocalized over the six atom Fe–C_4–Fe chain, but with a significant metallic contribution, and suggest that it is for this reason that depopulation of the HOMO does not affect the structure of the carbon bridge to a great extent.[262] Replacement of the phosphine ligands by carbonyl groups was calculated to decrease the interactions between the stabilized metal orbitals and the carbon π-orbitals, leading to increased carbon content in the HOMO and an overall decrease in the HOMO energy. The net result is that the oxidation of such carbonyl complexes should be less thermodynamically favorable than their phosphine-substituted analogues, a result which is entirely in agreement with experiment.[262]

In either event, the decrease in the metal d orbital energy expected to accompany such metal-centered oxidations would limit the metal contribution to the HOMO in the resulting dication $[\mathbf{107}]^{2+}$, which would be anticipated to display considerable carbon character. Indeed, the third oxidation of **107** gives the open-shell cation $[\mathbf{107}]^{3+}$, for which experimental evidence strongly supports a predominantly carbon-centered radical structure.[258]

Variable temperature magnetic susceptibility measurements have been carried out on $[\mathbf{107}]^{2+}$, with μ_{eff} decreasing from 2.8 μ_B to 1.1 μ_B as temperatures were lowered from 300 to 5 K.[397] The temperature dependence of the measurement, and the negative J parameter (-18.2 cm^{-1}) demonstrates antiferromagnetic coupling between the metal centers, and the dication is ESR-silent at room temperature. The energy gap between this singlet state and the corresponding triplet ($\Delta E_{ST} = -J$) is sufficiently small that the triplet can become thermally populated at liquid nitrogen temperatures.

As the ruthenium complex **109** is oxidized the carbon bridge becomes cumulenic, more in keeping with the Re complexes **96** than with the iron complex **107**. As indicated above, this has been attributed to a greater interaction between the higher lying metal d orbitals of the heavier metals with the filled carbon π-orbitals. The cumulenic dication is observed to be

diamagnetic and in agreement with this observation the $(35a')^2(22a')^0$ singlet state was found to be energetically favored over the $(35a')^1(22a')^1$ triplet by 0.1 eV. Hirschfeld analysis reveals a significant portion of the electron lost in the third oxidation originates from the carbon chain, much as was found for the iron series. For the electrochemically detected tetracation, unique to the Ru series, the singlet state $(21a'')^2(35a')^0$ was calculated to be significantly more stable than the corresponding triplet.[262]

Lengthening of the carbon chain results in decreased mixing of the metal and carbon orbitals associated with the HOMO of $\{ML_x\}_2\{\mu\text{-}(C{\equiv}C)_m\}$ complexes. This is to be expected on the basis of even a simple analysis as the C_n fragment π-orbitals must be partitioned over a greater number of atoms, decreasing the contribution at the terminal centers. Thus in the case of $\{Re(NO)(PPh_3)Cp^*\}_2\{\mu\text{-}(C{\equiv}C)_{10}\}$, the longest poly-yndiyl complex isolated to date, only a single, possibly two-electron, oxidation event is observed. When the trends in oxidation potentials within the series $m = 2\text{--}10$, which become thermodynamically less favorable with increasing chain length, are considered, it is reasonable to suggest that in this case the HOMO has considerable metal character. An electronic structure with predominantly $(C{\equiv}C)$ π-character would result in an increase in the HOMO energy level and a decrease in the observed oxidation potentials. In light of this argument, the most intense band in the UV–vis spectrum of these species, not the lowest energy band, has been assigned to the $(C{\equiv}C)$ $\pi \rightarrow \pi^*$ transition.

The electronic structures of $\{Ru(dHpe)Cp^*\}_2\{\mu\text{-}(C{\equiv}C)_4\}$ and $Hg\{C{\equiv}CC{\equiv}C[Ru(dHpe)Cp^*]\}_2$ $(dHpe = H_2PCH_2CH_2PH_2)$ were compared to examine the unusual bending found at C_a in the solid-state structure of the mercury complex.[298] Whereas electronic communication between the two Ru termini in the C_8 complex was little different from that in the analogous C_4 derivative, introduction of the Hg atom resulted in a significantly higher ionization potential. The HOMO has π-character and is non-bonding between the carbon and Hg atoms, i.e., there is no contribution to this orbital from the Hg atom. This result has significant implications if these complexes are considered as models for molecular wires, communication between the end-caps being prevented by insertion of the Group 12 atom into the carbon chain.

2. Odd-Numbered C_n Chains

As has been described above, metal complexes containing odd-numbered carbon chains are relatively rare in comparison with their even-numbered analogues and the data available suggest that the kinetic stability of these odd-carbon systems decreases more rapidly with increasing chain length

than is the case for the even-numbered examples. Valence forms **C** and **D** can be drawn without invoking radical formalisms. The Gladysz group have reported DFT analyses of a series of model complexes closely related to several isolated C_n (n odd) complexes (M = Re, Mn, W), while subsequent work by Belanzoni, Re and Sgamellotti has considered a set of hypothetical materials with Cr, Fe, and Mn using both DFT and qualitative Hückel methods.

It is convenient to consider first the Hückel results as an extension of the bonding schemes described for even-chain C_n complexes. The M–C_n–M σ framework is formed by overlap of the d_{z^2} and C(sp) orbitals from the terminal carbons, together with C(sp)–C(sp) overlaps to give the carbon skeleton. Provided the M(d_π) and C(p_π) orbitals are of comparable energy, the M–C_n–M π-system is described in terms of two sets of orthogonal $(n + 2)$-center MO's obtained from linear combinations of the M(d_{xz}) with C(p_x) and M(d_{yz}) with C(p_y). These orbitals can be designated 1π- $(n + 2)$π, and are illustrated in Fig. 10 for MC_3M.[390] The δ orbitals obtained from the bonding and anti-bonding combinations of d_{xy} and $d_{x^2-y^2}$ complete the π–δ framework. As has been stated previously, the exact positioning of these δ levels relative to the π levels is determined by the nature of the supporting ligands and the symmetry of the resulting metal-ligand fragment. For pseudo-octahedral fragments, the $d_{x^2-y^2}$ levels are destabilized by σ-interactions with the equatorial ligands and are well removed from the π framework, leaving only 1δ and 2δ near the 3π level.

For metal complexes containing $M(CO)_2Cp$ [M = Cr (d^5), Mn (d^6), Fe (d^7)] groups, there will be 14, 16, or 18 electrons, respectively, occupying the levels illustrated in Fig. 10, and cumulenic structures are predicted (the 3π level is essentially anti-bonding). Higher level DFT calculations suggest that singlet states are always lower in energy than the corresponding triplet states for the series $\{Cp(CO)_2M\}(\mu-C_n)\{M'(CO)_2Cp\}$ ($n = 3, 5, 7$).

DFT studies broadly support the conclusions reached from the Hückel work. Geometry optimization of the model cation $[\{Cp(NO)(PH_3)Re\}(\mu-C_3)\{Mn(CO)_2Cp\}]^+$ is in good agreement with the experimentally determined structure of the cation in $[\{Cp^*(NO)(PPh_3)Re\}(\mu-C_3)\{Mn(CO)_2Cp\}]$ BF_4.[391] The computed and observed structures both display a *cis* relationship between the Re–P and Mn–Cp centroid vectors, as a result of the overlap between the occupied metal fragment frontier orbitals with the orthogonal π-bonding orbitals at opposite ends of the =C=C=C= bridge. The resulting HOMO closely resembles the 3π level shown in Fig. 10. In comparison with symmetrical model complexes M–C_3–M , the Re–C_3–Mn complex displays longer Re–C and shorter Mn–C bond lengths, and natural bond order (NBO) and charge analyses indicate that these variations arise from electrostatic effects. The orbital coefficients indicate limited interaction
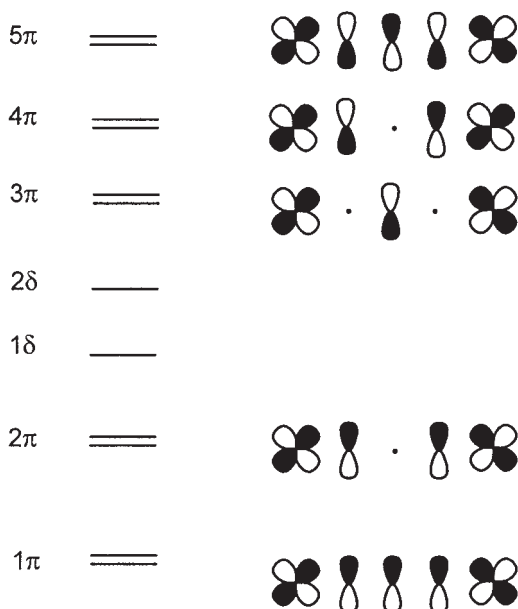
FIG. 10. Energy diagram for the π and δ frontier orbitals of an {L$_x$M}C$_3${ML$_x$} complex with pseudo-octahedral metal coordination spheres. Adapted from Ref. 390.

between the occupied Re(d$_\pi$) and the carbon chain, which together with the NBO data and the observed conformation suggests that the ground state is best described in terms of a dominant contribution from Re$^+$–C=C= C=Mn, with a highly polarized Re–C bond, and a cumulenic resonance form Re$^+$=C=C=C=Mn. The longer chain complexes Re$^+$=C= (C=C)$_n$=Mn behave similarly.[391] Exchange of the Mn(CO)$_2$Cp moiety for the more π-donating Re(CO)$_2$Cp fragment gave {Cp(NO)(PH$_3$)Re} (μ-C$_3$){Re(CO)$_2$Cp} for which geometry optimization and NBO analysis indicates a dominant {Cp(NO)(PH$_3$)Re}–C≡CC≡{Re$^+$(CO)$_2$Cp} resonance form. In contrast, NBO analyses of the symmetrical complexes Cp(CO)$_2$MC$_3$M(CO)$_2$Cp show more symmetrical cumulenic linkages.

The charge-neutral C$_3$ model compound {Cp(NO)(PH$_3$)Re}(μ-C$_3$){W (OMe)$_3$} was used to model the known complex {Cp*(NO)(PPh$_3$)Re} (μ-C$_3$){W(OBu^t)$_3$}.[391] The calculated geometrical parameters [Re–C 2.021 Å; W≡C 1.787 Å; ReC≡C 1.250 Å; C–CW 1.383 Å] are in good agreement with both calculated and experimental geometries of the monometallic reference compounds Re(C≡CC≡CR)(NO)(PPh$_3$)Cp* (R = H, Me) and W(≡CR)(OMe)$_3$ (R = H, Me, C≡CH, C≡CMe). The NBO results also indicate dominant Re–C single and W≡C triple bond character, and there is some evidence for ground-state charge transfer from Re to W.

3. Polymers

The electronic structures of several hypothetical $\{[ML_x]–C_n\}_y$ polymers have been considered.[388,392] In general, the band structure of these materials is derived from orbitals similar to those considered for the discrete molecular species $\{L_xM\}–C_n–\{ML_x\}$. Similar trends in variation of valence bond structure with metal d count are predicted, with the possibility of half-filled bands opening the way for Peierls distortions to give closed systems with greater band-gaps at the Fermi level. It is suggested that by raising the energy of the metal d_π orbitals through a judicious choice of metal–ligand fragments, a greater mixing between the filled metal d and empty carbon π^*-orbitals may be engineered.[388]

A collaborative study between the Bredas, Friend, and Lewis groups have examined the extent to which the Pt metal orbitals are involved in the conjugated backbone of polymers $Cl–\{[Pt(PMe_3)_2]–(C≡C)_m\}_x–PtCl(PMe_3)_2$ ($m = 2, 3; x = 1, 2, 3, 4, \infty$), and the effect of chain length on the energy of the lowest energy optical transition using EHMO methods.[393] The HOMO is derived from mixing of the d_π and C_π orbitals, while the LUMO is similarly comprised of empty metal and carbon orbitals. The calculated band gap decreases with increasing number of repeat units, although not to the same extent as found for purely organic poly-ynes $H–(C≡C)_m–H$, due to the increased stabilization of the LUMO and providing an indication of a degree of conjugation through the metal center. The smaller variation in band gap with number of repeat units in the longer chain systems points to a more localized electronic structure between the metal centers.

V

REACTIVITY

This section summarizes the reactions of metal supported C_n fragments towards non-metal based reagents, including addition of electrophiles and nucleophiles, cycloadditions, and insertions. Simple ligand substitution reactions, and modifications of the supporting metal fragment which give derivatives without modification of the C_n moiety have been detailed in the relevant parts of Section II. Reactions of these complexes with metallic reagents are summarized in Sections VI–VIII.

A. *Addition of Electrophiles*

Reactions of $\{Re(CO)_5\}_2(\mu\text{-}C≡C)$ (**51/Re**) with $HBF_4 \cdot Et_2O$ or $[Me_3O]^+$ give $[\{Re(CO)_5\}_2(\mu\text{-}\eta^1:\eta^2\text{-}C_2R)]^+$ (R = H, Me, respectively), although

reactions with HX (X = Cl, OTf) afford ReX(CO)$_5$.[175,176] The related complex [{Ru(CO)$_2$Cp^{Me}}$_2$(μ-η^1 : η^2-C$_2$H)]$^+$ is obtained by protonation of {Ru(CO)$_2$Cp^{Me}}$_2$(μ-C≡C), in a reaction reversed by NEt$_3$.[105]

The majority of C$_2$ complexes containing more than two metal centers are clusters with significant M–M bonding interactions (Section IX). In contrast, protonation of the Cp complex{Ru(CO)$_2$Cp}$_2$(μ-C≡C) with HBF$_4$·OEt$_2$ affords the orange trinuclear cation [{Ru(CO)$_2$Cp}$_3$(μ-C≡C)]$^+$ (189) in good yield, in which an Ru(CO)$_2$Cp fragment is η^2-bonded to a {Ru(CO)$_2$Cp}$_2$(μ-C≡C) ligand.[418] An alternative route to this cation is from the reaction of [Ag$_3${(C$_2$)Ru(CO)$_2$Cp′}$_3$]$^{3+}$ (Section VI) with RuCl(CO)$_2$Cp′ (Cp′ = Cp, Cp^{Me}). While the C–C distance [1.206(9) Å] is similar to that found in {Ru(CO)$_2$Cp}$_2$(μ-C≡C) [1.222(9) Å], the bend-back angles of the Ru(CO)$_2$Cp fragments are 152.5(4), 155.2(5)°. In solution, a facile fluxional process, even at −80 °C, renders all Cp groups equivalent, one possible process being the rotation of the C$_2$ unit within the Ru$_3$ triangle. Similar chemistry has been found for [{Fe(CO)$_2$Cp*}$_2$(μ-C≡CH)]$^+$.[35,181]

(189)
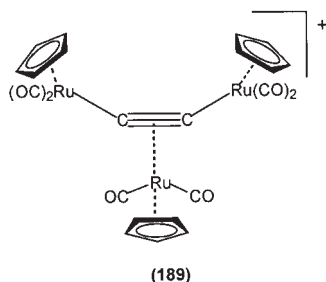
The complexes {Cp*(PP)Fe}(μ-C≡CC≡C){Fe(CO)$_2$Cp*} (PP = dppe 100, dippe 102) are protonated (HBF$_4$·Et$_2$O) or methylated (MeOTf) to give [{Cp*(PP)Fe}{μ-C=C=C=CR[Fe(CO)$_2$Cp*]}]BF$_4$ (190a–d) (R = H, Me), which can be isolated as moderately stable powders (Scheme 43). The UV–vis spectra of these deep purple butatrienylidene complexes have characteristic absorptions between 527 and 546 nm (ε ca. 15,000).[259] The absence of ν(CC) bands between 1500 and 1650 cm^{-1} excludes the ethynylvinylidene formulation, and bands at 1952, 1776 (dppe/H), 1945 (dippe/H), 1942, 1882, 1830 (dppe/Me), and 1946 cm^{-1} (dippe/Me) were tentatively assigned to ν(CC) modes. In ^{13}C NMR spectra, resonances beween 250 and 265 ppm [^{2}J(CP) ca. 35 Hz] were assigned to the carbon adjacent the Fe(PP)Cp* moiety. The other carbon resonances were assigned on the basis of J(CH) and the assumption that the chemical shifts will move upfield along the chain. The Mössbauer spectra contained two quadrupole doublets, with δ values similar to those shown by Fp*Me or allenylidene
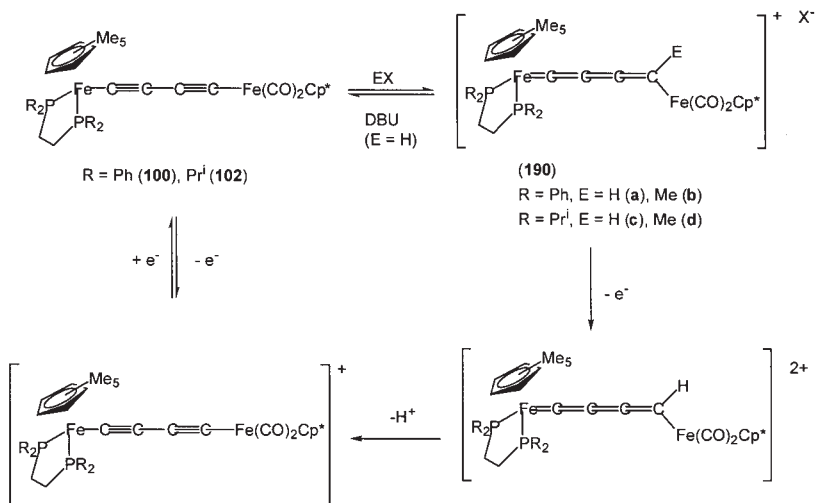
SCHEME 43

complexes containing the Fe(PP)Cp* group, which support the proposed regiochemistry of the electrophilic addition. The complex [{Cp*(dppe)Fe}{μ-C=C=C=CH[Fe(CO)₂Cp*]}]BF₄ (190a) was deprotonated by dbu (thf, −80 °C), and even partially deprotonated by water. The facile deprotonation leads to some complications in the electrochemical response of the secondary butatrienylidene complexes, which were rationalized in terms of Scheme 43. The tertiary butatrienylidene complexes display reversible one-electron oxidation processes (dppm + 0.40 V, dippe + 0.28 V), and an irreversible reduction in the case of the dppm complex at −1.13 V.[259]

B. Cycloaddition Reactions

Addition of $C_2(CN)_4$ (tcne) to {Ru(CO)₂Cp}₂(μ-C≡C) gives the buta-1,3-dien-2,3-diyl complex {Ru(CO)₂Cp}₂{μ-C[=C(CN)₂]C[=C(CN)₂]} (191).[398] With $C_2(CO_2Me)_2$, unusual coupling of both CO and the alkyne to the C₂ ligand gives Ru{η¹,η²-C(O)C(CO₂Me)=C(CO₂Me)C=C[Ru(CO)₂Cp]}(CO)Cp (192).

(191)
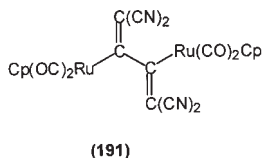
Cyclo-addition of tcne to {PtCl(PR$_3$)$_2$}$_2$(μ-C≡C) (R = Me, Et) gives yellow s-cis-{PtCl(PR$_3$)$_2$}$_2${μ-C[=C(CN)$_2$]C[=C(CN)$_2$]} (193), in which the torsion angle between the two C=C moieties is 55(1)°. In both cases, a green charge-transfer complex is the initial product, changing in hours to the product(s). An unobserved cyclobutenyl complex is probably formed which undergoes ring-opening to the kinetically favored s-cis product. The PEt$_3$ complex is accompanied by the s-trans isomer, a slow equilibrium between the two isomers occurring by slow rotation about the C–C single bond, as suggested by NMR data.[399,400] This is the first example of the s-trans geometry found for a tetracyanodienyl ligand. At higher temperatures (ca. 106 °C in C$_2$D$_2$Cl$_4$), ^{31}P NMR spectra of the PMe$_3$ complex show signals assigned to the s-trans isomer. Although the s-cis form is thermodynamically more stable, steric hindrance between the Pt(PEt$_3$)$_2$ groups in the cis isomer favors formation of the s-trans form in this case.

(192)

(193)
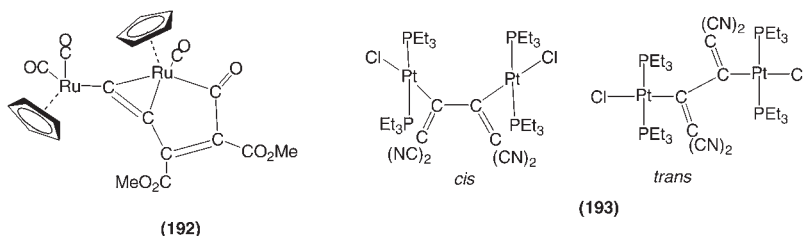
The heterometallic diyndiyl complexes {Cp(CO)$_3$W}(μ-C≡CC≡C){M(CO)(PPh$_3$)$_2$} (M = Rh, Ir) readily add tcne not to the C$_4$ moiety, but to the electron-deficient Group 9 metal center to give the simple adducts {Cp(CO)$_3$W}(μ-C≡CC≡C){M(CO)[η^2-C$_2$(CN)$_4$](PPh$_3$)$_2$}, but attempts to add a second equivalent of tcne were unsuccessful.[295] Nevertheless, addition of tcne to poly-yndiyl ligands occurs readily, as evidenced by the facile reactions with {Cp(CO)$_3$W}(μ-C≡CC≡C){Ru(PPh$_3$)$_2$Cp}.[261,401,402] The heterometallic diyndiyl complex afforded {Cp(CO)$_3$W}{μ-C[=C(CN)$_2$]C[=(CN)$_2$]C≡C}{Ru(PPh$_3$)$_2$Cp}, in which addition has occurred at the least hindered triple bond adjacent the W center. In the case of the homonuclear Ru-butadiyndiyl 103, cycloaddition and ring opening is followed by intramolecular displacement of a PPh$_3$ ligand to give an η^3-cyanocarbon ligand (194), which converts to the crystallographically characterized tetrametallic dimer 195 during preparative TLC (Scheme 44).[402]

Addition of tcne to the central C≡C moiety in {Ru(PPh$_3$)$_2$Cp}$_2${μ-(C≡C)$_3$} affords the dark-red symmetrical product {Ru(PPh$_3$)$_2$Cp}$_2${μ-C≡CC{=C(CN)$_2$}C{=C(CN)$_2$}C≡C} through a similar sequence of
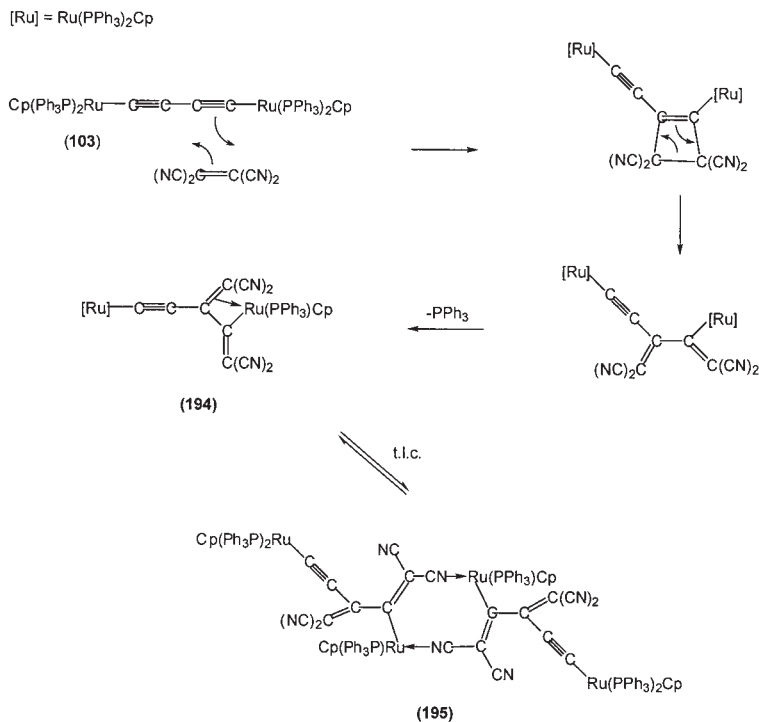
SCHEME 44

cycloaddition and subsequent ring-opening reactions. In this case, the stiff Ru–C≡C unit prevents the intramolecular displacement of a phosphine ligand, and the steric bulk of the end-capping Ru(PPh$_3$)$_2$Cp moieties prevent intramolecular reactions.[261] While only one tcne moiety adds to the triyne, the longer chain in {Ru(PPh$_3$)$_2$Cp}$_2${μ-(C≡C)$_4$} permits addition of two tcne units to give the red-brown bis-adduct, containing the first example of an octacyano ligand in **196**.[403] Addition to the inner C≡C triple bonds is dictated by steric considerations, although addition to triple bonds adjacent the metal center has been observed in related acetylide complexes.[404]

C. *Insertion into the M–C(sp) Bond*

The orange-yellow η^2-iminoacyl derivative ZrClCp$_2${η^2-Bu^{t}N=CC≡C[Ru(PMe$_3$)$_2$Cp]} (**197**) is formed by a rare insertion of Bu^{t}NC into the Zr–C bond of {ZrClCp$_2$}C≡C{Ru(PMe$_3$)$_2$Cp}, for which a small contribution from the zwitterionic form is proposed.[219]

(196)

(197)
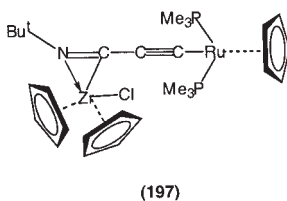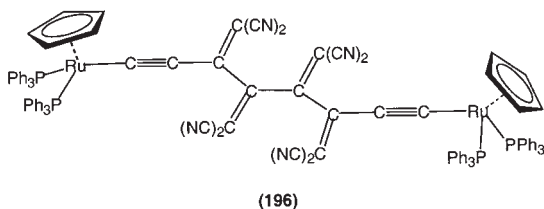
A selective double insertion of ArNC (Ar = Ph, $C_6H_4NO_2$-4) into one of the Pd–C(sp) bonds of {*trans*-PdX(PR$_3$)$_2$}$_2$(μ-C≡C) (X = Cl, I; R = Et, Bu) gives {*trans*-PdX(PR$_3$)$_2$}C≡CC(=NAr)C(=NAr){*trans*-PdX(PR$_3$)$_2$} (**198**; X = Cl, R = Et, Ar = Ph, $C_6H_4NO_2$-4, xy; X = I, R = Et, Ar = Ph; X = Cl, R = Bu, Ar = Ph, Scheme 45).[189,405] In the presence of KPF$_6$, the cationic intermediate [{Pd(CNPh)(PEt$_3$)$_2$}$_2$(μ-C≡C)]PF$_6$ was obtained; with [NEt$_4$]X (X = Cl, Br, I), insertion of PhNC gives {*trans*-PdX(PEt$_3$)$_2$}C≡CC(=NPh)C(=NPh){*trans*-PdX(PEt$_3$)$_2$}. The heterometallic complex {*trans*-PdCl(PEt$_3$)$_2$}C≡C{*trans*-PtCl(PEt$_3$)$_2$} (**73**) also undergoes specific double insertion of ArNC (Ar = Ph, tol, $C_6H_4NO_2$-4) into the Pd–C(sp) bond (refluxing thf). Alkyl isocyanides (R = Bu^t, Cy) do not insert.

In the presence of free PR$_3$ (R = Et, Bu), insertion of PhNC occurs into each Pd–C(sp) bond of {*trans*-PdCl(PR$_3$)$_2$}$_2$(μ-C≡C) to give the symmetrical product {*trans*-PdCl(PR$_3$)$_2$}$_2${μ-C(=NPh)C≡CC(=NPh)}; no polymerization occurs.[406,407] The cationic complex [{Pd(PR$_3$)$_3$}$_2${μ-C(=NPh)C≡CC(=NPh)}]Cl$_2$ could also be detected, suggesting the intermediate formation of [{PdCl(PR$_3$)$_2$}[C≡CC(=NPh)]{Pd(PR$_3$)$_3$}]Cl.

However, with an excess of isocyanide, oligomeric materials were obtained, e.g., with 10 equiv. of PhNC, yellow {PdCl(PEt$_3$)$_2$}{[C(=NAr)]$_n$}C≡C{*trans*-PtCl(PEt$_3$)$_2$} (**199**, $n \sim 10$, av. $M = 1850$) was formed (Scheme 46).[407,408] Similarly, 100 equiv. of PhNC gave a polymeric compound with $n \sim 100$. Other isocyanides ArNC (Ar = C_6H_4R'-4, R' = Bu, C_8H_{17}, NO$_2$, Me) behaved similarly, as did the PBu$_3$ complex, giving narrow molecular weight distributions, characteristic of living polymerization processes. Chain growth occurs on a cationic intermediate, similar to those isolated from stoichiometric reactions, with halide attack forming the termination step.
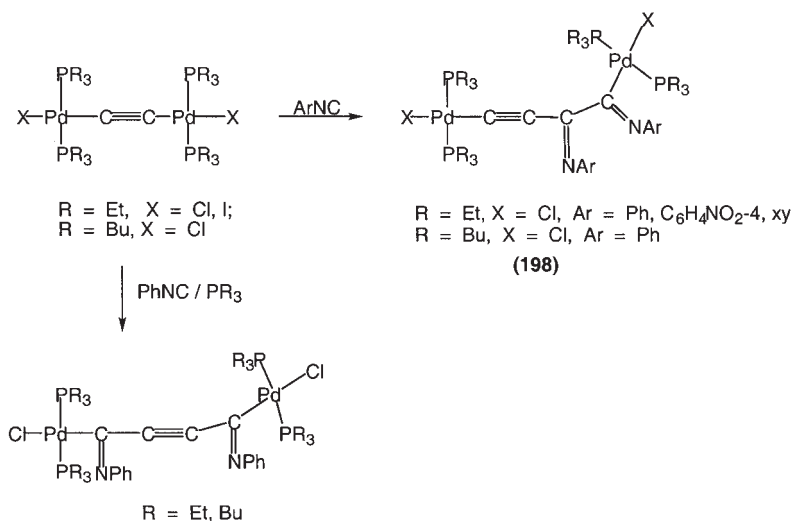
SCHEME 45
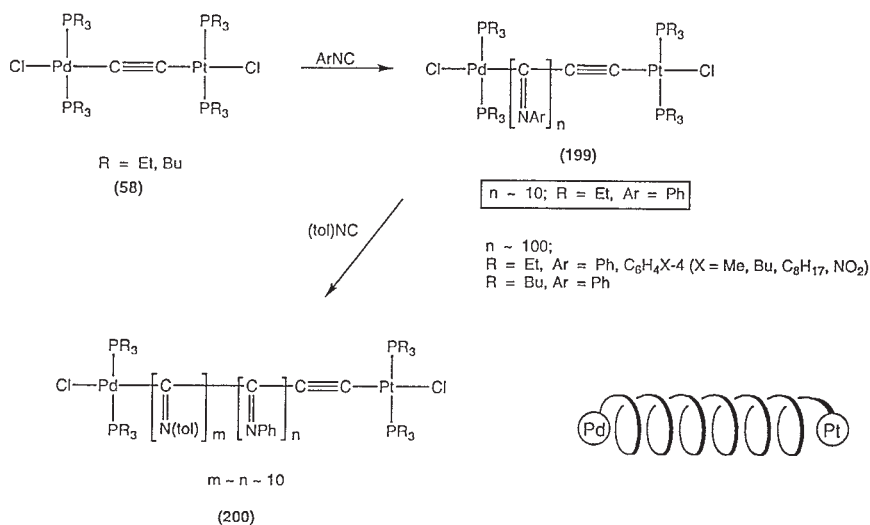
SCHEME 46

Further reactions include that of the bis-PhNC insertion product with an excess of PhNC to give the same polymer, and of the 10-oligomer of PhNC with tolNC to give block co-oligomers $\{PdCl(PEt_3)_2\}\{[C(=NPh)]_m[C(=Ntol)]_nC\equiv C\}\{trans\text{-}PtCl(PEt_3)_2\}$ (**200**, $m \sim n \sim 10$). Since the products still contain the active end-group $PdCl(PR_3)_2$, they are suitable for

preparing designed polymers with defined compositions, sequences, and molecular weights. Block co-polymers could be obtained when one polymer complex was used as initiator for the second isocyanide. However, the μ-butadiyndiyl complex {*trans*-PdCl(PBu$_3$)$_2$}$_2$(μ-C≡CC≡C) did not initiate polymerization, and even in the presence of a 100-fold excess of phenyl isocyanide only the single insertion complex (**201**) was obtained. The multiple, successive insertion of isocyanides into the Pd–C bond is therefore specific to the μ-ethynediyl complexes.

(**201**)

Many polyisocyanides have a helical structure. The Pd–Pt C$_2$ complex has been used to initiate living polymerization of chiral isocyanides. The products have helical chirality, the polymerization occurring with high screw-sense selectivity (Scheme 46). As found above, the chiral oligomers may also be used to initiate screw-sense selective polymerization of isocyanides with achiral but bulky groups; the single-hand helix is not preserved in polymerization of smaller isocyanides.[409,410] Thermodynamic control of the screw-sense occurs. A range of substituents has been employed: Ar* = (*L*)- and (*D*)-C$_6$H$_4$(CO$_2$men)-3 and -4, with different ratios from 1/10 to 1/200. Block co-polymers were prepared from various chiral oligomers and CNR' [R' = C$_6$H$_4$CO$_2$R-3 (R = Pr, Cy), C$_6$H$_4$CO$_2$Cy-4, C$_6$H$_3$(CO$_2$R)$_2$-3,5 (R = Pr, Bu, Cy)]. In all cases, products had narrow molecular weight distributions, in agreement with there being no significant differences in polymerization rates, and suggesting that the polymer backbone adopts the thermodynamically stable screw-sense.

D. *Thermal and Environmental Stability*

The majority of C$_n$ bridged complexes display impressive thermal stability. For example, the Re complexes up to **155/10** are stable in the solid-state, and it would seem that access to longer chains is precluded more by the instability of intermediates, particularly Re{(C≡C)$_6$H}(NO)(PPh$_3$)Cp* in the Re series[290] than any inherent instability of the dimetal products. Thermal decomposition of these reagents possibly involves initial inter-molecular cross-linking between chains, as found for 1,3-diynes,[411] to give polymeric materials containing C=C and C≡C units. However, it has

been noted that both $\{Au(PCy_3)\}_2\{\mu\text{-}(C{\equiv}C)_4\}$[315] and the expanded molecular square *cyclo*-$\{[Pt(dcpe)]C{\equiv}CC{\equiv}C[Pt(PBu_3)_2]C{\equiv}CC{\equiv}C\}_4$[284] are decomposed by halogenated solvents. In the case of the latter, $PtX_2(PP)$ [$PP = (PBu_3)_2$, dcpe; $X = Cl$, $C{\equiv}CC{\equiv}CH$] could be recovered. The selective cleavage of M–C bonds has been demonstrated for several polymeric materials containing Pt and Pd centers (see Section II.H).

VI

REACTIONS OF COMPLEXES CONTAINING LINEAR C_n LIGANDS WITH METAL SUBSTRATES

A. $\{ML_x\}_2(\mu\text{-}C_2)$

The reactions of alkynes with a variety of transition metal substrates have been a rich field of endeavor since the early days of organometallic chemistry. Attachment of ML_x residues to alkynes by M–C σ-bonds generally results in activation of the alkynyl fragment, since C_α becomes electron deficient and C_β becomes an electron-rich center. However, the general lack of metal-alkynyl back-bonding (see above) results in little change to the π bonding power of the $C{\equiv}C$ triple bond. Consequently, it is no surprise to find that ethynediyl complexes also take part in π-complex formation. For example, the ready reactions of alkynes with $Co_2(CO)_8$ to give C_2Co_2 derivatives are often paralleled by the C_2 complexes. However, the proximity of the σ-bonded metal center often results in metal–metal bond formation and construction of metal clusters, in which the C_2 ligand is attached to several metal atoms, in the process donating up to eight electrons (see Section IX.D). As demonstrated below, the C_2 complexes are now widely utilized as synthons for building clusters.

A survey of the reactions of C_2 complexes with other metal-containing fragments is conveniently organized in terms of the metal reagents by Group.

1. $M\{\eta^2\text{-}C_2(SiMe_3)_2\}(L)Cp_2$ ($M = Ti$, $L = -$; $M = Zr$, $L = thf$)

Reactions of $\{Ru(CO)_2Cp'\}_2(\mu\text{-}C{\equiv}C)$ ($Cp' = Cp$, Cp^{Me}) with $M\{\eta^2\text{-}C_2(SiMe_3)_2\}(L)Cp_2$ ($M = Ti$, $L = -$; $M = Zr$, $L = thf$)[121,154,155] gave **202**, in which the C_2 ligand is attached via an unsymmetrical π bond to the Group 14 element and one of the $Ru \cdots M$ vectors is bridged by a CO group. Under CO, the Ti derivative gives $Ti(CO)_2Cp_2$ and the C_2 complex, while with HCl, the binuclear complex $RuTi\{\mu\text{-}\eta^1:\eta^2\text{-}CHMe(C_5H_4)\}Cl_2(CO)_2$ $CpCp^{Me}$ (**203**) is obtained.[105]

2. $Fe_2(CO)_9$

Addition of $Fe_2(CO)_9$ to $\{Re(CO)_5\}_2(\mu\text{-}C\equiv C)$ affords orange-red $FeRe\{\mu\text{-}\eta^1_{Re}:\eta^2_{Fe}\text{-}C_2[Re(CO)_5]\}(\mu\text{-}CO)(CO)_7$ (**204**) with a structure related to that of $[FeRe(\mu\text{-}\eta^1:\eta^2\text{-}C_2Ph)(CO)_7Cp]^+$; the μ-CO group is semi-bridging to Re.[412,413]

(202) M = Ti, Zr

(203)

(204)
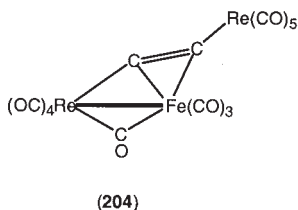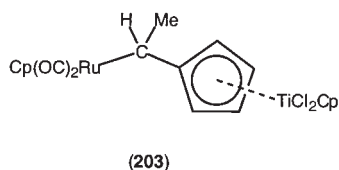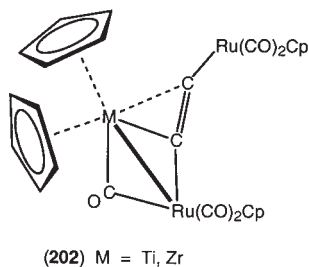
3. $Co_2(CO)_8$

The ready reactions of alkynes with $Co_2(CO)_8$ to give C_2Co_2 derivatives are paralleled by the C_2 complexes, although subsequent Co–M bond formation usually occurs and simple $Co_2(CO)_6$ adducts have not yet been reported.

4. $\{Ni(\mu\text{-}CO)Cp\}_2$

Alkynes react with $\{Ni(\mu\text{-}CO)Cp\}_2$ to give dimetallatetrahedrane complexes containing the C_2Ni_2 core. However, only $FeNi\,(\mu\text{-}CO)_2(CO)CpCp^*$ is obtained from this reagent and $\{Fe(CO)_2Cp^*\}_2(\mu\text{-}C\equiv C)$, the fate of the C_2 ligand being unknown.[414]

5. Pt Complexes

The reaction between $W_2(OBu^t)_6$ and $trans$-$Pt(C\equiv CH)_2(PMe_2Ph)_2$ gives $trans$-$Pt(C\equiv CH)\{C_2[W_2(OBu^t)_5]\}(PMe_2Ph)_2$, $trans$-$Pt\{C_2[W_2(OBu^t)_5]\}_2$ $(PMe_2Ph)_2$ (**205**), and $(Bu^tO)_3\equiv CC\equiv W(OBu^t)_3$.[415] Similar products containing OPr^i groups were characterized by NMR methods. The C_2 unit is σ-bonded to the Pt and attached to the W_2 moiety by an $\eta^1:\eta^2$ interaction, with a C–C distance of 1.336(13) Å. ^{13}C-Labeled samples were used to

assign the C_2 resonances at δ 235.2 and 302.1, and at 233.9 and 302.0 [^1J(CPt) 802, 801; ^2J(CPt) 78, 76, ^1J(CW) 132, 133] for C(1) and C(2) in the mono- and bis-C_2 complexes, respectively. Complex **205** decomposes in water, O_2, I_2, or BCl_3; with CO, stepwise addition to form (probably) *trans*-Pt{C_2[W_2(OBu^t)$_5$]}{C_2[W_2(μ-CO)(CO)$_5$]}(PMe$_2$Ph)$_2$ and *trans*-Pt{C_2 [W_2(μ-CO)(CO)$_5$]}$_2$(PMe$_2$Ph)$_2$ occurs.

In contrast to the reaction with Fe_2(CO)$_9$, that between {Re(CO)$_5$}$_2$(μ-C≡C) and Pt(η-C_2H_4)(PPh$_3$)$_2$ affords yellow PtRe{μ-η^1_{Pt} : η^2_{Re}-C_2[Re(CO)$_4$ (PPh$_3$)]}(CO)$_5$(PPh$_3$) (**206**) in which the C_2 unit is σ-bonded to Pt and Re; Re–C(sp) bond cleavage and exchange of CO and PPh$_3$ has occurred between Re and Pt.[413]

(205)   **(206)**
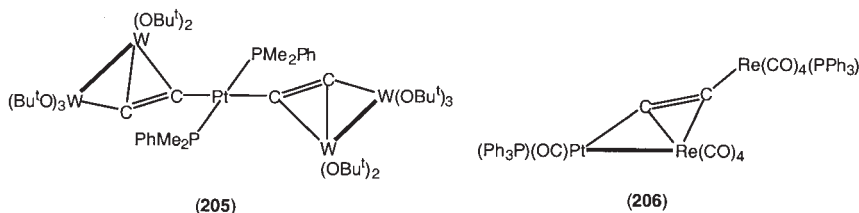
6. Group 11 Precursors

A detailed study of the reactions of {Re(CO)$_5$}$_2$(μ-C≡C) with Group 11 complexes shows that it behaves as a normal alkyne. With CuCl, bright red {Cu(μ-Cl)[η^2-C_2{Re(CO)$_5$}$_2$]}$_2$ (**207**) is formed, which decomposes readily to ReCl(CO)$_5$ on attempted recrystallization.[416] With [Cu(NCMe)$_4$]$^+$, the yellow dimetallatetrahedrane [Cu$_2${μ-η^2-C_2[Re(CO)$_5$]$_2$}(NCMe)$_4$]$^{2+}$ (**208**) is obtained, probably being formed via dimerization of an unisolated [Cu{η^2-C_2[Re(CO)$_5$]$_2$}(NCMe)$_2$]$^+$ intermediate with concomitant loss of MeCN. In this compound, which is similar to the well-known alkyne-Co_2 derivatives, the C–C bond is 1.2(3) Å, Cu–Cu 2.786(5) Å. Addition of water results in formation of the μ-O_2PF_2 derivative Cu_4{μ-C_2[Re(CO)$_5$]$_2$}$_2$(μ-O_2PF_2)$_4$ (**209**) with a structure similar to that of Cu_4{μ-C_2(SiMe$_3$)$_2$}$_2$(μ-O_2CMe)$_4$.[417] If a 1/2 ratio of reactants is used, [Cu{η^2-C_2[Re(CO)$_5$]$_2$}$_2$]$^+$ is formed.

Similar 1/2 silver(I) derivatives were obtained from AgBF$_4$ or AgOTf; an unstable intermediate formed with AgSbF$_6$ is thought to be [Ag$_2${μ-η^2-C_2[Re(CO)$_5$]$_2$}(thf)$_4$]$^{2+}$, but it rapidly decomposes to the η^2-alkyne complex. In thf, the triflate gives a 1/2 adduct, possibly with a structure related to that of **209**. All materials decompose to silver on standing. Related compounds have been obtained from {Re(CO)$_5$}$_2$(μ-C≡C) and Au$^+$ cations, further reaction with PPh$_3$ affording [Au(PPh$_3$){η^2-C_2[Re(CO)$_5$]$_2$}]$^+$ (**210**).

(207)   **(208)**
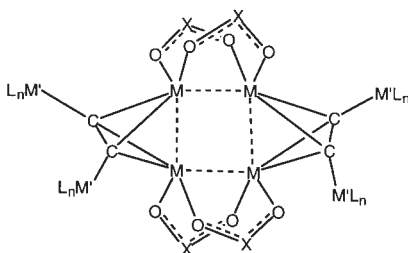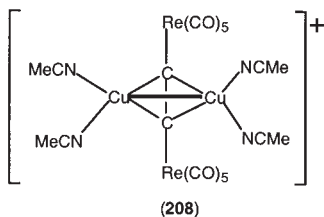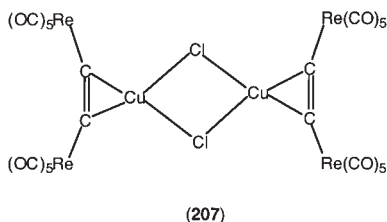
	(209)	(216)
M	Cu	Ag
X	PF_2	$C\text{-}CF_3$
M'L_n	$Re(CO)_5$	$Ru(CO)_2Cp$

With $[Au(PPh_3)]^+$, an equilibrium mixture of **210** with $[Au(PPh_3)_2]^+$ and $[Au\{\mu\text{-}\eta^2\text{-}C_2[Re(CO)_5]_2\}_2]^+$ is formed, while the latter was obtained pure from $[Au(SMe_2)]^+$.[416]

Reactions of $\{Ru(CO)_2Cp\}_2(\mu\text{-}C\equiv C)$ with CuCl give the chloro-bridged polymer $\{[Ru(CO)_2Cp]_2(\mu\text{-}C\equiv C)Cu(\mu\text{-}Cl)\}_n$ **(211)**, while $[Cu\{\eta^2\text{-}C_2[Ru(CO)_2Cp]_2\}_2]^+$ **(212)** and $[Cu_3\{C_2[Ru(CO)_2Cp]_2\}_3]^{3+}$ **(213)** are formed with $[Cu(NCMe)_4]^+$.[105] In solution, NMR spectra indicate that the Cp′ groups are equivalent and show only small shifts (ca. 15 ppm) for the resonances of the C_2 units.

Extensive studies of the reactions of $\{Ru(CO)_2Cp'\}_2(\mu\text{-}C\equiv C)$ (Cp′ = Cp, Cp^{Me}) with silver(I) cation have been made. If non-coordinating anions are present, cationic adducts $[Ag_3\{[Ru(CO)_2Cp']_2(\mu\text{-}C_2)\}_3]^{3+}$ **(214)** are obtained, in which the $\{Ru(CO)_2Cp'\}_2(\mu\text{-}C\equiv C)$ units are attached to the Ag^+ cations in either $\mu\text{-}\eta^1:\eta^1$ or $\mu\text{-}\eta^2:\eta^2$ modes.[105,418] A ^{1}H NMR study established that complexes with 1/2, 1/1, and 2/1 Ag^+/Ru_2 compositions are formed sequentially, and reactions with the appropriate stoichiometry enabled $[Ag\{[Ru(CO)_2Cp']_2(\mu\text{-}C_2)\}_2]^+$ **(215)** to be isolated. With $CF_3CO_2^-$ as counter-ion, complexes $Ag_4\{[Ru(CO)_2Cp']_2(\mu\text{-}C_2)\}_2(\mu\text{-}O_2CCF_3)_4$ **(216)** were obtained, with structures probably similar to those of the Cu–Re compounds above.

7. Other Routes

A by-product from the preparation of $\{Re(CO)_5\}_2(\mu\text{-}C\equiv C)$ is $\{(OC)_5Re\}(\mu\text{-}\eta^1:\eta^1:\eta^2\text{-}C_2)\{Re(CO)_4ReH(CO)_4\}$ **(217)**, which is fluxional
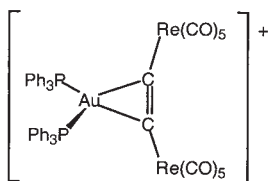
(210)
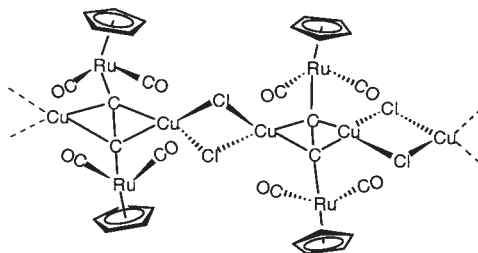
(211)
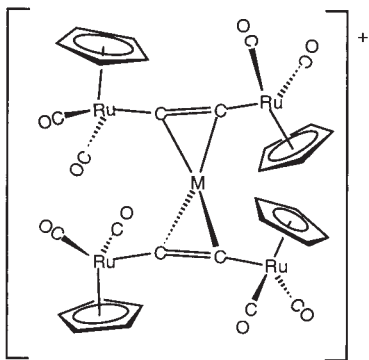
M = Cu **(212)**, Ag **(215)**

(213)

(214)
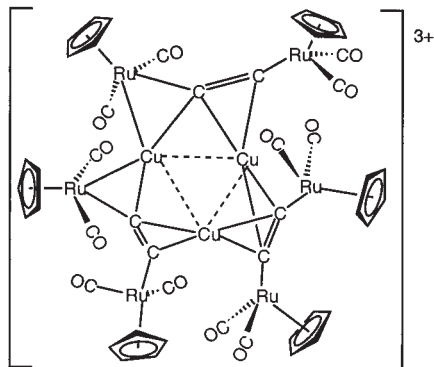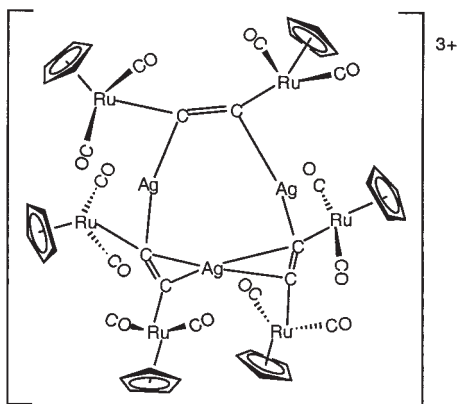
by σ,π exchange of the ethynyl ligand. Here, the C_2 ligand is π-bonded to the third $Re(CO)_4$ fragment, which is linked to one of the σ-bonded Re atoms, with an H atom bridging the resulting Re–Re bond.[172] Photolysis of $\{Re(CO)_5\}_2(\mu-C{\equiv}C)$ or treatment with Me_3NO results in the formation of tetranuclear $\{(OC)_5Re(\mu-\eta^1:\eta^1:\eta^2-C_2)Re(CO)_4\}_2$ (**218**); a by-product is $\{Re(\mu_3-OH)(CO)_3\}_4 \cdot 4H_2O$. The dimer is formed by the C_2 ligand of each monomer becoming π-bonded to one of the Re atoms of the other molecule, with loss of CO. In both cases, the usual bending of the acetylenic substituents results in Re–C–C angles between 150.1(12) and 161.1(9)°; in the Re_3 complex, the Re(1)–C(14)–C(15)–Re(3) adopts a transoid configuration.[172]

B. $\{ML_x\}_2(\mu-C_4)$

In contrast to the formation of Co_2W clusters in its reactions with $Co_2(CO)_8$ (see below), the reaction of $\{W(CO)_3Cp\}_2(\mu-C{\equiv}CC{\equiv}C)$ with $Co_2(\mu-dppm)(CO)_6$ gives a good yield of the simple mono-adduct $Co_2\{\mu-[Cp(OC)_3W]C_2C{\equiv}C[W(CO)_3Cp]\}(\mu-dppm)(CO)_4$ (**220**), perhaps because the presence of the bulky diphosphine precludes the formation of new W–Co bonds.[419] Reaction of $Co_2(CO)_8$ with the mixed-metal complex $\{Cp(OC)_3W\}C{\equiv}CC{\equiv}C\{Fe(CO)_2Cp\}$ results in addition of a $Co_2(CO)_6$ fragment to the sterically least hindered C≡C triple bond to give $Co_2\{\mu-[Cp(OC)_2Fe]C_2C{\equiv}C[W(CO)_3Cp]\}(\mu-dppm)(CO)_4$ (**221**).[419] No evidence for the formation of a bis-adduct was obtained.

(**217**)

(**218**)

M = W, n = 3 (**220**)
M = Fe, n = 2 (**221**)
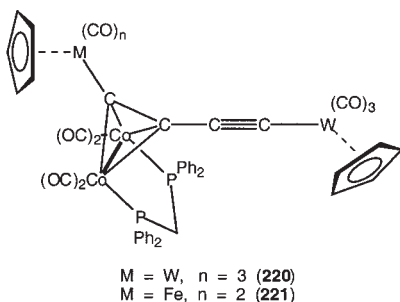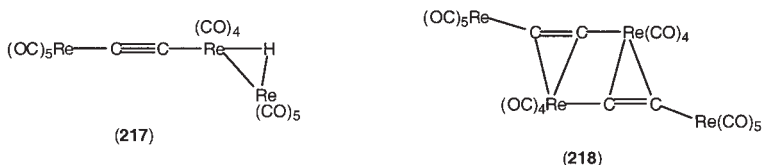
C. From $\{ML_x\}_2(\mu\text{-}C_n)$ $(n = 6, 8)$

1. With $Co_2(\mu\text{-dppm})_n(CO)_{8-2n}$ $(n = 0, 1)$

Reactions between $\{W(CO)_3Cp\}_2\{\mu\text{-}(C{\equiv}C)_4\}$ (**154/W**) and $Co_2(\mu\text{-}$dppm$)(CO)_6$ occur readily in thf at r.t.[421] A mono-adduct on an inner $C{\equiv}C$ triple bond and two isomers of the bis-adduct, in which the two outer (**222**) or two inner $C{\equiv}C$ triple bonds (**223**) were coordinated to $Co_2(\mu\text{-}$dppm$)(CO)_4$ groups, were isolated. The structural parameters of the C_2Co_2 fragments in these derivatives are similar to those found in the well-known $\mu\text{-}\eta^2$-alkyne-Co_2 complexes and show the usual bending of the substituents on the π-bonded carbons away from the Co_2 center, the distortion from linearity ranging between 33.8 and 38.2°. The bis-adducts consequently adopt a transoid or S-shaped conformation in which the W–C(1) vectors are approximately orthogonal to the central C(4)–C(4′) vector (range 82.6–92.6°). The bulk of the terminal substituent appears to have the major effect on the degree of bending of the C_8 chain, which is unaffected by the presence of the dppm ligand. Since the Co_2 unit can be readily displaced by oxidation with Ce(IV), for example, these complexes may serve as derivatives to aid characterization, especially by X-ray crystal structure determinations.

(**222**)

(**223**)
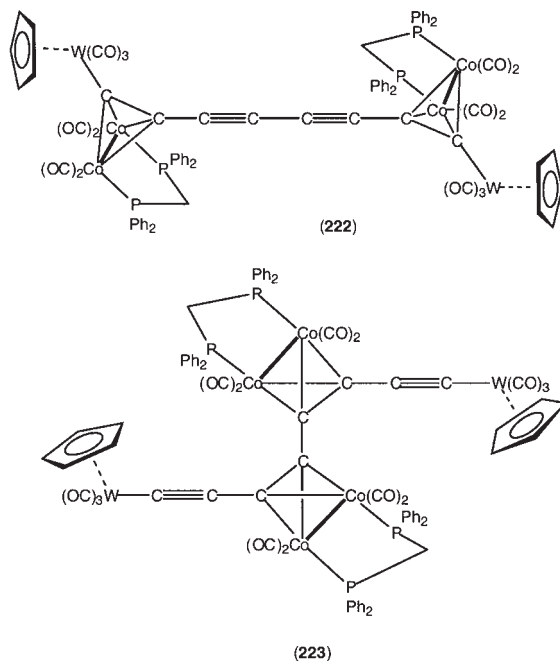
The complex $\{Co_2(CO)_6(\mu\text{-}\eta^2\text{-}C_2C\equiv CFp^*)\}_2$ (**224**) features two $Fp^*C\equiv CC_2[Co_2(CO)_6]$-moieties linked by a C–C single bond and is obtained from the reaction of the tetrayndiyl complex $Fp_2^*\{\mu\text{-}(C\equiv C)_4\}$ and $Co_2(CO)_8$.[422] The two C_2Co_2 cores, which again involve the inner $C\equiv C$ triple bonds, induce a transoid conformation (S-shaped) in the carbon chain, analogous to that described above for the tungsten complexes.

(**224**)

(**225**) $L_2 = (CO)_2$, dppm; m = 3, 4

(**226**)
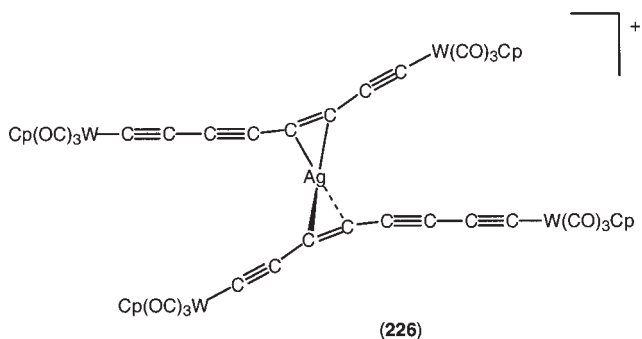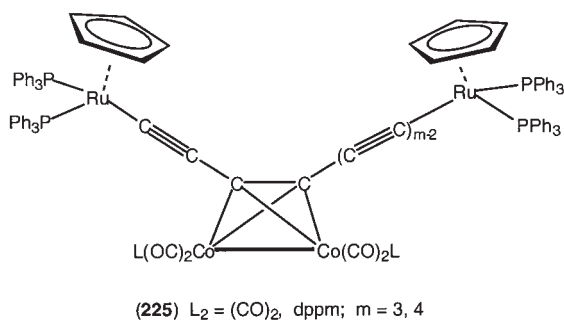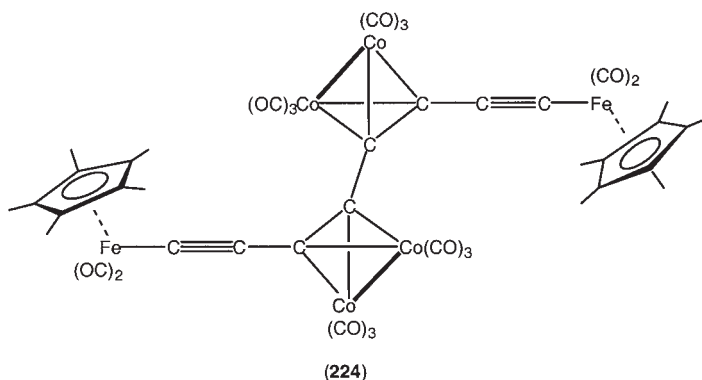
With $Co_2(CO)_8$ or $Co_2(\mu\text{-dppm})(CO)_6$, addition of the Co_2 fragment to the inner C≡C triple bonds in $\{Ru(PPh_3)_2Cp\}_2\{\mu\text{-}(C≡C)_m\}$ ($m = 3, 4$) occurs to give green $\{Ru(PPh_3)_2Cp\}_2\{\mu\text{-}C≡CC_2[Co_2(CO)_6](C≡C)_{m-2}\}$ (**225**); the brown dppm derivative is formed similarly from $Co_2(\mu\text{-dppm})(CO)_6$.[308]

2. With Group 11 Ions

The electrospray mass spectrum of $\{W(CO)_3Cp\}_2\{\mu\text{-}(C≡C)_4\}$ (**154/W**), when run with $AgNO_3$ as an aid to ionization, contained ions such as $[\{W_2(C_8)(CO)_6Cp_2\}Ag(NCMe)_2]^+$ and $[\{W_2(C_8)(CO)_6Cp_2\}_2Ag]^+$, for which structures such as **226**, involving η^2-bonding of the C_8 chains to silver center, can be proposed.[242]

VII

COMPLEXES CONTAINING ONE METAL CLUSTER MOIETY

A. *As End-Groups to C_n Chains*

In the next two sections are grouped complexes which contain metal cluster moieties at each end of the carbon chain. In general, these are attached via $\mu\text{-}\eta^1\text{-}C$ (**O**) or $\mu_3\text{-}\eta^1:\eta^2\text{-}C_2$ units (**P**) (Chart 5). Other complexes in which C_2 fragments are incorporated either partly (peripheral) or completely within metal clusters are considered in Section IX.

Initial coordination of a metal fragment to a C≡C triple bond directly attached to another metal center is often followed by formation of new metal–metal bonds and concomitant elimination of a 2-e donor ligand.
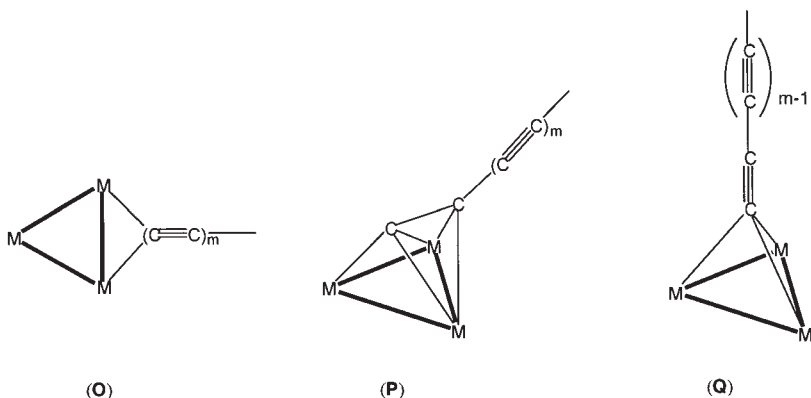
CHART 5

In this way, a general route to complexes of type **P**, containing μ_3-η^1 : η^2-$C_2\{ML_n\}$ ligands, becomes available. An alternative mode of bonding is via a μ_3-carbynic carbon as in **Q**. If the carbon chain is longer than two, uncoordinated carbons separate the cluster-bonded fragment from the metal center.

1. M–C_x–M_3 Complexes

(a) x = 1

Although we have chosen not to include cluster complexes containing fully or partially enclosed carbido atoms, such as $Fe_5C(CO)_{15}$, there are few complexes (so far) which contain a single sp^3-hybridized carbon supporting both a cluster and a single metal atom. This is in spite of several attempts to form such compounds. Thus, the reaction between $Mn(CX_3)(CO)_5$ (X = Cl, Br) and $[Co(CO)_4]^-$ afforded the ketenylidene cluster $[Co_2Mn(\mu_3$-$CCO)(CO)_9]^-$, possibly via coordination of CO onto the three-coordinate carbon atom which is produced when the $Mn(CO)_5$ group migrates from the carbide in $Co_3\{\mu_3$-$C[Mn(CO)_5]\}(CO)_9$ to the cluster with displacement of a $Co(CO)_3$ group.[423] The reducing agent is assumed to be excess $[Co(CO)_4]^-$. Similarly, attempts to replace the halogen in $Co_3(\mu_3$-$CX)(CO)_9$ (X = Cl, Br) in reactions with several anionic metal carbonyls resulted in incorporation of the metal (Cr, Mo, W) into the M_3C cluster.[424]

The reaction between $[Ru(CO)_2Cp]^-$ and $Co_3(\mu_3$-$CCl)\{\mu_3$-$(PPh_2)_3CH\}(CO)_6$ gives the tetranuclear complex $Co_3\{\mu_3$-$C[Ru(CO)_2Cp]\}\{\mu_3$-$(PPh_2)_3CH\}(CO)_6$ in 5–10% yield (**227**).[425] Considered as a permetallated methane, the angles around the solitary carbon atom range between ca. 80° (C–Co–C) and ca. 130° (Co–C–Ru), consistent with sp^3 hydridization. A radical mechanism involving a $Co_3C^{\bullet}$ species is suggested by the accompanying formation of $Co_3(\mu_3$-$CH)\{\mu_3$-$(PPh_2)_3CH\}(CO)_6$. A similar reaction carried out with $Co_3(\mu_3$-$CBr)(CO)_9$ afforded the heptanuclear carbido cluster $Co_4RuC\{\mu$-$Hg[Ru(CO)_2Cp]\}(\mu$-$CO)_2(CO)_{11}Cp$ (**228**), which incorporates a $[HgRu(CO)_2Cp]^+$ fragment [derived from the amalgam used to generate the $[Ru(CO)_2Cp]^-$ reagent, and hence $Hg\{Ru(CO)_2Cp\}_2]$.

(b) x = 2

Some of these complexes are obtained by reactions of $\{ML_n\}_2(\mu$-$C_2)$ with other metal complexes and they are given in order of metal substrate used in these reactions.

Group 6. A tetranuclear cluster now formulated as $Ru_3\{\mu_3$-$CC\equiv[Mo(CO)_2Cp]\}(\mu$-$CO)_3Cp'_3$ (**229**) is the major product from reactions of $\{Mo(CO)_2Cp\}_2$ and $\{Ru(CO)_2Cp'\}_2(\mu$-$C\equiv C)$ (Cp' = Cp, Cp^{Me}).[426,427] The two C_2 resonances are at δ_C 87.2 and 308.4. In air, slow formation of

(227)

(228)

(229)
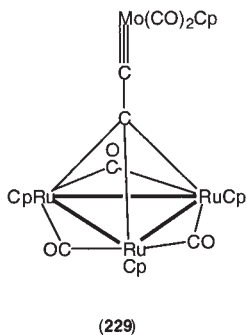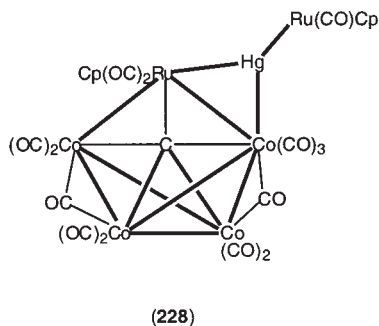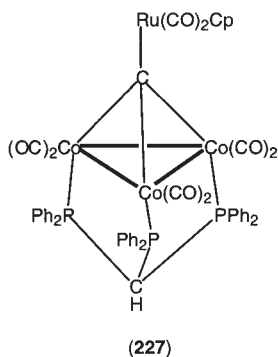
$Ru_3\{\mu_3\text{-}CC(O)R\}(\mu\text{-}CO)_3Cp'_3$ (R = H, OH) occurs, while among the many products obtained from reactions with CO, both $Ru_3\{\mu_3\text{-}CC(O)[ORu (CO)_2Cp]\}(\mu\text{-}CO)_3Cp_3$ and $\{Ru_2(\mu\text{-}CO)(CO)_2Cp_2^{Me}\}(\mu_4\text{-}C=C)\{MoRu(\mu\text{-}O)(O)(CO)CpCp^{Me}\}$ were isolated. The unusual electron-deficient cluster $Mo_3\{\mu_3\text{-}C_2[Ru(CO)_2Cp^{Me}]\}(\mu\text{-}CO)(Cl)_2(CO)Cp_3$ was obtained from a reaction with tetrachloroethene.

Group 8. Black trinuclear clusters $Fe_2M\{\mu_3\text{-}C_2[Fe(CO)_2(\eta\text{-}C_5Me_4R)]\}(\mu\text{-}CO)(CO)_4(\eta\text{-}C_5Me_4R)$ (**230**; M = Fe, Cp' = Cp*, $\eta\text{-}C_5Me_4Et$; M = Ru, Cp' = Cp*) are formed from $Fe_2(CO)_9$ and $\{M(CO)_2Cp'\}_2(\mu\text{-}C\equiv C)$.[428,429] Migration of one Ru center from a σ-bonded to a π-bonded position on the C_2 chain occurs during the reaction, perhaps via a "windscreen-wiper"-like motion with the σ,π-exchange of the alkynyl ligand, although apparently not in the homometallic reaction. As found elsewhere, the C–C separation is lengthened, with bending at both C atoms. The M–C σ-bond length is similar to that in the precursor. The complexes are dynamic, not only by rotation of the alkynyl group, but also by one of the processes shown in
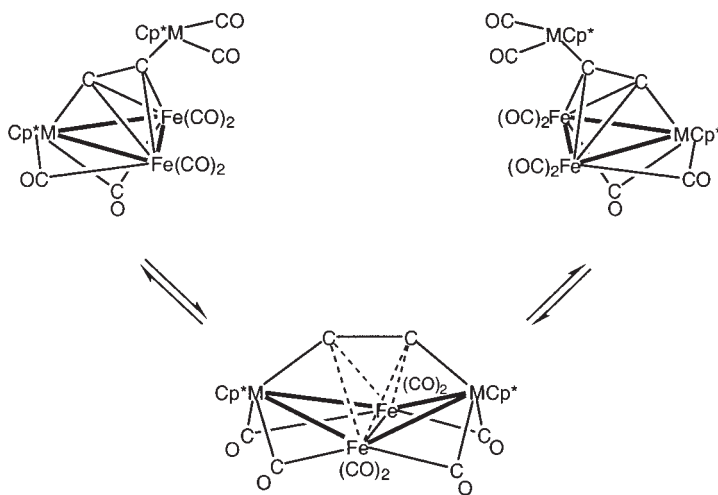
SCHEME 47

Scheme 47 whereby the two ML$_x$Cp groups are exchanged. The mechanism involves a relatively uncommon reversible M–M bond cleavage.

The oxygen of the ketenylidene ligand in [Fe$_3$(μ_3-CCO)(CO)$_9$]$^{2-}$ is readily acylated (MeCOCl) to give [Fe$_3$\{μ_3-C$_2$OC(O)Me\}(CO)$_9$]$^-$. Further attack of [Fe(CO)$_2$Cp]$^-$ occurs at the outer carbon with displacement of the acyl group to give red [Fe$_3$\{μ_3-C$_2$[Fe(CO)$_2$Cp]\}(CO)$_9$]$^-$ (231).[430] Rapid exchange of cluster CO groups occur. The structural study showed the C$_2$Fe fragment to incorporate a conventional μ_3-alkynyl group, for which the C$_2$ carbon resonances are at δ 206.3 (Fe$_3$C) and 99.0 (FeC). At $-20\,°$C, reversible oxidation occurs at $E° = +0.72$ V.[431]

Similar reactions of [Fe(CO)$_4$]$^{2-}$ with [Fe$_3$(μ_3-C$_2$OAc)(CO)$_9$]$^-$ proceed via the metalated ethynyl cluster [Fe$_3$\{μ_3-C$_2$[Fe(CO)$_4$]\}(CO)$_9$]$^{2-}$ (232) which exchanges isoelectronic Fe(CO)$_3$ and [Co(CO)$_3$]$^+$ groups upon reaction with Co$_2$(CO)$_8$ to give [CoFe$_2$\{μ_3-C$_2$[Fe(CO)$_4$]\}(CO)$_9$]$^-$ (233).[432] In the ^{13}C NMR spectrum, C$_\alpha$ and C$_\beta$ resonate at δ 201.6 and 114.8, respectively [^1J(CC) 23 Hz]. An 8 Hz coupling of C$_\beta$ to the Fe(CO)$_4$ groups was also observed. At $-70\,°$C, the C$_2$ ligand in 233 gives signals at δ 142.2 (C$_\beta$) and 193.1 (C$_\alpha$) [^1J(CC) 27 Hz], with the downfield resonance being broadened by the Co quadrupole, indicating it is σ-bonded to Co.[432] Further reactions with iron and cobalt carbonyls are discussed in Section VIII. Reactions of [ppn]$_2$[Fe$_3$\{μ_3-C$_2$[Fe(CO)$_4$]\}(CO)$_9$] with [Mn(CO)$_3$(NCMe)$_3$]$^+$ afforded a cation-exchanged product formulated as [ppn][Mn(CO)$_3$(NCMe)$_3$][Fe$_3$\{μ_3-C$_2$[Fe(CO)$_4$]\}(CO)$_9$]. In contrast to the reaction with Co$_2$(CO)$_8$ (above), that with \{Rh(μ-Cl)(CO)$_2$\}$_2$ gave the carbido cluster [ppn][Fe$_3$Rh$_3$C(CO)$_{15}$].[431]

Reactions of $Ru_3(CO)_{12}$ with $Fe(C\equiv CH)(CO)_2Cp'$ ($Cp' = Cp$, Cp^*) gave yellow-orange $Ru_3(\mu\text{-}H)\{\mu_3\text{-}C_2[Fe(CO)_2Cp']\}(CO)_9$ (**234**).[433] This complex has a structure similar to those of other μ_3-alkynyl-triruthenium clusters, with C–C 1.33(2) Å.

The reactions of $Re\{(C\equiv C)_mH\}(NO)(PPh_3)Cp^*$ ($m = 1$–3) with $Os_3(CO)_{10}(NCMe)_2$ gave $Os_3(\mu\text{-}H)\{\mu\text{-}\eta^1\text{-}(C\equiv C)_m[Re(NO)(PPh_3)Cp^*]\}(CO)_{10}$ (**235/m**) (Scheme 48) which contain unusual $\mu\text{-}\eta^1$-poly-ynyl ligands. For $m = 1$ and 2, decarbonylation in refluxing hexane affords the μ_3-diynyl complexes $Os_3(\mu\text{-}H)\{\mu_3\text{-}\eta^1,\eta^2\text{-}C_2(C\equiv C)_{m-1}[Re(NO)(PPh_3)Cp^*]\}(CO)_9$ (**236/m**).[434,435] In orange $Os_3(\mu\text{-}H)\{\mu\text{-}\eta^1\text{-}C\equiv C[Re(NO)(PPh_3)Cp^*]\}(CO)_{10}$ (**235/1**), both bridging groups symmetrically span the same Os–Os vector, the C_2 fragment being bonded in the $\mu\text{-}\eta^1$ mode. The Re–C_2 moiety tends towards the zwitterionic cumulenic form, with short Re–C [1.965(9) Å] and long C–C bonds [1.25(1) Å] and δ_C 245.4 [ReC; $J(CP)$ 8.8 Hz], 124.2 [$J(CC)$ 64.5 Hz]; the latter is close to those found for vinylidene–Re complexes, but
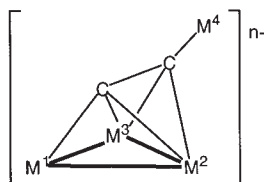
Complex	n	M^1	M^2	M^3	M^4
(**230**)	0	$Fe(CO)_3$	$Fe(CO)_3$	$M(CO)_2Cp$	$Fe(CO)_2Cp$
(**231**)	1-	$Fe(CO)_3$	$Fe(CO)_3$	$Fe(CO)_3$	$Fe(CO)_2Cp$
(**232**)	2-	$Fe(CO)_3$	$Fe(CO)_3$	$Fe(CO)_3$	$Fe(CO)_4$
(**233**)	1-	$Co(CO)_3$	$Fe(CO)_3$	$Fe(CO)_3$	$Fe(CO)_4$
(**234**)	0	$Ru(CO)_3$	$Ru(CO)_3$	$Ru(CO)_3(H)$	$Fe(CO)_2Cp'$
(**235/1**)	0	$Os(CO)_3$	$Os(CO)_3$	$Os(CO)_3$	$Re(NO)(PPh_3)Cp^*$
(**237**)	0	$Re(CO)_3$	$Co(CO)_3$	$Co(CO)_3$	$Re(CO)_5$
(**238/Fe**)	0	$FeCp$	$Co(CO)_2(\mu\text{-}CO)$	$Co(CO)_2(\mu\text{-}CO)$	$Fe(CO)_2Cp^*$
(**238/Ru**)	0	$RuCp$	$Co(CO)_2(\mu\text{-}CO)$	$Co(CO)_2(\mu\text{-}CO)$	$Ru(CO)_2Cp$
(**319**)	0	$Fe(CO)_3$	$Ru(CO)_3$	$Ru(\mu\text{-}H)(CO)_3$	Fp^*
(**326**)	1-	$Ru(CO)_3$	$Ru(CO)_3$	$Ru(CO)_3$	Fp

the $J(CC)$ value is similar to that found for a related $Re^+ = C = C = C = CRe^+$ cation. The $\nu(CC)$ absorption is at 1705 cm^{-1}. Decarbonylation occurs in refluxing hexane to give $Os_3(\mu\text{-}H)\{\mu_3\text{-}\eta^1,\eta^2\text{-}C_2[Re(NO)(PPh_3)Cp^*]\}(CO)_9$ (**236/1**), while a reversible protonation gives orange $[Os_3(\mu\text{-}H)_2\{\mu\text{-}C\equiv C[Re(NO)(PPh_3)Cp^*]\}(CO)_{10}]BF_4$, which contains a $Re^+ = C = C = Os_3$ contribution, with similar Re–C and C–C bond lengths to the neutral
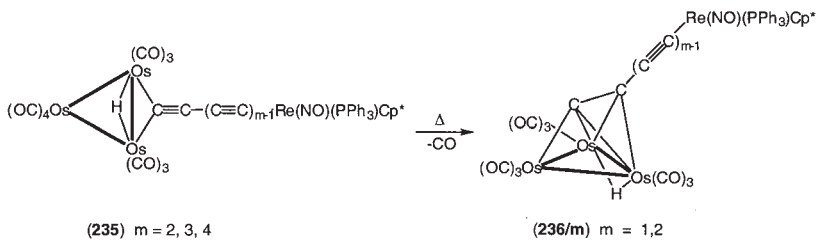
SCHEME 48

precursor.[435] No pure complexes were isolated from attempted substitution reactions with PMe_2Ph or PPh_3, nor was it possible to deprotonate the cluster (LiBu).

The absorption bands in the UV–vis spectra of the cluster-terminated complexes $Os_3(\mu\text{-H})\{\mu_2\text{-}\eta^1\text{-}(C{\equiv}C)_n[Re(NO)(PPh_3)Cp^*]\}(CO)_{10}$ (**235**/**m**) are not as intense as found for other poly-ynyl complexes featuring the same Re metal auxillary. There are minor shifts to longer wavelengths in the longer chain complexes.[435] Cyclic voltammetry of $Os_3(\mu\text{-H})\{\mu\text{-}\eta^1\text{-}(C{\equiv}C)_nRe(NO)(PPh_3)Cp^*\}(CO)_{10}$ (**235**/**m**, $m = 1–3$) showed that the longer chain complexes were more easily oxidized than their shorter chain analogues. However, all of these irreversible oxidations are found at more positive potentials than for the corresponding oxidation of $Re(C{\equiv}CR)(NO)(PPh_3)Cp$ reference complexes. This behavior, together with spectroscopic data [for $n = 1$, $\nu(NO)$ 1663 cm^{-1}], was interpreted in terms of contributions to the structure from a zwitterionic resonance form $Re^+{=}(C{=}C)_n{-}(Os_3)^-$ for the cluster species, which becomes less significant as the carbon bridge lengthens.[435]

Group 9. The green-black cluster $Co_2Re\{\mu_3\text{-}\eta^1:\eta^2:\eta^2\text{-}C_2[Re(CO)_5]\}(\mu\text{-}CO)_2(CO)_7$ (**237**) is formed from $\{Re(CO)_5\}_2(\mu\text{-}C{\equiv}C)$ and $Co_2(CO)_8$; the σ-type bonds from the C_2 unit to Re are preserved, the geometry resembling that of a conventional $\mu\text{-}\eta^1:\eta^2$-alkynyl cluster.[413]

With $Co_2(CO)_8$, both $\{M(CO)_2Cp'\}_2(\mu\text{-}C{\equiv}C)$ [**238**; M = Fe, Cp' = Cp*; M = Ru, Cp' = Cp] react to give $Co_2M\{\mu_3\text{-}C_2[M(CO)_2Cp']\}(\mu\text{-}CO)(CO)_5Cp'$.[436,437] The latter exhibit a dynamic process involving cluster rearrangement and CO scrambling.

(c) x = 3

The reaction between $Re(C{\equiv}CLi)(NO)(PPh_3)Cp^*$ and $Os_3(CO)_{12}$, followed by treatment with $[OMe_3]BF_4$, affords a rare example of an Os_3 cluster carbene complex, $Os_3(CO)_{11}\{=C(OMe)C{\equiv}C[Re(NO)(PPh_3)Cp^*]\}$ (**239**) (Scheme 49).[232] The structural parameters for the C_3 chain indicate
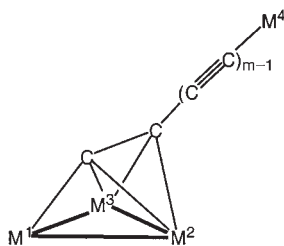
Complex	m−1	M^1	M^2	M^3	M^4
(236/2)	1	$Os(CO)_3$	$Os(CO)_3$	$Os(CO)_3(H)$	$Re(NO)(PPh_3)Cp^*$
(236/3)	2	$Os(CO)_3$	$Os(CO)_3$	$Os(CO)_3(H)$	$Re(NO)(PPh_3)Cp^*$
(248)	1	$Fe(CO)_3$	$Fe(CO)_3$	$M(CO)(PPh_3)$ (M = Rh, Ir)	$W(CO)_3Cp$
(257)	1	$Fe(CO)_3$	$Fe(CO)_3$	$Fe(\mu\text{-}CO)Cp^*$	$Fe(CO)_2Cp^*$
(245)	1	$Ru(CO)_3$	$Ru(CO)_3$	$Ru(CO)_3(H)$	$W(CO)_3Cp$
(246)	1	$Ru(CO)_3$	$Ru(CO)_2(dppm)$	$RuH(CO)_2$	$W(CO)_3Cp$

(239)   (240)
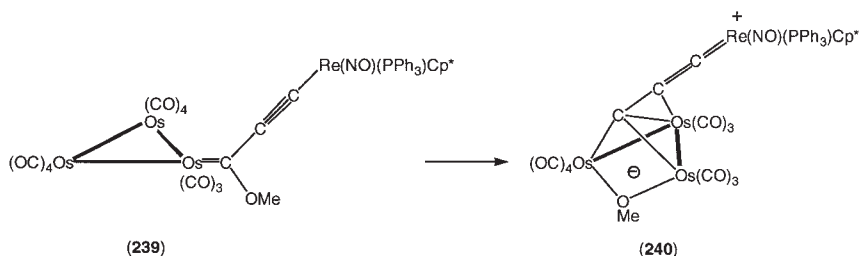
SCHEME 49

that there is a significant contribution from the $\{Re^+\}=C=C=C(OMe)–$ $\{Os_3^-\}$ resonance form [Re–C 1.983(7), Os–C 2.042(7), C–C 1.238(9), 1.364(10)Å; ReCC 174.5(6), CCC 174.2(8), CCOs 124.2(6)°]. No C_3 complex was obtained from its reaction with BF_3. Upon heating, however, OMe-migration to the cluster affords red-orange cumulenic $Os_3\{\mu_3\text{-}\eta^2\text{-}CC=C=[Re(NO)(PPh_3)Cp^*]\}(\mu\text{-}OMe)(CO)_9$ (240).[435] In the crystal, two forms are present (ca. 62/38), the minor form apparently containing a highly asymmetric μ-OMe group [Os–O 1.90, 2.25(2) Å]. Other structural data are consistent with a contribution from a zwitterionic structure.

Although $Co_3(\mu_3\text{-}CC\equiv CH)(CO)_9$ is very unstable,[438,439] its black $Co_2(CO)_6$ adduct (241) is one of the products obtained by heating $Co_3(\mu_3\text{-}CCl)(CO)_9$ in xylene or mesitylene (130 °C/30 min) under CO.[440] It is also a minor product from the reaction of ethyne with $Co_3(\mu_3\text{-}CBr)(CO)_9$, being

formed along with $Co_4(\mu_4\text{-}HC_2H)(CO)_{12}$.[441] The X-ray structure determination showed the $\mu_3\text{-}CC{\equiv}CH$ group to have C–C separations of 1.34, 1.46(2) Å and a C–C–C angle of 145.6(14)°. Coordination of the Co_2 fragment results in bending of the C(1)–C(2) vector away from the ideal perpendicular configuration as a consequence of close approaches of the CO groups within the molecule. The Pd(0)/Cu(I)-catalyzed reaction between $HC{\equiv}CSiMe_3$ and $Co_3(\mu_3\text{-}CBr)(\mu\text{-}dppm)(CO)_7$ affords $Co_3(\mu_3\text{-}CC{\equiv}CSiMe_3)(\mu\text{-}dppm)(CO)_7$, which on treatment with NaOMe and subsequent reaction with $AuCl(PPh_3)$, gives $Co_3\{\mu_3\text{-}CC{\equiv}C[Au(PPh_3)]\}(\mu\text{-}dppm)(CO)_7$ (**242**).[442]

Proto-desilylation (KOH) of $Co_3(\mu_3\text{-}CSiMe_3)(\mu_3\text{-}CC{\equiv}CSiMe_3)Cp_3$ affords $Co_3(\mu_3\text{-}CSiMe_3)(\mu_3\text{-}CC{\equiv}CH)Cp_3$ (**243**).[443] No reaction occurs between this complex and $Co_2(CO)_8$.

(**241**)   (**243**)
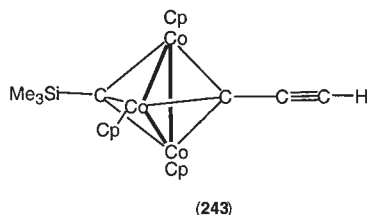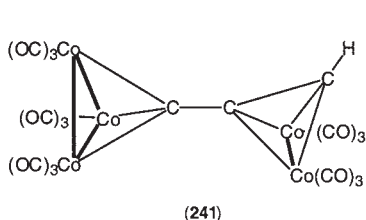
(d) x = 4

The chemistry of the C_4 chain is dominated by its varying electron-donor power, depending on the nature of the metal fragments with which it is associated. Zwitterionic species or intermediates are formed as a result of electron transfer through the C_n ligand, while if CO ligands are also present, terminal (2-e) or bridging CO (2 × 1-e) ligands may complete the coordination sphere.

The terminal diynyl ligand in $W(C{\equiv}CC{\equiv}CH)(CO)_3Cp$ has proved to be a convenient source of other complexes featuring σ,π-bonded diynyl ligands via reactions with multinuclear cluster reagents (Scheme 50). The reaction of the diynyl with $Ru_3(CO)_{10}(NCMe)_2$ proceeds via the μ_3-alkyne cluster (**244**) to give $Ru_3(\mu\text{-}H)\{\mu_3\text{-}\eta^1:\eta^2\text{-}C_2C{\equiv}C[W(CO)_3Cp]\}(CO)_9$ (**245**).[444,445] A similar reaction with $Ru_3(\mu\text{-}dppm)(CO)_{10}$ proceeded smoothly to give the oxidative adduct $Ru_3(\mu\text{-}H)\{\mu_3\text{-}\eta^1:\eta^2\text{-}C_2C{\equiv}C[W(CO)_3Cp]\}(\mu\text{-}dppm)(CO)_7$ (**246**) in high yield (92%). In solution, this complex exists as an interconverting mixture of isomers. The major component displays the usual "windscreen-wiper" motion often associated with cluster-bound acetylide ligands, while the minor isomer arises from trapping of the WC_4 portion of the molecule in the cleft formed by two phenyl rings from the dppm ligand.[241,445] A second molecule of $W(C{\equiv}CC{\equiv}CH)(CO)_3Cp$ adds to
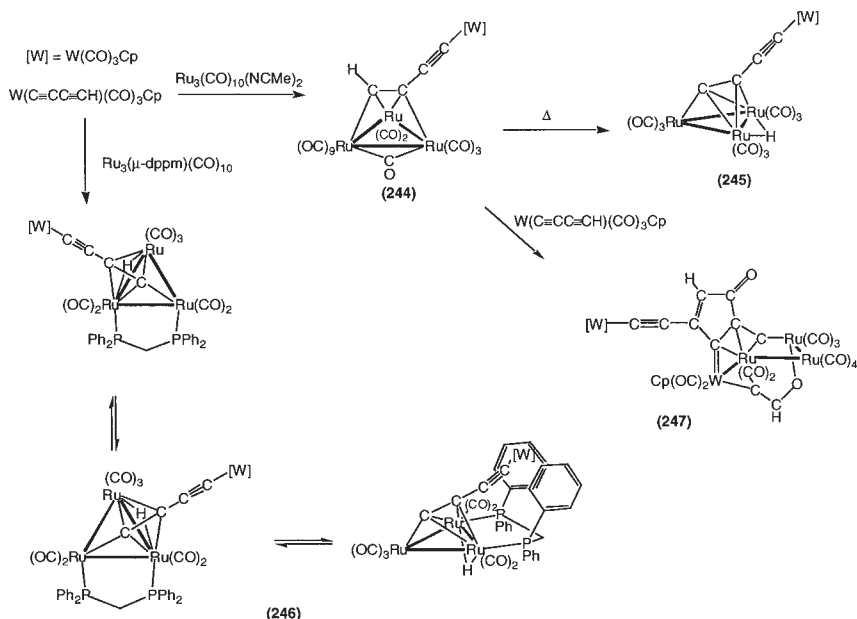
SCHEME 50

244, coupling with the uncoordinated C≡C triple bond of the diynyl ligand with subsequent cyclization to give cluster **247**, in which the new organic ligand is involved in carbenic bonding to the cluster tungsten atom.

The reactions of {Cp(OC)$_3$W}(μ-C≡CC≡C){M(CO)(PPh$_3$)$_2$} (M = Rh, Ir) with Fe$_2$(CO)$_9$ have given Fe$_2$M{μ$_3$-C$_2$C≡C[W(CO)$_3$Cp]}(CO)$_8$(PPh$_3$) (**248**; Scheme 51).[295] Interestingly, in **248**, the terminal carbon of the C$_4$ chain is σ-bonded to iron, rather than to the Group 9 metal center, as found in the precursor. As mentioned earlier, this type of rearrangement is frequently found (see Section VI) and indicates the ready mobility of alkynyl groups on metal clusters.

Red-orange Os$_3$(μ-H){μ-η^1-C≡CC≡C[Re(NO)(PPh$_3$)Cp*]}(CO)$_{10}$ (**235/2**) is obtained from Os$_3$(CO)$_{10}$(NCMe)$_2$ and the butadiynyl-rhenium complex.[434,435] The ReC resonance is at δ$_C$ 242.9. The UV–vis bands are at 296 (20,000), 388 (7500) and 500 nm (4900), while partially reversible oxidation occurs at 0.43 V. Thermolysis gave the μ$_3$-butadiynyl complex Os$_3$(μ-H){μ-C$_2$C≡C[Re(NO)(PPh$_3$)Cp*]}(CO)$_9$ (**236/2**) in which the ReC resonance is unchanged at δ$_C$ 242.9 [J(CP) 11.5 Hz].

Reactions between Fp*C≡CC≡CH and either {Mo(CO)$_2$Cp}$_2$, MoCo (CO)$_7$Cp or Co$_2$(CO)$_8$ gave the adducts Fp*C≡CC$_2$H{ML$_n$} [ML$_n$ = Mo$_2$ (CO)$_4$Cp$_2$ (**249/Mo**), MoCo(CO)$_5$Cp (**249/CoMo**), Co$_2$(CO)$_6$ (**249/Co**)]

(248)

+

(285)
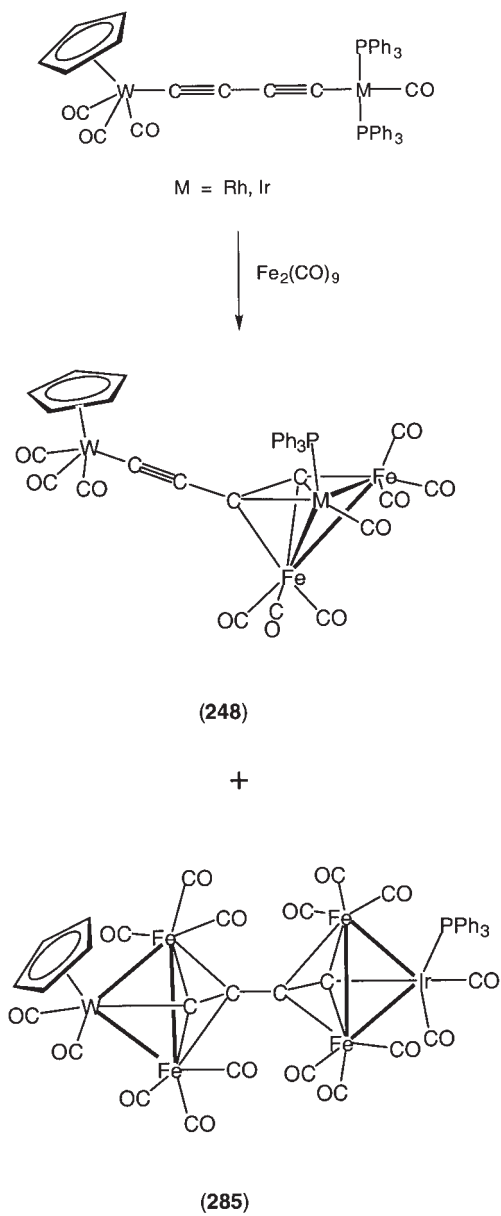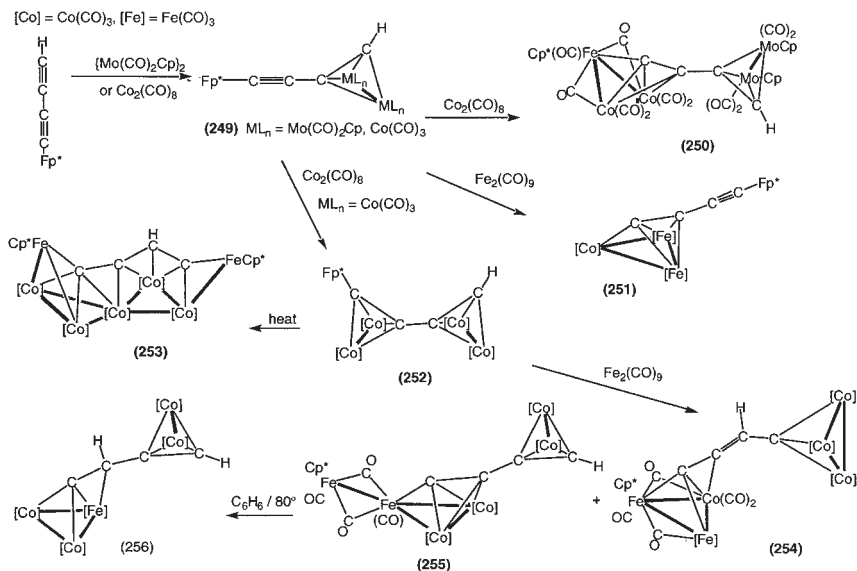
SCHEME 51

SCHEME 52

(Scheme 52).[420] Further reaction of **249**/**Mo** with $Co_2(CO)_8$ afforded red-grey $Co_2Fe\{\mu_3\text{-}C_2C_2H[Mo_2(CO)_4Cp_2]\}(\mu\text{-}CO)_2(CO)_4Cp^*$ (**250**). Similarly, **249**/**Co** and $Fe_2(CO)_9$ gives $CoFe_2(\mu_3\text{-}C_2C\equiv CFp^*)(CO)_9$ (**251**), possibly by addition of an $Fe(CO)_n$ fragment to the C_2Co_2 tetrahedron; the presumed intermediate Co_2Fe complex eliminates $CoH(CO)_n$ before adding a second $Fe(CO)_n$ fragment. The bis-adduct **252** is converted to the dark yellow Co_5Fe_2 cluster **253** in refluxing benzene, while reactions with $Fe_2(CO)_9$ give two isomeric complexes, purple **254**, containing $CoFe_2$ and Co_3 clusters linked by a C_3H ligand, and yellow **255**, containing an Fe-spiked $FeCo_2$ core. In refluxing benzene, the latter is converted into the vinylidene $Co_2Fe\{\mu_3\text{-}CCHC_2H[Co_2(CO)_6]\}(CO)_9$ (**256**).

The complex $Fp^*C\equiv CC\equiv CFp^*$ reacts with $Fe_2(CO)_9$ to give the grey-yellow alkynyl cluster $Fe_3(\mu_3\text{-}C_2C\equiv CFp^*)(\mu\text{-}CO)(CO)_6Cp^*$ (**257**) and the yellow ketenylidene complex $Fe_2\{\mu\text{-}\eta^3\text{-}C(Fp^*)CCC(CO)Fp^*\}(CO)_6$ (**258**), the latter being obtained in thf, but reverting to **257** in benzene after 44 h at r.t.[428] Structural data for **258** suggest contributions from propargylidene tautomers. In the product from $Fp^*C\equiv CC\equiv CRp$, the Fp^* group migrates to the $C\equiv C$ triple bond adjacent to the Ru center to give zwitterionic (**259**).[446]
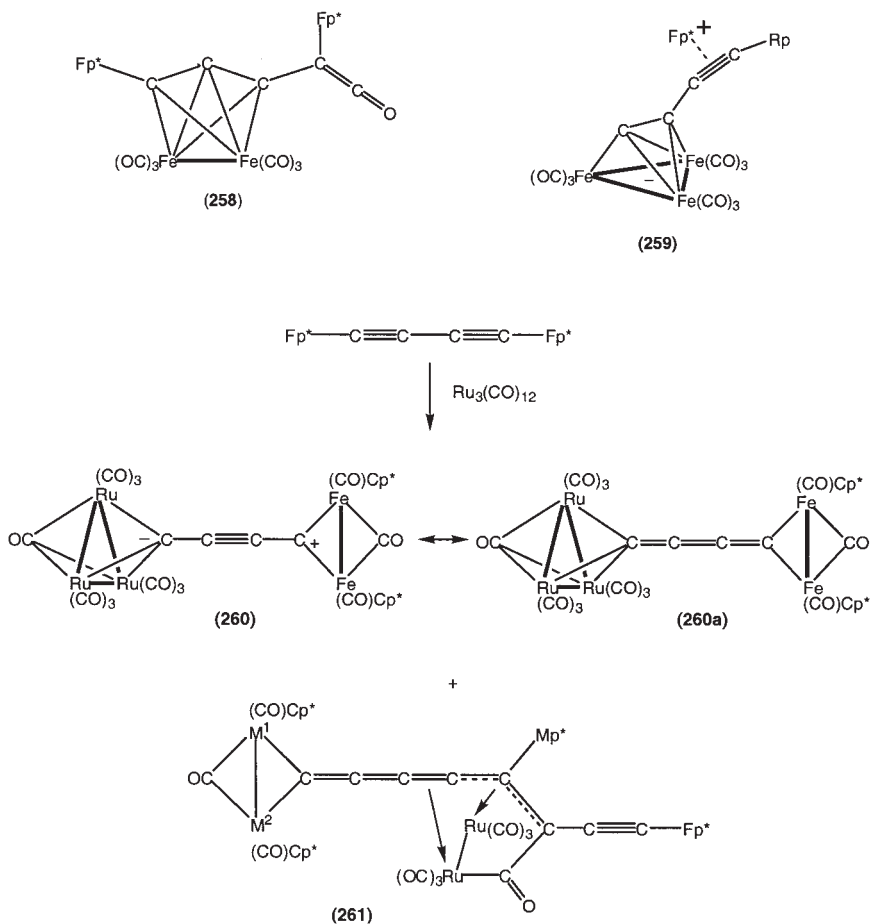
SCHEME 53

More extensive rearrangements occur in the reactions of $Fp^*C\equiv$
$CC\equiv CFp^*$ with $Ru_3(CO)_{12}$ (Scheme 53).[446] The products include **260**, also
formally zwitterionic but with a contribution from the butatrienetetra-yl
tautomer **260a**, and the coupled derivative (**261**, $M^1=M^2=Fe$), in which a
C_8 chain is present. In both cases migration of one Fp^* group gives end-
capping $Fe_2(\mu\text{-}CO)(CO)_2Cp_2^*$ groups. In a similar reaction with $Fp^*C\equiv$
$CC\equiv CRp^*$, inseparable isomers (**261**, $M^1/M^2=Fe/Ru$, Ru/Fe) were
obtained, both with an Rp^* group attached to the central allylic carbon.

Migration of a σ-bonded iron group in these complexes, either to a
π-bonded site in the cluster or with coupling to the second iron center, is
possibly as a result of steric congestion and electronic effects.[428,446]

With buta-1,3-diyne, $(AuCl)_2(\mu\text{-dppm})$ affords $\{Au(C{\equiv}CC{\equiv}CH)_2\}$ $(\mu\text{-dppm})$; serendipitous use of a stoichiometric amount of CuI catalyst resulted in migration of dppm from gold to copper and formation of the curious bis(diynyl) species $Cu_3(\mu_3\text{-}C{\equiv}CC{\equiv}CAuC{\equiv}CC{\equiv}CH)(\mu_3\text{-}I)(dppm)_3$ (**262**).[447] The reaction between $[ppn][Au(C{\equiv}CC{\equiv}CH)_2]$ and $[Cu_3(\mu_3\text{-}I)_2$ $(\mu\text{-dppm})_3]I$ gave the dumb-bell complex $\{Cu_3(\mu_3\text{-}I)(\mu\text{-dppm})_3\}_2(\mu_3:\mu_3\text{-}$ $C{\equiv}CC{\equiv}CAuC{\equiv}CC{\equiv}C)$ (**263**).[447]

(**262**)

(**263**)
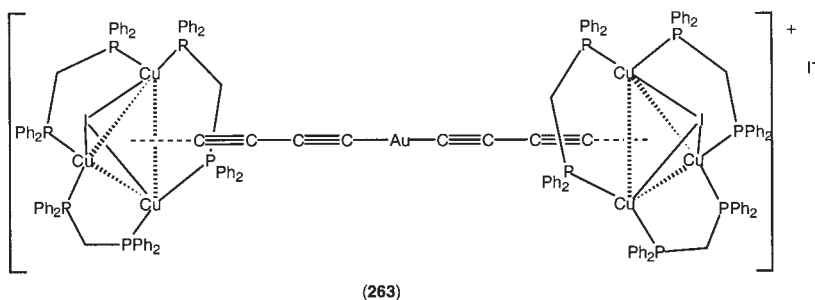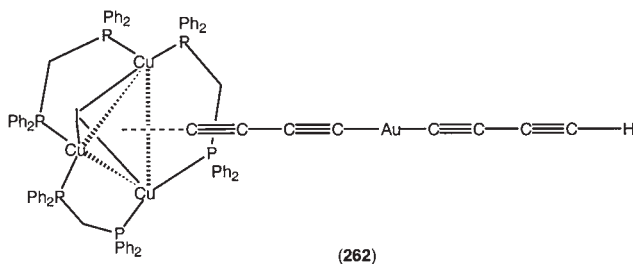
(e) x = 5

One product from coupling of $Co_3(\mu_3\text{-CBr})(CO)_9$ with $HC{\equiv}CC{\equiv}CH$ $(CuI/NHEt_2)$ is $Co_3\{\mu_3\text{-}C(C{\equiv}C)_2H\}(CO)_9$ which, although unstable, could be characterized via its $Co_2(CO)_6$ adduct. Attempted coupling reactions between $Co_3(\mu_3\text{-CBr})(CO)_9$ and the $Co_2(CO)_6$ derivative of $Co_3(\mu_3\text{-}CC{\equiv}CH)(CO)_9$ (CuCl, $NHEt_2$ in dioxan) give only $Co_3\{\mu_3\text{-}CC_2C(O)$ $NHEt[Co_2(CO)_6]\}(CO)_9$.[448] The red copper acetylide derivatives also separate during the reaction, together with black polymers similar to the Magnus product (see below). The reaction of $Co_3(\mu_3\text{-CBr})(CO)_9$ with $Me_3SiC{\equiv}CC{\equiv}CSiMe_3$ under Friedel–Crafts conditions afforded $Co_3\{\mu_3\text{-}C(C{\equiv}C)_2SiMe_3\}(CO)_9$ (**264**), but similar reactions did not occur with $Me_3Si(C{\equiv}C)_nSiMe_3$ ($n = 1, 4$). Both regioisomers of the $Co_2(CO)_6$ derivative of **264** were formed.[438]

The C_5 clusters $\{Cp(OC)_3W\}(\mu:\mu_3\text{-}C\equiv CC\equiv CC)\{Co_3(\mu\text{-dppm})_n(CO)_{9-2n}\}$ (**265/n**; $n=0$, 1) have been obtained in 16 and 80% yields, respectively, from the reactions between $W(C\equiv CC\equiv CH)(CO)_3Cp$ and $Co_3(\mu_3\text{-CBr})(\mu\text{-dppm})_n$ $(CO)_{9-2n}$ (CuI/NEt$_3$, r.t.). The X-ray structures show that the alternating short–long–short–long pattern of C–C bonds is preserved in these compounds. Reactions with $Co_2(CO)_8$ or tcne with the dppm-substituted complex have given the expected adducts, by reaction at the least hindered $C\equiv C$ triple bond.[449]

As with the tungsten analogue, the CuI-catalyzed reaction between $Ru(C\equiv CC\equiv CH)(dppe)Cp$ and $Co_3(\mu_3\text{-CBr})(\mu\text{-dppm})(CO)_7$ afforded the C_5 cluster $\{Cp(dppe)Ru\}(\mu:\mu_3\text{-}C\equiv CC\equiv CC)\{Co_3(\mu\text{-dppm})(CO)_7\}$ (**266**), although in only 26% yield. A side-product was the now-ubiquitous amidomethylidyne cluster $Co_3\{\mu_3\text{-CC(O)NEt}_2\}(\mu\text{-dppm})(CO)_7$.[442]

(f) $x=6$

Red-brown $Os_3(\mu\text{-H})\{\mu\text{-}\eta^1\text{-}C\equiv C(C\equiv C)_2[Re(NO)(PPh_3)Cp^*]\}(CO)_{10}$ (**235/3**) is obtained from $Os_3(CO)_{10}(NCMe)_2$ and the hexatriynyl–rhenium complex, but this could not be decarbonylated to the μ_3-derivative.[434,435] The ReC resonance is at δ_C 204.9. The UV–vis bands are at 306 (18,000) and 516 nm (3600), while partially reversible oxidation occurs at 0.44 V.

(g) $x=7$

The only example of a complex with a C_7 chain presently known is $Co_3\{\mu_3\text{-}C(C\equiv C)_3Fc\}(\mu\text{-dppm})(CO)_7$ (**267**) which was prepared from the reaction between $IC\equiv CFc$ and $Co_3\{\mu_3\text{-}C(C\equiv C)_2Au[P(tol)_3]\}(\mu\text{-dppm})(CO)_7$.[442]

(h) $x=8$

The Re–C_8–Os$_3$ complex **235/4**, analogous to the C_n ($n=2$, 4, 6) derivatives described above, could not be obtained.[434]

(i) $x=9$

The $Co_2(CO)_6$ complex of $Co_3\{\mu_3\text{-}C(C\equiv C)_4H\}(CO)_9$ is one of the products formed in the reaction between buta-1,3-diyne and $Co_3(\mu_3\text{-CBr})(CO)_9$.[438]

Reactivity of Re–C_n–Os$_3$ complexes.

The stabilities of the Os_3–C_x–Re complexes decrease with increasing x, the C_6 complex being thermally quite labile, although the nature of decomposition product has not been established. Tethering the redox-active $Re(PPh_3)(NO)Cp^*$ moiety to the cluster moiety $Os_3(\mu\text{-H})(CO)_{10}$ via a μ-$\eta^1(Re):\eta^1(Os_2)$–$(C\equiv C)_m$ bridge results in complexes **235/m** which undergo a single partially chemically reversible oxidation at more positive potentials

than comparable mono-nuclear complexes $Re\{(C\equiv C)_m R\}(PPh_3)Cp^*$ in each case.[434,435] In contrast to the $Re(C\equiv C)_m Re$ systems described above, these oxidations become more thermodynamically favorable as the chain length increases. These observations may be due to a greater contribution from a $^+Re=(C=C)_n=Os_3^-$ zwitterionic form in the ground-state, which becomes less important with increasing chain length.[435]

B. *Compounds Containing Two Carbon Chains Attached to a Single Cluster Unit*

Reactions of $\{ML_x\}_2\{\mu\text{-}(C\equiv C)_m\}$ $[ML_x = Fp^*, Ru(PPh_3)_2Cp; m = 3, 4]$ with $Fe_2(CO)_9$ under mild conditions result in cleavage of one of the central $C\equiv C$ triple bonds to give the carbyne clusters $\{ML_x\}C\equiv CC\{Fe_3(CO)_9\}$ $C(C\equiv C)_{m-2}\{ML_x\}$ (**268**).[308,422] The carbyne carbons are found between δ 265 and 280. These results contrast with reactions of the analogous $\mu\text{-}C_2$ and $\mu\text{-}C_4$ complexes, which give alkynyl clusters (above). These reactions result in cleavage of a $C\equiv C$ triple bond under mild conditions, possibly by formation of an electron-deficient trigonal prismatic C_2Fe_2 intermediate which adds a third $Fe(CO)_3$ group. The electron deficiency of this intermediate is relieved somewhat if electron donation from electron-rich ML_x groups can occur through the $C\equiv C$ triple bond.
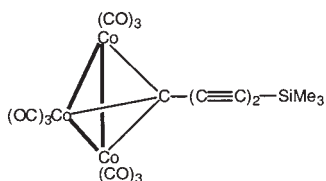
(264)
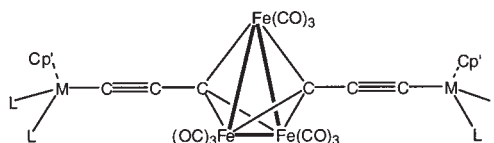
(268) $ML_nCp' = Fp^*, Ru(PPh_3)_2Cp$

VIII

COMPLEXES CONTAINING TWO CLUSTER END-GROUPS

A. *Compounds with a Single Carbon Atom*

Complexes containing a single carbon atom linking two trimetallic clusters have been obtained from the reaction between $Co_3(\mu_3\text{-}CCl)(CO)_9$ and $[PPh_4]_2[Fe_3(\mu_3\text{-}CCO)(CO)_9]$ in the presence of $TlBF_4$.[451] The Fe_3 cluster replaces the halide to give (**269**) which in turn is converted into the ethyl

ester (**270**) after treatment with EtOH. Subsequent reaction of **270** with AuCl(PPh$_3$) displaced the Co$_3$C cluster, affording Au$_3$Fe$_3$(μ_3-CCO$_2$Et) (CO)$_9$(PPh$_3$)$_3$.

(**269**) CR = C=O
(**270**) CR = C(O)OEt

n = 0 (**271**), 1 (**286**), 2 (**290**)
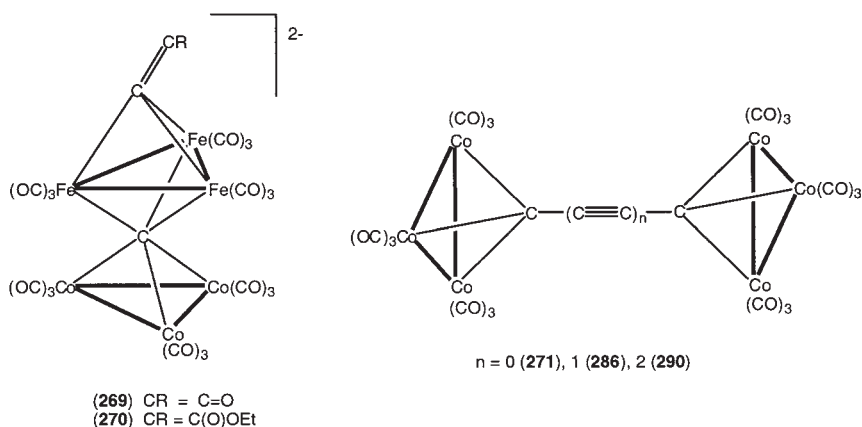
B. *Compounds with C$_2$ Ligands*

Two main methods have been used to produce metal clusters bearing C$_n$ ligands ($n \geq 2$) bridging two metal clusters:

(a) Addition of metal substrates to preformed complexes containing C$_n$ ligands;
(b) Thermal reactions involving dehalogenation of halomethylidyne precursors (especially cobalt).

As found with other complexes discussed in this chapter, the prevalence of even-numbered carbon chains is a result of the use of C$_n$ ($n =$ even) synthons in their construction. A few examples of odd-numbered chains, particularly when end-capped by trinuclear clusters which form μ_3-methylidyne complexes, are known. The following discussion will consider complexes in order of increasing n.

1. {Co$_3$(CO)$_9$}$_2$(μ_3:μ_3-C$_2$) (271)

The first example of a cluster containing two M$_3$C cores linked by a C–C bond was reported in 1966, when orange-brown {(OC)$_9$Co$_3$}(μ_3:μ_3-C$_2$){Co$_3$(CO)$_9$} (**271**) was obtained by heating Co$_3$(μ_3-CBr)(CO)$_9$ in toluene at 90 °C.[452] Other compounds formed include CoBr$_2$ and {Co$_3$(CO)$_9$ (μ_3-C)}$_2$CO. The best preparation appears to be Lewis base (AsPh$_3$)-induced

reductive coupling of $Co_3(\mu_3\text{-CBr})(CO)_9$, either at $100\,^\circ C$ (90%) or in hexane at $70\,^\circ C$ for 3 h (38%), the likely by-product being $AsBr_2$ Ph_3.[439,453,454] Under CO, however, a 63% yield of $\{Co_3(CO)_9(\mu_3\text{-C})\}_2CO$ is obtained.

The same compound has been reported on several occasions since then, often as a by-product from reactions involving other cobalt cluster carbides. Thus, it is one product of the reactions between $Co_3(\mu_3\text{-CX})(CO)_9$ ($X = Cl$, Br) and arenes.[440,455,456] Other products include $Co_5(C_3H)(CO)_{15}$, $Co_6C_4(CO)_{18}$ and $Co_6C_5(CO)_{17}$, together with $\{Co_3(CO)_9(\mu_3\text{-C})\}_2CO$, all complexes being obtained in low yield. Product distribution studies in reactions of $Co_2(CO)_8$ with either CX_4 ($X = Cl$, Br) or $Co_3(\mu_3\text{-CBr})(CO)_9$ have been used as evidence for the existence of the $Co_3(\mu_3\text{-C}^\bullet)(CO)_9$ radical as an intermediate.[457] The complex has also been isolated from reactions of $Co_3(\mu_3\text{-CCO}_2Pr^i)(CO)_9$ in propionic anhydride with aqueous HPF_6 [probably by reaction of $[Co_3(\mu_3\text{-CCO})(CO)_9]^+$ with $Co_3(\mu_3\text{-CCO}_2H)$ $(CO)_9$];[458] in trace amounts in the reaction of $Co_3(\mu_3\text{-CI})(CO)_9$ and $HgPh_2$ (benzene under CO, $58\,^\circ C$), or in 35% yield from $Co_3(\mu_3\text{-CBr})(CO)_9$, 4-$BrC_6H_4Me$ and activated copper–bronze in refluxing benzene under CO.[459] Low yields were also obtained from thermal or photochemical reactions of $Co_2(CO)_8$ with CF_3I (3.6%), C_2F_4 (7.7%) or C_2HF_3 in acetone (14%), along with $Co_3(\mu_3\text{-CF})(CO)_9$,[460] as a by-product from $[Co(CO)_4]^-$ with CCl_4 or $CHBr_3$, or of $Co_2(CO)_8$ with C_2Cl_6 (ca. 1% yield),[461] from $Co_2(CO)_8$ with 1,2,5-thiadiazolo[3,4-d][1,3]dithiole-2-thione,[462] or with dihaloethynes, particularly C_2I_2.[463,464]

The molecular structure of the monoclinic phase was first reported in 1971 and confirmed that two $CCo_3(CO)_9$ units were joined through a C–C bond [1.37(2) Å] with mean Co–C 1.96(1), Co–Co 2.457 Å.[465,466] The Co_3 clusters have average Co–Co and Co–C separations of 2.457(1) and 1.96(1) Å, respectively. Twisting of the Co_3C groups (ca. 28°) minimizes steric interactions between CO groups. The short C–C bond is consistent with approximate sp hybridization. A more recent structural determination, carried out on a trigonal phase, also found an inter-cluster twist of ca. 28°; the crystals are optically active by spontaneous resolution.[467] In this form, the C–C separation is longer at 1.426(9) Å, with Co–C 1.94, Co–Co 2.458 Å (av.).

The cluster does not undergo electron transfer-catalyzed CO substitution reactions because the lifetimes of the intermediate radical anions are too short (see below).

2. $[\{Co_2Fe(CO)_9\}(\mu_3:\mu_3\text{-C}_2)\{CoFe_2(CO)_9\}]^-$ (275) and Related Species

Addition of electrophilic metal reagents to ketenylidene (CCO) clusters is a source of several carbido clusters via cleavage of the C–CO bond.[468]

Cleavage of the CC–O bond to give C_2 derivatives can be achieved by using precursors containing good leaving groups, such as acetate, attached to alkynyl clusters. Ready attack on the μ_3-alkynyl group enables the nucleophilic metal reagent to become attached to the C_2 fragment. Further reactions to involve the added metal center in the cluster core (cluster expansion) affords dicarbido clusters.

Thus, attack of $[Fe(CO)_4]^{2-}$ on $[Fe_3(\mu_3\text{-}C_2OAc)(CO)_9]^-$ (272; Scheme 54) affords $[Fe_3\{\mu_3\text{-}C_2[Fe(CO)_4]\}(CO)_9]^{2-}$ (232) which with $Co_2(CO)_8$ gives $[\{Co_2Fe(CO)_9\}(\mu_3:\mu_3\text{-}C_2)\{CoFe_2(CO)_9\}]^-$ (273) via intermediate complexes $[CoFe_2\{\mu_3\text{-}C_2[Fe(CO)_4]\}(CO)_9]^-$ (274) and $[\{Co_2Fe(CO)_9\}(\mu_3:\mu_3\text{-}C_2)\{Fe_3(CO)_9\}]^{2-}$ (275).[432] Direct conversion of 272 to 275 occurs in its reaction with $Co_2(CO)_8$, but lower yields are obtained. Formation of 275 involves addition of a $Co_2(CO)_6$ fragment to the C_2 moiety, together with exchange of an $Fe(CO)_3$ group for $[Co(CO)_3]^+$. Since addition of $[Fe_2(CO)_8]^{2-}$ to 273 regenerates 275, similar structures are ascribed to these two clusters. The terminal CO ligands resonate at δ 200–225, with μ-CO signals at δ 240 and 245. Broad resonances at δ 285.9 and 293.7 arise from the C_2 ligand, which at $-70\,^\circ$C show $^1J(CC)$ of 34 Hz. For 275, the C_2 resonances are at δ 279.4 and 285.7, the former assigned to the carbon attached to the Co_2Fe cluster on the basis of quadrupolar broadening.

The X-ray structure of 273 shows that the C_2 ligand is $\mu_3:\mu_3$-bridging $CoFe_2$ and Co_2Fe clusters. Of the nine CO ligands, one bridges a Co–Fe edge on each cluster. The C–C separation is 1.362(8) Å, similar to that found in $\{Co_3(CO)_9\}_2$ $(\mu_3:\mu_3\text{-}C_2)$ (271) above. However, in contrast to this complex, in which the two Co_3 planes are parallel, the M_3 planes in 273 are
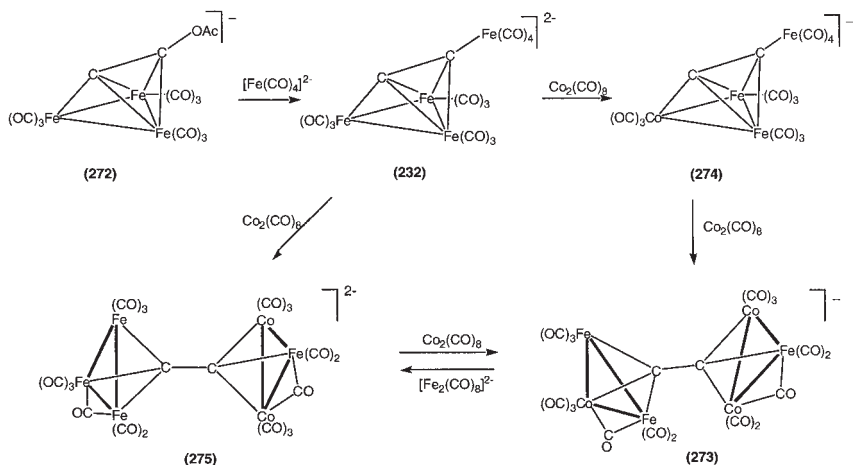
SCHEME 54

inclined towards each other by 18° so that the Co(3)···Fe(2) separation is only 2.899(1) Å, with concomitant effects on the CO coordination. The asymmetric interactions of the M_3 clusters with the C_2 ligand is seen from the M–C–C angles [range 110.0(4)–140.6(5)°] and some variation in M–C distances [Co(1)–C(1) 1.919(6), Fe(3)–C(2) 1.987(6) Å]. The tilt is ascribed to a second-order Jahn-Teller effect, which results in separation of the nearly degenerate HOMO and LUMO levels and full occupation of the former, leading to the observed diamagnetism for this 94 c.v.e. anion.

The related cluster anion $[Co_5Fe(C_2)(CO)_{17}]^-$ (**276**) has been prepared from $Co_3(\mu_3$-CCl)$(CO)_9$ and $[PPh_4]_2[Fe_3(CO)_{11}]$ in the presence of $TlBF_4$.[451] The structure is closely related to that of **273** by replacement of [2Fe(CO)$_3$ + CO] by two Co(CO)$_3$ groups. A similar but larger tilt (42°) of the Co$_2$Fe and Co$_3$ planes towards each other results in formation of a shorter Co–Co bond [2.643(2) Å]. The reaction probably proceeds via Tl-induced loss of Cl from $Co_3(\mu_3$-CCl)$(CO)_9$ and reduction to give $\{Co_3(CO)_9\}_2(\mu$-$C_2)$, followed by facile exchange of cobalt for iron.

(**276**)
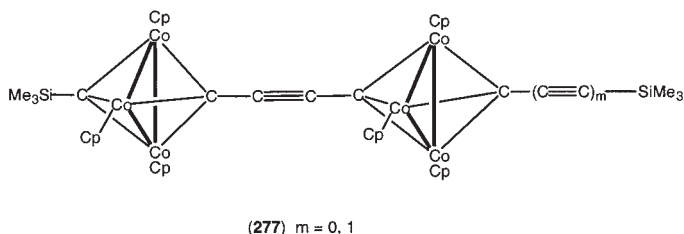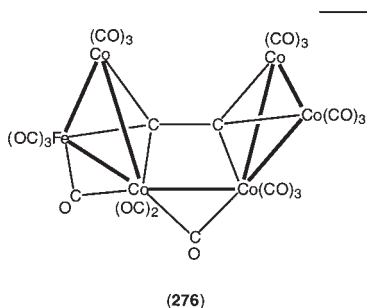
(**277**) m = 0, 1

3. Co$_3$Cp$_3$ Derivatives

The complexes $(\mu_3$-CSiMe$_3)\{Co_3Cp_3\}(\mu_3:\mu_3$-CC)$\{Co_3Cp_3\}\{\mu_3$-C(C≡C)$_m$ SiMe$_3\}$ (**277**, $m=0$, 1) were found in the plethora of products obtained from reactions of Co(CO)$_2$Cp with SiMe$_3$(C≡C)$_{m+2}$SiMe$_3$ (decalin, 195°), the cluster being formed with concomitant cleavage of one of the C≡C triple bonds.[469]

C. *Compounds with C_4 Chains*

1. Iron, Ruthenium, and Osmium

Cleavage of the CC–O bond in μ_3-ketenylidene clusters has been used as a route to dicarbido clusters, sometimes via an intermediate containing a ligand with a good leaving group, such as acetate. In the presence of an excess of triflic anhydride, ready loss of the resulting triflate group followed by oxidative coupling of the C_2Fe_3 cluster occurs instead to give red $[\{Fe_3(CO)_9\}_2(\mu_3:\mu_3-C_4)]^{2-}$ (**278**),[470,471] also obtained by loss of the Fp group in the reaction of $[Fe_3(\mu_3-C_2Fp)(CO)_9]^{2-}$ with $[Mn(CO)_3(NCMe)_3]^+$.[431] The C_4 chain is attached to each cluster through two carbons, in the familiar μ_3-$\eta^1,2\eta^2$ mode often found in μ_3-alkynyl ligands. The C_4 chain is bent [internal angle C–C–C 148.0(6)°] and the C–C distances are 1.306(7) and 1.42(1) Å, the ligand resembling a 1,3-diene with a rather larger internal angle from steric interactions.

Thermolysis (refluxing toluene with nitrogen purge) of the bis(cluster) complexes $\{M_3(CO)_{11}\}_2(\mu-PPh_2C\equiv CC\equiv CPPh_2)$ (**279**, $M = Ru$, Os) results in cleavage of both P–C(sp) bonds to give $\{M_3(\mu-PPh_2)(CO)_9\}_2(\mu_3:\mu_3-C_2C_2)$.[472,473] The C_4 fragment bridges two triangular M_3 clusters in the μ_3-$\eta^1,2\eta^2$ fashion. The two halves of each molecule are related by a crystallographic symmetry element.
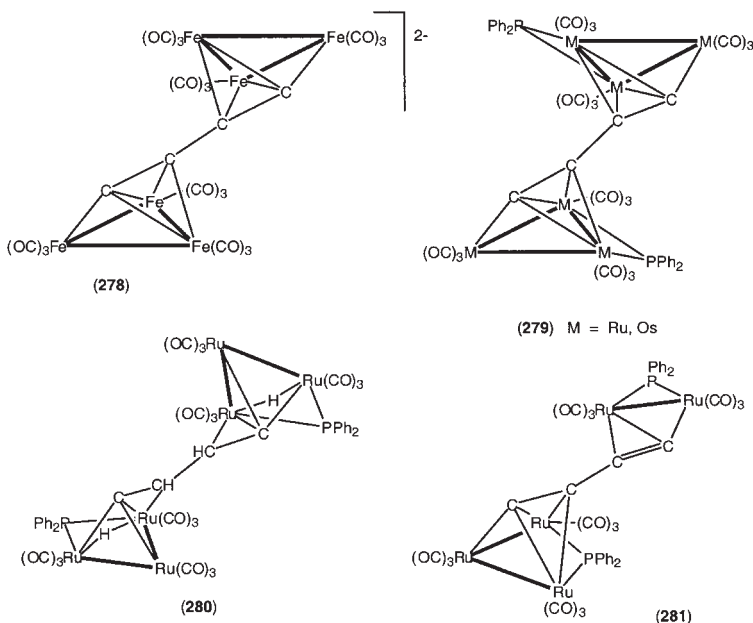
Reactions of **279** with H^-/H^+ ($\equiv H_2$) gave **280** in which hydrogen has added both to the cluster and to the central carbons of the C_4 unit. In contrast, the reaction of **279** with molecular dihydrogen resulted in cleavage of an $Ru(CO)_3$ fragment and formation of the pentanuclear complex **281**.[474]

The cluster $Ru_3\{\mu_3-\eta^1:\eta^2-HC_2C\equiv C[W(CO)_3Cp]\}(\mu-CO)(CO)_9$ (**244**) reacts readily with a further portion of $Ru_3(CO)_{12}$ to afford $\{Ru_3(\mu-H)(CO)_9\}(\mu_3:\mu_3-C_2C_2)\{Ru_2W(CO)_8Cp\}$ (**282**) in which both $C\equiv C$ moieties of the original diynyl ligand are engaged in σ/π bonding with a trimetallic fragment (Scheme 55).[444,445] A similar reaction with $Fe_2(CO)_9$ gave a mixture of complexes $\{Fe_mRu_{3-m}(\mu-H)(CO)_9\}(\mu_3:\mu_3-C_2C_2)\{Fe_nRu_{2-n}W(CO)_8Cp\}$ (**283**), while $Co_2(CO)_8$ gave the ethynylvinylidene-linked cluster $\{CoRu_2(CO)_9\}\{\mu_3:\mu_3-CCHC_2\}\{CoRuW(\mu-CO)(CO)_8Cp\}$ (**284**). The cluster-bonded H atom in the precursor has migrated to the C_4 chain in **284**. In both, X-ray studies showed the presence of extensive disorder, eventually resolved in terms of variable occupancies of the three sites M(1,5,6) in **283** of between 26, 52, 12 and 74, 92, 64% iron. In **284**, sites M(2,3) similarly have Co/Ru disorder. In these complexes, the two cluster-bonded C_2 units act independently, being linked by a formal C–C single bond.

(244)

(282) M = Ru
(283) Ru/Fe (disordered)

(284) M = Co/Ru disordered
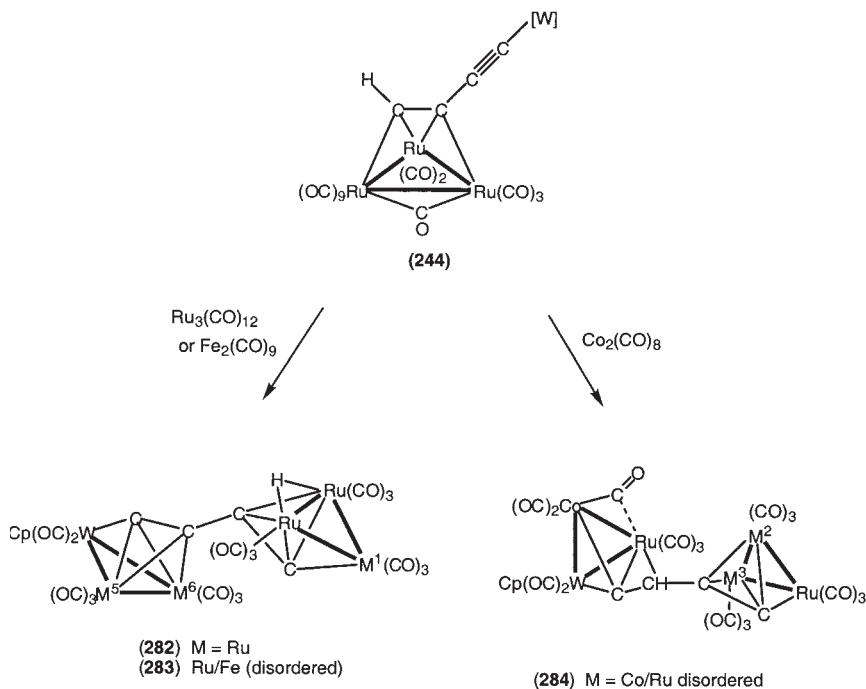
SCHEME 55

Reactions of $\{Cp(OC)_3W\}(\mu\text{-}C\equiv CC\equiv C)\{M(CO)(PPh_3)_2\}$ (M = Rh, Ir) with $Fe_2(CO)_9$ have given not only **248** but also $\{Fe_2M(CO)_6(PPh_3)\}(\mu_3:\mu_3\text{-}C_2C_2)\{Fe_2W(CO)_8Cp\}$ (**285**; Scheme 51, above) as the major products, which are formed sequentially.[295] Concomitantly with the formation of the two new metal–metal bonds, loss of PPh_3 has occurred from the Group 9 metal center and of CO from the tungsten atom. In contrast to **248**, the terminal carbon of the C_4 chain remains σ-bonded to the Group 9 metal center in **285**.

2. $\{Co_3(CO)_9\}_2(\mu_3:\mu_3\text{-}CC\equiv CC)$ (286)

Orange-brown $\{Co_3(CO)_9\}_2(\mu_3:\mu_3\text{-}CC\equiv CC)$ (**286**) is one of the products of thermolysis of $Co_3(\mu_3\text{-}CX)(CO)_9$ (X = Cl, Br) in xylene or mesitylene, and it is also obtained from $MgBr(C\equiv CH)$ and $Co_3(\mu_3\text{-}CBr)(CO)_9$,[448,456] $Co_2(CO)_8$ and $CFCl_3$, $Co_3(\mu_3\text{-}CBr)(CO)_9$ and C_6F_6, $Co_2(CO)_8$ and C_2F_4. However, the highest yielding reaction is that between $Co_2(CO)_8$ and $Fp^*C\equiv CC\equiv CFp^*$ (62%).[420] The crystal structure confirms the presence of a linear C_4 ligand, attached to a $Co_3(CO)_9$ cluster at each end by a $\mu_3\text{-}C$ atom, with a $C\equiv C$ unit linking the two.[456,466] The mean Co–Co and Co–C distances are 2.47(1) and 1.92(1) Å, while the C–C and $C\equiv C$ bond lengths are 1.37(1) and 1.24(2) Å, respectively, consistent with "partial π-delocalization". The $C\equiv C$ triple bond is sterically protected by the CO groups and does not react with $Co_2(CO)_8$, nor it is catalytically hydrogenated.

The mono- and bis-PPh_3 derivatives were prepared as brown neeedles from the parent complex and PPh_3 in refluxing hexane, or better, from $Pt(PPh_3)_4$ at r.t.;[456] mono- and bis-PCy_3 complexes are also described. IR ν(CO) data are given for complexes containing up to five PEt_2Ph ligands, but no preparative details are available. Reactions of **286** with $P(OMe)_3$ afforded di-, tri-, and tetra-substitution products as black crystalline materials.[439] The structure of $\{[(MeO)_3P](OC)_8Co_3\}(\mu_3:\mu_3\text{-}CC\equiv CC)\{Co_3(CO)_7[P(OMe)_3]_2\}$ (**287**) suggests that the distribution of $P(OMe)_3$ ligands minimizes steric interactions in the solid-state. The central C_4 ligand has C–C bond distances of 1.39, 1.26, and 1.38(2) Å and mean Co–C and Co–Co separations are 1.91 and 2.475 Å, respectively.

3. Mo/W–Co Clusters

Reactions of $Co_2(CO)_8$ with the C_4 complexes $\{M(CO)_3Cp\}_2(\mu\text{-}C\equiv CC\equiv C)$ (M = Mo, W) have given the cluster complexes $\{Co_2M(CO)_8Cp\}_2(\mu_3:\mu_3\text{-}CC\equiv CC)$ (**288**) in which the terminal carbons are attached to all three metal centers in each cluster.[419] All three compounds (Mo$_2$, MoW, W$_2$) have similar structures, which are closely related to that

(287)

(288) M = M' = Mo, W; M = Mo, M' = W
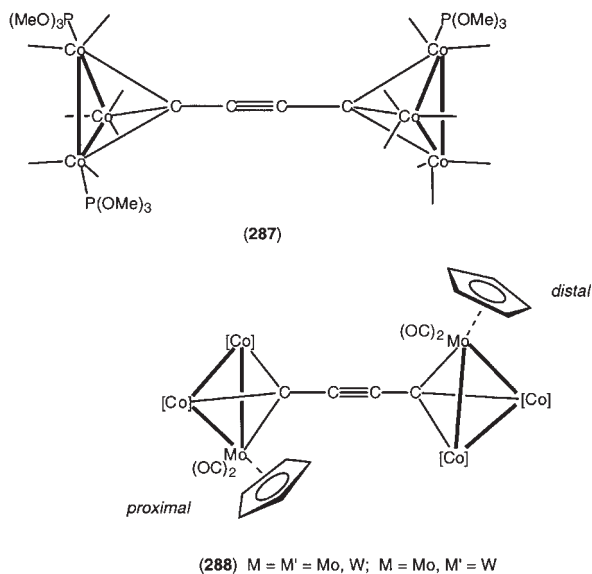
of $\{Co_3(CO)_9\}_2(\mu_3 : \mu_3\text{-}CC\equiv CC)$. The C–C separations suggest that the electronic rearrangement of the original diyndiyl chain has been altered to an acetylenic dicarbyne, $\equiv CC\equiv CC\equiv$, corresponding to a formal oxidation of the precursor. Of note also are the locations of the Cp groups, which in one cluster is *proximal*, in the second *distal*, to the C_4 chain. Cluster formation occurs as a result of the presence of the two sterically demanding $M(CO)_3Cp$ end-caps.

4. Co_3Cp_3 Derivatives

Products from reactions of $Co(CO)_2Cp'$ ($Cp' = Cp$, Cp^{Me}) and Me_3Si $(C\equiv C)_2SiMe_3$ include $(Me_3Si\text{-}\mu_3\text{-}C)\{Co_3Cp_3\}(\mu_3{:}\mu_3\text{-}CC\equiv CC)\{Co_3Cp_3\}(\mu_3\text{-}CSiMe_3)$ **(289)** (0.33%),[469,475] also formed by "deck shifting" (f.v.p. at 550 °C, or in pristane at 290 °C/6 h; 40%) of the isomeric $(Me_3SiC\equiv C\text{-}\mu_3\text{-}C)\{Co_3Cp_3\}(\mu_3 : \mu_3\text{-}CC)\{Co_3Cp_3\}(\mu_3\text{-}CSiMe_3)$. Compared with those of $Co_3(\mu_3\text{-}CSiMe_3)\{\mu_3\text{-}C(C\equiv C)_nR\}Cp_3$ ($n = 1$, $R = H$; $n = 1$, 2, $R = SiMe_3$), the electronic spectra of the more deeply colored $\{Co_3(\mu_3\text{-}CSiMe_3)Cp_3\}_2\{\mu_3 : \mu_3\text{-}C(C\equiv C)_nC)\}$ ($n = 2$, 4) are bathochromically shifted to 610 and 635 nm ($\varepsilon \sim 10{,}000$), respectively, indicating a reduced HOMO/LUMO separation.[443]

D. *Compounds with C_6 Chains*

1. Cobalt Carbonyl Clusters

The dark brown $Co_2(CO)_6$ derivative of $\{Co_3(CO)_9\}_2\{\mu_3 : \mu_3\text{-}C(C{\equiv}C)_2C\}$ (**290**) has been obtained on several occasions. It is a minor product from $Co_3(\mu_3\text{-CBr})(CO)_9$ in xylene (125 °C, 25 min),[476,477] from buta-1,3-diyne and $Co_3(\mu_3\text{-CBr})(CO)_9$ (with $CuCl/NHEt_2$),[438] and from the reaction between $Co_2(CO)_8$ and hexachlorocyclopropane in thf (13% yield).[478] In the $0.5C_6H_6$-solvate, C–C separations along the C_6 chain are 1.37, 1.37, 1.36, 1.20, 1.36(4) Å and corresponding angles of 140, 148, 172, and 175(3)°, or of a non-solvated form, which has C–C distances are 1.44, 1.37, 1.38, 1.19, and 1.36(3) Å, with mean Co–Co 2.454(7) and Co–C 1.92(3) Å.[476] Addition of a second $Co_2(CO)_6$ moiety is precluded for steric reasons. The short C–C distances suggest that electron delocalization along the carbon chain occurs, subsequently confirmed by electrochemical studies (see below).

The phosphine-substituted derivative $\{Co_3(\mu\text{-dppm})(CO)_7\}_2(\mu_3 : \mu_3\text{-}CC{\equiv}CC)$ (**291**) was initially isolated from the CuI-catalyzed reaction between $Co_3(\mu_3\text{-CBr})(\mu\text{-dppm})(CO)_7$ and $Au(C{\equiv}CC{\equiv}CH)(PPh_3)$, and can be prepared in 39% yield if $\{Au(PPh_3)\}_2(\mu\text{-}C{\equiv}CC{\equiv}C)$ is used. Presumably the basic solvent allowed dissociation of both the H and $Au(PPh_3)$ groups

m = 1 (**289**), 2 (**292**), 4 (**298**)

(**290**)
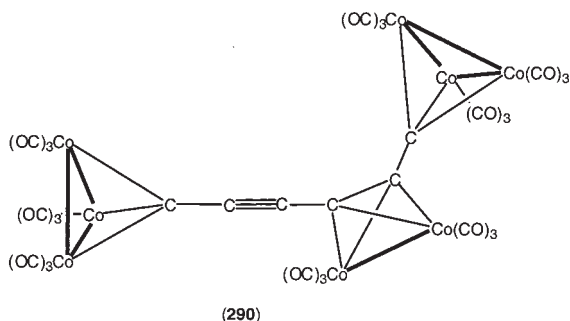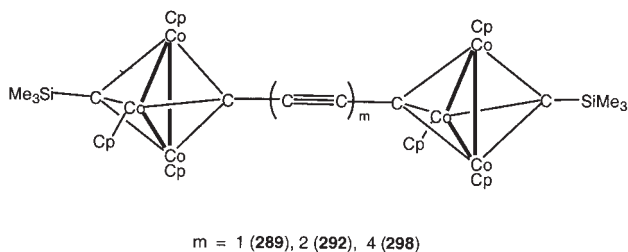
and subsequent attachment of the cobalt cluster fragments to each end of the C_4 chain.[442] An alternative route is from $Co_3(\mu_3\text{-CBr})(\mu\text{-dppm})(CO)_7$ and $Co_3\{\mu_3\text{-CC}\equiv C[Au(PPh_3)]\}(\mu\text{-dppm})(CO)_7$.

2. Co_3Cp_3 Derivatives

Proto-desilylation of $(Me_3Si\text{-}\mu_3\text{-C})\{Co_3Cp_3\}(\mu_3\text{-CC}\equiv CSiMe_3)$ and oxidative coupling of the resulting terminal alkyne ($CuCl$/tmed/acetone, O_2, $40\,°C$) afforded $\{Co_3(\mu_3\text{-CSiMe}_3)Cp_3\}_2(\mu_3:\mu_3\text{-CC}\equiv CC\equiv CC)$ (292), also obtained by coupling of $(Me_3Si\text{-}\mu_3\text{-C})\{Co_3Cp_3\}(\mu_3\text{-CC}\equiv CH)$ with $HC\equiv CSiMe_3$; the cluster $(Me_3Si\text{-}\mu_3\text{-C})\{Co_3Cp_3\}(\mu_3\text{-CC}\equiv CC\equiv CSiMe_3)$ (293) was formed as a major product in the latter reaction and also from $(Me_3Si\text{-}\mu_3\text{-C})\{Co_3Cp_3\}(\mu_3\text{-CC}\equiv CH)$ and $(I\text{-}\mu_3\text{-C})\{Co_3Cp_3\}(\mu_3\text{-CSiMe}_3)$. Complex 292 has an unusual intense dark green color rather than the usual purple.[443] The molecular structure contains two CCo_3 clusters capping a slightly bent buta-1,3-diyne chain (angles at C 178, 177, 175, 178°) with C–C bonds along the chain (1.42, 1.19, 1.36, 1.21, 1.43(2) Å) indicating some delocalization. There is no steric interaction between the Cp and $SiMe_3$ groups.

E. Compounds with C_8 Chains

The reaction between $Co_3(\mu_3\text{-CBr})(\mu\text{-dppm})(CO)_7$ and $\{Au[P(tol)_3]\}_2\{\mu\text{-}(C\equiv C)_3\}$ gives $\{Co_3(\mu\text{-dppm})(CO)_7\}_2\{\mu_3:\mu_3\text{-C}(C\equiv C)_3C\}$ (294) in 77%

(291) m = 2
(294) m = 3
(297) m = 4

(293)
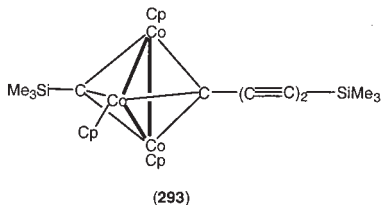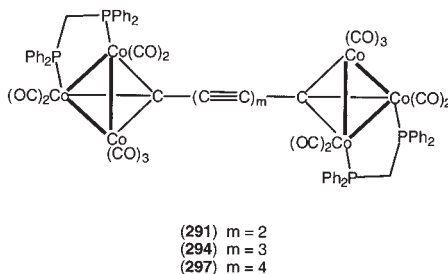
yield.[442] Subsequent reaction with tcne gave the mono-adduct $\{Co_3(\mu$-dppm$)(CO)_7\}_2\{\mu_3:\mu_3$-C(C≡C)$_2$C[=C(CN)$_2$]$_2$C$\}$ (295). Similarly, treatment of Ru$_3(\mu$-H)$_3(\mu_3$-CBr$)(CO)_9$ with $\{Au[P(tol)_3]\}_2\{\mu$-(C≡C)$_3\}$ afforded $\{Ru_3(\mu$-H)$_3(CO)_9\}_2\{\mu_3:\mu_3$-C(C≡C)$_3C\}$ (296).

(295)

(296)
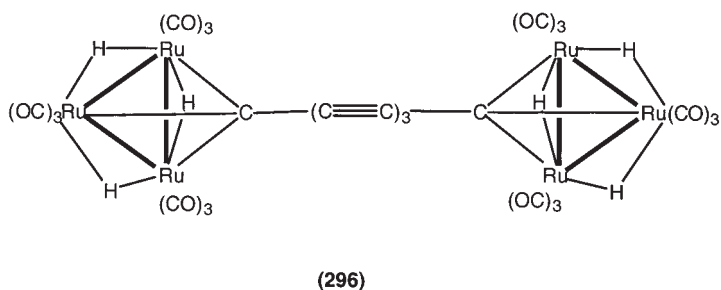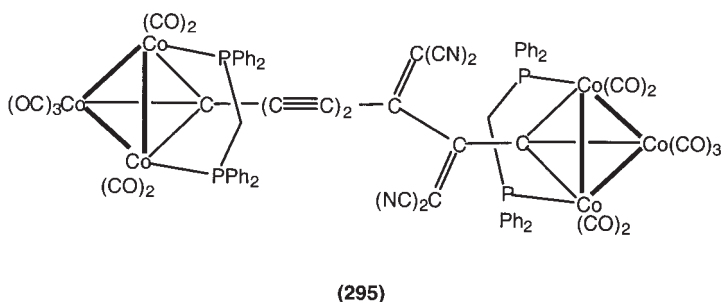
F. *Compounds with C₁₀ Chains*

The complex $\{Co_3(\mu$-dppm$)(CO)_7\}_2\{\mu_3:\mu_3$-C(C≡C)$_4$C$)\}$ (297) forms thin black hair-like crystals and is obtained in 91% yield from the reaction between Co$_3(\mu_3$-CBr$)(\mu$-dppm$)(CO)_7$ and $\{Au(PPh_3)\}_2\{\mu$-(C≡C)$_4\}$.[442]

Proto-desilylation of Co$_3(\mu_3$-CSiMe$_3)\{\mu_3$-C(C≡C)$_2$SiMe$_3\}$Cp$_3$ and oxidative coupling (CuCl/tmeda/acetone, O$_2$, 40 °C) *in situ* afforded dark green $\{Co_3(\mu_3$-CSiMe$_3)$Cp$_3\}_2\{\mu_3:\mu_3$-C(C≡C)$_4$C$\}$ (298), which is unstable both as a solid and in solution.[443] As found for the analogous C$_6$ cluster 292, the complex shows an intense band at 635 nm (ε ca. 10,000) and two reversible oxidation steps separated by ca. 0.14 V, again indicating some electronic communication via the carbon chain. The Co$_3$Cp$_3$ clusters provide steric hindrance to adjacent CC≡C moieties and only 298 reacted with Co$_2(CO)_8$ to give (Me$_3$Si-μ_3-C)$\{Co_3$Cp$_3\}\{\mu_3$-CC≡CC$_2$SiMe$_3$[Co$_2(CO)_6]\}$.[443]

G. *Polymeric Species*

Several copper(I)-catalyzed coupling reactions of alkynes or diynes with Co_3 clusters proceed with the deposition of insoluble black materials which have $\nu(CO)$ spectra typical to those of the $CCo_3(CO)_9$ clusters described above.[438] Similar products were obtained when $HC{\equiv}CMgBr$ was used. Thermal decomposition of **286** at 100 °C gives conducting aggregates, which continue to show $\nu(CO)$ absorptions and are soluble in non-aqueous solvents.[480] The conductivity appears to be associated with partial decarbonylation and formation of granular microcrystalline materials.

H. *Redox Chemistry of Complexes Containing Co₃ Clusters Linked by Carbon Chains*

Extensive studies of the redox chemistry of $[\{Co_3(CO)_9\}_2\{\mu\text{-}C(C{\equiv}C)_mC\}]$ ($m = 0$, **271**; 1, **286**) have been made independently by the groups of Robinson[439] and Osella[481,482] and the electrochemical behavior of the C_2 and C_4 complexes has been compared with that of $\{Co_2(CO)_6\}_2(\mu\text{-}\eta^2\text{-}PhC_2C_2Ph)$.[482,483] Two distinct one-electron reduction processes are found, of which the first shifts to more negative potentials as the carbon chain is lengthened. This is consistent with effective electronic communication between the redox centers. This is attenuated when a $Co_2(CO)_6$ group is attached to the carbon chain. All scans contain a wave due to the $[Co(CO)_4]^-$ anion formed by chemical decomposition.

Osella and co-workers observed that the absolute values of the electrochemical potentials are sensitive to the nature of the solvent (CH_2Cl_2 vs. acetone), which is consistent with the different degree of solvation around the metal cores, and the different reorganization energy associated with the ligand rearrangement proposed by Robinson.[481] However, as the difference in half-wave potential between the two electrochemical events is more or less independent of the dielectric constant of the medium (**271**/**286** ca. 340/200 mV CH_2Cl_2; 360/210 mV acetone), it is reasonable to suggest that a significant through-bond contribution to the electronic coupling between the metal centers is in operation. In thf the wave separation was found to increase to 470/300 mV, but this may be due to the greater stabilization of the radical anion in this solvent.[481]

1. $\{Co_3(CO)_9\}_2(\mu_3 : \mu_3\text{-}C_2)$ (**271**)

Solutions of $\{Co_3(CO)_9\}_2(\mu_3 : \mu_3\text{-}C_2)$ (**271**) and its reduction products are unstable at r.t., so conventional electrochemistry of this complex was carried out at low temperatures. Two chemically reversible 1-e transfers are found

at E° -0.41, -0.77 V; the 360 mV separation suggests that there is effective electronic communication between the redox centers, namely the Co_3 clusters which are kept 4.6 Å apart by the carbon chain. At higher temperatures, these processes become less reversible and a third process with $E^{\circ} \sim 0.1$ V is found. The latter is derived from the first reduced product via a slow chemical reaction.[439,481,482] Both reductions are associated with fast irreversible chemical processes, the first reduction to the radical anion being followed by a rapid conversion to a new CO-bridged species (**299**; Scheme 56), which can be oxidized back to the original neutral cluster at -0.33 V (vs. $[FcH]^{0/1+}$). The isomerization is probably induced by steric interactions between the CO groups, as well as by the tendency of bridging CO groups for the better removal of electron density from the cluster. The main features of the reduction have been confirmed by *in situ* spectro-electrochemistry, monitoring the $\nu(CO)$ bands of the five reduced species which account for the spectral and electrochemical changes observed in this system.[484] Solvent effects on the reduction potentials result from solvation of the anion and ion association processes.

Irreversible chemical reduction of **271** gives a dark brown solution, which also contains $[Co(CO)_4]^-$. Slow conversion to the μ-CO species occurs, which has a short half-life on oxidation, regenerating **271**. With $CoCp_2$, the ESR-silent CO-bridged product is formed quantitatively. Oxidation of this species regenerates **271** in an amount which is less by the $[Co(CO)_4]^-$ produced by decomposition. Attempted chemical oxidation (Ag^+) gave only unstable pale yellow materials.
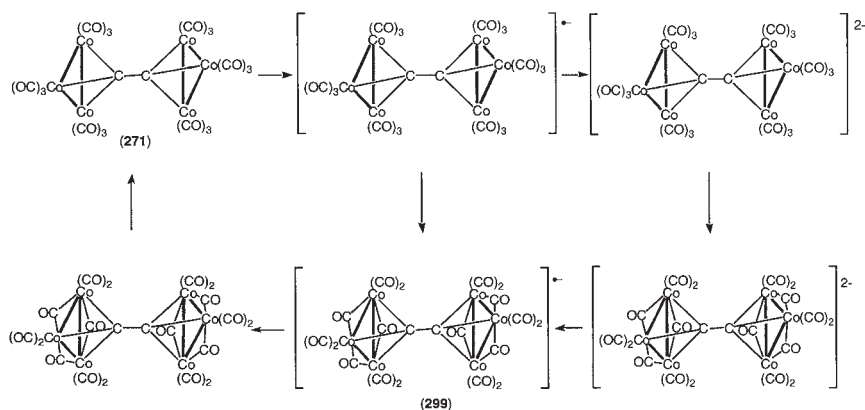
SCHEME 56

The rapid chemical transformation of the initial radical anion precludes the use of ETC-substitution chemistry to make substituted derivatives, because of the short lifetime and hence inactivity of the isomerized radical anion [**299**]$^{\cdot-}$ towards the CO/PR_3 replacement reaction.[484]

2. {$Co_3(CO)_9$}$_2(\mu_3:\mu_3$-CC≡CC) (**286**)

Strong electronic interactions between the two Co_3 clusters in the C_4 analogue **286**, which are separated by some 7.1 Å by the carbon chain, are suggested by the presence of two chemically reversible 1-e processes separated by 200–300 mV. The reduced species are more stable than the C_2 anions under electrochemical conditions and voltammograms were successfully collected at ambient temperature. At low temperatures (243 K) and moderate scan rates (200 mV/s) two reversible reductions are observed at $E_{1/2} = -0.39$ and -0.68 V. Above 243 K, a third reversible couple is found at ca. 0.85 V. In polar solvents (CH_2Cl_2, Me_2CO) ΔE° is 200–210 mV, whereas in thf, a value of 300 mV suggests that the monoanion is stabilized by the solvent interaction. The dianion also displays a tendency to generate electroactive species by subsequent chemical reactions, but if the cathodic scan is limited to the first two reduction waves (attributed to the [0,0/0,−1] and [0,−1/−1,−1] processes), the electrochemical response of each wave is as reversible as ferrocene under the same experimental conditions.[481]

3. {$Co_3(\mu_3$-CSiMe$_3$)Cp$_3$}$_2(\mu_3:\mu_3$-C(C≡C)$_m$C} ($m=2$, 4)

Less well-defined redox spectra are obtained for analogous Co_3Cp_3 complexes, which show two reversible 1-e oxidation processes at ca. 0.5, 0.8 V, separated by ca. 140 mV, again suggesting some electronic communication between the two clusters. Attempted chemical oxidation (Ag^+) gave unstable uncharacterized pale yellow compounds.

The cluster {$Co_3(\mu_3$-CSiMe$_3$)Cp$_3$}$_2${$\mu_3:\mu_3$-C(C≡C)$_4$C} (**298**) displays two reversible 1-e processes separated by ∼0.14 V, suggesting electronic communication between the two clusters. The oxidized species were not accessible by chemical oxidation (Ag^+), unstable uncharacterized pale yellow materials being obtained instead.[443]

IX

METAL CLUSTERS CONTAINING C_n LIGANDS

For reasons discussed above, this section will not include metal cluster carbide complexes containing only one carbide atom, for which several reviews are available.[35,37,38,40,485,486]
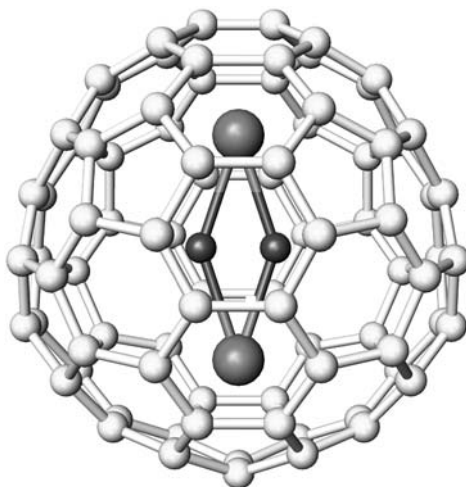
FIG. 11. Proposed structure for $Sc_2C_2@C_{84}$. (Reproduced with permission.)

An unusual C_2 complex contained within a carbon cluster is contained in the soot formed by an arc discharge between graphite containing Sc_2O_3. Purification of the endohedral scandium fullerenes by HPLC gave $Sc_2C_2@C_{84}$ (Fig. 11). X-ray powder diffraction and ^{13}C NMR data (δ 92) were interpreted in terms of a disordered Sc_2C_2 cluster encapsulated by D_{2d}–C_{84} (Sc–C 2.26, C–C 1.43 Å).[487]

Relatively few examples of metal clusters containing C_2 ligands have been reported, in comparison with the host of complexes containing a single carbon atom. There are two major classes of complexes, so-called "cage" or interstitial dicarbides, in which the C_2 unit is encompassed within the metal polyhedron, and "peripheral" dicarbides, where the C_2 unit lies on the periphery of the cluster or, alternatively, can be considered as part of a C_2M_n polyhedron. There is a continuum between clusters containing C_2 ligands in which the carbon atoms are separated by "normal" C–C bond distances (1.2–1.5 Å) and those in which the separation is up to 2.4 Å, i.e., too long for a conventional C–C bond (see Section IX.B below). The bonding electrons are delocalized between the carbon atoms and the metal clusters and rearrangements can occur readily.[35]

A. Peripheral C_n Clusters

Several clusters are known in which the C_2 ligand lies more-or-less exposed on the surface of an M_n cluster or within a cavity, but not completely encapsulated by the metal core. A theoretical study of these

compounds has been given by Frapper and Halet (Section IX.D).[488,489] In the complexes so far described, the C_2 unit acts as a four- or six-electron donor, while the distribution of electron density on the C_2 unit is revealed in the reactions with H–H, C–H or C–C bonds, or C–C bond-forming reactions. Often only one carbon is involved, the second becoming more closely bonded to the cluster. Synthetic approaches have included

(a) reactions of mono- or di-nuclear ethynyl complexes with other reactive metal substrates;
(b) cleavage of P–C(sp) bonds in 1,2-bis(phosphino)ethyne complexes;
(c) reactions of metal substrates with other easily cleaved C–X bonds.

Table XIII contains selected ^{13}C NMR and structural data for many of the C_2 complexes described below.

1. M_4 Complexes

(a) M_4C_2 clusters

The complexes $Fp'C{\equiv}CX$ [$Fp' = Fe(CO)_2Cp'$, $Cp' = Cp$, Cp^*; $X = H$, Fp'] react readily with iron, ruthenium, and cobalt carbonyls to give a range of homo- and hetero-metallic clusters containing C_2 and C_2H ligands.[35,433] Thermolysis (refluxing toluene) or oxidation ([FcH]PF$_6$) of $Ru_3(\mu\text{-}H)$ $(\mu_3\text{-}C_2Fp')(CO)_9$ affords the purple tetranuclear dicarbide cluster $Fe_2Ru_2(\mu_4\text{-}C_2)(\mu\text{-}CO)_2(CO)_8Cp'$ (**300**), also obtained from $Ru_3(CO)_{12}$ and $Fp^*C{\equiv}CFp^*$. The Cp^* complex contains the C_2 unit [C–C 1.27(1) Å] in a slightly twisted Fe_2Ru_2 framework (dihedral 24°). Each carbon bridges an Fe–Ru bond, with a long Ru–Ru separation [2.963(2) Å]; the complex is considered to be a permetallated ethene. Both carbons are equivalent, giving a singlet at δ 177.2; the CO groups are found between δ 191.1 and 217.8, with the μ-CO ligand resonating at δ 262.5. NMR studies suggest that protonation occurs either on the the Ru–Ru bond or to form an agostic C–H to the Ru atom (**301**).

Attempted protonation of the C_2 group with $MeCHClCO_2H$ resulted in addition of the acid across the Ru–Ru bond to give **302** (Scheme 57).[490] Reaction of the substituted cluster **303** with $HBF_4 \cdot OEt_2$ gave a cationic $\mu_4\text{-}C_2H$ complex **304**, which with SiH_2Ph_2 afforded $FeRu_2(\mu\text{-}H)$ $(\mu_3\text{-}HC_2H)(\mu\text{-}dppm)(CO)_5Cp^*$ (**305**), completing the formal hydrogenation of the C_2 ligand in **300**. Reaction of **304** with $[NEt_4][BH_4]$ gave $FeRu_2(\mu_3\text{-}C_2H)(\mu\text{-}dppm)(CO)_5Cp^*$ (**306**) while reaction of **303** with $Co_2(CO)_8$ formed $CoRu_2(\mu_3\text{-}C_2Fp)(\mu\text{-}dppm)(CO)_7$ (**307**).

Further examples of clusters containing the C_2M_4 framework have been obtained from $\{Ru(CO)_2Cp^R\}_2(\mu\text{-}C{\equiv}C)$ and two equivalents of $Ru(CO)_4(\eta\text{-}C_2H_4)$, which afford dark red $Ru_4(C_2)(\mu\text{-}CO)(CO)_8Cp'_2$ [$Cp' = Cp$ (**308a**),

(300)

MeCHClCO$_2$H

(302)

CHClMe

dppm

HBF$_4$.OEt$_2$

(303)

(304)

Co$_2$(CO)$_8$

[NEt$_4$]BH$_4$

SiH$_2$Ph$_2$

(307)

(306)

(305)
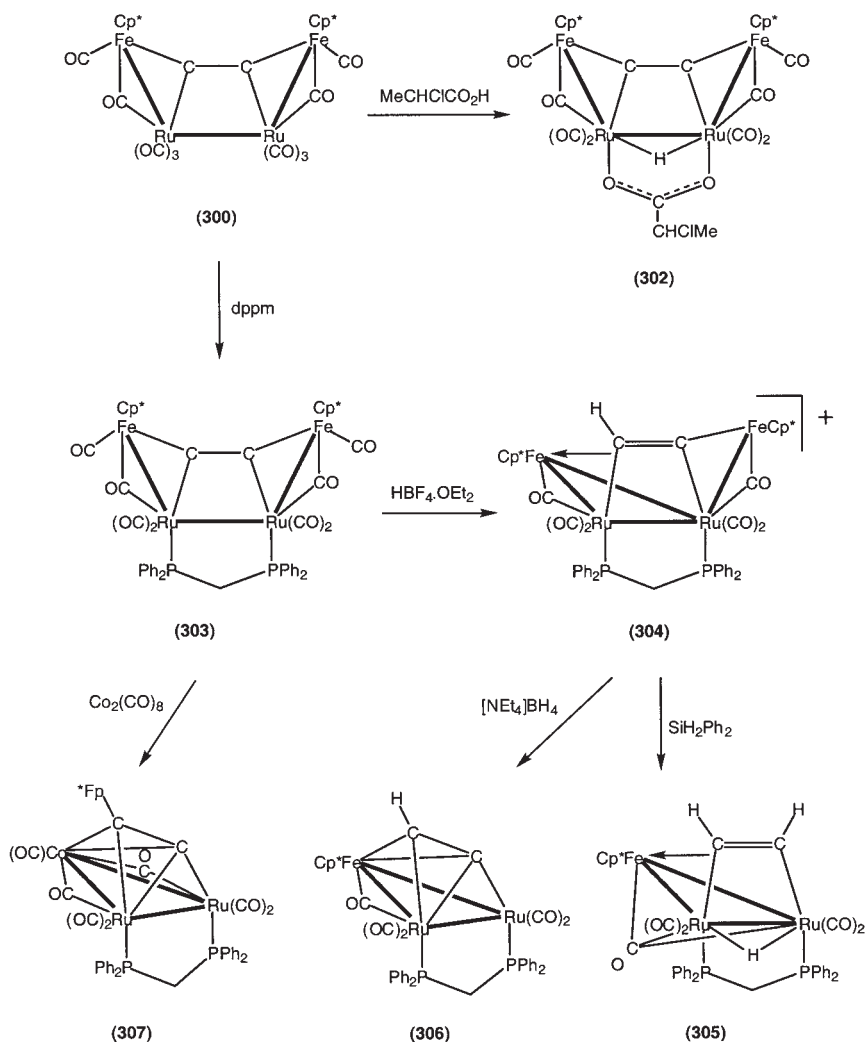
SCHEME 57

Cp^{Me}, (308b)] in moderate yield.[491] The reaction probably proceeds via the η^2 intermediate, followed by cluster build-up. The four metal atoms are almost co-planar with (308a) or slightly twisted (308b) with the C$_2$ unit, which is formulated as a permetallated ethene, and is similar to the Fe$_2$Ru$_2$ complex mentioned above. The unique Ru–Ru separation is long, at 3.0190(5) (Cp) or 3.0423(3), 3.0366(4) Å (Cp^{Me}) and the C–C separations are 1.258(5), 1.258(4) Å, respectively. The ^{13}C NMR spectrum of enriched

TABLE XIII
Peripheral C_2 Clusters

Complex	Structure	δ_C (J_{CP})	C–C/Å	M–C/Å	Ref.
300/Fe	$Fe_2Ru_2(\mu_4\text{-}C_2)(\mu\text{-}CO)_2(CO)_8Cp_2^*$	177.2	1.24(1)	1.946(7) (Fe), 2.204(7) (Ru)	498
302	$Fe_2Ru_2(\mu\text{-}H)(\mu_4\text{-}C_2)(\mu\text{-}O_2CCHClMe)$ $(\mu\text{-}CO)_2(CO)_6Cp_2^*$	178.3, 178.5	1.263(7)	1.923(4) (Fe), 2.173, 2.180(4) (Ru)	490
303/dppe	$Fe_2Ru_2(\mu_4\text{-}C_2)(\mu\text{-}dppe)(\mu\text{-}CO)_2(CO)_6Cp_2^*$	182.7	1.270(5)	1.921, 1.925(4) (Fe), 2.183, 2.202(4) (Ru)	490
303/dppm	$Fe_2Ru_2(\mu_4\text{-}C_2)(\mu\text{-}dppm)(\mu\text{-}CO)_2(CO)_6Cp_2^*$	180.9 (12.2)			490
308a	$Ru_4(\mu_4\text{-}C_2)(\mu\text{-}CO)(CO)_8Cp_2$	154.9	1.258(5)	2.030, 2.240(4)	491
308b	$Ru_4(\mu_4\text{-}C_2)(\mu\text{-}CO)(CO)_8Cp_2^{Me}$	157.1	1.258(4)	2.015, 2.212(3)	491
315	$Ru_5(\mu_4\text{-}C_2)(\mu\text{-}SMe)_2(\mu\text{-}PPh_2)_2(CO)_{13}$		1.20(4)	2.06–2.65(2)	495
316	$Ru_4(\mu_4\text{-}C_2)(\mu\text{-}SMe)_2(\mu\text{-}PPh_2)_2(CO)_{10}$		1.239(9)	2.027–2.499(6)	495
318	$Fe_2Ru_6(\mu_6\text{-}C_2)_2(\mu\text{-}CO)_3(CO)_{14}Cp_2$	203.2, 209.0	1.334(8), 1.354(7)	1.866, 1.908(6) (Fe), 1.997–2.205(5) (Ru)	498
320	$Ru_5(\mu_4\text{-}C_2Fp^*)_2(\mu\text{-}CO)_3(CO)_{10}$		1.32, 1.34(2)	1.93(2) (Fe), 2.14–2.26(1) (Ru)	497,498
321	$FeRu_6(\mu_5\text{-}C_2)(\mu_5\text{-}C_2H)(\mu\text{-}CO)(CO)_{15}Cp$		1.334(9)	1.877(7) (Fe), 1.939–2.282(7) (Ru)	497,498
322	$Ru_5(\mu_5\text{-}C_2)(\mu\text{-}dppm)(\mu\text{-}CO)_2(CO)_7Cp_2$	211.8, 248.6	1.29(1)	1.982–2.337(7)	499
322/Me	$Ru_5(\mu_5\text{-}C_2)(\mu\text{-}dppm)(\mu\text{-}CO)_2(CO)Cp_2^{Me}$	211.9, 251.3	1.308(9)	1.964–2.351(7)	499
325	$Ru_5(\mu_5\text{-}C_2)(\mu\text{-}SMe)_2(\mu\text{-}PPh_2)_2(CO)_{11}$	184.9, 206.66	1.305(5)	1.938–2.471(3)	520,521
335	$Ru_5(\mu_5\text{-}C_2)(\mu\text{-}SMe)_2(\mu\text{-}PPh_2)_2(CO)_{12}$		1.26(2)	2.06–2.45(1)	521
336	$Ru_5(\mu_5\text{-}C_2)(\mu\text{-}SMe)_2(\mu\text{-}PBu_2)_2(CO)_{11}$	187.44, 203.23 (7.8)			522
337	$Ru_5(\mu_5\text{-}C_2)(\mu\text{-}Cl)_2(\mu\text{-}PPh_2)_2(CO)_{11}$		1.32(1)	1.931(9)–2.25(1)	523

338	$Ru_5(\mu_5\text{-}C_2)(\mu\text{-}PPh_2)_2(CO)_{11}(py)_2$		1.301(5)	1.955–2.434(3)	525,526
340	$Co_6(\mu_6\text{-}C_2)(\mu_4\text{-}S)(\mu\text{-}CO)_4(CO)_{12}$		1.37(2)	1.81–2.03(2)	527
341/Fe	$FeRu_5(\mu_6\text{-}C_2)(\mu\text{-}SMe)_2(\mu\text{-}PPh_2)_2(CO)_{14}$		1.355(9)	2.05(1) (Fe), 2.079–2.120(6) (Ru)	529,530
341/Ru	$Ru_6(\mu_6\text{-}C_2)(\mu\text{-}SMe)_2(\mu\text{-}PPh_2)_2(CO)_{14}$		1.381(8)	1.998–2.058(6) (Fe), 2.093–2.119(7) (Ru)	529,530
342/Fe	$Fe_2Ru_5(\mu_6\text{-}C_2)(\mu_3\text{-}SMe)_2(\mu\text{-}PPh_2)_2(CO)_{16}$		1.38(1)	2.095–2.146(9)	529,530
342/Ru	$Ru_7(\mu_6\text{-}C_2)(\mu_3\text{-}SMe)_2(\mu\text{-}PPh_2)_2(CO)_{16}$		1.37(2)	2.09–2.21(1)	529,530
343	$Co_2Ru_6(\mu_7\text{-}C_2)(\mu_3\text{-}SMe)_2(\mu\text{-}PPh_2)_2(CO)_{16}$		1.36(2)	2.039(8) (Co), 2.12–2.20(1) (Ru)	529,531
344	$Co_4Ru_5(\mu_8\text{-}C_2)(\mu_3\text{-}SMe)_2(\mu\text{-}PPh_2)_2(CO)_{18}$		1.41(4)	1.94–2.13(3) (Co), 2.05–2.21(2) (Ru)	529,531
345	$NiRu_5(\mu_6\text{-}C_2)(\mu\text{-}SMe)_2(\mu\text{-}PPh_2)_2(CO)_9Cp_2$		1.328(7)	2.017, 2.038(6) (Ni), 2.163–2.199(6) (Ru)	532
346	$Ni_2Ru_4(\mu_6\text{-}C_2)(\mu\text{-}SMe)_2(\mu\text{-}PPh_2)_2(CO)_8Cp_2$		1.57(4)	1.72(3) (Ni), 2.24, 2.32(2) (Ru)	532
348	$Os_3W(\mu_4\text{-}C_2)(\mu_3\text{-}C_2Ph)(CO)_9Cp^*$	145.9, 172.2	1.25(3)	1.99–2.26(2) (Os), 2.25, 2.43(2) (W)	533
349	$Os_3W(\mu_4\text{-}C_2)(\mu_3\text{-}OC_2Ph)(CO)_9Cp^*$	119.9, 141.4	1.20(4)	2.04–2.23(3) (Os), 2.21, 2.47(3) (W)	533
350	$Os_3W(\mu_4\text{-}C_2)(\mu_3\text{-}CPh)(CO)_9Cp^*$	155.3, 162.5			533
352	$Ru_5(\mu_5\text{-}C_2)(\mu\text{-}SMe)_2(\mu\text{-}PPh_2)_2(CO)_{11}(CNBu^t)$	146.02 (15.7), 146.96 (14.6)	1.22(1)	2.10–2.38(1)	536,537
353	$Ru_5(\mu_5\text{-}C_2)(\mu\text{-}SMe)_2(\mu\text{-}PPh_2)_2(CO)_{10}(CNBu^t)$		1.36(2)	1.88–2.41(1)	536,537
354	$Ru_5(\mu_5\text{-}C_2)(\mu\text{-}SMe)_2(\mu\text{-}PPh_2)_2(CO)_{10}\{P(OMe)_3\}$		1.322(7)	1.953–2.416(5)	537

308a showed the dicarbide resonance at δ 154.9; weaker (ca. 15%) resonances in these regions were assigned to a second stereoisomer.

One of the two isomeric products formed from reactions between $C_2(CO_2Me)_2$ and **308** ($Cp' = Cp$, Cp^{Me}) was structurally identified as **309**, containing a ruthenacyclopentadiene unit attached to two other Ru fragments.[398] A likely route to this compound is by a formal 1,3-cycloaddition of the alkyne to an RuC_2 moiety of the cluster.
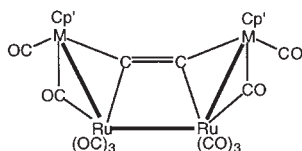
(300) M = Fe, Cp' = Cp*
(308) M = Ru, Cp' = Cp, Cp^{Me}
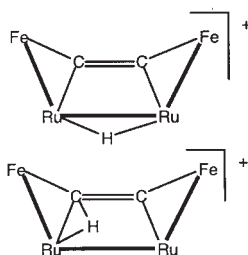
(301)
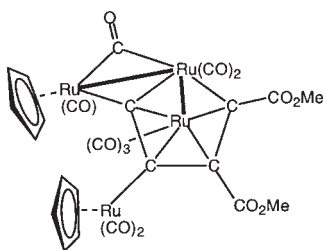
(309)
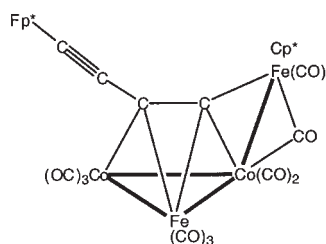
(310)

Orange $Co_2Fe_2\{\mu_4-C_2C\equiv CFp^*\}(\mu-CO)(CO)_9Cp^*$ (**310**) is obtained from the adduct from $Fp^*C\equiv CC\equiv CFp^*$ and $Co_2(CO)_8$ in a reaction with $Fe_2(CO)_9$.[420]

(b) M_2–C_4–M_2 complexes (see also Section II.G)

The complex $\{Fe_2(\mu-PPh_2)(CO)_6\}_2(\mu:\mu-C_4)$ (**311**, M = Fe; Scheme 58) is obtained directly from the reaction between $Fe_3(CO)_{12}$ and $PPh_2C\equiv C$ $C\equiv CPPh_2$ (bdpp) in thf by cleavage of the P–C(sp) bonds,[492] having been described earlier from the reaction between $Fe_2(CO)_9$ and bdpp, followed by thermolysis (PhMe, 100 °C, 2.5 h) of the resulting $\{Fe(CO)_4\}_2$ (μ-bdpp).[472,473] Carbonylation (20 atm, 100 °C, 16 h) of the phosphino-alkynyl cluster, $Ru_5(\mu_5-C_2PPh_2)(\mu-PPh_2)(CO)_{15}$ (**329**; see below) gives the

(311, M = Fe)

P(OMe)₃ →

(314)

NHEt₂ ↓

(312)

+

(313)
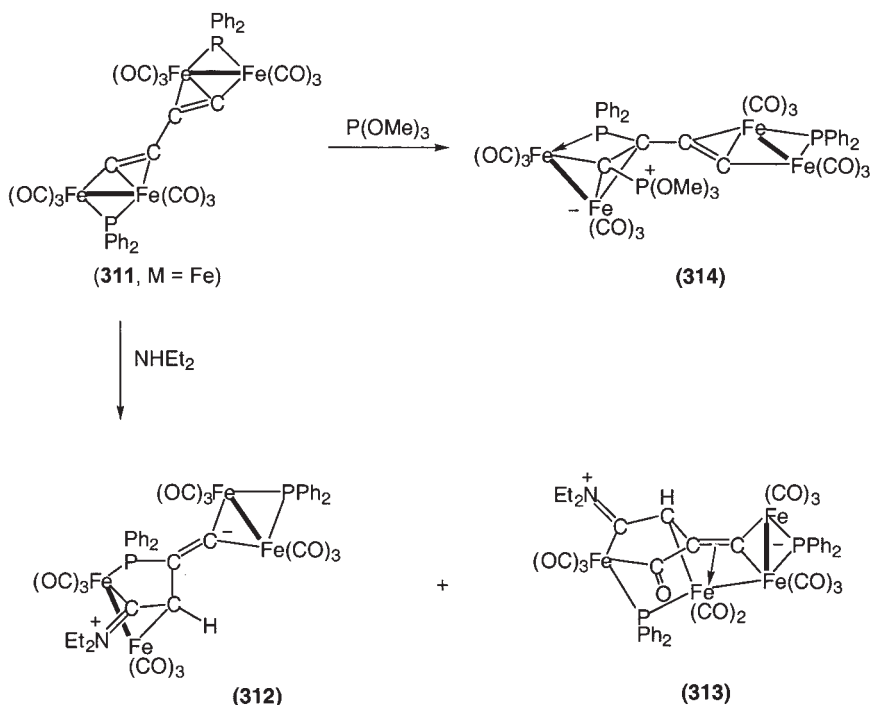
SCHEME 58

lemon-yellow ruthenium analogue (**311**, M = Ru) in 28% yield;[493] it is also obtained by thermolysis of $Ru_3(CO)_{11}\{PPh_2(C\equiv CC\equiv CSiMe_3)\}$.[494] The C_4 ligand bridges two $Ru_2(\mu\text{-}PPh_2)(CO)_6$ moieties by a σ,π interactions with each C_2 moiety, acting as a 6-electron donor. Steric demands of the other ligands present (particularly the CO groups) prevent the optimal overlaps of π-orbitals of the C_2 ligand, which would require the two Ru_2 systems to be orthogonal. This results in a relatively weak interaction, with long Ru–C π-bonds [2.326, 2.470(6) Å] and a short C–C separation [1.275(11) Å] and resulting bend-back angles of only 22.6°. The complex is stable to CO or H_2 under mild conditions.

Reactions of the carbon ligands with nucleophiles are rare, the reactivity being dominated by PPh₂-migration reactions. With NHEt₂, 1,2-addition of the sterically unencumbered secondary amine NHEt₂ to the C_4 chain is accompanied by migration of a PPh₂ or carbonyl ligand to give **312** and **313**, respectively (Scheme 58).[492] The former is formed by addition of the N–H bond across the $C_\alpha\equiv C_\beta$ bond and migration of a PPh₂ group to C(3), while the other (**313**) is formed by addition of the amine to C_α and migration of a CO ligand to give the metallacycle. In contrast, reaction with P(OMe)₃

results in facile addition of the phosphite to one of the C_α carbons to give a single adduct (**314**) in which substitution of one CO on iron by the phosphite is accompanied by migration of one PPh_2 group to C_β.[492] Simple CO substitution products are also formed.

This mode of addition of the amine is unusual when compared with the reactions of the corresponding mono-ynyl complexes, which give products derived exclusively from addition to C_β, and ruthenium diynyl complexes, which undergo 1,4-addition. These reactions, which demonstrate C–C, C–N, and C–P bond formation involving the C_4 moiety, proceed with total atom conservation.

Extrusion of an Ru_2 fragment from $Ru_5(\mu_5\text{-}C_2PPh_2)(\mu\text{-}SMe)_2(\mu\text{-}PPh_2)_2(CO)_{11}$ (**325**, see below) has occurred in both products **315** and **316** isolated from its reaction with CO, although this moiety is retained within the complex by virtue of the bridging C_2 ligand.[495] Again in **315**, excess electron density in the 50 c.v.e. system is accommodated in low-lying metal–metal antibonding MOs, resulting in long Ru–Ru separations [2.956–3.170(4) Å]. A short C–C bond [1.20(4) Å] and long Ru(5)–C(1) separation suggest that the C_2 ligand is a 4-electron donor, the Ru(4)–Ru(5) bond being short [2.694(6) Å] and suggesting a major contribution from tautomer **315a**. In **316**, non-bonded atoms Ru(3) and Ru(4) are bridged by two SMe groups and attached to the second Ru_2 fragment by the C_2 ligand, which is a tetra-metallated ethene.

(311) M = Fe, Ru

(315)

(315a)

(316)
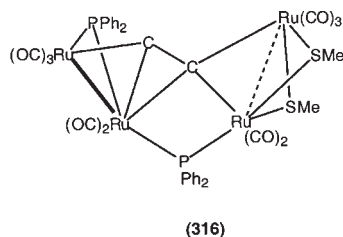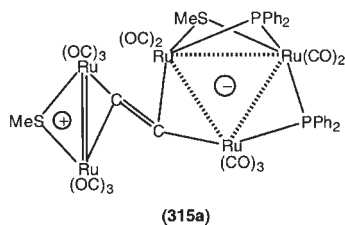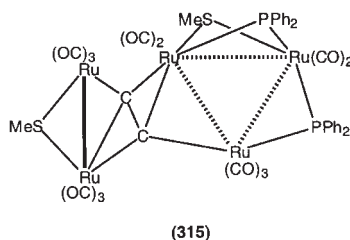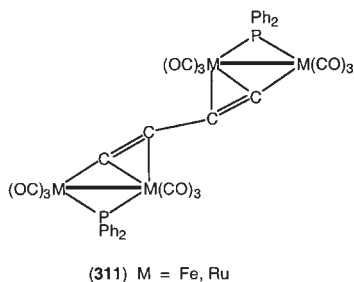
2. Complexes Containing > 4 Metal Atoms

(a) Iron–ruthenium

Much of the chemistry of peripheral C_2 clusters of iron and ruthenium has been reviewed.[35] Evolution of permetallated ethynes via cluster build-up to permetallated ethenes and ethynes is discussed, sequential additions of metal fragments occurring in addition to thermal redox and thermal condensation reactions.

Further transformations of the Fe_2Ru_2 cluster **300** (above) occur with gradual formation of **317** and Fe_2Ru_6 cluster **318**, suggesting formation of the latter either by reaction of **300** with $Ru_3(CO)_{12}$ or by dimerization of **317** (Scheme 59).[496,497] Compound **318** is thermodynamically the most stable species. Addition of $Fe_2(CO)_9$ to **300** gave a low yield of yellow $FeRu_2$ $(\mu\text{-H})(\mu_3\text{-}C_2Fp^*)(CO)_9$ (**319**). On heating **317** in refluxing toluene, black heptanuclear Fe_2Ru_5 (**320**) and $FeRu_6$ (**321**) clusters are formed by assembly of the metal fragments around the C_2 ligand. Thermolysis of **317** gives a trace of **318** and the black ethynyl-containing cluster **321**. Oxidation ($[FcH]^+$) of $[Ru_3\{\mu_3\text{-}C_2[Fe(CO)_2Cp]\}(CO)_9]^-$ (from **319**, KOH and [ppn]Cl) produces **318** in moderate yield, together with **320**.

The purple-grey Fe_2Ru_6 cluster **318** contains an Ru_4 square, the four edges each being bridged by Fe or Ru atoms and supporting two $\mu_6\text{-}C_2$ ligands on opposite sides of the square, which each interact with the boat-shaped Fe_2Ru_4 array, each C atom capping a triangular face; the c.v.e. count is 124 if the C_2 ligand is an 8-e donor. The C–C separations are 1.334(8), 1.354(7)(4) Å, i.e., similar to a C(sp)–C(sp) single bond, but the C_2M_6 arrangement is that of a permetallated ethane. In the ^{13}C NMR spectra, the C_2 resonances are at δ 203.2 and 209.0, with CO groups at δ 190.5–210.4 and at δ 243.4 (μ-CO). A rapid fluxional CO-exchange process on ruthenium is indicated by the ^{13}C NMR spectrum. The Fe_2Ru_5 complex **320** contains two $\mu_4\text{-}C_2Fp$ fragments attached to the butterfly portions of a 112 c.v.e. "arrowhead" Ru_5 cluster and is probably formed by dimerization of an intermediate radical species. Any dissociation of CO occurs from the more labile iron centre. In the black $FeRu_6$ cluster **321**, the $\mu_5\text{-}C_2$ ligand is attached to an open-envelope $FeRu_4$ portion and a $\mu_5\text{-}C_2H$ fragment is in extended interaction with the $FeRu_5$ portion of the open M_8 cluster, on opposite sides of the central $FeRu_3$ square. The C–C separations in the C_2 ligands in **320** and **321** are 1.334, 1.354(8) Å (C_2), and 1.334(9) (C_2), 1.420(9) Å (C_2H), respectively.

(b) Ruthenium

Products from $\{Ru(CO)_2Cp'\}_2(\mu\text{–}C{\equiv}C)$. Reactions of $\{Ru(CO)_2Cp'\}_2$ (μ-C≡C) (Cp$' =$ Cp, Cp*) with $Ru_3(\mu\text{-dppm})(CO)_{10}$ have given dark green

[M] = M(CO)$_3$, (M) = M(CO)$_2$

Fp*——C≡≡C——Fp*

Ru$_3$(CO)$_{12}$

Cp'(OC)Fe

(CO)Cp'
Fe

(300)

(OC)$_3$Ru

Cp'
Fe

(Ru)

(Ru)

(Ru)

(OC)$_3$Ru

(Ru)

Fe
Cp'

(318)

+ (317)

Fe$_2$(CO)$_9$
(M = Fe)

Fp*
C

C

[Ru]

[M]

[Ru]

H

(317) M = Ru
(319) M = Fe

(i) KOH, [ppn]Cl
(ii) [FcH]PF$_6$
(M = Ru)

PhMe, reflux
(M = Ru)

(Ru)

Fp—C

(Ru)

(Ru)

C—Fp

(Ru)

(Ru)

(320)

H—C

(Ru)

(Fe)

C

(Ru)

(C)

(Ru)

(Ru)

(Ru)

(Ru)

(321)
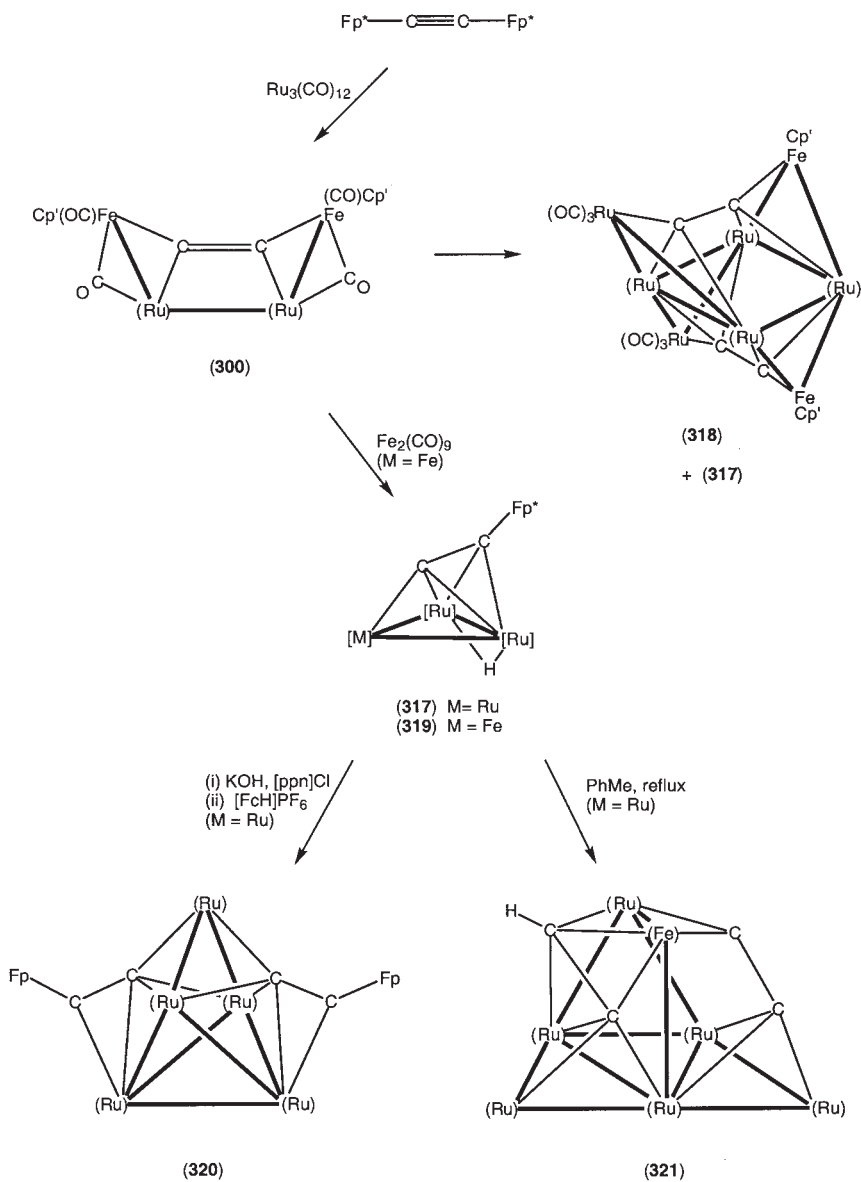
SCHEME 59

complexes $Ru_5(\mu_5\text{-}C_2)(\mu\text{-dppm})(\mu\text{-CO})_2(CO)_7Cp'$ ($Cp' = Cp$, Cp^{Me}) (**322**) (55–74%).[499] The reaction probably proceeds via a ring-opened Ru_3-dppm complex which coordinates the entering $\{Ru(CO)_2Cp'\}_2(\mu\text{-}C{\equiv}C)$ complex via the C_2 ligand. The resulting cluster is a flattened Ru-spiked butterfly, one edge of which is bridged by the dppm ligand. The C_2 ligand is attached to all five Ru atoms, two pairs being considered "substituents" to each of the carbons, while the C_2 unit is η^2 bonded to one of the hinge atoms; Ru–C distances are between 1.964 and 2.351(7) Å. The C–C separations are 1.29(1) (Cp) and 1.308(9) Å (Cp*). The geometry is similar to that found in $Ru_5(\mu_5\text{-}C_2)(\mu\text{-PPh}_2)_2(CO)_{11}(py)_2$ (below). The Cp ligands are inequivalent and two resonances are found for the dicarbide ligand.

On heating $Ru_4(C_2)(\mu\text{-CO})(CO)_8Cp_2$ (**308**) coupling and condensation to Ru_7 (**323**) and Ru_8 clusters (**324**) occurs, which are related by loss of CO and formation of an extra Ru–Ru bond.[105] Both contain similar arrangements for seven of the eight Ru atoms, while the multi-site attachments of the C_2 ligands appear to be unique.

$Ru_5(C_2)(\mu\text{-}SMe)_2(\mu\text{-}PPh_2)_2(CO)_{11}$. The best studied cluster of this type is $Ru_5(C_2)(\mu\text{-SMe})_2(\mu\text{-PPh}_2)_2(CO)_{11}$ (**325**) obtained from $Ru_3(CO)_{12}$ and $C_2(PPh_2)_2$ by a multi-step but efficient transformation which involves synthesis of $Ru_3(CO)_{11}\{PPh_2(C{\equiv}CPPh_2)\}$, its conversion to $Ru_5(\mu_5\text{-}C_2Ph_2)(\mu\text{-PPh}_2)(CO)_{13}$ by thermolysis and oxidation with Me_2S_2. The chemistry associated with these reactions has been reviewed.[500,501]

The ready migration of one H atom from a $\mu_3\text{-HC}_2H$ ligand in $Ru_3(\mu_3\text{-HC}_2H)(\mu\text{-CO})(CO)_9$ to give $Ru_3(\mu\text{-H})(\mu_3\text{-}C_2H)(CO)_9$[502,503] is not followed by cleavage of the second C–H bond to give a cluster-bonded C_2 unit. An alternative approach to the stabilization of reactive molecules on small metal clusters is by C–P bond cleavage.[504,505] In the case of P–Ph bonds, as found in tertiary phosphine ligands, this can be accompanied by C–H bond cleavage to give μ-benzyne complexes.[506–508] This work has been extended to acetylenic phosphines to give a multitude of unusual and interesting complexes.[509–513]

Synthesis and structure of **325**. The ease of cleavage of P–C bonds, usually by thermolytic reactions of their trinuclear Group 8 cluster carbonyl complexes, is P–C(sp) > P–C(aryl-sp^2) > P–C(vinyl-sp^2) > P–C(sp^3).[514] When applied to $\{Ru_3(CO)_{11}\}_2(\mu\text{-dppa})$ [**326**; dppa = $C_2(PPh_2)_2$], in which the C≡C triple bond is not coordinated to either cluster moiety, the product is formed by cleavage of one P–C(sp) bond and coordination of the resulting diphenylphosphinoethynyl group to a larger cluster formed by condensation of the two Ru_3 units with elimination of one "$Ru(CO)_4$" group (Scheme 60). The resulting complex (**327**) is the source of much
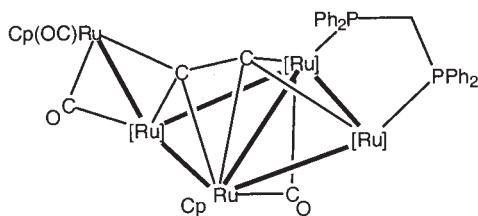
(322) [Ru] = Ru(CO)$_2$
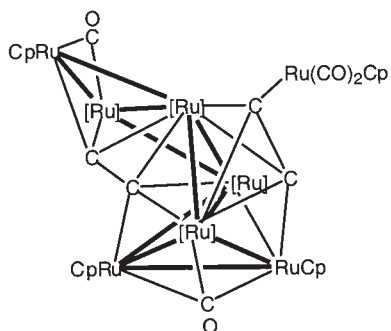
(323) [Ru] = Ru(CO)$_2$
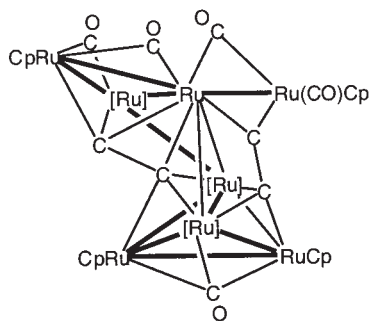
(324) [Ru] = Ru(CO)$_2$

(325) [Ru] = Ru(CO)$_2$

(326)

90°C
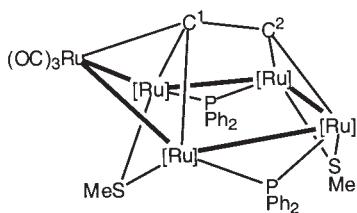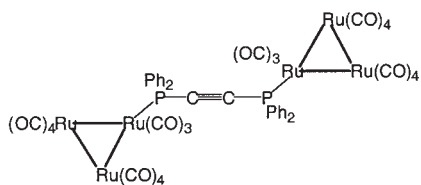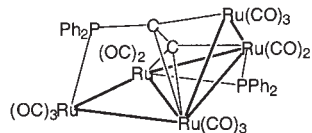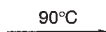
(327)

SCHEME 60

interesting chemistry, uncovered while searching for methods to break the remaining P–C bond.[500] An osmium analogue is also known.[515]

During these studies, several products indicated that cleavage of the second P–C(sp) bond had occurred, but it was not clear whether reaction occurred before or after further reaction of the reagent with the C_2PPh_2 ligand. Thus, in reactions with alkenes, products such as $Ru_5(\mu_4\text{-PPh})$ $\{\mu_4\text{-}C_2(CHCHR)CHCH_2R\}(\mu\text{-PPh}_2)(CO)_{12}$ (**328**, R = H, Me) and $Ru_5(\mu_4\text{-PPh})(\mu\text{-PPh}_2)(\mu\text{-CO})(CO)_{10}\{\eta^5\text{-}C_5H_3Me(CH=CH_2)\}$ (**329**) were formed.[516] With buta-1,3-diene, the product **330** contains a cyclohex-1-en-4-yne ligand (an isomer of benzene) formed by cycloaddition of the diene to a C_2 group.[517] The formation of the phenylethynyl complexes **331** and **332** in reactions of **327** with oxirane[518] or $Co(CO)_2Cp$,[519] respectively, occurs by formal elimination of PPh groups to the cluster. Successful formation of a C_2 complex was first achieved in the reaction between **327** and CO, which gave $\{Ru_2(\mu\text{-PPh}_2)(CO)_6\}_2(\mu\text{-}C_2)$ (see above).

The C_2 cluster **325** was obtained as the end-product of a series of reactions that occurs when **327** is treated with Me_2S_2 (Scheme 61).[520,521]

[Ru] = $Ru(CO)_2$
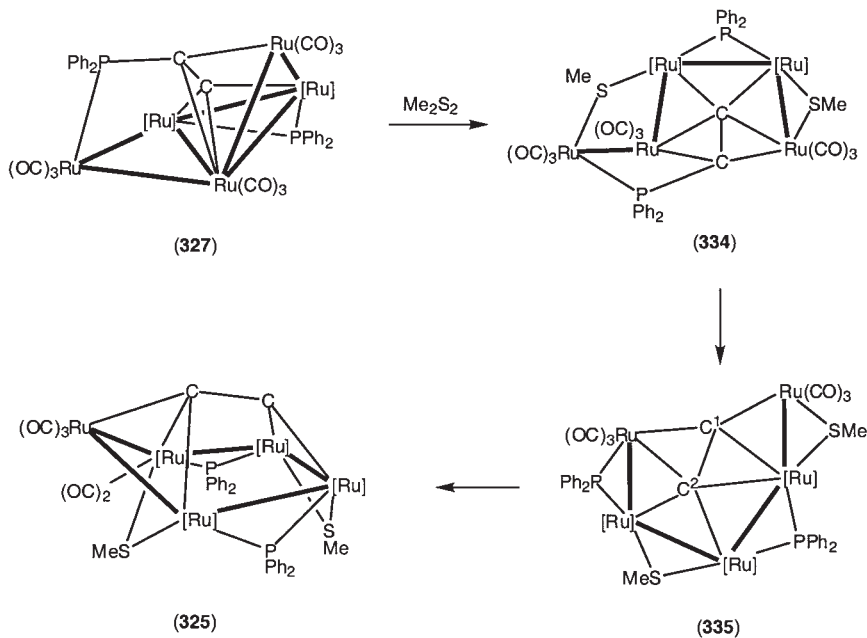
SCHEME 61
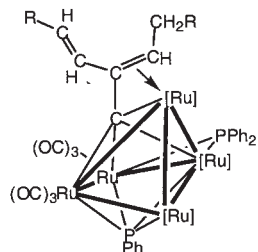
(328) R = H, Me; [Ru] = Ru(CO)$_2$
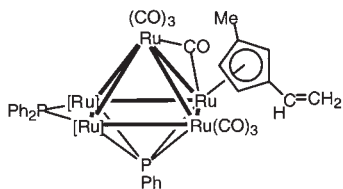
(329) [Ru] = Ru(CO)$_2$
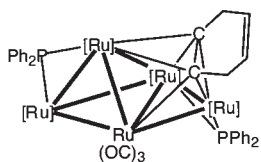
(330) [Ru] = Ru(CO)$_2$
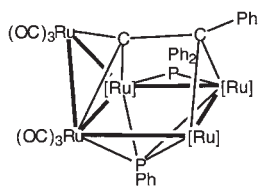
(331) [Ru] = Ru(CO)$_2$
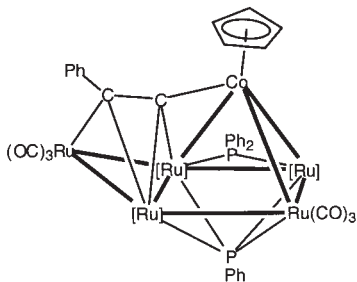
(332) [Ru] = Ru(CO)$_2$
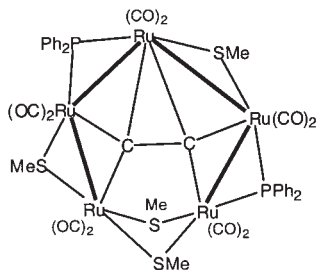
(333)
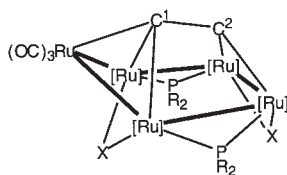
(336) R = Bu^n, X = SMe
(337) R = Ph, X = Cl

[Ru] = Ru(CO)$_2$

This series of transformations occurs under mild conditions at reasonable rates, allowing isolation of the various intermediates and demonstrating that each could be induced to complete the transformation into **325**. A second molecule of Me_2S_2 adds to **325** to give **333**, in which an Ru–Ru bond of the Ru_5 pentagon has been broken.

The first isolable product is **334** which on heating undergoes the desired P–C(sp) bond cleavage to give **335**, in which the C_2 ligand is attached to all five metal atoms in an asymmetric fashion. Thermal decarbonylation results in Ru–Ru bond formation to give **325**, in which the C_2 ligand sits atop the open pentagonal Ru_5 cluster. Notwithstanding the relatively large number of intermediates, **325** is isolated in over 80% yield. The analogous complexes $Ru_5(C_2)(\mu\text{-SMe})_2(\mu\text{-PBu}_2)_2(CO)_{11}$ (**336**)[522] and **337**[523] have also been reported. The latter was obtained from a reaction between **327** and $CH_2{=}CMeCH_2CMe(CH_2Cl)_2$, together with $Ru_5(\mu\text{-H})\{\mu_5\text{-CC(PPh}_2)\}$ $(\mu\text{-Cl})(\mu\text{-PPh}_2)(CO)_{12}$.

In **325**, the C_2 ligand sits atop the open puckered Ru_5 cluster, which allows ready attack by incoming reagents. The Ru–C separations range between 2.133 and 2.470(3) Å, with a C–C bond length of 1.307(5) Å, consistent with a multi-site attachment of the ethyndiyl ligand. Nuclei C(1) and C(2) resonate at δ_C 184.9 and 206.7, respectively. Theoretical studies have been carried out on **325** (see Section IX.D)[489] after a preliminary study of the model $Ru_5(\mu_5\text{-C}_2)(\mu\text{-SH})_2(\mu\text{-PH}_2)_2(CO)_{11}$.[524] The C_2 ligand carries an overall negative charge, resulting in its displaying nucleophilic character. To some extent, its reactivity is consistent with formulation as a metalled μ_3-vinylidene complex. Additionally, one of the HOMOs is centered on an SMe group bridging the non-bonded Ru(3)–Ru(4) vector, which results in its adopting μ_3 bonding in several of the reactions of **325**. The complex has 80 cluster valence electrons (c.v.e.) as expected for an M_5 system if the C_2 ligand acts as a 6-electron donor.

$Ru_5(\mu_5\text{-C}_2)(\mu\text{-PPh}_2)_2(CO)_{11}(py)_2$ (**338**). This complex was obtained from **327** and pyridine together with the ethynyl cluster $Ru_6(\mu_6\text{-C}_2H)$ $(\mu_3\text{-NC}_5H_4)(\mu\text{-PPh}_2)_2(\mu\text{-CO})(CO)_{12}$ (**339**) and other products formed by metallation of a pyridine ligand without cleavage of the P–C(sp) bond.[525,526]

(c) Cobalt

The reaction between $Co_2(CO)_8$ and CS_2 at r.t. for 2–3 h affords a mixture of solid materials and other complexes present in the supernatant. Repeated extractions of the solid phase gave black $Co_6(C_2)(\mu_4\text{-S})(CO)_{14}$ (**340**) which contains a boat-like Co_6 skeleton (a Co_4 square with two opposite edges each bridged by a Co atom) supporting a C_2 unit between the extremities.[527] The Co(basal)–Co(basal) and Co(basal)–Co(ap) separations

(338)

(339) [Ru] = Ru(CO)₂

(340) [Co] = Co(CO)₂
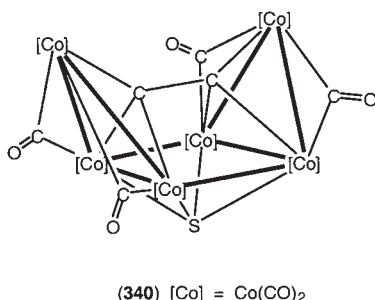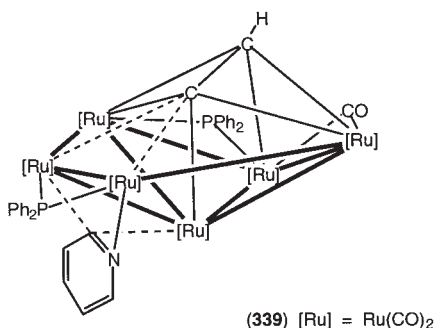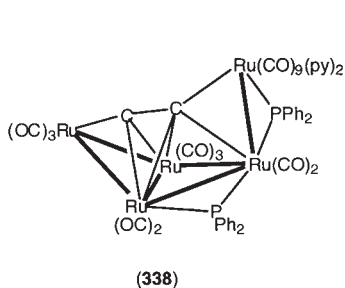
are 2.590–2.619(3) and 2.490–2.562(3) Å, respectively. The structure is derived from a trigonal prismatic Co₆ core (of idealized C_{2v} symmetry) by insertion of the C_2 group into one of the edges linking the triangular faces. Alternatively, it is related to the eclipsed rotamer of $\{Co_3(CO)_9\}_2C_2$ with some tilting, as in the related Co_3Fe_3 complex **275**. The two apical Co atoms and the C_2 unit are co-planar and inclined at 81° to the square Co_4 base which is capped by the sulfur atom. It is likely that π-electron density is delocalized along the Co(ap)CCCo(ap) unit. Each carbon of the C_2 unit is attached to the nearest Co_3 unit by one short (1.81 Å) and two long (2.01 Å) C–Co bonds, while the C–C separation is 1.37(2) Å. There are eight terminal CO and six μ-CO ligands, the latter bridging all peripheral edges. Detailed discussions of the ν(CO) and IR modes of the C_2SCo_6 core are given; the weak ν(CC) band is at 1444 cm^{-1}. A smooth reaction with CO gives $\{Co_3(CO)_9\}_2C_2$ (**271**; q.v.) (60%).

The olive-green selenium analogue of **340** has been isolated from the reaction of $Co_2(CO)_8$ and CSe_2 and identified from its IR spectrum [ν(CC) 1446 cm^{-1}].[528] Both complexes probably originate from mono-carbon species, such as $Co_3(\mu_3\text{-}CX)(CO)_9$ (X = S- or Se-containing group).

(d) Heterometallic complexes

$M_nRu_5(\mu\text{-}C_2)(\mu\text{-}SMe)_2(\mu\text{-}PPh_2)_2(CO)_{10+2n}$ (M = Fe, Ru; n = 1, 2). Reactions of **325** with Group 8 carbonyls result in cluster growth, the hexa- (**341**) and heptanuclear compounds (**342**) being formed.[529,530] In these, the C_2 ligand acts as a collar, allowing permetallabicyclo[2.2.0]hexane frameworks to be constructed. Each carbon is found associated with an approximately square face, the added $M(CO)_n$ groups forming the hinge atoms. The SMe groups span the outer metal atoms and probably prevent further encapsulation of the C_2 ligand.

(341) [Ru] = Ru(CO)₂

(342) [Ru] = Ru(CO)₂
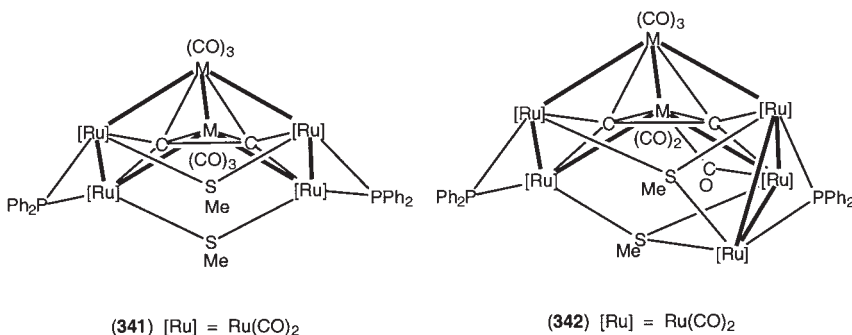
$Co_nRu_5(\mu\text{-}C_2)(\mu_3\text{-}SMe)_2(\mu\text{-}PPh_2)_2(CO)_{10+2n}$ (n = 3, 4). Related complexes are found in products from reactions between **325** and $Co_2(CO)_8$, in this case the CM_4 face being capped by $Co(CO)_n$ groups to give octa- (**343**) and nona-nuclear products (**344**).[529,531] In the latter, the C_2 unit interacts with eight of the nine metal atoms.

(343) [Ru] = Ru(CO)₂

(344)
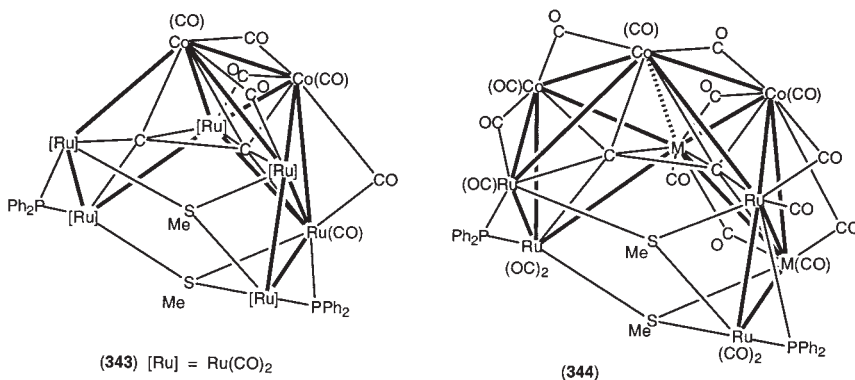
$Ni_nRu_{6-n}(\mu\text{-}C_2)(\mu\text{-}SMe)_2(\mu\text{-}PPh_2)_2(CO)_{10-n}Cp_n$ $(n=1, 2)$. Two products were obtained from the reaction between **325** and nickelocene. The metal core in **345** is closely related to those found in the Fe, Ru, and Co carbonyl adducts mentioned above, migration of Cp from Ni to Ru having occurred. In the second product **346**, an interesting disorder is found in the solid-state in which the C_2 ligand adopts a conformation either orthogonal to (**346a**) or parallel to the $Ni \cdots Ni$ vector (**346b**).[532]

(**345**) [Ru] = Ru(CO)$_2$

(**346**)

(**346a**)

(**346b**)
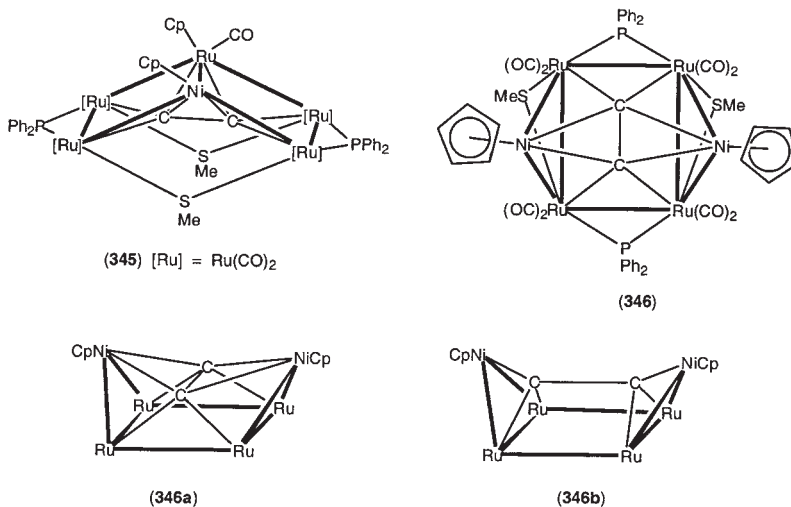
Other systems. Heating **347** (Scheme 62) [from Os$_3$(CO)$_{10}$(NCMe)$_2$ and W(C≡CC≡CPh)(CO)$_3$Cp*] in refluxing toluene results in incorporation of the tungsten atom in the cluster and cleavage of the central C–C bond in the diyne to give **348**.[533] Oxidation gives the ketenyl cluster **349** which loses CO on heating to form the benzylidyne (**350**), the yield increasing to 92% yield under CO. Notable is the oxidative conversion of alkynyl to carbyne and CO which has occurred:

$$R\text{-}C\equiv C\text{-} + O_2 \rightarrow R\text{-}C\text{=}C\text{=}O \rightarrow R\text{-}C\equiv + C\equiv O$$

3. Reactions of Peripheral C_2 Clusters

Although a relatively complicated molecule with several potentially reactive sites, the ready availability of **325** allowed a study of its reactions and led to the characterization of many other complexes containing cluster-bonded C_2 ligands. Although the details of reactions involving (i) substitution of CO by other donor ligands (PR$_3$, CNR),
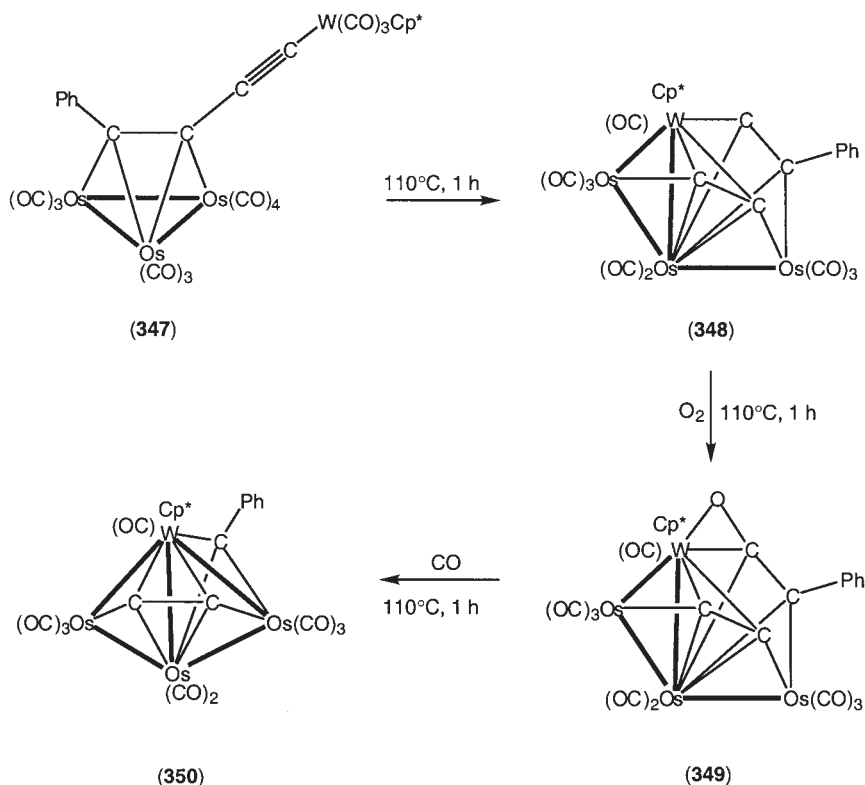
SCHEME 62

(ii) reactions of the C_2 unit with nucleophilic reagents, and (iii) construction of larger clusters retaining the C_2 ligand have been given elsewhere,[501,534] the following summarizes the salient points of the chemistry and brings the earlier surveys up-to-date. The Ru_5 core undergoes ready transformations by making and breaking of Ru–Ru bonds, so that during the course of these studies, examples of complexes with more than ten different cluster geometries have been identified.

General features found in these reactions suggest that one of the C_2 carbons enters into a reaction (insertion, addition, etc.) while the other becomes more tightly bound to at least four of the five Ru atoms, giving a CRu_4 system related to that found in metal cluster carbides such as $Ru_5C(CO)_{15}$. Other geometrical changes result from facile reorganization of the bridging SMe and PPh_2 ligands, coupled with the flexibility (or softness) of medium-sized cluster frameworks. When the cluster geometries are considered, we conclude that the conformations are determined by the

nature of the organic ligands present, again revealing the ready deformability of the cluster core.

(a) Reactions with donor ligands

With dihydrogen, one carbon of the C_2 ligand inserts into the H–H bond to give a μ_3-vinylidene in **351**.[524,535] The latter is fluxional via a windscreen-wiper-like oscillation between the two Ru_3 faces, with $\Delta G^{\ddagger}$ estimated at 60.3 kJ mol^{-1}. The 80 c.v.e. cluster exhibits lengthening of the Ru–Ru bonds (average 3.03 Å).

Expansion of the Ru_5 cluster (average Ru–Ru separation 2.961 Å) occurs in the reaction with CNBu^t to give **352**, pulling the C_2 ligand almost into the Ru_5 plane and shortening the C–C separation to 1.22 Å, again indicating that it is acting as a four-electron donor.[536,537] Decarbonylation affords **353**, with the isocyanide occupying a position opposite the shortest Ru–C vector. A mechanism involving reversible displacement of one of the SMe groups from Ru(3) has been suggested.

(351) R = H
(355) R = CH=CHR',
         R' = H, Me, Ph, CO$_2$Me
         [Ru] = Ru(CO)$_2$

(352)
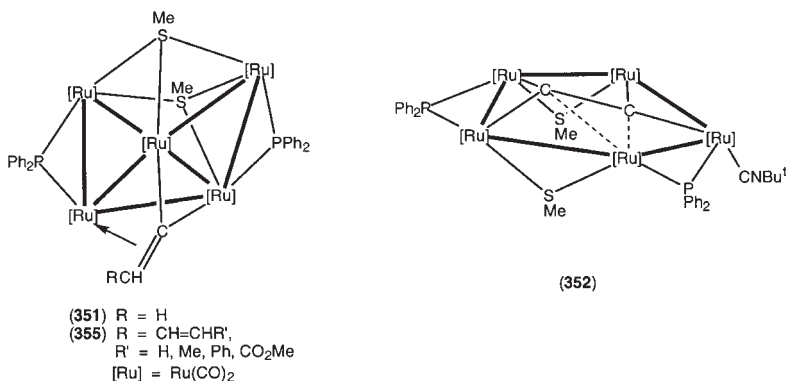
The usual Me$_3$NO-activation of **325** in the presence of MeCN affords a mono-MeCN derivative. Subsequent reactions with tertiary phosphines have given complexes **354** [L=PMe$_2$Ph, PPh$_3$, P(OMe)$_3$] in which L occupies the same site as CNBu^t in **353** above.[537] One Ru_5 cluster can be attached to each end of PPh$_2$C≡CPPh$_2$. With bidentate phosphines, such as dppm, or functional phosphines [PPh$_2$(C$_6$H$_4$NH$_2$-4), PPh$_2$(C$_6$H$_4$CH= CH$_2$-4)], a variety of Ru–Ru bond cleavage or C–C bond formation reactions, were described.[479,543]

(b) Reactions with unsaturated hydrocarbons

The major products from **325** and 1-alkenes are substituted vinylidenes **355** (R=CH=CHR', R'=H, Me, Ph, CO$_2$Me), resulting from insertion

Me
S
(OC)₂ Ru — Ru(CO)₂
Ph₂P   C² PPh₂
C¹
(OC)₂Ru — S — Ru(CO)₂
Me
Ru
(CO)₂(L)
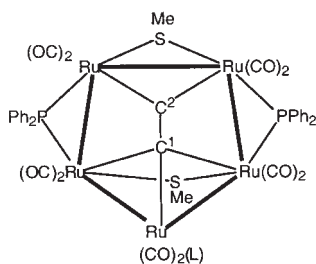
(353) L = CNBu^t
(354) L = P(OMe)₃, PMe₂Ph, PPh₃

MeS   [Ru]   PPh₂
Ph₂P   S
[Ru]   Me
[Ru]   [Ru]
[Ru]   C
C

(356) [Ru] = Ru(CO)₂

HC   C   CH
C   (CO)
[Ru]   Ru   PPh₂
[Ru]   [Ru]
SMe
Ph₂P
SMe
[Ru]
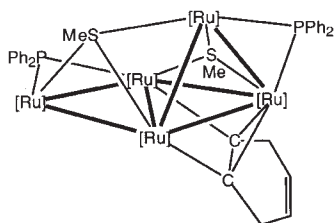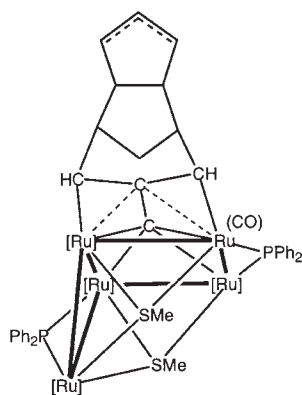
(357) [Ru] = Ru(CO)₂

of one carbon of the C₂ ligand into a C–H bond.[524,535] The fluxional process involving the vinylidene ligand is more facile than that found for **351**.

Cycloaddition of buta-1,3-diene to the C₂ ligand affords **356**, containing complexed cyclohex-1-en-4-yne, this time attached to an Ru₃ face.[538] With cyclopenta-1,3-diene, formal insertion of one of the C₂ carbons into a C=C double bond occurs (possibly via a three-membered ring and ring-opening) to give **357**.[539] Two molecules of the cyclic diene have been incorporated into the organic ligand, which shows C=C double bond disorder.

The four main types of complex obtained from **325** and alkynes are illustrated in Scheme 63.[540–542] Rather than insertion into the ≡C–H bond, coupling of the C₂ ligand with 1-alkynes gives **358** which contains a ruthenacycle which has an η⁴-interaction with a second Ru atom, as found in the dimerization of alkynes on Ru₃ clusters. The Ru₅ cluster becomes flattened, as found in **352**. Under CO, extrusion of an Ru(CO)ₙ group

[Ru] = Ru(CO)₂

(358) R = Ph, Buᵗ, SiMe₃

(359) R = Ph, SiMe₃

(360) R¹ = Ph; R² = Ph or C₂Ph

(361) R¹ = R² = Me, Ph
R¹ = H, R² = Ph, SiMe₃
R¹ = C₂Ph, R² = Ph
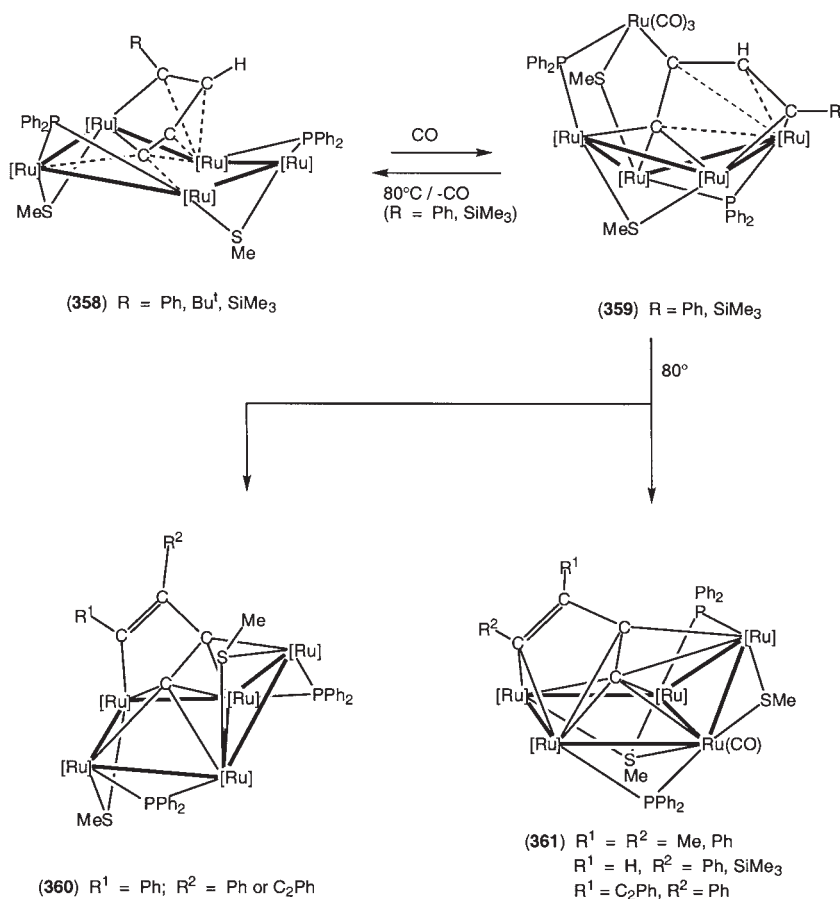
SCHEME 63

occurs, although this remains in the complex by virtue of attachment via the μ-SMe and μ-PPh₂ groups in **359**. Thermal decarbonylation is reversible (R = Ph, SiMe₃) and also affords **360** and **361**. While not formed by heating **358** directly, **360** and **361** are also formed in reactions of disubstituted alkynes with **325**. Again, heating **361** (R = Ph) results in decarbonylation to **360** (R = Ph). In the latter, the η^2 interaction is no longer found, a new Ru–Ru bond giving an open-envelope Ru₅ cluster (78 c.v.e.). Coupling of HC≡CR (R = Ph, SiMe₃), CO, and SMe with the C₂ group in **325** gives the RCCHC(C)C(O)SMe ligand in **362**.[543]

(362) $R^1 = H$, $R^2 = Ph$ or $SiMe_3$
[Ru] = $Ru(CO)_2$
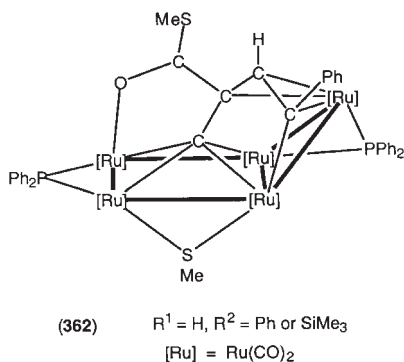
End-to-end coupling of the C_2 ligand with $HC\equiv CR$ ($R = Bu^t$, $SiMe_3$) gave the first examples of cluster-stabilized butatrienylidene ligands in **363**; one $SiMe_3$ group is lost from $C_2(SiMe_3)_2$ during the reaction. Treatment of **363** ($R = SiMe_3$) with KOH/MeOH affords the parent butatrienylidene complex **363** ($R = H$), which adds CO to give **364** via Ru–C and Ru–S bond making and breaking reactions (Scheme 64).[544,545] Other products obtained from the reaction between **325** and $C_2(SiMe_3)_2$ include **365**, formed by coupling two alkyne molecules to the C_2 ligand with partial desilylation and loss of one SMe group [possibly as $SiMe_3(SMe)$]. The formation of **366** in the same reaction suggests the intermediacy of a vinylidene ligand, since the vinylacyl ligand formally incorporates C_2, CO, HC_2SiMe_3, and $C=CHSiMe_3$.[545]

With 1,3-diynes such as $PhC\equiv CC\equiv CPh$, complexes of types **359**, **360**, and **361** are formed, the diyne behaving as a phenylethynyl-alkyne. Minor amounts of **367**, in which two diyne ligands have added to one carbon of the C_2 ligand to give a branched-chain C_{10} ligand, and **368**, in which one SMe group has inserted into an Ru–C bond to give a four-membered metallacycle, are also isolated.[546]

B. *Interstitial C_2 Clusters*

In this Section, transition metal clusters encapsulating C_2 ligands, and also those with two or more carbide (C) ligands, will be covered. Methods that have been used for the synthesis of dicarbide clusters include:

(a) thermolysis of mono-carbide clusters;
(b) *in situ* redox condensation reactions;
(c) reactions of anionic metal carbonyls with a C_2 source (C_2Cl_4 or C_2Cl_6).

$[Ru] = Ru(CO)_2$ **(325)**

$C_2(SiMe_3)_2$

Ph$_2$R

[Ru]

[Ru]

[Ru]

[Ru]

PPh$_2$

MeS

MeS

[Ru]

OH^-/H_2O **(363)** R = SiMe$_3$

(363) R = H

CO

H$_2$C

Ru(CO)$_3$

MeS

PPh$_2$

[Ru]

Ph$_2$P

[Ru]

[Ru]

[Ru]

S
Me

(364)

SCHEME 64
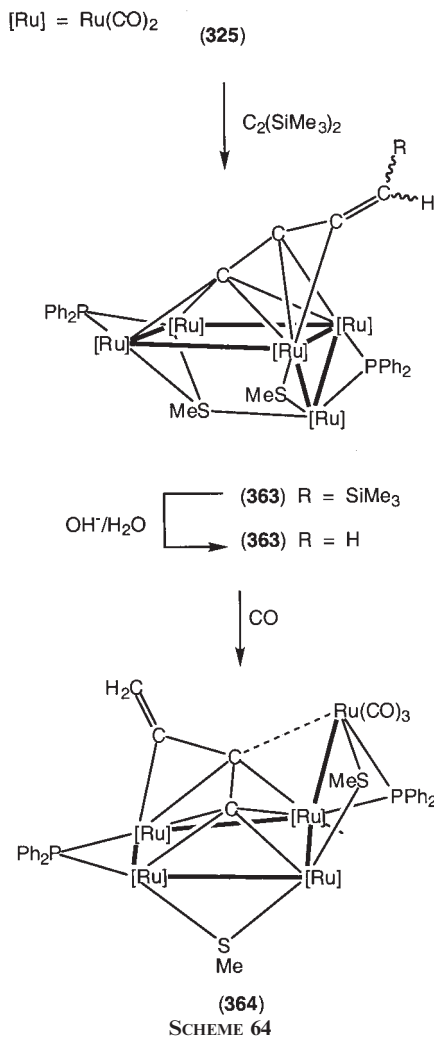
Table XIV summarizes the reported examples and includes systems with between 8 and 38 metal atoms; sketches of the central cluster cores of some of the complexes are given in Figs. 12, 13, and 14.

1. Homometallic Systems

(a) Iron and Ruthenium

On heating $Ru_5(\mu_5\text{-}C_2PPh_2)(\mu\text{-}PPh_2)(CO)_{13}$ (**325**; see above) with $Ru_3(CO)_{12}$ in cyclohexane under CO (45 bar), $Ru_8(C)_2(\mu\text{-}PPh_2)_2(CO)_{17}$

(365)

(366) [Ru] = Ru(CO)$_2$

(367) [Ru] = Ru(CO)$_2$

(368) R, R' = Ph, C≡CPh
[Ru] = Ru(CO)$_2$
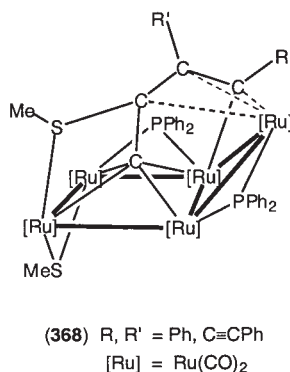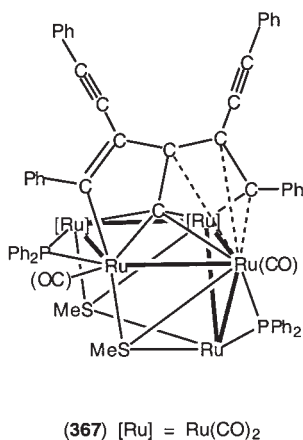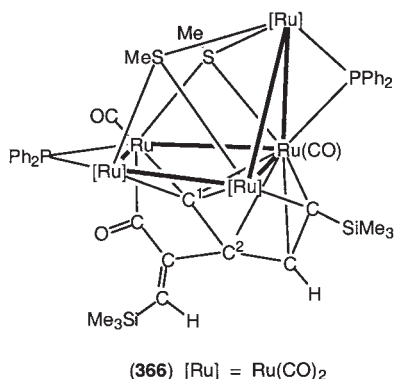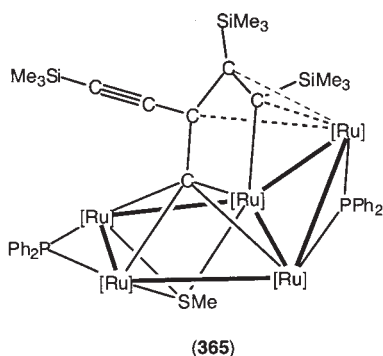
(**369/Ru**) is formed.[547] The cluster core is made up of a square pyramid fused to an octahedron, with one carbon atom in each fragment. The isostructural mixed-metal cluster Fe$_3$Ru$_5$(C)$_2$(μ-PPh$_2$)$_2$(CO)$_{17}$ (**369/Fe**) is found (35%) among the products obtained from heating **325** with Fe$_2$(CO)$_9$ (toluene, 100 °C, 40 h).[548,549]

Deep purple [NEt$_4$]$_2$[Ru$_{10}$(C)$_2$(μ-CO)$_4$(CO)$_{20}$] (**370**; Scheme 65) was first reported in 1982, being obtained in 35% yield by thermolysis of [NEt$_4$]$_2$[Ru$_6$C(CO)$_{16}$]$^{2-}$ (tetraglyme, 210–230 °C, 80 h).[40,550,551] The yield is sensitive to the counter-ion (Na$^+$, [ppn]$^+$, [NEt$_3$(CH$_2$Ph)]$^+$ resulted in decomposition), although a synthesis of the [ppn]$^+$ salt in up to 50% yield was achieved from Ru$_3$(CO)$_{12}$ and calcium carbide, followed by addition of [ppn]Cl.[552] The carbide resonance is at δ 457, with CO exchange between μ-CO and one set of terminal CO ligands (interchange of bridged

TABLE XIV

Some Structural Data for Interstitial Carbido Clusters

No.	Cluster	c.v.e.[a]	M–M/Å	M–C/Å	C–C/Å[b]	Ref.
A. Fe/Ru						
369/Fe	$Fe_3Ru_5(C)_2(\mu\text{-PPh}_2)_2(CO)_{17}$	112	2.648(3) (Fe–Fe)	1.89–1.94 (Fe)	[2.46]	547
			2.664–2.913(3) (Fe–Ru)	2.01–2.15 (Ru)		
			2.733–2.946(3) (Ru–Ru)			
369/Ru	$Ru_8(C)_2(\mu\text{-PPh}_2)_2(CO)_{17}$	112	2.738–2.984(3)	1.982–2.162(9)	[2.56]	548,549
370	$[Ru_{10}(C)_2(CO)_{24}]^{2-}$	138	2.803–3.098(2)	2.07 (av.)	[2.984]	550–552
			3.122, 3.138(2)*			
371	$[Ru_{10}(C)_2(\mu\text{-C}_2Ph_2)(CO)_{22}]^{2-}$	138	2.783–3.004(1)	2.06 (av.)	[3.001]	553
			2.711, 3.823(1)*			
372	$Ru_{10}(C)_2(\mu\text{-C}_2R_2)(CO)_{23}$ (R = Ph, tol)	138	2.786–3.076(2)	2.07 (av.)	[3.029]	554
			2.738, 3.892(2)*			
373	$[Ru_{10}(C)_2(\mu\text{-C}_3H_4)(CO)_{23}]^{2-}$	138	2.802–3.028(3)	2.045 (av.)	[2.994]	555
			3.049, 3.135(3)*			
374	$[Ru_{10}(C)_2(\mu\text{-C}_3H_4)_2(CO)_{20}]^{2-}$	138	2.819–2.990(1)	2.05 (av.)	[3.034]	555
			3.038, 3.084(1)*			
376	$Ru_{10}(C)_2(CO)_{23}(nbd)$	138	2.764–3.206(2)	1.95–2.08	[3.004]	556
			2.939, 3.876(2)*			
377	$Ru_{10}(C)_2(\mu\text{-C}_2Ph_2)(CO)_{22}(nbd)$	138	2.759–3.272(5)	2.065 (av.)	[3.016]	556
			2.748, 3.839(5)			
378	$Ru_{10}(C)_2(\mu\text{-CH}_2)(CO)_{22}(nbd)$	138	2.794–3.061(1)	2.074 (av.)	[3.039]	557
			3.071, 3.106(1)*			
379	$Ru_{10}(C)_2(\mu\text{-H})(\mu_3\text{-CH})(CO)_{22}(nbd)$	138				557
B. Co						
380	$[Co_9(C_2)(CO)_{19}]^{2-}$	127	2.514–2.780(4)	1.96, 2.04(2)	1.39(2)	558
			2.588 (av.)			
381	$[Co_{11}(C_2)(CO)_{22}]^{3-}$	152	2.48, 2.60	1.86–2.37	1.62, 1.66(5)	558

382	[Co$_{13}$(C$_2$)(CO)$_{24}$]$^{4-}$	175	2.390–2.789(5) 2.57 (av.)	1.90–2.06(2) (av. 1.98)	[2.986]	560
383	[Co$_{13}$(C$_2$)(CO)$_{24}$]$^{3-}$	174	2.387–2.745(4) 2.575 (av.)	1.97 (av.)	[2.554]	561

C. Rh

384	Rh$_{12}$(C$_2$)(CO)$_{25}$	164	2.67–2.97 2.79 (av.)	2.22–2.64	1.48(2)	562
385	[Rh$_{15}$(C)$_2$(CO)$_{28}$]$^-$	200	2.738–2.988 2.87 (av.)	1.93–2.12 (av. 2.04)		570,571
386	[Rh$_{12}$(C)$_2$(CO)$_{24}$]$^{2-}$	166	2.754–2.834 2.773 (av.)	2.12 (av.)	[3.30]	563
387	[Rh$_{12}$(C)$_2$(CO)$_{23}$]$^{4-}$	166	2.829 (av.)	2.13	[3.371]	563,567
388	[Rh$_{12}$(C)$_2$(CO)$_{23}$]$^{3-}$	165	2.660–3.157(2) 2.831 (av.)	2.125 (av.)	[3.20, 3.32]	565
389	[Rh$_{14}$(C)$_2$(CO)$_{23}$]$^{2-}$	182	2.570, 2.771–2.830(1) 2.778 (av.)	2.14 (av.)	[10.00]	568
390	[Rh$_{15}$(C)$_2$(μ-I)$_2$(CO)$_{24}$]$^{3-}$	200	2.694–3.173(1) 2.89 (av.)	2.06	[3.468]	572

D. Ni

391	[Ni$_{10}$(C$_2$)(CO)$_{16}$]$^{2-}$	140	2.42, 2.65, 2.92 (av.)	2.08 (av.)	1.405	573
392	[Ni$_{11}$(C$_2$)(CO)$_{15}$]$^{2-}$	148	2.541 (av.)	2.069 (av.)	1.46(2)	574
393	[Ni$_{12}$(C$_2$)(CO)$_{16}$]$^{4-}$	162	2.524 (av.)	2.062 (av.)	1.43(2)	574
394	[Ni$_{16}$(C$_2$)$_2$(CO)$_{23}$]$^{4-}$	222	2.355–3.028 2.604 (av.)	1.935–2.176 (av. 2.07)	1.38 (av.) [2.88]	575
395	[Ni$_{32}$(C)$_6$(CO)$_{36}$]$^{6-}$	422	2.397, 2.461, 2.634	2.062 (av.)	[3.17–3.28]	576
396	[Ni$_{32}$H(C)$_6$(CO)$_{36}$]$^{5-}$	422				577
398	[Ni$_{35}$(C)$_4$(CO)$_{36}$]$^{6-}$	444	2.350–2.975(2)		[3.62, 3.72]	578
399	[Ni$_{38}$H(C)$_6$(CO)$_{36}$]$^{5-}$	482	2.402–2.633	2.061	[3.25–3.32]	577,579

E. Ru–Pd

400	[Pd$_2$Ru$_{12}$(C)$_2$(CO)$_{30}$]$^{2-}$	184	Pd–Ru 2.776 (av.)	2.08 (av.)	[5.44]	580
401	[Pd$_4$Ru$_{12}$(C)$_2$(CO)$_{32}$]$^{2-}$	208	Pd–Pd 2.778 (av.)	2.08 (av.)	[6.72]	580

(*Continued*)

TABLE XIV

Continued

No.	Cluster	c.v.e.[a]	M–M/Å	M–C/Å	C–C/Å[b]	Ref.
402	$Pd_8Ru_{10}(C)_2(\mu\text{-}C_3H_5)_4(CO)_{27}$	234	Pd–Ru 2.813 (av.) Pd–Ru 2.917 (av.)	2.085 (av.)	[6.33]	580
F. Ru–Ag						
403	$[Ag_3Ru_{10}(C)_2(\mu\text{-}Cl)(CO)_{28}]^{2-}$	182	Ag–Ag 2.8074 (av.), 3.3498 Ag–Ru 2.917 (av.) Ru–Ru 2.855 (av.)	2.066 (av.)	[7.42]	581
G. Co–Ni						
404	$[Co_6Ni_2(C_2)(CO)_{16}]^{2-}$	114	2.603 (av.)	1.993 (av.)	1.49(1)	582,583
405	$[Co_6Ni_2(C_2)(CO)_{14}(NCMe)_2]^{2-}$	114	2.605 (av.)	1.998 (av.)	1.49	582
406	$[Co_3Ni_7(C_2)(CO)_{16}]^{2-}$	137	2.34–2.80	1.90–2.15 (av. 2.07)	1.48(2)	584
407	$[Co_3Ni_7(C_2)(CO)_{15}]^{3-}$	138			1.43	584
H. Rh–Au						
408	$Au_4Rh_{10}(C)_2(CO)_{20}(PPh_3)_4$	190	Au–Rh 2.826 (av.) Rh–Rh 2.895 (av.)	2.01–2.11	[2.98]	586
409	$Au_4Rh_{10}(C)_2(CO)_{18}(PPh_3)_4$	186	Au–Rh 2.825 (av.) Rh–Rh 2.888 (av.)	2.00–2.11	[2.99]	586

[a]Calculated with C giving 4 e, C_2 giving 6 e.

[b]Values in [ ] are non-bonded distances.
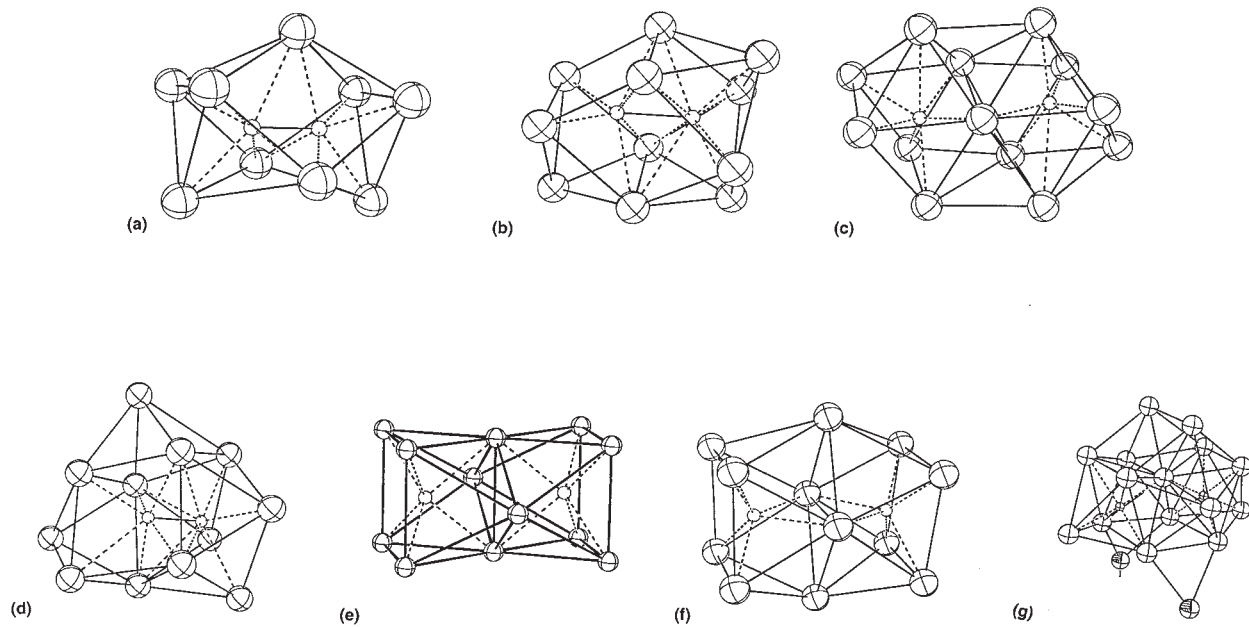
Fig. 12. Some cobalt and rhodium clusters containing interstitial C_2 ligands or two C atoms: (a) $[Co_9(C_2)(CO)_{19}]^{2-}$ (**380**); (b) $[Co_{11}(C_2)(CO)_{22}]^{3-}$ (**381**); (c) $[Co_{13}(C)_2(CO)_{24}]^{3-}$ (**382**); (d) $Rh_{12}(C_2)(CO)_{25}$ (**384**); (e) $[Rh_{12}(C)_2(CO)_{24}]^{2-}$ (**386**); (f) $Rh_{12}(C)_2(CO)_{23}]^{4-}$ (**387**); (g) $[Rh_{15}(C_2)(\mu\text{-I})_2(CO)_{24}]^{3-}$ (**390**).
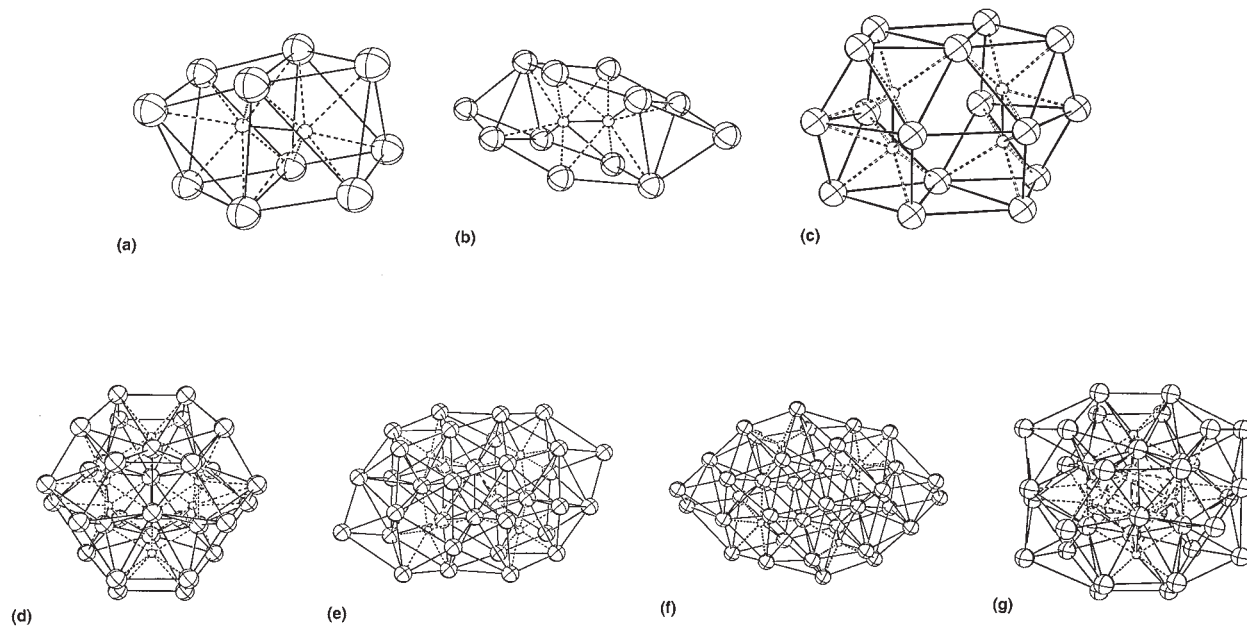
FIG. 13. Some nickel clusters containing interstitial C_2 ligands or four or six C atoms: (a) $[Ni_{10}(C_2)(CO)_{16}]^{2-}$ (**391**); (b) $[Ni_{12}(C_2)(CO)_{16}]^{4-}$ (**393**); (c) $[Ni_{16}(C)_4(CO)_{23}]^{4-}$ (**394**); (d) $[Ni_{32}(C)_6(CO)_{36}]^{6-}$ (**395**); (e) $[Ni_{34}H(C)_4(CO)_{38}]^{5-}$ (**397**); (f) $[Ni_{35}(C)_4(CO)_{39}]^{6-}$ (**398**); (g) $[Ni_{38}H(C)_6(CO)_{42}]^{5-}$ (**399**).
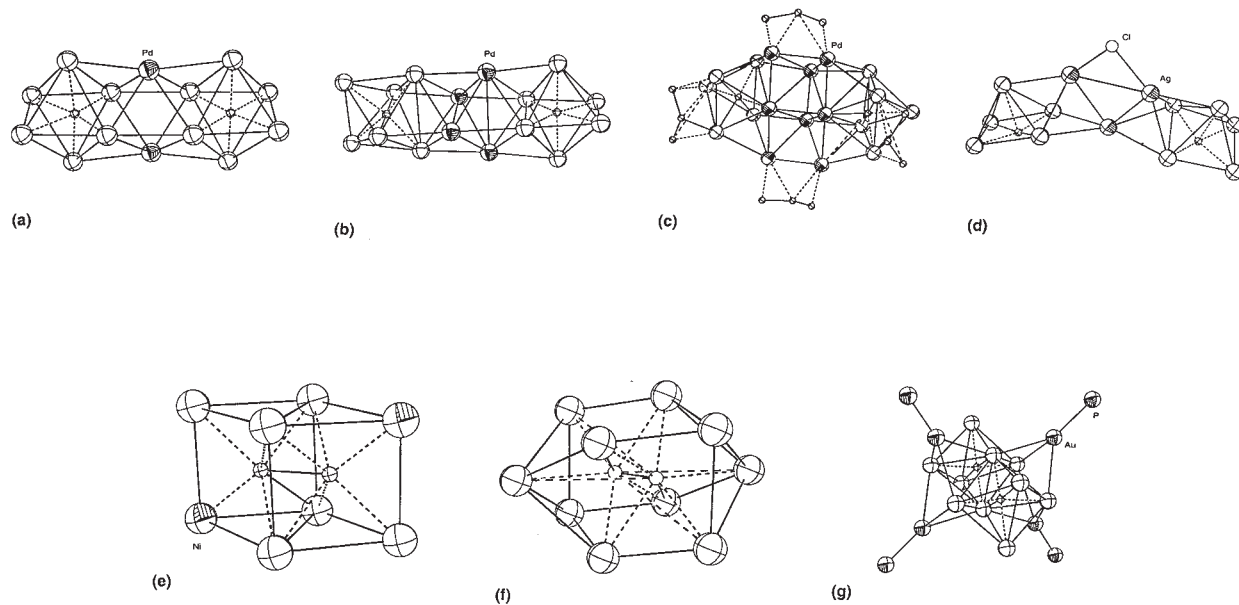
FIG. 14. Some heterometallic clusters containing interstitial C atoms: (a) $[Pd_2Ru_{12}(C)_2(CO)_{30}]^{2-}$ (**400**); (b) $[Pd_4Ru_{12}(C)_2(CO)_{32}]^{2-}$ (**401**); (c) $Pd_8Ru_{10}(C)_2(\mu-C_3H_5)_4(CO)_{27}$ (**402**); (d) $Ag_3Ru_{10}(C)_2(\mu-Cl)(CO)_{28}]^{2-}$ (**403**); (e) $[Co_6Ni_2(C_2)(CO)_{16}]^{2-}$ (**404**); (f) $[Co_3Ni_7(C_2)(CO)_{16}]^{2-}$ (**406**) (Co/ Ni atoms disordered); (g) $Au_4Rh_{10}(C)_2(CO)_{18}(PPh_3)_4$ (**409**).

$(CO)_2$
Ru
$(OC)_2$
Ru
Ph_2P
$Ru(CO)_2$
PPh_2
$(OC)_2Ru$
C
M
$(CO)_2$
C
$Ru(CO)_2$
M
$(CO)_2$
$(OC)_3M$

(369) M = Ru, Fe

$Ru_3(CO)_{12}$ 　　　 $[Ru_6C(CO)_{16}]^{2-}$ 　　　 $[Ru_{10}(C)_2(\mu\text{-}CH_2=C=CH_2)_2(CO)_{22}]^{2-}$ **(374)**

CaC_2, thf, 8 h 　　 tetraglyme 210–230°C, 80 h 　　 $CH_2=C=CH_2$ diglyme, 140°C

$[Ru_{10}(C)_2(\mu\text{-}RC_2R')(CO)_{22}]^{2-}$ **(371)** $\xrightarrow[\text{RC}_2\text{R'} \text{ diglyme, 125°C, 5 d}]{\text{CO, 3 d}}$ $[Ru_{10}(C)_2(CO)_{24}]^{2-}$ **(370)** $\xrightarrow[\text{diglyme, 90°C}]{CH_2=C=CH_2}$ $[Ru_{10}(C)_2(\mu\text{-}CH_2=C=CH_2)(CO)_{23}]^{2-}$ **(373)**

KOH / MeOH 　 RC_2R' [FcH]+

$Ru_{10}(C)_2(\mu\text{-}RC_2R')(CO)_{23}$ **(372)**

nbd, [FcH]+

nbd diglyme, 140°C

nbd diglyme, 140°C

$Ru_{10}(C)_2(CO)_{23}(nbd)$ **(376)**

$Ru_{10}(C)_2(\mu\text{-H})(\mu_3\text{-CH})(CO)_{22}(nbd)$ **(379)**

[FcH]+ 　 CO 　 80°C

nbd PhMe, 110°C

$Ru_{10}(C)_2(\mu\text{-}RC_2R')(CO)_{22}(nbd)$ **(377)** $\xleftarrow[\text{[FcH]}^+]{\text{RC}_2\text{R'}}$ $[Ru_{10}(C)_2(CO)_{22}(nbd)]^{2-}$ **(375)** $\xrightarrow[\text{[FcH]}^+]{CH_2N_2}$ $Ru_{10}(C)_2(\mu\text{-}CH_2)(CO)_{22}(nbd)$ **(378)**

SCHEME 65

and non-bridged apical–equatorial Ru–Ru edges results in racemization of the cluster). The structure of the cluster anion is closely related to that of the well-known $Ru_6C(CO)_{17}$ carbido-cluster and consists of two edge-fused octahedra, each containing a carbon atom [Ru–C 2.07 Å (av.)]. Each Ru has two terminal CO groups, four bridging CO ligands linking Ru_2 pairs (except on the fused edge). The triangular faces are alternately large and small, with individual Ru–Ru separations falling within five groups between 2.803 and 3.098(2) Å. The Ru(ap)···Ru(ap) separations are 3.122 and 3.138(2) Å, which is probably a result of apical

Ru(CO)$_2$ group repulsions, which also lead to a small twisting between the octahedra.

Unlike the other clusters considered in this Section, a limited chemistry has been described for the dianion. The thermal reaction with C$_2$Ph$_2$ at 125 °C affords red-purple [Ru$_{10}$(C)$_2$(μ-C$_2$Ph$_2$)(μ-CO)$_4$(CO)$_{18}$]$^{2-}$ (**371**, R = R′ = Ph), in which the two apical Ru atoms are now joined with the alkyne bridging this bond. Heating in diglyme under CO, the parent cluster anion is regenerated.[553] Oxidative substitution of the dianion with alkynes in the presence of [FcH]$^+$ gives green Ru$_{10}$(C)$_2$(μ-RC$_2$R′)(CO)$_{23}$ (**372**, R = Ph, R′ = Me, Ph; R = R′ = tol). Ready reduction to the dianions occurs with methanolic hydroxide.[554] Facile migration of CO occurs over the cluster framework.

The dianion reacts with allene to give bright purple mono- (**373**) and red-purple di-substitution products (**374**) at the apical positions. The allene can be removed under CO. In solution, dynamic processes involve the CO groups.[555] In contrast, the reaction with bicyclo[2.2.1]hepta-2,5-diene (norbornadiene) gives red-purple [Ru$_{10}$(C)$_2$(CO)$_{22}$(nbd)]$^{2-}$ (**375**) which can be oxidized to Ru$_{10}$(C)$_2$(CO)$_{23}$(nbd) (**376**) by [FcH]$^+$ under CO. In both clusters, the diene is coordinated to an outer Ru atom. In the red-purple mixed ligand derivatives Ru$_{10}$(C)$_2$(μ-C$_2$R$_2$)(CO)$_{22}$(nbd) (**377**; R = Ph, tol), the ligands occupy the same relative positions.[556] Similarly, the CH$_2$ group bridges the apical Ru atoms in purple-brown Ru$_{10}$(C)$_2$(μ-CH$_2$)(CO)$_{22}$(nbd) (**378**), which is formed from **376** and diazomethane/[FcH]$^+$. On heating, the brown hydrido-methylidyne tautomer **379** is formed reversibly, the equilibrium mixture containing a 77/13 ratio of CH$_2$/H(CH) at 80 °C.[557]

The Ru$_{10}$C$_2$ cluster dianion **370** has 138 c.v.e. and the HOMOs are occupied M–M bonding and anti-bonding MOs. The Ru(ap)–Ru(ap) separations are generally longer than 3.0 Å and are considered to be non-bonding. Comparison of the core structures in the dianion and its substitution products shows that coordination of the alkyne or allene results in shortening of the Ru(ap)–Ru(ap) separations, e.g., to 2.738(2) Å in the C$_2$Ph$_2$ complex (Table XIV). The formation of Ru(ap)–Ru(ap) bonds appears to be a consequence of increased back-bonding of the alkyne or allene, which changes the occupation of the two HOMOs. In addition, either one or two Ru(ap)–Ru(hinge) distances are very long [at 3.292(2) Å for the C$_2$Ph$_2$ derivative]. The difference in donor power between the two ligand sets (CH$_2$ 2-e, H/CH 4-e) likely results in the lengthening of some Ru–Ru bonds in the latter case, the cluster being able to accommodate varying steric and electronic demands. Where only one ligand bridges the apical Ru atoms, the octahedra bend about the equatorial hinge to reduce the separation between one pair of Ru(ap) atoms, the other necessarily increasing.

$$[Co_6C(CO)_{14}]^- \qquad\qquad [Co_6C(CO)_{15}]^{2-}$$

diglyme
130°C, 6-7 h

diglyme

140°C, 10-11 h

175°C, 8 h

$$[Co_9(C_2)(CO)_{19}]^{2-} \qquad [Co_{11}(C_2)(CO)_{22}]^{3-} \qquad [Co_{13}(C)_2(CO)_{24}]^{4-}$$

(380)   **(381)**   **(382)**

$[Co(CO)_4]^-$ ‖ CO   Zn ↕ I_2 / MeCN

$$\{Co_3(CO)_9(\mu_3\text{-}C)\}_2 \qquad\qquad [Co_{13}(C)_2(CO)_{24}]^{3-}$$

(271)   **(383)**
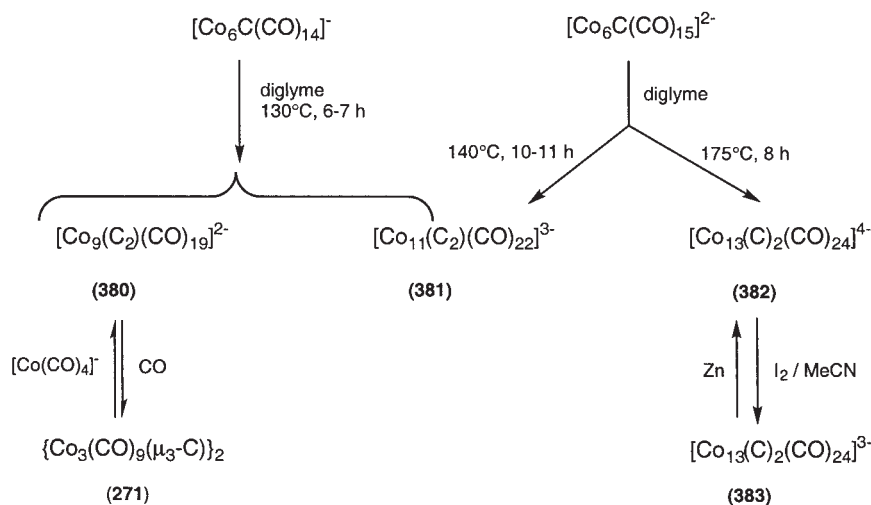
SCHEME 66

(b) Cobalt

Pyrolysis of paramagnetic $[Co_6C(CO)_{14}]^-$ (diglyme, 130 °C, 6–7 h) has given paramagnetic $[Co_9(C_2)(CO)_{19}]^{2-}$ (**380**; Scheme 66) [g = 2.027 (thf, 123 K), linewidth 200 G, no hyperfine splitting], together with $[Co_{11}(C_2)(CO)_{22}]^{3-}$ (**381**; see below).[558] The dianion (but not the expected trianion) has also been obtained from $[Co(CO)_4]^-$ and $\{Co_3(CO)_9(\mu_3\text{-}C)\}_2$. Degradation occurs under CO: extended reaction times give $[Co(CO)_4]^-$ and trace amounts of $\{Co_3(CO)_9\}_2C_2$. The Co_9 cluster is a staggered three-layer stack of Co_3 units forming a D_{3h} tricapped trigonal prism, the central one being non-bonded and resulting in a barrel-shaped cluster which perfectly fits the C_2 fragment, with av. Co–C 1.96, 2.02(2) Å. The C–C separation is short at 1.39(2) Å. In both the Co and Rh clusters [see (*c*) below], the distribution of terminal and bridging CO groups is generally consistent with balanced charge donation to the metals and is determined by non-bonded contacts on the surface of the cluster core.

Fractional crystallization of the mixture of anions (as $[NMe_3(CH_2Ph)]^+$ salts) obtained by thermolysis of $[Co_6C(CO)_{15}]^{2-}$ in diglyme (140 °C, 10–11 h)[559] or, better, $[Co_6C(CO)_{14}]^-$ (130 °C, 6–7 h)[558] affords $[Co_{11}(C_2)(CO)_{22}]^{3-}$ (**381**) in up to 5–10% yield. The Co_{11} polyhedron can be described approximately as either a tri-capped cube (idealized symmetry C_{2v}), with one stretched edge [Co(10)–Co(11)] reducing the symmetry to C_s-*m*, or as a trigonal prism sharing a square face with a square pyramid, of which two opposite edges are stretched, with the 11th Co capping a second square face of the prism. The lengthening appears to be a result of

accommodating a bonded C_2 fragment [1.62(5) Å], one C atom being in the prism and the other within the antiprism, since shortening of the two Co–Co distances would lead to lengthening of the C–C separation to ca. 1.8 Å. The Co–C distances average 2.10 (outer Co) and 2.26 Å (central Co).

Thermolysis of $[Co_6C(CO)_{15}]^{2-}$ in diglyme (175 °C, 8 h) afforded paramagnetic $[Co_{13}(C)_2(CO)_{24}]^{4-}$ (**382**) as the major product, isolated as the black $[NMe_3(CH_2Ph)]^+$ salt.[560] The ESR spectrum shows a strong absorption at −120 °C (but not at r.t.) for $S = 1/2$, while at 4.2 K, the anisotropy of the g tensor is found in the spectrum of the powder ($g_{zz} = 2.031$, $g_{yy,xx} = 2.183$). The anion is oxidatively very sensitive in solution, while under CO, it is slowly degraded to Co^{2+} and $[Co(CO)_4]^-$. Oxidation of the tetra-anion **382** with iodine in MeCN gives the trianion $[Co_{13}(C)_2(CO)_{24}]^{3-}$ (**383**) quantitatively.[561] The anion is stable in air for a few hours, but solutions are quickly oxidized. Reduction with zinc regenerates the tetra-anion, but reaction with CO leads to $[Co(CO)_4]^-$, $Co_3(\mu_3\text{-}CX)(CO)_9$, and other clusters. In MeCN, reduction with zinc gives the tetra-anion.

The cores of the two anions are isostructural with idealized C_2 symmetry. The closed Co_{13} polyhedron has "no resemblance to any simple geometrical solid" and is best described as a 4 (square)/5 (three fused triangles)/4 (square) stack. Two trigonal prismatic cavities each contain a carbon atom. There are two uncapped rectangular faces, the remainder being triangular. Of the 33 metal–metal interactions (36 are required for a closed packed M_{13} polyhedron), the two longest [2.735, 2.789(4) Å] are within the cluster. The connectivity of each cobalt ranges from four to eight, with all Co atoms being bonded to at least one carbide atom. The overall ranges of Co–Co distances in both anions tend to confirm the suggestion that the extra electron is used to widen the prismatic cavities to accommodate the carbide atoms.

(c) Rhodium

Treatment of $[Rh_6C(CO)_{15}]^{2-}$ with Fe^{III} gives $Rh_{12}(C_2)(CO)_{25}$ (**384**; Scheme 67) (79%), also formed by slow decomposition of $[Rh_{15}(C)_2(CO)_{28}]^-$ (**385**; see below).[562] Both anions are prepared by similar reactions, the precise conditions favoring one over the other not being determined. The metal core is one of the most irregular found, with the Rh atoms arranged in a nearly parallel 4 (rhomb)/5 (irregular pentagon)/3 (triangle) tri-layer core with average layer separation 2.2 Å. All but two rhombic faces are triangular. The Rh_{12} core is conceptually related to the Co_{11} core in **381** by adding a second μ_4-Rh capping atom. The central 10-vertex polyhedron in both is well-suited to accommodate the C_2 unit, the elongated edges being required for closer M–C bonding contacts. Thus,
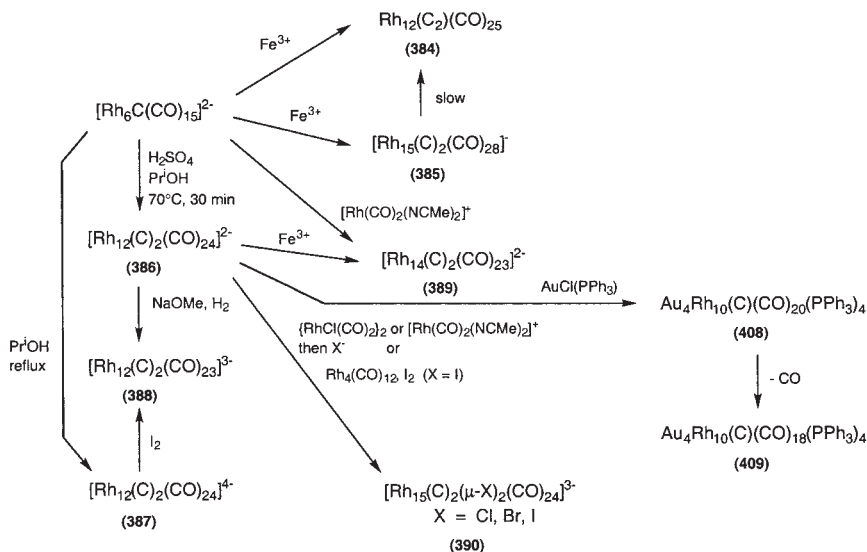
SCHEME 67

a more regular arrangement is inhibited by the presence of the carbon atoms. The C_2 unit occupies an irregular cavity derived from a trigonal prism and a tetragonal antiprism fused via a rhombic face.

In contrast to **384** and **385**, which readily fragment when treated with common basic solvents, the dianion $[Rh_{12}(C)_2(CO)_{24}]^{2-}$ (**386**) is more stable.[563] On heating $[Rh_6C(CO)_{15}]^{2-}$ and one equivalent of sulfuric acid in propan-2-ol (70 °C, 30 min), this dianion is obtained in 80–90% yield. The reaction proceeds via a reactive monohydrido cluster,[564] detected by NMR. In the absence of an acid, the prismatic Rh_6 dianion is converted into octahedral $[Rh_6C(CO)_{13}]^{2-}$ after brief heating, while longer times give $[Rh_{12}(C)_2(CO)_{23}]^{4-}$ (**387**) (below). The Rh_{12} cluster dianion has idealized D_{2h}-mmm symmetry, with a 4 (square)/4 (rhomb)/4 (square) layer structure which forms two prismatic cavities each containing one carbon atom. Metal connectivities range from four to seven, with most Rh–Rh separations lying in the range 2.754–2.834(2) Å. Comparison with the $Co_{13}C_2$ cluster (above) shows that they have closely related structures with an extra metal atom being attached to the central layer to form a third triangle. The dianion is isoelectronic with $Rh_{12}(C_2)(CO)_{25}$, but the presence of a discrete C_2 ligand in the latter means they are not isostructural.

The dianion is reduced to the unstable paramagnetic trianion $[Rh_{12}(C)_2(CO)_{23}]^{3-}$ (**388**) by NaOMe under hydrogen with 35–40% conversion; a diamagnetic species thought to be $[Rh_{12}H(C_2)(CO)_{23}]^{3-}$ (δ −15.25)

is also formed.[565] The latter is deprotonated by an excess of base. At 120 K, the trianion gives ESR signals with g_1 2.282, g_2 2.198, g_3 2.038; in solution, slow decomposition occurs. The core structure of the trianion is similar to that of the dianion, with a three-layer 4 (square)/4 (rhomb)/4 (square) stack. The two C atoms are in the two prismatic cavities (mean Rh–C 2.125 Å). Comparison with the dianion shows an increase in both values, indicating that the unpaired electron is in a delocalized anti-bonding cluster orbital. ESR studies are interpreted in terms of the atoms lying in the central plane, the unpaired electron residing in a HOMO derived from d_{z^2} and d_{xy} orbitals.[566]

The tetra-anion **387** is formed by treating the dianion with a large excess of KOH or by prolonged thermolysis (refluxing propan-2-ol or diglyme) of $[Rh_6C(CO)_{15}]^{2-}$, in 70–80% yield. With iodine, conversion to the trianion is found, also formed by traces of water in MeCN or acetone solvent; the tetra-anion is also unstable in methanol.[565,567] The core structure is similar to that of the dianion, with two prismatic cavities for the carbides, but loss of one CO from an acute apex of the equatorial layer is compensated by movement of two terminal CO ligands to the same bridging positions as in the trianion, thus alleviating overcrowding in the dianion. Compared with the dianion, the average Rh–Rh distance increases by 0.018 Å to 2.829 Å. With increasing charge, there is a general increase in back-donation to CO, giving shorter Rh–CO and longer C–O bonds The tetra-anion reacts with acids under CO to give the hydrido-trianion and then the dianion; the trianion is also formed by stoichiometric addition of iodine in acetonitrile solution.

The reaction between $[Rh(CO)_2(NCMe)_2]^+$ (in MeCN) and $[Rh_6C(CO)_{15}]^{2-}$ (in aqueous acid) under CO gives dark violet $[Rh_{14}(C)_2(CO)_{33}]^{2-}$ (**389**) by dimerization of a putative $[Rh_7C(CO)_{17}]^-$; under CO in MeCN, fragmentation occurs to the smaller clusters, while if halide is present, $[RhX_2(CO)_2]^-$ is formed.[568] Some **389** is also formed from $Rh_8C(CO)_{19}$ under CO in acetonitrile/CH_2Cl_2. The Rh_{14} core consists of two trigonal prismatic clusters bridged by an $Rh_2(\mu\text{-}CO)_3$ unit attached to one triangular face of each Rh_6C unit and, as such, does not strictly fall within the scope of this section.

Oxidation (Fe^{III}) of $[Rh_6C(CO)_{15}]^{2-}$ under mild conditions gives a solid which, when dissolved and kept under CO, affords $Rh_8C(CO)_{19}$.[569] Oxidation under nitrogen gives two different clusters, one of which has been characterized as black $[H_3O][Rh_{15}(C)_2(CO)_{28}]$ (**385**).[570,571] The anion has C_{2v} symmetry, two descriptions being (i) a centred pentagonal prism capped on two basal and two side faces, or (ii) two octahedra sharing a vertex, with four extra atoms forming tetrahedra with four faces also fused with themselves. A possible growth mechanism involves capping of a

trigonal prism (in the precursor dianion) and isomerization reactions. The central Rh atom is twelve-coordinate but not close-packed. Short non-bonding distances separate some Rh atoms atoms in the square faces which contain the carbon atoms. The cluster contains two octahedral cavities which contain the discrete carbon atoms with Rh–C distances somewhat shorter than those found in trigonal prismatic cavities.

Reactions of $[Rh_{12}(C)_2(CO)_{24}]^{2-}$ with $\{RhCl(CO)\}_2$ or $[Rh(CO)_2(NCMe)_2]^+$ give an uncharacterized, possibly unsaturated, intermediate which reacts with halides to give $[Rh_{15}(C)_2(\mu\text{-}X)_2(\mu\text{-}CO)_{14}(CO)_{10}]^{3-}$ (**390**; X = Cl, Br, I), which has also been obtained from the reaction of $[Rh_{12}(C)_2(CO)_{24}]^{2-}$ with $Rh_4(CO)_{12}$ and iodide.[572] The Rh_{15} core forms a centred tetracapped pentagonal prism with C_{2v} symmetry, closely related to that found in $[Rh_{15}(C)_2(CO)_{28}]^-$. The two halides span basal edges and replace four terminal CO ligands. The carbide atoms occupy octahedral cavities and give multiplet resonances at δ_C 388.

(d) Nickel

Selective formation of red $[Ni_{10}(C_2)(CO)_{16}]^{2-}$ (**391**; Scheme 68) occurs by reaction of $[Ni_6(CO)_{12}]^{2-}$ with C_2Cl_4 or C_2Cl_6 in yields up to 60%.[573] It has also been made by thermolysis of $[Ni_9C(CO)_{17}]^{2-}$ in diglyme (120 °C). The core consists of two Ni-capped trigonal prisms sharing a square face and closely resembles the Co_6Ni_2 cluster **404** (below). The C_2 unit resides in a single cavity (in contrast with others above) with each C atom being coordinated by seven Ni atoms. The C–C separation is 1.40 Å (the shortest
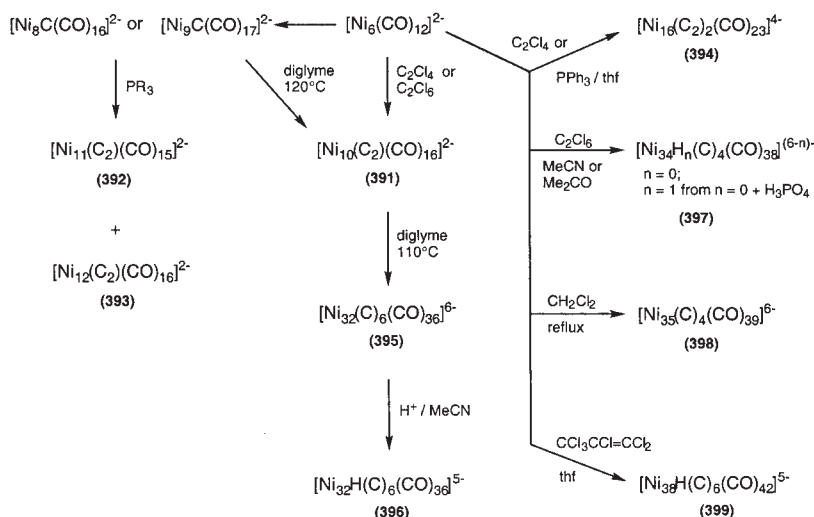
SCHEME 68

reported so far). Under CO, reversible degradation to $Ni(CO)_4$ and other reactive dicarbido clusters occurs.

Controlled degradation of $[Ni_8C(CO)_{16}]^{2-}$ or $[Ni_9C(CO)_{17}]^{2-}$ with tertiary phosphines has given $[Ni_{11}(C_2)(CO)_{15}]^{2-}$ (**392**) and $[Ni_{12}(C_2)(CO)_{16}]^{4-}$ (**393**) by a disproportionation-induced coupling via $[Ni_7C(CO)_{12}]^{2-}$.[574] The frameworks are derived by successive capping of an $Ni_{10}C_2$ cluster. Each C atom coordinated to seven Ni atoms (Ni–C 2.07 Å). Similarly, reaction of **391** with PPh_3 in thf affords $[Ni_{16}(C_2)_2(CO)_{23}]^{4-}$ (**394**) quantitatively, and this is also the main product (20%) from the reaction between $[Ni_6(CO)_{12}]^{2-}$ and C_2Cl_4 with $[NMe_4]^+$ counter-ion (rather than $[PPh_4]^+$ or $[ppn]^+$) being used.[575] The core has a truncated distorted v_2-octahedron (idealized symmetry C_{2h}) derived from fusion of two $Ni_{10}C_2$ units. Two C_2 units are incorporated into the cavity (C–C 1.38 Å, C$\cdots$C 2.88 Å) with Ni–C between 1.935 and 2.176 Å (av. 2.07 Å, as in Ni_{10}).

Thermolysis of **394** (diglyme, 110 °C) gives 394 and $[Ni_{32}(C)_6(CO)_{36}]^{6-}$ (**395**), together with $Ni(CO)_4$. The two larger clusters can be separated by virtue of their relative solubilities, the Ni_{32} cluster being the less soluble, its salts separating during the reaction.[576,577] The six carbon atoms cap six faces of the inner Ni_8 cube and form a non-bonded octahedron, being in square antiprismatic cavities formed with the outer Ni_{24} shell. All CO groups are edge-bridging [$v(CO)$ 1889 cm^{-1}] and resemble CO chemisorbed on a nickel surface at low coverage.

Addition of acid in acetonitrile to the hexa-anion gives only traces of $[Ni_{32}H(C)_6(CO)_{36}]^{5-}$ (**396**), although the penta-anion is stable in acetone. Reduction (sodium/naphthalene, dmf) affords the hepta- and octa-anions, which are stable for hours in solution, while oxidation ($C_7H_7^+$) regenerates the hexa-anion and ultimately gives the unstable penta-anion.[577] The odd-electron species do not give ESR spectra.

Reactions of $[Ni_6(CO)_{12}]^{2-}$ with C_2Cl_6 give $[Ni_{34}H_n(C)_4(CO)_{38}]^{(6-n)-}$ (**397**, $n = 0$, 1), accompanied by **391** and **394**. The monoprotonated Ni_{34} cluster is best obtained by addition of H_3PO_4 to the hexa-anion in MeCN.[578] Each carbon is thus seven-coordinate and caps a square face of the cubic-close packed Ni_{20} fragment. A trigonal prismatic cavity around each carbon is formed by further addition of two Ni atoms to each square face to give the $Ni_{28}C_4$ unit. There are 10 terminal CO, 26 μ-CO, and two μ_3-CO ligands, although the bridging groups are often unsymmetrical or semi-bridging.

The closely related $[Ni_{35}(C)_4(CO)_{39}]^{6-}$ (**398**), isolated from the products obtained by heating $[Ni_6(CO)_{12}]^{2-}$ in CH_2Cl_2, has a structure formed by formal addition of the extra Ni atom to either of the two centrosymmetrically related stepped faces in the Ni_{34} cluster.[578] The CO stereochemistry is the same as found for the $Ni_{34}C_4$ cluster, except for the extra Ni(CO)

group and change of one μ-CO to terminal. In both, the presence of the carbon atoms results in swelling of the lattice.

Even larger is the black $[Ni_{38}H(C)_6(CO)_{42}]^{5-}$ (**399**), which was obtained from $[Ni_6(CO)_{12}]^{2-}$ and hexachloropropene in tetrahydrofuran.[577,579] Deprotonation to the hexa-anion occurs in acetone, while reversible stoichiometric protonation (H_2SO_4) gives the penta-anion (in MeCN) or $[Ni_{38}H_{6-n}C_6(CO)_{42}]^{n-}$ ($n = 2$, 3) in acetone. The carbon atoms occupy square antiprismatic cavities (Ni–C 2.061, C$\cdots$C 3.25–3.32 Å). There are six terminal CO and 36 μ-CO ligands. Treatment with CO (1 atm., MeCN) generates the $Ni_{32}C_6$ hexa-anion by removal of nickel as $Ni(CO)_4$. The IR spectra suggests that a stepwise process proceeds through $[Ni_{38-n}C_6(CO)_{42-n}]^{6-}$ ($n = 1$–6), all of which have ($6n + 19$) valence orbitals.[576]

Reduction ($Na/C_{10}H_8$, dmf) gives the hepta- and octa-anions (and possibly nona-), which can be reoxidized with $C_7H_7^+$, finally giving the penta-anion. Addition of more oxidant results in decomposition to $Ni(CO)_4$ and black insoluble material.[577] Comparison of the hexa-anion with the protonated penta-anion shows that the former has four well-defined reversible redox processes (one oxidation, three reduction), while the four processes (4-/8-) for the hydrido-anion are not so well resolved. The presence of the hydride shifts the potentials by ca. 400 mV to more negative potentials. The penta-anion decomposes slowly and the tetra-anion is very unstable. Peak-to-peak separations > 60 mV probably arise from some structural rearrangements. The odd-electron species do not give ESR spectra. Electrochemical studies of the $Ni_{32}C_6$ and $Ni_{38}C_6$ clusters show sequences of five (5-/10-) or four (4-/8-) 1-e reduction steps in the CVs; the $HNi_{38}C_6$ cluster also gives four 1-e processes, each shifted by −400 mV compared with the non-protonated complex. Some structural changes may accompany the reductions, which are separated by more than 60 mV.

The structures of the larger nickel cluster cores are closely related. For **395**, the cluster has idealized O_h symmetry and is formed from an Ni_8 cube inside a truncated octahedral Ni_{24} shell (Ni–Ni 2.461 Å). The average Ni(inner)–Ni(outer) distance is 2.634 Å, the Ni(inner) atoms being 12-coordinate and lying 0.93 Å below the hexagonal face of the Ni_{24} shell. The $Ni_{32}C_6^{6-}$ core is the same as that found in the $Ni_{38}C_6$ cluster (see above) and identical to the $Cr_{32}C_6$ structural unit found in $Cr_{23}C_6$, although the carbide atoms in Ni_3C are enclosed in octahedral cavities in a hexagonal close-packed Ni lattice. The core of **397** consists of a cubic close-packed Ni_{20} core. Further, cluster build-up occurs by capping two of the square faces adjacent to the two pentagonal faces, also capped, which generates two stepped units (concave butterfly) on the surface, which are also capped by two Ni atoms. The two remaining square faces are uncapped.

In **398**, the extra Ni(CO) group caps one of the four stepped faces. In both clusters, the Ni–Ni separations range between 2.350 and 2.975 Å. Neither metal framework is related to a close-packed metal lattice. Six of the eight hexagonal faces of the truncated octahedral $Ni_{32}C_6$ core found in **395** are μ_3-capped by the extra Ni atoms in **399** (Ni–Ni 2.488, inter-layer Ni–Ni 2.633, outer edge Ni–Ni 2.459 Å; idealized D_{3d} symmetry). The geometry is similar to that found for $[Pt_{38}H_2(CO)_{44}]^{2-}$ except for the Pt_8 inner core of the latter, which is close-packed.

2. Heterometallic Systems

(a) Ru–Pd clusters

   Treatment of ruthenium cluster carbide anions $[Ru_5C(CO)_{14}]^{2-}$ or $[Ru_6C(CO)_{16}]^{2-}$ with $\{Pd(\mu\text{-Cl})(\eta\text{-}C_3H_5)\}_2$ or $[Pd(NCMe)_4]^{2+}$ afford high-nuclearity systems containing two carbido atoms. The complexes $[ppn]_2[Pd_2Ru_{12}(C)_2(CO)_{30}]$ (**400**), $[ppn]_2[Pd_4Ru_{12}(C)_2(CO)_{32}]$ (**401**) and $Pd_8Ru_{10}(C)_2(\mu\text{-}\eta\text{-}C_3H_5)_4(CO)_{27}$ (**402**) have been characterized crystallographically.[580] In these compounds, two octahedral $PdRu_5C$ or Ru_6C cores are linked by other metal atoms.

(b) Ru–Ag cluster

   Similarly, reactions between Ag^+ ions and $[Ru_5C(CO)_{14}]^{2-}$ have given $[Ag_3Ru_{10}(C)_2(\mu\text{-Cl})(CO)_{28}]^{2-}$ (**403**), which retains the square pyramidal Ru_5C core.[581] The Cl atom is presumably derived from the [ppn]Cl or $[AsPh_4]Cl$ used to provide counter-cations for this large anion. When anchored inside mesoporous silica (MCM-41), the intact cluster core acts a catalyst for hex-1-ene hydrogenation.

(c) Co–Ni clusters

   Redox condensation of $Co_3(\mu_3\text{-CCl})(CO)_9$ with $[Ni_6(CO)_{12}]^{2-}$ or better, $[Co_3Ni_9C(CO)_{20}]^{3-}$, gives $[Co_6Ni_2(C_2)(CO)_{16}]^{2-}$ (**404**; Scheme 69).[582] In thf, extended redox behavior involves reversible 1-e reduction and two 1-e oxidations: E(1-/2-) −0.04, (2-/3-) −1.24, (3-/4-) −1.48 V, each being stable enough for ESR measurements. Chemical reduction gives only one relatively stable complex which has not been fully characterized. Attempted crystallization from acetonitrile gave $[Co_6Ni_2(C_2)(CO)_{14}(NCMe)_2]^{2-}$ (**405**). In their $[NEt_4]^+$ salts, both clusters are similar, consisting of two trigonal prisms sharing a square face, with the carbon atoms in the prismatic cavities, i.e., a fragment of a hexagonal lattice stabilized by filling with carbon atoms.[583] In **404**, there are ten terminal CO and six μ-CO ligands; the two atoms with lower CO coordination are assumed to be nickel, and are those coordinated by MeCN in **405**. While the C–C separation is short at

$[Ni_6(CO)_{12}]^{2-}$ or
$[Co_3Ni_9C(CO)_{20}]^{3-}$

$[Co_6Ni_2(C_2)(CO)_{16}]^{2-}$ $\xrightarrow{\text{MeCN}}$ $[Co_6Ni_2(C_2)(CO)_{14}(NCMe)_2]^{2-}$
(404)   (405)

$Co_3(\mu_3\text{-CCl})(CO)_9$

$[Ni_9C(CO)_{18}]^{2-}$

$[Co_3Ni_7(C_2)(CO)_{16}]^{2-}$ $\xrightarrow{\text{NaOH / MeOH}}$ $[Co_3Ni_7(C_2)(CO)_{16}]^{3-}$
(406)   (407)
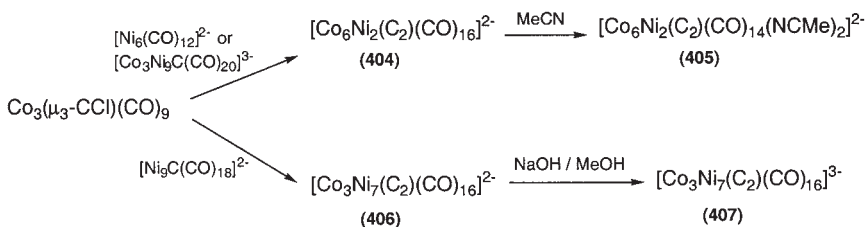
SCHEME 69

1.49 Å in both complexes, it is thought that the two atoms are kept close together by the delocalized interaction with all metal atoms.

Redox condensation of $Co_3(\mu_3\text{-CCl})(CO)_9$ with $[Ni_9C(CO)_{15}]^{2-}$ gives paramagnetic $[Co_3Ni_7(C_2)(CO)_{16}]^{2-}$ (406) [$g = 2.05$ (r.t.), some unresolved fine structure is seen at $-196\,^\circ$C], which can be reduced to the trianion by sodium in thf, the reaction being readily reversed by O_2 or H_2O (protic solvents). The high reactivity of the latter has precluded its structural characterization. Under a CO/H_2 mixture, 406 gives ethane, $[Co(CO)_4]^-$ and $Ni(CO)_4$, while 404 gives methane. All anions are oxidized in air to $Ni(CO)_4$, $CoCO_3$ and nickel.[584] Treatment of 406 with methanolic NaOH results in loss of CO to give $[Co_3Ni_7(C_2)(CO)_{15}]^{3-}$ (407), which is stable in protic solvents; treatment with acids gives 409 and $Ni(CO)_4$.[584,585]

The cores of 406 and 407 are each 3/4/3 stacks (alternatively described as a bi-octahedron with a broken shared edge or as two distorted fused trigonal prisms) with idealized symmetry C_{2h} which encloses a C_2 unit. The Co and Ni atoms cannot be distinguished and are probably distributed randomly. The carbides are in distorted seven-vertex cages (capped trigonal prisms) with M–C distances between 1.90–2.15 Å (mean 2.07 Å).

(d) Rh–Au clusters

Reactions of the dianion $[Rh_{12}(C)_2(CO)_{24}]^{2-}$ with $AuCl(PPh_3)$ proceed through several unidentified intermediates; with a large excess of $AuCl(PPh_3)$, only $[RhCl_2(CO)_2]^-$ remains in solution over a brown-red precipitate. After addition of four equiv., however, almost quantitative yields of dark red $Au_4Rh_{10}(C)_2(CO)_{20}(PPh_3)_4$ (408; Scheme 67) can be isolated.[586] This complex readily evolves CO to give brown $Au_4Rh_{10}(C)_2(CO)_{18}(PPh_3)_4$ (409) and under CO, a reversible equilibrium is established. Pure crystalline samples of both complexes have been obtained from 1-methylpyrrolidin-2-one. The cluster is constructed of two octahedra sharing an edge, each containing a carbon atom, with the six Rh(eq) and two carbons being coplanar. Four Rh(ap) atoms and two Rh(hinge) atoms define two tetrahedra, the outer faces of which are

capped by the four Au(PPh$_3$) units. The distribution of CO ligands is more symmetrical in **408**, with 10 terminal and eight bridging the outer Rh(ap)–Rh(eq) edges. In **408**, four Rh(eq)–Rh(hinge) edges are bridged by CO, whereas in **409**, the CO ligands attached to Rh(hinge) are disordered and bend towards the corresponding Rh(eq) atoms. The Rh–C distances are similar in both clusters. Addition of two CO ligands does not induce any significant differences in the core geometries of the two complexes. Conversion of the Rh$_{12}$C$_2$ precursor to **408** likely involves loss of two of the rhodium atoms above the Rh$_6$ plane, followed by core rearrangement to close-packing.

C. *C$_2$ Groups in Group 11 Metal Clusters*

1. Copper

The pale yellow tetranuclear ethyndiyl complex [Cu$_4$(μ_4-η^1:η^2-C$_2$) (μ-dppm)$_4$][BF$_4$]$_2$ (**410**) is formed in 46% yield from a mixture of LiBu and HC≡CSiMe$_3$ with [Cu$_2$(μ-dppm)$_2$(NCMe)$_2$][BF$_4$]$_2$.[587] The cation contains a saddle-like Cu$_4$(μ-dppm)$_4$ system, with the C$_2$ unit occupying the centre of a distorted rectangular Cu$_4$ array, each copper being three-coordinate. The C$_2$ ligand acts as a 6-e donor and is attached in both η^1 and η^2 modes. As found for other complexes [e.g., {Ru$_2$(μ-PPh$_2$) (CO)$_6$}$_2$(μ-C$_2$) (Section IX.A)], there is an approximately coplanar arrangement of the C$_2$Cu$_4$ core, whereas an orthogonal system might be expected from optimal overlap of the two π-orbitals. This conformation probably arises from steric hindrance between the dppm ligands. Consequently, the C–C distance is short [1.255 Å]. The Cu–C(η^1) separations are 1.913 Å and the Cu–C(η^2) distances 2.131 Å. The long Cu$\cdots$Cu separations are 3.245, 3.264(2) Å, much longer than the van der Waals sum (2.8 Å) and indicative of minimal metal–metal bonding.

VT ^{13}C and ^{31}P NMR studies have shown that the C$_2$ unit undergoes a rapid fluxional process, assigned to a rotation within the Cu$_4$ array with associated flipping of the dppm ligands. Coalescence of the ^{31}P resonances found at δ −9.6 (P attached to π-bonded Cu) and −12.3 (P attached to σ-bonded Cu) occurred at 182 K, while the carbon resonances in the ^{13}C-enriched complex coalesced at 208 K to give a nine-line resonance at δ 149.4 [*J*(CP) 13.3 Hz]. For the two processes, $\Delta G^{\#}$ values of ca. 38 and 47 kJ mol^{-1} were measured. The relatively facile process is indicative of a weak interaction between the C$_2$ ligand and the four copper atoms, which was confirmed by DFT calculations (calc. ΔG 32.9 kJ mol^{-1}). The UV–vis spectrum contains bands at 262 (dppm intra-ligand transfer), 374 nm (C$_2^{2-}$ → Cu$_4$ LMCT), while excitation (λ > 350 nm) produces intense

(410)

(411)
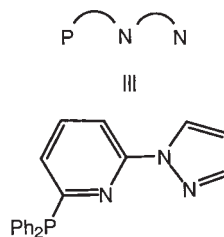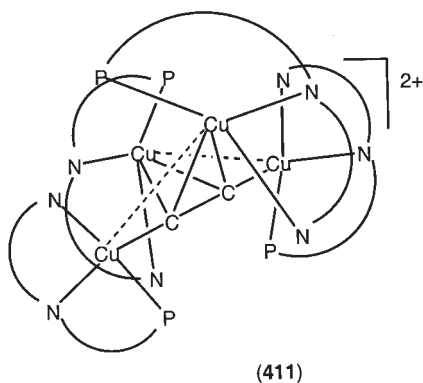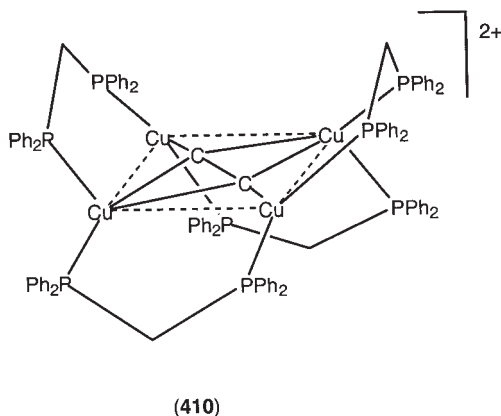
relatively long-lived emissions at ca. 560 nm, also observed in the solid at 509 (r.t.) or 551 nm (77 K), probably arising from a spin-forbidden transition from a triplet state. The luminescence is quenched by pyridinium ions. The reduction potential of the excited state $E°(3+/2+*)$ is -1.77 V (vs. SCE), i.e., it is a strong reducing agent.

The related complex $[Cu_4(\mu_4\text{-}C_2)(\mu\text{-}PPh_2\text{-}pypz)_4][ClO_4]_2$ (**411**; PPh_2-pypz $= 2$-PPh_2-6-pyrazol-1-ylpyridine) was obtained (60%) from $[Cu_2(\mu\text{-}PPh_2\text{-}pypz)_2(NCMe)_2][ClO_4]_2$ as air-stable orange crystals either by adding the salt to a mixture of LiBu and HC≡CSiMe$_3$, or in lower yield, NaC≡CH.[588] The carbons of the C_2 ligand resonate at δ 68.65 (cf. C$_2$H$_2$, δ 71.90). The C_2Cu_4 core has a butterfly conformation, containing two Cu$_2$ units attached in both η^1 and η^2 modes. The Cu–C–C planes have a dihedral angle of 129.0(3)°, probably because the phosphino-pyrazolyl ligand has less steric hindrance than dppm. The C–C separation is 1.26(1) Å,

with Cu–C distances of 1.931(6) (η^1) and 2.143, 2.215(6) Å (η^2). Both coppers are 4-coordinate with the two Cu–Cu separations 2.843, 3.735(1) Å, suggesting some cuprophilic interaction. In the electronic spectrum, absorption bands occur at 345, 364, 373, and 396 nm ($C_2^{2-} \rightarrow Cu_4$ LMCT), while excitation at $\lambda > 350$ nm gives a blue-green emission at 408, 430, 448, 475 nm, with vibronic structure (2188, 2203 cm^{-1}).

2. Silver

Reactions of ethyne with sources of Ag(I) afford insoluble yellow Ag_2C_2, which is explosive when dry; alternative preparations are from $AgNO_3$ and $C_2(CO_2Na)_2$ or Hg_2C_2. Although the structure of this material is unknown, a series of adducts of Ag_2C_2 with AgX (X = halide, ClO_4, NO_3, SO_4, etc.) was first described over half a century ago[589] and many of their interesting structures have been revealed by recent investigations by Mak and his group. A series of double, triple, and quadruple salts has been prepared by dissolving the carbide in aqueous solutions of silver(I) salts, which also contain $AgBF_4$, and allowing to crystallize. In some cases hydrothermal techniques have been used, such as heating the combined solution in a sealed tube followed by slow cooling to allow crystallization.

The structures of several of these materials have been described, a common feature being the encapsulation of the C_2 unit within a cage of ≥ 6 silver atoms. Examples of C_2 units enclosed in trigonal pyramidal, octahedral, capped polyhedral, rhombohedral, and triangulated dodecahedra have been found, while extended structures involving edge- or face-sharing Ag_7 or Ag_8 clusters are also known. The solubility of polymeric $\{Ag_2C_2\}_n$ in aqueous solutions of silver salts presumably results from breakup of the polymer by addition of the anion, or formation of cationic $[C_2@Ag_n]^{(n-2)+}$ species by addition of extra Ag^+ ions from the highly soluble $AgBF_4$, presumably driven by argentophilic interactions. These are stabilized by appropriate anions and crystallize directly. Many of these compounds are unstable in solution and cannot be recrystallized. Table XV summarizes many of the significant features, while Figs. 15–20 contain plots of the various $C_2@Ag_n$ fragments.

Polymeric layer or three-dimensional supramolecular structures are achieved by the sharing of common vertices of the $C_2@Ag_n$ clusters or by linking through bridging anions. Limitations to the degree of cross-linking by incorporation of hydrophobic end-groups, such as those of coordinated nitriles (RCN, R = Me, Et) or perfluoroalkylcarboxylate anions ($R_FCO_2^-$, $R_F = CF_3$, C_2F_5), or the use of hydrophobic cations, such as $[Ag(15\text{-}c\text{-}5)]^+$ or $[Ag(tmc)]^{2+}$ (tmc = 1,4,8,11-tetramethyl-1,4,8,11-tetra-azaclotetradecane) has enabled other discrete species to be isolated. If quaternary

TABLE XV

Structural Characteristics of Complexes Containing $C_2@Ag_n$ Cages

No.	Formulation	Ag···Ag	Ag–C	C–C	Cage/shape	Ref.
412	$Ag_2C_2 \cdot AgNO_3$		2.163(3) (bent σ) 2.432(1) (sym π)	1.225(7)	$C_2@Ag_6$ octahedral, shares corners to give slab	590
413	$Ag_2C_2 \cdot 2AgClO_4 \cdot 2H_2O$		2.087(3), 2.108(6) (σ) 2.3448(4)–2.596(4) (unsym π)	1.212(7)	$C_2@Ag_6$ octahedral, shares corners to give layer	591
414	$Ag_2C_2 \cdot 5.5AgNO_3 \cdot 0.5H_2O$	2.9073–3.3604(5)		1.180(4)	$C_2@Ag_7$ monocapped octahedron	590
415	$Ag_2C_2 \cdot 5AgNO_3$	2.712–3.361(2)	2.051(5)–2.416(6) (mixed σ,π)	1.22(1)	$C_2@Ag_7$ monocapped trigonal prism	590
416	$2Ag_2C_2 \cdot 12AgO_2CCF_3 \cdot 5H_2O$	2.909–3.182(2) [2.739–3.185(2)]	2.15(1)–2.46(2)		$C_2@Ag_7$ square-based basket	592
417	$4Ag_2C_2 \cdot 23AgO_2CCF_3 \cdot 7EtCN \cdot 2.5H_2O$	2.756–3.368(1)		1.20	$C_2@Ag_n$ (four types) (see text)	592
418	$Ag_2C_2 \cdot AgF \cdot 4AgO_2CCF_3 \cdot MeCN$	2.878–3.003(1)	2.14(1)–2.319(9)	1.21(1)	$C_2@Ag_7$ monocapped trigonal prism	593
418	$Ag_2C_2 \cdot AgF \cdot 4AgO_2CCF_3 \cdot EtCN$				$C_2@Ag_7$ monocapped trigonal prism	593
419	$Ag_2C_2 \cdot 3AgO_2C(CF_2)_2CO_2Ag \cdot 7H_2O$	2.8848–2.9526(8)	2.111–2.521(6)	1.21(1)	$C_2@Ag_7$ crown	594
420	$Ag_2C_2 \cdot 5AgO_2CCF_3 \cdot 2(15\text{-}c\text{-}5) \cdot H_2O$ (trihydrate)	shortest 2.954(1)	2.13–2.62	1.13–1.26(1)	$C_2@Ag_7$ pentagonal bpyramid	595
421	$2Ag_2C_2 \cdot 9AgO_2CCF_3 \cdot 2(15\text{-}c\text{-}5) \cdot 2H_2O$	shortest 2.847(1)		1.13–1.26(1)	$(C_2)_2@Ag_{13}$ 2 × distorted square antiprisms share Δ face	595
422	$Ag_2C_2 \cdot 6AgNO_3$	2.9546(5)–3.0521(6)	2.089(9)–2.488(8)	1.22(2)	$C_2@Ag_8$ elongated rhombohedron	590,597,599

423	$Ag_2C_2 \cdot 6AgO_2CCF_3 \cdot 3MeCN$	2.738–3.350(1)	2.20–2.31(1) (σ) 2.35–2.67(1) (π)		fused tetrahedra $\rightarrow$ distorted triangulated dodecahedron	592
424	$Ag_2C_2 \cdot 4AgO_2C(CF_2)_3CO_2Ag \cdot 17.5H_2O$	2.909–3.338(2)	2.12–2.61(1)	1.23(2)	$C_2@Ag_8$ square antiprism	594
425	$2Ag_2C_2 \cdot 6AgO_2C(CF_2)_2CO_2Ag \cdot AgNO_3 \cdot 12H_2O$	2.901–3.354(1), 2.849–3.379(2)	2.11(1)–2.63(2), 2.16–2.49(1)	1.21(1), 1.22(1)	$C_2@Ag_7$ pentagonal bipyramid	594
426	$[Ag(tmc)(BF_4)][Ag_6(C_2)(O_2CCF_3)_5(H_2O)] \cdot H_2O$	2.818–3.366(1)	2.172(8)–2.497(9) (σ-type to all 7 Ag)	1.17(1)	$C_2@Ag_8$ edge-sharing triangulated dodecahedra (fused tetrahedra, elongated and flattened)	601
427	$[Ag(tmc)][Ag(OH_2)(tmc)]_2[Ag_{11}(C_2)(tfa)_{12}(OH_2)_4]_2$	2.8693–3.3236(7)	2.138–2.563(6)	1.212(8)	$\{C_2@Ag_8\}Ag$ Ag-spiked bicapped trig prism	602
428	$\{Ag_7(C_2)(tfa)_6[NMe_3(CH_2Ph)]\}_n$	2.8076(9)–3.2835(8)	2.100–2.449(5)	1.203(8)	$C_2@Ag_8$ square antiprisms fused into column	603
429	$Ag_2C_2 \cdot 8AgF$	2.8441(4)–3.0863(5)	2.110–2.311(4)	1.175(7)	$C_2@Ag_9$ capped sq antiprism	604
430	$Ag_2C_2 \cdot 6AgO_2CCF_3 \cdot 2(15\text{-}c\text{-}5) \cdot H_2O$ (0.5 hydrate)	shortest 2.830(1)		1.13–1.26(1)	$C_2@Ag_7$ distort pentagonal bipyramid	595
431	$2Ag_2C_2 \cdot 3AgCN \cdot 15AgO_2CCF_3 \cdot 2AgBF_4 \cdot 9H_2O$	2.879–3.316(1)	2.145(9)–2.59(1)	1.16(1)	$(C_2)_2@Ag_{13}$ $2 \times C_2@Ag_8$ share Δ face	605
432	$Ag_2C_2 \cdot 10AgO_2CC_2F_5 \cdot 9.5H_2O$	2.811–3.265(1)	2.167–2.560(9)		$(C_2)_2@Ag_{14}$ $2 \times C_2@Ag_8$ square antiprisms sharing edge	592
433	$Ag_2C_2 \cdot 6AgO_2CC_2F_5 \cdot 2EtCN$	2.798–3.311(1)			$(C_2)_2@Ag_{14}$ distorted dodecahedron by shared edges of $C_2@Ag_8$	592
434	$[NEt_4]_3[2Ag_2C_2 \cdot AgCN \cdot 11Ag(tfa) \cdot (tfa)_3 \cdot 6H_2O]$		2.106–2.592(7)	1.221(9)	$C_2@Ag_8$ bicapped trigonal prism $C_2@Ag_8$ triangulated dodecahedron	606

(*Continued*)

TABLE XV
Continued

No.	Formulation	Ag$\cdots$Ag	Ag–C	C–C	Cage/shape	Ref.
434	$Ag_2C_2 \cdot 9AgO_2CC_2F_5 \cdot$ $3MeCN \cdot H_2O$	2.845–3.332(1)	2.167–2.596(8)		$(C_2)_2@Ag_{16}$ $2 \times C_2@Ag_9$ edge-sharing square antiprism with Ag capping Δ face	592
436	$[NEt_4]_6[\{2Ag_2C_2 \cdot 8Ag(tfa) \cdot$ $(tfa)_3 \cdot 2H_2O\}_2]$		2.11–2.59(1)	1.21(2), 1.18(2)	$(C_2)_4@Ag_{24}$ by shared edges of $(C_2)@Ag_{13}$	606
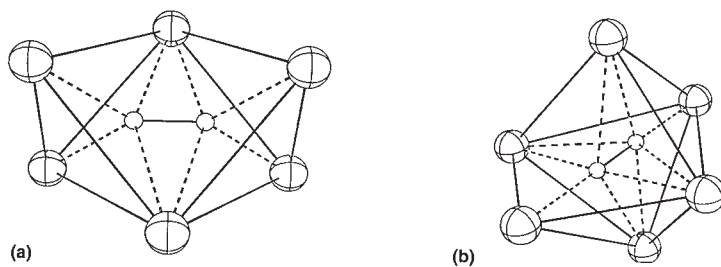
FIG. 15. $C_2@Ag_6$ clusters in (a) $Ag_2C_2 \cdot AgNO_3$ (**412**); (b) $Ag_2C_2 \cdot 2AgClO_4 \cdot 2H_2O$ (**413**).

ammonium cations are present, further examples of high nuclearity complexes are obtained.

In most cases, there is no significant lengthening of the C–C separation (range 1.13–1.26 Å), i.e., the C_2 unit retains the triple bond. The Ag$\cdots$Ag distances range from 2.71 to 3.38 Å and suggest some degree of argentophilic interaction (the Ag–Ag distance in metallic silver is 2.87 Å, the sum of van der Waals radii 3.4 Å). The Ag$\cdots$C interactions range from 2.05 to 2.67 Å and are interpreted in terms of mixed σ, π bonding, which affords more flexibility than say, the end-to-end arrangements found in $MAgC_2$[200] or the σ,π-bridging mode in $[Cu_4(\mu_4\text{-}C_2)(\mu\text{-dppm})_4]^{2+}$ (above). The usual σ and π orbital interactions are considered to operate, although filled–filled interactions may weaken the overall bonding [C–C 1.20; Ag–C (side-on) 2.45, 2.56; (end-on) 2.19 Å]. In some instances, however, unambiguous σ (end-on) Ag–C bonds are present, as are π (side-on) Ag–C interactions. It is suggested that as the size of the Ag_n cage increases, the structure of Ag_2C_2 should be approached.

$C_2@Ag_6$. Two extreme arrangements of the C_2 unit within an Ag_6 octahedron are shown. A hydrothermal technique, whereby a solution of Ag_2C_2 and $AgNO_3$ in water was heated (105 °C for 48 h, then slowly cooling to 80 °C) gave $Ag_2C_2 \cdot AgNO_3$ (**412**), in which octahedral $C_2@Ag_6$ units are linked by their apices, firstly into slabs which are further aggregated into a 3-D cationic network.[590] Within the octahedron, the C_2 unit is parallel to two longer Ag$\cdots$Ag edges, being π-bonded to equatorial Ag atoms [Ag–C 2.432(1) Å]. Other Ag atoms are attached by "bent" σ bonds [Ag–C 2.163(3) Å]. In consequence, the C–C bond is lengthened to 1.227(7) Å, while there is a shift in ν(CC) to lower energy. In $Ag_2C_2 \cdot 2AgClO_4 \cdot 2H_2O$, the C_2^{2-} dianion is enclosed in an octahedral Ag_6 cage and interacts with the Ag centres in a $\mu_6\text{-}\eta^1,\eta^1:\eta^2,\eta^2:\eta^2,\eta^2$ mode (**413**).[591] The C–C distance is 1.212(7) Å. An infinite linear chain
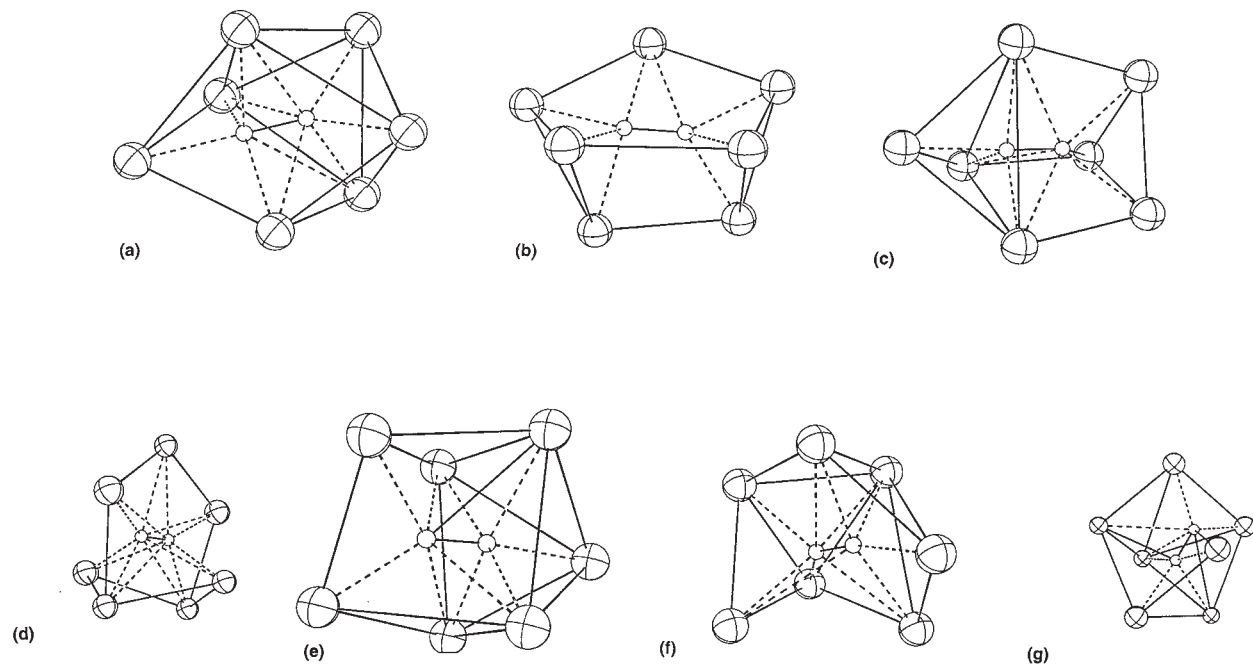
FIG. 16. $C_2@Ag_7$, clusters in (a) $Ag_2C_2 \cdot 5.5AgNO_3 \cdot 0.5H_2O$ (**414**); (b) $2Ag_2C_2 \cdot 12Ag(tfa) \cdot 5H_2O$ (**416**); (c) $Ag_2C_2 \cdot AgF \cdot 4AgOTf \cdot MeCN$ (**418**); (d) $Ag_2C_2 \cdot 3AgO_2C(CF_2)_2CO_2Ag \cdot 7H_2O$ (**419**); (e) $\{Ag_2C_2 \cdot 5Ag(tfa \cdot 2(15\text{-c-}5) \cdot H_2O\} \cdot 3H_2O$ (**420**); (f) $\{Ag_2C_2 \cdot 6Ag(tfa \cdot 2(15\text{-c-}5) \cdot H_2O)0.5H_2O$ (**421**); (g) $2\{Ag_2C_2 \cdot 6AgO_2C(CF_2)_2CO_2Ag \cdot AgNO_3 \cdot 12H_2O\}$ (**425**).
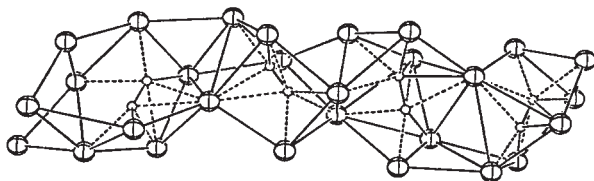
FIG. 17. Chain of $C_2@Ag_7$ clusters in $4Ag_2C_2 \cdot 23Ag(tfa) \cdot 7EtCN \cdot 2.5H_2O$ (**417**).

is formed between the C_2 unit and Ag(2) atoms, while unsymmetrical π bonds to Ag(3) serve to link adjacent chains.

$C_2@Ag_7$. Here, the C_2 ligand is enclosed in complete or incomplete capped trigonal prisms or octahedra; in some cases, the Ag$\cdots$Ag separations are > 3.0 Å. Addition of $AgNO_3$ to a slurry of Ag_2C_2 in water at 80 °C gave $Ag_2C_2 \cdot 5.5AgNO_3 \cdot 0.5H_2O$, which contains a monocapped octahedral Ag_7 cage enclosing the C_2 unit (**414**), which has the C_2 unit directed towards the capping Ag, with Ag–C and C–C separations of 2.108(3) and 1.180(4) Å, respectively.[590] The adduct $Ag_2C_2 \cdot 5AgNO_3$ was obtained from a mixture of Ag_2C_2 and AgO_2CCF_3 to which some $AgNO_3$ had been added and contains a monocapped trigonal prismatic Ag_7 cage with two long edges (**415**). Here, mixed σ, π-bonding of the C_2 unit is found [Ag–C 2.051–2.416(6) Å], the capping Ag being π-bonded; the C–C distance is 1.22(1) Å.

Several aggregates were obtained from aqueous solutions containing Ag_2C_2 with soluble $AgBF_4$ and AgO_2CR_f [$R_f = CF_3$ (tfa), C_2F_5 (pfp)].[592] In $2Ag_2C_2 \cdot 12Ag(tfa) \cdot 5H_2O$, two nearly identical $C_2@Ag_7$ baskets (**416**) are found, each having a square base. Each C is bonded to four of the Ag atoms [Ag–C 2.15(1)–2.46(2) Å]. The cages are linked by μ-tfa groups to give layers, which are further linked by tfa anions to give a 3-D network. If EtCN is present, the adduct $4Ag_2C_2 \cdot 23Ag(tfa) \cdot 7EtCN \cdot 2.5H_2O$ crystallizes. This has a 1-D structure made up of a double-walled Ag column consisting of four consecutive fused $C_2@Ag_7$ cages (**417**), two of which are monocapped trigonal prisms, one a basket with an Ag_4 base, and one a severely distorted pentagonal bipyramid. The Ag$\cdots$Ag distances range between 2.756 and 3.368(1) Å with all C–C separations ca. 1.20 Å.

Similarly, addition of Ag_2C_2 to an aqueous solution of AgOTf and $AgBF_4$ (1/1) containing a few drops of RCN (R = Me, Et) gave the triple salts, $Ag_2C_2 \cdot AgF \cdot 4AgOTf \cdot RCN$.[593] The structure contains a capped trigonal prism containing the C_2 unit (**418**) together with a lantern-shaped $Ag_6(\mu_3\text{-}F)(\mu_3\text{-}OTf)_2$ cage. The two polyhedra share Ag$\cdots$Ag edges to form a honeycomb layer containing OTf anions in the hexagonal voids. The nitrile is coordinated to the capping Ag(5) atom.
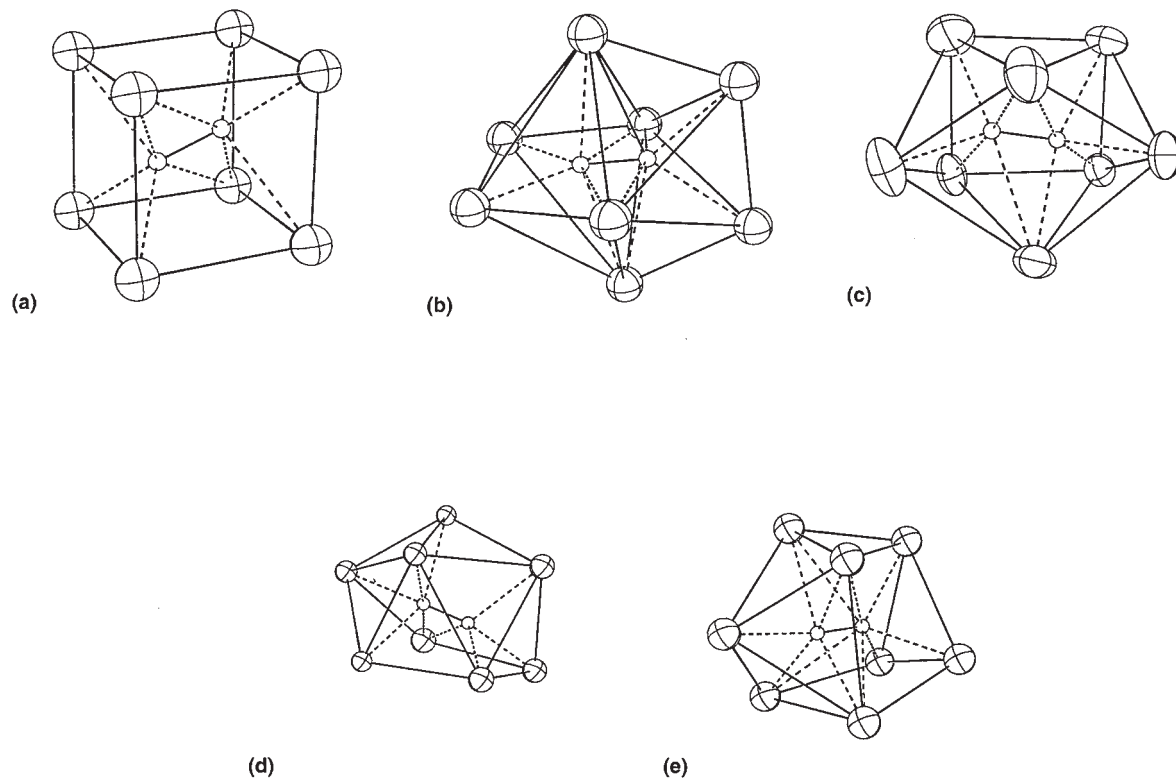
FIG. 18. $C_2@Ag_8$ clusters in (a) $Ag_2C_2 \cdot 6AgNO_3$ (**422**); (b) $Ag_2C_2 \cdot 6Ag(tfa) \cdot 3MeCN$ (**423**); (c) $Ag_2C_2 \cdot 4AgO_2C(CF_2)_3CO_2Ag \cdot 17.5H_2O$ (**424**); (d) $2Ag_2C_2 \cdot 6AgO_2 C(CF_2)_2CO_2Ag \cdot AgNO_3 \cdot 12H_2O$ (**425**); (e) $[Ag_6(C_2)(tfa)_5(OH_2)]^-$ (**426**).
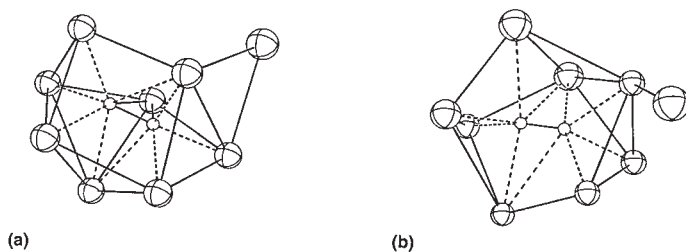
FIG. 19. $C_2@Ag_8Ag$ clusters in (a) $Ag_{11}(C_2)(tfa)_{12}(OH_2)_4]^-$ (**427**); (b) $\{[Ag_7(C_2)(tfa)_6$ $[NMe_3(CH_2Ph)]\}_n$. (**428**).
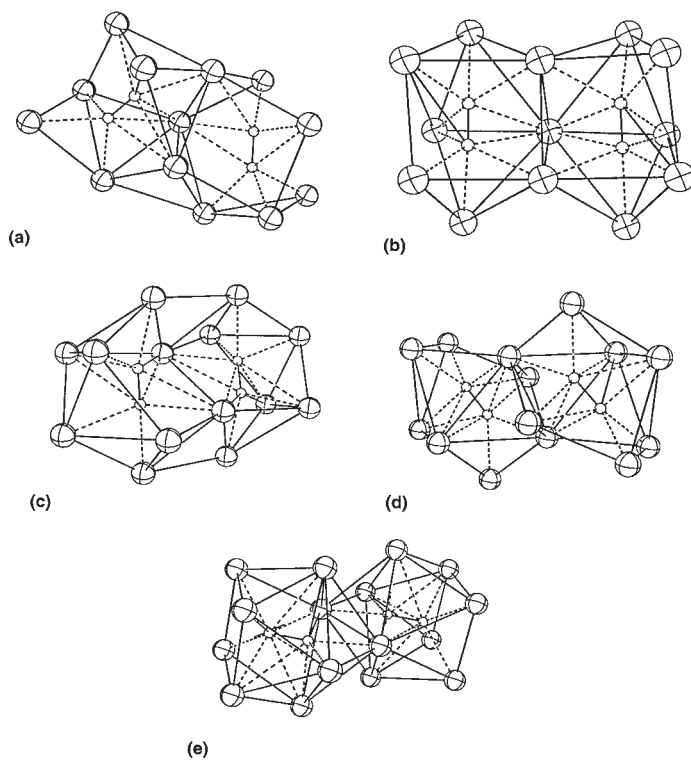
FIG. 20. $(C_2)_2@Ag_{13}$ clusters in (a) $2Ag_2C_2 \cdot 9Ag(tfa) \cdot 12(15\text{-}c\text{-}5) \cdot 2H_2O$ (**430**); (b) $2Ag_2C_2 \cdot 3AgCN \cdot 15Ag(tfa) \cdot 2AgBF_4 \cdot 9H_2O$ (**431**); $(C_2)_2@Ag_{14}$ clusters in (c) $Ag_2C_2 \cdot$ $10Ag(pfp) \cdot 9.5H_2O$ (**432**); (d) $Ag_2C_2 \cdot 6Ag(pfp) \cdot 2EtCN$ (**433**); $(C_2)_2@Ag_{16}$ cluster in (e) $Ag_2C_2 \cdot 9Ag(pfp) \cdot 3MeCN \, H_2O$ (**435**).

The $C_2@Ag_7$ unit **419** in $Ag_2C_2 \cdot 3AgO_2C(CF_2)_2CO_2Ag \cdot 7H_2O$ forms a crown-like cage, the C_2 fragment having both π-type and 3c-2e σ interactions with the Ag atoms.[594] Perfluorosuccinate dianions link the cages in a zig-zag chain.

A series of trifluoroacetate-containing clusters was obtained by dissolving Ag_2C_2 in solutions containing Ag(tfa) and 15-crown-5.[595] In $Ag_2C_2 \cdot 5Ag(tfa) \cdot 2(15-c-5) \cdot H_2O \cdot 3H_2O$, the $C_2@Ag_7$ cluster is a pentagonal bipyramid (**420**), with four equatorial edges bridged by CF_3CO_2 groups, while the two apical Ag atoms are each attached to a 15-c-5 ligand. One equatorial Ag is coordinated by monodentate CF_3CO_2 and H_2O. The C_2 unit has π interactions with three Ag atoms. A similar $C_2@Ag_7$ unit (**421**) is found in $Ag_2C_2 \cdot 6Ag(tfa) \cdot 2(15-c-5) \cdot H_2O \cdot 0.5H_2O$; here, the pentagonal bipyramid is distorted so that only two π interactions are found. All equatorial edges are bridged by CF_3CO_2, one Ag atom also carrying a H_2O ligand. Each apical Ag carries a 15-c-5 ligand. Two of these units are linked through an $Ag_2(tfa)_2$ bridge.

$C_2@Ag_8$. The first example of these cage structures was found in the compound $Ag_2C_2 \cdot 6AgNO_3$ prepared from ethyne and 30% aqueous $AgNO_3$.[596] Crystal data and a preliminary structure were reported in 1954[597] and again in 1964[598] but the structure was not fully resolved until 26 years later.[590,599,600] The C_2 unit is enclosed in a rhombohedral array of eight Ag atoms (i.e., $C_2@Ag_8$, **422**), two opposite corners of which are π bonded (side-on) to the C_2 ligand (Ag–C 2.45–2.56 Å); the other Ag atoms have a σ-type interaction with one or other carbon atom (Ag–C 2.19 Å). The C_2 unit retains its alkyne nature with C–C 1.22(2) Å.

Among the plethora of structures found for adducts containing Ag(tfa) or Ag(pfp) (see above), $Ag_2C_2 \cdot 6Ag(tfa) \cdot 3MeCN$ is obtained in the presence of MeCN and contains a distorted triangulated dodecahedral $C_2@Ag_8$ cage (**423**).[592] This is considered to be formed by fusion of elongated and flattened tetrahedra, the C_2 in the latter being π bonded. The formation of 3-centre/2-electron bonds [by overlap of Ag 5s and filled C(sp) orbitals] results in Ag–C distances of 2.20–2.31(1) Å. The adduct $Ag_2C_2 \cdot 4AgO_2C(CF_2)_3CO_2Ag \cdot 17.5H_2O$ contains the first example of square antiprismatic $C_2@Ag_8$ cages (**424**), which are linked by the hexafluoroglutarate dianions in a 2-D network.[594] In $2Ag_2C_2 \cdot 6AgO_2C(CF_2)_3CO_2Ag \cdot AgNO_3 \cdot 12H_2O$, a pentagonal bipyramidal $C_2@Ag_7$ unit similar to **420**, and a new type of $C_2@Ag_8$ cage (**425**) are both present. Both are linked by perfluorosuccinate dianions to give a 3-D network.[594]

The anion in mixed-valent $[Ag^{II}(tmc)(BF_4)][Ag_6(C_2)(tfa)_5(OH_2)].H_2O$ (tmc = 1,4,8,11-tetramethyl-1,4,8,11-tetra-azacyclotetradecane), which was obtained after adding the macrocycle to a mixture of Ag_2C_2 and $AgBF_4$

in aqueous Ag(tfa), consists of a chain of edge-sharing triangulated dodecahedral $C_2@Ag_8$ cages (**426**) (similar to **423**) [Ag–Ag 2.818–3.366(1) Å].[602] The Ag–C distances are 2.172(8)–2.497(9) Å, the C_2 group interacting with all Ag atoms. Weak axial coordination of BF_4 groups to square-planar $[Ag(tmc)]^{2+}$ cations results in formation of accompanying $[Ag^{II}(tmc)(FBF_3)]_{\infty}^+$ columns. Another example of an Ag(I)–Ag(II) complex is $[Ag^{II}(tmc)][Ag^{II}(OH_2)(tmc)]_2[Ag_{11}(C_2)(tfa)_{12}(OH_2)_4]_2$ which is formed from aqueous solutions containing Ag_2C_2 and Ag(tfa) after addition of tmc. The dimeric Ag_{11} anion contains bicapped trigonal prismatic $C_2@Ag_8$ cages with another Ag atom bridging one edge (**427**).[602] In both cases, addition of tmc has resulted in disproportionation to give cationic $Ag^{II}(tmc)$ and incorporation of the other Ag atoms within the cages.

$C_2@Ag_9$. In $Ag_2C_2 \cdot 8AgF$, the 10th Ag atom is exohedral to a $C_2@Ag_9$ cage (**428**).[603] The C_2 unit is attached to the cage in a delocalized fashion (Ag–C 2.1104–2.3114 Å), with C–C separation of 1.1757 Å. If the $[NMe_3(CH_2Ph)]^+$ cation is added to a mixture of Ag_2C_2, 4Ag(tfa), and $AgBF_4$, the polymeric complex $\{Ag_7(C_2)(tfa)_6[NMe_3(CH_2Ph)]\}_n$ is formed.[603] In addition to a $C_2@Ag_8$ cage also attached to a ninth pendant Ag atom (**429**), which form an infinite chain by edge-sharing, the structure contains the unusual feature of an exterior η^3 π-type interaction between the cation and one of the cage Ag atoms.

$(C_2)_2@Ag_{13}$. In $2Ag_2C_2 \cdot 9Ag(tfa) \cdot 2(15\text{-c-}5) \cdot 2H_2O$ trihydrate, an Ag_{13} cage formed by two distorted square antiprisms sharing a triangular face encapsulates two C_2 units (**430**).[595] The 15-c-5 ligands each bridge two Ag atoms, while the bridging tfa ligands are used to construct an infinite zig-zag chain. The C–C separations are between 1.13 and 1.26(1) Å, and short Ag$\cdots$Ag separations [2.954 (1), 2.830 (2), and 2.847(1) Å (3)] indicate argentophilic interactions.

The quadruple salt $2Ag_2C_2 \cdot 3AgCN \cdot 15Ag(tfa) \cdot 2AgBF_4 \cdot 9H_2O$ contains a $(C_2)_2@Ag_{13}$ cluster, (**431**), formed from two $C_2@Ag_8$ polyhedra, each consisting of a trigonal prism with two capped rectangular faces, sharing a triangular face.[605] The C_2 units point towards the capping atoms and the very short C–C separations [1.16(1) Å] indicate little back-bonding from the metal.

$(C_2)_2@Ag_{14}$. In $Ag_2C_2 \cdot 10Ag(pfp) \cdot 9.5H_2O$, two Ag_8 square antiprisms, each encapsulating a C_2 group, share an edge to give the centrosymmetric Ag_{14} double cage (**432**).[592] Similarly, $Ag_2C_2 \cdot 6Ag(pfp) \cdot 2EtCN$ contains a $(C_2)_2@Ag_{14}$ double cage formed by two edge-sharing distorted dodecahedral $C_2@Ag_8$ cages (**433**).

Addition of [NEt$_4$][BF$_4$] to a mixture of Ag$_2$C$_2$, AgCN, Ag(tfa), and AgBF$_4$ in water enables the complex [NEt$_4$]$_3$[(Ag$_2$C$_2$)$_2$(AgCN){Ag(tfa)}$_{11}$ (tfa)$_3$(H$_2$O)$_6$] to be isolated.[606] A double cage is built from two edge- and apex-sharing C$_2$@Ag$_8$ dodecahedra which are also attached to two external Ag atoms. The resulting {(C$_2$)$_2$@Ag$_{14}$}Ag$_2$ units (**434**) form an infinite column, in which the CN anions are also intercalated within a distorted tetrahedral Ag$_4$ moiety.

(C$_2$)$_2$@Ag$_{16}$. This double cage (**435**), formed from two edge-sharing C$_2$@Ag$_9$ square antiprisms of which the top faces are capped by the ninth Ag atom, is found in Ag$_2$C$_2$ · 9Ag(pfp) · 3MeCN · H$_2$O.[592] In each, the C$_2$ is bonded to all nine Ag atoms [Ag–C 2.167–2.596(8) Å].

(C$_2$)$_4$@Ag$_{24}$. The complex [NEt$_4$]$_6$[{(Ag$_2$C$_2$)$_2$[Ag(tfa)$_8$](tfa)$_3$(H$_2$O)$_2$}$_2$] is formed from Ag$_2$C$_2$, Ag(tfa), and AgBF$_4$ in aqueous solution, followed by addition of [NEt$_4$][BF$_4$].[606] The anion is built up from C$_2$@Ag$_n$ ($n = 7, 8$) cages, which share a triangular face to form a (C$_2$)$_2$Ag$_{13}$ double cage. Two of these share an edge to give a centrosymmetric (C$_2$)$_4$@Ag$_{24}$ cluster (**436**).

D. *Theory of C$_n$ Ligands in Metal Clusters*

While several groups have sought to rationalize the structural features of clusters containing C$_2$ units, perhaps the most comprehensive study is that by Halet and co-workers, who have considered transition metal carbonyl clusters containing interstitial Main Group atoms, including polycarbide clusters[39,607] and clusters containing peripheral C$_2$ ligands.[488,489] Simple electron counting rules (polyhedral skeletal electron pair theory) supported by extended Hückel and DF theory calculations have been used to rationalize the observed structures. In these complexes, it is considered that the C$_2^{2-}$ anion acts as an 8-e donor.

1. Peripheral Carbide Clusters

(a) M$_4$ complexes

Three common structural types (**R–T**; Chart 6) are found for the tetrametallic compounds, which are related to the 64 c.v.e. square by addition of electrons and bond cleavage (Scheme 70). In **R**, the C$_2$ unit bonds like an alkynyl group, with a fourth metal atom being attached by a σ bond to one carbon. An alternative approach is to consider it as a trigonal bipyramidal C$_2$M$_3$ cluster (52 c.v.e.) with an ML$_n$ substituent. Either way, the isolated ML$_n$ fragment is isolobal with an alkyl group. The HOMO and LUMO are mainly metallic in nature (only 3–6% carbon character), although the (LUMO + 1), which is an M–C antibonding orbital, is 17%

(R)

(S)

(T)

(U)

(V)

(W)

CHART 6

2e

2e

2e
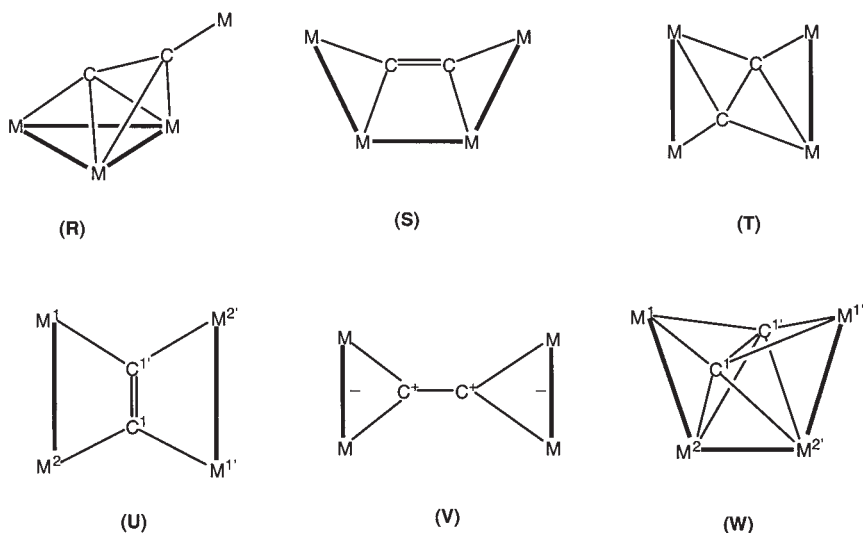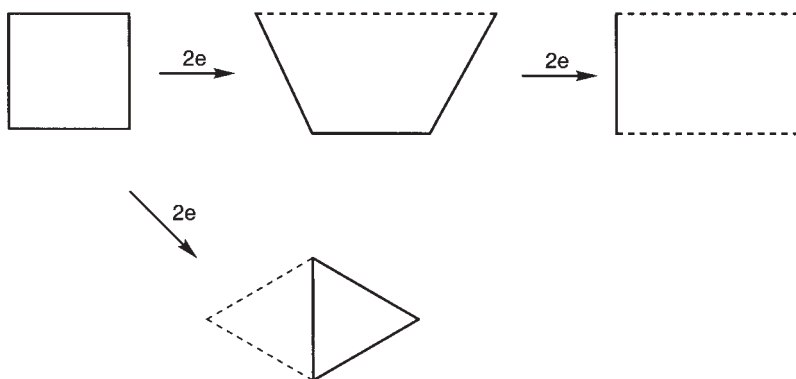
SCHEME 70

on the σ-bonded C atom and allows nucleophilic attack. The C_2 unit is immune to electrophilic attack. Heterometallic complexes have only a small energy preference for the symmetrical isomers, with the more electro-negative metal occupying the M(1) site (as found for Re_2Co_2 and Fe_2Co_2 clusters, but not for Fe_2Ru_2 complexes).

Structure **S** has the C_2 unit σ-bonded via each carbon to two metal atoms in a trapezoidal arrangement, which is electron-precise with 66 c.v.e. if C_2^{2-} is a 6-e donor. The short C–C distance (compared with ethene) results from reduced electron donation from C_2 to the cluster and reduced donation

from the metals to the C_2 π^* MOs. With two σ, one π, and one π^* orbitals, the description of **S** as a "permetallated ethene" is appropriate, although relatively low degrees of donation from C_2 to the metal framework and back-donation to the C_2 moiety result in short C–C separations. The HOMO has strong metallic character, whereas the LUMO has 18% carbon character, so that both nucleophilic and electrophilic reactions at carbon would be expected if these are orbital controlled. Conversion of **R** to **S** requires addition of a 2-e donor ligand and is initially a dissociative process, with break-up of the M_3 cluster (Scheme 71).

In **T**, asymmetric bonding from C_2 to two M_2 moieties (each attached via a σ, π system) results in an electron precise 68 c.v.e. count if C_2^{2-} is an 8-e donor. Here, the M–M bonds have a bond order > 1, since one of the metallic FMOs does not interact with the C_2 unit in the planar complex. Most of the interaction between the metals and the C_2 unit occurs via σ-type orbitals, with weak back-donation to π-type acceptor MOs. Better overlap would occur if the M–M bonds were orthogonal; the Ru_4 complex **311** has a twist of $42.5°$ (limited by steric interactions between ligands), leading to a significant increase in the calculated bonding energy. Whereas the planar system is predicted to be unstable, the twisted molecule is more robust, as found experimentally in reactions with H_2 or CO. However, the C_2 unit is electron deficient and therefore attack by nucleophilic reagents is expected and found in the case of the iron
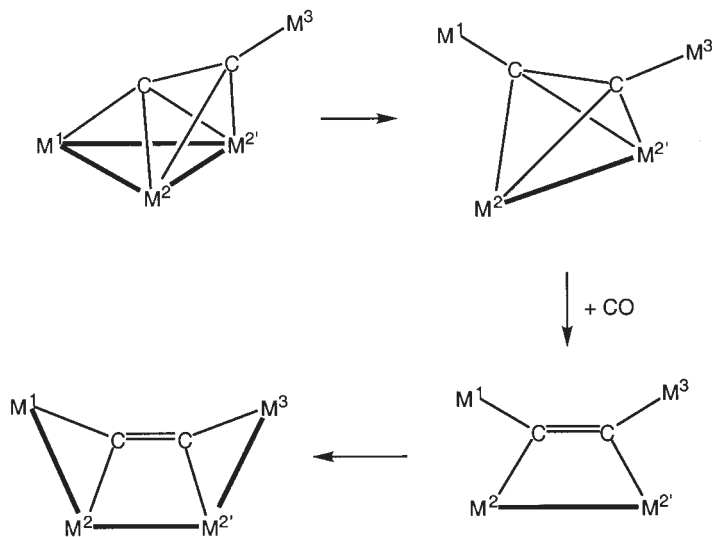
SCHEME 71

analogue. Both fluxional behavior and isomerization can be expected for these structures, via bond breaking/making reactions illustrated in Scheme 72. Calculations indicate that some suggested intermediates are relatively unstable; interconversion between C_2 units acting as 6-e or 8-e donors can also be envisaged.

Other geometries, such as **U**, **V**, and **W**, can be proposed, although **V**, as a double zwitterion, is considerably less stable than **U**. For **W**, geometric constraints probably preclude this arrangement, with normal M–C and M–M bond lengths leading to bond formation along the non-bonding M$\cdots$M vector and the C–C bond penetrating the resulting M square. The first example of this type of complex was obtained by thermolysis (PhMe, 140 °C, 2 h) of $Fe_2(\mu\text{-PPh}_2)(\mu\text{-}\eta^1 : \eta^2\text{-C}_2Ph)(CO)_6$ to give $Fe_4(\mu_4\text{-}\eta^1 : \eta^1 : \eta^2 : \eta^2\text{-PhC}_4Ph)(\mu\text{-PPh}_2)_2(CO)_8$ (**437**) in which the terminal alkynyl carbons are separated by ca. 1.6 Å.[608,609]

(437)
(Fe) = Fe(CO)$_2$
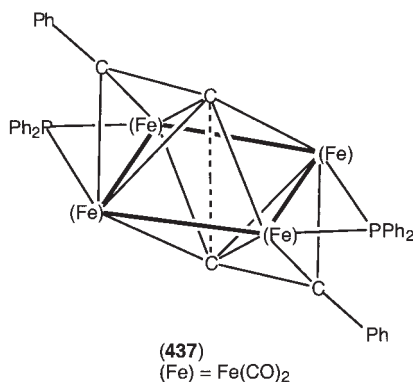
Two products, **315** and **316**, were obtained by carbonylation of **325**.[495] Addition of two CO ligands gives the first, in which two Ru–Ru bonds have been cleaved, resulting in an Ru_2 fragment linked to the Ru_3 cluster by the C_2 unit. Long Ru–Ru separations in the 50-e Ru_3 fragment (av. 3.07 Å) are consistent with accommodation of the extra two electrons in Ru–Ru anti-bonding orbitals, as found on other occasions for complexes with μ-PR$_2$ or μ-SR groups. Conversely, the Ru_2 unit is electron-poor and has an Ru=Ru double bond [2.694(6) Å] with the C_2 unit (1.20 Å) only weakly bonded to the Ru_3 cluster. The 68-e Ru_4 complex **315** is closely related to **308** (66-e) and **311** (68-e), with the C_2 unit acting as a formal 4-e donor. Calculations show one strong Ru–Ru (2.796 Å) and C–C bonds (1.24 Å) are consistent with a degree of multiple bonding, as shown in tautomers **315** and **315a**; the second Ru$\cdots$Ru separation (3.571 Å) is only weakly interacting at best.
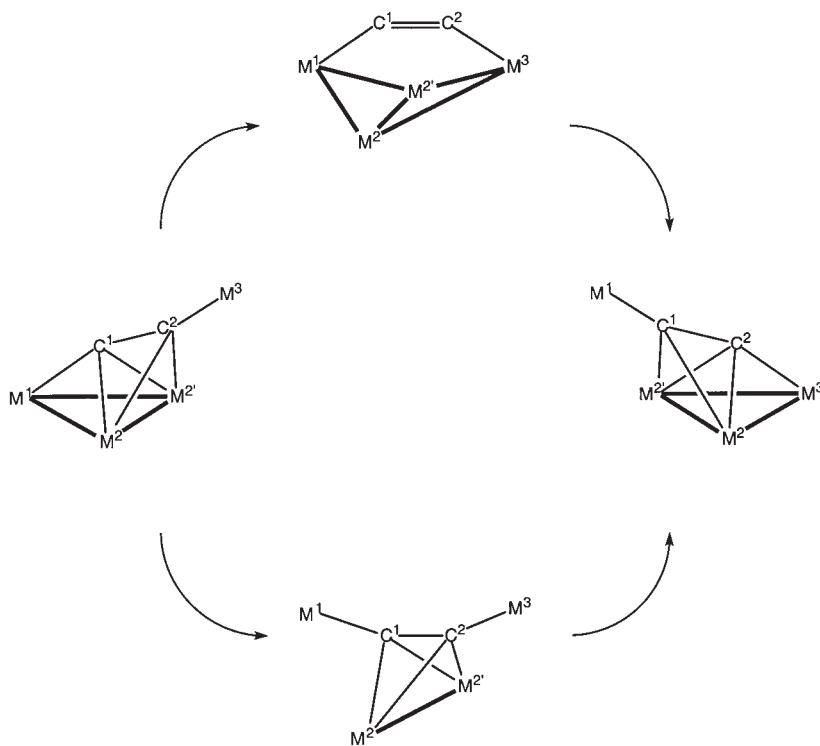
SCHEME 72

(b) Complexes with > 4 metal atoms

Several larger clusters containing C_2 units have also been studied.[489] In a series of C_2M_5 and C_2M_6 clusters, the metal cores are related to square pyramidal and trigonal prismatic geometries, respectively, by addition of electrons and consequent M–M bond cleavage (Schemes 73 and 74). Complexes with these structures have been described in Section IX.A. The incorporation of the larger C_2 units (compared to single atoms) results in the formation of open clusters. However, the different bonding modes of the C_2 unit (C_2^{2-} as a 6- or 8-e donor) can be accounted for by using extended Hückel calculations.

Generally, the C_2 unit has a synergic bonding interaction with the cluster, with donation from filled σ and π orbitals to the cluster and acceptance of electron density from the metal framework into the π^* orbitals. In all cases, the C_2 ligand is slightly negatively charged and charge-controlled reactions with electrophiles are expected. However, as the ligand is sterically well protected, reactions may occur at the metal

(78 c.v.e.)

$Ru_5(C_2)(PPh_2)_2(CO)_{11}(py)_2$ **(338)**

+ 4 e

(82 c.v.e.)

$Fe_2Ru_5(C_2)_2(CO)_{17}Cp_2$ **(320)**

+ 4 e

+ 8 e

(74 c.v.e.)

+ 4e

+ 8e

+ 6e

(78 c.v.e.)

$FeRu_6(C_2)(C_2H)(CO)_{16}Cp$ **(321)**

(82 c.v.e.)

$Ru_5(C_2)(SMe)_2(PPh_2)_2(CO)_{12}$ **(335)**
$Ru_5(C_2)(SMe)_4(PPh_2)_2(CO)_{10}$ **(333)**

+ 2e

+ 2e

(80 c.v.e.)

$Ru_5(C_2)(SMe)_2(PPh_2)_2(CO)_{11}$ **(325)**
$Ru_5(C_2)(SMe)_2(PPh_2)_2(CO)_{11}(CNBu^t)$ **(352)**

SCHEME 73

(96 c.v.e.)

NiRu$_5$(C$_2$)(SMe)$_2$(PPh$_2$)$_2$(CO)$_9$Cp$_2$ (**345**)
Ni$_2$Ru$_4$(C$_2$)(SMe)$_2$(PPh$_2$)$_2$(CO)$_8$Cp$_2$ (**346**)

+ 4 e   + 2 e

(92 c.v.e.)   (94 c.v.e.)

Fe$_2$Ru$_6$(C$_2$)$_2$(CO)$_{17}$Cp$_2$ (**318**)
Co$_6$(C$_2$)(S)(CO)$_{14}$ (**340**)   FeRu$_5$(C$_2$)(SMe)$_2$(PPh$_2$)$_2$(CO)$_{14}$ (**341**)

+ 2 e   + 4 e

+ 2 e

(90 c.v.e.)

+ 4 e   + 6 e

+ 2e

(94 c.v.e.)   (96 c.v.e.)

[Co$_3$Fe$_3$(C$_2$)(CO)$_{18}$]$^-$ (**275**)   {Co$_3$(CO)$_9$}$_2$(C$_2$) (**271**)

SCHEME 74

framework rather than at the C_2 centre. In Ru_5 clusters (Section IX.A), the C_2 is considered as part of a metallated vinylidene spanning an M_3 triangle. Efficient delocalization of electron density results in each carbon carrying a similar negative charge. In **325**, however, asymmetric attachment of the C_2 leads to C(2) being more electron-rich than C(1) and its reactions support the expectation of electrophilic attack at C(2). In **352**, reduced electron transfer in both directions results in a shorter C–C bond, with a μ_4-C_2 bonding mode and relatively long Ru–Ru separations. In **321**, the two additional electrons are in an Ru–Ru anti-bonding orbital; again, only four Ru atoms are involved in bonding to the C_2 unit. For **335**, weaker Ru–C and stronger C–C bonding are found, as a result of the longer π interactions, and result in a greater stability for this open-ring compound. In **320**, the C_2 unit is dipolar, with C atoms attached to two metal atoms being more electron-poor than those attached to four metal atoms. This may derive from the electron-withdrawing properties of the $Fe(CO)_2Cp$ group.

In C_2M_6 clusters, the C_2 unit is more strongly bound to the M_6 core than those in C_2M_5 clusters (above). The C–C separations are about 0.05 Å longer, but net charges are similar. Interestingly, with **271**, a 96 c.v.e. count results in full occupation of the HOMOs. With 94 c.v.e., there is a Jahn-Teller distortion, the M_3 triangles tilting to allow a long M–M bond to form between them, as is found in **275**. For **318** and **340**, similarly, two M–M bonds between the triangles result in M–M non-bonding orbitals becoming anti-bonding. In all of these, the C_2 unit is σ-bonded to the apical atoms and σ,π-bonded to the square. The calculations agree with the formulation as a permetallated ethane. For **341**, hypervalent carbons have several $(\sigma + \pi)$ interactions with the metal atoms. In **343**, further interaction with the apical metal atoms results in diminution of the electron density on carbon and hence a longer C–C distance. By normal c.v.e. counting rules this complex has four electrons too many: relatively long M–M distances suggest that these are accommodated into M–M anti-bonding orbitals. The final C–C separation depends on the geometry of the metal cage.

The structural determination of the Ni_2Ru_4 cluster **346** is consistent with the presence of two isomers in which the C_2 unit is either colinear with the two Ni atoms, or perpendicular to the Ni–Ni vector.[532] In the former, the 8-e $[C_2]^{2-}$ unit interacts strongly with six of the 12 FMOs, corresponding to six Ni–C σ bonds (as a permetallated ethane) and π-bonding to Ru. The second isomer is more highly delocalized, calculations showing π bonding to Ni and numerous C–Ru interactions of the $(\sigma + \pi)$ type. However, while there is a higher amount of electron transfer to the metal in **346a**, the net C–C overlap populations and forward and back-donation are similar in both, which are considered to be isoenergetic.

Although no examples of such compounds have been reported to date, calculations on clusters $Au_n(C_2)(PH_3)_n$ ($n = 8, 10, 12$) have found two c.v.e. counts are possible.[610] Stable clusters with $(12n + 10)$ c.v.e. will have short C–C distances, preserving some C–C multiple bonding. For $n = 10$, with a bicapped antiprismatic geometry, transfer of 2e from the C_2 π orbital to the Au_{10} core, and acceptance of 2.54 e into the π^* orbital occurs. On the other hand, in clusters with $(12n + 14)$ c.v.e., the C–C separation depends strongly on cluster geometry, with the C–C bond being preserved if Au–C bonds of ca. 2.0 Å can be formed. Clusters with $(12n + 16)$ c.v.e. are predicted to be unstable, forming monocarbido clusters, e.g., $[\{Au_5(PH_3)\}_5C]^+$ rather than $[\{Au_{10}(PH_3)_{10}\}(C_2)]^{2+}$, the choice being related to the presence of a frontier MO of symmetry b_2.

2. Cluster-Capped C_n Fragments

Extended Hückel MO studies of the CCo_3 skeleton have been reported[611,612] and used to interpret the UV-PE spectra of Co_3 $(\mu_3\text{-}CR)(CO)_9$.[613] If the C_2 ligand is considered to be the 8-e donor $[C_2]^{2-}$ dianion, the double cluster $\{(CO)_9Co_3\}_2(\mu_3:\mu_3\text{-}C_2)$ (**271**) has 96 c.v.e.[614] Combinations of orbitals from the Co_3 faces give two sets of six orbitals, the filled lower set being Co–Co bonding, while the partly filled second set can accept electron density from filled σ_{sp}^*, π, and σ_p orbitals of the C_2 ligand. The HOMO is delocalized over the Co–Co and Co–C bonds, with a lower energy MO involving the Co–Co and Co–CO π bonds. The apical carbon is electron-rich (-0.36 e), but the π system can act as an acceptor or donor. The LUMO is Co–Co anti-bonding and is 1.05 eV above the HOMO. Metal–C_2 back-bonding into empty π^* orbitals results in lengthening of the C–C bond to the observed 1.37(1) Å. Compared with encapsulated C_2 groups, donation from σ_p and back-bonding to the π^* orbitals is more favorable.[607]

The electronic structures of bis(cluster) fragments bridged by C_n ligands have been explored. Delocalization of HOMOs in tricobalt-carbon clusters involves contributions from metal, carbyne, and ligand orbitals. Initially, it was suggested that the a_1 orbitals of the $Co_3(\mu_3\text{-}C)$ units may interact with p_π-type C orbitals to give a filled molecular orbital encompassing the $Co_3C(C\equiv C)_nCCo_3$ unit.[439] For the cluster $\{(CO)_9Co_3\}_2(\mu_3:\mu_3\text{-}CC\equiv CC)$ (**286**) and its phosphine-substituted derivatives the HOMO is constructed from metal fragment molecular orbitals directed above the M_3 plane and the π-type $(2e_u)$ orbital set which is predominantly localized on the terminal carbon centres. Only six of the 16 MOs of a linear C_4 unit are able to interact with the Co_3 cluster and these are largely localized on the terminal carbon atoms. The six M–C bonding orbitals are well separated

from the six anti-bonding combinations. Replacement of one CO by PH_3 on each cluster fragment has little effect on the interactions, as shown by donation of 0.72 and 0.82 e, respectively, by the $Co_3(CO)_9$ and $Co_3(CO)_8(PH_3)$ fragments. The orbitals associated with the $M_3(\mu_3\text{-}C)$ and $C{\equiv}C$ moieties are strongly localized on these fragments and there is little evidence from the computational work for direct electronic interactions between the cluster cores via the carbon bridge. The degree of electronic communication between the clusters via the C_4 chain is low, since this would involve π^* FMOs of the C_4 chain being involved in bonding to the clusters. Formally, these complexes are best viewed as permetallated 2-butynes.

The observed electrochemical behavior (two reversible 1-e reductions)[439,481] may be associated with changes in geometry of the M_3 clusters and/or the C_4 chain. In contrast with the mononuclear systems discussed above ([Section IV.D](#)), in which the HOMOs are high energy and M–C anti-bonding, the HOMOs in the cluster complexes are low energy and strongly M–C bonding, while the LUMOs are M–C_a antibonding. Thus oxidation would result in M–C bond-breaking. Electrochemical studies have shown the symmetrical Co_6 species undergoes two 1-e reduction processes indicative of moderate electronic coupling between the $CCo_3(CO)_9$ moieties. It is possible that small changes in geometry involving the metal triangles and/or the C_4 bridge follow the intial reduction and result in some through-bond interactions not observed in the neutral complex,[419] or that the electronic interactions occur following a degree of orbital remixing in the radical anion as there is negligible orbital overlap between the cluster cores and the $C{\equiv}C$ bridge in the neutral species. However, for both **271** and **286**, the separations of the half-wave reduction potentials are relatively constant in solvents of markedly different polarity. This suggests that the electronic interaction occurs mainly through the carbon bridge as Coulombic (i.e., through-space) interactions should be highly dependent on the dielectric properties of the solvent.[481] There is a large HOMO–LUMO gap [1.25 eV (by DFT), 2.26 eV (by EH)] for **286** and the major bonding interaction between the Co_3 clusters and the C_4 chain occurs between the upper FMOs of each fragment.

Theoretical studies of $\{Cp(CO)_8Co_2M\}_2(\mu_3:\mu_3\text{-}CC{\equiv}CC)$ (**288**; M = Mo, W) have been carried out using extended Hückel and density functional MO calculations.[419] Replacement of Co by Mo in Co_3C clusters results in the FMOs being more heavily weighted towards the Mo atom. Some increased electron donation to the C_4 chain from Mo is found in the complex with *proximal* Cp groups, compared to the isomer with *distal* Cp groups. These heterometallic clusters differ in having significant electron donation from the Group 6 metal to C_α (the amount varies with

geometries of the two Cp groups), leading to the C_4 ligand being more negatively charged. Nevertheless, the C–C bonding is hardly affected and the electron distribution is similar to that calculated for a $(C_4)^{6-}$ ligand, because the C_4 FMOs are C–C non-bonding. Substitution of a $Co(CO)_3$ fragment by an isoelectronic $M(CO)_2Cp$ (M = Mo, W) group results in greater localization of the M_3C electron density in the FMO set at the heteroatom, but does not appreciably alter the interactions between the cluster core and the central C≡C moiety. The clusters remain electronically isolated from each other, the net bonding interactions between the clusters and the chain being reduced in the heterometallic complexes (11.7 eV vs. 12.88 eV). The computations indicate that the *proximal–proximal* arrangements of the two Cp groups are more stable, and the observed *proximal–distal* arrangement in the solid state is likely to be due to crystal packing forces.

3. Interstitial Carbido Clusters

The relationships between the various structures of the ruthenium, cobalt, and rhodium dicarbido clusters have been discussed in terms of their electron counts and the accommodation of some electrons in M–M anti-bonding orbitals. Such treatments have rationalized the paramagnetism of some clusters via partial occupation of such orbitals leading to swelling of the intra-cluster cavity to a point where the C_2 fragment can be accommodated.

For ruthenium derivatives, the carbide atoms are found at the centres of octahedral clusters, while in the Co, Rh, or Ni clusters, individual carbon atoms are sited in cavities derived from trigonal prismatic, capped trigonal prismatic, or square antiprismatic polyhedra sharing a square face. The separation of the carbon atoms within the cluster is dependent upon the geometry of the metal cage and effects of surrounding ligands. Consideration of the various geometries of the metal cage (Table XIV) shows that the favored geometry is that formed by two trigonal prisms, or a trigonal prism and a square antiprism, sharing a square face. The separation of the centroids of the cavities approximates to the length of a C–C single bond. The C–C bond order is calculated at between 1.0 and 1.5, as deduced from observed C–C bond lengths.

The cluster valence electron (c.v.e.) count usually corresponds to $12n + 22$ electrons. Bonding of the C_2 unit involves stabilization of σ, σ*, and π orbitals by interaction with radial metal MOs of the same symmetry, together with overlap of π* orbitals with filled metal MOs, i.e., a similar synergic interaction to the familiar bonding mode found in alkyne-metal complexes. For the model $[Co_8(C_2)(\mu\text{-L})(L)_8]^{4-}$ based on two trigonal

prisms sharing a square face, the HOMO/LUMO region is predominantly composed of metal orbitals, so that changes in c.v.e. count do not affect the C–C bond. The C–C separations in $[Co_3Ni_7(C_2)(CO)_{15}]^{3-}$ (138 c.v.e.) and $[Ni_{10}(C_2)(CO)_{16}]^{2-}$ (142 c.v.e.) are 1.430 and 1.405 Å, respectively. The structures of these clusters and the $Ru_{10}C_2$ complex are closely related, being derived from a bi-octahedron by successive cleavage of M–M bonds. The electron pair from the C_2 in Co_3Ni_7 and Ni_{10} clusters is used to stabilize the bis-octahedral Ru_{10} system, each C atom being enclosed in an octahedral cavity.[553]

Alternatively, a more spherical cluster, such as a bicapped square antiprism would incorporate a C_2 moiety with a C–C separation of 1.47 Å and the M–M and M–C separations between 2.54 and 2.80, and ca. 1.8–2.2 Å, respectively. The C_2 unit is not stabilized in a square antiprismatic cavity or in other frameworks, because the inter-centroid distances are > 2.0 Å, leading to C–C bond cleavage and formation of dicarbido complexes. The strength of the metal–carbide bonding is increased at the expense of the C–C bond. However, the cavity in $[Ni_{16}(C_2)_2(CO)_{23}]^{4-}$, is large enough to accommodate two C_2 moieties.

The strong tendency for cobalt to form paramagnetic clusters has been related to the accommodation of the unpaired electron in a low-lying cluster anti-bonding orbital derived mainly from the Co d_{z^2} orbitals , thereby enlarging the cluster to dimensions suitable for incorporation of the carbon atoms.[558,566]

The main conclusions are, that lengthening of the C–C bond is a soft process and that the symmetry-allowed C–C bond breaking/making process is influenced by the shape of the cavity. For instance, the two compounds $Rh_{12}(C_2)(CO)_{25}$ and $[Rh_{12}(C)_2(CO)_{24}]^{2-}$ are isoelectronic but have different polyhedra which allow formation of the C–C bond in the former but not in the latter. Formation of C_2 hydrocarbons from clusters containing isolated C atoms is consistent with a facile interconversion of the two extremes.

A theoretical study of $[Ni_{32}(C)_6(CO)_{36}]^{n-}$ (**400**) using combined linear combination of Gaussian orbitals (LCGTO)–local density functional (LDF) methods has been reported.[615] In the Ni_{32} core, the metal–metal bond strength derives from the d band, which are reorganized when the C atoms interact with the 4s orbitals. Addition of CO ligands results in the four unpaired electrons on the core being quenched by the C atoms, while the magnetization of the outer layer is quenched by the CO ligands. Addition of CO results in a large electronic rearrangement and increases the d character of the Ni atoms so that the cluster resembles a metal. However, while three levels near the Fermi level are almost degenerate, they are separated by 0.54 eV from the LUMO, i.e., the compound is an insulator.

X

ABBREVIATIONS

acac	acetylacetonato
ap	2-anilinopyridinate
bdpp	1,4-bis(diphenylphosphino)buta-1,3-diyne
bp	2,2′-biphenylyl
bpy	2,2′-bipyridyl
cod	1,5-cyclooctadiene
Cp	η-C_5H_5
Cp*	η-C_5Me_5
Cp^R	η-C_5H_4R
CV	cyclic voltammogram
dbu	diazabicyclo[5.4.0]undecene
dcype	1,2-bis(dicyclohexylphosphino)ethane
dippe	1,2-bis(di-i-propylphosphino)ethane
dmpe	1,2-bis(dimethylphosphino)ethane
dpf	1,3-diphenylformamidinate
dppa	1,2-bis(diphenylphosphino)ethyne
dppe	1,2-bis(diphenylphosphino)ethane
dppm	bis(diphenylphosphino)methane
dppp	1,3-bis(diphenylphosphino)propane
Fp	$Fe(CO)_2Cp$
Fp*	$Fe(CO)_2Cp*$
LDA	$LiNPr^i_2$
Me-im	*N*-methylimidazole
mes	mesityl
MLCT	metal-to-ligand charge transfer
nap	1-naphthyl
nbd	norbornadiene, bicyclo[2.1.0]hepta-2,5-diene
oepg	*meso*-octaethylporphyrinogen
ompg	*meso*-octamethylporphyrinogen
OTf	triflate
pc	phthalocyanine dianion
pfp	perfluoropropionate
phen	1,10-phenanthroline
porph	porphyrin dianion
ppn	bis(triphenylphosphine)iminium cation
RE	rare earth metal
r.t.	room temperature
silox	$Si(OBu^t)_3$
tbaf	tetrabutylammonium fluoride
tcne	tetracyanoethene
thf	tetrahydrofuran
tmc	1,4,8,11-tetramethyl-1,4,8,11-tetra-azacyclotetradecane
tmeda	1,1,2,2-tetramethyldiaminoethane, *N*,*N*,*N*′,*N*′-tetramethylethylenediamine
tol	4-tolyl
Tp	hydrotris(pyrazolyl)borate, $HB(pz)_3$
Tp*	hydrotris(3,5-dimethylpyrazolyl)borate, $HB(dmpz)_3$

tpp	tetraphenylporphyrin dianion
tpy	$2:2',6':6''$-terpyridyl
triphos	$MeC(CH_2PPh_2)_3$
xy	xylyl, $2,6\text{-}Me_2C_6H_3$

<div align="center">REFERENCES</div>

(1) Diederich, F.; Rubin, Y. *Angew. Chem.* **1992**, *104*, 1123; *Angew. Chem., Int. Ed. Engl.* **1992**, *31*, 1101.

(2) Kroto, H. W.; Allaf, A. W.; Balm, S. P. *Chem. Rev.* **1991**, *91*, 1213.

(3) Dresselhaus, M. S.; Dressselhaus, G.; Eklund, P. C. *Science of Fullerenes and Carbon Nanotubes*, Academic Press, San Diego, 1996.

(4) Kadish K. M.; Ruoff R. S., (Eds.), *Fullerenes: Chemistry, Physics and Technology*, Wiley-Interscience, Chichester, 2000.

(5) Prinzbach, H.; Weller, A.; Landenberger, P.; Wahl, F.; Wörth, J.; Scott, L. T.; Gelmont, M.; Olevano, D.; von Issendorf, B. *Nature* **2000**, *407*, 60.

(6) Douglas, A. E. *Astrophys. J.* **1951**, *114*, 466.

(7) Bettens, R. P. A.; Herbst, E. *Astrophys. J.* **1996**, *468*, 686; **1997**, *478*, 585.

(8) Hinkle, K. H.; Keady, J. J.; Bernath, P. F. *Science* **1988**, *241*, 1319; **1989**, *244*, 562.

(9) Blanksby, S. J.; McAnoy, A. M.; Dua, S.; Bowie, J. H. *Mon. Not. R. Astron. Soc.* **2001**, *328*, 89.

(10) Weltner, W. Jr.; Van Zee, R. J. *Chem. Rev.* **1989**, *89*, 1713.

(11) van Orden, A.; Zare, R.; Saykally, J. *Chem. Rev.* **1998**, *98*, 2313.

(12) Anderson, H. L.; Faust, R.; Rubin, Y.; Diederich, F. *Angew. Chem.* **1994**, *106*, 1427; *Angew. Chem., Int. Ed. Engl.* **1994**, *33*, 1366.

(13) Melnichenko, V. M.; Sladkov, A. M.; Nikulin, Yu. N. *Russ. Chem. Rev.* **1982**, *51*, 421.

(14) Smith, P. P. K.; Buseck, P. R. *Science* **1982**, *216*, 984.

(15) Lagow, R. J.; Kampa, J. J.; Wei, H.-C.; Battle, S. L.; Genge, J. W.; Laude, D. A.; Harper, C. J.; Bau, R.; Stevens, R. C.; Haw, J. F.; Munsen, E. *Science* **1995**, *267*, 362.

(16) Bohlmann, F. *Angew. Chem.* **1953**, *65*, 385.

(17) Sladkov, A. M.; Kudryatsev, Yu. P. *Russ. Chem. Rev.* **1963**, *32*, 229.

(18) Jones, E. R. H.; Lee, H. H.; Whiting, M. C. *J. Chem. Soc.* **1960**, 3483.

(19) Johnson, T. R.; Walton, D. R. M. *Tetrahedron* **1972**, *28*, 5221.

(20) Eastmond, R.; Johnson, T. R.; Walton, D. R. M. *Tetrahedron* **1972**, *28*, 4601.

(21) Schermann, G.; Grösser, T.; Hampel, F.; Hirsch, A. *Chem. Eur. J.* **1997**, *3*, 1105.

(22) Balaban, A. T.; Rentia, C. C.; Ciupitu, E. *Rev. Roum. Chim.* **1968**, *13*, 231.

(23) Hoffmann, R.; Hughbanks, T.; Kertesz, M.; Bird, P. H. *J. Am. Chem. Soc.* **1983**, *105*, 4831.

(24) Balaban, A. T., (C. Párkányi, Ed.) *Theoretical Organic Chemistry*, Elsevier, Amsterdam, 1998. p. 381.

(25) Diederich, F. *Nature* **1994**, *369*, 199.

(26) Diederich, F.; Gobbi, L. *Topics Curr. Chem.* **1999**, *201*, 43.

(27) Bunz, U. H. F.; Rubin, Y.; Tobe, Y. *Chem. Soc. Rev.* **1999**, *28*, 107.

(28) Bosshard, C.; Spreiter, R.; Gunter, P.; Tykwinski, R. R.; Schreiber, M.; Diederich, F. *Adv. Mater.* **1996**, *8*, 231.

(29) Tykwinski, R. R.; Schreiber, M.; Gramlich, V.; Seiler, P.; Diederich, F. *Adv. Mater.* **1996**, *8*, 226.

(30) Martin, R. E.; Diederich, F. *Angew. Chem.* **1999**, *111*, 1440; *Angew. Chem. Int. Ed.* **1999**, *38*, 1351.

(31) Wan, W. B.; Brand, S. C.; Pak, J. J.; Haley, M. M. *Chem. Eur. J.* **2000**, *6*, 2044.

(32) Diederich, F., (F. Diederich, P. J. Stang, (Eds.)) *Modern Acetylene Chemistry*, VCH, Weinheim, 1995. p. 443.

(33) Bunz, U. H. F. *Topics Curr. Chem.* **1999**, *201*, 131.

(34) Beck, W.; Niemer, B.; Wieser, M. *Angew. Chem.* **1993**, *105*, 969; *Angew. Chem., Int. Ed. Engl.* **1993**, *32*, 923 (a more general account of hydrocarbon-bridged metal complexes without metal-metal bonds).

(35) Akita, M.; Moro-oka, Y. *Bull. Chem. Soc. Jpn* **1995**, *68*, 420 (mainly the authors' work on metal complexes containing C_n ligands).

(36) Low, P. J.; Bruce, M. I. *Adv. Organomet. Chem.* **2001**, *48*, 71.

(37) Tachikawa, M.; Muetterties, E. L. *Prog. Inorg. Chem.* **1981**, *28*, 203.

(38) Bradley, J. S. *Adv. Organomet. Chem.* **1983**, *22*, 1.

(39) Halet, J.-F., (M. Gielen, Ed.) *Topics in Physical Organometallic Chemistry*, Vol. 4, Freund, Tel Aviv, 1992. p. 221.

(40) Dyson, P. J. *Adv. Organomet. Chem.* **1998**, *43*, 43.

(41) Bowser, J. R. *Adv. Organomet. Chem.* **1994**, *36*, 57.

(42) Stephens, A. H. H.; Green, M. L. H. *Adv. Inorg. Chem.* **1997**, *44*, 1.

(43) Balch, A. L.; Olmstead, M. M. *Chem. Rev.* **1998**, *98*, 2123.

(44) Sokolov, V. I. *Pure Appl. Chem.* **1998**, *70*, 789.

(45) Balch, A. L.; Giawalla, A. S.; Lee, J. W.; Noll, B. C.; Olmstead, M. M. *J. Am. Chem. Soc.* **1994**, *116*, 2227.

(46) Fagan, P. J.; Calabrese, J. C.; Malone, B. *J. Am. Chem. Soc.* **1991**, *113*, 9408.

(47) Balch, A. L.; Hao, L.; Olmstead, M. M. *Angew. Chem.* **1996**, *108*, 211; *Angew. Chem., Int. Ed. Engl.* **1996**, *35*, 188.

(48) Lahamer, A.; Ying, Z. C.; Haufler, R. E.; Hettich, R. L.; Crompton, R. N. *Adv. Met. Semicond. Clusters* **1998**, *4*, 179.

(49) Shinohara, H. *Adv. Met. Semicond. Clusters* **1998**, *4*, 205.

(50) Heaven, M. W.; Stewart, G. M.; Buntine, M. A.; Metha, G. F. *J. Phys. Chem.* A **2000**, *104*, 3308.

(51) Guo, B. C.; Castleman, A. W. Jr. *Adv. Met. Semi-Cond. Clusters* **1994**, *2*, 137.

(52) Rohmer, M.-M.; Bénard, M.; Poblet, J.-M. *Chem. Rev.* **2000**, *100*, 495.

(53) King, R. B. *Inorg. Chem.* **2000**, *39*, 2906.

(54) Harris, H.; Dance, I. G. *J. Phys. Chem.* A **2001**, *105*, 3340.

(55) Dance, I.; Wenger, E.; Harris, H. *Chem. Eur. J.* **2002**, *8*, 3497.

(56) Rohmer, M.-M.; Benard, M.; Poblet, J.-M., (P. Braunstein, L. A. Oro, P. R. Raithby, Eds.) *Metal Clusters in Chemistry*, Vol. 3, Wiley-VCH, Weinheim, 1999. Ch. 5.9, p. 1664.

(57) Pilgrim, J. S.; Duncan, M. A. *J. Am. Chem. Soc.* **1993**, *115*, 9724.

(58) van Heijnsberger, D.; von Helden, G.; Duncan, M. A.; van Roij, A. J. A.; Meijer, G. *Phys. Rev. Lett.* **1999**, *83*, 4983.

(59) Oyama S. T. (Ed.), *The Chemistry of Transition Metal Carbides and Nitrides*, Blackie, London, 1996.

(60) Li, J.; Hoffmann, R. *Chem. Mater.* **1989**, *1*, 83.

(61) King, R. B. *Izv. Akad. Nauk, Ser. Khim.* **1994**, 1358; *Russ. Chem. Bull.* **1994**, *43*, 1533.

(62) King, R. B. *J. Organomet. Chem.* **1997**, *536–537*, 7.

(63) Skell, P. S.; Havel, J. S.; McGlinchey, M. J. *Acc. Chem. Res.* **1973**, *6*, 97.

(64) Dyer, S. F.; Shevlin, P. B. *J. Am. Chem. Soc.* **1979**, *101*, 1303.

(65) Pan, W. T.; Shevlin, P. B. *J. Am. Chem. Soc.* **1996**, *118*, 1004.

(66) List, A. K.; Hillhouse, G. L.; Rheingold, A. L. *Organometallics* **1989**, *8*, 2010.

(67) Pan, W.; Armstrong, B. M.; Shevlin, P. B.; Crittell, C. H.; Stang, P. J. *Chem. Lett.* **1999**, 849.

(68) Stang, P. J., (P. J. Stang, F. Diederich, Eds.) *Modern Acetylene Chemistry*, VCH, Weinheim, 1995. p. 67.

(69) De Lucchi, O.; Cossu, S. *J. Chem. Soc., Chem. Commun.* **1992**, 1089; *Eur. J. Org. Chem.* **1998**, 2775.

(70) Goldberg, S. Z.; Duesler, E. N.; Raymond, K. N. *Inorg. Chem.* **1972**, *11*, 1397.

(71) Dahlenberg, L.; Weiss, A.; Moll, M. *J. Organomet. Chem.* **1997**, *535*, 195.

(72) Bestmann, H. J.; Behl, H.; Bremer, M. *Angew. Chem.* **1989**, *101*, 1303; *Angew. Chem., Int. Ed. Engl.* **1989**, *28*, 1219.

(73) Bestmann, H. J.; Hadawi, D.; Behl, H.; Bremer, M.; Hampel, F. *Angew. Chem.* **1993**, *105*, 1198; *Angew. Chem., Int. Ed. Engl.* **1993**, *32*, 1205.

(74) Schmidbaur, H. *Nachr. Chem. Tech. Lab.* **1979**, *27*, 620.

(75) Stang, P. J.; Arif, A. M.; Zhdankin, V. V. *Tetrahedron* **1991**, *47*, 4539.

(76) Bennison, A. C.; Grosshenny, V.; Harriman, A.; Ziessel, R. *Angew. Chem.* **1994**, *106*, 1956; *Angew. Chem., Int. Ed. Engl.* **1994**, *33*, 1884.

(77) Grosshenny, V.; Harriman, A.; Ziessel, R. *Angew. Chem.* **1995**, *107*, 1211; *Angew. Chem., Int. Ed. Engl.* **1995**, *34*, 1100.

(78) Lang, H. *Angew. Chem.* **1994**, *106*, 569; *Angew. Chem., Int. Ed. Engl.* **1994**, *33*, 547.

(79) Bunz, U. H. F. *Angew. Chem.* **1996**, *108*, 1047; *Angew. Chem., Int. Ed. Engl.* **1996**, *35*, 969.

(80) Schumm, J. S.; Pearson, D. L.; Tour, J. M. *Angew. Chem.* **1994**, *106*, 1445; *Angew. Chem., Int. Ed. Engl.* **1994**, *33*, 1360.

(81) Aviram, A. (Ed.), *Molecular Electronics: Science and Technology*, Am. Inst. Phys. Conf. 1992, 262.

(82) Bunz, U. H. F. *Angew. Chem.* **1994**, *106*, 1127; *Angew. Chem., Int. Ed. Engl.* **1994**, *33*, 1073.

(83) Giroud-Godquin, A.-M.; Maitlis, P. M. *Angew. Chem.* **1991**, *103*, 370; *Angew. Chem., Int. Ed. Engl.* **1991**, *30*, 375.

(84) Fyfe, H. B.; Mlekuz, M.; Zargarian, D.; Taylor, N. J.; Marder, T. B. *J. Chem. Soc., Chem. Commun.* **1991**, 188.

(85) Oriol, L.; Serrano, J. L. *Adv. Mater.* **1995**, *7*, 348.

(86) Oriol, L.; Pinol, M.; Serrano, J. L. *Prog. Polym. Chem.* **1997**, *22*, 873.

(87) Siemsen, P.; Livingston, R. C.; Diederich, F. *Angew. Chem. Int. Ed.* **2000**, *39*, 2632.

(88) Coat, F.; Guillevic, M.-A.; Toupet, L.; Paul, F.; Lapinte, C. *Organometallics* **1997**, *16*, 5988.

(89) Paul, F.; Lapinte, C. *Coord. Chem. Rev.* **1998**, *178–180*, 431.

(90) Manners, I. *Angew. Chem.* **1996**, *108*, 1712; *Angew. Chem., Int. Ed. Engl.* **1996**, *35*, 1603, but esp. p. 1616, Section 5.3: Rigid-rod organometallic polymers.

(91) Furstner, A.; Mathes, C.; Lehmann, C. W. *J. Am. Chem. Soc.* **1999**, *121*, 9453.

(92) Agapie, T.; Diaconescu, P. L.; Cummins, C. C. *J. Am. Chem. Soc.* **2002**, *124*, 2412.

(93) Peters, J. C.; Odom, A. L.; Cummins, C. C. *Chem. Commun.* **1997**, 1995.

(94) Cummins, C. C. *Chem. Commun.* **1998**, 1777.

(95) Greco, J. B.; Peters, J. C.; Baker, T. A.; Davis, W. M.; Cummins, C. C.; Wu, G. *J. Am. Chem. Soc.* **2001**, *123*, 5003.

(96) Enriquez, A. E.; White, P. S.; Templeton, J. L. *J. Am. Chem. Soc.* **2001**, *123*, 4992.

(97) Chen, Y.; Petz, W.; Frenking, G. *Organometallics* **2000**, *19*, 2698.

(98) Carlson, R. G.; Gile, M. A.; Heppert, J. A.; Mason, M. H.; Powell, D. R.; Velde, D. V.; Vilain, J. M. *J. Am. Chem. Soc.* **2002**, *124*, 1580.

(99) Caselli, A.; Solari, E.; Scopelliti, R.; Floriani, C. *J. Am. Chem. Soc.* **2000**, *122*, 538. See also: Floriani, C.; Floriani-Moro, R. *Adv. Organomet. Chem.* **2001**, *47*, 167.

(100) Miller, R. L.; Wolczanski, P. T.; Rheingold, A. L. *J. Am. Chem. Soc.* **1993**, *115*, 10422.

(101) Etienne, M.; White, P. S.; Templeton, J. L. *J. Am. Chem. Soc.* **1991**, *113*, 2324.

(102) Beck, W.; Breimar, J.; Fritz, P.; Knauer, W.; Weidmann, T., (F. R. Kreissl, Ed.) *Transition Metal Carbyne Complexes,* NATO ASI Ser., Vol. C392, 1993. p. 189.

(103) Latesky, S. L.; Selegue, J. P. *J. Am. Chem. Soc.* **1987**, *109*, 4731.

(104) Koutsantonis, G. A.; Selegue, J. P. *J. Am. Chem. Soc.* **1991**, *113*, 2316.

(105) Griffith, C. S.; Koutsantonis, G. A., unpublished work.

(106) Hejl, A.; Trnka, T. M.; Day, M. W.; Grubbs, R. H. *Chem. Commun.* **2002**, 2524.

(107) Mansuy, D. *Pure Appl. Chem.* **1980**, *52*, 681.

(108) Mansuy, D.; Lecomte, J.-P.; Chottard, J.-C.; Bartoli, J.-F. *Inorg. Chem.* **1981**, *20*, 3119.

(109) Goedken, V. L.; Deakin, M. R.; Bottomley, L. A. *J. Chem. Soc., Chem. Commun.* **1982**, 607.

(110) Tatsumi, K.; Hoffmann, R. *J. Am. Chem. Soc.* **1981**, *103*, 3328.

(111) English, D. R.; Hendrickson, D. N.; Suslick, K. S. *Inorg. Chem.* **1983**, *22*, 367.

(112) Rossi, G.; Goedken, V. L.; Ercolani, C. *J. Chem. Soc., Chem. Commun.* **1988**, 46.

(113) Ercolani, C.; Gardini, M.; Goedken, V. L.; Pennesi, G.; Rossi, G.; Russo, U.; Zanonato, P. *Inorg. Chem.* **1989**, *28*, 3097.

(114) Bakshi, E. N.; Delfs, C. D.; Murray, K. S.; Peters, B.; Homborg, H. *Inorg. Chem.* **1988**, *27*, 4318.

(115) Kienast, A.; Bruhn, C.; Homborg, H. *Z. Anorg. Allg. Chem.* **1997**, *623*, 967.

(116) Kienast, A.; Homborg, H. *Z. Anorg. Allg. Chem.* **1998**, *624*, 107.

(117) Galich, L.; Kienast, A.; Huckstadt, H.; Homborg, H. *Z. Anorg. Allg. Chem.* **1998**, *624*, 1235.

(118) Beck, W.; Knauer, W.; Robl, C. *Angew. Chem.* **1990**, *102*, 331; *Angew. Chem., Int. Ed. Engl.* **1990**, *29*, 318.

(119) Noda, I.; Kato, S.; Mizuta, M.; Yasuoka, N.; Kasai, N. *Angew. Chem.* **1979**, *91*, 85; *Angew. Chem., Int. Ed. Engl.* **1979**, *18*, 83.

(120) Tatsumi, K.; Hoffmann, R.; Whangbo, M.-H. *J. Chem. Soc., Chem. Commun.* **1980**, 509.

(121) Rosenthal, U.; Burlakov, V. V.; Arndt, P.; Baumann, W.; Spannenberg, A. *Organometallics* **2003**, *22*, 884.

(122) Scherbaum, F.; Grohmann, A.; Muller, G.; Schmidbaur, H. *Angew. Chem.* **1989**, *101*, 464; *Angew. Chem., Int. Ed. Engl.* **1989**, *28*, 463.

(123) Scherbaum, F.; Grohmann, A.; Huber, B.; Krüger, C.; Schmidbaur, H. *Angew. Chem.* **1988**, *100*, 1602; *Angew. Chem., Int. Ed. Engl.* **1988**, *27*, 1542.

(124) Schmidbaur, H.; Steigelmann, O. *Z. Naturforsch.* **1992**, *47b*, 1721.

(125) Matteson, D. S.; Castle, R. B.; Larson, G. L. *J. Am. Chem. Soc.* **1970**, *92*, 231.

(126) Grdenic, D.; Kamenar, B.; Korpar-Colig, B.; Sikirica, M.; Jovanovski, G. *J. Chem. Soc., Chem. Commun.* **1974**, 646.

(127) Breitinger, D.; Morell, W.; Grabetz, K. *Z. Naturforsch.* **1979**, *34b*, 390.

(128) Breitinger, D. K.; Kress, W.; Sendelbeck, R.; Ishiwada, K. *J. Organomet. Chem.* **1983**, *243*, 245.

(129) Mink, J.; Meic, Z.; Gal, M.; Korpar-Colig, B. *J. Organomet. Chem.* **1983**, *256*, 203.

(130) Breitinger, D.; Morell, W. *Z. Naturforsch.* **1977**, *32b*, 1022.

(131) O'Halloran, T. V.; Lippard, S. J.; Richmond, T. J.; Klug, A. *J. Molec. Biol.* **1987**, *194*, 705.

(132) Ceska, T. A.; Henderson, R. *J. Molec. Biol.* **1990**, *213*, 539.

(133) Auerbach, T.; Pioletti, M.; Avila, H.; Anagnostopoulos, K.; Weinstein, S.; Shulamith, F.; Francesci, F.; Yonath, A. *J. Biomolec. Sci. Dynam.* **2000**, *17*, 617.

(134) Kickham, J. E.; Guérin, F.; Stewart, J. C.; Stephan, D. W. *Angew. Chem. Int. Ed.* **2000**, *39*, 3263.

(135) Kickham, J. E.; Guérin, F.; Stewart, J. C.; Urbanska, E.; Stephan, D. W. *Organometallics* **2001**, *20*, 1175.

(136) Guérin, F.; Stephan, D. W. *Angew. Chem.* **1999**, *111*, 3910; *Angew. Chem. Int. Ed.* **1999**, *38*, 3698.

(137) Ong, C.; Kickham, J.; Clemens, S.; Guérin, F.; Stephan, D. W. *Organometallics* **2002**, *21*, 1646.

(138) Hoffmann, R.-D.; Jeitschko, W.; Boonk, L. *Chem. Mater.* **1989**, *1*, 580.

(139) Artlet, H. M.; Meyer, G. *Z. Anorg. Allg. Chem.* **1994**, *620*, 1527.

(140) Mattausch, H.; Warkentin, E.; Oeckler, O.; Simon, A. *Z. Anorg. Allg. Chem.* **2000**, *626*, 2117.

(141) Manning, M. C.; Trogler, W. C. *Inorg. Chim. Acta* **1981**, *50*, 247.

(142) Davies, J. A. *Asian J. Chem. Revs.* **1990**, *1*, 1.

(143) Ustynyuk, N. A.; Filatova, T. V.; Vinogradova, V. N.; Leont'eva, L. I.; Semeikin, O. V.; Epshtein, L. M.; Shubina, E. S.; Saitkulova, L. N.; Bakhmutova, E. V.; Chistyakov, A. L.; Stankevich, I. V. *Russ. Chem. Bull.* **1999**, *48*, 1165.

(144) Ramsden, J. A.; Agbossou, F.; Senn, D. R.; Gladysz, J. A. *J. Chem. Soc., Chem. Commun.* **1991**, 1360.

(145) Ramsden, J. A.; Weng, W.; Gladysz, J. A. *Organometallics* **1992**, *11*, 3635.

(146) Kawata, Y.; Sato, M. *Organometallics* **1997**, *16*, 1093.

(147) St Clair, M.; Schaefer, W. P.; Bercaw, J. E. *Organometallics* **1991**, *10*, 525.

(148) Evans, W. J.; Rabe, G. W.; Ziller, J. W. *J. Organomet. Chem.* **1994**, *483*, 21.

(149) Campazzi, E.; Solari, E.; Scopelliti, R.; Floriani, C. *Chem. Commun.* **1999**, 1617.

(150) Wailes, P. C.; Kautzner, B., unpublished results, cited in P. C. Wailes, R. S. P. Coutts, H. Weigold, *Organometallic Chemistry of Titanium, Zirconium and Hafnium*, Academic, New York, 1974. p. 220.

(151) Binger, P.; Müller, P.; Philipps, P.; Gabor, B.; Mynott, R.; Herrmann, A. T.; Langhauser, F.; Krüger, C. *Chem. Ber.* **1992**, *125*, 2209.

(152) DeAngelis, S.; Solari, E.; Floriani, C.; Chiesa-Villa, A.; Rizzoli, C. *Angew. Chem.* **1995**, *107*, 1200; *Angew. Chem., Int. Ed. Engl.* **1995**, *34*, 1092.

(153) Binger, P.; Müller, P.; Herrmann, A. T.; Philipps, P.; Gabor, B.; Langhauser, F.; Krüger, C. *Chem. Ber.* **1991**, *124*, 2165.

(154) Ohff, A.; Pulst, S.; Lefeber, C.; Peulecke, N.; Arndt, P.; Burlakov, V. V.; Rosenthal, U. *Synlett.* **1996**, 111.

(155) Rosenthal, U.; Pellny, P.-M.; Kirchbauer, F. G.; Burlakov, V. V. *Acc. Chem. Res.* **2000**, *33*, 119.

(156) Harlan, C. J.; Tunge, J. A.; Bridgewater, B. M.; Norton, J. R. *Organometallics* **2000**, *19*, 2365.

(157) Southard, G. E.; Curtis, M. D.; Kampf, J. W. *Organometallics* **1996**, *15*, 4667.

(158) Kreisel, G.; Scholz, P.; Seidel, W. *Z. Anorg. Allg. Chem.* **1980**, *460*, 51.

(159) LaPointe, R. E.; Wolczanski, P. T.; Mitchell, J. F. *J. Am. Chem. Soc.* **1986**, *108*, 6382.

(160) Neithamer, D. R.; LaPointe, R. E.; Wheeler, R. A.; Richeson, D. S.; Van Duyne, G. D.; Wolczanski, P. T. *J. Am. Chem. Soc.* **1989**, *111*, 9056.

(161) Wolczanski, P. T. *Polyhedron* **1995**, *14*, 3335.

(162) Ustynyuk, N. A.; Vinogradova, V. N.; Kravtsov, D. N. *Metallo-org. Khim.* **1988**, *1*, 85.

(163) Ustynyuk, N. A.; Vinogradova, V. N.; Kravtsov, D. N.; Oprunenko, Yu. F.; Piven', V. A. *Metallo-org. Khim.* **1988**, *1*, 884.

(164) Chen, M.-C.; Tsai, Y.-J.; Chen, C.-T.; Lin, Y.-C.; Tseng, T.-W.; Lee, G.-H.; Wang, Y. *Organometallics* **1991**, *10*, 378.

(165) Yang, Y.-L.; Wang, L. J.-J.; Lin, Y.-C.; Huang, S.-L.; Chen, M.-C.; Lee, G.-H.; Wang, Y. *Organometallics* **1997**, *16*, 1573.

(166) Woodworth, B. E.; White, P. S.; Templeton, J. L. *J. Am. Chem. Soc.* **1998**, *120*, 9028.

(167) Listemann, M. L.; Schrock, R. R. *Organometallics* **1985**, *4*, 74.

(168) Gilbert, T. M.; Rogers, R. D. *J. Organomet. Chem.* **1991**, *421*, C1.

(169) Gilbert, T. M.; Rogers, R. D. *Acta Crystallogr*. **1993**, *C49*, 677.

(170) Caulton, K. G.; Cayton, R. H.; Chisholm, M. H.; Huffman, J. C.; Lobkovsky, E. B.; Xue, Z. *Organometallics* **1992**, *11*, 321.

(171) Heidrich, J.; Steimann, M.; Appel, M.; Beck, W.; Phillips, J. R.; Trogler, W. C. *Organometallics* **1990**, *9*, 1296.

(172) Mihan, S.; Weidmann, T.; Weinrich, V.; Fenske, D.; Beck, W. *J. Organomet. Chem.* **1997**, *541*, 423.

(173) Davies, J. A.; El-Ghanam, M.; Pinkerton, A. A.; Smith, D. A. *J. Organomet. Chem.* **1991**, *409*, 367.

(174) Beck, W.; Niemer, B.; Breimair, J.; Heidrich, J. *J. Organomet. Chem.* **1989**, *372*, 79.

(175) Appel, M.; Heidrich, J.; Beck, W. *Chem. Ber.* **1987**, *120*, 1087.

(176) Herrmann W. A., (Ed.), *Synthetic Methods of Organometallic and Inorganic Chemistry*, Vol. 7, Georg Thieme, New York, 1995. p. 256.

(177) Herrmann, W. A.; Kühn, F. E.; Romão, C. C. *J. Organomet. Chem.* **1995**, *495*, 209.

(178) Akita, M.; Terada, M.; Oyama, S.; Sugimoto, S.; Moro-oka, Y. *Organometallics* **1990**, *9*, 816.

(179) Akita, M.; Terada, M.; Oyama, S.; Sugimoto, S.; Moro-oka, Y. *Organometallics* **1991**, *10*, 1561.

(180) Akita, M.; Terada, M.; Moro-oka, Y. *Organometallics* **1991**, *10*, 2961.

(181) Akita, M.; Takabuchi, A.; Terada, M.; Ishii, N.; Tanaka, M.; Moro-oka, Y. *Organometallics* **1994**, *13*, 2516.

(182) Akita, M.; Chung, M.-C.; Sakurai, A.; Sugimoto, S.; Terada, M.; Tanaka, M.; Moro-oka, Y. *Organometallics* **1997**, *16*, 4882.

(183) Sünkel, K.; Birk, U. *Polyhedron* **1999**, *18*, 3187.

(184) Weiss, M.; Ruschewitz, U. *Z. Anorg. Allg. Chem.* **1997**, *623*, 1208.

(185) Hemmersbach, S.; Zibrowius, B.; Kockelmann, W.; Ruschewitz, U. *Chem. Eur. J.* **2001**, *7*, 1952.

(186) Sünkel, K.; Birk, U.; Robl, C. *Organometallics* **1994**, *13*, 1679.

(187) Ogawa, H.; Joh, T.; Takahashi, S.; Sonogashira, K. *J. Chem. Soc.*, *Chem. Commun.* **1985**, 1220.

(188) Ogawa, H.; Onitsuka, K.; Joh, T.; Takahashi, S.; Yamamoto, Y.; Yamazaki, H. *Organometallics* **1988**, *7*, 2257.

(189) Onitsuka, K.; Ogawa, H.; Joh, T.; Takahashi, S.; Yamamoto, Y.; Yamazaki, H. *J. Chem. Soc., Dalton Trans.* **1991**, 1531.

(190) Back, S.; Lutz, M.; Spek, A. L.; Lang, H.; van Koten, G. *J. Organomet. Chem.* **2001**, *620*, 227.

(191) Berenguer, J. R.; Forniés, J.; Lalinde, E.; Martínez, F. *Organometallics* **1995**, *14*, 2532.

(192) *Gmelin's Handbook of Inorganic Chemistry*, *8th ed.,* Springer, Berlin. M = Cu: *Kupfer*, Vol. B2, 1961. p. 648; *Organo-copper Compounds*, 1985. Vol. 1, p. 1; M = Ag: *Silber*, Vol. B3 1977. p. 265; M = Au: *Gold* 1954. p. 722; *Organo-gold Compounds*, 1980. p. 296; *Supplement*, Vol. B2 1994. p. 264.

(193) Nast, R.; Pfab, W. *Z. Anorg. Allg. Chem.* **1957**, *292*, 287.

(194) Nast, R.; Pfab, W. *Chem. Ber.* **1956**, *89*, 415.

(195) Nast, R.; Schultze, C. *Z. Anorg. Allg. Chem.* **1960**, *307*, 15.

(196) Cataldo, F. *Eur. J. Solid State Inorg. Chem.* **1998**, *35*, 281.

(197) Cataldo, F. *Polym. Internat.* **1999**, *48*, 15.

(198) Cataldo, F. *Eur. J. Solid State Inorg. Chem.* **1998**, *35*, 293.

(199) Nast, R.; Schindel, H. *Z. Anorg. Allg. Chem.* **1963**, *326*, 201.

(200) Kockelmann, W.; Ruschewitz, U. *Angew. Chem.* **1999**, *111*, 3697; *Angew. Chem. Int. Ed.* **1999**, *38*, 3492.

(201) Matthews, A.; Waters, L. L. *J. Am. Chem. Soc.* **1900**, *22*, 108.

(202) Nast, R.; Kirner, U. *Z. Anorg. Allg. Chem.* **1964**, *330*, 311.

(203) Nast, R.; Schneller, P.; Hengefeld, A. *J. Organomet. Chem.* **1981**, *214*, 273.

(204) Offermanns, J.; Ruschewitz, U.; Kneip, C. *Z. Anorg. Allg. Chem.* **2000**, *626*, 649.

(205) Cross, R. J.; Davidson, M. F.; McLennan, A. J. *J. Organomet. Chem.* **1984**, *265*, C37.

(206) Cross, R. J.; Davidson, M. F. *J. Chem. Soc., Dalton Trans.* **1986**, 411.

(207) Bruce, M. I.; Grundy, K. R.; Liddell, M. J.; Snow, M. R.; Tiekink, E. R. T. *J. Organomet. Chem.* **1988**, *344*, C49.

(208) Lang, H.; Köcher, S.; Back, S.; Rheinwald, G.; van Koten, G. *Organometallics* **2001**, *20*, 1968.

(209) Müller, T. E.; Choi, S. W.-K.; Mingos, D. M. P.; Murphy, D.; Williams, D. J.; Yam, V. W.-W. *J. Organomet. Chem.* **1994**, *484*, 209.

(210) Kienast, A.; Galich, L.; Murray, K. S.; Mourbaki, B.; Lazarev, G.; Cashion, J. D.; Homborg, H. *J. Porph. Phthalocyan.* **1997**, *1*, 141.

(211) Müller, T. E.; Mingos, D. M. P.; Williams, D. J. *J. Chem. Soc., Chem. Commun.* **1994**, 1787.

(212) Mingos, D. M. P.; Müller, T. E. *J. Organomet. Chem.* **1995**, *500*, 251.

(213) Frad, W. A. *Adv. Inorg. Chem. Radiochem.* **1968**, *11*, 207.

(214) Spair, R. J.; Vogt, R. R.; Nieuwland, J. A. *J. Am. Chem. Soc.* **1933**, *55*, 2465.

(215) Borisov, A. E.; Borisova, A. I.; Kudryavtseva, L. V. *Izv. Akad. Nauk SSSR, Ser. Khim.* **1968**, 2287.

(216) Sebald, A.; Wrackmeyer, B. *Spectrochim. Acta* **1982**, *38A*, 163.

(217) Lemke, F. R.; Szalda, D. J.; Bullock, R. M. *J. Am. Chem. Soc.* **1991**, *113*, 8466.

(218) Gu, X.; Sponsler, M. B. *Organometallics* **1998**, *17*, 5920.

(219) Lemke, F. R.; Bullock, R. M. *Organometallics* **1992**, *11*, 4261.

(220) Frank, K. G.; Selegue, J. P. *J. Am. Chem. Soc.* **1990**, *112*, 6414.

(221) Sharma, S. B.; Tewari, I. N. *Synth. React. Inorg. Met.-Org. Chem.* **1992**, *22*, 217.

(222) Akita, M.; Ishii, N.; Takabuchi, A.; Tanaka, M.; Moro-oka, Y. *Organometallics* **1994**, *13*, 258.

(223) Ramsden, J. A.; Weng, W.; Arif, A. M.; Gladysz, J. A. *J. Am. Chem. Soc.* **1992**, *114*, 5890.

(224) Weng, W.; Bartik, T.; Brady, M.; Bartik, B.; Ramsden, J. A.; Arif, A. M.; Gladysz, J. A. *J. Am. Chem. Soc.* **1995**, *117*, 11922.

(225) Gamasa, M. P.; Gimeno, J.; Godefroy, I.; Lastra, E.; Martin-Vaca, B. M.; García-Granda, S.; Gutierrez-Rodriguez, A. *J. Chem. Soc., Dalton Trans.* **1995**, 1901.

(226) Onitsuka, K.; Joh, T.; Takahashi, S. *Bull. Chem. Soc. Jpn* **1992**, *65*, 1179.

(227) Woodworth, B. E.; Templeton, J. L. *J. Am. Chem. Soc.* **1996**, *118*, 7418.

(228) Weng, W.; Ramsden, J. A.; Arif, A. M.; Gladysz, J. A. *J. Am. Chem. Soc.* **1993**, *115*, 3824.

(229) Bartik, T.; Weng, W.; Ramsden, J. A.; Szafert, S.; Falloon, S. B.; Arif, A. M.; Gladysz, J. A. *J. Am. Chem. Soc.* **1998**, *120*, 11071.

(230) Weng, W.; Bartik, T.; Gladysz, J. A. *Angew. Chem.* **1994**, *106*, 2272; *Angew. Chem., Int. Ed. Engl.* **1994**, *33*, 2199.

(231) Weng, W.; Arif, A. M.; Gladysz, J. A. *Angew. Chem.* **1993**, *105*, 937; *Angew. Chem., Int. Ed. Engl.* **1993**, *32*, 891.

(232) Falloon, S. B.; Weng, W.; Arif, A. M.; Gladysz, J. A. *Organometallics* **1997**, *16*, 2008.

(233) Dembinski, R.; Szafert, S.; Haquette, P.; Lis, T.; Gladysz, J. A. *Organometallics* **1999**, *18*, 5438.

(234) Shostakovskii, M. F.; Bogdanova, A. V. *The Chemistry of Diacetylenes*, Wiley, New York, 1974.

(235) Zweifel, G.; Rajagopalan, S. *J. Am. Chem. Soc.* **1985**, *107*, 700.

(236) Jones, G. E.; Kendrick, D. A.; Holmes, A. B. *Org. Synth., Coll. Vol. VIII* **1993**, 63.

(237) Holmes, A. B.; Jennings-White, C. L. D.; Schulthess, A. H.; Akinde, B.; Walton, D. R. M. *J. Chem. Soc., Chem. Commun.* **1979**, 840.

(238) Crescenzi, R.; Lo Sterzo, C. *Organometallics* **1992**, *11*, 4301.

(239) Stang, P. J.; Tykwinski, R. *J. Am. Chem. Soc.* **1992**, *114*, 4411.

(240) Hlavaty, J.; Kavan, L.; Sticha, M. *J. Chem. Soc., Perkin Trans.* **2002**, *1*, 705.

(241) Bruce, M. I.; Ke, M.; Low, P. J. *Chem. Commun.* **1996**, 2405.

(242) Bruce, M. I.; Ke, M.; Low, P. J.; Skelton, B. W.; White, A. H. *Organometallics* **1998**, *17*, 3539.

(243) Roberts, R. L.; Puschmann, H.; Howard, J. A. K.; Yamamoto, J. H.; Carty, A. J.; Low, P. J. *J. Chem. Soc., Dalton Trans.* **2003**, 1099.

(244) Moreno, C.; Arnanz, A.; Delgado, S. *Inorg. Chim. Acta* **2001**, *312*, 139.

(245) Woodworth, B. E.; White, P. S.; Templeton, J. L. *J. Am. Chem. Soc.* **1997**, *119*, 828.

(246) Kheradmandan, S.; Heinze, K.; Schmalle, H. W.; Berke, H. *Angew. Chem.* **1999**, *111*, 2412; *Angew. Chem. Int. Ed.*, **1999**, *38*, 2270.

(247) Fernández, F. J.; Blacque, L.; Alfonso, M.; Berke, H. *Chem. Commun.* **2001**, 1266.

(248) Zhou, Y.; Sweyler, J. W.; Weng, W.; Arif, A. M.; Gladysz, J. A. *J. Am. Chem. Soc.* **1993**, *115*, 8509.

(249) Brady, M.; Weng, W.; Zhou, Y.; Seyler, J. W.; Amoroso, A. J.; Arif, A. M.; Böhme, M.; Frenking, G.; Gladysz, J. A. *J. Am. Chem. Soc.* **1997**, *119*, 775.

(250) Brady, M.; Weng, W.; Gladysz, J. A. *J. Chem. Soc., Chem. Commun.* **1994**, 2655.

(251) Meyer, W. E.; Amoroso, A. J.; Horn, C. R.; Jaeger, M.; Gladysz, J. A. *Organometallics* **2001**, *20*, 1115.

(252) Seyler, J. W.; Weng, W.; Zhou, Y.; Gladysz, J. A. *Organometallics* **1993**, *12*, 3802.

(253) Yam, V.W.-W.; Lau, V.C.-Y.; Cheung, K.-K. *Organometallics* **1996**, *15*, 1740.

(254) Nast, R.; Urban, F. *Z. Anorg. Allg. Chem.* **1957**, *289*, 244.

(255) Wong, A.; Kang, P. C. W.; Tagge, C. D.; Leon, D. R. *Organometallics* **1990**, *9*, 1992.

(256) Kim, P. J.; Masai, H.; Sonogashira, K.; Hagihara, N. *Inorg. Nucl. Chem. Lett.* **1970**, *6*, 181.

(257) Akita, M.; Chung, M.-C.; Sakurai, A.; Moro-oka, Y. *Chem. Commun.* **2002**, 1284.

(258) Guillemot, M.; Toupet, L.; Lapinte, C. *Organometallics* **1998**, *17*, 1928.

(259) Coat, F.; Guillemot, M.; Paul, F.; Lapinte, C. *J. Organomet. Chem.* **1999**, *578*, 76.

(260) Bruce, M. I.; Hinterding, P.; Tiekink, E. R. T.; Skelton, B. W.; White, A. H. *J. Organomet. Chem.* **1993**, *450*, 209.

(261) Bruce, M. I.; Hall, B. C.; Kelly, B. D.; Low, P. J.; Skelton, B. W.; White, A. H. *J. Chem. Soc., Dalton Trans.* **1999**, 3719.

(262) Bruce, M. I.; Low, P. J.; Costuas, K.; Halet, J.-F.; Best, S. P.; Heath, G. A. *J. Am. Chem. Soc.* **2000**, *122*, 1949.

(263) Bruce, M. I.; Smith, M. E.; Skelton, B. W.; White, A. H., unpublished work.

(264) Bruce, M. I.; Ellis, B. G.; Low, P. J.; Skelton, B. W.; White, A. H. *Organometallics* **2003**, *22*, 3184.

(265) Bruce, M. I.; Denisovich, L. I.; Low, P. J.; Perudova, S. M.; Ustynyuk, N. A. *Mendeleev Commun.* **1996**, 200.

(266) Coat, F.; Thominot, P.; Lapinte, C. *J. Organomet. Chem.* **2001**, *629*, 39.

(267) Bruce, M. I.; Smith, M. E., unpublished work.

(268) Stein, E.; Oki, S. Y.; Vichi, E. J. S. *J. Braz. Chem. Soc.* **2000**, *11*, 252.

(269) Le Narvor, N.; Lapinte, C. *J. Chem. Soc., Chem. Commun.* **1993**, 357.

(270) Le Narvor, N.; Toupet, L.; Lapinte, C. *J. Am. Chem. Soc.* **1995**, *117*, 7129.

(271) Bruce, M. I.; Kramarczuk, K. A.; Skelton, B. W.; White, A. H., unpublished work.

(272) Bonomo, L.; Stern, C.; Solari, E.; Scopelliti, R.; Floriani, C. *Angew. Chem. Int. Ed.* **2001**, *40*, 1449.

(273) Marder, T. B.; Lesley, G.; Yuan, Z.; Fyfe, H. B.; Chow, P.; Stringer, G.; Jobe, I. R.; Taylor, N. J.; Williams, I. D.; Kurtz, S. K. *ACS Symp. Ser.* **1991**, *455* (Mater. Nonlinear Opt.), 605.

(274) Fyfe, H. B.; Mlekuz, M.; Stringer, G.; Taylor, N. J.; Marder, T. B. *NATO ASI Ser., Series E* **1992**, *206*, 331.

(275) Rappert, T.; Nürnberg, O.; Werner, H. *Organometallics* **1993**, *12*, 1359.

(276) Werner, H.; Lass, R. W.; Gervert, O.; Wolf, J. *Organometallics* **1997**, *16*, 4077.

(277) Gil-Rubio, J.; Laubender, M.; Werner, H. *Organometallics* **1998**, *17*, 1202.

(278) Gil-Rubio, J.; Weberndörfer, B.; Werner, H. *Angew. Chem. Int. Ed.* **2000**, *39*, 786.

(279) Gil-Rubio, J.; Laubender, M.; Werner, H. *Organometallics* **2000**, *19*, 1365.

(280) Gervert, O.; Wolf, J.; Werner, H. *Organometallics* **1996**, *15*, 2806.

(281) Sonogashira, K.; Kataoka, S.; Takahashi, S.; Hagihara, N. *J. Organomet. Chem.* **1978**, *160*, 319.

(282) Takahashi, S.; Ohyama, Y.; Murata, E.; Sonogashira,K.; Hagihara, N. *J. Polym. Sci., Polym. Chem. Ed.* **1980**, *18*, 349.

(283) Klein, A.; Klinkhammer, K.-W.; Scheiring, T. *J. Organomet. Chem.* **1999**, *592*, 128.

(284) AlQaisi, S. M.; Galat, K. J.; Chai, M.; Ray, D. G. III; Rinaldi, P. L.; Tessier, C. A.; Youngs, W. J. *J. Am. Chem. Soc.* **1998**, *120*, 12149.

(285) Bruce, M. I.; Costuas, K.; Halet, J.-F.; Hall, B. C.; Low, P. J.; Nicholson, B. K.; White, A. H. *J. Chem. Soc., Dalton Trans.* **2002**, 383.

(286) Cherevko, P. P.; Kucher, R. V. *Spektrosk. At. Mol.* **1969**, 411.

(287) Low, P. J.; Bruce, M. I., unpublished work.

(288) Che, C.-M.; Chao, H.-Y.; Miskowski, V. M.; Li, Y.; Cheung, K.-K. *J. Am. Chem. Soc.* **2001**, *123*, 4985.

(289) Bruce, M. I.; Hall, B. C.; Skelton, B. W.; Smith, M. E.; White, A. H. *J. Chem. Soc., Dalton Trans.* **2002**, 995.

(290) Dembinski, R.; Bartik, T.; Bartik, B.; Jaeger, M.; Gladysz, J. A. *J. Am. Chem. Soc.* **2000**, *122*, 810.

(291) Bartik, T.; Bartik, B.; Brady, M.; Dembinksi, R.; Gladysz, J. A. *Angew. Chem.* **1996**, *108*, 467; *Angew. Chem., Int. Ed. Engl.* **1996**, *35*, 414.

(292) Dembinksi, R.; Lis, T.; Szafert, S.; Mayne, C. L.; Bartik, T.; Gladysz, J. A. *J. Organomet. Chem.* **1999**, *578*, 229.

(293) Bruce, M. I.; Hall, B. C.; Low, P. J.; Smith, M. E.; Skelton, B. W.; White, A. H. *Inorg. Chim. Acta* **2000**, *300–302*, 633.

(294) Bruce, M. I.; Low, P. J.; Ke, M.; Kelly, B. D.; Skelton, B. W.; Smith, M. E.; White, A. H.; Witton, N. B. *Aust. J. Chem.* **2001**, *54*, 453.

(295) Bruce, M. I.; Ellis, B. G.; Skelton, B. W.; White, A. H. *J. Organomet. Chem.* **2000**, *607*, 137.

(296) Paul, F.; Meyer, W. E.; Toupet, L.; Jiao, H.; Gladysz, J. A.; Lapinte, C. *J. Am. Chem. Soc.* **2000**, *122*, 9405.

(297) Bruce, M. I.; Ellis, B. G.; Lapinte, C.; Smith, M. E., unpublished work.

(298) Bruce, M. I.; Halet, J.-F.; Le Guennic, B.; Skelton, B. W.; Smith, M. E.; White, A. H. *Inorg. Chim. Acta.* **2003**, *350*, 175.

(299) Jia, G.; Xia, H. P.; Wu, W. F.; Ng, W. S. *Organometallics* **1996**, *15*, 3634.

(300) Xia, H. P.; Wu, W. F.; Ng, W. S.; Williams, I. D.; Jia, G. *Organometallics* **1997**, *16*, 2940.

(301) Xia, H. P.; Ng, W. S.; Ye, J. S.; Li, X.-Y.; Wong, W. T.; Lin, Z.; Yang, C.; Jia, G. *Organometallics* **1999**, *18*, 4552.

(302) Gibtner, T.; Hampel, F.; Gisselbrecht, J.-P.; Hirsch, A. *Chem. Eur. J.* **2002**, *8*, 408.

(303) Grösser, T.; Hirsch, A. *Angew. Chem.* **1993**, *105*, 1390; *Angew. Chem., Int. Ed. Engl.* **1993**, *32*, 1340.

(304) Bartik, B.; Dembinski, R.; Bartik, T.; Arif, A. M.; Gladysz, J. A. *New J. Chem.* **1997**, *21*, 739.

(305) Horn, C. R.; Martin-Alvarez, J. M.; Gladysz, J. A. *Organometallics* **2002**, *21*, 5386.

(306) Sakurai, A.; Akita, M.; Moro-oka, Y. *Organometallics* **1999**, *18*, 3241.

(307) Coat, F.; Lapinte, C. *Organometallics* **1996**, *15*, 477.

(308) Bruce, M. I.; Kelly, B. D.; Skelton, B. W.; White, A. H. *J. Organomet. Chem.* **2000**, *604*, 150.

(309) Rigault, S.; Pernichon, J.; Le Pichon, L.; Touchard, D.; Dixneuf, P. H. *J. Organomet. Chem.* **2003**, *670*, 37.

(310) Peters, T. B.; Bohling, J. C.; Arif, A. M.; Gladysz, J. A. *Organometallics* **1999**, *18*, 3261.

(311) Mohr, W.; Stahl, J.; Hampel, F.; Gladysz, J. A. *Inorg. Chem.* **2001**, *40*, 3263.

(312) Wong, W.-Y.; Wong, C.-K.; Lu, G.-L.; Cheah, K.-W.; Shi, J.-X.; Lin, Z. *J. Chem. Soc., Dalton Trans.* **2002**, 4587.

(313) Lewis, J.; Khan, M. S.; Kakkar, A. K.; Johnson, B. F. G.; Marder, T. B.; Fyfe, H. B.; Wittmann, F.; Friend, R. H.; Dray, A. E. *J. Organomet. Chem.* **1992**, *425*, 165.

(314) Stahl, J.; Bohling, J. C.; Bauer, E. B.; Peters, T. B.; Mohr, W.; Martín-Alvarez, J. M.; Hampel, F.; Gladysz, J. A. *Angew. Chem.* **2002**, *41*, 1872.

(315) Lu, W.; Xiang, H.-F.; Zhu, N.; Che, C.-M. *Organometallics* **2002**, *21*, 2343.

(316) Lu, W.; Zhu, N.; Che, C.-M. *J. Organomet. Chem.* **2003**, *670*, 11.

(317) Bruce, M. I.; Low, P. J.; Zaitseva, N. N., unpublished results.

(318) Ren, T.; Zou, G.; Alvarez, J. C. *Chem. Commun.* **2000**, 1197.

(319) Ren, T.; Xu, G.-L. *Comments Inorg. Chem.* **2002**, *23*, 355.

(320) Wong, K.-T.; Lehn, J.-M.; Peng, S.-M.; Lee, G.-H. *Chem. Commun.* **2000**, 2259.

(321) No reference.

(322) Xu, G.L.; Zou, G.; Ni, Y.-H.; DeRosa, M.C.; Crutchley, R. J.; Ren, T. *J. Am. Chem. Soc.* **2003**, *125*, 10057.

(323) Bear, J. L.; Han, B.; Wu, Z.; Camelbaeke, E. V.; Kadish, K. M. *Inorg. Chem.* **2001**, *40*, 2275.

(324) Miguel, D.; Moreno, M.; Perez, J.; Riera, V.; Churchill, D. G.; Churchill, M. R.; Janik, T. S. *J. Am. Chem. Soc.* **1998**, *120*, 417.

(325) Fraser, C. C.; Guha, S.; Chen, W. P.; Cockerham, M. P.; Porter, P. L.; Chauchard, E. A.; Lee, C. H. *Polymer* **1987**, *28*, 553.

(326) Porter, P. L.; Guha, S.; Kang, K.; Frazier, C. C. *Polymer* **1991**, *32*, 1756.

(327) Yang, M. J.; Zhang, L. J.; Lei, Z. Q.; Ye, P. X.; Si, J. H.; Yang, Q. G.; Wang, Y. G. *J. Appl. Polym. Sci.* **1998**, *70*, 1165.

(328) Kingsborough, R. P.; Swager, T. M. *Prog. Inorg. Chem.* **1999**, *48*, 123.

(329) Nguyen, P.; Gomez-Elipe, P.; Manners, I. *Chem. Rev.* **1999**, *99*, 1515.

(330) Markwell, R. D.; Butler, I. S.; Kakkar, A. K.; Khan, M. S.; Al-Zakwani, Z. H.; Lewis, J. *Organometallics* **1996**, *15*, 2331.

(331) Le Stang, S.; Paul, F.; Lapinte, C. *Organometallics* **2000**, *19*, 1035.

(332) Sonogashira, K.; Takahashi, S.; Hagihara, N. *Macromolecules* **1977**, *10*, 879.

(333) Takahashi, S.; Morimoto, H.; Murata, E.; Kataoka, S.; Sonogashira, K.; Hagihara, N. *J. Polym. Sci., Polym. Chem. Ed.* **1982**, *20*, 565.

(334) For a related study of cuprous ion catalysed ligand redistribution reactions see Osakada, K.; Hamada, M.; Yamamoto, T. *Organometallics*, **2000**, *19*, 458.

(335) Songashira, K.; Ohga, K.; Takahashi, S.; Hagihara, N. *J. Organomet. Chem.* **1980**, *188*, 237.

(336) Blau, W. J.; Byrne, H. J.; Cardin, D. J.; Davey, A. P. *J. Mater. Chem.* **1991**, *1*, 245.

(337) Fujikura, Y.; Sonogashira, K.; Hagihara, N. *Chem. Lett.* **1975**, 1067.

(338) Takahashi, S.; Murata, E.; Sonogashira, K.; Hagihara, N. *J. Polm. Sci., Polym. Chem. Ed.* **1980**, *18*, 661.

(339) Johnson, B. F. G.; Kakkar, A. K.; Khan, M. S.; Lewis, J.; Dray, A. E.; Friend, R. H.; Whitmann, F. *J. Mater. Chem.* **1991**, *1*, 485.

(340) Lewis, J.; Khan, M. S.; Kakkar, A. K.; Johnson, B. F. G.; Marder, T. B.; Fyfe, H. B.; Wittmann, F.; Friend, R. H.; Day, A. E. *J. Organomet. Chem.* **1992**, *425*, 165.

(341) Wilson, J. S.; Kohler, A.; Friend, R. H.; Al-Suti, M. K.; Al-Mandhary, M. R. A.; Khan, M. S.; Raithby, P. R. *J. Chem. Phys.* **2000**, *113*, 7627.

(342) Chawdhury, N.; Kohler, A.; Friend, R. H.; Wong, W. Y.; Lewis, J.; Younis, M.; Raithby, P. R.; Corcoran, T. C.; Mandhury, M. R. A.; Khan, M. S. *J. Chem. Phys.* **1999**, *110*, 4963.

(343) For a closely related study see Liu, Y.; Jiang, S.; Glusac, K.; Powell, D. H.; Anderson, D. F.; Schanze, K. S. *J. Am. Chem. Soc.* **2002**, *124*, 12412.

(344) Magnus, P.; Becker, D. P. *J. Chem. Soc., Chem. Commun.* **1985**, 640.

(345) Sautet, P.; Eisenstein, O.; Canadell, E. *New J. Chem.* **1987**, *11*, 797.

(346) Cox, M. K. *Mol. Cryst. Liq. Cryst.* **1987**, *6*, 981.

(347) Whittall, I. R.; McDonagh, A. M.; Humphrey, M. G.; Samoc, M. *Adv. Organomet. Chem.* **1998**, *42*, 291.

(348) Whittall, I. R.; McDonagh, A. M.; Humphrey, M. G.; Samoc, M. *Adv. Organomet. Chem.* **1999**, *43*, 349.

(349) Long, N. J. *Angew. Chem.* **1995**, *107*, 37; *Angew. Chem., Int. Ed. Engl.* **1995**, *34*, 21.

(350) Davey, A. P.; Page, H.; Blau, W. *Synth. Met.* **1993**, *55*, 3980.

(351) Davey, A. P.; Cardin, D. J.; Byrne, H. J.; Blau, W. J., (J. Messier, F. Kajzar, P. Prasad, D. Ulrich, Eds.) *Organic Molecules for Nonlinear Optics*, Kluwer, Dordrecht, The Netherlands, 1991. p. 361.

(352) Page, H.; Blau, W.; Davey, A. P.; Lou, X.; Cardin, D. J. *Synth. Met.* **1994**, *63*, 179.

(353) Morton, M. S.; Selegue, J. P. *J. Am. Chem. Soc.* **1995**, *117*, 7005.

(354) Morton, M. S.; Selegue, J. P. *J. Organomet. Chem.* **1999**, *578*, 133.

(355) Morton, M. S.; Selegue, J. P.; Carrillo, A. *Organometallics* **1996**, *15*, 4664.

(356) Re, N.; Sgamellotti, A.; Floriani, C. *Organometallics* **1996**, *15*, 5330.

(357) Amiet, G.; Nicholas, K.; Pettit, R. *Chem. Commun.* **1970**, 161.

(358) Kuzmina, L. G.; Ginzburg, A. G.; Struchkov, Yu.T.; Kursanov, D. N. *J. Organomet. Chem.* **1983**, *253*, 329.

(359) Bunz, U. H. F.; Enkelmann, V.; Rader, J. *Organometallics* **1993**, *12*, 4745.

(360) Kur, S. A.; Heeg, M. J.; Winter, C. H. *Organometallics* **1994**, *13*, 1865.

(361) Boev, V. I.; Dombrovskii, A. V. *Zh. Obshch. Khim.* **1977**, *47*, 727 (*Chem. Abstr. 87*, 23452).

(362) Boev, V. I.; Dombrovskii, A. V. *Izv. Vyssh. Uchebn. Zaved., Khim. Khim. Tekhnol.* **1977**, *20*, 1789 (*Chem. Abstr. 88*, 136762).

(363) Han, Y.-H.; Heeg, M. J.; Winter, C. H. *Organometallics* **1994**, *13*, 3009.

(364) Winter, C. H.; Han, Y.-H.; Ostrander, R. L.; Rheingold, A. L. *Angew. Chem.* **1993**, *105*, 1247; *Angew. Chem., Int. Ed. Engl.* **1993**, *32*, 1161.

(365) Winter, C. H.; Han, Y.-H.; Heeg, M. J. *Organometallics* **1992**, *11*, 3169.

(366) Pitzer, K. S.; Clementi, E. *J. Am. Chem. Soc.* **1959**, *81*, 4477.

(367) Hoffmann, R. *Tetrahedron* **1966**, *22*, 521.

(368) Bernholc, J.; Phillips, J. C. *J. Chem. Phys.* **1986**, *85*, 3258.

(369) Tobe, Y.; Fujii, T.; Matsumoto, H.; Tsumuraya, K.; Noguchi, D.; Nakagawa, N.; Sonoda, M.; Naemura, K.; Achiba, Y.; Wakabayashi, T. *J. Am. Chem. Soc.* **2000**, *122*, 1762.

(370) Diederich, F.; Rubin, Y.; Knobler, C. B.; Whetten, R. L.; Schriver, K. E.; Houk, K. N.; Li, Y. *Science* **1989**, *245*, 108.
(371) Rubin, Y.; Knobler, C. B.; Diederich, F. *J. Am. Chem. Soc.* **1990**, *112*, 4966.
(372) Rubin, Y.; Knobler, C. B.; Diederich, F. *J. Am. Chem. Soc.* **1990**, *112*, 1607.
(373) Rubin, Y.; Kahr, M.; Knobler, C. B.; Diederich, F.; Wilkins, C. L. *J. Am. Chem. Soc.* **1991**, *113*, 495.
(374) Rubin, Y.; Diederich, F. *J. Am. Chem. Soc.* **1989**, *111*, 6870.
(375) Tobe, Y.; Fujii, T.; Matsumoto, H.; Naemura, K.; Achiba, Y.; Wakabayashi, T. *J. Am. Chem. Soc.* **1996**, *118*, 2758.
(376) Diederich, F.; Rubin, Y.; Chapman, O. L.; Goroff, N. S. *Helv. Chim. Acta* **1994**, *77*, 1441.
(377) Yam, V.W.-W. *Acc. Chem. Res.* **2002**, *35*, 555.
(378) Yam, V.W.-W. *Pure Appl. Chem.* **2001**, *73*, 543.
(379) Yam, V.W.-W. *Chem. Commun.* **2001**, 789.
(380) Hong, X.; Cheung, K.-K.; Guo, C.-X.; Che, C.-M. *J. Chem. Soc., Dalton Trans.* **1994**, 1867.
(381) Bruce, M. I. *Chem. Rev.* **1998**, *98*, 2797.
(382) Toto, J. L.; Toto, T. T.; de Melo, C. P.; Kirtman, B.; Robins, K. *J. Chem. Phys.* **1996**, *104*, 8586.
(383) Bruce, M. I.; Kelly, B. D.; Skelton, B. W.; White, A. H. *J. Chem. Soc., Dalton Trans.* **1999**, 847.
(384) Connelly, N. G.; Geiger, W. E. *Chem. Rev.* **1996**, *96*, 877.
(385) Frohnapfel, D. S.; Woodworth, B. E.; Thorp, H. H.; Templeton, J. L. *J. Phys. Chem.* A. **1998**, *102*, 5665.
(386) Cruetz, C. *Prog. Inorg. Chem.* **1983**, *30*, 1.
(387) Belanzoni, P.; Re, N.; Sgamellotti, A.; Floriani, C. *J. Chem. Soc., Dalton Trans.* **1997**, 4773.
(388) Re, N.; Sgamellotti, A.; Floriani, C. *J. Chem. Soc., Dalton Trans.* **1998**, 2521.
(389) Belanzoni, P.; Sgamellotti, A.; Re, N.; Floriani, C. *Inorg. Chem.* **2000**, *39*, 1147.
(390) Belanzoni, P.; Re, N.; Sgamellotti, A. *J. Organomet. Chem.* **2002**, *656*, 156.
(391) Jiao, H. J.; Gladysz, J. A. *New J. Chem.* **2001**, *25*, 551.
(392) Frapper, G.; Kertesz, M. *Inorg. Chem.* **1993**, *32*, 732.
(393) Lhost, O.; Toussaint, J. M.; Bredas, J. L.; Whittmann, H. F.; Fuhrmann, K.; Friend, R. H.; Khan, M. S.; Lewis, J. *Synth. Met.* **1993**, *55–57*, 4525.
(394) Sponsler, M. B. *Organometallics* **1995**, *14*, 1920.
(395) Belanzoni, P.; Re, N.; Rosi, M.; Sgamellotti, A.; Floriani, C. *Organometallics* **1996**, *15*, 4264.
(396) Belanzoni, P.; Re, N.; Sgamellotti, A.; Floriani, C. *J. Chem. Soc., Dalton Trans.* **1998**, 1825.
(397) Le Narvor, N.; Lapinte, C. *C.R. Acad. Sci., Paris, Serie IIc* **1998**, *1*, 745.
(398) Byrne, L. T.; Hos, J. P.; Koutsantonis, G. A.; Sanford, V.; Skelton, B. W.; White, A. H. *Organometallics* **2002**, *21*, 3147.
(399) Onitsuka, K.; Takahashi, S. *J. Chem. Soc., Chem. Commun.* **1995**, 2095.
(400) Onitsuka, K.; Ose, N.; Ozawa, F.; Takahashi, S. *J. Organomet. Chem.* **1999**, *578*, 169.
(401) Thomas, D.; Peulecke, N.; Burlakov, V. V.; Heller, B.; Baumann, W.; Spannenberg, A.; Kempe, R.; Rosenthal, U.; Beckhaus, R. *Z. Anorg. Allg. Chem.* **1998**, *624*, 919.
(402) Bruce, M. I.; Low, P. J.; Skelton, B. W.; White, A. H. *New J. Chem.* **1998**, *22*, 419.
(403) Bruce, M. I.; Kelly, B. D.; Skelton, B. W.; White, A. H. *J. Organomet. Chem.* **2000**, *604*, 150.
(404) Bruce, M. I.; Hambley, T. W.; Snow, M. R.; Swincer, A. G. *Organometallics* **1985**, *4*, 494.
(405) Ogawa, H.; Joh, T.; Takahashi, S. *J. Chem. Soc., Chem. Commun.* **1988**, 561.

(406) Onitsuka, K.; Joh, T.; Takahashi, S. *J. Organomet. Chem.* **1994**, *464*, 247.

(407) Onitsuka, K.; Yanai, K.; Takei, F.; Joh, T.; Takahashi, S. *Organometallics* **1994**, *13*, 3862.

(408) Onitsuka, K.; Joh, T.; Takahashi, S. *Angew. Chem.* **1992**, *104*, 893; *Angew. Chem.*, *Int. Ed. Engl.* **1992**, *31*, 851.

(409) Takei, F.; Yanai, K.; Onitsuka, K.; Takahashi, S. *Angew. Chem.* **1996**, *108*, 1634; *Angew. Chem.*, *Int. Ed. Engl.* **1996**, *35*, 1554.

(410) Takei, F.; Yanai, K.; Onitsuka, K.; Takahashi, S. *Chem. Eur. J.* **2000**, *6*, 983.

(411) Foley, J. L.; Li, L.; Sandman, D. J. *Chem. Mater.* **1998**, *10*, 3984, and references therein.

(412) Fritz, P. M.; Polborn, K.; Steimann, M.; Beck, W. *Chem. Ber.* **1989**, *122*, 889.

(413) Weidmann, T.; Weinrich, V.; Wagner, B.; Robl, C.; Beck, W. *Chem. Ber.* **1991**, *124*, 1363.

(414) Akita, M.; Terada, M.; Tanaka, M.; Moro-oka, Y. *Organometallics* **1992**, *11*, 3468.

(415) Blau, R. J.; Chisholm, M. H.; Folting, K.; Wang, R. J. *J. Chem. Soc., Chem. Commun.* **1985**, 1582; *J. Am. Chem. Soc.* **1987**, *109*, 4552.

(416) Mihan, S.; Sünkel, K.; Beck, W. *Chem. Eur. J.* **1999**, *5*, 745.

(417) Lang, H.; Kohler, K.; Zsolnai, L. *Chem. Ber.* **1995**, *128*, 519.

(418) Griffith, C. S.; Koutsantonis, G. A.; Skelton, B. W.; White, A. H. *Chem. Commun.* **2002**, 2174.

(419) Bruce, M. I.; Halet, J.-F.; Kahal, S.; Low, P. J.; Skelton, B. W.; White, A. H. *J. Organomet. Chem.* **1999**, *578*, 155.

(420) Chung, M.-C.; Sakurai, A.; Akita, M.; Moro-oka, Y. *Organometallics* **1999**, *18*, 4684.

(421) Bruce, M. I.; Kelly, B. D.; Skelton, B. W.; White, A. H. *J. Chem. Soc., Dalton Trans.* **1999**, 847.

(422) Akita, M.; Sakurai, A.; Moro-oka, Y. *Chem. Commun.* **1999**, 101.

(423) Crespi, A. M.; Went, M. J.; Sunshine, S. S.; Shriver, D. F. *Organometallics* **1988**, *7*, 214.

(424) Duffy, N. D.; Kassis, N. M.; Rae, A. D. *J. Organomet. Chem.* **1993**, *460*, 97.

(425) Takahashi, Y.; Akita, M.; Moro-oka, Y. *Chem. Commun.* **1997**, 1557.

(426) Griffith, C. S.; Koutsantonis, G. A.; Skelton, B. W.; White, A. H. *Chem. Commun.* **1998**, 1805.

(427) Griffith, C.S.; Koutsantonis, G. A.; Skelton, B. W.; White, A. H., *J. Organomet. Chem.* **2003**, *672*, 17.

(428) Akita, M.; Chung, M.; Terada, M.; Miyauti, M.; Tanaka, M.; Moro-oka, Y. *J. Organomet. Chem.* **1998**, *565*, 49.

(429) Koutsantonis, G. A.; Selegue, J. P.; Wang, J. *Organometallics* **1992**, *11*, 2704.

(430) Jensen, M. P.; Sabat, M.; Shriver, D. F. *J. Cluster Sci.* **1990**, *1*, 75.

(431) Norton, D. M.; Shriver, D. F. *J. Organomet. Chem.* **2000**, *614–615*, 318.

(432) Jensen, M. P.; Phillips, D. A.; Sabat, M.; Shriver, D. F. *Organometallics* **1992**, *11*, 1859.

(433) Frank, K. G. Ph.D. thesis, University of Kentucky, 1990.

(434) Falloon, S. B.; Arif, A. M.; Gladysz, J. A. *Chem. Commun.* **1997**, 629.

(435) Falloon, S. B.; Szafert, S.; Arif, A. M.; Gladysz, J. A. *Chem. Eur. J.* **1998**, *4*, 1033.

(436) Akita, M.; Terada, M.; Moro-oka, Y. *Organometallics* **1992**, *11*, 1825.

(437) Selegue, J. P., unpublished work.

(438) Worth, G. H.; Robinson, B. H.; Simpson, J. *Organometallics* **1992**, *11*, 501.

(439) Worth, G. H.; Robinson, B. H.; Simpson, J. *Organometallics* **1992**, *11*, 3863.

(440) Dellaca, R. J.; Penfold, B. R.; Robinson, B. H.; Robinson, W. T.; Spencer, J. L. *Inorg. Chem.* **1970**, *9*, 2197.

(441) Allegra, G.; Valle, S. *Acta Crystallogr.* **1969**, *B25*, 107.

(442) Bruce, M. I.; Zaitseva, N. N.; Skelton, B. W.; White, A. H., unpublished work.

(443) Elder, S. M.; Robinson, B. H.; Simpson, J. *J. Organomet. Chem.* **1990**, *398*, 165.

(444) Bruce, M. I.; Skelton, B. W.; White, A. H.; Zaitseva, N. N. *J. Chem. Soc., Dalton Trans.* **1996**, 3151.

(445) Bruce, M. I.; Low, P. J.; Zaitseva, N. N.; Kahlal, S.; Halet, J.-F.; Skelton, B. W.; White, A. H. *J. Chem. Soc., Dalton Trans.* **2000**, 2939.
(446) Akita, M.; Chung, M.-C.; Sakurai, A.; Moro-oka, Y. *Chem. Commun.* **2000**, 1285.
(447) Bruce, M. I.; Hall, B. C.; Skelton, B. W.; White, A. H. *J. Chem. Soc., Dalton Trans.* **2002**, 995.
(448) Worth, G. H.; Robinson, B. H.; Simpson, J. *J. Organomet. Chem.* **1993**, *450*, 219.
(449) Bruce, M. I.; Kramarczuk, K. A.; Zaitseva, N. N.; Skelton, B. W.; White, A. H., unpublished work.
(450) Lapinte, C., personal communication.
(451) Reina, R.; Riba, O.; Rossell, O.; Seco, M.; Font-Bardia, M.; Solans, X. *Organometallics* **2002**, *21*, 5307.
(452) Allegra, G.; Ercoli, R.; Peronaci, E. M. *Chem. Commun.* **1966**, 549.
(453) Robinson, B. H.; Tham, W. *J. Organomet. Chem.* **1968**, *16*, P45.
(454) Matheson, T. W.; Robinson, B. H.; Tham, W. S. *J. Chem. Soc. (A)* **1971**, 1457.
(455) Robinson, B. H.; Spencer, J. L.; Hodges, R. *Chem. Commun.* **1968**, 1480.
(456) Dellaca, R. J.; Penfold, B. R.; Robinson, B. H.; Robinson, W. T.; Spencer, J. L. *Inorg. Chem.* **1970**, *9*, 2204.
(457) Palyi, G.; Varada, G.; Schmiedeknecht, K. *C1 Mol. Chem.* **1985**, *1*, 297 (*Chem. Abstr.* *104*, 140945).
(458) Mlekuz, M.; D'Agostino, M. F.; Kolis, J. W.; McGlinchey, M. J. *J. Organomet. Chem.* **1986**, *303*, 361.
(459) Seyferth, D.; Hallgren, J. E.; Spohn, R. J.; Williams, G. H.; Nestle, M. O.; Hung, P. L. K. *J. Organomet. Chem.* **1974**, *65*, 99.
(460) Beveridge, A. D.; Clark, H. C. *J. Organomet. Chem.* **1968**, *11*, 601.
(461) Bor, G.; Marko, L.; Marko, B. *Chem. Ber.* **1961**, *95*, 333.
(462) Le Coustumer, G.; Mollier, Y. *J. Chem. Soc., Chem. Commun.* **1980**, 38.
(463) Varadi, G.; Palyi, G. *Inorg. Chim. Acta* **1976**, *20*, L33.
(464) Varadi, G.; Palyi, G. *Magy. Kem. Foly.* **1977**, *83*, 323 (*Chem. Abstr. 87*, 201727).
(465) Brice, M. D.; Dellaca, R. J.; Penfold, B. R.; Spencer, J. L. *J. Chem. Soc., Chem. Commun.* **1971**, 72.
(466) Brice, M. D.; Penfold, B. R. *Inorg. Chem.* **1972**, *11*, 1381.
(467) Geiser, U.; Kini, A. M. *Acta Crystallogr.* **1993**, *C49*, 1322.
(468) Kolis, J. W.; Holt, E. M.; Hriljac, J. A.; Shriver, D. F. *Organometallics* **1984**, *3*, 469.
(469) Fritch, J. R.; Vollhardt, K. P. C. *Angew. Chem.* **1980**, *92*, 570; *Angew. Chem., Int. Ed. Engl.* **1980**, *19*, 560.
(470) Norton, D. M.; Stern, C. L.; Shriver, D. F. *Inorg. Chem.* **1994**, *33*, 2701.
(471) Norton, D. M.; Shriver, D. F. *Inorg. Chem.* **2000**, *39*, 5118.
(472) Adams, C. J.; Bruce, M. I.; Horn, E.; Skelton, B. W.; Tiekink, E. R. T.; White, A. H. *J. Chem. Soc., Dalton Trans.* **1993**, 3299.
(473) Adams, C. J.; Bruce, M. I.; Skelton, B. W.; White, A. H. *J. Organomet. Chem.* **1993**, *450*, C9.
(474) Adams, C. J.; Bruce, M. I.; Humphrey, P. A.; Skelton, B. W.; White, A. H. *Aust. J. Chem.* **2001**, *54*, 325.
(475) Allison, N. T.; Fritch, J. R.; Vollhardt, K. P. C.; Walborsky, E. C. *J. Am. Chem. Soc.* **1983**, *105*, 1984.
(476) Dellaca, R. J.; Penfold, B. R. *Inorg. Chem.* **1971**, *10*, 1269.
(477) Robinson, B. H.; Spencer, J. L. *J. Organomet. Chem.* **1971**, *30*, 267.
(478) Seyferth, D.; Spohn, R. J.; Churchill, M. R.; Gold, K.; Scholer, F. *J. Organomet. Chem.* **1970**, *23*, 237.

(479) Adams, C. J.; Bruce, M. I.; Skelton, B. W.; White, A. H. *J. Organomet. Chem.* **1996**, *513*, 255.
(480) Worth, G. H.; Robinson, B. H.; Simpson, J. *Appl. Organomet. Chem.* **1990**, *4*, 481.
(481) Osella, D.; Gambino, O.; Nevi, C.; Ravera, M.; Bertolino, D. *Inorg. Chim. Acta* **1993**, *206*, 155.
(482) Osella, D.; Milone, L.; Nervi, C.; Ravera, M. *J. Organomet. Chem.* **1995**, *488*, 1.
(483) Osella, D.; Gobetto, R.; Nervi, C.; Ravera, M.; D'Amato, R.; Russo, M. V. *Inorg. Chem. Commun.* **1998**, *1*, 239.
(484) Brooksby, P. A.; Duffy, N. W.; McQuillan, A. J.; Robinson, B. H.; Simpson, J. *J. Organomet. Chem.* **1999**, *582*, 183.
(485) Chini, P.; Longoni, G.; Albano, V. G. *Adv. Organomet. Chem.* **1976**, *14*, 285.
(486) Mak, T. C. W.; Zhou, G.-D. *Crystallography in Modern Chemistry*, Wiley, New York, 1992. Ch. 6.8, p. 1074.
(487) Wang, C.-R.; Kai, T.; Tomiyama, T.; Yoshida, T.; Kobayashi, Y.; Nishibori, E.; Takata, M.; Sakata, M.; Shinohara, H. *Angew. Chem. Int. Ed.* **2001**, *40*, 397.
(488) Frapper, G.; Halet, J.-F. *Organometallics* **1995**, *14*, 5044.
(489) Frapper, G.; Halet, J.-F.; Bruce, M. I. *Organometallics* **1997**, *16*, 2590.
(490) Terada, M.; Akita, M. *Organometallics* **2003**, *22*, 355.
(491) Byrne, L. T.; Hos, J. P.; Koutsantonis, G. A.; Skelton, B. W.; White, A. H. *J. Organomet. Chem.* **2000**, *598*, 28.
(492) Low, P. J.; Carty, A. J.; Udachin, K. A.; Enright, G. D. *Chem. Commun.* **2001**, 411.
(493) Bruce, M. I.; Snow, M. R.; Tiekink, E. R. T.; Williams, M. L. *J. Chem. Soc., Chem. Commun.* **1986**, 701.
(494) Blenkiron, P.; Enright, G. D.; Low, P. J.; Corrigan, J. F.; Taylor, N. J.; Chi, Y.; Saillard, J.-Y.; Carty, A. J. *Organometallics* **1998**, *17*, 2447.
(495) Adams, C. J.; Bruce, M. I.; Skelton, B. W.; White, A. H.; Frapper, G.; Halet, J.-F. *J. Chem. Soc., Dalton Trans.* **1997**, 371.
(496) Koutsantonis, G. A.; Hos, J. P.; Skelton, B. W.; White, A. H., unpublished work.
(497) Akita, M.; Hirakawa, H.; Tanaka, M.; Moro-oka, Y. *J. Organomet. Chem.* **1995**, *485*, C14.
(498) Akita, M.; Sugimoto, S.; Hirakawa, H.; Kato, S.; Terada, M.; Tanaka, M.; Moro-oka, Y. *Organometallics* **2001**, *20*, 1555.
(499) Byrne, L. T.; Griffith, C. S.; Hos, J. P.; Koutsantonis, G. A.; Skelton, B. W.; White, A. H. *J. Organomet. Chem.* **1998**, *565*, 259.
(500) Bruce, M. I. *J. Organomet. Chem.* **1990**, *394*, 365.
(501) Bruce, M. I. *Coord. Chem. Rev.* **1997**, *166*, 91.
(502) Aime, S.; Gobetto, R.; Milone, L.; Osella, D.; Violano, L.; Arce, A. J.; De Sanctis, Y. *Organometallics* **1991**, *10*, 2854.
(503) Bruce, M. I.; Zaitseva, N. N.; Skelton, B. W.; White, A. H. *J. Chem. Soc., Dalton Trans.* **1999**, 1445.
(504) Cullen, W. R.; Harbourne, D. A.; Liengme, B.; Sams, J. R. *Inorg. Chem.* **1970**, *9*, 702.
(505) Cullen, W. R. *Adv. Inorg. Chem. Radiochem.* **1972**, *15*, 323.
(506) Bradford, C. W.; Nyholm, R. S.; Gainsford, G. J.; Guss, J. M.; Ireland, P. R.; Mason, R. *J. Chem. Soc., Chem. Commun.* **1972**, 87.
(507) Gainsford, G. J.; Guss, J. M.; Ireland, P. R.; Mason, R.; Bradford, C. W. *J. Organomet. Chem.* **1972**, *40*, C70.
(508) Bradford, C. W.; Nyholm, R. S. *J. Chem. Soc., Dalton Trans.* **1973**, 529.
(509) Smith, W. F.; Yule, J.; Taylor, N. J.; Paik, H. N.; Carty, A. J. *Inorg. Chem.* **1977**, *16*, 1593.
(510) MacLaughlin, S. A.; Taylor, N. J.; Carty, A. J. *Organometallics* **1983**, *2*, 1194.
(511) Doherty, S.; Corrigan, J. F.; Carty, A. J. *Adv. Organomet. Chem.* **1995**, *37*, 39.

(512) Blenkiron, P.; Corrigan, J. F.; Pilette, D.; Taylor, N. J.; Carty, A. J. *Can. J. Chem.* **1996**, *74*, 2349.

(513) Blenkiron, P.; Enright, G. D.; Low, P. J.; Corrigan, J. F.; Taylor, N. J.; Chi, Y.; Saillard, J.-Y.; Carty, A. J. *Organometallics* **1998**, *17*, 2447.

(514) Carty, A. J. *Pure Appl. Chem.* **1982**, *54*, 113.

(515) Daran, J.-C.; Cabrera, E.; Bruce, M. I.; Williams, M. L. *J. Organomet. Chem.* **1987**, *319*, 239.

(516) Adams, C. J.; Bruce, M. I.; Liddell, M. J.; Tiekink, E. R. T.; Skelton, B. W.; White, A. H. *J. Organomet. Chem.* **1993**, *445*, 187.

(517) Adams, C. J.; Bruce, M. I.; Skelton, B. W.; White, A. H. *J. Organomet. Chem.* **1992**, *430*, 181.

(518) Adams, C. J.; Bruce, M. I.; Skelton, B. W.; White, A. H. *J. Organomet. Chem.* **1991**, *420*, 87.

(519) Adams, C. J.; Bruce, M. I.; Skelton, B. W.; White, A. H. *J. Organomet. Chem.* **1991**, *420*, 95.

(520) Adams, C. J.; Bruce, M. I.; Skelton, B. W.; White, A. H. *J. Chem. Soc., Chem. Commun.* **1992**, 26.

(521) Adams, C. J.; Bruce, M. I.; Skelton, B. W.; White, A. H. *J. Chem. Soc., Dalton Trans.* **1997**, 2937.

(522) Adams, C. J.; Bruce, M. I. *Aust. J. Chem.* **1996**, *49*, 517.

(523) Adams, C. J.; Bruce, M. I.; Skelton, B. W.; White, A. H. *J. Organomet. Chem.* **1996**, *506*, 191.

(524) Adams, C. J.; Bruce, M. I.; Liddell, M. J.; Skelton, B. W.; White, A. H. *J. Chem. Soc., Chem. Commun.* **1992**, 1314.

(525) Adams, C. J.; Bruce, M. I.; Skelton, B. W.; White, A. H. *J. Organomet. Chem.* **1992**, *423*, 97.

(526) Adams, C. J.; Bruce, M. I.; Skelton, B. W.; White, A. H. *J. Organomet. Chem.* **1993**, *445*, 211.

(527) Gervasio, G.; Rossetti, R.; Stanghellini, P. L.; Bor, G. *Inorg. Chem.* **1984**, *23*, 2073.

(528) Gervasio, G.; Kettle, S. F. A.; Musso, F.; Rossetti, R.; Stanghellini, P. L. *Inorg. Chem.* **1995**, *34*, 298.

(529) Adams, C. J.; Bruce, M. I.; Skelton, B. W.; White, A. H. *J. Chem. Soc., Chem. Commun.* **1993**, 446.

(530) Adams, C. J.; Bruce, M. I.; Skelton, B. W.; White, A. H. *J. Organomet. Chem.* **1998**, *551*, 235.

(531) Adams, C. J.; Bruce, M. I.; Skelton, B. W.; White, A. H. *Polyhedron* **1998**, *17*, 2795.

(532) Adams, C. J.; Bruce, M. I.; Halet, J.-F.; Kahlal, S.; Skelton, B. W.; White, A. H. *J. Chem. Soc., Dalton Trans.* **2001**, 414.

(533) Huang, T.-K.; Chi, Y.; Peng, S.-M.; Lee, G.-H.; Wang, S.-L.; Liao, F.-L. *Organometallics* **1995**, *14*, 2164.

(534) Bruce, M. I. *J. Cluster Sci.* **1997**, *8*, 293.

(535) Adams, C. J.; Bruce, M. I.; Schulz, M.; Skelton, B. W.; White, A. H. *J. Organomet. Chem.* **1994**, *472*, 285.

(536) Adams, C. J.; Bruce, M. I.; Skelton, B. W.; White, A. H. *Chem. Commun.* **1996**, 975.

(537) Adams, C. J.; Bruce, M. I.; Skelton, B. W.; White, A. H. *J. Organomet. Chem.* **1998**, *561*, 97.

(538) Adams, C. J.; Bruce, M. I.; Skelton, B. W.; White, A. H. *J. Organomet. Chem.* **1999**, *573*, 134.

(539) Adams, C. J.; Bruce, M. I.; Skelton, B. W.; White, A. H. *J. Organomet. Chem.* **1993**, *444*, C44.

(540) Adams, C. J.; Bruce, M. I.; Skelton, B. W.; White, A. H. *J. Chem. Soc., Chem. Commun.* **1996**, 969.

(541) Adams, C. J.; Bruce, M. I.; Skelton, B. W.; White, A. H. *J. Chem. Soc., Dalton Trans.* **1999**, 1283.

(542) Adams, C. J.; Bruce, M. I.; Skelton, B. W.; White, A. H. *J. Chem. Soc., Dalton Trans.* **1999**, 2451.

(543) Adams, C. J.; Bruce, M. I.; Skelton, B. W.; White, A. H. *Aust. J. Chem.* **1999**, *52*, 409.

(544) Adams, C. J.; Bruce, M. I.; Skelton, B. W.; White, A. H. *J. Chem. Soc., Chem. Commun.* **1996**, 2663.

(545) Adams, C. J.; Bruce, M. I.; Skelton, B. W.; White, A. H. *J. Organomet. Chem.* **1999**, *584*, 254.

(546) Adams, C. J.; Bruce, M. I.; Skelton, B. W.; White, A. H. *J. Organomet. Chem.* **1999**, *589*, 213.

(547) Adams, C. J.; Bruce, M. I.; Skelton, B. W.; White, A. H. *Aust. J. Chem.* **1993**, *46*, 1811.

(548) Adams, C. J.; Bruce, M. I.; Skelton, B. W.; White, A. H. *Inorg. Chem.* **1992**, *31*, 3336.

(549) Adams, C. J.; Bruce, M. I.; Skelton, B. W.; White, A. H. *J. Organomet. Chem.* **1992**, *423*, 105.

(550) Hayward, C.-M.T.; Shapley, J. R.; Churchill, M. R.; Bueno, C.; Rheingold, A. L. *J. Am. Chem. Soc.* **1982**, *104*, 7347.

(551) Churchill, M. R.; Bueno, C.; Rheingold, A. L. *J. Organomet. Chem.* **1990**, *395*, 85.

(552) Bruce, M. I.; Skelton, B. W.; White, A. H.; Zaitseva, N. N. *J. Chem. Soc., Dalton Trans.* **2002**, 3879.

(553) Ma, L.; Rodgers, D. P. S.; Wilson, S. R.; Shapley, J. R. *Inorg. Chem.* **1991**, *30*, 3591.

(554) Benson, J. W.; Ishida, T.; Lee, K.; Wilson, S. R.; Shapley, J. R. *Organometallics* **1997**, *16*, 4929.

(555) Lee, K.; Shapley, J. R. *Organometallics* **1998**, *17*, 4030.

(556) Lee, K.; Shapley, J. R. *Organometallics* **1998**, *17*, 4368.

(557) Lee, K.; Shapley, J. R. *Organometallics* **1998**, *17*, 4113.

(558) Martinengo, S.; Noziglia, L.; Fumagalli, A.; Albano, V. G.; Braga, D.; Grepioni, F. *J. Chem. Soc., Dalton Trans.* **1998**, 2493.

(559) Albano, V. G.; Braga, D.; Ciani, G.; Martinengo, S. *J. Organomet. Chem.* **1981**, *213*, 293.

(560) Albano, V. G.; Braga, D.; Chini, P.; Ciani, G.; Martinengo, S. *J. Chem. Soc., Dalton Trans.* **1982**, 645.

(561) Albano, V. G.; Braga, D.; Fumagalli, A.; Martinengo, S. *J. Chem. Soc., Dalton Trans.* **1985**, 1137.

(562) Albano, V. G.; Chini, P.; Martinengo, S.; Sansoni, M.; Strumolo, D. *J. Chem. Soc., Dalton Trans.* **1978**, 459.

(563) Albano, V. G.; Braga, D.; Chini, P.; Strumolo, D.; Martinengo, S. *J. Chem. Soc., Dalton Trans.* **1983**, 249.

(564) Heaton, B. T.; Stroma, L.; Martinengo, S.; Strumolo, D.; Goodfellow, R. J.; Sadler, I. H. *J. Chem. Soc., Dalton Trans.* **1982**, 1499.

(565) Strumolo, D.; Seregni, C.; Martinengo, S.; Albano, V. G.; Braga, D. *J. Organomet. Chem.* **1983**, *252*, C93.

(566) Beringhelli, T.; Morazzoni, F.; Strumolo, D. *J. Organomet. Chem.* **1982**, *236*, 109.

(567) Albano, V. G.; Braga, D.; Strumolo, D.; Seregni, C.; Martinengo, S. *J. Chem. Soc, Dalton Trans.* **1985**, 1309.

(568) Martinengo, S.; Strumolo, D.; Chini, P.; Albano, V. G.; Braga, D. *J. Chem. Soc., Dalton Trans.* **1984**, 1837.

(569) Albano, V. G.; Sansoni, M.; Chini, P.; Martinengo, S.; Strumolo, D. *J. Chem. Soc., Dalton Trans.* **1975**, 305.

(570) Albano, V. G.; Chini, P.; Martinengo, S.; Sansoni, M.; Strumolo, D. *J. Chem. Soc., Chem. Commun.* **1974**, 299.
(571) Albano, V. G.; Sansoni, M.; Chini, P.; Martinengo, S.; Strumolo, D. *J. Chem. Soc., Dalton Trans.* **1976**, 970.
(572) Fumagalli, A.; Martinengo, S.; Bernasconi, G.; Noziglia, L.; Albano, V. G.; Monari, M.; Castellari, C. *Organometallics* **2000**, *19*, 5149.
(573) Ceriotti, A.; Longoni, G.; Manassero, M.; Masciocchi, N.; Resconi, L.; Sansoni, M. *J. Chem. Soc., Chem. Commun.* **1985**, 181.
(574) Ceriotti, A.; Piro, G.; Longoni, G.; Manassero, M.; Masciocchi, N.; Sansoni, M. *New J. Chem.* **1988**, *12*, 501.
(575) Ceriotti, A.; Longoni, G.; Manassero, M.; Masciocchi, N.; Piro, G.; Resconi, L.; Sansoni, M. *J. Chem. Soc., Chem. Commun.* **1985**, 1402.
(576) Calderoni, F.; Demartin, F.; Iapalucci, M. C.; Longoni, G. *Angew. Chem.* **1996**, *108*, 2393; *Angew. Chem., Int. Ed. Engl.* **1996**, *35*, 2225.
(577) Calderoni, F.; Demartin, F.; Fabrizi de Biani, F.; Femoni, C.; Iapalucci, M. C.; Longoni, G.; Zanello, P. *Eur. J. Inorg. Chem.* **1999**, 663.
(578) Ceriotti, A.; Fait, A.; Longoni, G.; Piro, G.; Resconi, L.; Demartin, F.; Manassero, M.; Masciocchi, N.; Sansoni, M. *J. Am. Chem. Soc.* **1986**, *108*, 5370.
(579) Ceriotti, A.; Fait, A.; Longoni, G.; Pino, G.; Demartin, F.; Manassero, M.; Masciocchi, N.; Sansoni, M. *J. Am. Chem. Soc.* **1986**, *108*, 8091.
(580) Nakajima, T.; Ishiguro, A.; Wakatsuki, Y. *Angew. Chem. Int. Ed.* **2000**, *39*, 1131.
(581) Shephard, D. S.; Maschmeyer, T.; Johnson, B. F. G.; Thomas, J. M.; Sankar, G.; Ozkaya, D.; Zhou, W.; Oldroyd, R. D.; Bell, R. G. *Angew. Chem.* **1997**, *109*, 2337; *Angew. Chem., Int. Ed. Engl.* **1997**, *36*, 2242.
(582) Ceriotti, A.; Della Pergola, R.; Garlaschelli, L.; Longoni, G.; Manassero, M.; Masciocchi, N.; Sansoni, M.; Zanello, P. *Gazz. Chim. Ital.*, **1992**, *122*, 365 (*Chem. Abstr. 118*, 159796).
(583) Arrigoni, A.; Ceriotti, A.; Della Pergola, R.; Longoni, G.; Manassero, M.; Masciocchi, N.; Sansoni, M. *Angew. Chem.* **1984**, *96*, 290; *Angew. Chem., Int. Ed. Engl.* **1984**, *23*, 322.
(584) Arrigoni, A.; Ceriotti, A.; Della Pergola, R.; Longoni, G.; Manassero, M.; Sansoni, M. *J. Organomet. Chem.* **1985**, *296*, 243.
(585) Longoni, G.; Ceriotti, A.; Della Pergola, R.; Manassero, M.; Perego, M.; Piro, G.; Sansoni, M. *Phil. Trans. R. Soc. London* **1982**, *A308*, 47.
(586) Fumagalli, A.; Martinengo, S.; Albano, V. G.; Braga, D.; Grepioni, F. *J. Chem. Soc., Dalton Trans.* **1993**, 2047.
(587) Yam, V. W.-W.; Fung, W. K.-M.; Cheung, K.-K. *Angew. Chem.* **1996**, *108*, 1213; *Angew. Chem., Int. Ed. Engl.* **1996**, *35*, 1100.
(588) Song, H.-B.; Wang, Q.-M.; Zhang, Z.-Z.; Mak, T. C. W. *Chem. Commun.* **2001**, 1658.
(589) R. Vestin, *Acta Chem. Scand.* **1949**, *3*, 101, 107.
(590) Guo, G.-C.; Zhou, G.-D.; Mak, T. C. W. *J. Am. Chem. Soc.* **1999**, *121*, 3136.
(591) Guo, G.-C.; Wang, Q.-G.; Zhou, G.-D.; Mak, T. C. W. *Chem. Commun.* **1998**, 339.
(592) Wang, Q.-M.; Mak, T. C. W. *J. Am. Chem. Soc.* **2001**, *123*, 7594.
(593) Wang, Q.-M.; Mak, T. C. W. *J. Am. Chem. Soc.* **2000**, *122*, 7608.
(594) Wang, Q.-M.; Guo, G.-C.; Mak, T. C. W. *J. Cluster Sci.* **2002**, *13*, 63.
(595) Wang, Q.-M.; Mak, T. C. W. *Angew. Chem. Int. Ed.* **2001**, *40*, 1130.
(596) Shaw, J. A.; Fisher, E. *J. Am. Chem. Soc.* **1946**, *68*, 2745.
(597) Osterlof, J. *Acta Crystallogr.* **1954**, 7, 637.
(598) Redhouse, A. D.; Woodward, P. *Acta Crystallogr.* **1964**, *17*, 616.
(599) Jin Xiabglin, Zhou Gongdu, Wu Nianzu, Tang Youqi, Huang Haochun, *Huaxue Xuebao (Acta Chim. Sin.)* **1990**, *48*, 232 (*Chem. Abstr. 113*, 88547).

(600) Mak, T. C. W.; Zhou, G.-D. *Crystallography in Modern Chemistry: a Resource Book of Crystal Structures*, Wiley-Interscience, New York, 1992. p. 288.

(601) Wang, Q.-M.; Mak, T. C. W. *Chem. Commun*. **2001**, 807.

(602) Wang, Q.-M.; Lee, H. K.; Mak, T. C. W. *New J. Chem*. **2002**, *26*, 513.

(603) Wang, Q.-M.; Mak, T. C. W. *Chem. Commun*. **2002**, 2682.

(604) Guo, G.-C.; Zhou, G.-D.; Wang, Q.-G.; Mak, T. C. W. *Angew. Chem.* **1998**, *110*, 652; *Angew. Chem., Int. Ed.* **1998**, *37*, 630.

(605) Wang, Q.-M.; Mak, T. C. W. *J. Am. Chem. Soc.* **2001**, *123*, 1501.

(606) Wang, Q.-M.; Mak, T. C. W. *Angew. Chem. Int. Ed.* **2002**, *41*, 4135.

(607) Halet, J.-F.; Mingos, D. M. P. *Organometallics* **1988**, *7*, 51.

(608) Halet, J.-F., (M. Gielen, Ed.) *Topics in Physical Organometallic Chemistry*, Vol. 4, Freund, London, 1992. p. 221.

(609) Carty, A. J.; Hogarth, G.; Enright, G.; Frapper, G. *Chem. Commun*. **1997**, 1883.

(610) Davies, J. E.; Mays, M. J.; Raithby, P. R.; Sarveswaran, K. *Angew. Chem.* **1997**, *109*, 2784; *Angew. Chem., Int. Ed. Engl.* **1997**, *36*, 2668.

(611) Mingos, D. M. P.; Kanters, R. P. F. *J. Organomet. Chem.* **1990**, *384*, 405.

(612) Schilling, B. E. R.; Hoffmann, R. *J. Am. Chem. Soc.* **1979**, *101*, 3456.

(613) Pinhas, A. R.; Albright, T. A.; Hofmann, P.; Hoffmann, R. *Helv. Chim. Acta* **1980**, *63*, 929.

(614) Chesky, P. T.; Hall, M. B. *Inorg. Chem.* **1981**, *20*, 4419.

(615) Rosch, N.; Ackkermann, L.; Pacchioni, G. *J. Am. Chem. Soc.* **1992**, *114*, 3549.

ADDENDUM

In the few months since finishing our review and receiving proofs, several important papers have appeared, surely a sign of a rapidly developing field of contemporary interest. These are summarized below in order of the above Sections.

I. Some aspects of the chemistry of metal alkynyls including $M–C_n–M$ complexes have been reviewed,[616] while volume 670 (2003) of *J. Organomet. Chem*. is dedicated to carbon-rich organometallics and contains several relevant articles.

II. A couple of complexes have been inadvertently omitted: $\{Cu(\mu-C_2)Ti(C\equiv CSiMe_3)Cp^{SiMe3}\}_2$[617] and $\{ZrCp_2\}_2(\mu_4-C_4)\{Zr(C\equiv CSiMe_3)Cp_2\}_2$.[618] Yam has described luminescent $[\{4,4',4''-Bu^t_3-trpy)Pt\}_2\{(\mu-C\equiv C)_m\}]^{2+}$ ($m = 1, 2, 4$; all structurally characterized).[619]

II.B. Rosenthal has written an important highlight in which the various coordination modes of C_2 are highlighted and rationalized.[620] He concludes that the isolobal relationships between $[M]_2C_2$ complexes and alkynes C_2R_2, coupled with the extreme mobility of the C_2 ligand, might lead to further unusual rearrangements of the former. Principles of structure and reactivity can be extended to the longer carbon chains, in which "walking" of the metal center along the carbon chain, already observed for poly-ynes,

is expected for multi-metal species. The acid-base chemistry of $\{Ru(CO)_2 Cp\}_2(\mu\text{-}C\equiv C)$ involves protonation to give on occasion trinuclear $[\{Ru(CO)_2Cp^R\}_3(\mu_3\text{-}C\equiv C)]^+$ and, more reliably and reversibly, $[\{Ru(CO)_2 CpR\}_2(\mu\text{-}\eta^1{:}\eta^2\text{-}C_2H)]^{+}.$[621] Aurophilic interactions are present in $\{Au (PR_3)\}_2(\mu\text{-}C\equiv C)$ $(PR_3 = PMe_3, PMe_2Ph)$ but not with the larger PEt_3 analogue.[622]

II.D. The preparation and structures of W(II), W(VI) diyndiyl complexes $\{W(CO)_3Cp^*\}_2(\mu\text{-}C\equiv CC\equiv C)$, $\{W(O)_2Cp^*\}_2(\mu\text{-}C\equiv CC\equiv C)$ have been reported.[623] Reactions of $[Ag_2(\mu\text{-}dppm)_2(NCMe)_2]^{2+}$ with $Re(C\equiv CC\equiv CH)(CO)_3(NN)$ $(NN = Me_2\text{-}bpy, Bu^t_2\text{-}bpy, phen, Br_2\text{-}phen)$ have given $[Ag_6\{\mu_3\text{-}C\equiv CC\equiv C[Re(CO)_3(NN)]\}_4(\mu\text{-}dppm)_4]^{2+}$ (X-ray for Me_2-bpy, Br_2-phen).[624] The syntheses, structures and spectro-electrochemistry of $\{Ru(PP)Cp^*\}_2(\mu\text{-}C\equiv CC\equiv C)$ $(PP = dppe, dppm)$ and the mono- and di-oxidized species have been reported. This study includes the structural characterization of the cumulenic dication.[625] Trimetallic systems $Hg\{C\equiv CC\equiv C[Ru(dppe)Cp']\}_2$ $(Cp' = Cp, Cp^*)$ have been obtained, the Cp^* derivative showing an unusual bend at the $\equiv C$–Hg carbon [166.5(2)°]. Calculations showed only limited mixing of the Hg d and $C\equiv C$-based π orbital, suggesting that the chain distortion results from crystal lattice forces.[626] A C–C coupling reaction occurs in the reaction of $\{Rh(=C=CHFc)(PPr^i_3)_2\}_2(\mu\text{-}C\equiv CC\equiv C)$ [from $RhF(=C=CHFc)(PPr^i_3)_2$ and $Ph_3SnC\equiv CC\equiv CSnPh_3$] with CO to give $\{Rh(CO)(PPr^i_3)_2\}_2\{\mu\text{-}C(=CHFc)C\equiv CC\equiv CC(=CHFc)\}$.[627]

II.F. Oxidative coupling $[Cu(OAc)_2/py]$ of labile $Re(C\equiv CC\equiv CH)(NO)\{PPh_2(CH_2)_nPPh_2\}Cp^*$ $(n = 10, 14)$ afforded the analogous binuclear C_8 complexes, which each undergo two 1-e oxidations.[628] The synthesis and spectroscopic and electrochemical studies of $\{Fe(dppe)Cp^*\}_2\{\mu\text{-}(C\equiv C)_4\}$ have been reported, together with its structure and time-dependent DFT calculations.[629] Oxidative coupling $[Cu(OAc)_2/py]$ of *trans*-$RuCl\{(C\equiv C)_3H\}(dppe)_2$ afforded the corresponding binuclear C_{12} complex, for which $K_C = 10^4$.[630] A full account of the chemistry of $\{Pt(C_6F_5)[P(tol)_3]_2\}_2\{\mu\text{-}(C\equiv C)_m\}$ describes the syntheses of compounds with $m = 3, 4, 6, 8$, together with trace quantities of $m = 10, 12$. Effects of m on IR, UV/vis, NMR and redox properties, together with the degree of chain bending in the solid state, are discussed.[631]

II.G. The chemistry of carbon chains end-capped by binuclear metal–ligand fragments has been reviewed.[319,632] Extensive spectroscopic and electrochemical studies of $\{Ru_2(ap)_4\}_2(\mu\text{-}(C\equiv C)_m\}$ $(m = 1\text{–}4, 6; $ X-ray for $m = 2, 4)$ have been reported.[633]

III.B. Four oxidation waves are found for $CoCp(\eta^4\text{-}C_4Fc_4)$ and the mono- and dications behave as Class II and Class II/III mixed-valence species, respectively.[634]

IV.D. Bonding within $[L_mMC_4M'L'_n]^{z+}$ $[ML_m, M'L'_n = Fe(dppe)Cp',$ $Re(NO)(PR_3)Cp'; z = 0–4]$ has been explored using DFT which confirms the occurrence of cumulenic singlet dications which have nearly isoenergetic triplet states with diyndiyl structures.[635] X-ray structures of {Fe(dppe) Cp*}$_2$(μ-C≡CC≡C) and [{Fe(dippe)Cp*}$_2$(μ-C$_4$)][PF$_6$]$_3$ are given.

IX.A. Akita and colleagues have reviewed the chemistry of cluster complexes derived from Fp*$_2${μ-(C≡C)$_m$} $(m = 1, 2)$.[636,637] Reaction of Fe$_2$Ru$_2$(μ$_4$-C$_2$)(CO)$_{10}$Cp*$_2$ (**300**) with C$_2$Ph$_2$ afforded Fe$_2$Ru$_2$(μ$_4$-C$_2$)(μ-PhC$_2$Ph)(CO)$_6$Cp*$_2$ containing an unprecedented dimetallacyclobutatriene fragment.[638]

IX.B. The synthesis and structure of [PPh$_4$]$_2$[Pt$_3$Ru$_{10}$(C)$_2$(CO)$_{32}$] have been described.[639]

IX.C. Further examples of C$_2$@Ag$_n$ clusters were found in complexes obtained from Ag$_2$C$_2$ and Ag(tfa) and various *N*-donor ligands,[640] Ag(tfa) or Ag(OTf) with (4-hydroxymethyl)pyridine,[641] Ag(tfa) or Ag(pfp) with crown ethers,[642] and an anionic Ag(I) double cage formed from Ag(tfa), AgNO$_3$ and [NMe$_3$(CH$_2$Ph)]$^+$.[643]

References

(616) Long, N. J.; Williams, C. K. *Angew. Chem. Int. Ed.* **2003**, *42*, 2586.

(617) Jansen, M. D.; Herres, M.; Zsolnai, L.; Grove, D. M.; Spek, A. L.; Lang, H.; van Koten, G. *Organometallics*, **1995**, *14*, 1098.

(618) Pellny, P.-M.; Peulecke, N.; Burlakov, V. V.; Tillack, A.; Baumann, W.; Spannenberg, A.; Kempe, R.; Rosenthal, U. *Angew. Chem.* **1997**, *109*, 2728; *Angew. Chem., Int. Ed. Engl.* **1997**, *36*, 2615.

(619) Yam, V. W.-W.; Wong, K. M.-C.; Zhu, N. *Angew. Chem. Int. Ed.* **2003**, *42*, 1400.

(620) Rosenthal, U. *Angew. Chem. Int. Ed.* **2003**, *42*, 1794.

(621) Griffith, C. S.; Koutsantonis, G. A.; Skelton, B. W.; White, A. H. *J. Organomet. Chem.* **2003**, *670*, 198.

(622) Liau, R.-Y.; Schier, A.; Schmidbaur, H. *Organometallics*, **2003**, *22*, 3199.

(623) Roberts, R. L.; Puschmann, H.; Howard, J. A. K.; Yamamoto, J. H.; Carty, A. J.; Low, P. J. *J. Chem. Soc., Dalton Trans.* **2003**, 1099.

(624) Yam, V. W.-W.; Lo, W.-Y.; Zhu, N. *Chem. Commun.* **2003**, 2446.

(625) Bruce, M. I.; Ellis, B. G.; Low, P. J.; Skelton, B. W.; White, A. H. *Organometallics* **2003**, *22*, 3184.

(626) Bruce, M. I.; Halet, J.-F.; Le Guinnec, B.; Skelton, B. W.; White, A. H. *Inorg. Chim. Acta* **2003**, *350*, 175.

(627) Callejas-Gaspar, B.; Laubender, M.; Werner, H. *J. Organomet. Chem.* **2003**, *684*, 144.

(628) Horn, C. R.; Gladysz, J. A. *Eur. J. Inorg. Chem.* **2003**, 2211.

(629) Coat, F.; Paul, F.; Lapinte, C.; Toupet, L.; Costuas, K.; Halet, J.-F. *J. Organomet. Chem.* **2003**, *683*, 386.

(630) Rigaut, S.; Perruchon, J.; Le Pichon, L.; Touchard, D.; Dixneuf, P. H. *J. Organomet. Chem.* **2003**, *670*, 37.

(631) Mohr, W.; Stahl, J.; Hampel, F.; Gladysz, J. A. *Chem. Eur. J.* **2003**, *9*, 3324.

(632) Hurst, S. K.; Ren, T. *J. Organomet. Chem.* **2003**, *670*, 188.

(633) Xu, G.-L.; Zou, G.; Ni, Y.-H.; DeRosa, M. C.; Crutchley, R. J.; Ren, T. *J. Am. Chem. Soc.* **2003**, *125*, 10057.
(634) Jiao, J.; Long, G. J.; Grandjean, F.; Beatty, A. M.; Fehlner, T. P. *J. Am. Chem. Soc.* **2003**, *125*, 7522.
(635) Jiao, H.; Costuas, K.; Gladysz, J. A.; Halet, J.-F.; Guillemot, M.; Toupet, L.; Paul, F.; Lapinte, C. *J. Am. Chem. Soc.* **2003**, *125*, 9511.
(636) Akita, M.; Sakurai, A.; Chung, M.-C.; Moro-oka, Y. *J. Organomet. Chem.* **2003**, *670*, 2.
(637) Terada, M.; Akita, M. *Organometallics* **2003**, *22*, 355.
(638) Terada, M.; Higashihara, G.; Inagaki, A.; Akita, M. *Chem. Commun.* **2003**, 2910.
(639) Khimyak, T.; Johnson, B. F. G.; Hermans, S.; Bond, A. D. *Dalton Trans.* **2003**, 2651.
(640) Wang, Q.-M.; Mak, T. C. W. *Inorg. Chem.* **2003**, *42*, 1637.
(641) Wang, Q.-M.; Guo, G.-C.; Mak, T. C. W. *J. Organomet. Chem.* **2003**, *670*, 235.
(642) Wang, Q.-M.; Mak, T. C. W. *Chem. Eur. J.* **2003**, *9*, 44.
(643) Wang, Q.-M.; Mak, T. C. W. *Chem. Commun.* **2003**, 25.

Index

N

O

P

Cumulative List of Contributors
for Volumes 1–36

Abel, E. W., **5,** 1; **8,** 117
Aguiló. A., **5,**321
Akkerman, O. S., **32,** 147
Albano, V. G., **14,** 285
Alper, H., **19,** 183
Anderson, G. K., **20,** 39; **35,** 1
Angelici, R. J., **27,** 51
Aradi, A. A., **30,**189
Armitage, D. A., **5,** 1
Armor, J. N., **19,** 1
Ash, C. E., **27,** 1
Ashe, A. J., III. **30,** 77
Atwell, W. H., **4,** 1
Baines. K. M., **25,** 1
Barone, R., **26,** 165
Bassner, S. L., **28,** 1
Behrens, H., **18,** 1
Bennett, M. A., **4,** 353
Bickelhaupt, F., **32,** 147
Binningham, J., **2,** 365
Blinka, T. A., **23,** 193
Bockman, T. M., **33,** 51
Bogdanović, B., **17,** 105
Bottomley, F., **28,** 339
Bradley, J. S., **22,** 1
Brew, S. A., **35,** 135
Brinckman, F. E., **20,** 313
Brook. A. G.. 7, 95; **25,** 1
Bowser, J. R., **36,** 57
Brown, H. C., **11,** 1
Brmcn, T. L., **3,** 365
Bruce, M. 1., **6,** 273, **10,** 273; **11,** 447: **12,** 379:
  22, 59
Brunner, H., **18,** 151
Buhro, W. E., **27,** 311
Byers, P. K., **34,** 1
Cais, M., **8,** 211
Calderon, N., **17,** 449
Callahan, K. P., **14,** 145
Canty, A. J., **34,** 1
Cartledge, F. K., **4,** 1
Chalk, A. J., **6,** 119
Chanon, M., **26,** 165

Chatt, J., **12, 1**
Chini, P., **14,**285
Chisholm, M. H., **26,** 97; **27,**311
Chiusoli, G. P., **17,** 195
Chojinowski, J., **30,** 243
Churchill, M. R., **5,** 93
Coates, G. E., **9,** 195
Collman, J. P., **7,**53
Compton, N. A., **31,** 91
Connelly, N. G., **23,** 1; **24,** 87
Connolly, J. W., **19,** 123
Corey, J. Y., **13,** 139
Corriu, R. J. P., **20,** *265*
Courtney, A., **16,** 241
Coutts, R. S. P., **9,** 135
Coville, N. J., **36,** 95
Coyle. T. D., **10,** 237
Crabtree, R. H., **28,** 299
Craig, P J., **11,** 331
Csuk, R., **28,** 85
Cullen, W R., **4,** 145
Cundy, C. S., **11,** 253
Curtis, M. D., **19,** 213
Darensbourg, D. J., **21,** 113; **22,** 129
Darensbourg, M. Y., **27,** 1
Davies, S. G., **30,** 1
Deacon, G. B., **25,** 337
de Boer, E., **2,** 115
Deeming, A. J., **26,** 1
Dessy, R. E., **4,** 267
Dickson, R. S., **12,** 323
Dixneuf, P H., **29,** 163
Eisch, J. J., **16,** 67
Ellis, J. E., **31,** 1
Emerson, G. F., **1,** 1
Epstein, P. S., **19,** 213
Erker. G., **24,** 1
Ernst, C. R., **10,** 79
Errington, R. J., **31,** 91
Evans, J., **16,** 319
Evan, W. J., **24,** 131
Faller, J. W., **16,** 211
Farrugia, L. J., **31,** 301

Stone, F. G. A., **1,** 143; **31,** 53; **35,** 135
Su, A. C. L., **17,** 269
Suslick, K. M., **25,** 73
Süss-Fink, G., **35,** 41
Sutin, L., **28,** 339
Swincer, A. G., **22,** 59
Tamao, K., **6,** 19
Tate, D. P., **18,** 55
Taylor, E. C., **11,** 147
Templeton, J. L., **29,** 1
Thayer, J. S., **5,** 169; **13,** 1; **20,** 313
Theodosiou, I., **26,** 165
Timms, P. L., **15,** 53
Todd, L. J., **8,** 87
Touchard, D., **29,** 163
Traven, V. F., **34,** 149
Treichel, P. M., **1,** 143; **11,** 21
Tsuji, J., **17,** 141
Tsutsui, M., **9,** 361; **16,** 241
Turney, T. W., **15,** 53
Tyfield, S. P., **8,** 117
Usón, R., **28,** 219
Vahrenkamp, H., **22,** 169
van der Kerk, G. J. M., **3,** 397

van Koten, G., **21,** 151; **35,** 241
Veith, M., **31,** 269
Vezey, P. N., **15,** 189
von Ragué Schleyer, P., **24,** 353; **27,** 169
Vrieze, K., **21,** 151
Wada, M., **5,** 137
Walton, D. R. M., **13,** 453
Wailes, P. C., **9,** 135
Webster, D. E., **15,** 147
Weitz, E., **25,** 277
West, R., **5,** 169; **16,** 1; **23,** 193
Werner, H., **19,** 155
White, D., **36,** 95
Wiberg, N., **23,** 131; **24,** 179
Wiles, D. R., **11,** 207
Wilke, G., **8,** 29
Williams, R. E., **36,** 1
Winter, M. J., **29,** 101
Wojcicki, A., **11,** 87; **12,** 31
Yamamoto, A., **34,** 111
Yashina, N. S., **14,** 63
Ziegler, K., **6,** 1
Zuckerman, J. J., **9,** 21
Zybill, C., **36,** 229

Cumulative Index
for Volumes 37–50